The role of serotoninergic neurons in amyotrophic lateral sclerosis

Hajer El Oussini-Ben Chaabane

UNIVERSITÉ DE STRASBOURG

ÉCOLE DOCTORALE 414

Sciences de la vie et de la santé

INSERM U1118

THÈSE présentée par :

Hajer EL OUSSINI-BEN CHAABANE

Soutenue le : **12 juillet 2016**

Pour obtenir le grade de : **Docteur de l'université de Strasbourg**

Discipline/ Spécialité : Neurosciences

Rôle des neurones sérotoninergiques dans la sclérose latérale amyotrophique

THÈSE dirigée par :

Mr. DUPUIS Luc	Directeur de recherches, université de Strasbourg

RAPPORTEURS :

Mme. BOILLEE Séverine	Directrice de recherches, ICM Paris
Mr. BRANCHEREAU Pascal	Professeur, université de Bordeaux

PRESIDENT DU JURY :

Mr. CASSEL Jean Christophe	Directeur de recherches, université de Strasbourg

ACKNOWLEDGMENT

There are no proper words to convey my deepest and sincere gratitude for my thesis and research advisor **Dr. Luc DUPUIS** for the continuous support during my master and PhD. I would like to thank him for his patience, motivation, immense knowledge and his guidance that helped me in all the time of research and writing of the thesis. He has inspired me to become an independent researcher and helped me to realize the power of critical reasoning. Ever since, Luc has supported me not only by providing a research assistantship over almost five years, but also for the moral support and his trust through the rough road to finish this thesis. Thanks to him I had the opportunity to build my scientific knowledge and a huge technical background. I could not have imagined having a better advisor and mentor for my Ph.D study.

Besides my advisor, I would like to thank my thesis committee: **Dr. Séverine BOILLEE**, **Prof. Jean Christophe CASSEL** and **Prof. Pascal BRANCHEREAU** for their time and for reviewing my thesis.

My sincere thanks also go to Dr. **Jean Philippe LOEFFLER**, who provided me an opportunity to join his team, and who gave me access to the laboratory and research facilities. Without his precious support it would not be possible to conduct this research.

A special acknowledgement goes to **Frederique, RENÉ**, **Sylvie GROSCH** and **Annie PICCHINENNA** for their joyful spirits and technical help all this time and for being supportive in every way.

I would like to thank specially **Caroline ROUAUX, Marc de TAPIA** and **José-Luis GONZALEZ DE AGUILAR** for their help and previous advice and for being an inspiration on how to make things 'perfect'.

I would like to thank **Brigitte KUENEMANN** and **Marie Jo RUIVO** for keeping their office door open and being available every time when we needed you.

There is no way to express how much it meant to me to have been a member of Laboratory. These brilliant friends and colleagues inspired me over the many years: Special thanks must go to **Pauline VERCRUYSSE, Stephane DIETLERE, Alexandre HENRIQUES**, **Christine MARQUES, Mathieu FISCHER, Laura ROBELIN, Gina PICCHIARELLI, Robin WAEGAERT, Thibaut BURG** and **Alexia MENUET** for all exchanges, for all the fun we have had in the last five years, for their precious friendship and for being a source of energy ever since.

Thank you to those who helped the project as graduate students: **Coraline KOSTAL, Marc-Antoine GOY and Sebastien FREISMUTH.**

My endless acknowledgement goes to **Jelena SCEKIC-ZAHIROVIC** and **Jérôme SINNIGER**, my true friends since we began working together. They have been my best friends and great companion, loved, supported, encouraged, entertained, and helped me to get through all in the most positive way. Thank you for being in my life and may our friendship last for the rest of our life.

My deepest acknowledgement goes to my family, my source of joy, my source of inspiration and my permanent source of motivation. Their support and endless love has been unconditional all these years, they have given up many things for me to be, and they supported me whenever I needed it and believed in me. Special thanks go To "**Les hommes de Hajer"**: **My husband**, **my father** and **my best friend François**. My biggest thanks goes also to **my mother** and **my sisters**.

Last, I am thankful for who gave me the first push to go further, my dearest **Grandfather** (May his spirit rest in peace).

TABLE OF CONTENT

ABBREVIATION

5-HT	5-hydroxytryptamine
5-HTTP	5-hydroxytryptophan
ALS	Amyotrophic lateral sclerosis
Ca^{2+}	Calicium
CNS	Central nervous system
cAMP	Cyclic adenosine 3',5'-monophosphate
DNA	Deoxyribonucleic Acid
DR	Dorsal raphe
EEC	El Escorial Criteria
EMG	Electromyography
FALS	Familial amyotrophic lateral sclerosis
FLTD	Frontotemporal dementia
GABA	Gamma-aminobutyric acid
LLR	Long lasting reflex
LMN	Lower motor neurons
MRI	Magnetic resonance imaging
MrR	Median raphe
MAO	Monoamine oxidase
MN	Motor neurons
NCS	Nerve conduction studies
PIC	Persistent inward currents
K^{+}	Potasium
KCC2	Potassium-chloride cotransporter 2
RMg	Raphe magnus
RNA	Ribonucleic Acid
P62	Sequestosome 1
Na^{+}	Sodium
SALS	Sporadic amyotrophic lateral sclerosis
SOD1	*Superoxide dismutase 1*
TDP43	TAR DNA-binding protein 43
UMN	Upper motor neurons

FOREWORD

The subject of my thesis was to investigate the role of serotonin neurons during amyotrophic lateral sclerosis (ALS).

This manuscript will be divided in an introductory part that describes ALS clinical and pathological features, the serotoninergic system and one major symptom of ALS, spasticity.

In the first result section, I will present how we have been elucidating the role of one serotonin receptor, serotonin receptor 2B (HTr2B) in ALS mouse models and patients.

A second major part of my results focused on understanding the role of mutant SOD1 toxicity in serotoninergic neurons during disease progression. The knock down of human mutant SOD1 (G37R) in serotoninergic neurons accelerated disease onset and abolished spasticity. The results of this study are presented as a manuscript in preparation in the results part.

The result section is followed by a concise discussion of my results along with some future perspectives.

Importantly, I included at the end of the manuscript of four published studies where I participated in during my PhD and my master. Since these papers were not directly related with my major topic, I will not discuss them, but include them in annex.

Introduction

I. Amyotrophic lateral sclerosis

1. Clinical and pathological definition

Amyotrophic lateral sclerosis (ALS) is a fatal neurodegenerative disease of adult onset. ALS is characterized by the simultaneous degeneration of upper motor neurons (UMN) in the motor cortex and lower motor neurons (LMN) in the brainstem and spinal cord. The term “amyotrophic” means “atrophy of muscle”, and this muscle atrophy leads to muscle weakness, paralysis and visible fasciculations. The term “Lateral sclerosis” refers to the hardening and degeneration of axons in the lateral corticospinal tracts (Cleveland & Rothstein, 2001; Wijesekera & Leigh, 2009; Dengler, 2010; Pratt *et al.*, 2012; Renton *et al.*, 2014; Swinnen & Robberecht, 2014; Zarei *et al.*, 2015)(Figure1).

Since 1824 several observations of the clinical and pathological features of ALS were described by Bell (1824), Aran (1850), Duchenne (1851), Cruveilher (1853) and last by Charcot (1869)(Cleveland & Rothstein, 2001; Wijesekera & Leigh, 2009). ALS patients develop several clinical signs in different levels. Two thirds of ALS patients have a so-called spinal form of the disease. They develop focal muscle weakness distally or proximally in the upper and lower limbs. Fasciculation or cramps are also observed in the majority of the cases characterized by noticed involuntary muscle twitching.

Patients gradually develop spasticity that consists in excess activation and hyperreflexia of the flexor arc in the limb, this appears mostly in the regions with marked atrophy. In the later stage patients develop bulbar and respiratory symptoms. The bulbar symptoms lead to sialorrhoea due to swallowing difficulties and facial weakness. For the respiratory symptoms patients present respiratory failure and hypoventilation with disturbed sleep and anorexia (Cleveland & Rothstein, 2001; Wijesekera & Leigh, 2009; Dengler, 2010; Pratt *et al.*, 2012; Renton *et al.*, 2014; Swinnen & Robberecht, 2014; Zarei *et al.*, 2015).

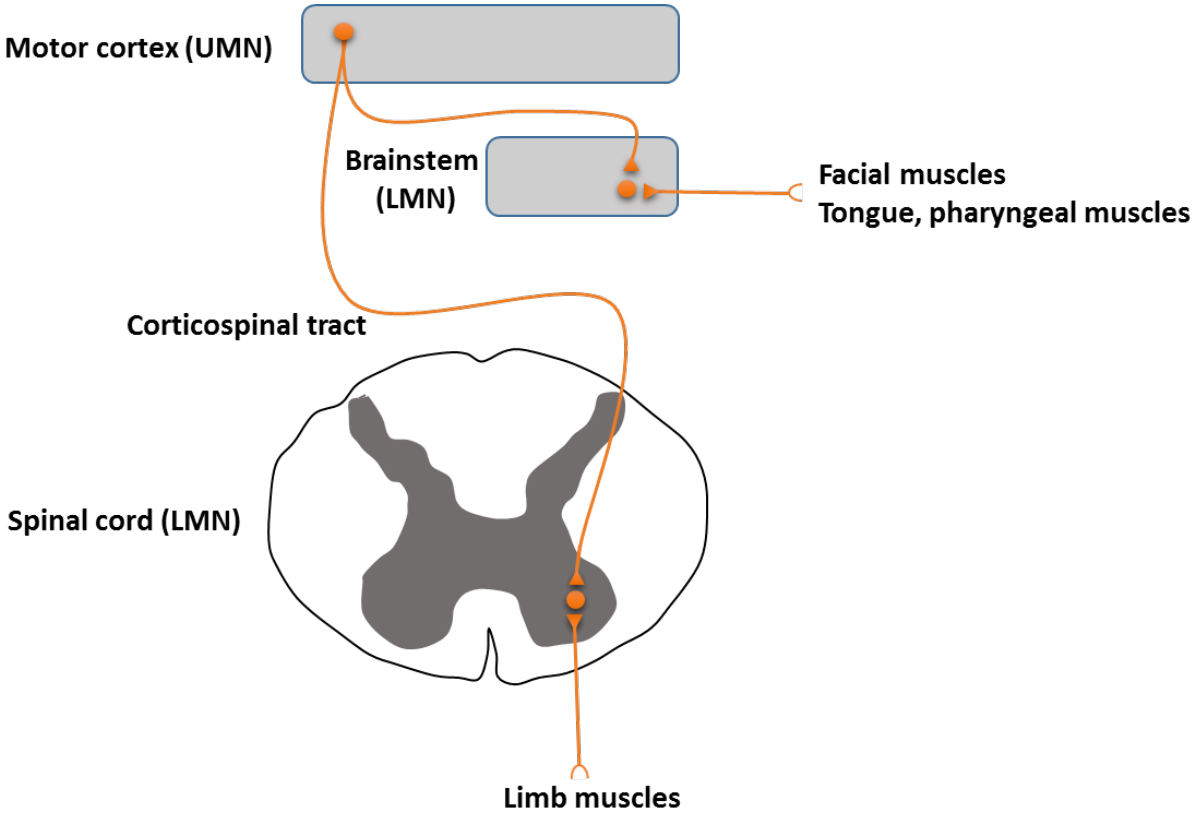

Figure 1: Amyotrophic lateral sclerosis: loss of upper and lower motor neurons (simplified scheme)

2. Clinical features

i. Hallmarks

The clinical definition of ALS implies that both upper motor neurons in the motor cortex and lower motor neurons in the brainstem and spinal cord degenerate. The main phenotypes of ALS include: **(1) limb onset** with first signs observed in the muscles of one limb and **(2) bulbar onset** with first signs observed in the muscles of the head and face.

ii. Phenotype diversity: site of onset

a. Bulbar onset

About 20% of ALS patients initially present with a bulbar onset affecting pharynx, tongue and larynx muscles. The bulbar onset is characterized by flail-arm-syndrome, dysarthria, dysphagia, tongue fasciculation and pseudobulbar affect with emotional imbalance. In clinical examination patients mostly show speech and swallowing disabilities. Bulbar onset patients usually show shorter survival as compared with spinal onset patients (Wijesekera & Leigh, 2009; Renton *et al.*, 2013; Swinnen & Robberecht, 2014).

b. Spinal onset

About 80% of ALS patients initially present with a spinal onset, characterized by an asymmetric painless weakness of limb. This symptom can occur distally or proximally, either in upper or lower limb. Clinical examination in patients reveals LMN and UMN signs. LMN signs are characterized by muscle atrophy, muscle weakness and visible fasciculations. UMN signs are characterized by marked hyperreflexia and hypertonia (Wijesekera & Leigh, 2009; Renton *et al.*, 2013; Swinnen & Robberecht, 2014).

c. Respiratory onset

About 5% of patients have respiratory onset with orthopnoea or dyspnoea with mild spinal or bulbar signs. Like bulbar onset, patients with respiratory onset have a shorter survival (Wijesekera & Leigh, 2009; Renton *et al.*, 2013; Swinnen & Robberecht, 2014).

iii. UMN syndrome

In ALS patients, **UMN signs** are characterized by increased tone and involuntary spasms called spasticity or hyperreflexia, and hypertonia (WADE, 2001).

In ALS **LMN signs** are characterized by lower limb muscle atrophy and denervation. These signs involve several muscles of the hands, forearms or shoulders. Clinical examination shows also lower muscle fasciculation and atrophy (Cleveland & Rothstein, 2001; Swinnen & Robberecht, 2014) (Figure 2 and 3).

iv. Others symptoms

Clinical examinations in patients showed emotional disequilibrium, decreased concentration, irritability and mood changes. ALS patients could also develop metabolic dysfunction with massive loss of weight due to hypermetabolism (Jelsone-Swain *et al.*, 2012; Zarei *et al.*, 2015).

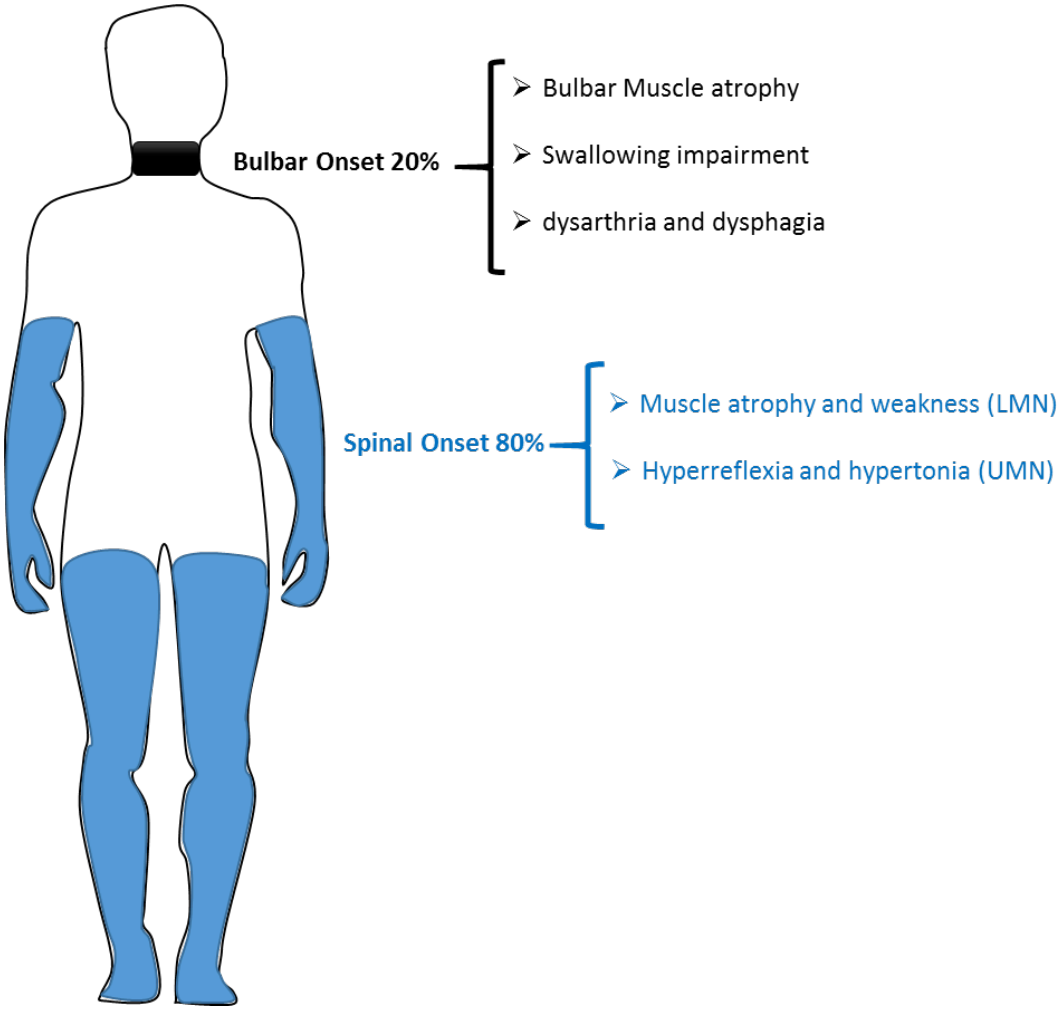

Figure 2: ALS major symptoms and site of onset reproduced from (Swinnen & Robberecht, 2014)

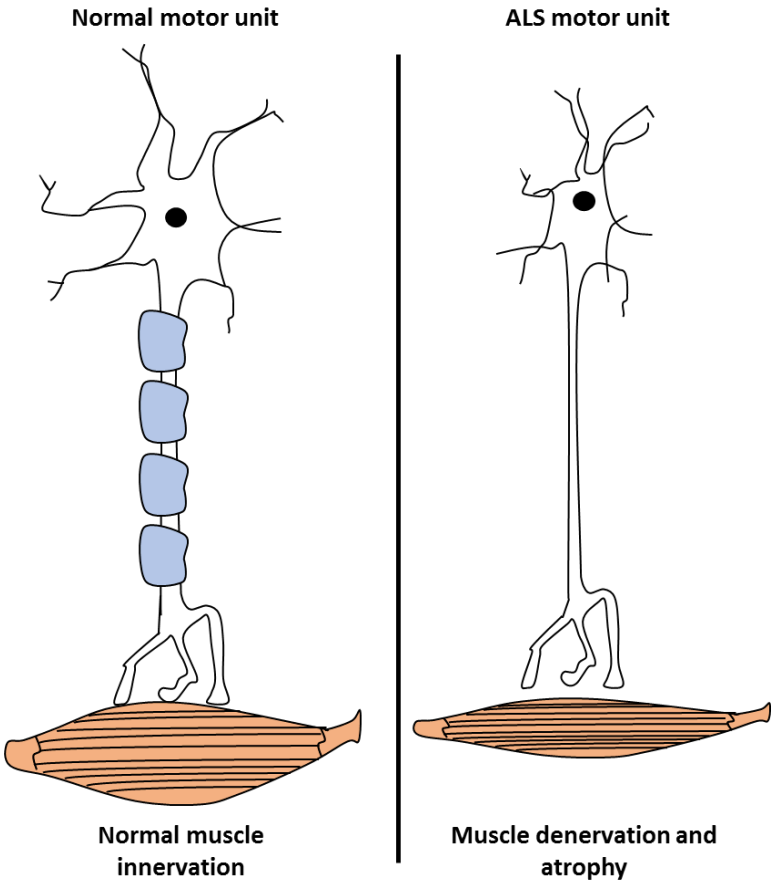

Figure 3: Amyotrophic lateral sclerosis: muscle denervation and atrophy upon lower motor neurons loss

3. Diagnostic methods and criteria

In ALS, different diagnostic methods are used for disease characterization such as nerve conduction studies, electromyography, neuroimaging, muscle biopsy and neuropathological studies.

i. Electrophysiological studies

Electrophysiological studies include two methods: nerve conduction studies (NCS) for motor and sensory nerves and electromyography (EMG) for motor unit. NCS are important to define and exclude other peripheral nerve and motor unit disorder. In ALS patients distal motor latency and motor conduction velocity remain normal whereas muscle potential is small which help clinicians during diagnosis to exclude multifocal motor neuropathy. EMG provides more clinical evidence specific for ALS, more precisely for LMN degeneration. For this, concentric needle electromyography examination is required to identify chronic denervation and muscle fasciculation signs (Figure 4a). In ALS patients muscle denervation signs consist of large motor unit potential with an increased amplitude and duration (Figure 4b). Quantitative EMG is used also to quantify and estimate the number of axons innervating to follow LMN loss during disease progression (Julien *et al.*, 2001; WADE *et al.*, 2001; Trompetto *et al.*, 2014; Teng *et al.*, 2015).

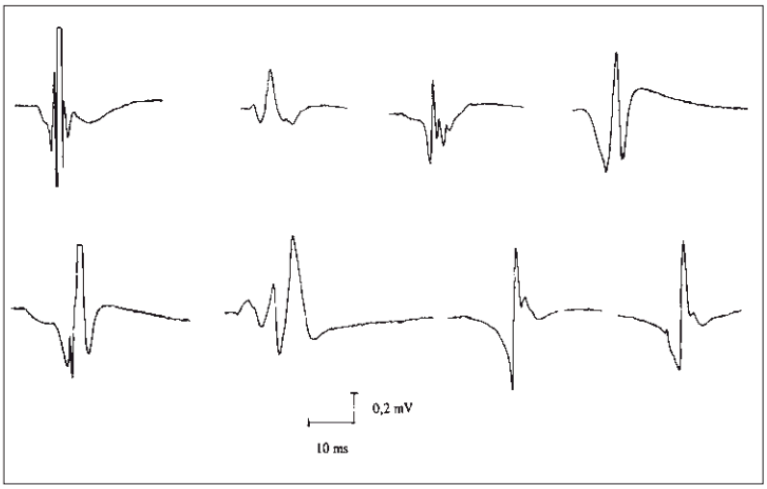

Figure 4a: Fasciculation potentials in the vastus lateral muscle of ALS patient (Dengler, 2010)

Figure 4b: EMG profile of motor unit potentials in the biceps muscle of ALS patient (Dengler, 2010)

ii. Neuroimaging studies

Neuroimaging is used to exclude other motor disease or structural lesion. The main two neuroimaging techniques used are magnetic resonance imaging (MRI) and X-rays. MRI is used in brain regions visualization during disease course and for revealing lesions in corticospinal tracts. Thorax X rays and neck MRI are also performed depending on the site of the onset in case of confirmed ALS (Wijesekera & Leigh, 2009; Dengler, 2010).

iii. Muscle biopsy and neuropathological studies

Upon clinical and electrophysiological examinations muscle biopsy is required for some cases to identify and confirm LMN dysfunction. Histological analysis of muscle biopsy in ALS are characterized by muscle hypotrophy and necrotic muscle fibers (Wijesekera & Leigh, 2009; Dengler, 2010).

iv. El Escorial Research Diagnostic Criteria protocol (Brooks *et al.*, 2000; Traynor *et al.*, 2000)

The standard protocol for clinical exam on ALS is the El Escorial Criteria (EEC). EEC is based on clinical and electrophysiological observations in order to identify ALS at an early stage of the disease and in clinical trials. **The EEC requires two major sets of criteria to approve ALS phenotype: The presence of A set criteria and absence of B set criteria.**

Table1: EEC criteria reproduced from (Wijesekera & Leigh, 2009; Dengler, 2010):

Presence of A-Criteria	Absence of B-Criteria
A1-Degeneration of LMN clinically, electrophysiologically and neuropathologically approved	**B1-**Electrophysiological or neuropathological UMN and LMN degeneration typical for other disease
A2-Degeneration of UMN clinically approved	**B2-**Imaging analysis showing clinical symptoms
A3- Progressive dissemination beyond typical nerve supply areas	

v. Airlie House criteria (Brooks *et al.*, 1994)

After clinical examination patients are classified into 4 categories:

- '**Clinically definite**' ALS with UMN and LMN signs in 3 regions.
- '**Clinically probable**' ALS with UMN and LMN signs in 2 regions and some UMN signs rostral to LMN signs.
- '**Clinically probable laboratory supported**' ALS UMN signs in 1 or 2 more regions and LMN signs defined by EMG in at least 2 regions.
- '**Clinically possible**' ALS with UMN and LMN signs in 1 region or UMN signs in 2 regions or UMN and LMN signs in 2 regions with no UMN signs rostral to LMN signs.

vi. ALS overlap with other neurodegenerative diseases

Frontotemporal dementia (FTLD) is a neurodegenerative disease described first by Arnold Pick in 1892, originally called Pick's disease. FTLD occurs between 55 and 65 years old. It is characterized by progressive aphasia and anterior temporal lobar atrophy. The atrophy is due to the degeneration of neurons in the superficial layers of the frontotemporal cortex and in the dentate gyrus of the hippocampus. FTLD have a strong genetic contribution compared to ALS, up to 30-50% of patient have familial history (Hodges *et al.*, 2003; Ng *et al.*, 2015).

There is a clinical overlap between ALS and frontotemporal lobar dementia (FTLD). 30-50% of ALS patients show at least some executive function deficits and 15% meet clinical criteria for FTLD. More over 50% of FTLD patients present with some forms of motor neuron dysfunction and 15% meet criteria for ALS (Lillo & Hodges, 2009; Mackenzie *et al.*, 2010; Burrell *et al.*, 2011; Strong & Yang, 2011). Ubiquitinated TDP-43 is a common pathological hallmark in both diseases (Neumann *et al.*, 2006).

4. Sporadic and familial ALS

Most ALS cases do not show family history of ALS or FTD, and are thus termed "sporadic ALS" (SALS). However, 10-15% of ALS cases shows a positive history for either ALS, or FTD, and is classified as familial (FALS). The mean age of onset for SALS is between 58-63 years and FALS is between syounger ages around 40-60 years. Several forms of FALS lead to an earlier onset at about 20 years of age. FALS cases are caused

by various mutations (see below), while no clear genetic linkage is observed in SALS. Besides genetic risks, several risk factors have been linked with ALS (Ingre *et al.*, 2015). These related risk factors are associated with dietary habits (food intake, hypermetabolism), gender, age, lifestyle (smoking, sport) and environment (viruses, pesticides, metals) (Wijesekera & Leigh, 2009; Ingre *et al.*, 2015).

5. Epidemiology and ALS incidence

ALS is an adult-onset neurodegenerative disease of unknown etiology. Most of ALS cases onset is between 55 and 65 years. Rare ALS cases are reported before the age of 40 years or at the 20th. Men have higher risk than women (ratio 1.3:1). The overall lifetime risk of developing the ALS is 1:350 for men and 1:400 for women.

The incidence is defined as the number of new cases per year. In Europe, within a population of 100,000 people, there are between 2 to 3 cases each year over the age of 15 years.

The prevalence or the number of people living with ALS is variable depending on geographic regions in the world. In France, the prevalence is around 5000 cases living with ALS. Every year there are 1000 new cases of ALS in France.

Several risk factors have been identified in sporadic and familial ALS. These risks factors are due to genetic history and population ancestry. Environmental toxicity was also reported as a risk factor in ALS such as smoking, heavy metals, pesticides and chemicals exposures. Special diet or lifestyle might be also a risk factor such as excessive exercise or football sport (Jelsone-Swain *et al.*, 2012; Zarei *et al.*, 2015).

6. Genetics of ALS (Table 2, figure 5)

i. Major ALS genes

a. *ALS1/Superoxide dismutase 1* (*SOD1*) mutation in ALS

In 1993, dominant missense mutations in *the superoxide dismutase 1 (SOD1)* gene were found associated with FALS cases. These mutations are one of the most common FALS causes (20% of FALS) and are found in a smaller percentage of SALS. SOD1 is a homodimer of ubiquitously expressed 153 amino-acid polypeptide. The polypeptide has a stabilizing zinc ion and a catalytic copper ion in each subunit. SOD1 enzyme is found in all cell types. SOD1 regulates dismutation reaction where superoxide free radical is reduced to water by glutathione peroxidase. Different types of mutations were detected in *SOD1* gene like, missense mutations in codons leading to the exchange of one amino acid, non-sense mutations truncating the polypeptide and variant or intronic mutations that are silent DNA (Andersen, 2006). Up to date 150 of these mutations were associated in ALS (Deng *et al.*, 1993; Borchelt *et al.*, 1994; Gurney *et al.*, 1994; Wong *et al.*, 1995; Ripps *et al.*, 1995; Beckman *et al.*, 2001; Andersen, 2006; Marchetto *et al.*, 2008; TURNER & TALBOT, 2008; Gertz *et al.*, 2012; Vinsant *et al.*, 2013; Rotunno & Bosco, 2013; Zwiegers *et al.*, 2014).

Animal studies have showed that the toxicity of *SOD1* mutations was not caused by a loss of function but rather was due to a toxic gain of function. SOD1 toxicity triggers ALS through different mechanisms such as, aggregates formation, oxidative stress, protein instability leading motor neurons death (Borchelt *et al.*, 1994; Julien, 2001).

Several well known human mutations in *SOD1* gene were studied using animal models carrying mutations, for example: mutations resulting in glycine to alanine substitution at position 93 (G93A), arginine to glycine in position 37 (G37R) and finally glycine to arginine in position 86 (G86R) in *SOD1* gene (Ripps *et al.*, 1995; Wong *et al.*, 1995; TURNER & TALBOT, 2008).

b. *ALS10/TAR DNA binding protein (TDP-43/TARDBP)* mutation in ALS

Since 2008, 40 different autosomal dominant ALS mutations were discovered in *TAR DNA binding protein (TDP-43)* gene in 4% of FALS and 1% of SALS. TDP-43 is a protein encoded by six exons containing two RNA recognition motifs and C-terminal glycine rich region. TDP-43 is DNA/RNA binding protein involved in gene transcription, RNA splicing and mRNA transport. Most of the TDP-43 mutations are dominant missense. Ubiquitinated TARDBP is one of major cytoplasmic inclusions in ALS (Neumann *et al.*, 2006; Lagier-Tourenne *et al.*, 2010; Ling *et al.*, 2013; Cirulli *et al.*, 2015).

c. *ALS6/Fused in sarcoma (FUS)* mutation in ALS

ALS patients with *Fused in sarcoma (FUS) gene* mutation can have an early disease onset 26-80 years with a short disease progression around 33 months. More than 50 mutations in FUS gene have been identified in 4% of FALS and 1% of SALS. FUS gene encodes a DNA/RNA binding protein involved in transcriptional activation, splicing regulation, mRNA biogenesis, stress granule formation, transportation and stabilization of long introns. Most of *FUS* gene mutations that co-segregate with ALS are in the C-terminus, which leads to FUS mislocalization from nucleus to cytoplasm with the formation of stress granules. *FUS* mutations rarely are also associated with frontotemporal dementia (Kwiatkowski *et al.*, 2009; Lagier-Tourenne *et al.*, 2010; Dormann & Haass, 2013; Deng *et al.*, 2014).

d. *Chromosome 9 open reading frame 72 (C9orf72)* mutation in ALS

A massive hexanucleotide repeat expansion was identified in noncoding region of *chromosome 9 open reading frame 72 (C9ORF72).* This repeat expansion causes ALS in 40% of FALS and 6 - 10% of SALS. The underlying mechanisms leading to ALS are not well known. However, repeat expansions are known to disrupt RNA metabolism in several neurodegenerative diseases. In some studies it has been shown that the repeat expansion leads to the formation of toxic nuclear RNA foci causing transcriptome

defect. *C9ORF72* mutations are also associated with FLTD (DeJesus-Hernandez *et al.*, 2011; Renton *et al.*, 2011).

e. TANK-binding kinase 1 (TBK1)

TANK-binding kinase (TBK1) is a non-canonical IkB kinase (IKK) involved in NF-kB signal transduction, innate immune defense and autophagy. Recently *TBK1* was identified as ALS gene (Freischmidt *et al.*, 2015) .

ii. Minor ALS genes

a. *ALS8/Vesicle associated membrane protein associated protein B (VAPB)*

Vesicle associated membrane protein associated protein B (VAPB) is a protein member of VAP family involved in vesicle trafficking and resident in the endoplasmic reticulum (ER). *VAPB* mutations were identified in a large Brazilian family and in UK ALS patients. The onset was between 31 and 45 years with postural tremor, fasciculations and limb weakness with long disease course. The investigation for VAPB in ALS showed that *VAPB* mutation could be a risk factor (Chen *et al.*, 2013; Han *et al.*, 2013; Kabashi *et al.*, 2013).

b. *ALS14/Valosin-containing protein (VCP) mutation in ALS*

Valsin-containing protein (VCP) is a hexameric type II ATPase of the AAA family involved in protein homeostasis, Golgi biogenesis, vesicle transport and fusion, autophagy and ER stress. *VCP* mutation in ALS leads to an adult onset autosomal dominant motor neuropathy in 1-2% of FALS. The age of onset is around 49 years with limb onset and rapid disease progression (Wijesekera & Leigh, 2009; Chen *et al.*, 2013; Renton *et al.*, 2014; Swinnen & Robberecht, 2014).

c. *ALS12/Optineurin (OPTN)* mutation in ALS

In 2010 an autosomal recessive mutation in *Optineurin (OPTN)* gene was described in ALS families. *OPTN* had previously been involved in glaucoma. OPTN regulates membrane trafficking, protein secretion, cell division, Golgi homeostasis, autophagy and immune response. In ALS *OPTN* mutation is characterized by lower limb onset and slow disease progression with predominant UMN signs (Wijesekera & Leigh, 2009; Chen *et al.*, 2013; Renton *et al.*, 2013; Swinnen & Robberecht, 2014).

d. *Sequestosome 1(SQSTM1)* mutation in ALS

Sequestosome 1 (SQSTM1) missense and deletion variants are found in 1% of ALS cases. *SQSTM1* encodes for p62, a protein that regulates ubiquitin binding and activation of nuclear factor kappa-B signaling. P62 aggregates in motor neurons are one of the pathological hallmarks of ALS, especially in C9ORF72 cases (Wijesekera & Leigh, 2009; Chen *et al.*, 2013; Renton *et al.*, 2013; Swinnen & Robberecht, 2014).

e. *ALS2/ RHO guanine nucleotide exchange factors (ALSIN)* mutation in ALS

ALS2/ RHO guanine nucleotide exchange factors (ALSIN) mutation in ALS is a rare, autosomal recessive mutation. ALSIN mutation is characterized by a juvenile onset around 6.5 years old with slow progression. Indeed, mutations in *ALS2* are now more commonly thought to lead to hereditary spastic paraplegia, rather than true ALS. ALSIN mutations in ALS are characterized by predominant UMN signs with fascial spasticity(Wijesekera & Leigh, 2009; Chen *et al.*, 2013; Renton *et al.*, 2013; Swinnen & Robberecht, 2014).

f. *ALS15/ALS X/Ubiquilin-2 protein (UBQLN2)* mutation in ALS

Ubiquilin-2 mutation (UBQLN2) causing ALS is X-linked dominant missense mutation. It is an adult and juvenile onset with UMN signs. UBQLN2 belong to ubiquitin like protein family that regulates ubiquitin proteasome system triggering protein degradation. UBQLN2 inclusions are one of the pathological hallmarks of ALS

(Wijesekera & Leigh, 2009; Chen *et al.*, 2013; Renton *et al.*, 2013; Swinnen & Robberecht, 2014).

g. *Dynactin (DCTN1)* mutation in ALS

A mutation in p150 subunit of *dynactin* gene *(DCTN1)* is responsible for progressive autosomal dominant distal motor neuropathy in familial and sporadic ALS. Dynein is a microtubule motor protein involved in axonal transport of vesicles. The mutation trigger neurodegeneration by impairing axonal transport (Wijesekera & Leigh, 2009; Chen *et al.*, 2013; Renton *et al.*, 2013; Swinnen & Robberecht, 2014). Importantly, mutations in *DCTN1* are also causing atypical forms of Parkinsonism, in particular the so-called Perry Syndrome (Farrer *et al.*, 2009).

Table 2: ALS mutant genes in sporadic and familial forms

Gene	**Location**	**Function**	**Clinical features**
ALS1/ SOD1	21q22.1	Superoxide metabolism	Classical ALS
ALS2/ ALSIN	2q33-2q35	Vesicle trafficking	Young onset
ALS4/ SETX	9q34	RNA metabolism	Young onset
ALS6/ FUS	16q11.2	RNA metabolism	Juvenile/ adult ALS
ALS8/ VAPB	20q13.3	Vesicle trafficking	Classical ALS
ALS9/ ANG	14q11.2	Angiogenesis	Classical ALS
ALS10/ TARDBP	1q36.2	RNA metabolism	Classical ALS
ALS12/ OPTN	10q13	Vesicle trafficking	Classical ALS
ALS14/ VCP	9q13.3	Proteasome, vesicle trafficking	Classical ALS
ALS15/ALSX/UBQLN2	Xp11	Proteasome	Juvenile/ adult ALS
ALS-FTD2/ C9ORF72	9q21	Proteasome	ALS-FTD
DCTN1	2q13	autophagy and axonal transport	LMND/ ALS
SQSTM1	5q35	Ubiquination and autophagy	Classical ALS

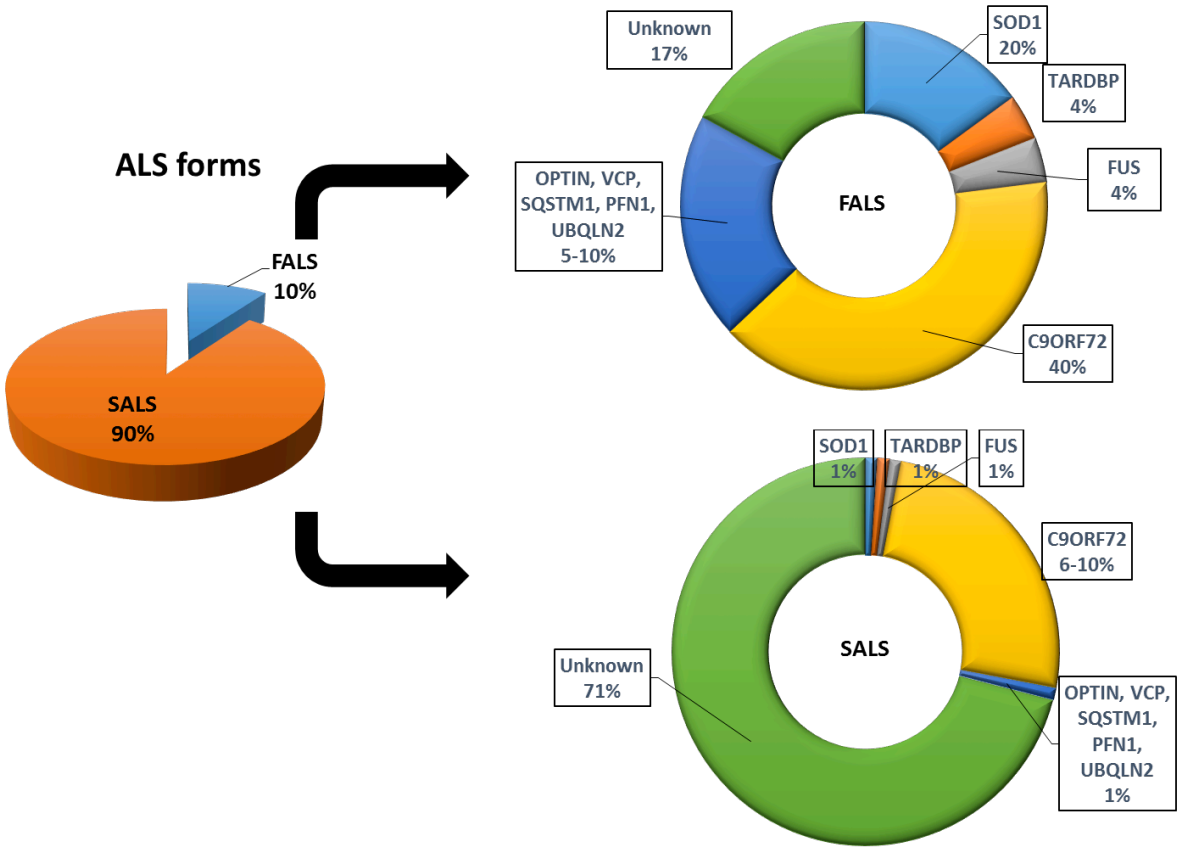

Figure 5: Percentage of ALS mutant genes in sporadic and familial forms

7. ALS pathology

i. Histological features in ALS

ALS is characterized by a number of specific pathological hallmarks. First, as initially described by Charcot and later colleagues, UMN and LMN are degenerating, concomitantly with activated gliosis. The degeneration of LMN in ALS patient leads to MN atrophy in the ventral horn of spinal cord and the loss of 50% of cell bodies.

The degenerating motor neurons accumulate cytoplasmic inclusions and protein aggregates. These inclusions are not restricted only to spinal cord but in other affected brain regions (Blokhuis *et al.*, 2013).

There are two types of known inclusions. First, ubiquitinated aggregates that are either Lewy bodies-like hyaline or skein-like inclusions. They appear as a randomly oriented filament covered by fine granules due to the accumulation of abnormal proteins (Mather *et al.*, 1993). Second, Bunina bodies that are mostly intracytoplasmic, small eosinophilic and round hyaline inclusions, without halo due to proteins materials accumulations (Okamoto *et al.*, 2008). Bunina bodies are present in more than 70% of ALS cases (Okamoto *et al.*, 2008; Blokhuis *et al.*, 2013).

One of the first proteins identified in these inclusions was mutant SOD1, that is found exclusively in cases with *SOD1* mutations forms (Blokhuis *et al.*, 2013).

In non-*SOD1* cases, the predominant pathological aggregates of ALS are ubiquitinated TDP43 aggregates. In ALS patients TDP43 aggregates are present in spinal cord motor neurons, hippocampal and frontal cortex neurons and glial cells. These aggregates are cytoplasmic due to the mislocalisation of TDP43 from nucleus to cytoplasm (Braak *et al.*, 2010; Magran *et al.*, 2014; Wang *et al.*, 2015). These cytoplasmic aggregates are accompanied by nuclear clearance of the protein. TDP43 aggregates are seen in 95% of cases (Neumann *et al.*, 2006b; Lee *et al.*, 2012).

Dysfunction in ubiquitin-proteasome system is linked to ALS. In ALS patient's spinal cord, ubiquitinated inclusions appear as fine granules with filamentous profile. These inclusions reflect protein degradation and autophagy (Stieber *et al.*, 2000). TDP-43 aggregates are indeed ubiquitinated.

P62 (sequestosome 1) aggregates are present in spinal cord ALS animal models and patients. They are accumulated in parallel with the increase of mutant SOD1 aggregates (Gal *et al.*, 2007). It is noteworthy that P62 pathology is extremely robust in ALS patients with *C9ORF72* mutation.

FUS cytoplasmic aggregates are found in ALS patients with *FUS* mutations, and in a large subset of sporadic FTD cases. Importantly mutations linked to ALS cause the mislocalisation of FUS from nucleus to cytoplasm (Takanashi & Yamaguchi, 2014).

Neurofilament (NF) accumulation is also one of the hallmarks of ALS. They are found in axon hillock of MN and are associated mostly with FALS. This NF toxic accumulations leads to axonal transport dysfunction and neurodegeneration (Julien; Dale & Garcia, 2012).

ii. Molecular mechanisms of ALS

A number of mechanisms have been involved in ALS-related motor neuron degeneration. These mechanisms are not mutually exclusive and could, in principle all participate in motor neuron death. The next section will present a non-exhaustive selection of the different mechanisms that were postulated (Figure 6).

a. Motor neurons intrinsic events

Some of the toxic events leading to MN death occur in motor neurons themselves.

- Oxidative stress:

Oxidative stress originates from an imbalance between the generation and removal of reactive oxygen (ROS). Oxidative stress could arise as a consequence of expression of ALS-related proteins. Indeed, expression of mutant SOD1 is known to cause oxidative stress (Barber *et al.*, 2006). Many different mechanisms have been postulated over the years to link SOD1 mutations with oxidative stress. However, the importance of oxidative stress in motor neuron degeneration remains controversial (Borchelt *et al.*, 1994; Wong *et al.*, 1995a; Beckman *et al.*, 2001; Andersen, 2006).

More recently, it was shown that oxidative stress induces stress granule formation that incorporates other ALS related proteins such as TDP-43 and FUS. The interplay between oxidative stress, stress granules and ALS related mutations is the subject of intense investigations in the last years (Li *et al.*, 2013) (Figure 6).

- Mitochondrial dysfunction:

Mitochondrial morphological and functional abnormalities are observed in ALS patients and mice models. This has been especially studied in mutant SOD1 based animal models. Mutant SOD1 (mSOD1) protein accumulates in mitochondria on the outer membrane and inside the intermembrane space (Taylor *et al.*, 2002). The accumulation of mSOD1 affects mitochondrial protein expressions involved in energy metabolism and impairs calcium buffering. Mitochondrial dysfunction is especially observed in skeletal muscle and spinal cord motor neurons (Ferraiuolo *et al.*, 2011; Calvo *et al.*, 2014; Magran *et al.*, 2014)(Figure 6).

- Endoplasmic Reticulum (ER) Stress:

ER and Golgi morphological abnormalities are pathological hallmarks of ALS. The ER stress triggers signaling pathways collectively known as the unfolded protein response (UPR). The UPR is a homeostatic mechanism, which is initially protective by the upregulation of chaperone proteins, inhibition of general protein translation, and expansion of ER volume. In ALS intracellular inclusions due to the accumulation of misfolded or unfolded proteins are observed in early stage of the disease. In mSOD mice ER-resident chaperone and UPR markers are activated and co-localize with mSOD1 inclusions (Ferraiuolo *et al.*, 2011; Calvo *et al.*, 2014; Chen *et al.*, 2015; Wang *et al.*, 2015). UPR activation appears as a very early event in vulnerable motor neurons (Saxena & Caroni, 2011; Kaplan *et al.*, 2014), and contributes to motor neuron degeneration (Saxena & Caroni, 2011) (Figure 6).

- Dysregulated transcription and RNA processing:

Altered RNA processing is implicated in the pathophysiological mechanism of motor neuron injuries, especially upon TDP-43 and FUS involvement. Dysregulated RNA is observed in mutant TDP43 and FUS. TDP43 and FUS are implicated in transcriptional regulation, alternative splicing, nucleus-cytoplasm shuttling and microRNA processing (Lagier-Tourenne *et al.*, 2010) Most of the TDP43 and FUS mutations disrupt these RNA processing and in several cases induce stress granules formations (Ferraiuolo *et al.*, 2011; Calvo *et al.*, 2014). Loss of FUS or TDP43 induces large defects in RNA metabolism, especially affecting splicing of brain specific large introns (Polymenidou *et al.*, 2011, 2012; Lagier-Tourenne *et al.*, 2012) (Figure 6).

- Axonal failure:

Motor neurons are highly polarized cells with long axons within the corticospinal tract. The axonal transport uses microtubule-dependent kinesin and cytoplasmic dynein molecular motors that mediate transport towards neuromuscular junction (anterograde transport) and toward cell body (retrograde transport). The inhibitory effects on axonal outgrowth or dysfunction of transport process lead to denervation of neuromuscular system and axonal degeneration. In ALS defective axonal transport occurs early in the disease. Several mutations in *dynactin* genes are involved in vesicle and axonal transport along microtubule. Dynactin mutations, cause lower motor neurons syndrome and are shown to be associated with ALS. Other mutation in the *neurofilament Heavy chain* and *profilin 1*, essential for the polymerization of actin were also observed in ALS. Moreover, light neurofilament chain (NFL) abundance is decreased in ALS. The binding of TDP43 and FUS to NFL mRNA, leads to the formation of stress granules and induces motor neurons injuries (Ferraiuolo *et al.*, 2011; Calvo *et al.*, 2014, Gerardo et al., 2009).

- Excitotoxicity:

Excitotoxicity is the neuronal death elicited by excessive activation of glutamate receptors, due to increased synaptic glutamate or increased sensitivity of the postsynaptic neurons to glutamate. Glutamate binds to AMPA receptors. AMPA receptor is a non-NMDA type ionotropic transmembrane receptor for glutamate that mediates fast synaptic transmission. It is known that motor neurons are especially vulnerable to AMPA-mediated excitotoxicity. ALS patients have increased levels of glutamate in the cerebrospinal fluid. In presymptomatic and early stages of ALS, patients have shown hyperexcitability of the motor system. The mSOD1 models showed altered AMPA receptor subunit expression, increased glutamate efflux from spinal cord nerve terminals and a reduction in the motor neuron inhibitory-excitatory synaptic ratio (Ferraiuolo *et al.*, 2011; Calvo *et al.*, 2014). Of note, riluzole, the only drug that extends survival of ALS patients has some anti-glutamatergic properties. However, no other glutamate based medication has shown efficacy, and it remains questionable as to whether riluzole exerts its protective effects through its anti-glutamatergic properties.

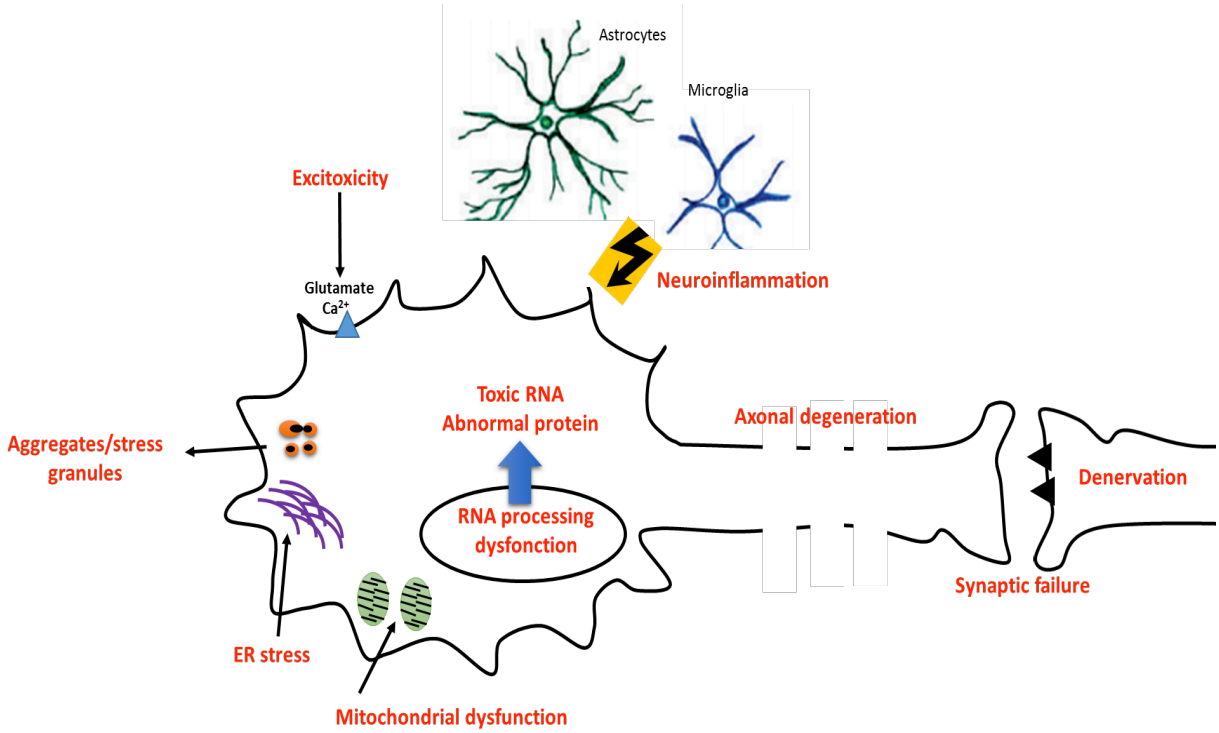

Figure 6: ALS molecular mechanisms triggering motor neurons death, aggregates, stress granules, ER stress, RNA processing dysfunction, mitochondrial dysfunction, excitoxicity, axonal denervation and transport dysfunction and neuroinflammation

b. Neuroinflammation (Figure 7)

- **Microglia triggering neuroinflammation**

Microglia is a resident macrophage that triggers innate and adaptive immunity in the CNS. In normal conditions, microglia and peripheral immune cells communicate to keep tissues homeostasis. In pathological state, they are activated during inflammation to ensure balance, repair and protection of cells. During inflammation microglia passes from resting state to activated state characterized by enlargement of the cell body and thickness of processes (Appel *et al.*, 2011).

There are two activated state of microglia polarization, pro-inflammatory state called M2 and anti-inflammatory state called M1. Upon activation microglia acquires an amoeboid appearance and secretes M1 pro-inflammatory markers to repair damage and after M2 anti-inflammatory markers to prevent neuronal death. Neuroinflammation is considered as a double-edged sword that executes beneficial and suppressing effect on the neurons (Crain *et al.*, 2013; Orihuela *et al.*, 2015; Tang & Le, 2015).

In ALS gliosis occurs in different brain regions and spinal cord. More precisely, around dying cells bodies of motor neurons in the motor cortex and motor nuclei in the brainstem along the corticospinal tract. Microglia interacts with astrocytes and T cells during inflammation. During M1 state there is a production of inflammatory cytokines such as tumor necrosis factor alpha (TNF-α), interleukin 1β (IL-1 β), IL-6, IL-23, IL-12, IL-8. Moreover neurotoxic mediators such as nitric oxide (NO) and reactive oxygen species (ROS) are synthetized from NADPH oxidase 2 (NOX2). Under M1 state there is an increased expression of CD86, MCH-II cell surface receptors that contribute to antigen presenting activity. There is also an upregulation of following chemokines COX2, CLL2, CCL4 and CCL20. These responses aim to the clearance of tissue debris and the resolution of the inflammatory response induced by necrotic neurons. In some cases M1 prolonged state leads to a chronic neuroinflammation that can be neurotoxic and induce apoptosis or microglia can become over activated and widespread damage to neighboring neurons.

Upon neuronal repair there is a switch of microglia to M2 state. Firstly, it starts with an acquired inactivation to alleviate acute inflammation and secondly, an alternative activation to promote anti-inflammatory response. During M2 state there is a production of anti-inflammatory cytokines such as IL-13, IL-4 (alternative activation), IL-10, and transforming growth factor- β (TGF- β) (acquired inactivation). The anti-inflammatory release of cytokines antagonizes pro-inflammatory response by suppressing the production of IL-6 and IL-8 and reducing NO release. Moreover, during M2 state there is an upregulation of neurotrophic factors such as insulin-like growth factor 1 (IGF-1) and brain-derived neurotrophic factor (BDNF) to promote neuronal survival and an increase in phagocytosis. M2 phase is also characterized by an increase in arginase 1 (ARG1) that promotes wound healing and tissue remodeling. There is also an upregulation of the expression of CD206 and CD204 cell surface receptors. Several markers are also present during M2 state such as triggering receptor expressed on myeloid cells 2 (Trem2) that promotes anti-inflammatory response and debris clearance. Trem2 is considered as a gateway influencing balance between phagocytic and pro-inflammatory activity. Last, there are an upregulation of YM1 (chitinase-like 3) that prevent degradation of extracellular matrix components, FIZZ1 that inhibit inflammation and enhance tissue remodeling and neurite growth and DNAX activation protein (Dap12) that mediates cell surface receptors and activates natural killer cells (Turnbull & Colonna, 2007; Graeber & Streit, 2010; Appel *et al.*, 2011; Philips & Robberecht, 2011; Hu *et al.*, 2012, 2015; Boche *et al.*, 2013; Chiu *et al.*, 2013; Crain *et al.*, 2013; Prinz & Priller, 2014; Xanthos & Sandkühler, 2014; Cherry *et al.*, 2014; Nayak *et al.*, 2014; Orihuela *et al.*, 2015; Tang & Le, 2015; Heppner *et al.*, 2015).

- **Neuroinflammation in ALS**

Several studies showed the presence of M2 state at the disease onset that is followed by a switch from M2 state to M1 to face neuronal death during disease progression. This neuroinflammation upon neuronal death is associated in some cases with the accumulation of misfolded mutant forms of SOD1 or TDP43 in motor neurons (Appel et al., 2015)

An intense glial activation is observed in ALS, which involves glial cell types, in particular astrocytes and microglia. Moreover infiltration of circulating monocytes has also been observed in the CNS in ALS. These cells, either glial or infiltrated are the source of an intense neuroinflammatory response contributing neurodegeneration.

A large body of evidence suggests that non neuronal cells contribute to MN loss in ALS animal models. First, reactive microglia, astrocytes and infiltrated lymphocytes T have been identified during ALS disease progression especially at end stage. They express high levels of proinflammatory mediators and effectors (Bowerman *et al.*, 2013; Frakes *et al.*, 2015).

In ALS, neuroprotection is decreased at end stage of the disease due to acute prolonged neuroinflammation. Mutant $SOD1^{G93A}$ mice had increased levels of YM1, BDNF and IGF-1 and decreased NOX2 at disease onset compared to end stage mice (Angelica & Fong, 2008).

The role of monocyte/macrophage was demonstrated using mice with floxed gene of the SOD1 G37R human mutation. These floxed mice allowed the knock-down of SOD1 toxicity in microglia upon CRE recombination. Indeed, mice with decreased SOD1 toxicity in microglia and monocytes have longer survival with an increase in late disease progression (Beers *et al.*, 2006; Boillée *et al.*, 2006; Trias *et al.*, 2013).

Astrocytes also contribute to neuroinflammation and the knock-down of mutant SOD1 in astrocytes did not affect disease onset but delayed microglia activation and slower later disease progression. Consistently, the transplantation of $SOD1^{G93A}$ glial-restricted precursor cell glial progenitor that differentiate into astrocytes in WT rats induced MN death (Yamanaka *et al.*, 2008; Diaz-Amarilla *et al.*, 2011; Papadeas *et al.*, 2011; Trias *et al.*, 2013)

Infiltrated lymphocytes are also implicated in ALS during disease progression through promotion of immune response and MN injury along with glial cells (Henderson et al., 2011).

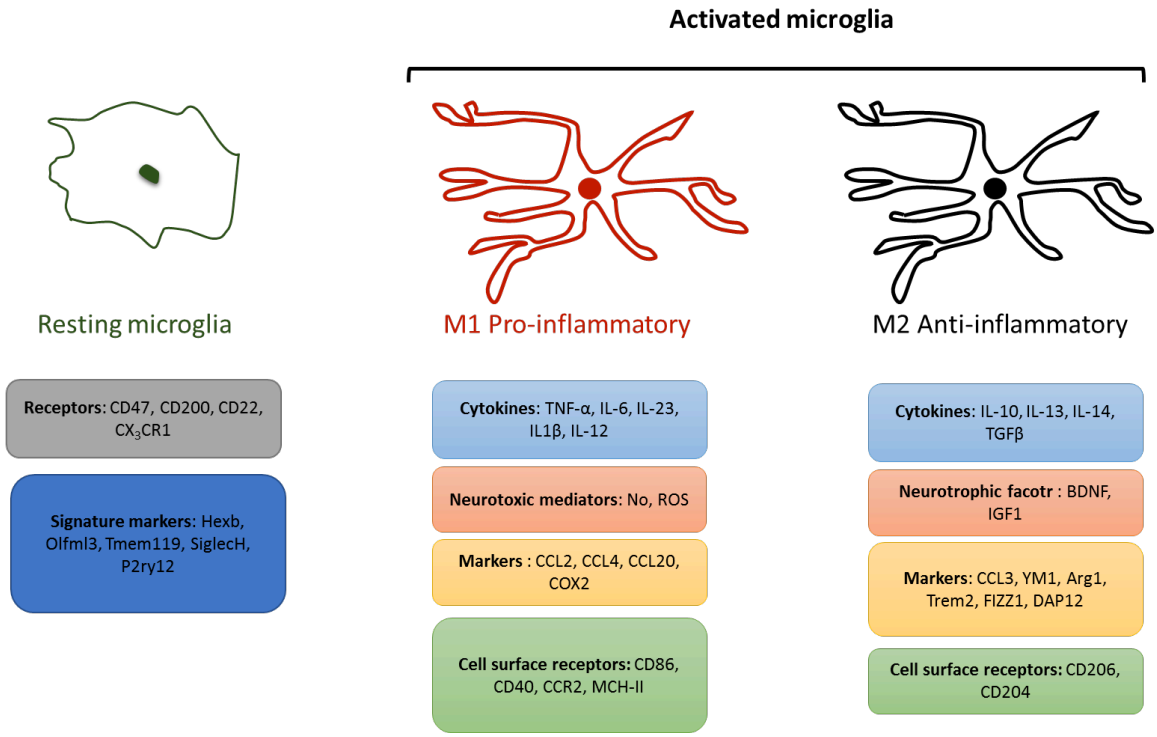

Figure 7: M1/M2 inflammatory profile upon neuronal injury, signature markers of microglia, cell surface expressed receptors, cytokines, and neurotoxic mediators

8. Treatment and clinical trials in ALS

Table 3: Treatment strategies and drugs used for ALS patients reproduced from (Radunović *et al.*, 2007; Wijesekera & Leigh, 2009)

Strategie of treatement	Stage of use	Name of the treatement	The aim of treatement
Pharmacological intervention	Symptomatic stage	Crabamazepine, Phenytoin, Quinine	Cramps
		Atropine, Hyoscine hydrobromide, Hyosine butylbromide, Hyoscine scopoderm, Glyocopyrronium, Amitriptyline	Excessive watery Saliva
		Carbocisteine, Propranolol, Metoprolol	Excessive branchial secretion
		Lorazepam	Anxiety and laryngospasm
		Analgesics, Opioids	Pain
		Tricyclic antidepressant, Levodopa, Dextrometorphan,	Emotional lability

		Riluzole	
Physical therapy	Symptomatic and later stages	Physiotherapy	Spasticity and cramps
		Physical exercises	
		Massage	
		Hydrotherapy	
Monitoring devices	Symptomatic and later stages	Brain computer interfaces	Communication difficulties
		Speaking technics and light writers	
		Voice amplifier	
Ventilatory management device	50% decline of vital respiration capacity	Non-invasive ventilation	Comfort, sleeping and respiration
Nutritional management	Early stage and during disease progression	Percutaneous endoscopic gastrostomy	Increase caloric intake and decrease swallowing disabilities
		Percutaneous radiologic gastrostomy	
		Radiologically inserted gastrostomy	
		Nasogastric tube	
		High-fat diet/ High-protein diet	

9. ALS in vivo models (Table 4)

Table 4: TDP43 and SOD1 ALS mutant animal models reproduced from (Wong *et al.*, 1995; Wang *et al.*, 2003, 2005)

Transgene	Pathology	Symptoms onset	Survival
Human TDP-43 cDNA	Increased ubiquitin in some neurons	*	30-60 days
Human TDP-43 cDNA	Axonal degeneration/ no glial activation/ Rare phospho-TDP43 inclusions/ C-terminal TDP-43 fragments/ Mitochondrial accumulations	*	30-60 days
Human TDP-43 cDNA A315T mutation N-terminal Flag	UMN, LMN and axonal degeneration/ Glial activation/ Rare phospho-TDP43 inclusions/ Loss of nuclear TDP-43/ C-terminal TDP-43 fragments	90 days	150 days
Human TDP-43 cDNA A315T mutation (line 23)	Muscle denervation/ Astrocytic activation/ Rare phospho-TDP-43 inclusions/ C-terminal TDP-43 fragments	28 days	75 days
Human TDP-43 cDNA	UMN and LMN degeneration/ Glial activation/ Rare TDP-43 and phospho-TDP-43 inclusions/ Loss of nuclear TDP-43/ C-terminal TDP-43 fragments	*	30-200 days

Human TDP-43 cDNA	Abnormal NMJ staining/ Axonal atrophy/ Mitochondrial accumulations	14-18 (Males) 90 (Females) days	30-60/ 30-200 days
Mouse TDP-43 cDNA	Brain atrophy and neuronal apoptosis/ Cortical neurons atrophy	*	*
Human TDP-43 minigene	No ALS	*	*
Human TDP-43 cDNA M337V mutation	LMN and axonal degeneration/ Glial activation/ Rare phospho-TDP-43 inclusions in cortical regions	32-34 days	46-49 days
genomic hSOD1 G37R	Active glia/ Aberrant neurofilament accumulation/ Motor neurons degeneration/ Loss of myelinated axons/ Paralysis/ Muscle atrophy/ Accumulation of SOD1 aggregates and ubiquitin	3,5-8 months	9-12 months
genomic hSOD1 G85R		3 months	4 months
genomic mSOD1 G86R		90 days	105 days
genomic hSOD1 G93A		3-4 months	5-6 months
genomic hSOD1		307 days	407 days

D90A			
genomic hSOD1 L126Z (stop)	Accumulation of ubiquitin in spinal cord/ Massive loss of MN and fibers tracts	*	*
genomic hSOD1 L126delTT	Reactive gliosis/ Hyaline inclusions/ Hindlimb paraparesis/ Forelimb weakness/ Muscle atrophy	Homo 120 days/ Hetero 340-445 days	Homo 126 days/ Hetero 372-480 days
genomic hSOD1 H46R/ H48Q/ H63G/ H120G Quad	Hind limb paralysis/ Increased gliosis/ Ubiquitinated body inclusions in spinal cord	8-11 months	10-12 months

II. Serotoninergic system and ALS

1. Serotonin synthesis and neuroanatomy

Serotonin or 5-hydroxytryptamine (5-HT) is a monoamine neurotransmitter. The major source of serotonin is food intake. Serotonin is catabolized through intestinal wall and liver than lungs destroy the excess. A subset of serotonin is found in the brain and produced by different biochemical pathways. Importantly, serotonin does not cross the blood brain barrier, and peripheral and central pools of serotonin are thus independent.

Serotonin is biochemically derived from tryptophan. The essential amino acid tryptophan is hydroxylated to 5-hydroxytryptophan (5-HTP) by tryptophan hydroxylase (TPH). There are two isoforms of TPH, TPH1 being the peripheral isoform, and TPH2 being responsible for central nervous system synthesis of 5-HT. In a second step 5-HTP is decarboxylated by the aromatic amino acid decarboxylase (AADC) to form 5-HT. The monoamine transporter MAT transports 5-HT into vesicles.

10% of serotonin is synthesized and stored in pre-synaptic serotoninergic neurons, cathecholaminergic neurons and pineal gland in the central nervous system (CNS). 90% of serotonin is synthesized in the peripheral system (PNS) mainly in enterochromaffin cells. The major storage site of peripheral serotonin are blood platelets (Amireault *et al.*, 2013).

The concentration of serotonin depends on synthesis and metabolism rate. The monoamine oxidase (MAO), ubiquitinated enzyme presents the metabolic pathway of serotonin. There are two isoforms of MAO, MAO-A form that inactivates serotonin and MAO-B form that is the predominant form of MAO in platelets. MAO metabolic activity oxidizes serotonin to 5-hydroxyindole acetic acid aldehyde (5-HIAC). This is followed by oxidation by aldehyde dehydrogenase to 5-hydroxyindole acetic acid (5-HIAA).

In the CNS upon neuronal depolarization, serotonin is released into the synaptic cleft. Serotonin binds to postsynaptic 5-HT receptors or 5-HT autoreceptors on the presynaptic membrane as a negative feedback loop. The serotonin transporter

(SERT) is critical to the functioning of the 5-HT system. SERT limits 5-HT neurotransmission by removing 5-HT synaptic neurotransmitter across the presynaptic membrane (Moses, 2008; Pytliak *et al.*, 2011) (Figure 8).

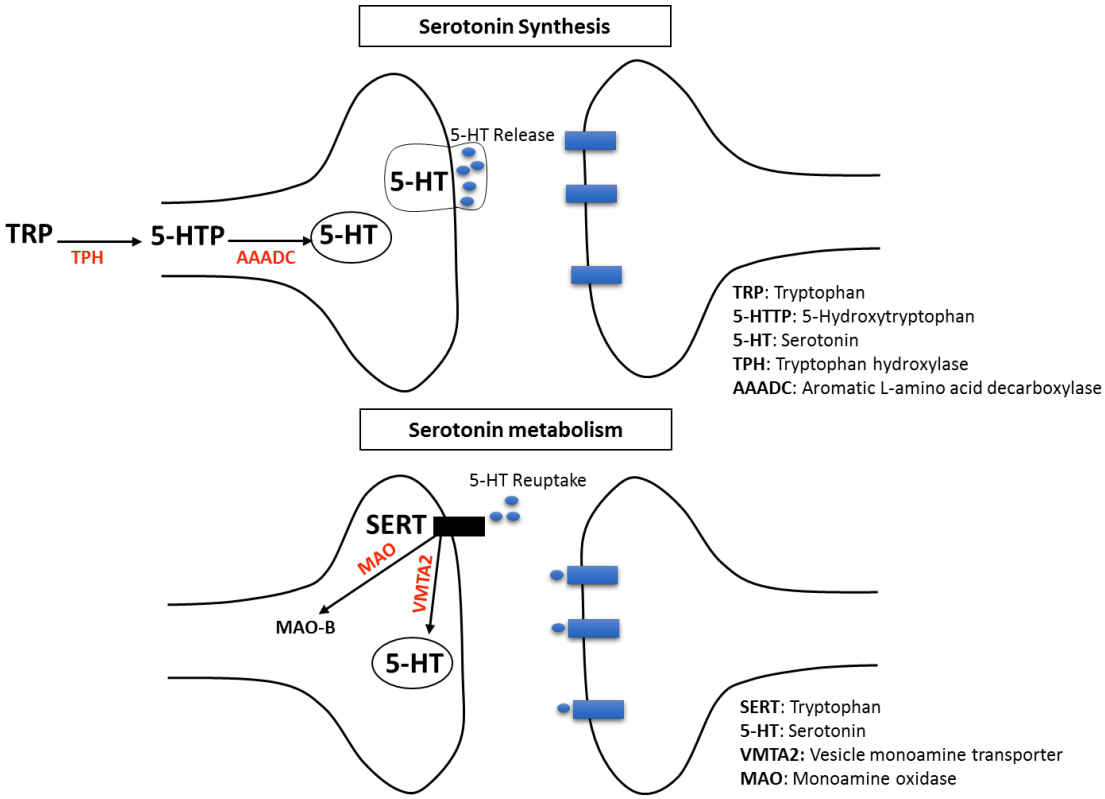

Figure 8: Serotonin synthesis and metabolism in central nervous system

2. Serotoninergic neurons major nuclei

The brain serotoninergic system is a complex network. The major 5-HT nuclei are are located in the brainstem. The 5-HT nuclei have ascending projection to different region of the brain and descending projections to the inferior structure -spinal cord. Two groups of 5-HT neurons are known; the first is a superior rostral group at the boundary between midbrain and pons (Törk, 1990). This rostral group includes B5, B6, B7, B8 and B9 5-HT neuronal cells. The second inferior group stretches from the caudal pons to the cervical spinal cord. This second group includes B1, B2 and B3 5-HT neuronal cells (Dahlström & Fuxe, 1964)

i. The rostral serotoninergic group

There are three raphe nuclei in the rostral group located in the caudal mesencephalon to the mid pons.

a. Caudal linear nucleus (CLi)

The CLi belongs to the ventral mesencephalic tegmentum and represent the rostral population of the B8 group (Dahlström & Fuxe, 1964). The 5-HT neurons have an elongated dendritic arborization (Halliday & Törk, 1986).

b. Dorsal raphe nucleus (DR)

The DR presents the largest collection of serotoninergic neurons and represents the population of B7 and B6 groups (Dahlström & Fuxe, 1964).

DR includes 5 subnuclei located between the mesencephalic and the medial longitudinal fasciculus. The dorsal raphe spreads in the anteroposterior axis between the oculomotor and the abducens nuclei, with the widest expansion at the level of the trochlear nucleus. There are three division of the DR. First, the dorsal division (DRD) contains medium multipolar 5-HT neurons. Second, the ventrolateral division (DRVL) that spreads dorsally and laterally to the eye muscle MN and contains small multipolar 5-HT neurons. Third, the intermediate division (DRI) that lies between the two-parasagittal tracts of the medial longitudinal fasciculus, with elongated dendritic arborization (Törk, 1990; Baker *et al.*, 1991; Bjarkam *et al.*, 1997).

c. Median raphe nucleus (MnR)

The MnR is made of midline and a paramedian division below and caudal to the superior cerebellar decussation. The midline group is contiguous dorsaly with the DRI, with elongated dendritic arborization (Törk, 1990).

d. 5-HT neurons of the pontomesencephalic reticular formation

5-HT neurons are located also in two distinct clusters in the lateral reticular formation. One is located in the oral pontine nucleus (PnO) and the second in the supralemniscal nucleus (SLN)(Baker *et al.*, 1991; Bjarkam *et al.*, 1997).

ii. The caudal serotoninergic group

There are three raphe nuclei in the caudal group that extend from the caudal mesencephalon to the decussation of the pyramidal tract at the brainstem-spinal cord junction.

a. Raphe magnus nucleus (RMg)

The RMg is located between the pons and the medulla and represents the population of B3 group (Dahlström & Fuxe, 1964). RMg extends from the rostral superior olive back to cranial nerve XII (Törk, 1990).

b. Raphe obscurus nucleus (ROb)

The ROb is located dorsaly to the RMg and extends from the facial nucleus to the decussation of the pyramidal tract. The nucleus is more dense caudally in the medulla ROb corresponds to the population of B2 group (Dahlström & Fuxe, 1964). ROb neurons are medium-sized with dendrites oriented dorsoventrally (Loewy, 1981; Loewy & McKellar, 1981).

c. Raphe pallidus nucleus (RPa)

RPa is the smallest raphe nucleus that corresponds to the population of B1 group (Dahlström & Fuxe, 1964). The nucleus stretches from the cranial nerve XII to the anterior end of the inferior olive. 5-HT neurons of RPa are medium-sized, slender and elongated neurons with few dendritic processes oriented dorsoventrally (Loewy, 1981; Loewy & McKellar, 1981; Nakamura *et al.*, 2002).

3. Serotoninergic neurons projection regions in the CNS (Figure 9)

The rostral group of 5-HT neurons project mostly to the brain and the upper part of the brainstem. The caudal group of neurons project to the lower brainstem and the spinal cord.

i. Rostral group projections

There are five ascending pathways of 5-HT rostral projections. The rostral group projects mostly towards the forebrain. There are two parallel, dorsal and ventral, pathways. The dorsal pathways connect and collect projection from the DR and the MnR in the dorsolateral PnO and project to the medial forebrain and lateral cortex (Lidov & Molliver; Steinbusch *et al.*, 1980; Waterhouse *et al.*, 1986; Aitken & Törk, 1988; Vertes, 1991). The ventral pathway is located in the midline MnR and project to the basal forebrain and the medial cortex. The ascending projection of MnR modulates motor system and the basal ganglia through striatal projection and nigral and intralaminar thalamic projection. The MnR innervates the cingulate cortex, septal nuclei and the hippocampus (dentate gyrus) (Azmitia & Segal, 1978; Köhler & Steinbusch, 1982; Vertes & Crane, 1997; Vertes *et al.*, 1999).

The dorsal raphe (DR) nucleus projects to cerebral cortex, neostriatum, the amygdala, nucleus accumbens and the substantion nigra. The DR projects to the hippocampus, lateral septum and thalamus (Kazakov *et al.*, 1993; Van Bockstaele *et al.*, 1993). The 5-HT fibers are presented in all cortical layers, mostly in the granule cell layers but also in the motor region of the frontal lobe. The DR projects caudally to the RMg and Rob (Köhler & Steinbusch, 1982; Köhler *et al.*, 1982; Imai *et al.*, 1986; Vertes & Crane, 1997).

ii. Caudal group projections

The caudal group projects mostly to the caudal brainstem and spinal cord (CARLSSON *et al.*; Brodal *et al.*, 1960). The ROb and RPa project to the brainstem somatic motor nuclei, the motor trigeminal nucleus, the facial nucleus, the retrofacial and ambiguous nuclei (Arita *et al*. 1995; Arita *et al.*, 1993; Li *et al.*, 1993; Ridet *et al.*, 1993).

There are two population of 5-HT descending projection into the spinal cord (Felten & Sladek, 1983): small axonal varicosities in the dorsal division and large axonal varicosities in the intermediate and ventral division of the spinal cord (Lidov & Molliver; Törk, 1990; Ridet *et al.*, 1993). There is a dense 5-HT neurons innervation in lamina 1 and 2 of the spinal cord trigeminal nucleus. The RMg projects laterally to the dorsal horn in the spinal cord via the dorsolateral funiculus (Wu & Wessendorf, 1992; Ridet *et al.*, 1993). The ROb and RPa project medially and ventrally in to the ventral horn in lumbar and autonomic MN nuclei via the ventral and ventrolateral funiculi respectively (Arita *et al*. 1995; Arita *et al.*, 1993; Li *et al.*, 1993; Ridet *et al.*, 1993). The RMg and RPa have ascending projection to the rostral group (Behzadi *et al.*, 1990).

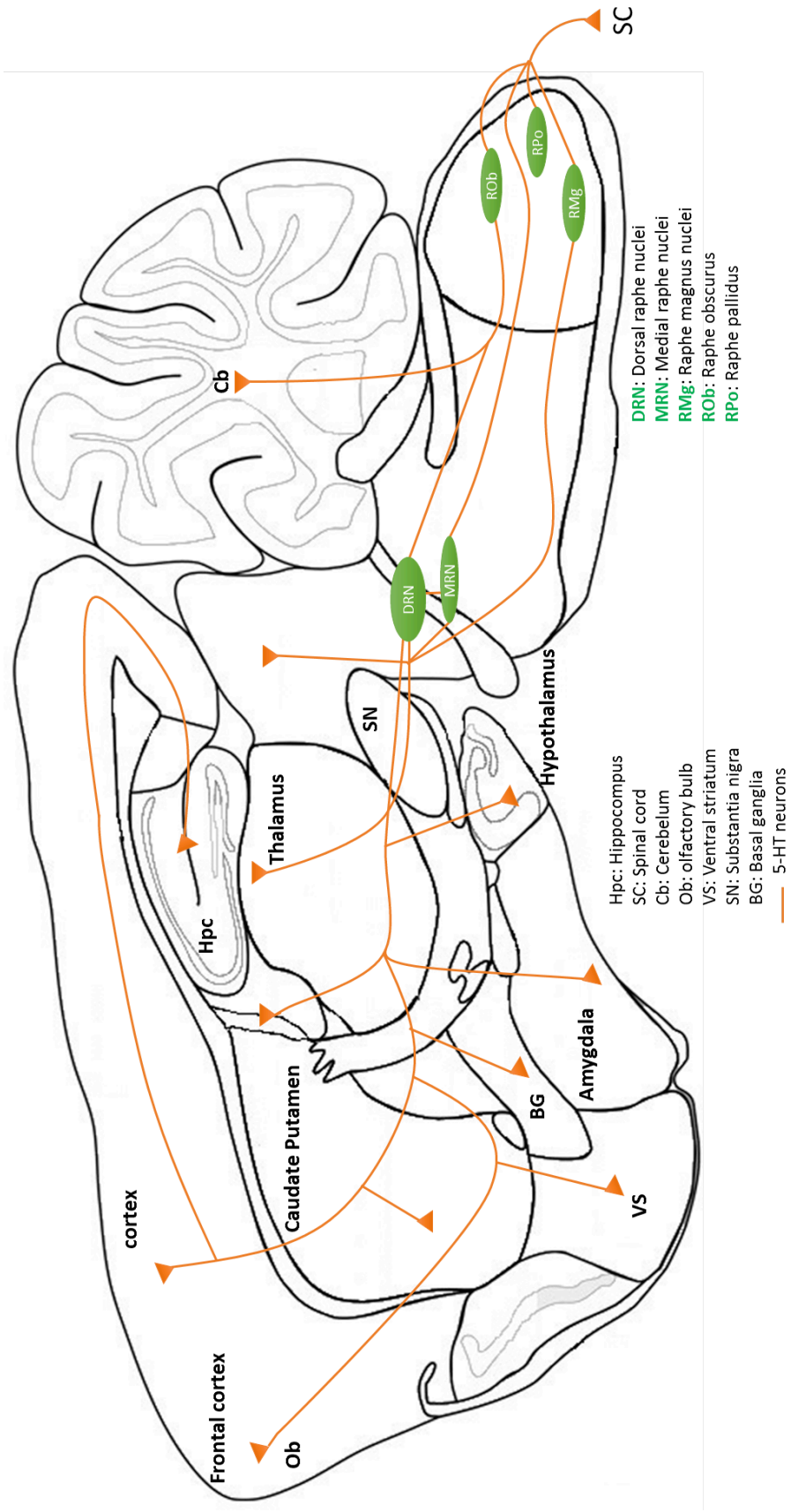

Figure 9: Major rostral and caudal projections of serotoninergic system in the brain

4. Serotonin receptors pharmacology and localization (Figure 10, 11, Table 5)

Serotoninergic receptors are composed of 7 families 5-HT1-7 with 14 receptor subtypes which are structurally and pharmacologically different. The characterization of 5-HT receptors comes from radioligand binding studies with high affinity binding site for (3H)-5HT.

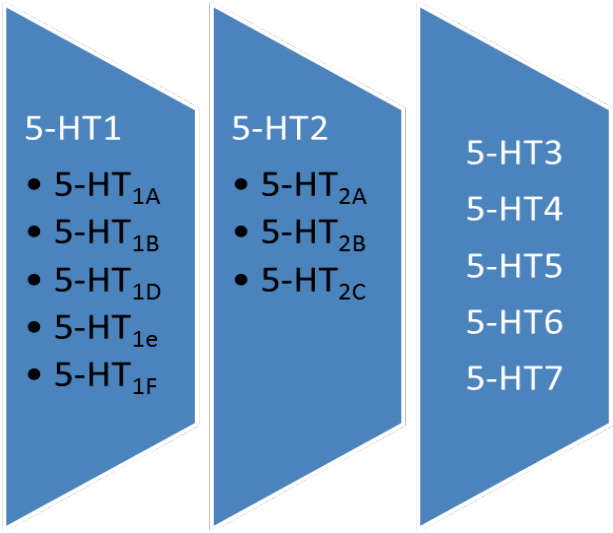

Figure 10: Serotonin receptors subtypes: 7 families of 5-HT receptors.

i. 5-HT1

The 5-HT1 receptors contain 5 different subtypes. They have high amino acid sequence homology. They are members of the G- protein coupled receptors. All 5-HT1 receptors are coupled negatively to adenylate cyclase and reduce Cyclic adenosine 3',5'-monophosphate (cAMP) levels (Raymond *et al.*, 2001). Several of these receptors act as autoreceptors that regulate the excitability of serotoninergic neurons and release of serotonin. They are also expressed in other types of neurons.

a. 5-HT_{1A}

5-HT_{1A} receptors are distributed in the CNS in soma, dendrites, axons, cell body of neurons and processes of astrocytes. They are highly located in limbic brain areas,

hippocampus (pyramidal and granular neurons), lateral septum (cholinergic neurons), cortical area (pyramidal neurons) and mesencephalic raphe nuclei in 5-HT neurons (postsynaptic membrane). The activation of 5-HT_{1A} receptor in neurons is generally inhibitory and reduce neuronal firing rate. Electrophysiological studies showed that 5-HT_{1A} receptor activation causes neuronal hyperpolarization through G-protein coupled opening K^+ channels (Raymond *et al.*, 2001). 5-HT_{1A} receptor specific pharmacological ligands are the therapeutic targets for neuropsychiatric disorders like anxiety, depression and schizophrenia. 5-HT_{1A} receptors distribution in the PNS is mainly in the intestinal tract. 5-HT1A receptor knockout mice are more anxious. Several basic and clinical data showed that 5-HT_{1A} receptor agonists induce hyperphagia, hypothermia, altered sexual behavior and acts as anxiolytic and antidepressant. 5-HT1A receptor antagonists facilitate the effect of 5-HT reuptake inhibitors, monoamine oxidase inhibitors and certain tricyclic antidepressant drugs on 5-HT release. Two polymorphisms were identified in the N-terminal region of the receptor and several polymorphisms also were associated with Tourette syndrome (Hoyer *et al.*, 1990; De Vry, 1995; Barnes & Sharp, 1999; Celada *et al.*, 2004; Moses, 2008; Nichols & Nichols, 2008; Savitz *et al.*, 2009; Pytliak *et al.*, 2011).

b. 5-HT_{1B}

5-HT1B receptors are distributed in serotonergic and non-serotonergic neurons mainly in axonal terminals. In 5-HT neurons 5-HT_{1B} receptors are located in presynaptic and postsynaptic membranes. They are highly distributed in the basal ganglia (substantia nigra, globus pallidus, ventral pallidum and entopeduncular nucleus), forebrain region (striatum), dorsal and median raphe nuclei (postsynaptic and presynaptic membranes), hippocampus (granule and pyramidal cells) and caudate putamen (medium spiny GABAergic neurons) (Barnes & Sharp, 1999). 5-HT_{1B} receptor is negatively coupled to adenylate cyclase (Raymond *et al.*, 2001). 5-HT_{1B} receptor knockout mice have increased aggression and in most cases predisposition for addiction-like behaviors. 5-HT_{1B} autoreceptors reduce 5-HT synthesis and release and enhance reuptake via the serotonin transporter. 5-HT_{1B} heteroreceptors inhibit the

release of a range of different neurotransmitters (glutamate) or modulate their release (acetylcholine, dopamine), depending on the neuron types that is expressing 5-HT_{1B} receptor. 5-HT_{1B} receptor agonists are effective as antimigraine drug and induce learning deficit. 5-HT_{1B} treatments modulate behavior including increased locomotion, change in brain reward mechanisms, increased corticosterone and prolactin secretion, hypophagia, hypothermia and decreased aggression. 5-HT_{1B} selective antagonist's treatments act as aggression-enhancing compounds (Bruinvels *et al.*, 1994; Barnes & Sharp, 1999; Clark & Neumaier, 2001; Tepper *et al.*, 2002; Goadsby & Classey, 2003; Olivier & van Oorschot, 2005; Moses, 2008; Nichols & Nichols, 2008; Pytliak *et al.*, 2011).

c. 5-HT_{1D}

5-HT_{1D} receptor is less expressed than 5-HT_{1B} receptor. 5-HT_{1D} receptors are found in serotonergic (raphe nuclei) and non-serotonergic neurons (hippocampus, olfactory tubercle, caudate putamen) in presynaptic and postsynaptic membranes like 5-HT_{1B} receptors. 5-HT_{1D} receptors are implicated in cardiovascular regulation (Hoyer *et al.*, 1990; Bruinvels *et al.*, 1994; Barnes & Sharp, 1999; Tepper *et al.*, 2002; Goadsby & Classey, 2003; Moses, 2008; Nichols & Nichols, 2008; Pytliak *et al.*, 2011).

d. 5-hT_{1e}

5-HT_{1e} receptors are found in cortical regions, caudate membranes, caudate putamen and claustrum, hippocampus (subiculum), amygdala and raphe nuclei (postsynaptic). 5-HT_{1e} receptor is negatively coupled to adenylate cyclase (Raymond *et al.*, 2001). The physiological significance of this receptor remains unclear (Bruinvels *et al.*, 1994; Barnes & Sharp, 1999; Bai *et al.*, 2004; Moses, 2008; Nichols & Nichols, 2008; Klein *et al.*, 2011; Pytliak *et al.*, 2011; Klein et al., 2011; Klein & Teitler, 2012).

e. 5-HT_{1F}

5-HT_{1F} receptors are detected in hippocampus (CA1-CA3 cell layers), cortex, dorsal raphe nucleus, caudate nucleus and hypothalamus and thalamus nuclei. 5-HT_{1D} receptors are found in serotonergic (raphe nuclei) and non-serotonergic neurons (Barnes & Sharp, 1999). Like other 5-HT1 receptor family this receptor inhibits adenylyl cyclase (Raymond *et al.*, 2001). The physiological significance of this receptor remains not well understood but current studies are indicating a possible use of 5-HT_{1F} receptor agonist in the treatment of migraine (Bruinvels *et al.*, 1994; Barnes & Sharp, 1999; Goadsby & Classey, 2003; Ramadan *et al.*, 2003; Moses, 2008; Nichols & Nichols, 2008; Neeb *et al.*, 2010; Olesen, 2010; Pytliak *et al.*, 2011; Mitsikostas & Tfelt-Hansen, 2012).

ii. 5-HT2

5-HT2 receptors contain 3 different subtypes. They have a seven-transmembrane domain motif, coupled positively to phospholipase C that lead to increased accumulation of inositol phosphates and intracellular calcium (Raymond *et al.*, 2001). The gene structure of 5-HT2 receptors family has either two introns like in 5-HT_{2A} and 5-HT_{2B} receptors subtypes or three introns like in the 5-HT_{2C} in the coding sequence. The 5-HT2 receptors are well characterized at the molecular and pharmacological levels.

a. 5-HT_{2A}

5-HT_{2A} receptors are densely expressed in the forebrain regions, more precisely in the cortical membrane, neocortex (pyramidal and interneurons), entorhinal and pyriform cortex. They are also expressed in the caudate nucleus, nucleus accumbens, olfactory tubercle and hippocampus. 5-HT_{2A} receptors are present in 5-HT neurons (dorsal raphe nuclei) and non 5-HT neurons in glial cells, GABAergic interneurons and glutamatergic pyramidal neurons in the cortex. In the periphery 5-HT_{2A} receptors are

expressed mainly in blood vessels and stomach fundus (Barnes & Sharp, 1999). In animal models 5-HT_{2A} antagonists have antipsychotic action and modulate noradrenaline release. 5-HT_{2A} agonists mediate hyperthermia and neuroendocrine responses such as increased secretion of cortisol and prolactin. The Knock-out for 5-HT_{2A} receptors mice had an effect on their sleeping rhythms (Barnes & Sharp, 1999; Bhattacharyya *et al.*, 2002; Williams *et al.*, 2002; Marek *et al.*, 2003; Raote *et al.*, 2007; Moses, 2008; Nichols & Nichols, 2008; Pytliak *et al.*, 2011).

b. 5-HT_{2B}

5-HT_{2B} receptors are distributed in CNS in the cerebellum, lateral septum, dorsal hypothalamus and medial amygdala and in the periphery in stomach fundus, liver, kidney and mainly in the heart (Schmuck *et al.*, 1994). The 5-HT_{2B} has many different physiological roles in cardiac function, morphogenesis, memory and learning, smooth muscle contraction. 5-HT_{2B} receptor agonist modulates anxiety (Barnes & Sharp, 1999). The activation of 5-HT_{2B} receptors induces valvulopathy. The over-expression of 5-HT_{2B} receptors leads to ventricular hypertrophy and mitochondrial alteration (Barnes & Sharp, 1999; Hoyer *et al.*, 2002). 5-HT_{2B} receptors are also expressed on macrophages(de las Casas-Engel *et al.*, 2013). In the central nervous system, the 5-HT_{2B} receptor is expressed on serotonergic nuclei and regulates serotonin role on food intake. It was recently shown that the 5-HT_{2B} receptor is expressed on microglial cells and regulates chemotaxis of microglia (Nebigil *et al.*, 2000, 2003; Doly *et al.*, 2008; Diaz & Maroteaux, 2011; Diaz *et al.*, 2012, 2016; Launay *et al.*, 2012).

c. 5-HT_{2C}

5-HT_{2C} receptors are distributed in CNS in the midbrain (raphe nuclei), area of the cortex (olfactory nucleus, piriform, cingulate and retrosplenial), limbic system (nucleus accumbens, hippocampus and amygdala), basal ganglia (caudate nucleus, substantia nigra), hypothalamic nuclei and poorly present in the brainstem and spinal

cords. The activation of 5-HT_{2C} receptors increased phospholipase C activity (Raymond *et al.*, 2001). 5-HT_{2C} receptors agonist mediates the activation of motorneurons and induces hypophagia, hypolocomotion and anxiety. The receptors antagonists are shown to stimulate long-term memory increase the release of noradrenaline and dopamine and in humans increase slow wave sleep. 5-HT_{2C} -/- mice has impairment in cognitive function increased food intake, mid-life obesity, glucose intolerance and seizures (Millan; Ni & Miledi, 1997; Barnes & Sharp, 1999; Moses, 2008; Nichols & Nichols, 2008; Pytliak *et al.*, 2011).

5-HT_{2C} receptor has been extremely well studied for its role in the regulation of food intake on melanocortin neurons of the arcuate nucleus. Indeed, deletion of 5-HT_{2C} leads to obesity due to increased food intake, while, conversely 5-HT_{2C} agonists decrease sharply food intake. Re-expression of 5-HT_{2C} in POMC neurons of the arcuate nucleus is sufficient to revert these phenotypes in 5-HT_{2C} knockout mice (Lam *et al.*, 2008; 2010; Sohn *et al.*, 2011; Berglund *et al.*, 2013)

5-HT_{2C} encoding transcript undergoes RNA editing by conversion of adenosine to inosine (A to I). There are 5 A to I editing events that generate 24 different protein isoforms and 32 mRNA that differ by up to three amino-acids within second intracellular loop of the receptor, the region involved in receptor G-coupled protein coupling. Several editing variants decrease the receptor affinity, constitutive activity and G-protein coupling efficacy. Alterations in 5-HT_{2C} receptor editing have been observed in suicide victims with depression and schizophrenia history and bipolar disorders (Hoyer *et al.*, 2002; Iwamoto *et al.*, 2011).

iii. 5-HT3

5-HT3 receptors contain 2 different subtypes, 5-HT_{3A} and 5-HT_{3B}. They are the only receptors members of the Cys-loop ligand gated ion channel family. The 5-HT3 receptor complex is a non-selective cation channels (Ca2+, Na+ and K+) (Barnes & Sharp, 1999; Hoyer *et al.*, 2002). 5-HT3 expression is in the CNS and PNS. 5-HT3 receptors are distributed mostly in CNS in the dorsal vagal complex in the brainstem, in

the basal ganglia, hippocampus, amygdala, superficial layers of the cerebral cortex and forebrain. The 5-HT3 receptor is associated with GABAergic neurons (cerebral cortex and hippocampus) and interneurons (CA1-CA3 in the hippocampus), Glutamatergic and dopaminergic neurons. The 5-HT3 receptor activation enhances the release of serotonin. The 5-HT3 receptors have many different physiological roles in learning and behavior (Barnes & Sharp, 1999). 5-HT3 receptor antagonist modulates cognitive processes and long term potentiation (LTP). The activation of 5-HT3 receptors inhibits LTP and increase dopamine release. 5-HT3 receptor agonist potentiated the hyperactivity (Maricq *et al.*, 1991; Barnes & Sharp, 1999; Hoyer *et al.*, 2002; Thompson & Lummis, 2006, 2007; Moses, 2008; Nichols & Nichols, 2008; Pytliak *et al.*, 2011).

iv. 5-HT4

5-HT4 receptors have seven putative transmembrane domains. 5-HTreceptors are G-protein coupled receptors positively to adenylate cyclase with ten different isoforms (Raymond *et al.*, 2001). Expression of 5-HT receptor is present in the CNS and PNS (cardiovascular tissues). 5-HT4 receptors are mostly with postsynaptic localisation distributed in the basal ganglia, substantia nigra, caudate nucleus, globus pallidus, the striatum, nucleus accumbens, putamen, hippocampus (CA1 and subiculum) and cortical regions. The 5-HT4 receptor is associated with cholinergic and dopaminergic neurons. 5-HT4 receptor modulates dopamine release. The 5-HT4 receptors have many different physiological roles in learning, locomotion, cognition and anxiety. 5-HT4 receptor activation facilitates cognitive performance and enhances short and long term memory. 5-HT4 receptor antagonist has an anxiolytic-like action. 5-HT4 receptor agonist increase serotonin release and modify locomotor activity (Hegde & Eglen, 1996; Barnes & Sharp, 1999; Bharucha, 2000; Hoyer *et al.*, 2002; De Maeyer *et al.*, 2008; Moses, 2008; Nichols & Nichols, 2008; Camilleri, 2010; Manabe *et al.*, 2010; Ahmad & Nirogi, 2011; Pytliak *et al.*, 2011).

v. 5-HT5

5-HT5 receptors are members of the seven putative transmembrane domain-G-protein coupled family coupled positively with adenylate cyclase (Raymond *et al.*, 2001). Their distribution is in different brain regions, hippocampus (pyramidal cell layer in CA1-3), hypothalamus, cerebral cortex, dorsal raphe, striatum, thalamus, cerebellum (granule cell layer), olfactory bulb (tufted cells) pons and medulla. The 5-HT5 receptors have many different physiological roles in cognition, Alzheimer disease, and anxiety (Plassat *et al.*, 1992; Barnes & Sharp, 1999; Hoyer *et al.*, 2002; Nelson, 2004; Moses, 2008; Nichols & Nichols, 2008; Ahmad & Nirogi, 2011; Pytliak *et al.*, 2011).

vi. 5-HT6

5-HT6 is a G-coupled seven putative transmembrane domain receptor family (Raymond *et al.*, 2001). They are distributed in the striatum, olfactory, nucleus accumbens, hippocampus (pyramidal and granule cell neurons) and substantia nigra. 5-HT6 is associated with depression and Alzheimer disease (Barnes & Sharp, 1999; Hoyer *et al.*, 2002; Moses, 2008; Nichols & Nichols, 2008; Upton *et al.*, 2008; Pytliak *et al.*, 2011; Ramírez, 2013; Benhamú *et al.*, 2014).

vii. 5-HT7

5-HT7 receptor is a G-coupled receptor (Raymond *et al.*, 2001). The distribution of 5-HT7 receptors is in the thalamus, hypothalamus, amygdala and cerebral cortex. 5-HT7 receptors are implicated in the regulation of circadian rhythms, vasodilation and behavior. 5-HT7 receptors are also expressed on macrophage cells and appear important in their polarization. The knockout of the receptor leads to reduced immobility in forced swim test. 5-HT7 receptor antagonist has a role in the treatment of epilepsy (Barnes & Sharp, 1999; Hoyer *et al.*, 2002; Moses, 2008; Nichols & Nichols,

2008; Hedlund, 2009; Bonaventure *et al.*, 2011; Pytliak *et al.*, 2011; Mnie-Filali *et al.*, 2011; de las Casas-Engel *et al.*, 2013a; Nikiforuk *et al.*, 2013; Naumenko *et al.*, 2014).

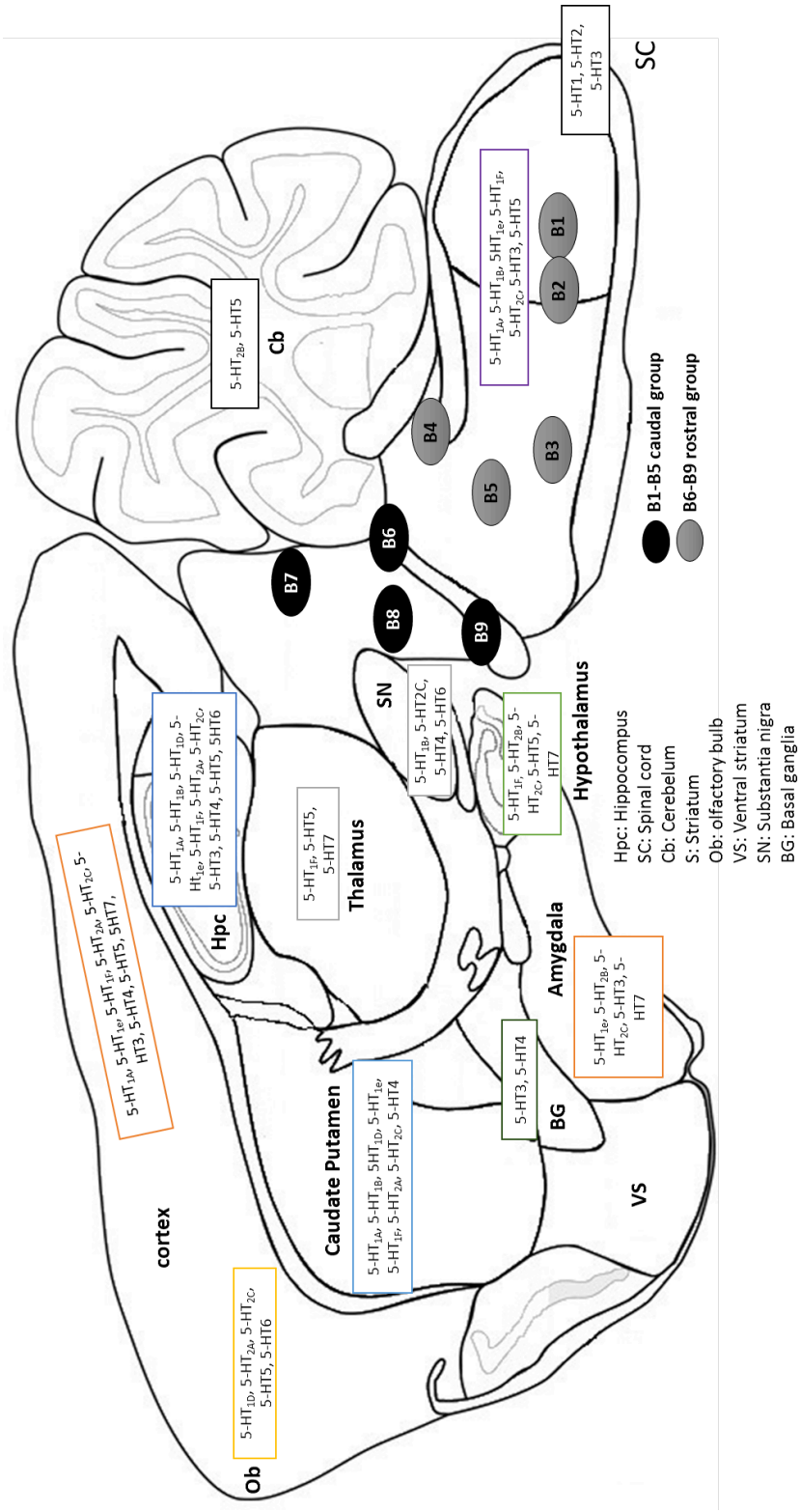

Figure 11: Major serotoninergic receptors localization in the brain

Table 5: Major serotoninergic receptors gene localization and function

Gene receptor	Gene location	Effect on neurotransmissions	Function
Htr1A	5q11.2-q13	ACTH (+) Prolactin (+), 5-HT release (−) Noradrenaline release (+) Acetylcholine release (+) Glutamate release (−)	CNS: Aggression, Anxiety, Addiction, Appetite, Emesis, Impulsivity, Memory, Mood, Nausea, Nociception, Respiration, Sleep, Sociability, Thermoregulation, Sexual behavior Cardiovascular system: Blood pressure, Heart rate, Cardiovascular function, Vasoconstriction, Penile erection Other: Pupil dilation
Htr1B	6q13	5-HT release (−) Acetylcholine release (−)	CNS: Aggression, Anxiety, Learning, Addiction, Locomotion, Memory, Mood, Sexual behavior Vessels: Pulmonary vasoconstriction
Htr1D	1p34.3-36,3	Acetylcholine release (−)	CNS: Locomotion, Anxiety Vessels: Cerebral vasoconstriction
Htr1e	6q14-q15	_	Memory
Htr1F	3q11	_	Memory

Htr2A	13q14-q21	Noradrenaline release (−) Cortisol ACTH	CNS: Anxiety, Appetite, Addiction, Cognition, Imagination, Learning, Memory, Mood, Perception, Sexual behaviour, Sleep, Thermoregulation Smooth muscles: Contraction Vessels: Vasoconstriction, Vasodilation Platelets: Aggregation
Htr2B	2q36.3-q37.1	Adenylate cyclase (+)	Muscle contraction, CNS: Anxiety, Appetite, Sleep, Neuroinflammation, Gastrointestinal tract: GI motility Vessels: Vasoconstriction Cardiovascular system: Cardiovascular function
Htr2C	Xq24	Noradrenaline/Dopamine release (−)	CNS: Anxiety, Appetite, Addiction, Locomotion, Mood, Sexual behaviour, Sleep, Thermoregulation Gastrointestinal tract: GI motility Vessels: Vasoconstriction, Penile erection
Htr3	11q23.1–q23.2	5-HT release (+) Acetylcholine release (−) GABA release (+) CCK release (+) Dopamine release (+)	CNS, PNS: Anxiety, Addiction, Anxiety, Nausea, Emesis, Learning, Memory, Neuronal excitation Gastrointestinal tract: GI motility, Nausea, Emesis
Htr4	5q31-q33	5-HT release (+) Acetylcholine release (+) Dopamine release (+) cAMP (+)	CNS: Anxiety, Appetite, Learning, Memory, Mood, Respiration Gastrointestinal tract: GI motility

Htr5A	1p35–36	cAMP (-)	Locomotion, Sleep
Htr5B	2q11 –q13		
Htr6	1p35-p36	cAMP (+)	CNS: Anxiety, Cognition, Learning, Memory, Mood
Htr7	10q21-q24	Adenylate cyclase (+), cAMP (+)	CNS: Anxiety, Memory, Mood, Respiration, Sleep, Thermoregulation Vessels: Vasoconstriction

5. Serotonin and serotoninergic neurons loss in ALS

In ALS patients, levels of serotonin and its metabolites are decreased in brain tissues. Moreover a decreased binding of 5-HT1A ligands where observed in ALS patients autopsy in the raphe nuclei and cortex (Bertel *et al.*, 1991; Sofic *et al.*, 1991; Forrest *et al.*, 1996; Turner *et al.*, 2005).

Recently two major studies from our team brought up important findings. First it has been shown that peripheral serotonin levels were modified during disease course. In ALS patients platelet's serotonin levels were decreased. Interestingly, serotonin levels were positively correlated with longer survival (Dupuis *et al.*, 2010).

Second, in SOD1 (G86R) mutant mice, serotonin levels were decreased in the brainstem and spinal cord even before disease onset. In autoptic brains of ALS patients, Tph2 positive cells loss were observed in the serotoninergic nuclei. Moreover, ubiquitinated cytoplasmic aggregates were observed in the raphe magnus and gigantocellular nuclei. Serotoninergic neurons degeneration in ALS patients was characterized with neurite and cell body loss (Dentel *et al.*, 2013).

III. Spasticity: an ALS symptom, mostly studied in spinal cord injury (Figure 12)

A large part of my thesis work was dedicated to elucidate the role of serotonin neurons in spasticity during ALS.

In this last part of the introduction, I will present the current knowledge on spasticity in ALS, as well as in spinal cord injury in which this symptom has been intensely studied.

1. Spasticity, a typical sign of the so-called UMN syndrome

Spasticity and hypertonia are one of the common consequences of UMN lesions in the pyramidal and extrapyramidal pathways during ALS progression. Lance defined the spasticity in 1980 as « a motor disorder characterized by a velocity-dependent increase in tonic reflexes (muscle tone) with exaggerated tendon jerks, resulting from hyperexcitability of the stretch reflex as one component of the upper motor neuron syndrome » (Lance, 1980). The development of spasticity, which is gradual over several months, interferes with residual motor function, induces pain and can be violent enough to expel a person out of a wheelchair. Importantly, the involuntary muscle spasms and tone in extensor muscles can facilitate walking, standing and transfers which give patients the ability to keep low level of their motor functions. Besides ALS, spasticity occurs in a number of neurological diseases, either genetic (hereditary spastic paraplegia), traumatic (spinal cord injury) or after stroke. It remains unknown whether spasticity mechanisms are indeed the same in these disparate diseases.

Spasticity has been widely studied after spinal cord injury (SCI). Spasticity intensity depend on muscle length, it is stronger with short muscles compared to long ones. It occurs more often in flexor muscle of upper limb (fingers, wrist, elbow flexors) and in extensor muscle of lower limb (knee and ankle extensors) (Rushworth, 1960; Moor & Rehabilitation, 1998; Sheean, 2002; Trompetto *et al.*, 2014).

The current paradigm regarding the cause of spasticity in ALS is that this results from the loss of UMN (cortical motor neurons) leading to the disruption of

communication between brain and spinal cord and producing a state of net inhibition of spinal reflexes (Sheean, 2002; Bhimani & Anderson, 2014; de Carvalho *et al.*, 2014). Over months, the loss of upper controls is postulated to induce local plasticity that leads to hyperexcitability of motor neurons and hyperreflexia (see below).

Cortical motor neurons (CMN), the major source of descending motor commands for voluntary movement, are located in layer V of motor cortex referred to corticospinal tract (CST) neurons. These neurons are characterized by a large pyramidal cell body and single apical dendrite with very long axon that projects toward spinal cord. CST axons terminate in spinal cord interneurons to make connection with spinal MN and second type of CTS axons terminate in the ventral horn of the spinal cord to make monosynaptic connection with α-MN (Lance, 1980; de Carvalho *et al.*, 2014). The current hypothesis is that the degeneration of UMN is sufficient to trigger spasticity. To our knowledge, this has not been addressed experimentally.

2. Structural mechanisms of spasticity in ALS and SCI

The spinal cord plastic changes upon injury and/or UMN degeneration induce the disruption in the balance between excitatory and inhibitory inputs to LMN. Several mechanisms were proposed to explain the pathophysiology of spasticity.

i. Fusimotor hyperexcitability

Stretch reflexes are mediated by excitatory connections between Ia afferent fibers from muscles spindles and α-MN. Upon excitation, α-MN sends efferent impulse to muscles to contract. The mechanisms inducing hyperreflexia upon UMN loss include muscle spindles hyperexcitability changes and excessive reflex activation is followed by prolonged firing of α-MN. This feedback system is disrupted after UMN loss and leads to abnormal muscle activation by increasing their contraction (Rekling *et al.*, 2000; Murray *et al.*, 2011; de Carvalho *et al.*, 2014,Wilson *et al.*, 1999)(Figure12).

ii. Reduction in presynaptic inhibition (PSI)

The PSI adjusts the strength of synaptic inputs to neurons by regulating the levels of neurotransmitter release. In spastic patients PSI was reduced in resting and contracting muscles (Katz, 1999; Li & Bennett, 2003; Kitzman, 2005)(Figure12).

iii. Enhancement in the excitability of motor neurons

In spastic patients, the ratio of potentials resulting from electrical stimulation of the sensory and motor axons in resting position is increased. Consistently, the amplitude of the F-wave due to activation of motor neurons is also increased in spastic cases (Rushworth, 1960; Moor & Rehabilitation, 1998; Rekling *et al.*, 2000; Sheean, 2002; Nardone & Schieppati, 2005; Sheean & McGuire, 2009; Chang *et al.*, 2013; Bhimani & Anderson, 2014; Trompetto *et al.*, 2014; D'Amico *et al.*, 2014; de Carvalho *et al.*, 2014). The mechanisms underlying this increased excitability are unknown.

iv. Enhancement in the excitability of interneurons

In spinal networks, a number of interneurons mediate inhibition of the antagonist muscles or increase action potentials in the sensory neurons from the muscle spindle. During spasticity, these inhibitory interneurons are disrupted in their functioning, leading to hypertonia (Rushworth, 1960; Moor & Rehabilitation, 1998; Chang *et al.*, 2013; Bhimani & Anderson, 2014; de Carvalho *et al.*, 2014).

v. Activation of persistent inward currents (PIC)

In MN, persistent inward currents (PIC) are located in dendrites and are activated by monoaminergic drive from brainstem. These PICs allow the amplifying of the synaptic inputs allowing motor neurons to fire repeatedly. During spasticity related to SCI, PICs are no longer physiologically activated. However, a few weeks after injury, PICs appear chronically activated, thus inducing high firing rate of MN. Indeed, a PIC activation underlies the appearance of long-lasting reflex and muscle spasms due to increased MN excitability (Sheean, 2002; Li & Bennett, 2003; Murray *et al.*, 2011)**(** Figure12).

3. Molecular mechanisms underlying spasticity

i. Neuromodulator dysfunction in controlling motor neurons excitability

MNs are under the control of a number of neurotransmitters such as acetylcholine, thyroid releasing hormone, substance P, adenosine and monoamines (serotonin and norepinephrine). Monoamines drive differential effects on the ventral and dorsal horns of spinal cord. In the ventral horn monoamines have excitatory effect on MN and low-threshold muscle afferents leading to the increase of cell excitability.

Monoamines also inhibit sensory inputs to MN (high-threshold muscle afferents) and suppress inputs to deep dorsal horn interneurons from high-threshold afferents. The losses of monoamines reduce the excitability of neurons in the ventral horn and increase sensory inputs in the dorsal horn. After chronic injury, MNs become highly sensitive to residual monoamines, and this restores motoneuronal excitability and activates the long-lasting reflexes (Thilmann *et al.*, 1991; Sheean & McGuire, 2009; Murray *et al.*, 2011) (Figure12).

ii. Potassium-chloride cotransporter 2 (KCC2) dysregulation

KCC2 is a cation-chloride cotransporter expressed in neurons. KCC2 participates in Cl^- homeostasis (DeFazio *et al.*, 2000). KCC2 plays an important role in establishing neuronal Cl^- and control neuronal processes such as migration, dendritic growth, formation of synaptic connection and spine morphology (Edgerton & Roy, 2010; Tanis *et al.*, 2010; Medina *et al.*, 2014). In animal models of SCI that develop spasticity, a down regulation of KCC2 in MN membranes was observed (Boulenguez *et al.*, 2010). KCC2 is important to maintain low intracellular Cl^- concentrations in adult neurons, thus allowing GABA and glycine to mediate entry of Cl^- in neurons, leading to their inhibitory properties. KCC2 activity is modulated by many different signals. KCC2 activity is stimulated by serotonin, through 5-HT_{2A} receptor (Bos *et al.*, 2013). KCC2 localization and activity is also modulated by growth factors such as brain-derived neurotrophic factor (BDNF), insulin-like growth factor 1 (IGF-1) and neurturin indicating a potential role in neuroinflammation upon axonal and MN loss (Tanis *et al.*,

2010; Medina *et al.*, 2014; Mòdol *et al.*, 2014; Ford *et al.*, 2015). In ALS, there was a report stating that KCC2 is not modified in end-stage mutant SOD1 mice (Mòdol *et al.*, 2014), while Fuchs and collaborators observed decreased KCC2 mRNA in vulnerable motor neurons (Fuchs *et al.*, 2010). In general, the role of KCC2 in ALS remains unclear.

4. Spasticity and serotonin in spinal cord

5-HT present in the spinal cord comes from 5-HT containing neurons in B1, B3 and B3 caudal nucleus. The major raphe nuclei that project to the spinal cord are the RMg, RPa and ROb. Approximately 50% of the raphe magnus neurons, 80% of raphe pallidus neurons and the majority of raphe obscuris neurons contain 5-HT. Only 47 to 28% of spinal-projection neurons in the raphe nuclei contain 5-HT. The axons containing 5-HT project to lamina I and II in the dorsal horn dominated by 5-HT1 receptors that mediate hyperpolarization response. 5-HT2 receptors are found mainly in the ventral horn near motor neurons where they mediate depolarization response. 5-HT3 receptors are present in dorsal horn where they modulate pain.

Serotonin has been shown to participate in the development of spasticity after spinal cord injury, and this was mostly postulated to occur through 5-HT2 receptors. Indeed, the activation of persistent inward currents and pre/post-synaptic sensory transmission requires the activation of 5-HT or noradrenergic receptors on MNs. 5-$HT2_{B/C}$ receptors activate PICs on MNs in physiological conditions. After SCI, serotonergic input to motor neurons is lost, and PICs are transiently decreased, participating in initial flaccid paralysis. When spasticity and long lasting reflexes develop, PICs are simultaneously reemerging, together with constitutively active forms of 5-HT2 receptors. Indeed, only inverse agonists of 5-$HT2_{B/C}$ receptors, that binds to the receptor and block its active or inactive state, reduce PIC-mediated Long lasting reflex (LLR), while neutral antagonists do not show these anti-spastic properties. This indicates that the constitutive activity of 5-HT2 receptors, likely caused by 5-HT loss, is responsible for PICs and LLRs. 5-HT2 agonists significantly increase LLR consistent with an hypersensitivity of MNs upon 5-HT loss (DAHLSTROEM & FUXE, 1964; Hökfelt *et al.*, 1978; Bowker *et al.*, 1983; Skagerberg & Björklund, 1985; Holstege & Kuypers, 1987;

Bowker & Abbott, 1990; Leanza *et al.*, 1991, 1995; Jones & Light, 1992; Maxwell *et al.*, 1996; Schmidt & Jordan, 2000, 2001; Machacek *et al.*, 2001; Release *et al.*, 2010; Tanis *et al.*, 2010; Edgerton & Roy, 2010; Bruinstroop *et al.*, 2012; Andrade & Haj-Dahmane, 2013; D'Amico *et al.*, 2014).

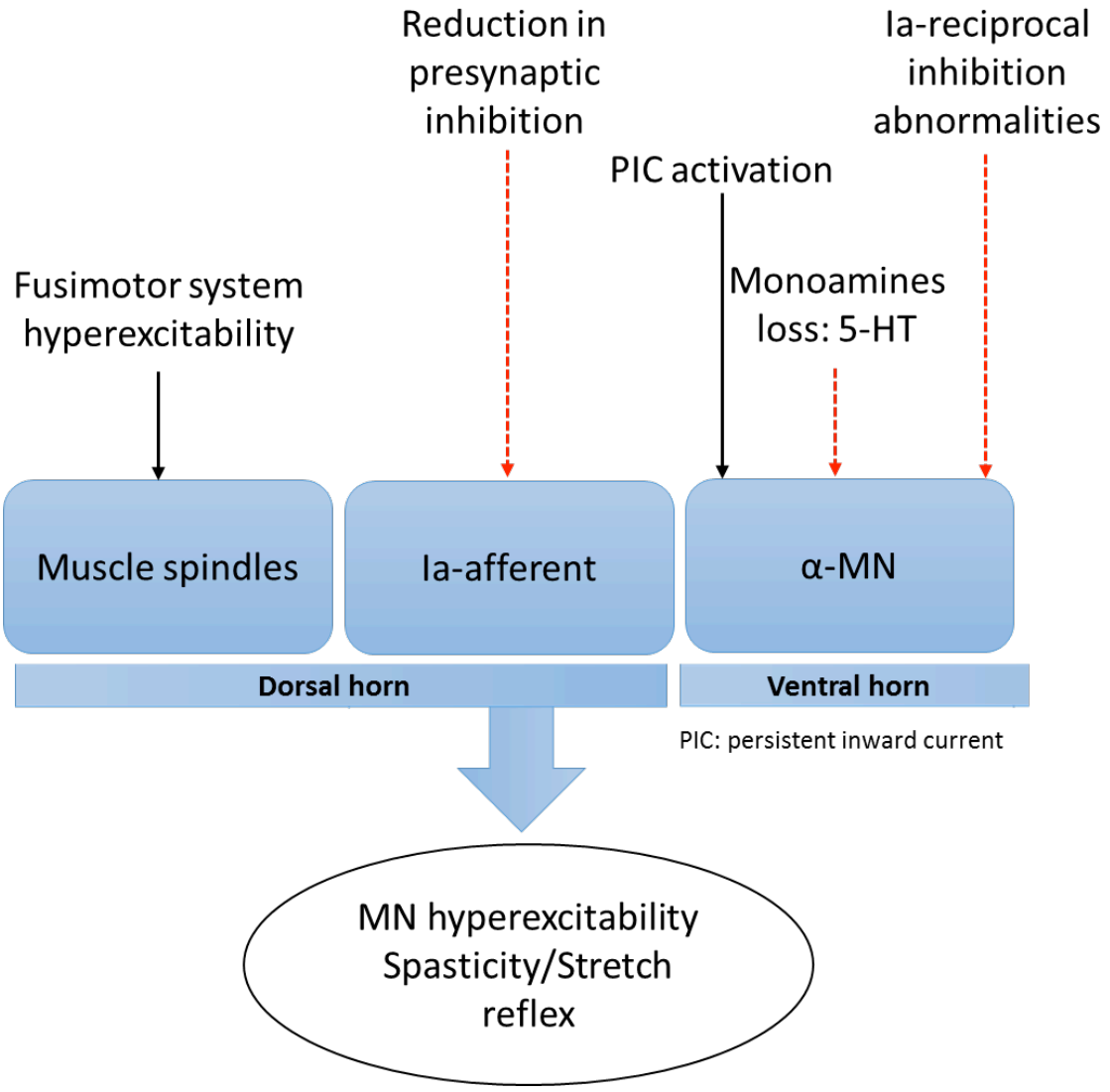

Figure 12: Motor neurons hyperexcitability major mechanisms inducing spasticity

5. Management of spasticity

Spasticity is a painful and disabling symptom. The intensity and level of spread of spasticity are variable from one ALS patient to the other depending on the disease state and site of onset. There are two types of therapy used for the management of spasticity: Non-invasive procedures where they use pharmacological modulation and invasive procedures based on surgeries. Most of these therapies were assessed for spasticity due to SCI but most of them were also used in ALS patients.

i. Antispastic drugs

Antispastic drugs are used in patients with diffuse spasticity.

a. Centrally acting drugs

The most used one are baclofen, clonidine, tizanidine, benzodiazepine and gabapentin. The side effect of some of these drugs is the loss of neuronal activity and liver toxicity. They target mostly the MN and interneurons of spinal cord.

Baclofen is a GABA B receptor agonist at the spinal level, leading to membrane hyperpolarization. This restricts calcium influx, which subsequently (1) restricts endogenous excitatory neurotransmitters from being released such as glutamate and (2) inhibits mono- and polysynaptic spinal reflexes

Tizanidine and clonidine are alpha-2 receptors agonists. They inhibit the poly-synaptic spinal excitatory pathways. Tizanidine decreases tone by increasing presynaptic inhibition of MN and decreases the release of excitatory amino acids from spinal cord interneurons. Clonidine, inhibit excessive afferent sensory transmission and decrease spasms.

Benzodiazepine is a GABA A receptor agonist that acts mostly on flexor muscles. Gabapentin inhibit calcium current. It is used for patients that suffer from neuropathic pain caused by spasms.

Tizanidine and baclofen are used for treating spasticity in ALS patients (Moor & Rehabilitation, 1998; WADE, 2001; Thuret *et al.*, 2006; Elbasiouny *et al.*, 2009; Chang *et al.*, 2013; Trompetto *et al.*, 2014)(Figure13).

b. Peripherally acting drugs

Dantrolene in one of the most used drug for spasticity that acts on muscle in the periphery. It suppresses the release of calcium ions from the sarcoplasmic reticulum of muscle. The decrease of Ca^{2+} in intrafusal and extrafusal muscle fibers reduces muscle contraction. It is also used for spasticity proposed treatment in ALS patients (Ellis & Carpenter, 1974) (Figure13).

ii. Interventionnal treatement

a. Chemical neurolysis

Chemical neurolysis is used for patients with focal spasticity. The intervention consists on the injection of phenol or alcohol solution in the peripheral nerve that innervates the spastic muscle. The injection destroys myelination of the nerve causing spasticity. Repeated injection are required in this procedure to maintain the effect (Moor & Rehabilitation, 1998; WADE, 2001; Thuret *et al.*, 2006; Chang *et al.*, 2013; Trompetto *et al.*, 2014) (Figure13).

b. Toxin injections

Botulinum toxin can be injected intramuscularly in spastic patients. The toxin acts on NMJs to inhibit the release of acetylcholine from pre-synaptic nerve terminals. It causes chemical denervation of intrafusal and extrafusal muscles fibers. Botulinum decreases muscle spasms causing excessive weakness of treated muscle. It is used for treating spasticity in ALS patients (BURGEN *et al.*, 1949; Picelli *et al.*, 2012; Phadke *et al.*, 2015) (Figure13).

iii. Surgical technics

Surgery is used when spasticity could not be handled with other non-invasive methods. It is used mainly for focal spasticity. The surgery consists of the ablation of motor neurons or rhizotomy of sensory spinal roots (Moor & Rehabilitation, 1998; Thuret *et al.*, 2006; Chang *et al.*, 2013) (Figure13).

iv. Electrical stimulation

Several electrical modalities have been used to reduce spasticity level especially in animal models of spasticity. There are two types of electrical stimulation. The first type is the surface electrical stimulation of muscle on spastic muscle and their antagonist that result to the decrease of MN PIC and excitability. The second type is the peripheral/central electrical stimulation of nerves in order to block exaggerated motor activity (Moor & Rehabilitation, 1998; Elbasiouny *et al.*, 2009; Chang *et al.*, 2013).

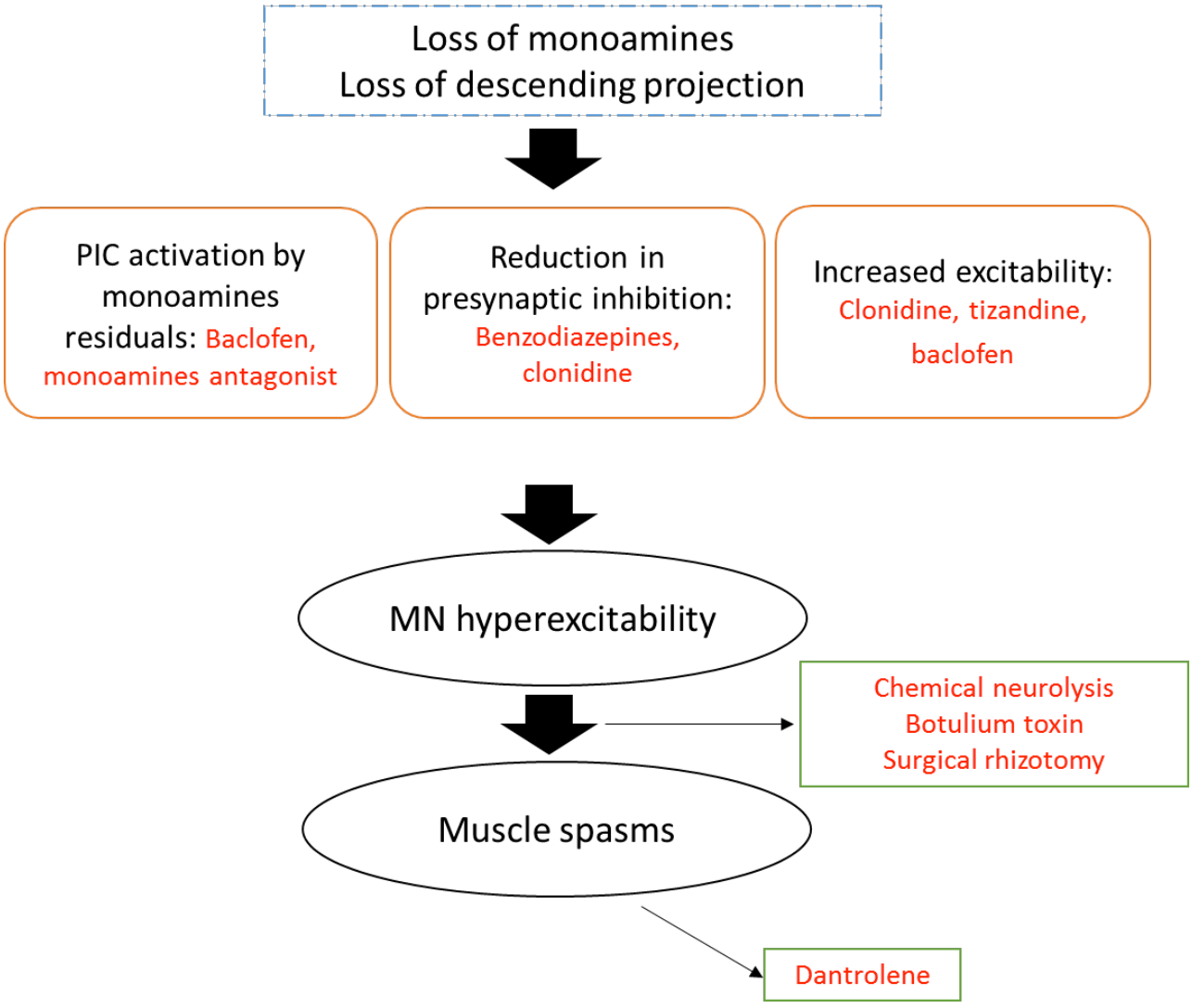

Figure 13: Spasticity management and drugs effect on spastic mechanisms

Results

Résultats #1

Le rôle du récepteur 5-HT_{2B} dans la SLA

Les neurones sérotoninergiques dégénèrent chez les patients atteints de SLA ainsi que chez les souris SOD1(G86R), modèles de la maladie. La perte des neurones 5-HT, induit l'augmentation de l'expression du gène codant pour le récepteur 2B de la sérotonine (5-HT_{2B}) chez les souris SOD1(G86R) au stade final de la maladie. Les neurones sérotoninergiques centraux ont des actions régulatrices sur de nombreuses fonctions physiologiques, notamment la prise alimentaire, la mémoire ou la contraction musculaire, et leur dégénérescence pourrait donc affecter de nombreuses régions cérébrales et spinales.

- Notre objectif est d'étudier les conséquences de la perte des neurones 5-HT sur la progression de la maladie. Pour cela les principales questions sont :

- L'augmentation transcriptionnelle du récepteur 5-HT_{2B} est-elle une réponse protectrice suite à la perte des neurones 5-HT au cours de la maladie ?
- Quels types cellulaires sur-expriment le récepteur 5-HT_{2B} ?
- Quel est le rôle du récepteur 5-HT_{2B} dans la SLA ?

Le récepteur 5-HT_{2B} (5-HT_{2B}R) est impliqué dans la physiopathologie de l'hypertension artérielle pulmonaire, les fonctions cardiaques et la réponse inflammatoire. Au niveau central, 5-HT_{2B}R est impliqué dans de nombreuses fonctions comme la prise alimentaire ou l'impulsivité. Au niveau du système nerveux central, 5-HT_{2B}R est exprimé dans quelques rares populations neuronales, et est exprimé de façon prédominante dans les cellules microgliales.

Pour la caractérisation du rôle fonctionnel du récepteur 5-HT_{2B} dans la SLA, nous avons en premier lieu mesuré son expression dans différentes souris transgéniques modèles de SLA, les souris SOD1(G86R), TDP43 et Dynactin au stade avancé de la maladie. Le niveau d'expression du récepteur 5-HT_{2B} était augmenté chez tous les modèles animaux étudiés. Nous avons donc décidé de réaliser des études fonctionnelles sur ce récepteur.

Il n'existe pas de molécules pharmacologiques entièrement sélectives du récepteur 5-HT_{2B}, et nous avons donc utilisé une approche génétique en croisant des souris Knock-out (KO) du récepteur 5-HT_{2B} avec les souris SOD1(G86R).

L'ablation du récepteur 5-HT_{2B} chez les souris modèle de SLA a accéléré la progression de la maladie. Les souris SOD1 sans le récepteur fonctionnel 5-HT_{2B} présentaient une perte de poids plus importants et une diminution des performances et de la force motrices. Au niveau histologique la perte de 5-HT_{2B}R a provoqué une atrophie des motoneurones plus sévères que chez les souris SOD1(G86R) avec le récepteur 5-HT2B fonctionnel.

Afin de déterminer l'origine cellulaire de l'augmentation de l'expression du récepteur 2B, nous avons utilisé un tri magnétique sélectif pour isoler la fraction des cellules CD11b de la moelle épinière des souris SOD1 (G86R) à un stade final de la maladie.. Nous avons observé que la surexpression de 5-HT_{2B}R avait pour origine les cellules CD11b+, probablement les microglies.

Ensuite, notre but était de déterminer la conséquence de cette augmentation de l'expression du récepteur spécifique aux cellules CD11b+, qui semble avoir un rôle protecteur dans la maladie étant donné l'aggravation du phénotype SLA suite à l'ablation de ce dernier.

Nous avons mesuré l'expression de différents marqueurs de signature de la microglie, du profil pro-inflammatoire et anti-inflammatoire. L'ablation de 5-HT_{2B} a diminué le niveau d'expression de nombreux marqueurs. Les gènes signature des microglies étaient aussi moins exprimés chez les souris KO du récepteur 5-HT_{2B}. Le profil histologique des microglies de souris SOD1(G86R) sans 5-HT_{2B}R a montré des structures plus fréquemment fragmentées, traduisant une dégénérescence accélérée de ce type cellulaire en absence de 5-HT_{2B}. De fait, la sur-expression du récepteur 5-HT_{2B} module la réponse neuroinflammatoire et semble donc indispensable au maintien des microglies dans le cas de SLA.

Nous avons ensuite étudié les polymorphismes génétiques du gène codant pour 5-HT_{2B}R (*HTR2B*) chez les patients SLA. Dans une cohorte de patients néerlandais, nous avons observé que l'allèle C du SNP rs10199752 présent dans le gène *HTR2B* était associé à une survie plus longue des patients. De plus, comparés aux patients présentant deux copies de l'allèle A, les patients porteurs d'une copie de cet allèle C du SNP rs10199752 présentent des niveaux augmentés de l'ARNm de 5-HT_{2B}R dans la moelle épinière et une diminution de la fréquence de la dégénérescence des microglies.

Ces résultats démontrent que le récepteur à la sérotonine 2B tarde la progression de la maladie et empêche la dégénérescence des microglies dans le cas d'une SLA.

Abstract graphique:

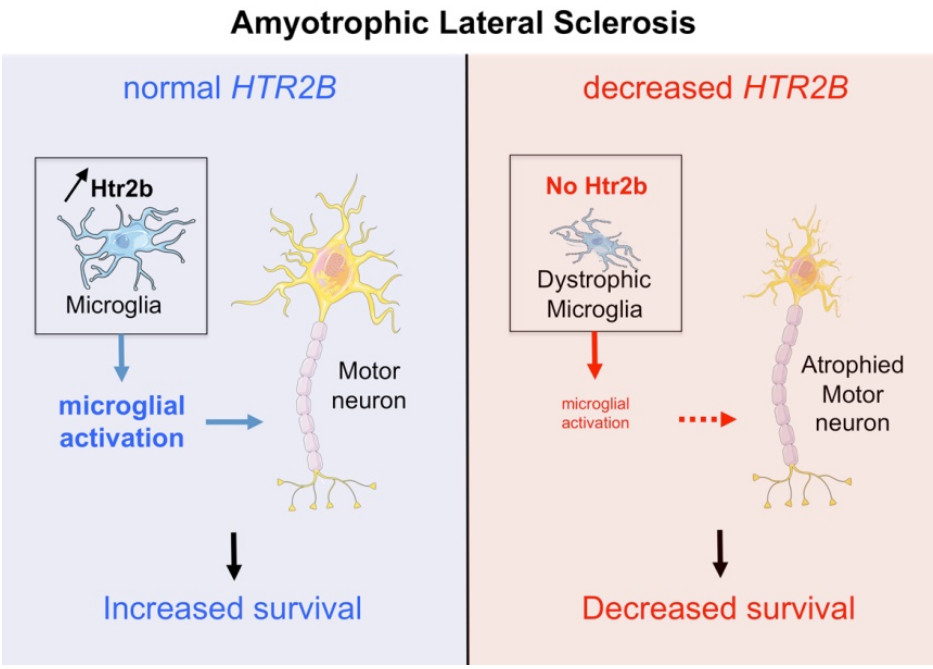

Acta Neuropathol (2016) 131:465–480
DOI 10.1007/s00401-016-1534-4

ORIGINAL PAPER

Serotonin 2B receptor slows disease progression and prevents degeneration of spinal cord mononuclear phagocytes in amyotrophic lateral sclerosis

Hajer El Oussini[1,2] · Hanna Bayer[3] · Jelena Scekic-Zahirovic[1,2] · Pauline Vercruysse[1,2,3] · Jérôme Sinniger[1,2] · Sylvie Dirrig-Grosch[1,2] · Stéphane Dieterlé[1,2] · Andoni Echaniz-Laguna[1,2,4] · Yves Larmet[1,2] · Kathrin Müller[3] · Jochen H. Weishaupt[3] · Dietmar R. Thal[5,6] · Wouter van Rheenen[7] · Kristel van Eijk[7] · Roland Lawson[2,4] · Laurent Monassier[2,4] · Luc Maroteaux[8,9,10] · Anne Roumier[8,9,10] · Philip C. Wong[11] · Leonard H. van den Berg[7] · Albert C. Ludolph[3] · Jan H. Veldink[7] · Anke Witting[3] · Luc Dupuis[1,2]

Received: 20 October 2015 / Revised: 17 December 2015 / Accepted: 1 January 2016 / Published online: 7 January 2016

Abstract Microglia are the resident mononuclear phagocytes of the central nervous system and have been implicated in the pathogenesis of neurodegenerative diseases such as amyotrophic lateral sclerosis (ALS). During neurodegeneration, microglial activation is accompanied by infiltration of circulating monocytes, leading to production of multiple inflammatory mediators in the spinal cord. Degenerative alterations in mononuclear phagocytes are commonly observed during neurodegenerative diseases, yet little is known concerning the mechanisms leading to their degeneration, or the consequences on disease progression. Here we observed that the serotonin 2B receptor (5-HT_{2B}), a serotonin receptor expressed in microglia, is upregulated in the spinal cord of three different transgenic mouse models of ALS. In mutant SOD1 mice, this upregulation was restricted to cells positive for CD11b, a marker of mononuclear phagocytes. Ablation of 5-HT_{2B} receptor in transgenic ALS mice expressing mutant SOD1 resulted in increased degeneration of mononuclear phagocytes, as evidenced by fragmentation of Iba1-positive cellular processes. This was accompanied by decreased expression of key neuroinflammatory genes but also loss of expression of homeostatic microglial genes. Importantly, the dramatic effect of 5-HT_{2B} receptor ablation on mononuclear phagocytes was associated with acceleration of disease progression. To determine the translational relevance of these results, we studied polymorphisms in the human *HTR2B* gene, which encodes the 5-HT_{2B} receptor, in a large cohort of ALS patients. In this cohort, the C allele of SNP rs10199752 in *HTR2B* was associated with longer survival. Moreover, patients carrying one copy of the C allele of SNP rs10199752 showed increased 5-HT_{2B} mRNA in spinal cord and displayed less pronounced degeneration of Iba1

Electronic supplementary material The online version of this article (doi:10.1007/s00401-016-1534-4) contains supplementary material, which is available to authorized users.

✉ Luc Dupuis
ldupuis@unistra.fr

1 INSERM UMR-S1118, Faculté de Médecine, bat 3, 8e etage, 11 rue Humann, 67085 Strasbourg Cedex, France

2 Université de Strasbourg, Fédération de Médecine Translationnelle, Strasbourg, France

3 Department of Neurology, University of Ulm, Ulm, Germany

4 Neurology Department, Hopitaux Universitaires de Strasbourg, Strasbourg, France

5 Laboratory of Neuropathology, Institute of Pathology, University of Ulm, Ulm, Germany

6 Laboratory of Neuropathology, Department of Neuroscience, KU-Leuven, Leuven, Belgium

7 Department of Neurology, Brain Center Rudolf Magnus, University Medical Center Utrecht, Utrecht, The Netherlands

8 Inserm, UMR-S839, Paris 75005, France

9 Sorbonne Universités, UPMC University Paris 06, UMR-S839, Paris 75005, France

10 Institut du Fer à Moulin, Paris 75005, France

11 Division of Neuropathology, Department of Pathology and Neuroscience, The Johns Hopkins University School of Medicine, Baltimore, USA

positive cells than patients carrying two copies of the more common A allele. Thus, the 5-HT_{2B} receptor limits degeneration of spinal cord mononuclear phagocytes, most likely microglia, and slows disease progression in ALS. Targeting this receptor might be therapeutically useful.

Keywords Amyotrophic lateral sclerosis · Motor neuron · Serotonin · Microglia · SOD1

Introduction

Amyotrophic lateral sclerosis (ALS) is the major adult onset motor neuron disease with a lifetime risk of 1/400, and represents the third most frequent neurodegenerative disease after Alzheimer's and Parkinson's diseases. ALS is characterized by the selective degeneration of upper motor neurons in the cerebral cortex and lower motor neurons in spinal cord and brainstem, and leads to progressive paralysis and death within 3–5 years after onset [41]. A number of ALS cases are dominantly inherited and more than 20 genes have been associated with ALS, in particular *C9ORF72*, *TARDBP*, *FUS* and *SOD1* [48]. Most experimental research has involved expression of mutant SOD1 in transgenic mice, leading to development of typical ALS symptoms.

In recent years it has become increasingly clear that progression of ALS symptoms is not caused exclusively by intrinsic events within motoneurons, but rather involves many other cell types [4, 57]. In particular, mononuclear phagocytes, that collectively refers to both microglia and infiltrating monocytes [23, 28, 34, 40], are activated during ALS [57, 58, 75]. This activation is characterized by appearance of an amoeboid morphology, increased phagocytic activity and production of a number of cytokines and chemokines [52, 75]. Activation of mononuclear phagocytes could either be protective by providing support to neurons and astrocytes in response to injury and by cleaning debris through phagocytosis or deleterious by creating an inflammatory environment contributing to neuronal degeneration [51, 57]. Importantly, decreased expression of mutant SOD1 in CD11b-positive cells, i.e. in all mononuclear phagocytes, prolongs disease progression suggesting that mutant SOD1 exerts toxic action in these cells thereby accelerating disease [5]. Furthermore, decreased activation of the pro-inflammatory transcription factor NF-kappaB in microglial cells potently slowed down disease progression [26]. Mononuclear phagocytes appear themselves affected during disease progression. Indeed, the recently identified molecular signature of homeostatic microglia [7–9, 12] is heavily altered during disease progression in ALS [7, 12]. This loss of typical microglial expression patterns could be directly correlated with degeneration of mononuclear phagocytes, documented in different neurodegenerative diseases [62, 63, 74] including a transgenic model of ALS [25, 63]. Whether mononuclear phagocytes degeneration is microglia specific or also occurs in infiltrating monocytes, and whether this degeneration might be involved in neurodegeneration is not known.

Recently, we observed that serotonin 2B receptor (5-HT_{2B}R) mRNA levels were strongly upregulated in the spinal cord of a mouse model of ALS–SOD1(G86R) mice, notably at later stages and coincident with development of spasticity [15]. 5-HT_{2B}R is expressed in microglia in the CNS, with expression in a few other cell types such as brain serotonin neurons [16]. In human peripheral macrophages, 5-HT_{2B}R mediates the response to serotonin by skewing macrophages to a M2, anti-inflammatory, phenotype [14]. More relevant to ALS, we showed that 5-HT_{2B}R is the major serotonin receptor expressed on perinatal microglia and regulates chemotaxis of microglial processes in response to serotonin [44]. These findings raise the possibility that the observed 5-HT_{2B}R upregulation could be linked to microglial activation and function in the pathogenesis of ALS.

Here, we show that the lack of 5-HT_{2B}R is associated with degeneration of spinal cord mononuclear phagocytes in ALS mouse models and human patients, and slows down disease progression of ALS. This has broad consequences for our understanding of serotonin function during disease, and provides a plausible pharmacological target to modulate neuroinflammation in ALS and other neurodegenerative diseases.

Materials and methods

Patients

Two independent populations of patients were studied here. In the human genetic study, cases from the Netherlands were diagnosed with probable or definite ALS according to the revised El-Escorial Criteria by neurologists specialized in motor neuron diseases [6]. Tertiary referral centers for ALS were University Medical Center Utrecht, Academic Medical Centre Amsterdam and Radboud University Medical Center Nijmegen. All participants gave written informed consent, and approval was obtained from the relevant local ethical committees for medical research. Characteristics of ALS patients included in this genetic study are presented in Table S1. Control individuals were free of any neuromuscular disease and matched for age, gender and ethnicity ascertained through a population based study on ALS in the Netherlands [35]. Patients included in the neuropathology study were from Ulm University. All autopsy brains were collected in

accordance with local ethical committee guidelines and the federal law governing the use of human tissue for research in Germany. The characteristics of these patients are described in Table S2.

Animals

Transgenic mice were housed in the animal facility of the medicine faculty of Strasbourg University, with 12 h/12 h of light/dark and unrestricted access to food and water. In all experiments, littermates were used for comparison, and mice compared are thus in the same genetic background. Transgenic mice carrying SOD1 G86R mutation [18] and their non-transgenic littermates on a FVB/N background were genotyped and onset of symptoms was defined according to previous studies [15]. Dynactin mice expressing G59S mutation of $P150^{Glued}$ have been previously described [47], and were used according to previous studies [72]. SOD1(G37R) mice were kindly provided by Dr Don W. Cleveland and have been described previously [5]. *Htr2b*$^{-/-}$ mice in a 129S2/Sv PAS background have been described previously [49, 53]. All animal experimentation was performed in accordance with institutional guidelines, and protocols were approved by the local ethical committee from Strasbourg University (CREMEAS) under number AL/30/37/02/13 and AL/29/36/02/13 in accordance with European regulations.

Mouse breeding, survival and motor phenotyping

SOD1 (G86R) mice were crossed with *Htr2b*$^{-/-}$ mice to obtain the F1 generation. Male *Htr2b*$^{+/-}$ carrying SOD1 (G86R) transgene were then crossed with female *Htr2b*$^{+/-}$ from the F1 generation to obtain the F2 generation with the genotypes of interest. *Htr2b*$^{-/-}$ mice carrying SOD1 (G86R) transgene ($n = 16$) were compared with littermate *Htr2b*$^{+/+}$ mice carrying SOD1 (G86R) transgene ($n = 12$), *Htr2b*$^{+/-}$ mice carrying SOD1 (G86R) transgene ($n = 19$), and *Htr2b*$^{-/-}$ or *Htr2b*$^{+/+}$ littermate mice negative for SOD1 (G86R) transgene were used as control.

Mice were visually inspected daily and weekly monitored for body weight and motor symptoms from 4 weeks of age until end stage of the disease. To evaluate muscle strength, we used a gripmeter test (Bioseb, ALG01; France). Disease course and survival were assessed daily by visual inspection. The muscle force was averaged as the mean of three consecutive trials per session. Disease onset was calculated as time of peak of body weight. Disease duration was the time between the peak of body weight and death. After disease onset mice were followed daily and end stage was defined by full paralysis and when mice were unable to return after 10 s placed on the back. End stage mice were immediately euthanized.

Histological techniques

Muscle tissues and spinal cords were dissected and fixed by immersion in 4 % paraformaldehyde in 0.1 M phosphate buffer pH 7.4 overnight. The whole muscles were dissected into fibre bundles, stained using α-Bungarotoxin labeled with tetramethylrhodamine(Sigma, T195; 1:500) for nicotinic acetylcholine receptors (AchRs), anti-synaptophysin (Millipore, 5258; 1:250) and anti-neurofilament (Abcam, Ab24574, 1/100) for pre-synaptic elements, followed by fluorescent secondary antibodies anti-mouse Alexa 488 (Life Technologies, A11001), and Draq 5 for nuclei (Cell Signaling, 4084; 1:1000). Single-layer images or merged Z-Stack images (1 µm optical section, for 10 µm thickness of merged z-stacks) were acquired using a laser-scanning microscope (confocal Leica SP5 Leica Microsystems CMS GmbH) equipped with 63× oil objective (NA1.4). Excitation wavelengths were sequentially argon laser 488 nm, diode 561 nm, and helium neon laser 633 nm. Emission bandwidths are 500–550 nm for Alexa488, 570–620 nm for Alexa594, and 650–750 nm for draq5.

The lumbar parts of spinal cords were dissected and the L3–L5 region was identified according to previous studies [29]. Tissue was cryoprotected in 30 % sucrose and snap frozen in melting isopropanol in TissueTek (O.C.T.Compound, SAKURA#4583). Cryosections (Leica CM 3050S) of 16 µm were obtained for histological analysis of end stage mice (10 sections per animal). Spinal cord sections were incubated in phosphate buffered saline (PBS) 0.1 % Triton with anti-choline acetyl transferase (ChAT) (Millipore, AB144-P; diluted 1:50) for motor neuron quantification and anti-Iba1 (Abcam ab5076, 1/100) antibody followed by biotinylated species-specific secondary antibody. The staining was revealed using the ABC kit (Vectastain), by the avidin–biotin complex immunoperoxidase technique or immunofluorescence. Identical techniques and antibodies were used to stain paraffin sections of ALS patients for Iba1 immunostaining.

Quantification of histological results

Motoneuron counting was performed in L3–L5 ventral horn in every tenth section for ten sections in total per animal (160 µm thick in total, spread over 1.6 mm). Only $ChAT^+$ neurons located in a position congruent with that of motoneuron groups were counted [13]. All $ChAT^+$ profiles located in the ventral horns of immunostained sections and clearly displayed in the plane of section were counted. Total estimated motoneuron numbers were obtained using a computer-assisted microscope (Nikon Eclipse E800) and associated software (Nis Elements version 4.0). Total numbers of motoneurons and the mean area of individual cells were obtained using ImageJ freeware (http://rsbweb.nih.gov/ij/) after image acquisition at 20X under the same

exposition parameters with a digital camera (Nikon Digital Sight DS-U3) [61]. The observer was blinded to the genotype of studied mice.

To quantify ventral horn atrophy, the total surface of the ventral horn was measured using Nis Elements version 4.0.

For staining of mononuclear phagocytes, measurement of Iba1 immunoreactivity was performed on images acquired from Iba1 immunostaining at 10× magnification. A standardized rectangle was drawn in the ventral horn and the surface of Iba1 staining relative to background was calculated using the Pixel classifier algorithm of Nikon Nis-element 3.10 SP3 software, using the intensity profile measurement function. The observer was blinded to the genotype of studied mice. >10 images per animal were quantified, with $n = 5$ animals per genotype.

Iba1 positive cells morphology was defined according to previous work [63]: (i) resting phagocyte with small branched cellular processes and small cell soma, (ii) activated state with greater distal arborization, (iii) phagocytic state with increased cell soma size, and (iv) dystrophic state with fragmented cytoplasm. Iba1-immunopositive cells were categorized according to their state in each ventral horn section of the spinal cord by an observer blinded to the genotype (HEO). Percentage of each state was then calculated for each genotype of interest.

To quantify degeneration of Iba1 positive cells in ALS patients, an observer blinded to the genotype scored from 0 to 4 the occurrence of degeneration in 2–5 sections per patient, with a score of 0 for sections showing non-degenerating phagocytes. Features of microglial degeneration were according to Streit and collaborators [63]. Similar results were obtained by two independent blinded observers (HEO and LD).

Isolation of CD11b positive cells

Isolated spinal cords and brain stems from end stage SOD1 (G86R) mice were transferred into a 2 ml sterile tube with 1 ml of Hank's balanced salt solution (HBSS) (Invitrogen), then triturated to single-cell suspension using Miltenyi's Neural Tissue Dissociation Kit (P) (Miltenyi Biotec). After a final wash in HBSS containing $CaCl_2$ and $MgCl_2$, the cell suspension was incubated with anti-myelin magnetic microbeads using Myelin removal kit (Miltenyi Biotec). The cell suspension was passed onto LS columns (Miltenyi Biotec) exposed to a strong magnetic field. The flow through (demyelinated cells) was incubated with anti-CD11b magnetic microbeads using CD11b kit (Miltenyi Biotec). The cell suspension was passed onto LS columns (Miltenyi Biotec) exposed to a strong magnetic field. The flow through (non-CD11b cells) was subsequently used as a negative control and the suspension obtained once the magnetic field was switched off (CD11b cells) used as a positive fraction. Both fractions were used for gene expression analysis.

Real–time quantitative polymerase chain reaction

Total RNA was extracted from the spinal cord and the brain stem of end stage mice using TRIzol (Invitrogen). RNA was reverse transcribed using 1 µg of RNA and the iScript cDNA synthesis kit (BioRad). We performed real-time PCR using IQ SYBR green Supermix (BioRad) and data were normalized with GeNorm software [69] using two standard genes (Tata-box binding protein, and RNA polymerase 2 subunit). For microglia experiments total RNA was extracted by using RNeasy Micro Kit (Qiagen), RNA was reverse transcribed using 1 µg of RNA and the iScript cDNA synthesis kit. Quantitative PCR was performed on a CFX96 Real-time System (BioRad) using iQ SYBR Green supermix (BioRad). Relative mRNA levels were calculated with BioRad CFX Manager 3.1 using $\Delta\Delta C_t$ method.

Primer sequences are provided in Table S3.

Echocardiography

Animals were analyzed for cardiac anatomy and function on a Sonos 5500 (Hewlett Packard, USA) with a 15 MHz linear transducer (15L6). All the examinations were performed in mice anesthetized with 1–1.5 % isoflurane. The heart was first imaged in the two-dimensional (2D) mode in the parasternal long-axis view to obtain the aortic root dimensions. The aortic flow velocity and the heart rate (HR) were measured with pulsed-wave Doppler on the same section. The cardiac output (CO) was calculated from the following equation: $CO = 0.785 \times D2 \times VTI \times HR$ where D is the diameter of the aortic root and VTI is the velocity–time integral of the Doppler aortic spectrum. Left ventricular cross sectional internal diameters in end-diastole (EDLVD) and end-systole (ESLVD) were obtained by an M-mode analysis of a 2D-short axis view at the papillary muscle level. The shortening fraction was calculated as $SF = (EDLVD\text{-}ESLVD/EDLVD) \times 100$. From this view, the diastolic septum (SW) and posterior wall (PW) thicknesses were measured. The left ventricular mass (LVM) was calculated with the following formula: $LVM = 1.055 \times [(SW + PW + EDLVD)^3 - (EDLVD)^3]$. All the measurements were performed on at least three beats, according to the guidelines of the American Society of Echocardiography.

Microglial culture

Mouse microglial cells in primary culture were prepared as described previously [73]. Briefly, 1–5 day old C57Bl/6

mice were decapitated according to the guidelines of the animal research center of Ulm University, Ulm, Germany. Meninges were removed from the brains. Neopallia were dissected and dissociated by enzyme treatment (1 % trypsin, Invitrogen, 0.05 % DNAse, Worthington, 2 min) and then mechanically dissociated. The cells were centrifuged (200×*g*, 10 min), suspended in Dulbecco's modified Eagle's medium (DMEM, Invitrogen) supplemented with penicillin (100 U/ml), streptomycin (100 µg/ml) (Invitrogen) and 10 % heat-inactivated fetal bovine serum (FBS, PAA), and plated into 75-cm^2 flasks (BD Falcon) pre-coated with 1µg/ml poly-L-ornithine (Sigma). Cells from the neopallia of two brains were plated at 10 ml per flask. After 3 days, adherent cells were washed three times with Dulbecco's phosphate buffered saline (DPBS) (Invitrogen) and incubated with serum-supplemented culture media. After 7–14 days in culture, floating and loosely attached microglial cells were manually shaken off, centrifuged (200×*g*, 10 min) and seeded into 96-well plates or 6-well plates (PRIMARIA, BD Falkon) at a density of 4 × 10^4 or 6 × 10^5 cells/well, respectively, in DMEM without serum (Invitrogen) supplemented with penicillin (100 U/ml), streptomycin (100 µg/ml) (Invitrogen) and Glutamax (Invitrogen). Cells in the flasks were reincubated with serum-supplemented media after shaking. Repopulating microglial cells were removed every 3–4 days for a total of 3 weeks until fewer microglial cells were observed.

LDH and WST-1 assays

The lactate dehydrogenase (LDH) assay and water soluble tetrazolium salt (WST-1) assay were performed as described in the manual for the LDH-Cytotoxicity Assay Kit (Bio Vision) and the WST-1 Assay Kit (Quick Cell Proliferation Assay Kit; BioVision). For a positive cell death control, microglia were treated with 1 % Triton-X100 (Sigma) for 30 min. Results were expressed as a percentage of Triton treatment, with 0 % being untreated control.

HTR2B Polymorphisms in human ALS

In total 1923 cases and 2881 controls were genotyped on two different platforms; IlluminaOmniExpress (n = 3488) and Illumina2.5 M (n = 1316). Extensive quality control using standard procedures was performed as described [68]. Following this, 612,666 SNPs and 3344 individuals (1207 cases and 2137 controls) were retained on the IlluminaOmniExpress chip, and the Illumina 2.5 M chip yielded 1,481,461 single nucleotide polymorphisms (SNPs) and 1294 individuals (679 cases and 615 controls). After this extensive quality control, seven *HTR2B* SNPs were extracted and used for analyses.

Statistical analysis

All data are presented as mean ± standard error of the mean.

When the measured values were not detectable in some of the experimental points (Fig. 1), these values were considered to be null. Comparison of discrete values for two groups (Figs. 1, 2d, e, 8b, c) was performed using Student's *t* test. Comparison of discrete values for more than two groups (Figs. 3d, e, 4a, c, d, 5c, 6a, 7) was performed using One Way ANOVA followed by Tukey's post hoc test. Differences in survival or disease onset of animals (Fig. 2a–c) was evaluated using log rank (Mantel Cox) test. To test for the effect of dose of *Htr2b* ablation, a log rank test for trend was performed (Figure S2). For repeated measures (Figure S1), a repeated measures two way ANOVA was performed to test for the effect of age and the effect of genotype.

These statistical analyses were performed using Prism 6 (GraphPad software).

All differences were considered significant at $p < 0.05$.

To investigate the association of these seven SNPs with ALS, a logistic regression was performed in PLINK, corrected for dataset and 2 principle components. These seven SNPs are strongly correlated ($D' = 1$, and five out of seven SNPs have an R^2 between 0.7 and 1, with a minor allele frequency >0.4). Therefore the strongest correlated SNP was tested for association with survival (rs10199752). A Cox proportional hazards

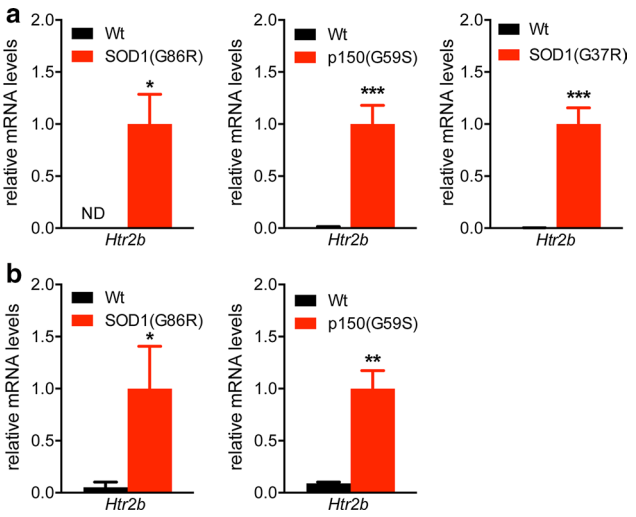

Fig. 1 Increased relative mRNA levels of 5-HT$_{2B}$ receptor in ALS mice. mRNA levels of 5-HT$_{2B}$R (Htr2b) in the spinal cord (**a**) and brainstem (**b**) of end stage SOD1 (G86R) mice (Wt N = 7, SOD11(G86R) N = 7), p150(G59S) mice (Wt N = 7, p150(G59S) N = 7), SOD1 (G37R) (Wt N = 8, SOD1(G37R) N = 7) relative to their respective wildtype (Wt) littermates. ND: not detected. *$p < 0.05$, **$p < 0.01$, ***$p < 0.001$ versus corresponding wild type, by Student's *t* test

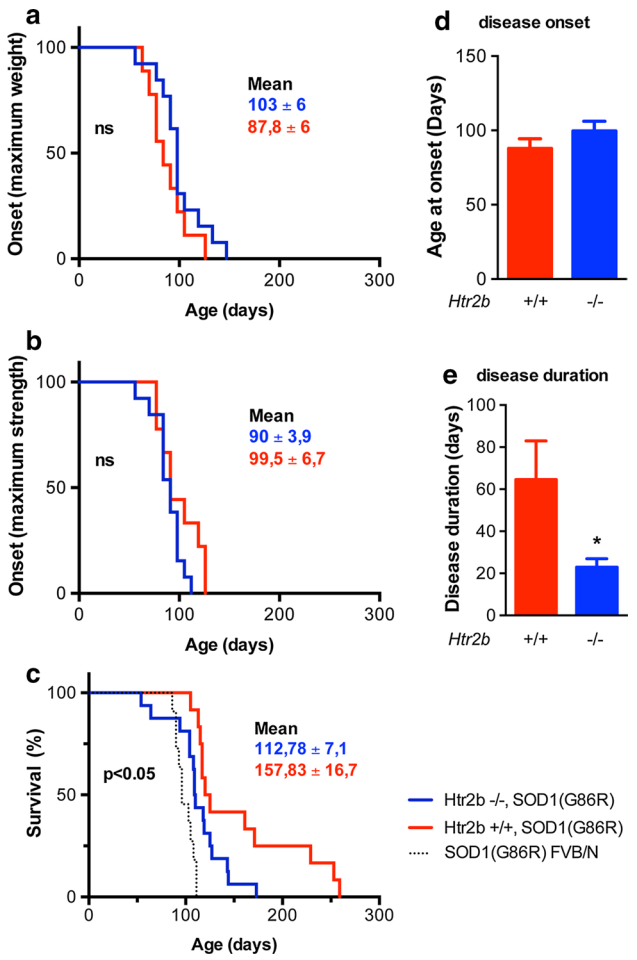

Fig. 2 The ablation of *Htr2b* in SOD1 (G86R) mice decreases life span and accelerates disease progression. Kaplan–Meier plot of disease onset, as determined by the peak weight (**a**) or the peak of grip strength (**b**), and of survival (**c**) for SOD1(G86R) mice wild type for *Htr2b* (*red*, $n = 12$) or knock-out for *Htr2b* (*blue*, $n = 16$). The mean of each group ± SEM is indicated on *each panel*. $p < 0.05$, log rank (Mantel–Cox) between *Htr2b* +/+ SOD1(G86R) mice and *Htr2b*−/−SOD1(G86R) mice in *panel* **c**. There were no significant difference (ns) in survival curves for *panels* **a** and **b.** The survival curve of SOD1 (G86R) mice in the original FVB/N background is indicated in *dashed line*. Duration of early disease (**d**, from birth to peak weight) and late disease (**e**, from peak weight to death) for SOD1(G86R) mice wild type for *Htr2b* (+/+, *red*) or knock-out for *Htr2b* (−/−, *blue*). $p < 0.05$, unpaired Student's *t* test

(coxph) regression model in R was performed with survival and death as time and event, respectively, genotype as predictor, and sex, age at onset, and site at onset as covariates. Patients with a maximum survival of 15 years were included in this analysis ($n = 1677$). This coxph regression was conducted using a dominant model, comparing a wildtype homozygous reference group versus a variant group (combined homozygous variant and heterozygous).

Results

5-HT_{2B} receptor upregulation during murine ALS

We first asked whether 5-HT_{2B}R upregulation is a general feature of ALS mouse models. For this, we measured mRNA levels of the gene encoding 5-HT_{2B}R (*Htr2b*), in spinal cord and brainstem of three different mouse models of ALS at a late stage of disease progression, i.e. when both hindlimbs were paralyzed. We used mice expressing the G86R SOD1 mutation in the murine gene (SOD1(G86R) mice), or the G37R mutation in the human gene [5]. Consistent with previous results [15], levels of *Htr2b* mRNA were strongly upregulated in spinal cord of SOD1(G86R) mice (Fig. 1a) but also of SOD1(G37R) mice (Fig. 1a). Importantly, *Htr2b* mRNA upregulation was also observed in non-SOD1 ALS mouse models, in particular in the spinal cord of mice expressing the G59S mutation in the p150 subunit of dynactin [47] (Fig. 1a). Last, *Htr2b* mRNA upregulation was also observed in the brainstem of SOD1(G86R) mice and p150(G59S) mice (Fig. 1b). Thus, 5-HT_{2B}R mRNA is upregulated in various ALS mouse models.

The lack of 5-HT_{2B} receptor accelerates disease progression in mice

To determine the effect of 5-HT_{2B}R on motoneuron disease progression, we ablated the *Htr2b* gene in SOD1(G86R) mice. We crossed SOD1(G86R) mice with $Htr2b^{-/-}$ mice generated previously [53]. After two breeding steps, we obtained SOD1(G86R); $Htr2b^{+/+}$mice, SOD1(G86R) $Htr2b^{+/-}$ mice and SOD1(G86R); $Htr2b^{-/-}$ mice, that were followed longitudinally until death. These mice were in a mixed FVB/N x 129S2/Sv PAS background. Ablation of *Htr2b* led to reduction in body weight in SOD1(G86R) mice as compared to SOD1(G86R) mice expressing *Htr2b* (Fig. S1). Complete ablation of *Htr2b* shortened survival of SOD1(G86R) mice by 30 % (Fig. 2a–c), while ablation of only one allele of *Htr2b* yielded an intermediate effect ($p < 0.05$, log rank test for trend, Fig. S2). Disease onset, as assessed either by peak of body weight [5] or by peak of grip strength, was not changed (Fig. 2a, b). Indeed, ablation of *Htr2b* did not modify the age of peak weight as a measure of disease onset (Fig. 2d), while drastically shortening disease duration after peak weight (Fig. 2e).

Since 5-HT_{2B}R has been implicated in cardiac development and function [53, 55, 56], we hypothesized that *Htr2b* ablation could affect cardiac function in SOD1(G86R) mice, leading to accelerated death. However, echocardiographic examinations did not show major reduction of cardiac contractility or output in SOD1(G86R); $Htr2b^{-/-}$ mice. In

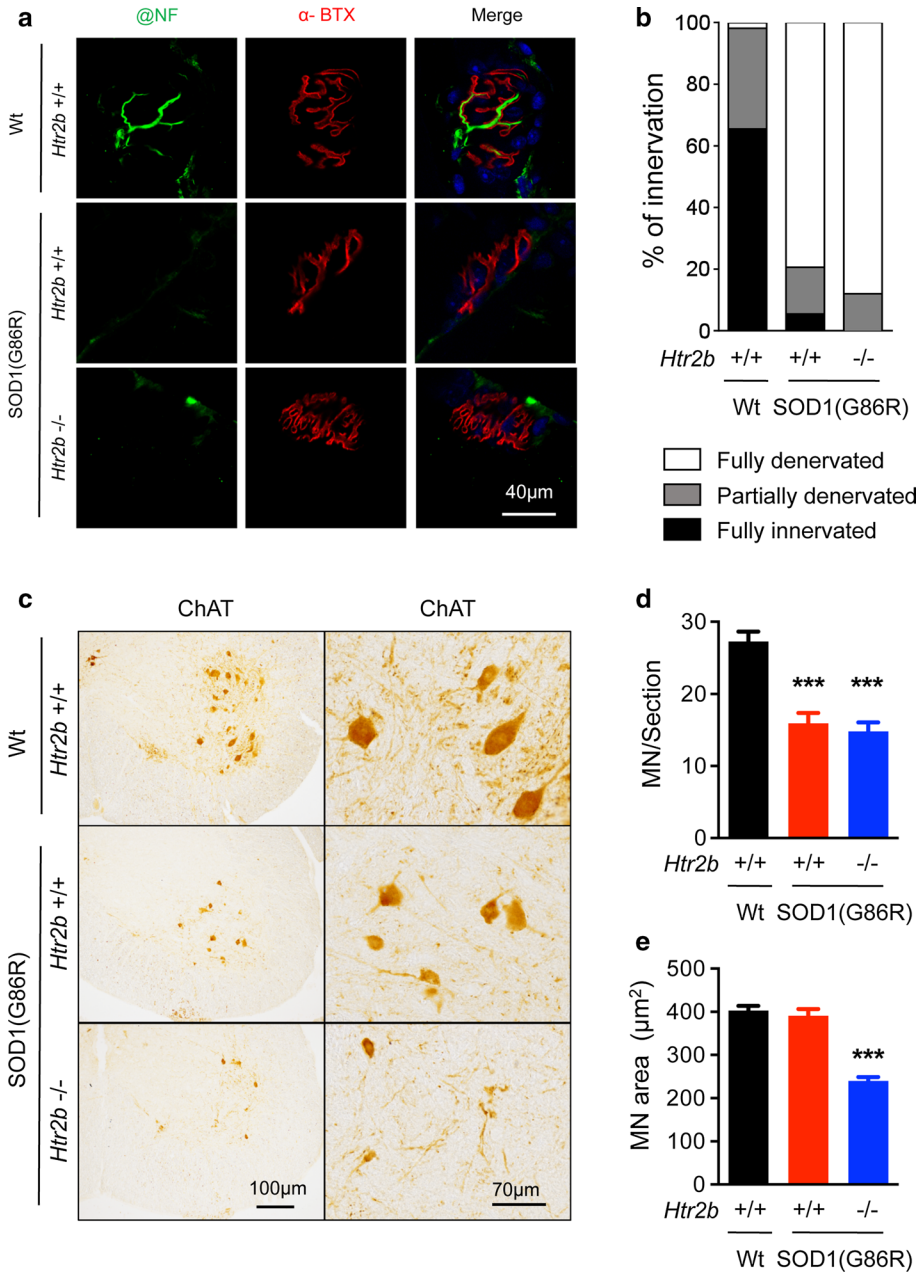

Fig. 3 The ablation of *Htr2b* in SOD1 (G86R) mice exacerbates neurodegeneration. **a** Representative confocal images of post and pre-synaptic apparatus of the neuromuscular junction in Tibialis muscle of end stage mice. Axons were labeled with anti-neurofilament (@NF, *green*), acetylcholine receptors with fluorescently labeled bungarotoxin (α-BTX, *red*) and nuclear with Draq 5 (*blue*) in wild type mice (+/+), and SOD1(G86R) mice wild type for *Htr2b* (+/+) or knock-out for *Htr2b* (−/−) at end stage. $N = 5$ for all genotypes. **b** Distribution of innervation profiles in the tibialis anterior of wild type mice (Wt), and SOD1(G86R) mice wild type for *Htr2b* (+/+) or knock-out for *Htr2b* (−/−) at end stage ($n = 5$ independent animals per genotype). **c** Representative ChAT immunohistochemistry images in wild type mice (Wt), and SOD1(G86R) mice wild type for *Htr2b* (+/+) or knock-out for *Htr2b* (−/−). Two magnifications are shown. $N = 5$ for all genotypes. Motor neuron numbers (**d**) and area (**e**) in wild type mice (Wt, *black columns*), and SOD1(G86R) mice wild type for *Htr2b* (+/+ *red columns*) or knock-out for *Htr2b* (−/− *blue columns*). ***$p < 0.001$ vs wild type, One way ANOVA followed by Tukey post hoc test. $N = 5$ for all genotypes

particular, they did not exhibit echocardiographic signs of heart failure that could explain body weight loss (Fig. S3). To determine whether SOD1(G86R); *Htr2b*$^{-/-}$ mice actually died of motoneuron disease, we examined neuromuscular junction histology in end-stage mice. All SOD1(G86R) mice examined at end-stage, irrespective of their *Htr2b* genotype, displayed heavily denervated neuromuscular junctions (Fig. 3a, b). Consistent with this, SOD1(G86R); *Htr2b*$^{+/+}$ mice displayed motoneuron degeneration similar to SOD1(G86R); *Htr2b*$^{-/-}$ mice (Fig. 3c, d), and ventral horn atrophy was not modified by the *Htr2b* genotype (Fig. S4). Motor neuron loss was similar in this mixed background to previous studies in the original FVB/N background [19, 20]. However, *Htr2b* ablation in SOD1(G86R) mice triggered atrophy of motoneuron cell bodies that was not present in SOD1(G86R); *Htr2b*$^{+/+}$ mice (Fig. 3e). Thus, consistent with its overexpression at symptom onset in SOD1(G86R) spinal cord [15], the lack of 5-HT_{2B}R potently accelerates disease progression of SOD1(G86R) mice after onset.

5-HT2B receptor is upregulated in CD11b-positive cells and is required for activation of mononuclear phagocytes during ALS

Microgliosis occurs at symptom onset in brainstem and spinal cord of transgenic models of ALS [4, 5, 57]. Since

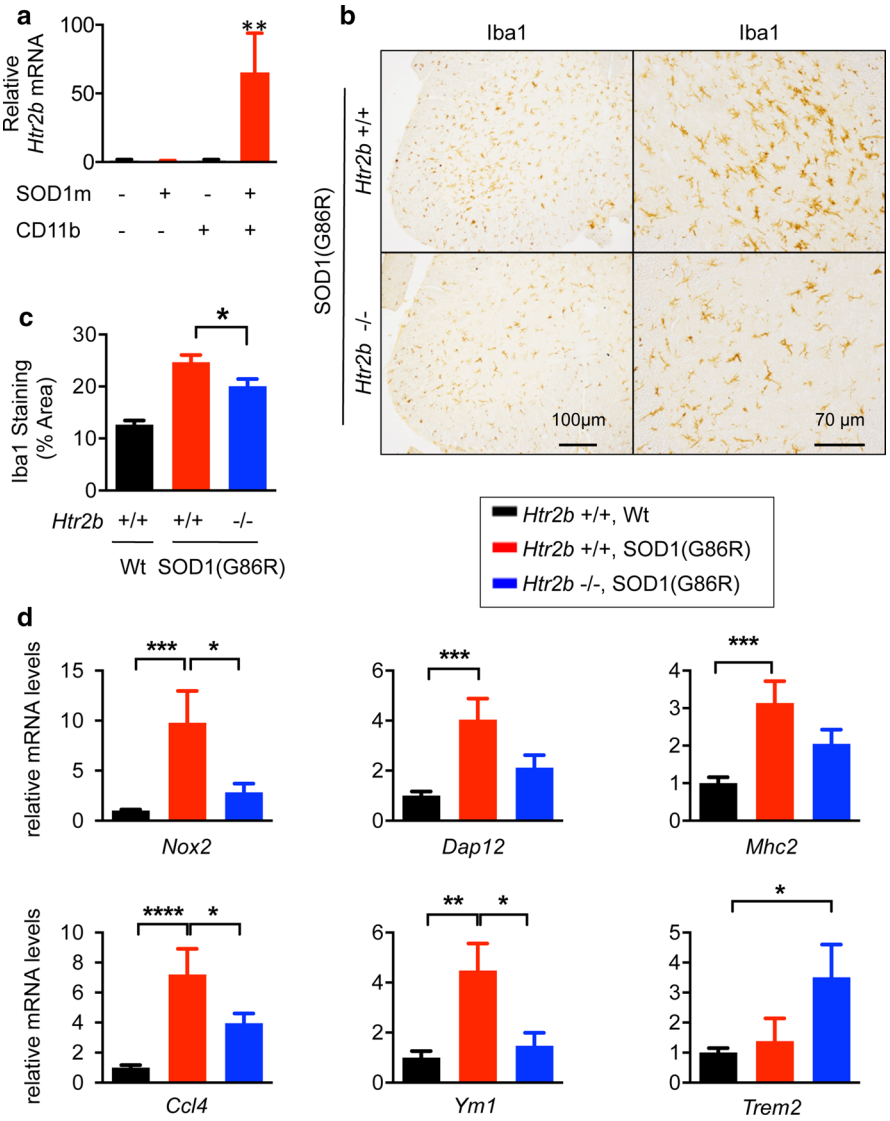

Fig. 4 The ablation of *Htr2b* in SOD1 (G86R) mice compromises activation of mononuclear phagocytes. **a** *Htr2b* mRNA levels in CD11b-positive cells ($CD11^{Pos}$) and CD11b-negative cells ($CD11b^{Neg}$) in brainstem and spinal cord of end stage SOD1(G86R) mice (SOD1) relative to wild-type littermates (Wt). $N = 5$ for all genotypes $^{**}p < 0.01$, Student's *t* test. **b** Representative Iba1 immunohistochemical images in ventral spinal cord of SOD1(G86R) mice wild type for *Htr2b* (+/+) or knock-out for *Htr2b* (−/−). $N = 5$ for all genotypes. **c** Quantification of Iba1 staining coverage in lumbar spinal cord of wild type mice (Wt, *black columns*), and SOD1(G86R) mice wild type for *Htr2b* (+/+ *red columns*) or knock-out for *Htr2b* (−/− blue columns). $^{*}p < 0.05$, One way ANOVA followed by Tukey post hoc test. $N = 5$ for all genotypes. **d** mRNA levels of the indicated genes in brainstem SOD1(G86R) mice wild type for *Htr2b* (+/+ *red columns*) or knock-out for *Htr2b* (−/− *blue columns*) relative to wild type mice (*black columns*). $^{*}p < 0.05$, $^{**}p < 0.01$; $^{***}p < 0.001$ One way ANOVA followed by Tukey post hoc test. $N = 4$–5 per genotype

5-HT_{2B}R is expressed in microglia and peripheral M2 macrophages [14, 44], increased 5-HT_{2B}R expression could reflect activation of microglia and/or of infiltrated monocytes. To address this question, we purified CD11b positive cells from late stage SOD1(G86R) mice using magnetic bead cell sorting, followed by RT-qPCR. To enable purification of CD11b positive cells from single individuals, we chose to pool brainstem and spinal cord from individual mice. Importantly, these areas are associated with strong microgliosis in mutant SOD1 models [25]. Using this procedure, we obtained CD11b positive fractions with a >300 fold enrichment in Iba1 mRNA, and corresponding 5-10 fold decrease in GFAP and ChAT mRNA content (Fig. S5). Importantly, we observed that *Htr2b* upregulation was strictly limited to mRNA enriched from CD11b positive cells (Fig. 4a). Activation of mononuclear phagocytes was reduced by *Htr2b* ablation, with decreased Iba1 staining in the spinal cord (Fig. 4b, c). Consistently, the disease-elicited induction of multiple genes involved in neuroinflammatory responses was decreased in the brainstem of the same animals (Fig. 4d). Interestingly, genes involved in the pro-inflammatory action of microglia (Fig. 4d, *Nox2, Ccl4, Mhc2*), as well as genes involved in anti-inflammatory responses (Fig. 4d, *Ym1, Dap12*) showed similar blunted expression upon *Htr2b* ablation. Notably, *Trem2*- a cell surface receptor associated with neurodegeneration—was especially upregulated in SOD1(G86R); $Htr2b^{-/-}$ brainstem (Fig. 4d). Thus, 5-HT_{2B}R is required for the activation of mononuclear phagocytes during motoneuron disease.

5-HT_{2B} receptor improves microglial survival

Searching for a role for 5-HT_{2B}R in mononuclear phagocytes, we re-examined the phenotype of these cells in SOD1(G86R); $Htr2b^{-/-}$ mice. We observed that spinal cord Iba1-positive cells of SOD1(G86R); $Htr2b^{-/-}$ mice frequently displayed

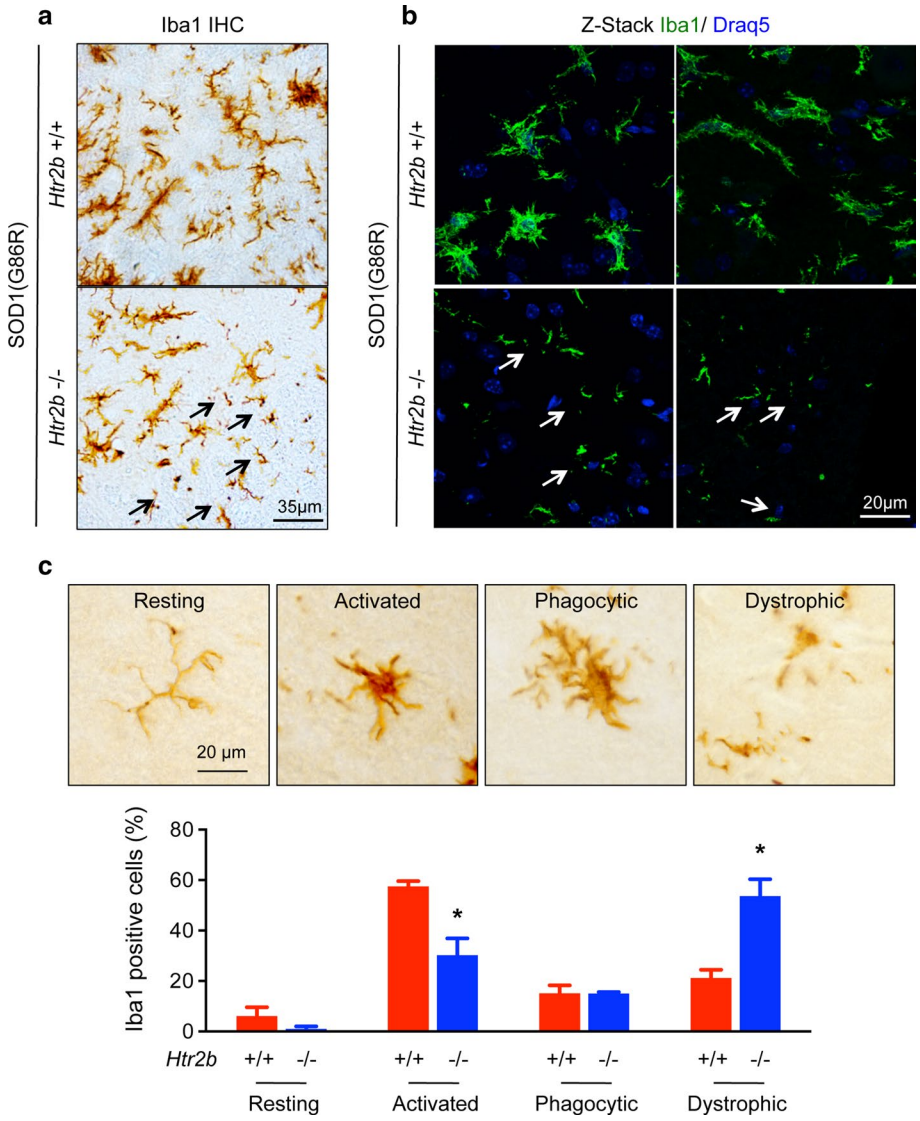

Fig. 5 The ablation of *Htr2b* in SOD1 (G86R) mice leads to degeneration of Iba1 positive cells. **a** Representative Iba 1 immunostaining in spinal cord of SOD1(G86R) mice wild type for *Htr2b* (+/+) or knock-out for *Htr2b* (−/−) showing cytorrhexia of Iba1+ cells (*arrows*). $N = 5$ for all genotypes. **b** Merged Z-stack confocal images of Iba1 immunofluorescence (*green*) counterstained with nuclear DRAQ5 staining in SOD1(G86R) mice wild type for *Htr2b* (+/+) or knock-out for *Htr2b* (−/−). Microglial cytorrhexia is shown with *arrows*. $N = 5$ for all genotypes. **c** Relative proportions of resting, activated, phagocytic and dystrophic (cytorrhexia) Iba1+ cells in SOD1(G86R) mice wild type for *Htr2b* (+/+ *red columns*) or knock-out for *Htr2b* (−/− *blue columns*). Representative examples of the different categories are illustrated. $^*p < 0.05$ vs corresponding *Htr2b* +/+ category, One way ANOVA followed by Tukey post hoc test. 10 sections per animal, with $N = 4$–5 for all genotypes

cytoplasmic fragmentation (also called cytorrhexia, Fig. 5a). This was further confirmed on z-stacks of Iba1immunostained sections obtained using confocal microscopy (Fig. 5b and Fig S6). Quantitative analysis demonstrated that about half of Iba1-positive cells displayed cytorrhexia in SOD1(G86R); *Htr2b*$^{-/-}$ mice (Fig. 5c), suggesting that the loss of *Htr2b* was associated with degeneration of mononuclear phagocytes in end stage SOD1(G86R) mice. To determine whether this degeneration of mononuclear phagocytes affected microglia and/or monocytes, we measured expression levels of genes known to be part of the homeostatic microglial signature [7–9, 12], in particular *Cx3cr1*, *Hexb, Tmem119, P2ry12, Olfml3* and *SiglecH*. All these genes displayed lower expression in SOD1(G86R) mice lacking the *Htr2b* gene than in SOD1(G86R) mice with the *Htr2b* gene (Fig. 6). The establishment of the homeostatic microglial signature is dependent upon TGFß and *Tgfbr1*, the microglial receptor of TGFß [8]. Consistent with previous work, we observed induction of TGFß and its receptor in SOD1(G86R) mice [24], and these two inductions were blunted in SOD1(G86R) mice lacking the *Htr2b* gene (Fig. 6b). Importantly expression levels of *Ly6c1*, a cell surface marker expressed on monocytes, but not microglia [9], were unaltered in SOD1(G86R) mice, irrespective of the *Htr2b genotype* (Fig. 6c). To define the relationships between 5-HT_{2B}R and microglial survival, we stimulated primary microglial cultures with 5-HT_{2B}R-targeted drugs. We selected 5-HT_{2B}R ligands classically used to target the 5-HT_{2B}R, in particular SB204741, a fairly selective antagonist of the 5-HT_{2B}R with 50 fold selectivity for 5-HT_{2B}R over other type 2 serotonin receptors, BW723C86, a preferential 5-HT_{2B}R agonist, with 50 fold selectivity for 5-HT_{2B}R over other type 2 serotonin receptors, and SB206553, an inverse agonist of both 5-HT_{2B}/5-HT_{2C}Rs [2, 43]. Microglial viability was decreased after 48 h in the presence of 1 µM of SB204741 (Fig. 7a), and increased in the presence of 3 µM of BW723C86. There was consistently more LDH

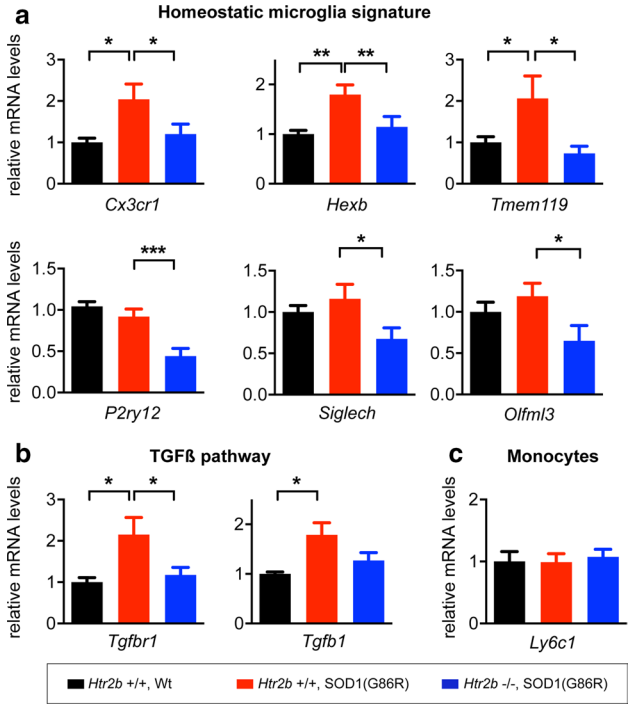

Fig. 6 The ablation of *Htr2b* in SOD1 (G86R) mice decreases expression of homeostatic microglia genes, while not affecting monocyte marker *Ly6c1*. **a–c** mRNA levels of the genes typical of the homeostatic microglia signature (**a**), TGFß pathway (**b**), and of *Ly6c1*, a monocyte marker, in brainstem of SOD1(G86R) mice wild type for *Htr2b* (+/+ *red columns*) or knock-out for *Htr2b* (−/− *blue columns*) relative to wild type mice (Wt, *black columns*). *$p < 0.05$, **$p < 0.01$; ***$p < 0.001$ One way ANOVA followed by Tukey post hoc test. $N = 7$

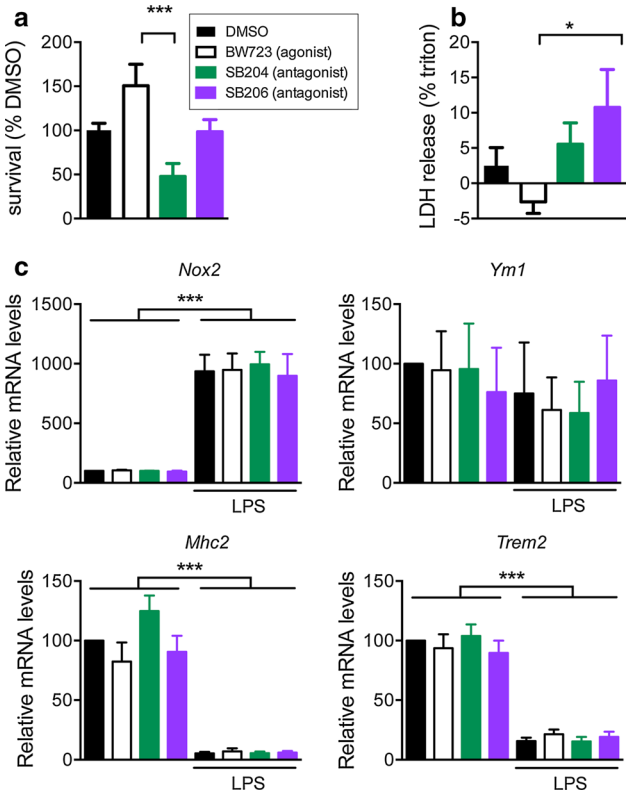

Fig. 7 Pharmacological modulation of the 5-HT_{2B} receptor modulates microglial survival in culture but not gene expression. WST-1 survival (**a**) and LDH release (**b**) assays of primary microglial cells treated with 1 µM SB204741 (5-HT_{2B} antagonist), 1 µM SB206553 (5-HT_{2B} inverse agonist), or 1 µM BW723C86 (5-HT_{2B} agonist). The WST-1 values are relative to vehicle, (DMSO). LDH release is expressed as a percentage of positive control (triton treatment), that releases all LDH contained in cells after subtracting the value of untreated cells. Note that treatment with BW723C86 (5-HT_{2B} agonist) leads to decrease in basal LDH release, leading to negative values. ***$p < 0.001$; *$p < 0.05$ as indicated by *brackets*; One way ANOVA followed by Tukey post hoc test. The experiments were performed in triplicate in three independent experiments. **c** mRNA levels of the indicated genes in primary mouse microglia incubated with 3 µM of BW723C86 (5-HT_{2B} agonist), 1 µM of SB204741 (5-HT_{2B} antagonist), 3 µM of SB206553 (5-HT_{2B} inverse agonist) relative to vehicle (DMSO) with or without 1 µg/ml LPS for 48 h. mRNA levels are given in % of control. Data are presented as mean ± SEM of $n = 3$–5 experiments ***$p < 0.001$ significantly different (One-way ANOVA followed by Tukey post hoc test)

release after 48 h in the presence of SB206553 as compared with 3 µM BW723C86 (Fig. 7b). To determine whether the 5-HT_{2B}R could also modulate microglial gene expression beyond survival, we measured mRNA levels of genes strongly modulated by *Htr2b* genotype in SOD1(G86R) mice (Fig. 4d) in primary microglia treated with 5-HT_{2B}R drugs and/or lipopolysaccharide (LPS) as a neuroinflammatory stimulus. 5-HT_{2B}R pharmacological modulation was not sufficient to alter the expression levels of *Nox2, Ym1, Mhc2* or *Trem2* whether in the absence or presence of LPS for 48 h (Fig. 7c). Thus, acute modulation of 5-HT_{2B}R modifies survival of primary microglia, but does not affect—neuroinflammatory gene expression. Taken together, our results indicate that 5-HT_{2B}R actively promotes microglial survival during neurodegeneration.

HTR2B polymorphisms associated with differential levels of 5-HT_{2B}R mRNA affect morphology of mononuclear phagocytes and survival in ALS

Next, we studied whether the *HTR2B* gene was a modifier of ALS. To this end, we interrogated genome wide association study (GWAS) results of 1886 ALS cases and 2752 controls of Dutch origin. In these samples, we identified seven different intronic SNPs. None of these SNPs showed differential frequencies between cases and controls, showing that at least in this Dutch population *HTR2B* polymorphisms are not a risk factor for ALS. However, a significant association with survival was found for SNP rs10199752 as a prototypical example of these highly correlated SNPs. We isolated patients in whom all phenotype data were available (Table S1), and used a dominant

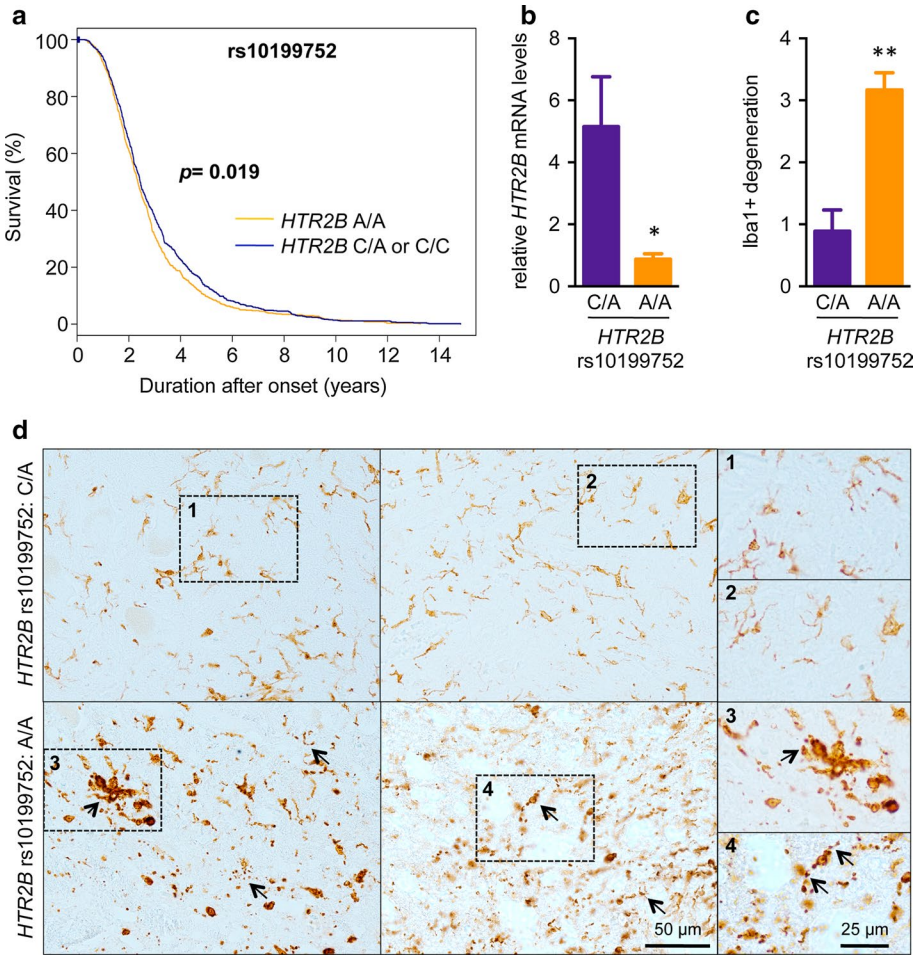

Fig. 8 *HTR2B* polymorphisms in gene expression and degeneration of Iba1 positive cells. **a** Kaplan–Meier plot for a dominant SNP model associated with patient survival. Patients with the variant genotypes (C/A and C/C, $n = 918$) have a longer survival compared to the wildtype homozygous reference group (AA, $n = 759$), hazard ratio = 0.88 (confidence interval 0.79–0.98), p value = 0.019. **b** *HTR2B* mRNA levels in the spinal cord of ALS patients with *HTR2B* C/A relative to patients with *HTR2B* A/A genotype for the rs10199752 SNP. *$p < 0.05$, Student's t test. No patient with the C/C genotype was present in this cohort. **c** quantification of degeneration of Iba1+ cells. Degeneration was semi-quantitatively scored (from 0 to 4) by an observer blinded to the genotype in Iba1-stained spinal cord sections of ALS patients with *HTR2B* A/A relative to C/A genotype for the rs10199752. **$p < 0.01$, Student's t test. **d** Representative Iba1 immunostaining in 4 ALS patients with *HTR2B* C/A (*upper row*) or A/A genotype (*lower row*) for the rs10199752 SNP. Magnifications of *rectangles* 1–4 is shown on the *right*. Note that microglial cells in *HTR2B* C/A carriers show the typical pattern of resident microglial cells with ramified processes (*rectangles* 1–2) whereas the A/A carriers frequently exhibited degenerating microglial cells (*arrows*), with fragmented and beaded processes (*rectangles* 3–4, *arrows*)

model to compare the survival of the variant group (combined genotypes C/A and C/C, $n = 918$) with the wild type homozygous reference group (A/A, $n = 759$). This analysis revealed that patients with the variant genotypes have a longer survival time compared to the homozygous reference group (hazard ratio = 0.88; confidence interval 0.79–0.98; p value = 0.019) (Fig. 8a). To determine whether *HTR2B* polymorphisms were associated with changes in *HTR2B* expression levels, we genotyped a cohort of autopsied ALS patients (Table S2). In this cohort, 6 patients carried an A/A genotype, and 10 patients carried a C/A genotype. There was no patient with the C/C genotype. In patients who carried the C/A genotype of rs10199752, we observed decreased spinal cord *HTR2B* mRNA levels as compared with patients carrying the A/A genotype of rs10199752 (Fig. 8b). We then performed Iba1 immunohistochemistry on lumbar spinal cord sections of these same patients and conducted a semi-quantitative evaluation of the degeneration of Iba1-positive cells (Fig. 8c). Notably, degenerating Iba1-positive cells—as evidenced by the presence of fragmented and/or beaded processes—were frequently observed in patients with the A/A genotype of rs10199752 (Fig. 8d, arrows in lower panels), but much less frequently in patients with the C/A genotype (Fig. 8d, upper panels).

Quantification revealed more frequent and severe degeneration of spinal cord Iba1 positive cells in patients with the A/A genotype than in patients with the C/A genotype (Fig. 8c). As a whole, *HTR2B* polymorphisms associated with higher spinal cord mRNA levels were also associated with increased survival and less pronounced degeneration of mononuclear phagocytes.

Discussion

Our current study provides multiple lines of evidence supporting that the 5-HT_{2B}R is a disease modifier of ALS progression by regulating survival and function of mononuclear phagocytes during neurodegeneration.

Our first important result is that *HTR2B* expression levels affect ALS progression, both in patients and in a transgenic mouse model. *Htr2b* ablation did not modify disease onset, but sharply accelerated disease progression in mutant SOD1 mice. The effect was observed despite compound transgenic mice were generated in the mixed FVB/N × 129 Sv background. The background was identical in all mice, as we used the F1 generation littermates to generate the F2 generation of interest. Interestingly, as illustrated in Fig. 2c, the mixed background increased overall survival of SOD1(G86R) mice and increased heterogeneity in survival. This effect of mixed genetic background has been previously reported, including by us [30, 38]. Accelerated death of mutant SOD1 mice ablated of *Htr2b* was due to accelerated neurodegeneration, and not to potential confounding effects on cardiac patho-physiology. Consistently, ALS patients carrying common haplotypes associated with higher spinal cord *HTR2B* mRNA expression levels survived longer than patients with low expression haplotypes. The relationship between *HTR2B* polymorphisms and survival will have to be investigated in larger cohorts, and different genetic backgrounds, but constitutes an example of a common polymorphism modifying disease progression but not disease risk. An interesting open question is whether *HTR2B* might affect other phenotypes associated with ALS. It is conceivable that *HTR2B* modulates the development of frontal symptoms commonly associated with ALS [64]. Indeed, *Htr2b*$^{-/-}$ mice were recently shown to display deficits in social interactions, as well as in learning and memory processes [59], and these processes require intact frontal lobe function. Along the same lines, the Q20* polymorphism, only found in the Finnish population, is associated with severe impulsivity [3], possibly caused by frontal lobe degeneration. Further work is thus required to elucidate the extent of the contribution of *HTR2B* in ALS-associated phenotypes, in particular in relation with frontal symptoms.

The second major result is that 5-HT_{2B}R could regulate morphology and function of central nervous mononuclear phagocytes, including microglia, in ALS. Here again we provide multiple complementary lines of evidence. Abnormalities of mononuclear phagocytes include (i) decreased overall Iba1 immunostaining, (ii) decreased induction of multiple pro- or anti-inflammatory genes, and (iii) fragmentation of Iba1-positive cells. A reasonable mechanism underlying all these different observations would be that 5-HT_{2B}R function is critical for survival of mononuclear phagocytes during prolonged neuroinflammation such as occurs in ALS. Survival of primary microglia was improved by 5-HT_{2B}R stimulation and decreased by its inhibition, consistent with previous work showing a protective function of 5-HT_{2B}R in newborn cardiomyocytes [54]. These studies will have to be extended to adult spinal cord microglia to determine the effect of aging, as well as the potential role of microglial location in their response to 5-HT_{2B}R stimulation. Our current work does not formally determine whether degenerating Iba1-positive cells are microglia and/or infiltrating monocytes. The extent of monocyte infiltration remains controversial in the field of ALS [1, 9, 12, 46, 50], contrary to Alzheimer's disease in which monocyte infiltration has been repeatedly observed [31, 32]. Our gene expression results demonstrate consistent loss of expression of multiple genes typical of homeostatic microglia while the monocyte marker *Ly6c1* remained unaffected (Fig. 6). Such loss of homeostatic microglial gene expression in whole tissue could be due to cell loss, leading to decreased proportion of microglial mRNAs. Alternatively, disease progression could also affect microglial phenotype, and a recent study performed on isolated microglia of mutant SOD1 mice observed that mutant SOD1 microglia lost their typical expression patterns with disease progression [7]. However, our in vitro experiments provide an initial proof of concept that microglial survival could be influenced by serotonergic stimulation of the 5-HT_{2B}R. Further work is required to determine the relative contributions of microglial cell death and altered microglial phenotypes in the observed degenerative phenotype in vivo as well as the importance of monocyte degeneration. Interestingly, degeneration of mononuclear phagocytes is commonly associated with human neurodegenerative diseases, and commonly referred to as microglial degeneration [63], whereas rodent models appear less affected by this phenotype. However, previous studies observed degeneration of mononuclear phagocytes in a transgenic mutant SOD1 rat [25], similar to our current results in mutant SOD1 mice carrying a wild type *Htr2b* gene. Loss of *Htr2b* almost doubled the proportion of fragmented Iba1-positive cells, showing the importance of this receptor in preventing phagocyte degeneration during disease, although detailed molecular pathways remain to be elucidated.

The processes underlying degeneration of mononuclear phagocytes during ALS remain elusive, and the

relationships between microglial activation, for instance through inflammasomes [70], and microglial survival are not understood. Paradoxically, *Trem2* was found to be upregulated in SOD1(G86R) mice in the absence of *Htr2b*. Trem2 is a scavenger receptor found on the surface of myeloid cells, and *TREM2* mutations leading to impaired phagocytic activity [42] are strong risk factors for multiple neurodegenerative diseases, including ALS [10, 27, 39]. Whether increased expression of *Trem2* in SOD1(G86R); *Htr2b*$^{-/-}$ mice is beneficial or deleterious remains unknown. However, recent work demonstrated that loss of *Trem2* leads either to microglial degeneration in different diseases of the central nervous system [11, 60, 71], or conversely to protection [37]. Thus, the exact mechanisms underlying 5-HT$_{2B}$R-mediated regulation of microglial survival and the role of scavenger receptors in this response will have to be investigated in further studies.

A major question arising from our work is whether the lack of 5-HT$_{2B}$R accelerates ALS progression through its effects on degeneration of mononuclear phagocytes. The hypothesis that degeneration of mononuclear phagocytes is directly linked to the lack of 5-HT$_{2B}$R in this cell type is plausible for several reasons. First, *Htr2b* expression has been detected in newborn brain microglia [44] although it remains low in basal conditions [7, 8, 12, 33]. *Htr2b* is also highly expressed in peripheral macrophages [14]. *Htr2b* expression was restricted to CD11b-positive cells purified from spinal cord and brainstem, thus originating from mononuclear phagocytes, either microglia or infiltrating monocytes. Second, the late occurrence of *Htr2b* upregulation [15] coincides with activation of mononuclear phagocytes in SOD1(G86R) mice. Third, the effects of *Htr2b* ablation on ALS progression are strikingly similar to interventions performed on mononuclear phagocytes. For instance, knocking out mutant SOD1 or NF-kappaB signaling from CD11b-positive cells improved disease progression, but had no effect on disease onset [5, 26]. Despite these parallels, our current results cannot exclude that at least part of the effects of *Htr2b* ablation are caused by its expression in other cell types. Besides mononuclear phagocytes, *Htr2b* is expressed at detectable levels in serotonergic neurons themselves [16], and is known to regulate serotonin release [2, 17]. It is therefore possible that the observed decrease in weight in SOD1(G86R) mice devoid of the *Htr2b* gene was due to serotonergic neurons indirectly affecting hypothalamic circuitry, consistent with our recent results (Vercruysse et al., Brain, in press). To date, no conditional knock-out model of *Htr2b* gene has been characterized. Thus, the current knowledge of the function of *Htr2b* in microglial cells remains limited to in vitro studies (this study (Fig. 7) or previous results [44]). The generation and characterization of knock-out mice in which *Htr2b* deletion is restricted to microglia will yield invaluable insights into this question.

To our knowledge, these results provide the first genetic evidence for an involvement of the serotoninergic system in ALS. We previously showed that platelet serotonin content correlated with survival [22]. Brain-derived serotonin was decreased in ALS patients and mice [15], and imaging studies consistently report dramatic reduction in the binding of 5-HT$_{1A}$ ligand [66, 67]. Pharmacological interventions targeting serotonin provided some evidence for its involvement. For instance, perinatally administered fluoxetine accelerated weight loss and disease onset in ALS rats [45], while 5-hydroxytryptophan, the serotonin precursor, delayed disease in mutant SOD1 mice [65]. Furthermore, spasticity appears linked to serotonergic abnormalities [15]. Here we provide genetic evidence that the serotonin system is involved in disease progression and microglial function. The observation that lack of *Htr2b* accelerated weight loss in ALS mice raises questions on the role of serotonin in weight loss during ALS progression [21], and our most recent results show that loss of serotonin is involved in the development of melanocortin defects (Vercruysse et al., Brain, in press).

Collectively, our results suggest that the 5-HT$_{2B}$R might be an interesting target to prolong survival of ALS patients after onset. However, this should be tempered by the known cardiovascular side effects of 5-HT$_{2B}$R agonists. Chronic use of 5-HT$_{2B}$R agonists has been associated with cardiac valvulopathies and pulmonary hypertension [36], and a therapeutic strategy targeting 5-HT$_{2B}$R should consider the balance between potential benefits and cardiovascular risks in a currently intractable and rapidly progressive disease like ALS, in which patients are most often in good cardiovascular health. Since we identify common *HTR2B* polymorphisms as differentially associated with *HTR2B* expression in the CNS, eventual clinical studies should also take into account *HTR2B* genetic variations.

Acknowledgments We thank Dr David Hicks (INCI, Strasbourg) for careful english editing. We acknowledge the technical help of Marie Jo Ruivo, Annie Picchinenna and Sébastien Freismuth. This work was supported by Fondation "Recherche sur le Cerveau" (call 2015, to LD and LMa), and the Fondation Thierry Latran (SpastALS, to LD). Research leading to these results has received funding from the European Community's Health Seventh Framework Programme (FP7/2007–2013; EuroMOTOR). This study was supported by The Netherlands Organization for Health Research and Development (Vici Scheme (to LvdB), under the frame of E-Rare-2 (to JHV) and JPND (STRENGTH, to LvdB and JHV), the ERA Net for Research on Rare Diseases (PYRAMID). This study was supported by the ALS Foundation Netherlands and the MND association (UK) (Project MinE, http://www.projectmine.com). Work in our laboratories is supported by ALS Association Investigator Initiated Award (Grants 2235, 3209 and 8075; to LD); the Frick Foundation (award 2013 to LD); Association Française contre les Myopathies (Grant #18280; to LD); Virtual Helmholtz Institute "RNA dysmetabolism in ALS and FTD" (WP2, to LD, AW and ACL). This study was supported by the ALS Foundation Netherlands and the MND association (UK) (Project MinE, http://www.projectmine.com). LMa is supported by the *Fondation pour la*

Recherche Médicale "Equipe FRM DEQ 2014039529", the French Ministry of Research (Agence Nationale pour la Recherche) ANR-12-BSV1-0015-01 and the *Investissements d'Avenir* program managed by the ANR under reference ANR-11-IDEX-0004-02.

References

1. Ajami B, Bennett JL, Krieger C, Tetzlaff W, Rossi FM (2007) Local self-renewal can sustain CNS microglia maintenance and function throughout adult life. Nat Neurosci 10:1538–1543. doi:10.1038/nn2014
2. Banas SM, Doly S, Boutourlinsky K, Diaz SL, Belmer A, Callebert J, Collet C, Launay JM, Maroteaux L (2011) Deconstructing antiobesity compound action: requirement of serotonin 5-HT2B receptors for dexfenfluramine anorectic effects. Neuropsychopharmacology 36:423–433. doi:10.1038/npp.2010.173
3. Bevilacqua L, Doly S, Kaprio J, Yuan Q, Tikkanen R, Paunio T, Zhou Z, Wedenoja J, Maroteaux L, Diaz S, Belmer A, Hodgkinson CA, Dell'osso L, Suvisaari J, Coccaro E, Rose RJ, Peltonen L, Virkkunen M, Goldman D (2010) A population-specific HTR2B stop codon predisposes to severe impulsivity. Nature 468:1061–1066. doi:10.1038/nature09629
4. Boillee S, Vande Velde C, Cleveland DW (2006) ALS: a disease of motor neurons and their nonneuronal neighbors. Neuron 52:39–59
5. Boillee S, Yamanaka K, Lobsiger CS, Copeland NG, Jenkins NA, Kassiotis G, Kollias G, Cleveland DW (2006) Onset and progression in inherited ALS determined by motor neurons and microglia. Science 312:1389–1392
6. Brooks BR, Miller RG, Swash M, Munsat TL (2000) El Escorial revisited: revised criteria for the diagnosis of amyotrophic lateral sclerosis. Amyotroph Lateral Scler Other Motor Neuron Disord 1:293–299
7. Butovsky O, Jedrychowski MP, Cialic R, Krasemann S, Murugaiyan G, Fanek Z, Greco DJ, Wu PM, Doykan CE, Kiner O, Lawson RJ, Frosch MP, Pochet N, Fatimy RE, Krichevsky AM, Gygi SP, Lassmann H, Berry J, Cudkowicz ME, Weiner HL (2015) Targeting miR-155 restores abnormal microglia and attenuates disease in SOD1 mice. Ann Neurol 77:75–99. doi:10.1002/ana.24304
8. Butovsky O, Jedrychowski MP, Moore CS, Cialic R, Lanser AJ, Gabriely G, Koeglsperger T, Dake B, Wu PM, Doykan CE, Fanek Z, Liu L, Chen Z, Rothstein JD, Ransohoff RM, Gygi SP, Antel JP, Weiner HL (2014) Identification of a unique TGF-beta-dependent molecular and functional signature in microglia. Nat Neurosci 17:131–143. doi:10.1038/nn.3599
9. Butovsky O, Siddiqui S, Gabriely G, Lanser AJ, Dake B, Murugaiyan G, Doykan CE, Wu PM, Gali RR, Iyer LK, Lawson R, Berry J, Krichevsky AM, Cudkowicz ME, Weiner HL (2012) Modulating inflammatory monocytes with a unique microRNA gene signature ameliorates murine ALS. J Clin Invest 122:3063–3087. doi:10.1172/JCI62636
10. Cady J, Koval ED, Benitez BA, Zaidman C, Jockel-Balsarotti J, Allred P, Baloh RH, Ravits J, Simpson E, Appel SH, Pestronk A, Goate AM, Miller TM, Cruchaga C, Harms MB (2014) TREM2 variant p. R47H as a risk factor for sporadic amyotrophic lateral sclerosis. JAMA Neurol 71:449–453. doi:10.1001/jamaneurol.2013.6237
11. Cantoni C, Bollman B, Licastro D, Xie M, Mikesell R, Schmidt R, Yuede CM, Galimberti D, Olivecrona G, Klein RS, Cross AH, Otero K, Piccio L (2015) TREM2 regulates microglial cell activation in response to demyelination in vivo. Acta Neuropathol 129:429–447. doi:10.1007/s00401-015-1388-1
12. Chiu IM, Morimoto ET, Goodarzi H, Liao JT, O'Keeffe S, Phatnani HP, Muratet M, Carroll MC, Levy S, Tavazoie S, Myers RM, Maniatis T (2013) A neurodegeneration-specific gene-expression signature of acutely isolated microglia from an amyotrophic lateral sclerosis mouse model. Cell Rep 4:385–401. doi:10.1016/j.celrep.2013.06.018
13. d'Errico P, Boido M, Piras A, Valsecchi V, De Amicis E, Locatelli D, Capra S, Vagni F, Vercelli A, Battaglia G (2013) Selective vulnerability of spinal and cortical motor neuron subpopulations in delta7 SMA mice. PLoS One 8:e82654. doi:10.1371/journal.pone.0082654
14. de las Casas-Engel M, Dominguez-Soto A, Sierra-Filardi E, Bragado R, Nieto C, Puig-Kroger A, Samaniego R, Loza M, Corcuera MT, Gomez-Aguado F, Bustos M, Sanchez-Mateos P, Corbi AL (2013) Serotonin skews human macrophage polarization through HTR2B and HTR7. J Immunol 190:2301–2310
15. Dentel C, Palamiuc L, Henriques A, Lannes B, Spreux-Varoquaux O, Gutknecht L, Rene F, Echaniz-Laguna A, Gonzalez de Aguilar JL, Lesch KP, Meininger V, Loeffler JP, Dupuis L (2013) Degeneration of serotonergic neurons in amyotrophic lateral sclerosis: a link to spasticity. Brain 136:483–493. doi:10.1093/brain/aws274
16. Diaz SL, Doly S, Narboux-Neme N, Fernandez S, Mazot P, Banas SM, Boutourlinsky K, Moutkine I, Belmer A, Roumier A, Maroteaux L (2012) 5-HT(2B) receptors are required for serotonin-selective antidepressant actions. Mol Psychiatry 17:154–163. doi:10.1038/mp.2011.159
17. Doly S, Valjent E, Setola V, Callebert J, Herve D, Launay JM, Maroteaux L (2008) Serotonin 5-HT2B receptors are required for 3,4-methylenedioxymethamphetamine-induced hyperlocomotion and 5-HT release in vivo and in vitro. J Neurosci 28:2933–2940. doi:10.1523/JNEUROSCI.5723-07.2008
18. Dupuis L, de Tapia M, Rene F, Lutz-Bucher B, Gordon JW, Mercken L, Pradier L, Loeffler JP (2000) Differential screening of mutated SOD1 transgenic mice reveals early up-regulation of a fast axonal transport component in spinal cord motor neurons. Neurobiol Dis 7:274–285
19. Dupuis L, Fergani A, Braunstein KE, Eschbach J, Holl N, Rene F, Gonzalez De Aguilar JL, Zoerner B, Schwalenstocker B, Ludolph AC, Loeffler JP (2009) Mice with a mutation in the dynein heavy chain 1 gene display sensory neuropathy but lack motor neuron disease. Exp Neurol 215:146–152
20. Dupuis L, Oudart H, Rene F, Gonzalez de Aguilar JL, Loeffler JP (2004) Evidence for defective energy homeostasis in amyotrophic lateral sclerosis: benefit of a high-energy diet in a transgenic mouse model. Proc Natl Acad Sci 101:11159–11164
21. Dupuis L, Pradat PF, Ludolph AC, Loeffler JP (2011) Energy metabolism in amyotrophic lateral sclerosis. Lancet Neurol 10:75–82. doi:10.1016/S1474-4422(10)70224-6
22. Dupuis L, Spreux-Varoquaux O, Bensimon G, Jullien P, Lacomblez L, Salachas F, Bruneteau G, Pradat PF, Loeffler JP, Meininger V (2010) Platelet serotonin level predicts survival in amyotrophic lateral sclerosis. PLoS One 5:e13346. doi:10.1371/journal.pone.0013346
23. ElAli A, Rivest S (2015) Microglia in Alzheimer's disease: a multifaceted relationship. Brain Behav Immun. doi:10.1016/j.bbi.2015.07.021
24. Endo F, Komine O, Fujimori-Tonou N, Katsuno M, Jin S, Watanabe S, Sobue G, Dezawa M, Wyss-Coray T, Yamanaka K (2015) Astrocyte-derived TGF-beta1 accelerates disease progression in ALS mice by interfering with the neuroprotective functions of microglia and T cells. Cell Rep 11:592–604. doi:10.1016/j.celrep.2015.03.053
25. Fendrick SE, Xue QS, Streit WJ (2007) Formation of multinucleated giant cells and microglial degeneration in rats expressing

a mutant Cu/Zn superoxide dismutase gene. J Neuroinflammation 4:9. doi:10.1186/1742-2094-4-9
26. Frakes AE, Ferraiuolo L, Haidet-Phillips AM, Schmelzer L, Braun L, Miranda CJ, Ladner KJ, Bevan AK, Foust KD, Godbout JP, Popovich PG, Guttridge DC, Kaspar BK (2014) Microglia induce motor neuron death via the classical NF-kappaB pathway in amyotrophic lateral sclerosis. Neuron 81:1009–1023. doi:10.1016/j.neuron.2014.01.013
27. Guerreiro RJ, Lohmann E, Bras JM, Gibbs JR, Rohrer JD, Gurunlian N, Dursun B, Bilgic B, Hanagasi H, Gurvit H, Emre M, Singleton A, Hardy J (2013) Using exome sequencing to reveal mutations in TREM2 presenting as a frontotemporal dementia-like syndrome without bone involvement. JAMA Neurol 70:78–84. doi:10.1001/jamaneurol.2013.579
28. Guilliams M, van de Laar L (2015) A Hitchhiker's guide to myeloid cell subsets: practical implementation of a novel mononuclear phagocyte classification system. Front Immunol 6:406. doi:10.3389/fimmu.2015.00406
29. Harrison M, O'Brien A, Adams L, Cowin G, Ruitenberg MJ, Sengul G, Watson C (2013) Vertebral landmarks for the identification of spinal cord segments in the mouse. Neuroimage 68:22–29. doi:10.1016/j.neuroimage.2012.11.048
30. Heiman-Patterson TD, Sher RB, Blankenhorn EA, Alexander G, Deitch JS, Kunst CB, Maragakis N, Cox G (2011) Effect of genetic background on phenotype variability in transgenic mouse models of amyotrophic lateral sclerosis: a window of opportunity in the search for genetic modifiers. Amyotroph Lateral Scler 12:79–86. doi:10.3109/17482968.2010.550626
31. Hickman SE, El Khoury J (2010) Mechanisms of mononuclear phagocyte recruitment in Alzheimer's disease. CNS Neurol Disord: Drug Targets 9:168–173
32. Hickman SE, El Khoury J (2013) The neuroimmune system in Alzheimer's disease: the glass is half full. J Alzheimers Dis 33(Suppl 1):S295–S302. doi:10.3233/JAD-2012-129027
33. Hickman SE, Kingery ND, Ohsumi TK, Borowsky ML, Wang LC, Means TK, El Khoury J (2013) The microglial sensome revealed by direct RNA sequencing. Nat Neurosci 16:1896–1905. doi:10.1038/nn.3554
34. Hoeffel G, Ginhoux F (2015) Ontogeny of tissue-resident macrophages. Front Immunol 6:486. doi:10.3389/fimmu.2015.00486
35. Huisman MH, de Jong SW, van Doormaal PT, Weinreich SS, Schelhaas HJ, van der Kooi AJ, de Visser M, Veldink JH, van den Berg LH (2011) Population based epidemiology of amyotrophic lateral sclerosis using capture-recapture methodology. J Neurol Neurosurg Psychiatry 82:1165–1170. doi:10.1136/jnnp.2011.244939
36. Hutcheson JD, Setola V, Roth BL, Merryman WD (2011) Serotonin receptors and heart valve disease–it was meant 2B. Pharmacol Ther 132:146–157. doi:10.1016/j.pharmthera.2011.03.008
37. Jay TR, Miller CM, Cheng PJ, Graham LC, Bemiller S, Broihier ML, Xu G, Margevicius D, Karlo JC, Sousa GL, Cotleur AC, Butovsky O, Bekris L, Staugaitis SM, Leverenz JB, Pimplikar SW, Landreth GE, Howell GR, Ransohoff RM, Lamb BT (2015) TREM2 deficiency eliminates TREM2+ inflammatory macrophages and ameliorates pathology in Alzheimer's disease mouse models. J Exp Med 212:287–295. doi:10.1084/jem.20142322
38. Jokic N, Gonzalez de Aguilar JL, Dimou L, Lin S, Fergani A, Ruegg MA, Schwab ME, Dupuis L, Loeffler JP (2006) The neurite outgrowth inhibitor Nogo-A promotes denervation in an amyotrophic lateral sclerosis model. EMBO Rep 7:1162–1167
39. Jonsson T, Stefansson H, Steinberg S, Jonsdottir I, Jonsson PV, Snaedal J, Bjornsson S, Huttenlocher J, Levey AI, Lah JJ, Rujescu D, Hampel H, Giegling I, Andreassen OA, Engedal K, Ulstein I, Djurovic S, Ibrahim-Verbaas C, Hofman A, Ikram MA, van Duijn CM, Thorsteinsdottir U, Kong A, Stefansson K (2013) Variant of TREM2 associated with the risk of Alzheimer's disease. N Engl J Med 368:107–116. doi:10.1056/NEJMoa1211103
40. Kettenmann H, Hanisch UK, Noda M, Verkhratsky A (2011) Physiology of microglia. Physiol Rev 91:461–553. doi:10.1152/physrev.00011.2010
41. Kiernan MC, Vucic S, Cheah BC, Turner MR, Eisen A, Hardiman O, Burrell JR, Zoing MC (2011) Amyotrophic lateral sclerosis. Lancet 377:942–955. doi:10.1016/S0140-6736(10)61156-7
42. Kleinberger G, Yamanishi Y, Suarez-Calvet M, Czirr E, Lohmann E, Cuyvers E, Struyfs H, Pettkus N, Wenninger-Weinzierl A, Mazaheri F, Tahirovic S, Lleo A, Alcolea D, Fortea J, Willem M, Lammich S, Molinuevo JL, Sanchez-Valle R, Antonell A, Ramirez A, Heneka MT, Sleegers K, van der Zee J, Martin JJ, Engelborghs S, Demirtas-Tatlidede A, Zetterberg H, Van Broeckhoven C, Gurvit H, Wyss-Coray T, Hardy J, Colonna M, Haass C (2014) TREM2 mutations implicated in neurodegeneration impair cell surface transport and phagocytosis. Sci Transl Med 6:243ra286. doi:10.1126/scitranslmed.3009093
43. Knight AR, Misra A, Quirk K, Benwell K, Revell D, Kennett G, Bickerdike M (2004) Pharmacological characterisation of the agonist radioligand binding site of 5-HT(2A), 5-HT(2B) and 5-HT(2C) receptors. Naunyn Schmiedebergs Arch Pharmacol 370:114–123. doi:10.1007/s00210-004-0951-4
44. Kolodziejczak M, Bechade C, Gervasi N, Irinopoulou T, Banas SM, Cordier C, Rebsam A, Roumier A, Maroteaux L (2015) Serotonin modulates developmental microglia via 5-HT receptors: potential implication during synaptic refinement of retinogeniculate projections. ACS Chem Neurosci. doi:10.1021/cn5003489
45. Koschnitzky JE, Quinlan KA, Lukas TJ, Kajtaz E, Kocevar EJ, Mayers WF, Siddique T, Heckman CJ (2014) Effect of fluoxetine on disease progression in a mouse model of ALS. J Neurophysiol 111:2164–2176. doi:10.1152/jn.00425.2013
46. Kunis G, Baruch K, Miller O, Schwartz M (2015) Immunization with a myelin-derived antigen activates the brain's choroid plexus for recruitment of immunoregulatory cells to the CNS and attenuates disease progression in a mouse model of ALS. J Neurosci 35:6381–6393. doi:10.1523/JNEUROSCI.3644-14.2015
47. Laird FM, Farah MH, Ackerley S, Hoke A, Maragakis N, Rothstein JD, Griffin J, Price DL, Martin LJ, Wong PC (2008) Motor neuron disease occurring in a mutant dynactin mouse model is characterized by defects in vesicular trafficking. J Neurosci 28:1997–2005. doi:10.1523/JNEUROSCI.4231-07.2008
48. Lattante S, Ciura S, Rouleau GA, Kabashi E (2015) Defining the genetic connection linking amyotrophic lateral sclerosis (ALS) with frontotemporal dementia (FTD). Trends Genet. doi:10.1016/j.tig.2015.03.005
49. Launay JM, Herve P, Peoc'h K, Tournois C, Callebert J, Nebigil CG, Etienne N, Drouet L, Humbert M, Simonneau G, Maroteaux L (2002) Function of the serotonin 5-hydroxytryptamine 2B receptor in pulmonary hypertension. Nat Med 8:1129–1135. doi:10.1038/nm764
50. Lewis CA, Solomon JN, Rossi FM, Krieger C (2009) Bone marrow-derived cells in the central nervous system of a mouse model of amyotrophic lateral sclerosis are associated with blood vessels and express CX(3)CR1. Glia 57:1410–1419. doi:10.1002/glia.20859
51. Liao B, Zhao W, Beers DR, Henkel JS, Appel SH (2012) Transformation from a neuroprotective to a neurotoxic microglial phenotype in a mouse model of ALS. Exp Neurol 237:147–152. doi:10.1016/j.expneurol.2012.06.011
52. Mosher KI, Wyss-Coray T (2014) Microglial dysfunction in brain aging and Alzheimer's disease. Biochem Pharmacol 88:594–604. doi:10.1016/j.bcp.2014.01.008
53. Nebigil CG, Choi DS, Dierich A, Hickel P, Le Meur M, Messaddeq N, Launay JM, Maroteaux L (2000) Serotonin 2B receptor is required for heart development. Proc Natl Acad Sci 97:9508–9513

54. Nebigil CG, Etienne N, Messaddeq N, Maroteaux L (2003) Serotonin is a novel survival factor of cardiomyocytes: mitochondria as a target of 5-HT2B receptor signaling. FASEB J 17:1373–1375. doi:10.1096/fj.02-1122fje
55. Nebigil CG, Hickel P, Messaddeq N, Vonesch JL, Douchet MP, Monassier L, Gyorgy K, Matz R, Andriantsitohaina R, Manivet P, Launay JM, Maroteaux L (2001) Ablation of serotonin 5-HT(2B) receptors in mice leads to abnormal cardiac structure and function. Circulation 103:2973–2979
56. Nebigil CG, Jaffre F, Messaddeq N, Hickel P, Monassier L, Launay JM, Maroteaux L (2003) Overexpression of the serotonin 5-HT2B receptor in heart leads to abnormal mitochondrial function and cardiac hypertrophy. Circulation 107:3223–3229. doi:10.1161/01.CIR.0000074224.57016.01
57. Philips T, Robberecht W (2011) Neuroinflammation in amyotrophic lateral sclerosis: role of glial activation in motor neuron disease. Lancet Neurol 10:253–263. doi:10.1016/S1474-4422(11)70015-1
58. Philips T, Rothstein JD (2014) Glial cells in amyotrophic lateral sclerosis. Exp Neurol 262(Pt B):111–120. doi:10.1016/j.expneurol.2014.05.015
59. Pitychoutis PM, Belmer A, Moutkine I, Adrien J, Maroteaux L (2015) Mice lacking the serotonin Htr receptor gene present an antipsychotic-sensitive schizophrenic-like phenotype. Neuropsychopharmacology. doi:10.1038/npp.2015.126
60. Poliani PL, Wang Y, Fontana E, Robinette ML, Yamanishi Y, Gilfillan S, Colonna M (2015) TREM2 sustains microglial expansion during aging and response to demyelination. J Clin Invest 125:2161–2170. doi:10.1172/JCI77983
61. Schneider CA, Rasband WS, Eliceiri KW (2012) NIH Image to ImageJ: 25 years of image analysis. Nat Methods 9:671–675
62. Streit WJ, Braak H, Xue QS, Bechmann I (2009) Dystrophic (senescent) rather than activated microglial cells are associated with tau pathology and likely precede neurodegeneration in Alzheimer's disease. Acta Neuropathol 118:475–485. doi:10.1007/s00401-009-0556-6
63. Streit WJ, Xue QS, Tischer J, Bechmann I (2014) Microglial pathology. Acta Neuropathol Commun 2:142. doi:10.1186/s40478-014-0142-6
64. Strong MJ, Yang W (2011) The frontotemporal syndromes of ALS. Clinicopathological correlates. J Mol Neurosci 45:648–655. doi:10.1007/s12031-011-9609-0
65. Turner BJ, Lopes EC, Cheema SS (2003) The serotonin precursor 5-hydroxytryptophan delays neuromuscular disease in murine familial amyotrophic lateral sclerosis. Amyotroph Lateral Scler Other Motor Neuron Disord 4(3):171–176. doi:10.1080/14660820310009389
66. Turner MR, Rabiner EA, Al-Chalabi A, Shaw CE, Brooks DJ, Leigh PN, Andersen PM (2007) Cortical 5-HT1A receptor binding in patients with homozygous D90A SOD1 vs sporadic ALS. Neurology 68:1233–1235. doi:10.1212/01.wnl.0000259083.31837.64
67. Turner MR, Rabiner EA, Hammers A, Al-Chalabi A, Grasby PM, Shaw CE, Brooks DJ, Leigh PN (2005) [11C]-WAY100635 PET demonstrates marked 5-HT1A receptor changes in sporadic ALS. Brain 128:896–905. doi:10.1093/brain/awh428
68. van Es MA, Veldink JH, Saris CG, Blauw HM, van Vught PW, Birve A, Lemmens R, Schelhaas HJ, Groen EJ, Huisman MH, van der Kooi AJ, de Visser M, Dahlberg C, Estrada K, Rivadeneira F, Hofman A, Zwarts MJ, van Doormaal PT, Rujescu D, Strengman E, Giegling I, Muglia P, Tomik B, Slowik A, Uitterlinden AG, Hendrich C, Waibel S, Meyer T, Ludolph AC, Glass JD, Purcell S, Cichon S, Nothen MM, Wichmann HE, Schreiber S, Vermeulen SH, Kiemeney LA, Wokke JH, Cronin S, McLaughlin RL, Hardiman O, Fumoto K, Pasterkamp RJ, Meininger V, Melki J, Leigh PN, Shaw CE, Landers JE, Al-Chalabi A, Brown RH Jr, Robberecht W, Andersen PM, Ophoff RA, van den Berg LH (2009) Genome-wide association study identifies 19p13.3 (UNC13A) and 9p21.2 as susceptibility loci for sporadic amyotrophic lateral sclerosis. Nat Genet 41:1083–1087. doi:10.1038/ng.442
69. Vandesompele J, De Preter K, Pattyn C, Poppe B, Van Roy N, De Paepe A, Speleman F (2002) Accurate normalization of real-time quantitative RT-PCR data by geometric averaging of multiple internal control genes. Genome Biol 3:research0034.1–research0034.11. doi:10.1186/Gb-2002-3-7-Research0034
70. Walsh JG, Muruve DA, Power C (2014) Inflammasomes in the CNS. Nat Rev Neurosci 15:84–97. doi:10.1038/nrn3638
71. Wang Y, Cella M, Mallinson K, Ulrich JD, Young KL, Robinette ML, Gilfillan S, Krishnan GM, Sudhakar S, Zinselmeyer BH, Holtzman DM, Cirrito JR, Colonna M (2015) TREM2 lipid sensing sustains the microglial response in an Alzheimer's disease model. Cell 160:1061–1071. doi:10.1016/j.cell.2015.01.049
72. Wiesner D, Sinniger J, Henriques A, Dieterle S, Muller H, Rasche V, Ferger B, Dirrig-Grosch S, Soylu-Kucharz R, Petersen A, Walther P, Linkus B, Kassubek J, Wong PC, Ludolph AC, Dupuis L (2014) Low dietary protein content alleviates motor symptoms in mice with mutant dynactin/dynein mediated neurodegeneration. Hum Mol Genet 15:2228–2240. doi:10.1093/hmg/ddu741
73. Witting A, Moller T (2011) Microglia cell culture: a primer for the novice. Methods Mol Biol 758:49–66. doi:10.1007/978-1-61779-170-3_4
74. Xue QS, Streit WJ (2011) Microglial pathology in Down syndrome. Acta Neuropathol 122:455–466. doi:10.1007/s00401-011-0864-5
75. Zhao W, Beers DR, Appel SH (2013) Immune-mediated mechanisms in the pathoprogression of amyotrophic lateral sclerosis. J Neuroimmune Pharmacol 8:888–899. doi:10.1007/s11481-013-9489-x

El Oussini and collaborators
Serotonin 2B receptor slows disease progression and prevents degeneration of spinal cord mononuclear phagocytes in amyotrophic lateral sclerosis

Supplementary Material

Supplementary Figures

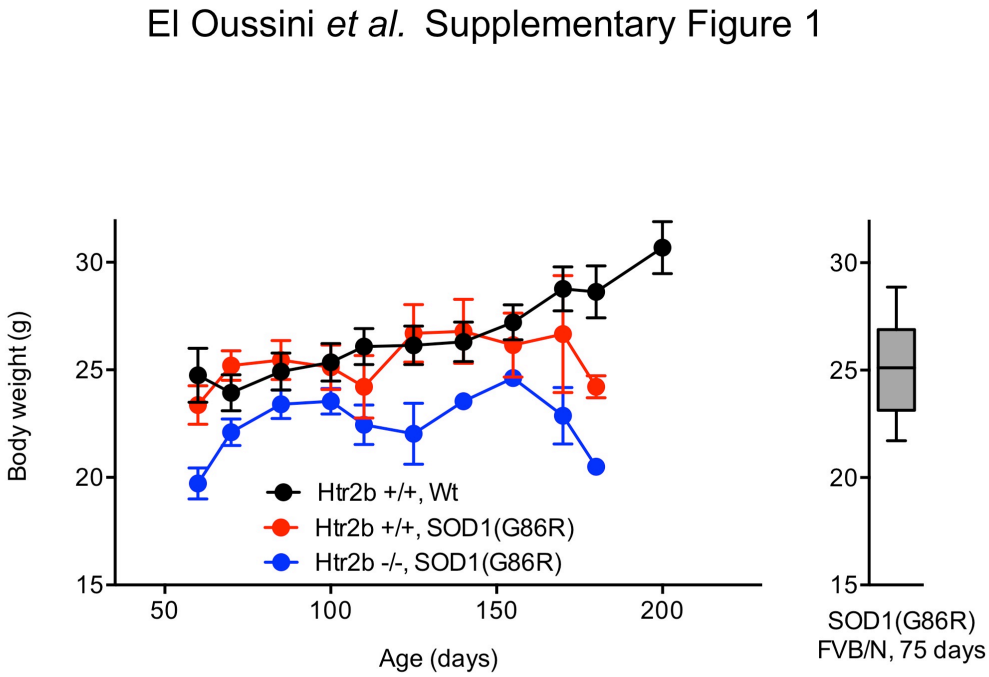

Fig. S1: *Htr2b* ablation decreases body weight in SOD1(G86R) mice
Body weight curves of SOD1(G86R) mice wild type for *Htr2b* (+/+) ,
or knock-out for *Htr2b* (-/-) and wild type littermate mice. N=10-16 per genotype.
The right panel shows the body weight of SOD1(G86R) mice in the initial FVB/N background (n=12).
P<0.05 for genotype between Htr2b -/- SOD1(G86R) and Htr2b +/+ SOD1(G86R), Repeated measures two way ANOVA.

El Oussini *et al.* Supplementary Figure 2

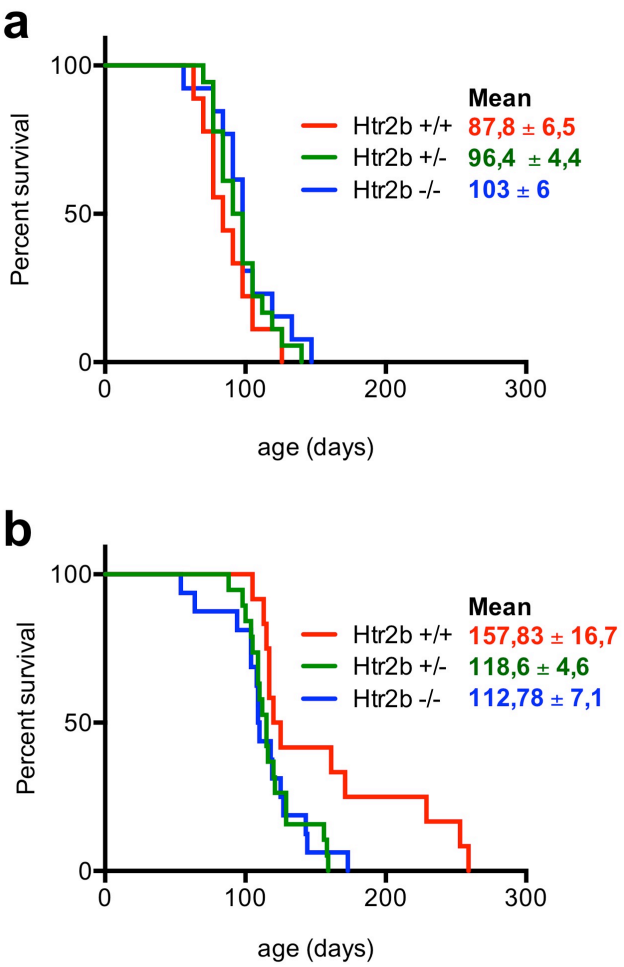

Fig. S2: *Htr2b* haploinsufficiency exacerbates SOD1(G86R) disease progression
Kaplan Meier plot of disease onset, as determined by the peak weight (a) and of survival (b) for SOD1(G86R) mice wild type for *Htr2b* (n=12, red), heterozygous for *Htr2b* (n=19, green) or homozygous for *Htr2b* (n=16, blue). The mean of each group +/- SEM is indicated on each panel.

P<0.05, log rank (Mantel cox) for panel b (+/+ vs +/- and +/+ vs -/-). The log rank test for trend has a p-value of 0.0149, showing the dose dependence of survival towards the number of functional *Htr2b* alleles.

El Oussini *et al.* Supplementary Figure 3

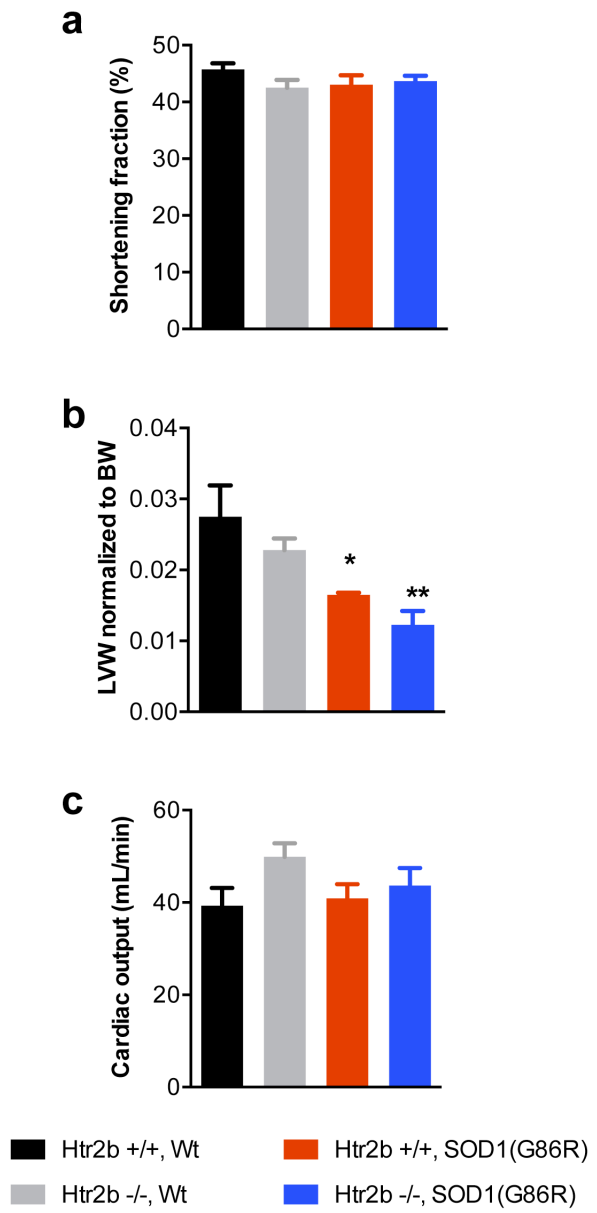

Fig. S3: *Htr2b* ablation does not exacerbate SOD1(G86R) cardiac phenotype

Shortening fraction (in %, A), left ventricular volume (LVW) and cardiac output (in mL/min) wild type mice (Htr2b +/+, Wt), mice knock-out for *Htr2b* (-/-)(Htr2b -/-, Wt) or littermate SOD1(G86R) mice wild type for *Htr2b* (+/+) , or knock-out for *Htr2b* (-/-). Note that the SOD1(G86R) genotype leads to a significant cardiac atrophy, not modified by *Htr2b* genotype.

El Oussini *et al.* Supplementary Figure 4

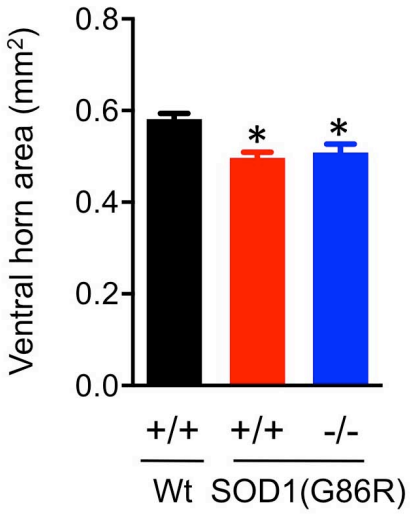

Fig. S4: *Htr2b* ablation does not modify ventral horn atrophy in SOD1(G86R)
Ventral horn area in wild type mice (Htr2b +/+, Wt), SOD1(G86R) mice wild type for *Htr2b* (+/+) , or knock-out for *Htr2b* (-/-). Note that the SOD1(G86R) genotype leads to a significant atrophy of ventral horn, not modified by *Htr2b* genotype.

Ventral horn was defined anatomically and measured in >10 sections per animal, with n=7 independent animals per genotype.
*$p<0.05$ significantly different (One-way ANOVA followed by Tukey *post hoc* test).

El Oussini *et al.* Supplementary Figure 5

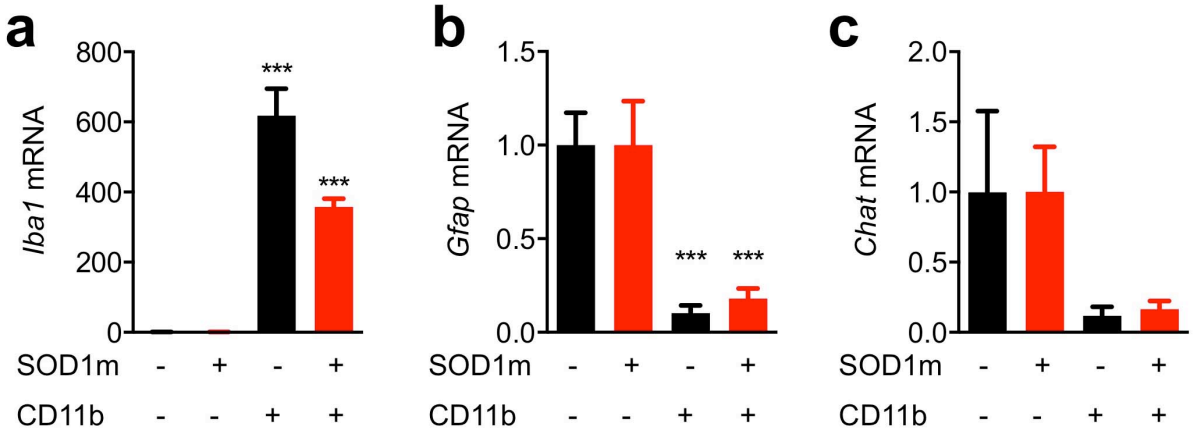

Fig. S5: controls for purification of CD11b positive cells.
Iba1 (**a**), *Gfap* (**b***) and Chat* (**c***)* mRNA levels in CD11b-positive cells ($CD11^{Pos}$) relative to CD11b-negative cells ($CD11b^{Neg}$) in brainstem and spinal cord of end stage SOD1(G86R) mice (SOD1) and control littermates (Wt). ***p<0.01 significantly different vs corresponding CD11b negative fraction (One-way ANOVA followed by Tukey *post hoc* test).

El Oussini *et al.* Supplementary Figure 6

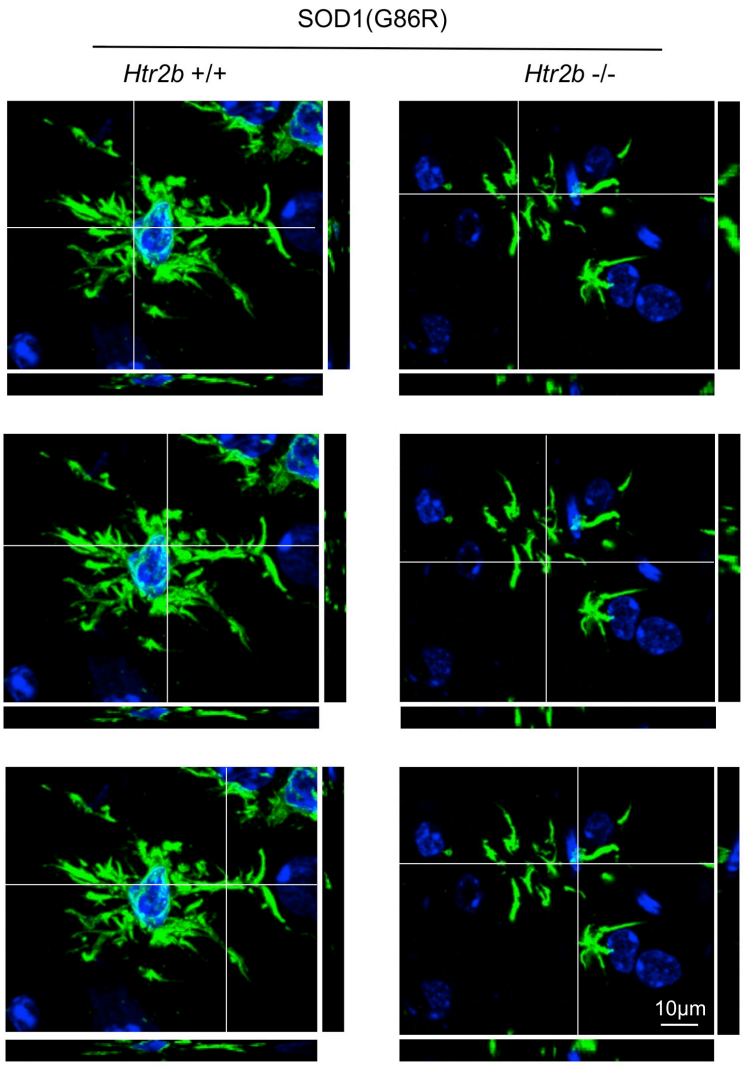

Fig. S6: side views of Iba1 immunofluorescence.
Orthogonal views of one Iba1 positive cell of a SOD1(G86R) mouse wild type for *Htr2b* (+/+) (left) and one Iba1 positive cell of a SOD1(G86R) mouse knock-out for *Htr2b* (-/-) (right).
z-stacks of 10-15µm thickness were merged and are shown in XY. Orthogonal side views are shown for XZ and YZ axes with white lines in merged images showing location of section.
Iba1 immunolabeling is shown in green, and nucleus in blue.

Table S1: Patient characteristics for survival analysis

Shown is the number of patients, gender (M=male, F=female), age at onset (AAO), age at inclusion (AAI), site of onset, Survival in years, percentage deceased.

Number	Gender (M/F)	AAO mean (range)	AAI mean (range)	Site of onset (bulbar (%))	Survival (y) mean/median	Deceased (%)
1677	998/679	62 (19-90)	66 (21-91)	563 (33.7%)	2.36/2.02 (0.0017-14.8)	80.1

Table S2: characteristics of ALS patients included in autoptic studies.

16 ALS patients were genotyped and included. 6 carried *HTR2B* A/A rs10199752 haplotype (patients 1-6) and 10 carried *HTR2B* C/A rs10199752 haplotypes (7-16).

Corresponding genotypes are indicated for each patient, as well as inclusion in qPCR and/or microglial degeneration score depending on material availability.

All patients were diagnosed with ALS, except patient 2, with a diagnosis of combined ALS and Lewy body disease (LBD). When available, the extent of TDP-43 pathology and Braak staging is indicated.

patient	rs10199752	qPCR	microglial fragmentation	age at death	Gender	diagnosis
1	A/A	+	3,5	63	m	ALS
2	A/A	+	3,5	75	m	ALS + LBD
3	A/A	+	3	66	f	ALS + AD
4	A/A	+	2	74	m	ALS (stage1/ 16% TDP-43 affected areas)
5	A/A	+	4	43	m	ALS (stage4/ 58% TDP-43 affected areas)
6	A/A	+	3	66	m	ALS
7	C/A	+	1	69	m	ALS (stage4/ 52% TDP-43 affected areas)
8	C/A	N/A	0,5	75	m	ALS (stage4/ 69% TDP-43 affected areas)
9	C/A	+	N/A	61	m	ALS (stage4/ 61% TDP-43 affected areas)
10	C/A	+	0,5	75	m	ALS (stage4/ 55% TDP-43 affected areas)
11	C/A	+	0	84	m	ALS
12	C/A	+	N/A	46	f	ALS (no TDP-43 lesions – only p62-lesions/ C9Orf72 mutation carrier)
13	C/A	+	0	25	m	ALS (stage3/ 40% TDP-43 affected areas)
14	C/A	+	N/A	76	f	ALS (stage4/ 60% TDP-43 affected areas)
15	C/A	+	1	56	f	ALS
16	C/A	N/A	0			ALS

Table S3: primers for RT-qPCR studies.
All primers are murine except where indicated.

mRNA		Sequence
Ccl4 For	Chemokine (C-C motif) ligand 4	CAA-GCC-AGC-TGT-GGT-ATT-CCT
Ccl4 Rev		GCT-GCT-CAG-TTC-AAC-TCC-AAG
Nox2 For	NADPH oxidase	ACA-CTG-ACC-TCT-GCT-CCT-GA
Nox2c Rev		AGG-CAT-CTT-GGA-ACT-CCT-GC
Mch2 For	Musculus histocompatibility 2, class II	AGG-AGA-GCC-TTA-TTC-ATC-GCT
Mch2 Rev		GAT-GGC-GCT-CTC-GTT-CTG-T
Dap12For	DNAX activation protein	TGA-CTC-TGC-TGA-TTG-CCC-TG
Dap12 Rev		GGC-GAC-TCA-GTC-TCA-GCA-AT
Ym1 For	Secretory protein precursor	GAA-GGA-CCA-TGG-AGC-AGC-TT
Ym1 Rev		GGG-GCA-CCA-ATT-CCA-GTC-TT
Hexb For	Beta-hexosaminidase subunit beta	GGA-CTT-CAG-CAT-CGA-CCA-CA
Hexb Rev		GTA-ATA-TCG-CCG-AAA-CGC-CTC
Olfml3 For	Olfactomedin-like protein 3	GAT-ATG-GTG-ACG-GAC-TGT-AGC
Olfml3 Rev		CTG-AAC-CAC-CAA-ACC-GCT-TC
Tmem119 For	Transmembrane Protein 119	ACC-CAG-AGC-TGG-TTC-CAT-AG
Tmem119 Rev		GAG-TGA-CAC-AGA-GTA-GGC-CA
Siglec-H For	Sialic acid binding Ig-like lectin H	TGC-TCT-GGG-TGC-TTA-AGT-GG
Siglec-H Rev		AAC-TCC-AGT-GTC-AGT-GAC-GG
Trem2 For	Triggering receptor expressed on myeloid cells 2	CTG-GAG-GAC-CCT-CTA-GAT-GAC
Trem2 Rev		CCA-CAG-GAT-GAA-ACC-TGC-CT
Iba1 For	Allograft inflammatory factor 1	AGC-TTT-TGG-ACT-GCT-GAA-GG
Iba1 Rev		CAG-CTC-TAG-GTG-GGT-CTT-GG
Htr2B For	5-hydroxytryptamine (serotonin) receptor 2B	GAA-GCC-ACA-GAA-GAC-AAG-CG
Htr2B Rev		GAT-TCA-GGC-TCT-CGA-AGA-TGG
ChaT For	Choline O-acetyltransferase	TAC-CTA-AGT-TGC-CAG-TGC-CC
ChaT Rev		CCC-CAA-ACC-GCT-TCA-CAA-TG
GFAP For	Glial fibrillary acidic protein	TCG-AGA-TCG-CCA-CCT-ACA-G
GFAP Rev		GTC-TGT-ACA-GGA-ATG-GTG-ATG-C
P2y12 For	Purinergic receptor P2Y, G-protein coupled 12	ACC-ACC-CCT-GTT-TTT-CCA-GTT
P2y12 Rev		AGC-CTT-GAG-TGT-TTC-TGT-AGG-G
Cx3cr1 For	Chemokine (C-X3-C motif) receptor 1	AGC-TCA-CGA-CTG-CCT-TCT-TC
Cx3cr1 Rev		GGT-TGT-TCA-TGG-AGT-TGG-CG
Ly6c1 For	Lymphocyte antigen 6 complex	ATC-TGT-GCA-GCC-CTT-CTC-TG
Ly6c1 Rev		GTA-GCA-CTG-CAG-TCC-CTG-AG
Tgfbeta1 For	Transforming growth factor, beta 1	ATG-CTA-AAG-AGG-TCA-CCC-GC
Tgfbeta1 Rev		TGC-TTC-CCG-AAT-GTC-TGA-CG
Tgfbeta1R For	Transforming growth factor receptor, beta 1	TGC-TGC-AAT-CAG-GAC-CAC-TG
Tgfbeta1R Rev		GGC-CAG-CTG-ACT-GCT-TTT-CT
HTR2B Hum For	Human 5-hydroxytryptamine (serotonin) receptor 2B, G protein-coupled	AGC-ACA-TTT-TGC-AGA-GCA-CC
HTR2B Hum Rev		GTG-CAG-TTT-ATT-TCC-CTG-TTC-CT

Résultat #2

Le rôle des neurones sérotonergiques dans la SLA liée aux mutations SOD1

La spasticité et l'hypertonie sont parmi les conséquences de la lésion des neurones moteurs supérieurs. La spasticité est un trouble moteur caractérisé par des réflexes musculaires toniques, exagérés et douloureux. La perte du contrôle supérieur induit l'hyperexcitabilité des neurones moteurs et l'altération des mécanismes du contrôle d'inhibition synaptiques. La spasticité est aussi parmi les symptômes douloureux observés dans le cas de SLA.

Plusieurs mécanismes sont à l'origine de la spasticité. La plupart de ces mécanismes ont été décrits dans le cas du traumatisme de la moelle épinière. La perte des monoamines dont la sérotonine, et la perte des projections spinales des neurones sérotoninergiques, participent au développement de la spasticité.

Dans le cas de la sclérose amyotrophique latérale (SLA) la perte des neurones sérotoninergiques est observée au stade final de la maladie chez les patients et les souris SOD (G86R). Les rôles des neurones sérotoninergiques dans le cas de SLA sont encore inconnus.

Pour cela nos principales questions sont:

- Etudier le rôle de la toxicité SOD1 dans les neurones sérotoninergiques au cours de la progression de la maladie.
- Comprendre comment la perte de sérotonine induit la spasticité.

Pour déterminer le rôle de la toxicité SOD1 dans les neurones sérotonergiques au cours de la SLA, nous avons utilisé les souris G37R, un modèle conditionnel de SLA exprimant un gène SOD1 humain muté en position G37R, flanqués de sites LoxP. Les SOD1(G37R) LoxP ont été croisées avec des souris exprimant la CRE sous le contrôle du promoteur Tph2. L'ablation sélective de la SOD1 (G37R) dans les neurones serotonergiques a restauré la

dégénérescence des neurones 5-HT observées chez les souris G37R. G37R$^{\Delta Tph2}$ présentaient une dégénérescence des neurones sérotoninergiques plus faible que les souris G37R.

La préservation des neurones sérotoninergiques chez les souris G37R$^{\Delta Tph2}$ diminue très fortement la spasticité, ce qui accélère l'établissement de la paralysie. La survie n'est par contre pas affectée. Ces résultats suggèrent que la spasticité dans le cas de SLA est d'origine sérotoninergique.

L'ablation partielle de la toxicité SOD1 dans les neurones 5-HT a aggravé le phénotype de SLA. Les neurones moteurs chez les souris G37R$^{\Delta Tph2}$ sont plus atrophiés en le comparant avec les souris G37R au stade final de la maladie.

Ces résultats démontrent que les neurones sérotoninergiques ont un rôle indispensable dans le déclenchement de la spasticité au cours de la SLA. Pour cette raison les stratégies anti-spastiques devraient cibler le système sérotoninergiques.

--Manuscript in preparation--

Degeneration of serotonin neurons is necessary to elicit spasticity in amyotrophic lateral sclerosis

Hajer El Oussini[1,2], Jelena Scekic-Zahirovic[1,2], Pauline Vercruysse[1,2,3], Stéphane Dieterlé[1,2], Gina Picchiarelli[1,2], Jérôme Sinniger[1,2], Sylvie GROSCH[1,2], Caroline Rouaux[1,2] & Luc Dupuis[1,2,*]

[1]INSERM UMR-S1118, faculté de médecine, Strasbourg, 67085 France.
[2]Université de Strasbourg, fédération de Médecine Translationnelle, Strasbourg, France.
[3]Department of Neurology, University of Ulm, Germany.

*Corresponding author: ldupuis@unistra.fr

Abstract

Amyotrophic lateral sclerosis (ALS) is characterized by the degeneration of both upper motor neurons (UMN), located in the motor cortex, and lower motor neurons in the brainstem and spinal cord. Degeneration of UMN is considered to constitute the primary cause of a number of symptoms, including spasticity, a painful symptom restricting everyday life, but participating in the maintenance a low level of motor function in impaired patients. Here we show that deleting the ALS-causing transgene selectively in brainstem serotonin neurons is sufficient to rescue the degeneration of this neuronal type and abolish spasticity. Consistently, this selective deletion worsened motor function and accelerated the onset of paralysis. These findings demonstrate that degeneration of serotonin neurons is necessary to trigger at least part of the typical symptoms commonly attributed to UMN loss. Thus the wide range of drugs targeting the serotonergic system could be useful to treat spasticity in ALS, and other neurodegenerative diseases characterized by spasticity.

Introduction

Spasticity occurs in a wide range of neurological diseases, including neurodegenerative diseases (*eg* amyotrophic lateral sclerosis, ALS or multiple sclerosis), genetic (*eg* hereditary spastic paraplegia), traumatic (*eg* spinal cord injury, SCI) or after stroke. Spasticity is characterized by involuntary muscle activity, and includes hyper-reflexia, muscles spasms, clonus and co-contraction of antagonist muscles [1-3]. Spasticity is a painful symptom and can severely restrict everyday life, but might also participate in maintaining a low level of motor function in severely impaired patients.

A number of mechanisms have been shown to participate in the development of spasticity after spinal cord injury. First, hyperreflexia might arise from increased synaptic input to motor neurons caused by remodeling of spinal pathways involving sensory afferents (Ia, Ib) or Renshaw cells [2,3]. Second, increased excitability of motor neurons themselves is able to lead to more sustained contractions in response to a sensory stimulus after SCI [2,4-6]. Such SCI-induced motor neuron hyperexcitability has been postulated to occur through BDNF-dependent downregulation of KCC2, a potassium-chloride co-transporter responsible for chloride extrusion in adult neurons [7]. Indeed BDNF application reverted both hyperreflexia and KCC2 downregulation after SCI in mice [7]. Alternatively, motor neuron hyperexcitability could be a late consequence of the deprivation of monoaminergic input to the motor neuron. Ligand-independent activity of serotonin (5-HT2B/C) and norepinephrine (alpha1) receptors could indeed be responsible for the development of spastic long lasting reflexes [8-11] and the maintenance of locomotion after partial SCI [8,12]. The sequence of events, as well as their relative importance in the development of spasticity remain however elusive.

Spasticity also occurs in amyotrophic lateral sclerosis, yet, contrary to SCI, ALS-associated spasticity has been barely studied. Spasticity in ALS is paradigmatically considered to result from the degeneration of upper motor neurons themselves [13,14]. Upper motor neurons (UMNs) are glutamatergic neurons located in layer V of motor cortex, project to spinal motor neurons through the corticospinal tract, and are the major source of descending motor commands for voluntary movement [15]. While there is a general consensus to attribute the development of spasticity to UMN degeneration in ALS, this specific question has, to our knowledge, not been addressed experimentally. Indeed, our recent work has shown that brainstem serotonin neurons degenerate in ALS mouse models and in ALS patients, and inverse agonists of the 5-$HT_{2B/C}$ receptors were potently anti-spastic in ALS mice [16]. This raised the possibility that degeneration

of serotonin neurons could, at least in part, be involved in the development of ALS-associated spasticity. In this study, we took advantage of the existence of a conditional mouse model of ALS [17] to investigate the role of serotonin neurons in ALS-related spasticity. The selective rescue of serotonin neurons abolished the development of spasticity in this mouse model. These findings demonstrate that a large part of the typical symptoms attributed to UMN degeneration in ALS are in fact caused by the degeneration of another neuronal type, widely accessible to pharmacological intervention.

Results

Targeting mutant SOD1 expression in adult serotonergic neurons

To determine the role of serotonergic neurons in ALS, we used floxed SOD1(G37R) mice, that express the ALS-linked G37R mutation in the human SOD1 gene that can be excised through CRE-mediated recombination [17]. These mice have been widely used to determine the respective roles of motor neurons, microglia, astrocytes or oligodendrocytes in ALS phenotypes[17-21]. SOD1(G37R) mice were crossed with transgenic mice expressing CRE-ERT2 upon control of the Tph2 promoter (Tph2-CRE mice). SOD1(G37R) mice carrying the Tph2-CRE transgene are denoted as G37R$^{\Delta Tph2}$ mice, whereas littermate SOD1(G37R) mice without the Tph2-CRE transgene are denoted as G37R mice. Crossing Tph2-CRE mice with Rosa26 STOP YFP (YFP CRE reporter) mice, that express YFP only after CRE mediated recombination, led to robust YFP immunoreactivity after 5 days of tamoxifen treatment in virtually all Tph2 positive neurons in the brainstem (Figure 1a and Figure S1a). Contrastingly, YFP was not detected in cholinergic neurons (Figure S1b) nor in microglial cells (Figure S1b), showing that CRE activity was restricted to serotonin neurons in Tph2-CRE mice. Expression of SOD1(G37R) was decreased in microdissected raphe magnus nucleus but not in cortex or cerebellum of G37R$^{\Delta Tph2}$ mice as compared with littermate G37R mice (Figure 1b). Importantly, a subset of serotonin neurons developed large aggregates positive to human SOD1 in G37R mice, but such aggregates were not observed in G37R$^{\Delta Tph2}$ serotonin neurons, although they were readily detectable in neighbouring cells (Figure 1c). Thus, our data are consistent with a selective rescue of mutant SOD1 expression in adult serotonergic neurons of G37R$^{\Delta Tph2}$ mice.

Serotonin neuron degeneration is cell autonomous in SOD1(G37R) mice

We first asked whether rescue of mutant SOD1 expression in serotonergic neurons was sufficient to rescue serotonin neurons themselves. To this aim, we performed Tph2 immunohistochemistry in endstage G37R$^{\Delta Tph2}$ mice and littermate G37R mice (Figure 2a). Consistent with previous results, we observed that Tph2 positive neurons displayed atrophy of the cell body in the dorsal raphe and median raphe nuclei of G37R mice (Figure 2b). This atrophy was entirely reverted in G37R$^{\Delta Tph2}$ mice (Figure 2b). Tph2 immunoreactivity was generally weaker in G37R mice, as compared with G37R$^{\Delta Tph2}$ mice, as observed also using immunofluorescence (Figure 1c). We further studied the morphology of a major serotonergic tract, located in the arcuate nucleus of the hypothalamus (Figure 1d). This serotonergic tract was strongly

degenerating in G37R mice, similar to what previously observed in SOD1(G86R) mice [22], and mostly preserved in G37R$^{\Delta Tph2}$ mice (Figure 1d-e). Thus, rescuing mutant SOD1 expression in serotonergic neurons prevents their degeneration.

Rescuing serotonin neurons eliminates spasticity

Spasticity is a major symptom of ALS, and previous evidence suggested that spasticity associated with ALS was caused by constitutive activity of 5-HT$_{2B}$/5-HT$_{2C}$ receptors. In mice, the development of spasticity is visually observed by spastic contractions of tail muscles at end stage. Tail spasticity was prominently observed in 10 out of 13 G37R mice at end stage, while, contrastingly, only 1 out of 11 G37R$^{\Delta Tph2}$ mice showed this phenotype (p=0.0013, Fisher's exact test; Figure 3a). To further quantify this effect, we measured long lasting reflex (LLR) using electromyography in awake mice at end stage. This quantitative method is correlated with spasticity after spinal cord injury, and allows to measure the biological effects of classical anti-spastic drugs [9,23]. We previously showed that 5-HT$_{2B}$/5-HT$_{2C}$ inverse agonists, such as SB206553 (later referred as SB206), are able to completely block existing LLRs, suggesting their anti-spastic potential [16]. We observed that while robust LLRs are observed in end-stage G37R mice and blocked by SB206 application, such LLRs did not develop in G37R$^{\Delta Tph2}$ mice (Figure 3b, and 3c-d for quantification). Thus the degeneration of serotonin neurons is necessary to trigger spasticity in mutant SOD1 mice.

Rescuing serotonin neurons hastens onset of paralysis and worsens motor neuron atrophy

Spasticity is thought to represent a compensatory mechanism activated by motorneurons enabling to maintain their function despite loss of excitatory input. Consistent with this, the absence of spasticity in G37R$^{\Delta Tph2}$ mice was associated with worsened grip strength (Figure 4a), and with earlier onset of paralysis (Figure 4b). Indeed, G37R$^{\Delta Tph2}$ mice displayed earlier age at onset of motor symptoms (Figure 4c), but reached end stage at similar ages than G37R mice, leading to increased disease duration (Figure 4c-d). G37R$^{\Delta Tph2}$ mice displayed similar loss in motor neurons at end stage (Figure 4e-f), but motor neuron atrophy was much more pronounced (Figure 4g). Importantly, astrocytosis and microgliosis appeared normally activated in G37R$^{\Delta Tph2}$ spinal cord (Figure S2), suggesting that the most deleterious effects of rescuing spasticity were on motor neurons.

Thus, rescuing serotonin neurons accelerates disease progression and worsens motor neuron function.

Discussion

Our current study demonstrates that the degeneration of brainstem serotonin neurons is responsible for the development of spasticity in ALS mice, and that spasticity compensates for motor deficits allowing the maintenance of motor function after disease onset. These findings have important consequences for our understanding of ALS pathophysiology and management, as well as for all the diseases involving spasticity.

A first major result of the current study is that degeneration of serotonin neurons is cell autonomous in ALS. This is demonstrated by the rescue of serotonin neurons observed upon deletion of the mutant SOD1 transgene in adult serotonergic neurons. To this aim, we used a conditional CRE transgene that allowed the rescue in adult mice, thereby avoiding the potential confounding developmental effects. Multiple indexes of serotonin neuron degeneration were rescued in G37R$^{\Delta Tph2}$ mice, including decreased TPH2 immunoreactivity, decreased size of cell bodies and occurence of degenerating serotonergic fibers. This cell autonomous nature of serotonin neuron degeneration contrasts with the situation observed in motor neurons in which the local environment appears critical [17,18,24,25]. Such a difference could be due to intrinsic properties of serotonergic neurons. Indeed, we observed very few SOD1 positive aggregates in Tph2 neurons, contrasting with other cell types that accumulated large amounts of aggregated SOD1. This is consistent with our previous observation of a lack of TDP43 aggregates in serotonergic neurons of ALS patients [16] and suggests that serotonin neurons display distinct mechanisms of clearance of aggregate prone proteins than other neuronal types. Our demonstration of the cell autonomous nature of serotonergic neuron degeneration in ALS opens the way for studying mechanisms of degeneration in cultured serotonergic neurons, in particular in transdifferentiated serotonergic neurons of ALS patients, using protocols recently published [26,27].

The selective rescue of serotonin neurons in G37R$^{\Delta Tph2}$ mice allowed us to identify the primary consequences of this degeneration. Interestingly, and despite the important roles of serotonin neurons in multiple brain functions, many phenotypes developed by G37R mice were not affected. For instance, the rescue of serotonin neurons did not modify the extent of motor neuron degeneration, of astrocytosis or microgliosis. Despite the well documented role of serotonin in food intake and energy homeostasis, body weight was only affected in female but not male G37R$^{\Delta Tph2}$ mice. As a consequence, survival of G37R$^{\Delta Tph2}$ mice was not significantly different from G37R mice. It is important to mention that we performed the rescue of serotonin neurons in adults, and alterations in motor neuron excitability and locomotor rythms, presumably

serotonin dependent, were documented in embryonic or perinatal mice in others mutant SOD1 mice [28-31]. Thus, we cannot completely exclude that early, embryonic alterations in serotonin neurons contribute to other aspects of ALS pathogenesis. Last, mutant SOD1 mice, like SOD1 ALS patients, do not exhibit frontal symptoms, and our current study was thus not able to determine whether degeneration of serotonin neurons could be related with frontal symptoms in ALS and FTD. Indeed, serotonin neurons are deeply involved in the regulation of mood, social behaviour or executive functions [32-34], that could all potentially be impaired during frontal symptoms of ALS or during FTD. Thus further studies are required to study the role of serotonin neurons in frontal lobe related symptoms.

The major consequence of the rescue of serotonin neurons in G37R$^{\Delta Tph2}$ mice was a complete absence of spasticity. This was obvious from visual inspection of tail spasticity and quantified using electrophysiological characterization of long lasting reflexes in the tail muscles, a well documented measure of spasticity in rodents [8,35]. We observed that G37R$^{\Delta Tph2}$ mice developed earlier paralysis onset, associated with decreased muscle strength. This is in perfect agreement with the lack of spasticity in these mice as spasticity allows some compensatory rescue of motor function. In SCI models, similar worsening of motor function was observed after pharmacological ablation of spasticity [8,12]. It was already known that serotonergic signaling was critical in the development of ALS muscle spasms as 5-HT$_{2B/2C}$ inverse agonists are able to abolish muscle spasms [16], yet it was unclear whether the degeneration of serotonin neurons themselves was required to elicit spasticity. Indeed, spasticity in ALS is paradigmatically associated with degeneration of upper motor neurons that are located in the motor cortex and fine tune the motor activity. Spasticity is indeed a cardinal symptom of the so-called “UMN syndrome”, presumably caused by UMN loss, and development of UMN syndrome is central to the diagnosis of ALS [13,14]. Our current data establish that this direct connection between UMN loss and spasticity is wrong, and that degeneration of serotonin neurons is essential in triggering spasticity in ALS. It is important to mention that this does not rule out that UMN loss contribute to spasticity or other symptoms of ALS, but this would have to be specifically studied using other CRE drivers.

Our model system will allow dissecting out the hierarchy of events leading to spasticity downstream of serotonin. Indeed, it will be interesting to determine whether increased mRNA levels of 5-HT$_{2B}$ receptor [16,36] and/or altered editing of the mRNA encoding the 5-HT$_{2C}$ receptor [8,16] return to baseline wild type levels in G37R$^{\Delta Tph2}$ mice. In spinal cord injury, spasticity has been found to involve a number of signaling mechanisms

such as downregulation of the sodium/chloride transporter KCC2 [7] or the calpain-dependent cleavage of voltage gated channels [6]. Whether these mechanisms occur during ALS and are downstream of serotonin loss remains an open question.

Summarizing, our current study demonstrate that the classical view of spasticity arising from UMN loss in ALS is, at best, incomplete. The demonstration that the degeneration of serotonin neurons is necessary to elicit spasticity suggests that anti-spastic strategies should focus on the serotonergic drugs widely available to improve the treatment of this painful symptom. Multiple neurological diseases are associated with spasticity, and our current results might thus be of critical importance for treating spasticity in diseases as diverse as spinal cord injury, hereditary spastic paraplegia or ALS.

Materials and methods

Animals

Transgenic mice were housed in the animal facility of the medicine faculty of Strasbourg University, with 12h/12h of light/dark and unrestricted access to food and water. In all experiments, littermates were used for comparison. Transgenic mice carrying a floxed SOD1 G37R human transgene on a C57BL/6 background were kindly provided by Dr Don W. Cleveland[17]. As described previously, these mice carry a 12 kb genomic DNA fragment encoding the human SOD1(G37R) transgene, under its endogenous promoter, flanked by LoxP sequences and were used as heterozygous, with their non-transgenic littermates as controls. Onset of symptoms was defined according to previous studies [17]. Tph2-iCreER (referred to as Tph2 CRE) transgenic mice (Jax strain #016854) expressing a tamoxifen-inducible Cre recombinase under the control of mouse *Tph2* promoter were genotyped with their non-transgenic littermates on a C57BL/6 background. YFP CRE reporter mice were R26-stop-EYFP mice (Jax strain #006148) carrying a loxP-flanked STOP sequence followed by the Enhanced Yellow Fluorescent Protein gene (EYFP) inserted into the Gt(ROSA)26Sor locus. All animal experimentation was performed in accordance with institutional guidelines, and protocols were approved by the local ethical committee from Strasbourg University (CREMEAS) under number AL/29/36/02/13 in accordance with European regulations.

Mouse breeding, survival and motor phenotyping

SOD1 (G37R) mice were crossed with Tph2 CRE mice to obtain double transgenic mice in F1. At 56 days of age 100µL of tamoxifen/corn oil solution at a dose of 75 mg/kg body weight was administrered through oral gavage every day during 5 consecutive days on all mice. Mice single transgenic for the SOD1 (G37R) transgene (G37R, n=14) were compared with littermate double transgenic mice carrying both SOD1 (G37R) transgene and Tph2 CRE transgene ($G37R^{\Delta Tph2}$, n=15). Mice negative for SOD1 (G37R) transgene were used as controls (Wt, n=15).

Mice were visually inspected daily and weekly monitored for body weight and motor symptoms from two months of age until end stage of the disease. To evaluate muscle strength, we used a gripmeter test (Bioseb, ALG01; France). The muscle force (in Newton) was measured three times per mouse. Results are the mean of two weeks sessions. Disease course and survival were assessed daily by visual inspection. Disease onset was calculated as time of peak of body weight. Disease duration was the time between the peak of body weight and death. After disease onset mice were followed daily and end stage was defined by

full paralysis and when mice were unable to return after 10 seconds placed on the back. End stage mice were immediately euthanized.

Histological techniques

Spinal cords and brains were dissected and fixed by immersion in 4% paraformaldehyde in 0.1 M phosphate buffer pH 7.4 overnight.

The lumbar parts of spinal cords were dissected and the L3-L5 region was identified according to previous studies (Harrison *et al.*, 2013). Tissue was cryoprotected in 30% sucrose and snaps frozen in melting isopropanol in TissueTek (O.C.T.Compound, SAKURA#4583). Cryosections (Leica CM 3050S) of 16µm were obtained for histological analysis of end stage mice (10 sections per animal). Spinal cord and brains sections were incubated in phosphate buffered saline (PBS) 0.1% Triton with anti-choline acetyl transferase (ChAT) (Millipore, AB144-P; diluted 1:50) for motor neuron, Tph2 (Abcam; ab121013; diluted 1:500, human SOD1 (Abcam, ab52950; diluted 1:100) and for glial cells anti-Iba1 (Abcam; ab5076, 1:100), GFAP (Dakocytomation; Z0334; diluted 1:500) antibodies followed by biotinylated species-specific secondary antibody. The staining was revealed using the ABC kit (Vectastain), by the avidin-biotin complex immunoperoxidase technique or using fluorescent secondary antibodies for immunofluorescence.

Single-layer images or Z-Stack images (1µm optical section) were acquired using a laser-scanning microscope (confocal Leica SP5 Leica Microsystems CMS GmbH) equipped with 63× oil objective (NA1.4). Excitation wavelengths were sequentially argon laser 488nm, diode 561nm, and helium neon laser 633nm. Emission bandwidths are 500-550nm for Alexa488, 570-620nm for Alexa594, and 650-750nm for draq5.

Quantification of motor neurons in mice spinal cord

Motoneuron counting was performed in L3-L5 ventral horn in every tenth section for ten sections in total per animal (160 µm thick in total, spread over 1.6 mm). Only ChAT+ neurons located in a position congruent with that of motoneuron groups were counted [37]. All $ChAT^+$ profiles located in the ventral horns of immunostained sections and clearly displayed in the plane of section were counted. Total estimated motoneuron numbers were obtained using a computer-assisted microscope (Nikon Eclipse E800) and associated software (Nis Elements version 4.0). Total numbers of motoneurons and the mean area of individual cells were obtained using ImageJ freeware (http://rsbweb.nih.gov/ij/) after image acquisition at 20X under the same exposition parameters with a digital camera (Nikon Digital Sight DS-U3). The observer was blinded to the genotype of studied mice.

Quantification of Iba1 and GFAP in mice spinal cord

For staining of microglia and astrocytes, measurement of Iba1 and GFAP immunoreactivity was performed on images acquired from Iba1/GFAP immunostaining at 10x magnification. A standardized rectangle was drawn in the ventral horn and the surface of staining relative to background was calculated using the Pixel classifier algorithm of Nikon Nis-element 3.10 SP3 software, using the intensity profile measurement function. The observer was blinded to the genotype of studied mice. >10 images per animal were quantified, with n=5 animals per genotype.

Quantification of Tph2 positive neurons in mice brain

For Tph2 positive neurons quantification in the brainstem we used the technics previously described [16]. At least three sections per region were selected and anatomically matched. We selected sections encomprising raphe dorsal, median raphe and raphe magnus nuclei according to Paxinos Atlas. Acquired image at 20X under the same exposition parameters with a digital camera (Nikon Digital Sight DS-U3) were taken in specific regions. Total mean area of individual cells was obtained using ImageJ freeware (http://rsbweb.nih.gov/ij/).

For quantification of axonal density in the brain, staining was processed to binary images using NIH ImageJ as described previously [38]. After changing tiff images to 8-bit images, images were inverted and processed with Feature J plugin for ImageJ (version 1.50d) to select the smallest Hessian values and « smoothing scale » of 1.0. The resulting images were transformed into binary images by thresholding. Threshold was determined on one cut of a WT animal and same threshold was applied to every image. The intensity of white pixel, referring to the axonal staining, and black pixel, referring to the, background is measured.

Real–time quantitative polymerase chain reaction

Total RNA was extracted from the spinal cord of end stage mice using TRIzol (Invitrogen). RNA was reverse transcribed using 1µg of RNA and the iScript cDNA synthesis kit (BioRad). We performed real-time PCR using IQ SYBR green Supermix (BioRad) and data were normalized with GeNorm software [39]. Two standard genes (Tata-box binding protein, and RNA polymerase 2 subunit). Quantitative PCR was performed on a CFX96 Real-time System (BioRad) using iQ SYBR Green supermix (BioRad). Relative mRNA levels were calculated with BioRad CFX Manager 3.1 using $\Delta\Delta C_t$ method.

Electromyographical evaluation of tail spasticity

Long lasting reflex (LLR) was determined and quantitated as previously described [16]. Briefly, tail muscle spasticity was performed with percutaneous EMG wires inserted in segmental tail muscles as described for rats [35]. Paralyzed mice were kept in a chamber during the recording with the tail free to move. During EMG recording, muscle spasms were evoked with mechanical stimulation of the tail. EMG was sampled at 5 kHz (0.2mv/1s per div). For quantification, we measured LLR signal-to noise ratio intensity by a standardized rectangle that was drawn before and after (>1s) mechanical stimulation. The signal intensity ratio relative to background was calculated using the Pixel classifier algorithm of Nikon Nis-element 3.10 SP3 software, using the intensity profile measurement function. The raw signal was obtained by deducing the noise before mechanical stimulation. 3 EMG signal recordings per animal were quantified, with n=12 animals per genotype. For signal processing only positive amplitude values were analyzed. Maximal amplitude threshold measurements were obtained from LLR signal upon mechanical stimulation. For each EMG signal recording the maximum amplitude of LLR was determined.

Statistical analysis

All data are presented as mean ± standard error of the mean. Analysis was performed using Prism6 (Graph Pad software). All difference were considered significant at $p<0.05$. For the comparison of discrete values for two groups was performed using student's T test. For the comparison of discrete values for more than two groups was performed using ordinary one-way ANOVA followed Tukey's post hoc test. For survival and disease onset analysis, animals were evaluated using Log rank (Mantel Cox) test. For repeated measurement, a repeated measure two-way ANOVA was performed to test the effect of age and the genotype (Figure).

Figures and figures legends

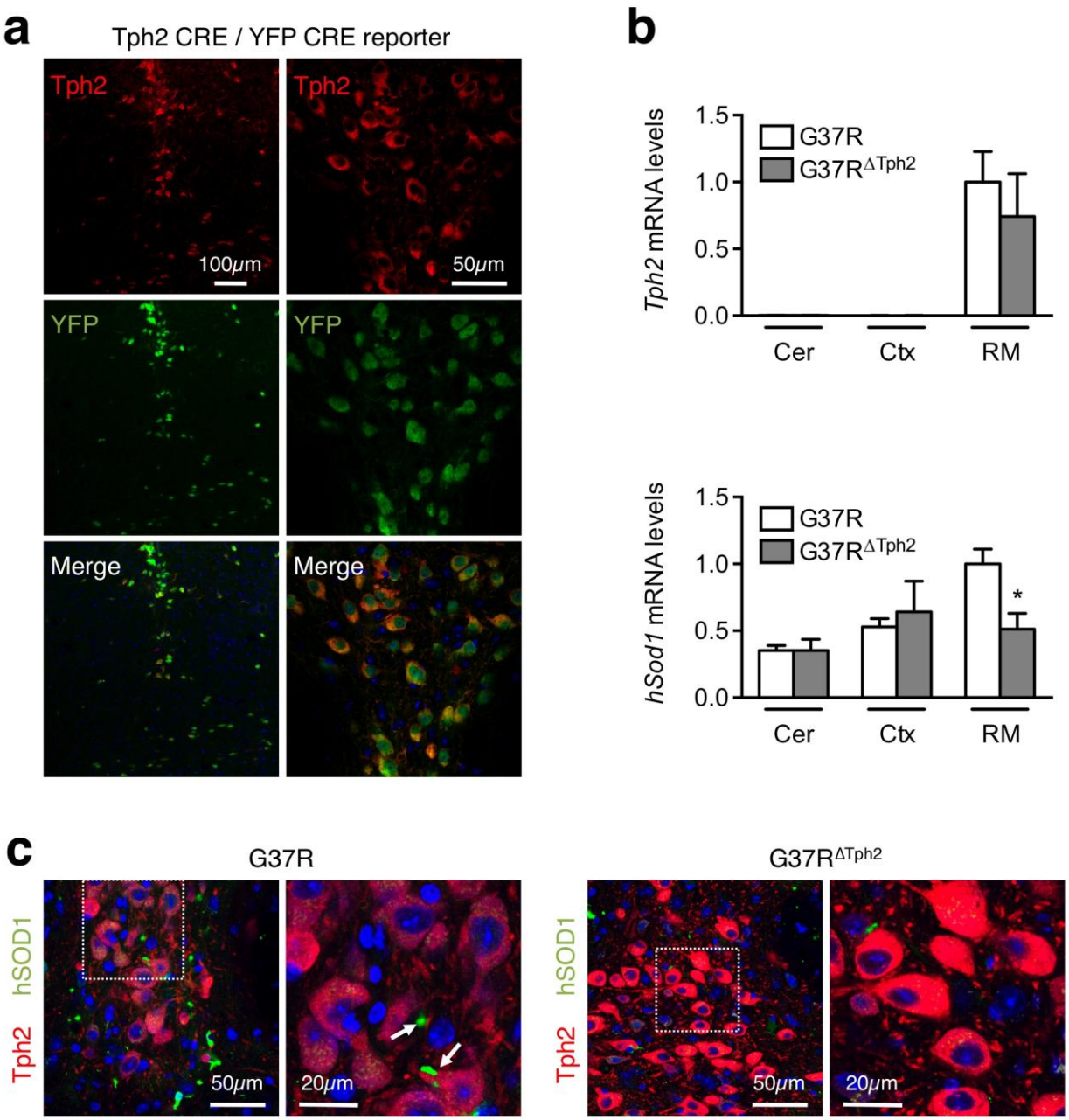

Figure 1: Efficient recombination in in adult serotoninergic neurons.
(a) Representative confocal image of serotoninergic neurons labeled with Tph2 antibody (red) and YFP (CRE reporter, green) in mice doubly transgenic for Tph2-Cre and YFP Cre reporter alleles. N=5 mice treated with Tamoxifen at 56 days of age and sacrificed one month after gavage. We observed a complete overlap between Tph2 and YFP immunoreactivities.
(b) mRNA levels of *Tph2* (upper panel) and human SOD1 (*hSOD1,* lower panel*)* in micro dissected cerebellum, cortex and raphe magnus of G37R (n=5-7) and G37R$^{\Delta Tph2}$ (n=3-6) mice one month after recombination induction. * p<0.05 Student's t test. Note that *Tph2* mRNA is only detected in raphe magnus, and *hSOD1* expression is selectively decreased in the raphe magnus of G37R$^{\Delta Tph2}$ mice
(c) Representative confocal image of Tph2 (red) and human SOD1 (green) immunoreactivities in G37R and G37R$^{\Delta Tph2}$ end stage mice. N=5 for all genotypes. Note the presence of bright hSOD1 positive aggregates (arrows) in G37R serotonergic neurons, but not in G37R$^{\Delta Tph2}$ serotonergic nuclei.

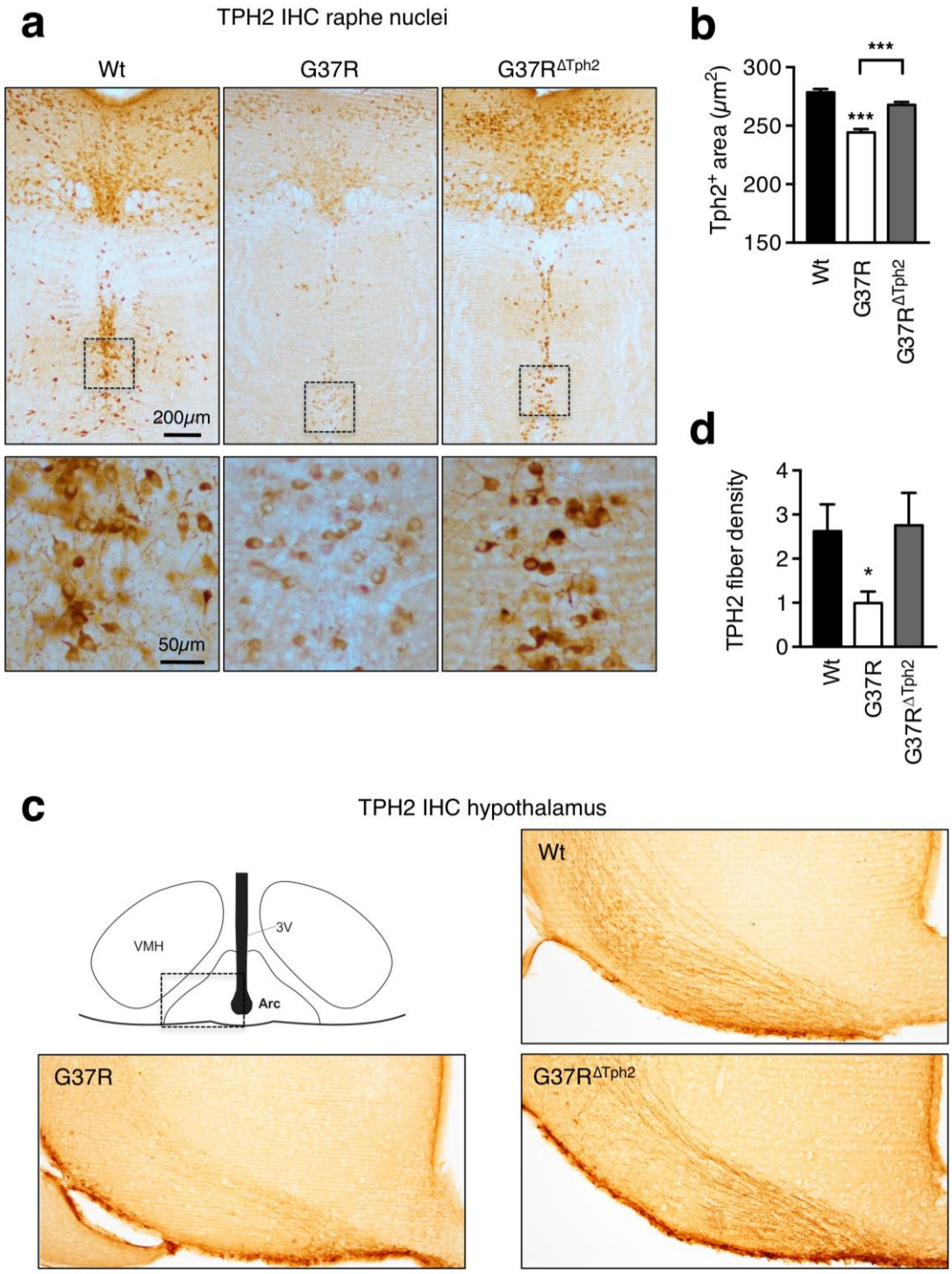

Figure 2: Serotoninergic neurons degeneration is cell autonomous in SOD1G37R mice.
(a) Representative Tph2 immunoreactivity in the brainstem (dorsal and median raphe) of Wt, G37R and G37R$^{\Delta Tph2}$ end stage mice. N=5 for all genotypes. Note that Tph2 immunoreactivity is weaker in G37R serotonergic neurons than in G37R$^{\Delta Tph2}$ serotonergic neurons.
(b) Mean area of Tph2 positive neurons in Wt (black columns), G37R (white columns) and G37R$^{\Delta Tph2}$ (grey columns) end stage mice. *** $p<0.001$ vs wild type, one way ANOVA. N=5 for all genotypes, N=4 brainstem sections/animal.
(c) Representative Tph2 immunoreactivity in the hypothalamus of of Wt, G37R and G37R$^{\Delta Tph2}$ end stage mice. A major serotonergic tract is visible in the arcuate nucleus of wild type and G37R$^{\Delta Tph2}$ mice, but almost absent in G37R mice. A scheme depicting the location of the picture is provided. *, $p<0.05$ in one way ANOVA

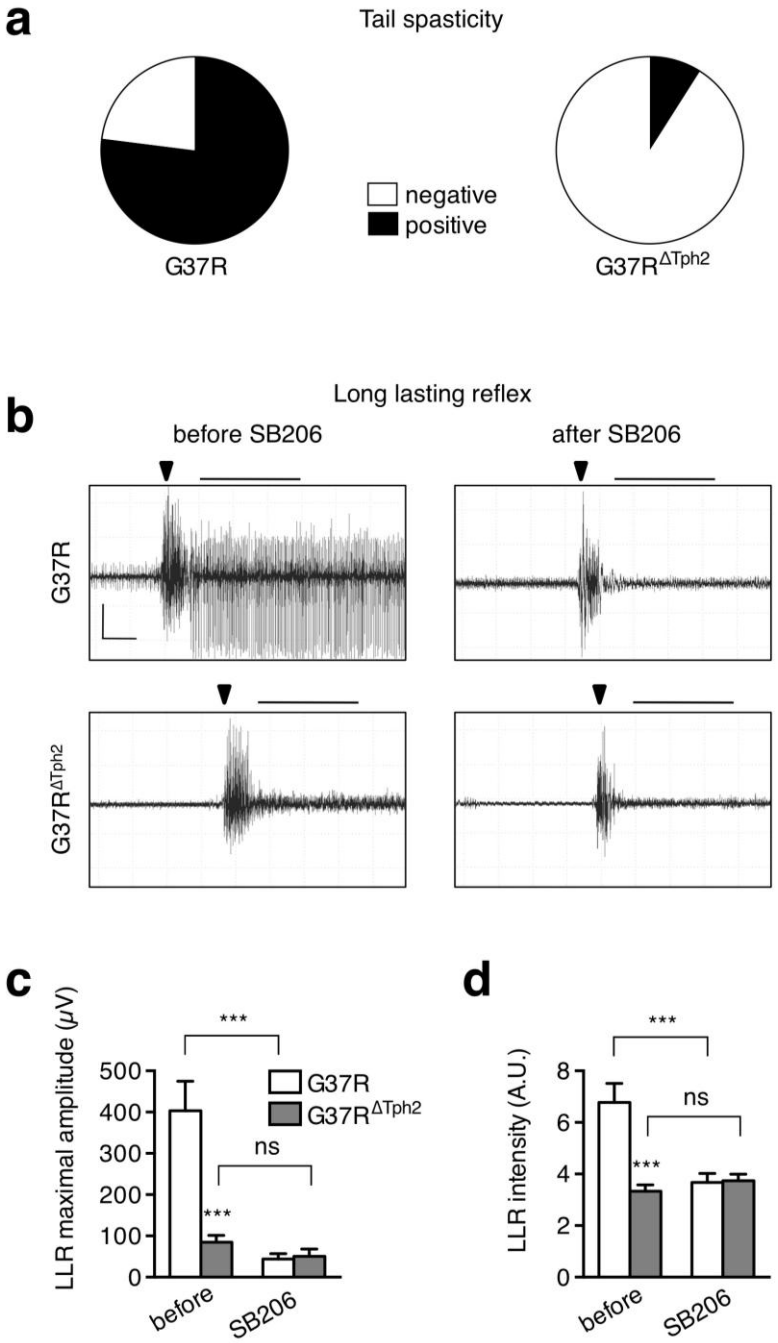

Figure 3: Rescuing serotonin neurons eliminates spasticity.

(a) Frequency of tail spasticity in G37R and G37R$^{\Delta Tph2}$ end stage mice as recorded from visual inspection.

(b) Representative recordings of long-lasting reflex (LLR) using tail EMG in G37R and G37R$^{\Delta Tph2}$ end stage mice. Recordings panel presented before and 5 minutes after SB206553 injection.

(**c-d)** Quantitative analysis of maximal LLR amplitude (μV) (c) and mean LLR signal intensity (d, A.U.) in tail EMG per animal before and 5 minutes after injection. G37R (white columns n=15); G37R$^{\Delta Tph2}$ (grey columns n=12) end stage mice. ***p<0.001 vs wild type, one way ANOVA followed by Tukey post hoc test.

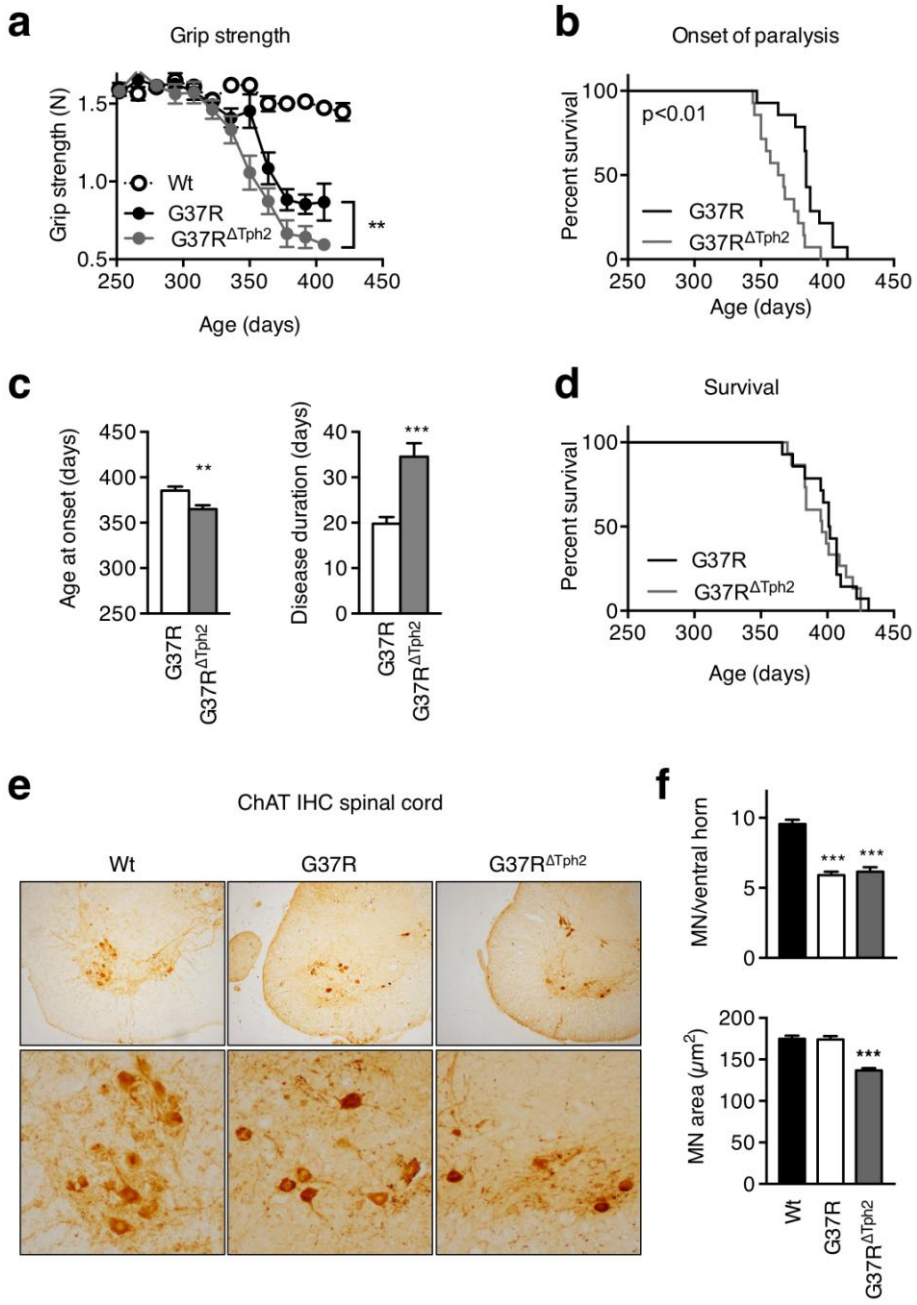

Figure 4: Rescuing serotonin neurons hastens onset of paralysis and worsens motor neuron atrophy.

(a) Muscle grip strength (Newton) curves in Wt, G37R and G37R$^{\Delta Tph2}$ mice. N=10-15 mice per genotype. **p<0.005 for genotypes between G37R and G37R$^{\Delta Tph2}$ mice, repeated two way ANOVA.

(b-d) Kaplan-Meier plot of onset of paralysis (b) and survival (d) in G37R (in black n=14) and G37R$^{\Delta Tph2}$ (in grey n=14). Representative histograms of age at disease onset (from birth to the peak of weight) and disease duration (from peak of weight to death) in G37R (white columns n=13) and G37R$^{\Delta Tph2}$ (grey columns n=11) are shown in (c). ** p<0.001, *** p<0.0001 unpaired Student's t test. Log rank test (Mantel cox) for onset of paralysis: p=0.0014; Log rank test (Mantel cox) for survival: p=0.7.

(e) Representative ChAT immunohistochemistry images in Wt, G37R and G37R$^{\Delta Tph2}$ mice. Two magnifications are shown. *N* = 5 for all genotypes.

(f) Motor neuron mean numbers and area in Wt (*black columns*), G37R (white columns) and G37R$^{\Delta Tph2}$ (grey columns) mice. ****p* < 0.001 vs wild type, One way ANOVA followed by Tukey post hoc test. *N* = 5 and 2 section per animal for all genotypes.

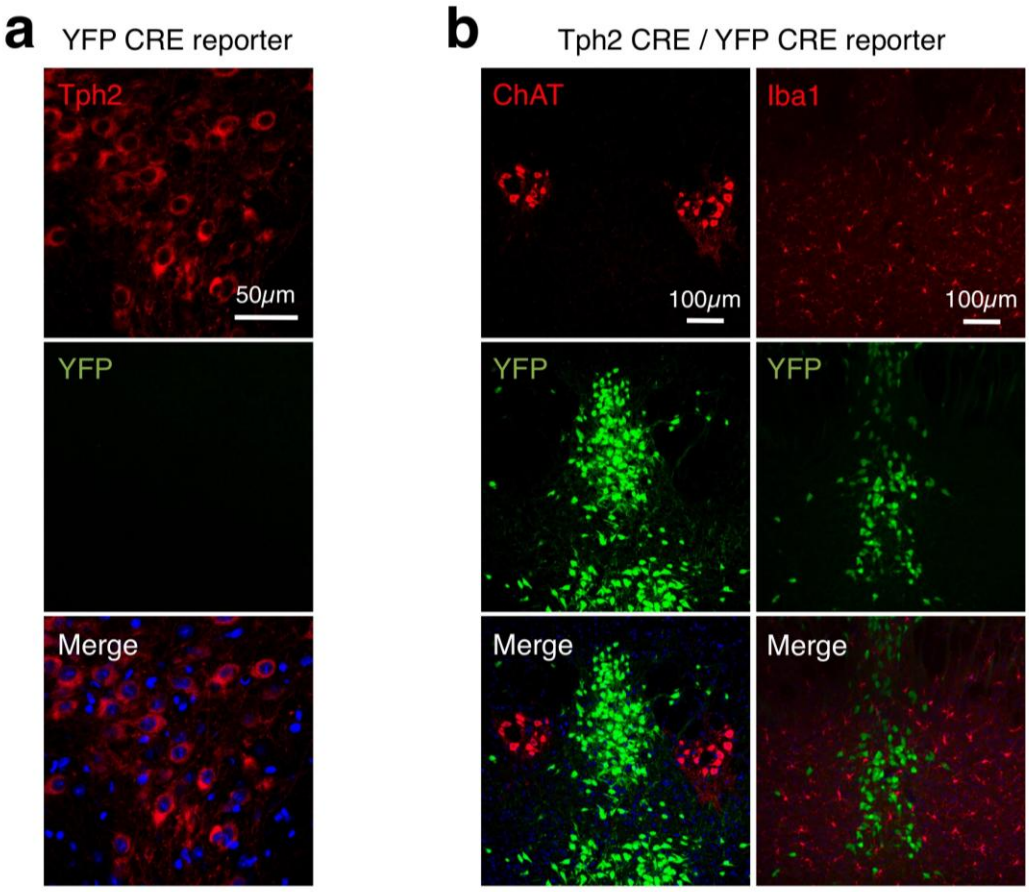

Figure S1: supplementary controls for selectivity of recombination in adult serotoninergic neurons.
(a) Representative confocal image of serotoninergic neurons labeled with Tph2 antibody (red) and YFP (CRE reporter, green) in mice single transgenic for YFP Cre reporter alleles. N=3 mice treated with Tamoxifen at 56 days of age and sacrificed one month after gavage. No leakage of YFP expression is observed
(b) Representative confocal image of cholinergic neurons labeled with Chat antibody (red, left column) or of microglia labeled with Iba1 antibody (red, right column) and YFP (CRE reporter, green) in mice doubly transgenic for Tph2-Cre and YFP Cre reporter alleles. N=5 mice treated with Tamoxifen at 56 days of age and sacrificed one month after gavage. All YFP positive cells lack ChAT or Iba1 staining.

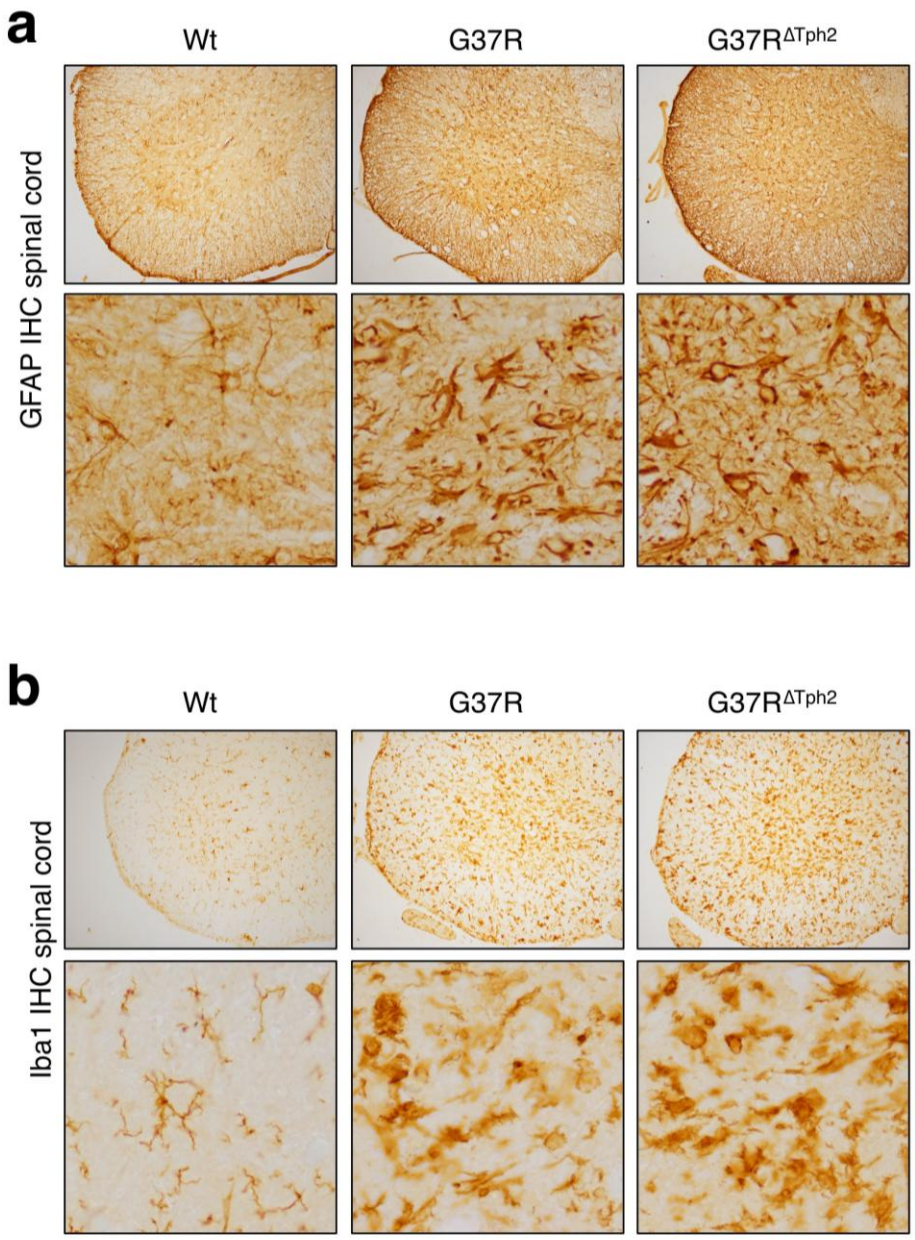

Figure S2: Rescuing serotonin neurons does not modify astrocytosis or microgliosis

(a) Representative GFAP immunohistochemistry images in Wt, G37R and G37R$^{\Delta Tph2}$ mice. Two magnifications are shown. *N* = 5 for all genotypes. Expression of human SOD1 leads to strong astrocytosis, independently of the presence of a Tph2-CRE allele.

(b) Representative Iba immunohistochemistry images in Wt, G37R and G37R$^{\Delta Tph2}$ mice. Two magnifications are shown. *N* = 5 for all genotypes. Expression of human SOD1 leads to strong microgliosis, independently of the presence of a Tph2-CRE allele.

References

1. Lance, J.W. Symposium synopsis. in *Spasticity: Disordered Motor Control* (eds Feldman, R.G., Young, R.R. & Koella, W.P.) 485-494 (Year Book Medical Publisher, Chicago, 1980).
2. Nielsen, J.B., Crone, C. & Hultborn, H. The spinal pathophysiology of spasticity--from a basic science point of view. *Acta Physiol (Oxf)* **189**, 171-80 (2007).
3. D'Amico, J.M., Condliffe, E.G., Martins, K.J., Bennett, D.J. & Gorassini, M.A. Recovery of neuronal and network excitability after spinal cord injury and implications for spasticity. *Front Integr Neurosci* **8**, 36 (2014).
4. Gorassini, M.A., Knash, M.E., Harvey, P.J., Bennett, D.J. & Yang, J.F. Role of motoneurons in the generation of muscle spasms after spinal cord injury. *Brain* **127**, 2247-58 (2004).
5. Norton, J.A., Bennett, D.J., Knash, M.E., Murray, K.C. & Gorassini, M.A. Changes in sensory-evoked synaptic activation of motoneurons after spinal cord injury in man. *Brain* **131**, 1478-91 (2008).
6. Brocard, C. *et al.* Cleavage of Na channels by calpain increases persistent Na current and promotes spasticity after spinal cord injury. *Nat Med* (2016).
7. Boulenguez, P. *et al.* Down-regulation of the potassium-chloride cotransporter KCC2 contributes to spasticity after spinal cord injury. *Nat Med* **16**, 302-7 (2010).
8. Murray, K.C. *et al.* Recovery of motoneuron and locomotor function after spinal cord injury depends on constitutive activity in 5-HT2C receptors. *Nat Med* **16**, 694-700 (2010).
9. Rank, M.M. *et al.* Adrenergic receptors modulate motoneuron excitability, sensory synaptic transmission and muscle spasms after chronic spinal cord injury. *J Neurophysiol* **105**, 410-22 (2011).
10. Murray, K.C., Stephens, M.J., Ballou, E.W., Heckman, C.J. & Bennett, D.J. Motoneuron excitability and muscle spasms are regulated by 5-HT2B and 5-HT2C receptor activity. *J Neurophysiol* **105**, 731-48 (2011).
11. D'Amico, J.M. *et al.* Constitutively active 5-HT2/alpha1 receptors facilitate muscle spasms after human spinal cord injury. *J Neurophysiol* **109**, 1473-84 (2013).
12. Fouad, K. *et al.* Locomotion after spinal cord injury depends on constitutive activity in serotonin receptors. *J Neurophysiol* **104**, 2975-84 (2010).
13. Swinnen, B. & Robberecht, W. The phenotypic variability of amyotrophic lateral sclerosis. *Nat Rev Neurol* **10**, 661-70 (2014).
14. Kiernan, M.C. *et al.* Amyotrophic lateral sclerosis. *Lancet* **377**, 942-55 (2011).
15. Lemon, R.N. Descending pathways in motor control. *Annu Rev Neurosci* **31**, 195-218 (2008).
16. Dentel, C. *et al.* Degeneration of serotonergic neurons in amyotrophic lateral sclerosis: a link to spasticity. *Brain* **136**, 483-93 (2013).
17. Boillee, S. *et al.* Onset and progression in inherited ALS determined by motor neurons and microglia. *Science* **312**, 1389-92 (2006).
18. Yamanaka, K. *et al.* Astrocytes as determinants of disease progression in inherited amyotrophic lateral sclerosis. *Nat Neurosci* **11**, 251-3 (2008).
19. Zhong, Z. *et al.* ALS-causing SOD1 mutants generate vascular changes prior to motor neuron degeneration. *Nat Neurosci* **11**, 420-2 (2008).
20. Lobsiger, C.S. *et al.* Schwann cells expressing dismutase active mutant SOD1 unexpectedly slow disease progression in ALS mice. *Proc Natl Acad Sci U S A* **106**, 4465-70 (2009).

21. Kang, S.H. *et al.* Degeneration and impaired regeneration of gray matter oligodendrocytes in amyotrophic lateral sclerosis. *Nat Neurosci* **16**, 571-9 (2013).
22. Vercruysse, P. *et al.* Alterations in the hypothalamic melanocortin pathway in amyotrophic lateral sclerosis. *Brain* **139**, 1106-22 (2016).
23. Li, Y., Li, X., Harvey, P.J. & Bennett, D.J. Effects of baclofen on spinal reflexes and persistent inward currents in motoneurons of chronic spinal rats with spasticity. *J Neurophysiol* **92**, 2694-703 (2004).
24. Boillee, S., Vande Velde, C. & Cleveland, D.W. ALS: a disease of motor neurons and their nonneuronal neighbors. *Neuron* **52**, 39-59 (2006).
25. Clement, A.M. *et al.* Wild-type nonneuronal cells extend survival of SOD1 mutant motor neurons in ALS mice. *Science* **302**, 113-7 (2003).
26. Xu, Z. *et al.* Direct conversion of human fibroblasts to induced serotonergic neurons. *Mol Psychiatry* **21**, 62-70 (2016).
27. Vadodaria, K.C. *et al.* Generation of functional human serotonergic neurons from fibroblasts. *Mol Psychiatry* **21**, 49-61 (2016).
28. Martin, E., Cazenave, W., Cattaert, D. & Branchereau, P. Embryonic alteration of motoneuronal morphology induces hyperexcitability in the mouse model of amyotrophic lateral sclerosis. *Neurobiol Dis* **54**, 116-26 (2013).
29. Amendola, J., Verrier, B., Roubertoux, P. & Durand, J. Altered sensorimotor development in a transgenic mouse model of amyotrophic lateral sclerosis. *Eur J Neurosci* **20**, 2822-6 (2004).
30. Durand, J., Amendola, J., Bories, C. & Lamotte d'Incamps, B. Early abnormalities in transgenic mouse models of amyotrophic lateral sclerosis. *J Physiol Paris* **99**, 211-20 (2006).
31. Bories, C., Amendola, J., Lamotte d'Incamps, B. & Durand, J. Early electrophysiological abnormalities in lumbar motoneurons in a transgenic mouse model of amyotrophic lateral sclerosis. *Eur J Neurosci* **25**, 451-9 (2007).
32. Puig, M.V. & Gener, T. Serotonin Modulation of Prefronto-Hippocampal Rhythms in Health and Disease. *ACS Chem Neurosci* **6**, 1017-25 (2015).
33. Challis, C. & Berton, O. Top-Down Control of Serotonin Systems by the Prefrontal Cortex: A Path toward Restored Socioemotional Function in Depression. *ACS Chem Neurosci* **6**, 1040-54 (2015).
34. Puglisi-Allegra, S. & Andolina, D. Serotonin and stress coping. *Behav Brain Res* **277**, 58-67 (2015).
35. Bennett, D.J., Sanelli, L., Cooke, C.L., Harvey, P.J. & Gorassini, M.A. Spastic long-lasting reflexes in the awake rat after sacral spinal cord injury. *J Neurophysiol* **91**, 2247-58 (2004).
36. El Oussini, H. *et al.* Serotonin 2B receptor slows disease progression and prevents degeneration of spinal cord mononuclear phagocytes in amyotrophic lateral sclerosis. *Acta Neuropathol* (2016).
37. d'Errico, P. *et al.* Selective vulnerability of spinal and cortical motor neuron subpopulations in delta7 SMA mice. *PLoS One* **8**, e82654 (2013).
38. Grider, M.H., Chen, Q. & Shine, H.D. Semi-automated quantification of axonal densities in labeled CNS tissue. *J Neurosci Methods* **155**, 172-9 (2006).
39. Vandesompele, J. *et al.* Accurate normalization of real-time quantitative RT-PCR data by geometric averaging of multiple internal control genes. *Genome Biology* **3**, research0034.1–0034.11 (2002).

Discussion

This section will be dedicated to the discussion of the project and the different results obtained. First, I will discuss the role of SOD1 toxicity in serotoninergic neurons in ALS. Then I will focus on the role of the 5-HT_{2B} receptor in ALS. Last, I will discuss the clinical perspectives of the current work and possible mechanisms triggering spasticity downstream serotonin in ALS.

Since the discovery of ALS in 1874, clinicians considered ALS as a motor disease where only upper and lower motor neurons degenerate in patients. This description is not accurate, and, indeed, the strong clinical and pathological link between ALS and FTLD demonstrates that other cell types are indeed affected in ALS.

Since 2010, a study from our team described that platelet serotonin levels were significantly decreased in ALS patients. Platelet serotonin levels did not correlate with disease duration but were positively correlated with survival of the patients (Dupuis *et al.*, 2010b). These findings indicated an alteration in serotonin in case of ALS that raised the question about what is the role of serotonin and serotoninergic neurons in ALS.

I. Role of Serotoninergic neurons in ALS

In 2013, our team described the loss of Tph2 positive neurons in raphe superior central nucleus and raphe magnus nucleus in six autopsy brains of ALS patients. Few patients showed an ubiquitinated and TDP43 pathology in serotoninergic nuclei. This loss of serotoninergic neurons was also observed in SOD1 (G86R) mice. At disease onset levels of serotonin and messenger RNA levels of serotonin specific markers were decreased. Moreover, an atrophy of Tph2 positive neurons and neurite fragmentation was observed in SOD1 (G86R) mice (Dentel, Palamiuc, Henriques, Lannes, Spreux-Varoquaux, Gutknecht, René, *et al.*, 2013). This initial study did not however demonstrate directly any pathological role for serotonergic neurons.

During my PhD we aimed to investigate the role of serotoninergic neurons loss in other ALS models, and extended our initial characterization of the G86R model to the G37R model. In this new SOD1 mouse model, we also observed atrophy of the cell body of Tph2 positive cell in the dorsal raphe, median raphe and magnus raphe in end stage mice. Importantly, serotoninergic fibers were decreased in projection regions of the brain, in the lateral hypothalamus and arcuate nuclei. More interestingly the partial rescue of SOD1 (G37R) through the deletion of SOD1 toxicity in serotoninergic neurons using our conditional models was able to rescue serotoninergic neurons atrophy in different brainstem nuclei and projection regions. This demonstrates that the observed degeneration is cell autonomous. Further investigations are required in order to study whether serotoninergic neurons are also lost in non-SOD1 based ALS models such as the $FUS^{\Delta NLS}$ recently identified ALS mice model (Scekic-Zahirovic, EMBO J, 2016).

A second important question was the description of the degeneration of serotoninergic outputs in brain and projection regions during disease progression. We asked the following questions:

What are the affected regions?

What are the kinetics of serotoninergic degeneration during different disease courses?

To answer these questions, we used a reporter mouse expressing the yellow fluorescent protein under the control of Tph2 promoter (Tph2-YFP) and crossed it with SOD1 (G86R) mouse. At disease onset we observed a significant decrease in YFP positive fibers density in the arcuate and lateral hypothalamus. The loss of serotoninergic inputs in these two regions could explain food intake and body weight alteration observed in SOD1 (G86R) mice. These data were included into the study by Vercruysse et al., that is in annex of the current manuscript (Vercruysse *et al.*, 2016). Unpublished data showed that other serotoninergic projection regions are affected by neuronal loss at disease onset. We observed decreased of YFP positive fibers in the motor cortex and hippocampus (CA1, CA3) regions. Further work is required to confirm this loss in a larger group of mice at different stage of the disease.

The loss of serotoninergic neurons in brainstem major nuclei and projection regions at least in two ALS mice models raised the question about the pathogenic consequence of this neuronal loss on disease parameters and ALS hallmarks.

The rescue of serotoninergic neurons in G37R mice using SOD1 (G37R) LoxP mice and Tph2-cre mice, expressing Cre recombinase under the control of Tph2 promoter, reverted serotoninergic neurons loss. These results indicated that the loss of serotoninergic neurons is cell autonomous in case of ALS.

Moreover the rescue did not modify astrocytes and microglia profile at the end stage of disease, suggesting that microgliosis and astrocytosis are not directly due to degeneration of serotonin neurons. On the other hand the conditional rescue affected motor neurons phenotype in end stage mice. $G37R^{\Delta Tph2}$ mice displayed similar loss in motor neurons at end stage, but motor neuron atrophy was much more pronounced compared to G37R mice. It is known that serotoninergic descending axons project through the ventral horn of spinal cord and innervate alpha and gamma motor neurons. Serotoninergic input in motor neurons modulate motor activity and locomotion (Stifani, 2014; Barreiro-Iglesias *et al.*, 2015) through 5-$HT_{2A/2B/2C}$ (Release *et al.*, 2010) and 5-HT_{1D} receptors (Enjin *et al.*, 2012). Interestingly, the rescue of serotoninergic neurons was not sufficient to rescue motor neurons death on the contrary it exaggerated the phenotype. This result raised the provocative question, that a neurodegeneration event could, contrary to what is usually perceived, be protective.

II. Serotoninergic neurons loss trigger spasticity

Spasticity is a major phenotype of upper motor neurons. The underlying mechanisms of spasticity are well established in spinal cord injury but not in case of ALS. In the previous study of Dentel and al in 2013 (Dentel, Palamiuc, Henriques, Lannes, Spreux-Varoquaux, Gutknecht, René, *et al.*, 2013) they observed tail spasticity with persistent long lasting reflex in SOD1 (G86R) end stage mice. Moreover, the administration of the inverse agonist of 5-$HT_{2B/2C}$ receptors abolished the long lasting reflex in spastic mice. These data along with previous study confirmed the implication of receptors in spasticity (Machacek *et al.*, 2001; Schmidt & Jordan, 2001; Release *et al.*, 2010; D'Amico *et al.*, 2014). More precisely the loss of serotoninergic neurons in of ALS triggers spasticity at least in SOD1 (G86R) mice.

Interestingly, in G37R mice the frequency of spasticity was significantly higher compared to $G37R^{\Delta Tph2}$ where most of mice tested did not show any spastic phenotype at the end stage. In addition the maximal amplitude of the long lasting reflex signal and its intensity were highly increased in G37R mice. These results indicate that compensatory mechanisms are set up to recover from serotoninergic neurons loss through 5-$HT_{2B/2C}$ constitute activity in lower motor neurons. Additionally, in a previous study it was shown that spasticity is associated with serotoninergic receptors denervation and loss of the ligand which increase motor neuronal and segmental reflex excitability (Schmidt & Jordan, 2001).

Spasticity can interfere with residual motor functions and induce pain yet involuntary muscle spasms can facilitate walking, standing and transfer in spastic patients. Moreover spastic patients have longer survival (Satkunam, 2003; Adams & Hicks, 2011). These previous studies correlates with what we observed in G37R mice where disease onset was delayed compared to $G37R^{\Delta Tph2}$. All these, the loss of serotoninergic neurons triggered spasticity and delaied paralysis at least in G37R mice indicating a beneficial role of serotonin loss triggering spasticity.

III. Serotoninergic neurons loss increase food intake

ALS patient witness a massive loss of weight since disease onset. This weight loss is usually due to reduced food intake, hypermetabolism (Slowie *et al.*, 1983; Kasarskis *et al.*, 1996; Desport *et al.*, 2001; Marin *et al.*, 2011) and increased energy expenditure (Dupuis *et al.*, 2011). Changes in serotonin levels are correlated with changes in food habits and food intake (Schwartz *et al.*, 2000; Morton *et al.*, 2006; Lam *et al.*, 2010). The neuronal pathways underlying the regulation of food intake are composed mainly of serotoninergic and melanocortin neuronal networks (Heisler *et al.*, 2006; Diano *et al.*, 2011).

Interestingly recent work from our team (Vercruysse *et al.*, 2016) showed that hypothalamic melanocortin system is defected in ALS patients and SOD1 (G86R) mice. SOD1 (G86R) mice showed an alteration in food intake upon fasting compared to wild type mice. The administration of fluoxetine, serotonin reuptake inhibitor, increased food intake in SOD1 (G86R) mice and reverted the alteration observed in melanocortin system genes expression levels. Moreover, there was a trend of decreased levels of serotonin in the hypothalamus of SOD1 (G86R) mice at the end stage.

These results suggested that the degeneration of serotoninergic neurons induced abnormal food intake behavior. The loss of serotoninergic neurons innervation is contributing to the melanocortin defects observed in SOD1 (G86R) mice.

In all serotoninergic neurons loss seem to have two major roles in case of ALS. First, the loss of serotoninergic neurons induce spasticity at the end stage of the disease at least in two ALS mice models, SOD1 (G86R and G37R). Second, the loss of serotonin connexions seems to participate in the observed alteration of body weight and food intake in SOD1 (G86R) mice.

IV. Serotoninergic neurons loss consequence on receptors and transduction signal

Our major results indicated that serotoninergic neurons loss modulates disease parameters along with motor neurons degeneration. Our next question was: What are the molecular and mechanistic consequences of serotoninergic neurons loss in ALS?

To address this question we used candidate strategy and focused mainly on serotonin receptors and their transduction signal parameters. The screening of serotonin receptors at different stage of the disease showed a high upregulation of 5-HT_{2B} receptor in the end stage SOD1 (G86R) mice in the brainstem and spinal cord. This upregulation was observed in G37R, TDP43 and G59S dynactin mutant mice.

The ablation of 5-HT_{2B} receptor in SOD1 (G86R) mice significantly shortened the survival. The 5-HT_{2B} -/- SOD1 (G86R) mice had lower body weight and decreased muscle strength compared to SOD1 (G86R) mice. Moreover, 5-HT_{2B} did not modify disease onset but accelerated its progression. The motor neurons atrophy in knockout mice was more prominent compared to SOD1 (G86R) mice with functional 5-HT_{2B} receptor.

These results revealed that 5-HT_{2B} upregulation was a protective response during disease progression. For this, we aimed to understand the mechanisms behind 5-HT_{2B} late upregulation in case of ALS. Interestingly, the overexpression of 5-HT_{2B} receptor was strictly limited to CD11b positive cells fractions.

5-HT_{2B} is the major serotoninergic receptor expressed in microglia and peripheral M2 macrophages (de las Casas-Engel *et al.*, 2013b; Kolodziejczak *et al.*, 2015). Moreover microgliosis present also one of the major pathological features of ALS and occurs at disease onset. Gene expression analysis of the neurinflammatory profile in 5-HT_{2B} -/- SOD1 (G86R) and 5-HT_{2B} +/+ SOD1 (G86R) end stage mice showed that the loss of 5-HT_{2B} receptor decreased expression of pro and anti-inflammatory signature genes. Our results showed the important role the receptor in maintaining normal inflammatory response.

In vitro analysis indicated a potential role of 5-HT_{2B} receptor for maintaining microglia survival. Additionally, the histological analysis of microglia in mice with

knockout receptor displayed cytorrhexia with cytoplasmic fragmented in more than 50% quantified microglia.

Interestingly, and contrary to our initial hypothesis, we observed similar upregulation of 5-HT_{2B} receptor at the end stage of the disease in both G37R and G37R$^{\Delta Tph2}$ mice. Indeed, similar microgliosis response or morphology alterations were observed in G37R and G37R$^{\Delta Tph2}$ mice. Thus 5-HT_{2B} induction is not a consequence of serotonin loss, but rather a consequence of neuroinflammation.

Up to now 5-HT_{2B} was mainly described in cardiac valvulopathy, cardiovascular system (Schmuck *et al.*, 1994; Choi & Maroteaux, 1996; Rothman *et al.*, 2000; Janssen *et al.*, 2015) and as a gene candidate in obsessive compulsive disorder (Kim *et al.*, 2000). In ALS 5-HT_{2B} seems to be a disease modifier modulating inflammatory response and microglia survival. In patients HTR2B genes polymorphisms are associated with survival. Moreover in patient with common haplotypes associated with higher HTR2B mRNA expression levels had longer survival compared to other haplotypes.

V. Potential mechanisms triggering spasticity downstream serotonin

An important question remaining open at the end of my PhD work is how the loss of serotonin neurons might lead to spasticity during ALS. Indeed, serotonin descending projection innervates motor neurons, and motor neurons persistent inward current are mainly modulated by monoamines receptors and peptides through the activation of 5-$HT_{2B/2C}$ receptors. These two receptors were found involved in both ALS and SCI induced spasticity, and it is tempting to speculate that the loss of descending serotonin leads to chronic activation of these receptors.

1. Does the loss of serotonin trigger spasticity through 5-HT$_{2B/2C}$ receptors constitutive activity in ALS?

It is known from previous studies that the activation of persistent inward currents (PICs) and pre/post-synaptic sensory transmission requires the activation of serotoninergic or noradrenergic receptors expressed on motor neurons. After spinal cord injuries and upper motor neurons loss PICs are transiently decreased, participating in initial flaccid paralysis. Upon these, compensatory mechanisms take place where PICs are simultaneously reemerging, together with constitutively active forms of 5-HT2 receptors. These lead to long lasting reflex development (Machacek *et al.*, 2001; Shay *et al.*, 2005; Cramer *et al.*, 2008; Edgerton & Roy, 2010; Release *et al.*, 2010; D'Amico *et al.*, 2014).

Indeed, in Dentel paper (Dentel, Palamiuc, Henriques, Lannes, Spreux-Varoquaux, Gutknecht, René, *et al.*, 2013) as well as in our recent results in SOD1 (G86R and G37R), we showed that inverse agonists of 5-HT$_{2B/2C}$ receptors, that bind to the receptor and block its active or inactive state, reduce mediated long lasting reflex in end stage mice. These results confirmed a possible mechanism triggering spasticity in ALS, through 5-HT$_{2B/2C}$ receptors, and opened new perspectives for the development of therapeutic strategies to manage spasticity in ALS patients.

2. Does KCC2 contribute to serotonin loss induced spasticity?

In spasticity upon spinal cord injury and neuropathic pain various studies showed an impaired potassium-chloride co-transporter-2 (KCC2) activity and expression. KCC2 is one of nine cation-chloride cotransporters encoded by SLC12 family genes. KCC2 have many function in central nervous system such as Cl^- neuronal regulation, development and the control of neuronal migration, dendritic outgrowth and formation of synaptic connections (Boulenguez *et al.*, 2010; Tanis *et al.*, 2010; Medina *et al.*, 2014; Mòdol *et al.*, 2014a; Ford *et al.*, 2015).

There are several described mechanisms of KCC2 triggering spasticity. Boulenguez and al, postulated that the loss of inhibitory tone below the lesion is

mediated by the down regulation of KCC2 in spinal cord motor neurons (Boulenguez *et al.*, 2010).

We are currently studying whether KCC2 expression and/or localization is affected by serotonin neuron degeneration. To this aim, we are currently analyzing the mRNA expression levels of KCC2 in G37R spastic and compare it to G37R$^{\Delta Tph2}$ mice. In parallel, we investigate if there is a decrease of KCC2 expression in motor neurons membranes in G37R mice at the end stage of the disease.

3. Calpain, a possible mechanism, triggering spasticity

As described in several reviews, the spasticity disturbs chloride homeostasis due to PICs reductions in motor neurons. Moreover increased $_{5\text{-HT2B/2C}}$ receptors activity induce the upregulation of Ca^{2+} PICs and the persistent sodium current (I_{NaP}) in the chronic phase after the injury. Calpain is activated by intracellular Ca^{2+} and BDNF neurotropic factor. Calpain activation leads to specific cleavage of synaptic substrate in response to intense synaptic activity. Calpain is an intracellular calcium-dependent cysteine proteases (Sorimachi *et al.*, 2011; Puskarjov *et al.*, 2012; Sorimachi & Ono, 2012; Kahle *et al.*, 2015).

Brocard et al recently demonstrated that calpain mediated cleavage of α-subunits of Na^+ channel increase long lasting reflex and the upregulation of I_{NaP} in lumbar motor neurons. Interestingly, the inhibition of calpain reduced spasticity. For these they suggest a possible mechanisms underlying spasticity saying that, activation of 5-HT2 receptor and increased I_{NaP} might regulate long lasting reflex in case of spinal cord injury (Brocard *et al.*, 2016). However, it is unknown whether this pathway is also involved in ALS spasticity. We will thus modulate pharmacologically the calpain complex and investigate the effect of calpain inhibition on long lasting reflex in case of ALS.

Conclusion

To conclude, our major results demonstrated first, that 5-HT_{2B} receptor is a disease modulator in case of ALS. Importantly, 5-HT_{2B} receptor might be an interesting target to regulate neuroinflammation and prolong survival. Moreover, *HTR2B* polymorphisms in patients and their correlation with survival opened the door for eventual clinical and pharmacological studies to target *HTR2B* genetic variations. In a second part we demonstrated that SOD1 toxicity in serotoninergic neurons trigger spasticity at least in one ALS animal model, G37R. These indicated that the degeneration of serotonin neurons is necessary to elicit spasticity in ALS. Last, serotoninergic neurons degeneration leads to melanocortin system and food intake dysfunction in SOD1 (G86R) mice. The results presented in this thesis showed how serotoninergic neurons are implicated in triggering ALS and several symptoms such as food intake, neuroinflammation and spasticity.

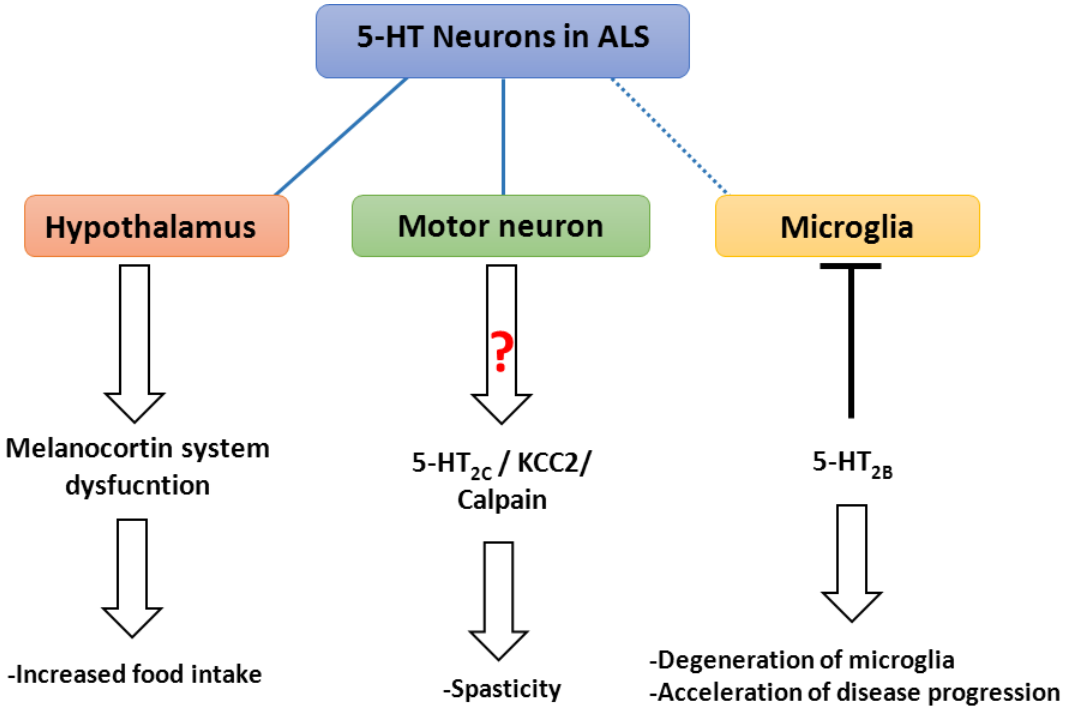

Bibliography

Adams, M.M. & Hicks, A.L. (2011) Comparison of the effects of body-weight-supported treadmill training and tilt-table standing on spasticity in individuals with chronic spinal cord injury. *J. Spinal Cord Med.*, **34**, 488–494.

Ahmad, I. & Nirogi, R. (2011) 5-HT_4 Receptor Agonists for the Treatment of Alzheimer's Dsease. *Neurosci. Med.*, **02**, 87–92.

Aitken, A.R. & Törk, I. (1988) Early development of serotonin-containing neurons and pathways as seen in wholemount preparations of the fetal rat brain. *J. Comp. Neurol.*, **274**, 32–47.

Al-Chalabi, A. & Hardiman, O. (2013) The epidemiology of ALS: a conspiracy of genes, environment and time. *Nat. Rev. Neurol.*, **9**, 617–628.

Amireault, P., Sibon, D., & Côté, F. (2013) Life without peripheral serotonin: insights from tryptophan hydroxylase 1 knockout mice reveal the existence of paracrine/autocrine serotonergic networks. *ACS Chem. Neurosci.*, **4**, 64–71.

Andersen, P.M. (2006) Amyotrophic lateral sclerosis associated with mutations in the CuZn superoxide dismutase gene. *Curr Neurol Neurosci Rep*, **6**, 37–46.

Andrade, R. & Haj-Dahmane, S. (2013) Serotonin neuron diversity in the dorsal raphe. *ACS Chem. Neurosci.*, **4**, 22–25.

Appel, S.H., Zhao, W., Beers, D.R., & Henkel, J.S. (2011) The microglial-motoneuron dialogue in ALS. *Acta Myol.*, **30**, 4–8.

Appel SH. (2005). Protective and Toxic Neuroinflammation in Amyotrophic Lateral Sclerosis. Neurotherapeutics., **12(2)**, 364-75.

ARITA, H., ICHIKAWA, K., & SAKAMOTO, M. (1995) Serotonergic cells in nucleus raphe pallidus provide tonic drive to posterior cricoarytenoid motoneurons via 5-hydroxytryptamine2 receptors in cats. *Neurosci. Lett.*, **197**, 113–116.

Arita, H., Sakamoto, M., Hirokawa, Y., & Okado, N. (1993) Serotonin innervation patterns differ among the various medullary motoneuronal groups involved in upper airway control. *Exp. brain Res.*, **95**, 100–110.

Azmitia, E.C. & Segal, M. (1978) An autoradiographic analysis of the differential ascending projections of the dorsal and median raphe nuclei in the rat. *J. Comp. Neurol.*, **179**, 641–667.

Bai, F., Yin, T., Johnstone, E.M., Su, C., Varga, G., Little, S.P., & Nelson, D.L. (2004) Molecular cloning and pharmacological characterization of the guinea pig 5-HT1E receptor. *Eur. J. Pharmacol.*, **484**, 127–139.

Baker, K.G., Halliday, G.M., Hornung, J.P., Geffen, L.B., Cotton, R.G., & Törk, I. (1991) Distribution, morphology and number of monoamine-synthesizing and substance P-containing neurons in the human dorsal raphe nucleus. *Neuroscience*, **42**, 757–

775.

Barber, S.C., Mead, R.J., & Shaw, P.J. (2006) Oxidative stress in ALS: A mechanism of neurodegeneration and a therapeutic target. *Biochim. Biophys. Acta - Mol. Basis Dis.*, **1762**, 1051–1067.

Barnes, N.M. & Sharp, T. (1999) A review of central 5-HT receptors and their function. *Neuropharmacology*, **38**, 1083–1152.

Barreiro-Iglesias, A., Mysiak, K.S., Scott, A.L., Reimer, M.M., Yang, Y., Becker, C.G., & Becker, T. (2015) Serotonin Promotes Development and Regeneration of Spinal Motor Neurons in Zebrafish. *Cell Rep.*, **13**, 924–932.

Beckman, J.S., Estévez, a G., Crow, J.P., & Barbeito, L. (2001) Superoxide dismutase and the death of motoneurons in ALS. *Trends Neurosci.*, **24**, S15–S20.

Beers, D.R., Henkel, J.S., Xiao, Q., Zhao, W., Wang, J., Yen, A. a, Siklos, L., McKercher, S.R., & Appel, S.H. (2006) Wild-type microglia extend survival in PU.1 knockout mice with familial amyotrophic lateral sclerosis. *Proc. Natl. Acad. Sci. U. S. A.*, **103**, 16021–16026.

Beghi, E., Logroscino, G., Chi, A., Hardiman, O., Mitchell, D., Swingler, R., & Traynor, B.J. (2006) The epidemiology of ALS and the role of population-based registries. *Biochim. Biophys. Acta - Mol. Basis Dis.*, **1762**, 1150–1157.

Behzadi, G., Kalén, P., Parvopassu, F., & Wiklund, L. (1990) Afferents to the median raphe nucleus of the rat: retrograde cholera toxin and wheat germ conjugated horseradish peroxidase tracing, and selective D-[3H]aspartate labelling of possible excitatory amino acid inputs. *Neuroscience*, **37**, 77–100.

Benhamú, B., Martín-Fontecha, M., Vázquez-Villa, H., Pardo, L., & López-Rodríguez, M.L. (2014) Serotonin 5-HT6 receptor antagonists for the treatment of cognitive deficiency in Alzheimer's disease. *J. Med. Chem.*, **57**, 7160–7181.

Bergemalm, D., Jonsson, P.A., Graffmo, K.S., Andersen, P.M., Brännström, T., Rehnmark, A., & Marklund, S.L. (2006) Overloading of stable and exclusion of unstable human superoxide dismutase-1 variants in mitochondria of murine amyotrophic lateral sclerosis models. *J. Neurosci.*, **26**, 4147–4154.

Berglund, E.D., Liu, C., Sohn, J.-W., Liu, T., Kim, M.H., Lee, C.E., Vianna, C.R., Williams, K.W., Xu, Y., & Elmquist, J.K. (2013) Serotonin 2C receptors in pro-opiomelanocortin neurons regulate energy and glucose homeostasis. *J. Clin. Invest.*, **123**, 5061–5070.

Bertel, O., Malessa, S., Sluga, E., & Hornykiewicz, O. (1991) Amyotrophic lateral sclerosis: changes of noradrenergic and serotonergic transmitter systems in the spinal cord. *Brain Res.*, **566**, 54–60.

Bharucha, A.E. (2000) Effects of a serotonin 5-HT4 receptor antagonist SB-207266 on gastrointestinal motor and sensory function in humans. *Gut*, **47**, 667–674.

Bhattacharyya, S., Puri, S., Miledi, R., & Panicker, M.M. (2002) Internalization and recycling of 5-HT2A receptors activated by serotonin and protein kinase C-mediated mechanisms. *Proc. Natl. Acad. Sci. U. S. A.*, **99**, 14470–14475.

Bhimani, R. & Anderson, L. (2014) Clinical Understanding of Spasticity: Implications for Practice. *Rehabil. Res. Pract.*, **2014**, 1–10.

Bjarkam, C.R., Sørensen, J.C., & Geneser, F.A. (1997) Distribution and morphology of serotonin-immunoreactive neurons in the brainstem of the New Zealand white rabbit. *J. Comp. Neurol.*, **380**, 507–519.

Blokhuis, A.M., Groen, E.J.N., Koppers, M., Van Den Berg, L.H., & Pasterkamp, R.J. (2013) Protein aggregation in amyotrophic lateral sclerosis. *Acta Neuropathol.*, **125**, 777–794.

Boche, D., Perry, V.H., & Nicoll, J.A.R. (2013) Review: Activation patterns of microglia and their identification in the human brain. *Neuropathol. Appl. Neurobiol.*, **39**, 3–18.

Boillée, S. & Cleveland, D.W. (2008) Revisiting oxidative damage in ALS: Microglia, Nox, and mutant SOD1. *J. Clin. Invest.*, **118**, 474–478.

Boillée, S., Yamanaka, K., Lobsiger, C.S., Copeland, N.G., Jenkins, N. a, Kassiotis, G., Kollias, G., & Cleveland, D.W. (2006) Onset and progression in inherited ALS determined by motor neurons and microglia. *Science*, **312**, 1389–1392.

Bonaventure, P., Aluisio, L., Shoblock, J., Boggs, J.D., Fraser, I.C., Lord, B., Lovenberg, T.W., & Galici, R. (2011) Pharmacological blockade of serotonin 5-HT_7 receptor reverses working memory deficits in rats by normalizing cortical glutamate neurotransmission. *PLoS One*, **6**, e20210.

Borchelt, D.R., Leeo, M.K., Sluntt, H.S., Guarnierit, M., Xu, Z., Wong, P.C., Brown, R.H., Price, D.L., Sisodia, S.S., & Clevelandt, D.O.N.W. (1994) Superoxide amyotrophic. *Neurobiology*, **91**, 8292–8296.

Bos, R., Sadlaoud, K., Boulenguez, P., Buttigieg, D., Liabeuf, S., Brocard, C., Haase, G., Bras, H., & Vinay, L. (2013) Activation of 5-HT2A receptors upregulates the function of the neuronal K-Cl cotransporter KCC2. *Proc. Natl. Acad. Sci. U. S. A.*, **110**, 348–353.

Boulenguez, P., Liabeuf, S., Bos, R., Bras, H., Jean-Xavier, C., Brocard, C., Stil, A., Darbon, P., Cattaert, D., Delpire, E., Marsala, M., & Vinay, L. (2010) Down-regulation of the potassium-chloride cotransporter KCC2 contributes to spasticity after spinal cord injury. *Nat. Med.*, **16**, 302–307.

Bowerman, M., Vincent, T., Scamps, F., Camu, W., & Raoul, C. (2013) The Neuroinflammation in the Physiopathology of Amyotrophic Lateral Sclerosis. *Curr. Adv. Amyotroph. Lateral Scler.*,.

Bowker, R.M. & Abbott, L.C. (1990) Quantitative re-evaluation of descending serotonergic and non-serotonergic projections from the medulla of the rodent:

evidence for extensive co-existence of serotonin and peptides in the same spinally projecting neurons, but not from the nucleus raphe ma. *Brain Res.*, **512**, 15–25.

Bowker, R.M., Westlund, K.N., Sullivan, M.C., Wilber, J.F., & Coulter, J.D. (1983) Descending serotonergic, peptidergic and cholinergic pathways from the raphe nuclei: A multiple transmitter complex. *Brain Res.*, **288**, 33–48.

Braak, H., Ludolph, A., Thal, D.R., & Del Tredici, K. (2010) Amyotrophic lateral sclerosis: dash-like accumulation of phosphorylated TDP-43 in somatodendritic and axonal compartments of somatomotor neurons of the lower brainstem and spinal cord. *Acta Neuropathol.*, **120**, 67–74.

Brocard, C., Plantier, V., Boulenguez, P., Liabeuf, S., Bouhadfane, M., Viallat-Lieutaud, A., Vinay, L., & Brocard, F. (2016) Cleavage of Na+ channels by calpain increases persistent Na+ current and promotes spasticity after spinal cord injury. *Nat. Med.*, **22**.

Brodal, A., Taber, E., & Walberg, F. (1960) The raphe nuclei of the brain stem in the cat. II. Efferent connections. *J. Comp. Neurol.*, **114**, 239–259.

Brooks BR. (1994) El Escorial World Federation of Neurology criteria for the diagnosis of amyotrophic lateral sclerosis. J.Neurol Sci., **124**, 96 – 107.

Brooks, B.R., Miller, R.G., Swash, M., & Munsat, T.L. (2000) El Escorial revisited: revised criteria for the diagnosis of amyotrophic lateral sclerosis. *Amyotroph. Lateral Scler. Other Motor Neuron Disord.*, **1**, 293–299.

Bruinstroop, E., Cano, G., Vanderhorst, V.G.J.M., Cavalcante, J.C., Wirth, J., Sena-Esteves, M., & Saper, C.B. (2012) Spinal projections of the A5, A6 (locus coeruleus), and A7 noradrenergic cell groups in rats. *J. Comp. Neurol.*, **520**, 1985–2001.

Bruinvels, A.T., Landwehrmeyer, B., Gustafson, E.L., Durkin, M.M., Mengod, G., Branchek, T.A., Hoyer, D., & Palacios, J.M. (1994) Localization of 5-HT1B, 5-HT1Dα, 5-HT1E and 5-HT1F receptor messenger RNA in rodent and primate brain. *Neuropharmacology*, **33**, 367–386.

BURGEN, A.S. V, DICKENS, F., & ZATMAN, L.J. (1949) The action of botulinum toxin on the neuro-muscular junction. *J. Physiol.*, **109**, 10–24.

Burrell, J.R., Kiernan, M.C., Vucic, S., & Hodges, J.R. (2011) Motor neuron dysfunction in frontotemporal dementia. *Brain*, **134**, 2582–2594.

Calvo, A.C., Manzano, R., Mendonça, D.M.F., Muñoz, M.J., Zaragoza, P., & Osta, R. (2014) Amyotrophic lateral sclerosis: a focus on disease progression. *Biomed Res. Int.*, **2014**, 925101.

Camilleri, M. (2010) Role of prucalopride, a serotonin (5-HT4) receptor agonist, for the treatment of chronic constipation. *Clin. Exp. Gastroenterol.*, **Volume 3**, 49.

CARLSSON, A., FALCK, B., FUXE, K., & HILLARP. (2008) Cellular localization of

monoamines in the spinal cord. *Acta Physiol. Scand.*, **60**, 112–119.

Celada, P., Puig, M., Amargós-Bosch, M., Adell, A., & Artigas, F. (2004) The therapeutic role of 5-HT1A and 5-HT2A receptors in depression. *J. Psychiatry Neurosci.*, **29**, 252–265.

Chang, E., Ghosh, N., Yanni, D., Lee, S., Alexandru, D., & Mozaffar, T. (2013) A review of spasticity treatments: Pharmacological and interventional approaches. *Crit. Rev. Phys. Rehabil. Med.*, **25**, 11–22.

Chen, D., Wang, Y., & Chin, E.R. (2015) Activation of the endoplasmic reticulum stress response in skeletal muscle of G93A*SOD1 amyotrophic lateral sclerosis mice. *Front. Cell. Neurosci.*, **9**, 170.

Chen, S., Sayana, P., Zhang, X., & Le, W. (2013) Genetics of amyotrophic lateral sclerosis: an update. *Mol. Neurodegener.*, **8**, 28.

Cherry, J.D., Olschowka, J.A., & O'Banion, M.K. (2014) Neuroinflammation and M2 microglia: the good, the bad, and the inflamed. *J. Neuroinflammation*, **11**, 98.

Chi, A., Logroscino, G., Traynor, B.J., Collins, J., Simeone, J.C., Goldstein, L.A., & White, L.A. (2013) Global epidemiology of amyotrophic lateral sclerosis: A systematic review of the published literature. *Neuroepidemiology*, **41**, 118–130.

Chiu, I.M., Morimoto, E.T.A., Goodarzi, H., Liao, J.T., O'Keeffe, S., Phatnani, H.P., Muratet, M., Carroll, M.C., Levy, S., Tavazoie, S., Myers, R.M., & Maniatis, T. (2013) A neurodegeneration-specific gene-expression signature of acutely isolated microglia from an amyotrophic lateral sclerosis mouse model. *Cell Rep.*, **4**, 385–401.

Choi, D.S. & Maroteaux, L. (1996) Immunohistochemical localisation of the serotonin 5-HT2B receptor in mouse gut, cardiovascular system, and brain. *FEBS Lett.*, **391**, 45–51.

Cirulli, E.T., Lasseigne, B.N., Petrovski, S., Sapp, P.C., Dion, P.A., Leblond, C.S., Couthouis, J., Lu, Y., Wang, Q., Krueger, B.J., Ren, Z., Keebler, J., Han, Y., Levy, S.E., Boone, B.E., Wimbish, J.R., Waite, L.L., Jones, A.L., Carulli, J.P., Day-williams, A.G., Staropoli, J.F., Xin, W.W., Chesi, A., Raphael, A.R., Mckenna-yasek, D., Cady, J., Jong, J.M.B.V. De, Kenna, K.P., Smith, B.N., Topp, S., Swarup, S., Landers, J., Baas, F., Allen, A.S., Bedlack, R.S., Harper, J.W., Gitler, A.D., Rouleau, G.A., Brown, R., Harms, M.B., Cooper, G.M., Harris, T., Myers, R.M., & Goldstein, D.B. (2015) Exome sequencing in amyotrophic lateral sclerosis identifies risk genes and Pathways. *Science*, **347**, 1436.

Clark, M.S. & Neumaier, J.F. (2001) The 5-HT1B receptor: behavioral implications. *Psychopharmacol. Bull.*, **35**, 170–185.

Cleveland, D.W. & Rothstein, J.D. (2001) From Charcot to Lou Gehrig: deciphering selective motor neuron death in ALS. *Nat. Rev. Neurosci.*, **2**, 806–819.

Crain, J.M., Nikodemova, M., & Watters, J.J. (2013) Microglia express distinct M1 and

M2 phenotypic markers in the postnatal and adult central nervous system in male and female mice. *J. Neurosci. Res.*, **91**, 1143–1151.

Cramer, S.W., Baggott, C., Cain, J., Tilghman, J., Allcock, B., Miranpuri, G., Rajpal, S., Sun, D., & Resnick, D. (2008) The role of cation-dependent chloride transporters in neuropathic pain following spinal cord injury. *Mol. Pain*, **4**, 36.

D'Amico, J.M., Condliffe, E.G., Martins, K.J.B., Bennett, D.J., & Gorassini, M.A. (2014) Recovery of neuronal and network excitability after spinal cord injury and implications for spasticity. *Front. Integr. Neurosci.*, **8**, 36.

DAHLSTROEM, A. & FUXE, K. (1964) Evidence for the existence of monoamine-containing neurons in the central nervous system. i. demonstration of monoamines in the cell bodies of brain stem neurons. *Acta Physiol. Scand. Suppl.*, SUPPL 232:1–55.

Dahlström, A. & Fuxe, K. (1964) Localization of monoamines in the lower brain stem. *Experientia*, **20**, 398–399.

Dale, J.M. & Garcia, M.L. (2012) Neurofilament Phosphorylation during Development and Disease: Which Came First, the Phosphorylation or the Accumulation? *J. Amino Acids*, **2012**, 382107.

de Carvalho, M., Eisen, A., Krieger, C., & Swash, M. (2014) Motoneuron firing in amyotrophic lateral sclerosis (ALS). *Front. Hum. Neurosci.*, **8**, 719.

de las Casas-Engel, M., Domínguez-Soto, A., Sierra-Filardi, E., Bragado, R., Nieto, C., Puig-Kroger, A., Samaniego, R., Loza, M., Corcuera, M.T., Gómez-Aguado, F., Bustos, M., Sánchez-Mateos, P., & Corbí, A.L. (2013) Serotonin skews human macrophage polarization through HTR2B and HTR7. *J. Immunol.*, **190**, 2301–2310.

De Maeyer, J.H., Lefebvre, R.A., & Schuurkes, J.A.J. (2008) 5-HT4 receptor agonists: similar but not the same. *Neurogastroenterol. Motil.*, **20**, 99–112.

De Vry, J. (1995) 5-HT1A receptor agonists: recent developments and controversial issues. *Psychopharmacology (Berl).*, **121**, 1–26.

DeFazio, R.A., Keros, S., Quick, M.W., & Hablitz, J.J. (2000) Potassium-Coupled Chloride Cotransport Controls Intracellular Chloride in Rat Neocortical Pyramidal Neurons. *J. Neurosci.*, **20**, 8069–8076.

DeJesus-Hernandez, M., Mackenzie, I.R., Boeve, B.F., Boxer, A.L., Baker, M., Rutherford, N.J., Nicholson, A.M., Finch, N.A., Flynn, H., Adamson, J., Kouri, N., Wojtas, A., Sengdy, P., Hsiung, G.-Y.R., Karydas, A., Seeley, W.W., Josephs, K.A., Coppola, G., Geschwind, D.H., Wszolek, Z.K., Feldman, H., Knopman, D.S., Petersen, R.C., Miller, B.L., Dickson, D.W., Boylan, K.B., Graff-Radford, N.R., & Rademakers, R. (2011) Expanded GGGGCC hexanucleotide repeat in noncoding region of C9ORF72 causes chromosome 9p-linked FTD and ALS. *Neuron*, **72**, 245–256.

Deng, H., Gao, K., & Jankovic, J. (2014) The role of FUS gene variants in

neurodegenerative diseases. *Nat. Rev. Neurol.*, **10**, 337–348.

Deng, H., Hentati, A., Tainer, J., & Iqbal, Z. (1993) Amyotrophic lateral sclerosis and structural defects in Cu, Zn superoxide dismutase. *Science (80-.).*,.

Dengler, R. (2010) Diagnostic Criteria of Amyotrophic Lateral Sclerosis (ALS). *Rom. J. Neurol.*, **9**, 165–171.

Dentel, C., Palamiuc, L., Henriques, A., Lannes, B., Spreux-Varoquaux, O., Gutknecht, L., René, F., Echaniz-Laguna, A., Gonzalez de Aguilar, J.-L., Lesch, K.P., Meininger, V., Loeffler, J.-P., & Dupuis, L. (2013) Degeneration of serotonergic neurons in amyotrophic lateral sclerosis: a link to spasticity. *Brain*, **136**, 483–493.

Desport, J.C., Preux, P.M., Magy, L., Boirie, Y., Vallat, J.M., Beaufrère, B., & Couratier, P. (2001) Factors correlated with hypermetabolism in patients with amyotrophic lateral sclerosis. *Am. J. Clin. Nutr.*, **74**, 328–334.

Diano, S., Liu, Z.-W., Jeong, J.K., Dietrich, M.O., Ruan, H.-B., Kim, E., Suyama, S., Kelly, K., Gyengesi, E., Arbiser, J.L., Belsham, D.D., Sarruf, D.A., Schwartz, M.W., Bennett, A.M., Shanabrough, M., Mobbs, C. V, Yang, X., Gao, X.-B., & Horvath, T.L. (2011) Peroxisome proliferation-associated control of reactive oxygen species sets melanocortin tone and feeding in diet-induced obesity. *Nat. Med.*, **17**, 1121–1127.

Diaz, S.L., Doly, S., Narboux-Nême, N., Fernández, S., Mazot, P., Banas, S.M., Boutourlinsky, K., Moutkine, I., Belmer, A., Roumier, A., & Maroteaux, L. (2012) 5-HT(2B) receptors are required for serotonin-selective antidepressant actions. *Mol. Psychiatry*, **17**, 154–163.

Diaz, S.L. & Maroteaux, L. (2011) Implication of 5-HT(2B) receptors in the serotonin syndrome. *Neuropharmacology*, **61**, 495–502.

Diaz, S.L., Narboux-Nême, N., Boutourlinsky, K., Doly, S., & Maroteaux, L. (2016) Mice lacking the serotonin 5-HT2B receptor as an animal model of resistance to selective serotonin reuptake inhibitors antidepressants. *Eur. Neuropsychopharmacol.*, **26**, 265–279.

Diaz-Amarilla, P., Olivera-Bravo, S., Trias, E., Cragnolini, a., Martinez-Palma, L., Cassina, P., Beckman, J., & Barbeito, L. (2011) From the Cover: Phenotypically aberrant astrocytes that promote motoneuron damage in a model of inherited amyotrophic lateral sclerosis. *Proc. Natl. Acad. Sci.*, **108**, 18126–18131.

Doly, S., Valjent, E., Setola, V., Callebert, J., Hervé, D., Launay, J.-M., & Maroteaux, L. (2008) Serotonin 5-HT2B receptors are required for 3,4-methylenedioxymethamphetamine-induced hyperlocomotion and 5-HT release in vivo and in vitro. *J. Neurosci.*, **28**, 2933–2940.

Dormann, D. & Haass, C. (2013) Fused in sarcoma (FUS): An oncogene goes awry in neurodegeneration. *Mol. Cell. Neurosci.*, **56**, 475–486.

Dupuis, L., Pradat, P.-F., Ludolph, A.C., & Loeffler, J.-P. (2011) Energy metabolism in

amyotrophic lateral sclerosis. *Lancet. Neurol.*, **10**, 75–82.

Dupuis, L., Spreux-Varoquaux, O., Bensimon, G., Jullien, P., Lacomblez, L., Salachas, F., Bruneteau, G., Pradat, P.F., Loeffler, J.P., & Meininger, V. (2010) Platelet serotonin level predicts survival in amyotrophic lateral sclerosis. *PLoS One*, **5**, 6–10.

Edgerton, V.R. & Roy, R.R. (2010) Spasticity: a switch from inhibition to excitation. *Nat. Med.*, **16**, 270–271.

Elbasiouny, S.M., Moroz, D., Bakr, M.M., & Mushahwar, V.K. (2009) Management of Spasticity After Spinal Cord Injury: Current Techniques and Future Directions. *Neurorehabil. Neural Repair*, **24**, 23–33.

Ellis, K.O. & Carpenter, J.F. (1974) Mechanism of control of skeletal-muscle contraction by dantrolene sodium. *Arch. Phys. Med. Rehabil.*, **55**, 362–369.

Enjin, A., Leão, K.E., Mikulovic, S., Le Merre, P., Tourtellotte, W.G., & Kullander, K. (2012) Sensorimotor function is modulated by the serotonin receptor 1d, a novel marker for gamma motor neurons. *Mol. Cell. Neurosci.*, **49**, 322–332.

Farrer, M.J., Hulihan, M.M., Kachergus, J.M., Dächsel, J.C., Stoessl, A.J., Grantier, L.L., Calne, S., Calne, D.B., Lechevalier, B., Chapon, F., Tsuboi, Y., Yamada, T., Gutmann, L., Elibol, B., Bhatia, K.P., Wider, C., Vilariño-Güell, C., Ross, O.A., Brown, L.A., Castanedes-Casey, M., Dickson, D.W., & Wszolek, Z.K. (2009) DCTN1 mutations in Perry syndrome. *Nat. Genet.*, **41**, 163–165.

Felten, D.L. & Sladek, J.R. (1983) Monoamine distribution in primate brain V. Monoaminergic nuclei: anatomy, pathways and local organization. *Brain Res. Bull.*, **10**, 171–284.

Ferraiuolo, L., Kirby, J., Grierson, A.J., Sendtner, M., & Shaw, P.J. (2011) Molecular pathways of motor neuron injury in amyotrophic lateral sclerosis. *Nat. Rev. Neurol.*, **7**, 616–630.

Ford, A., Castonguay, A., Cottet, M., Little, J.W., Chen, Z., Symons-Liguori, A.M., Doyle, T., Egan, T.M., Vanderah, T.W., De Konnick, Y., Tosh, D.K., Jacobson, K.A., & Salvemini, D. (2015) Engagement of the GABA to KCC2 signaling pathway contributes to the analgesic effects of A3AR agonists in neuropathic pain. *J. Neurosci.*, **35**, 6057–6067.

Forrest, V., Ince, P., Leitch, M., Marshall, E.F., & Shaw, P.J. (1996) Serotonergic neurotransmission in the spinal cord and motor cortex of patients with motor neuron disease and controls: quantitative autoradiography for 5-HT1a and 5-HT2 receptors. *J. Neurol. Sci.*, **139**, 83–90.

Frakes, A.E., Ferraiuolo, L., Haidet-phillips, A.M., Schmelzer, L., Braun, L., Miranda, C.J., Ladner, K.J., Bevan, A.K., Kevin, D., Godbout, J.P., Popovich, P.G., Guttridge, D.C., & Brian, K. (2015) Pathway in Amyotrophic Lateral Sclerosis **81**, 1009–1023.

Freischmidt, A., Wieland, T., Richter, B., Ruf, W., Schaeffer, V., Müller, K., Marroquin, N., Nordin, F., Hübers, A., Weydt, P., Pinto, S., Press, R., Millecamps, S., Molko, N.,

Bernard, E., Desnuelle, C., Soriani, M.-H., Dorst, J., Graf, E., Nordström, U., Feiler, M.S., Putz, S., Boeckers, T.M., Meyer, T., Winkler, A.S., Winkelman, J., de Carvalho, M., Thal, D.R., Otto, M., Brännström, T., Volk, A.E., Kursula, P., Danzer, K.M., Lichtner, P., Dikic, I., Meitinger, T., Ludolph, A.C., Strom, T.M., Andersen, P.M., & Weishaupt, J.H. (2015) Haploinsufficiency of TBK1 causes familial ALS and fronto-temporal dementia. *Nat. Neurosci.*, **18**, 631–636.

Fuchs, A., Ringer, C., Bilkei-Gorzo, A., Weihe, E., Roeper, J., & Schütz, B. (2010) Downregulation of the potassium chloride cotransporter KCC2 in vulnerable motoneurons in the SOD1-G93A mouse model of amyotrophic lateral sclerosis. *J. Neuropathol. Exp. Neurol.*, **69**, 1057–1070.

Gal, J., Strom, A.L., Kilty, R., Zhang, F., & Zhu, H. (2007) P62 Accumulates and Enhances Aggregate Formation in Model Systems of Familial Amyotrophic Lateral Sclerosis. *J. Biol. Chem.*, **282**, 11068–11077.

Gertz, B., Wong, M., & Martin, L.J. (2012) Nuclear Localization of Human Superoxide Dismutase 1 (SOD1) and Mutant SOD1-Specific Disruption of Survival Motor Neuron Protein Complex in Transgenic Amyotrophic Lateral Sclerosis Mice. *J Neuropathol Exp Neurol*, **71**, 162–177.

Gerardo A. (2009). Axonal Transport Defects in Neurodegenerative Diseases. The Journal of Neuroscience., **29(41)**, 12776 –12786.

Goadsby, P.J. & Classey, J.D. (2003) Evidence for serotonin (5-HT)1B, 5-HT1D and 5-HT1F receptor inhibitory effects on trigeminal neurons with craniovascular input. *Neuroscience*, **122**, 491–498.

Gomez Perdiguero, E., Klapproth, K., Schulz, C., Busch, K., Azzoni, E., Crozet, L., Garner, H., Trouillet, C., de Bruijn, M.F., Geissmann, F., & Rodewald, H.-R. (2014) Tissue-resident macrophages originate from yolk-sac-derived erythro-myeloid progenitors. *Nature*, **518**, 547–551.

Graeber, M.B. & Streit, W.J. (2010) Microglia: Biology and pathology. *Acta Neuropathol.*, **119**, 89–105.

Gurney, M.E., Pu, H., Chiu, A.Y., Dal Canto, M.C., Polchow, C.Y., Alexander, D.D., Caliendo, J., Hentati, A., Kwon, Y.W., & Deng, H.X. (1994) Motor neuron degeneration in mice that express a human Cu,Zn superoxide dismutase mutation. *Science*, **264**, 1772–1775.

Halliday, G.M. & Törk, I. (1986) Comparative anatomy of the ventromedial mesencephalic tegmentum in the rat, cat, monkey and human. *J. Comp. Neurol.*, **252**, 423–445.

Han, S.M., El Oussini, H., Scekic-Zahirovic, J., Vibbert, J., Cottee, P., Prasain, J.K., Bellen, H.J., Dupuis, L., & Miller, M. a (2013) VAPB/ALS8 MSP ligands regulate striated muscle energy metabolism critical for adult survival in caenorhabditis elegans. *PLoS Genet.*, **9**, e1003738.

Harrison, M., O'Brien, A., Adams, L., Cowin, G., Ruitenberg, M.J., Sengul, G., & Watson, C. (2013) Vertebral landmarks for the identification of spinal cord segments in the mouse. *Neuroimage*, **68**, 22–29.

Hedlund, P.B. (2009) The 5-HT7 receptor and disorders of the nervous system: an overview. *Psychopharmacology (Berl).*, **206**, 345–354.

Hegde, S.S. & Eglen, R.M. (1996) Peripheral 5-HT4 receptors. *FASEB J.*, **10**, 1398–1407.

Heisler, L.K., Jobst, E.E., Sutton, G.M., Zhou, L., Borok, E., Thornton-Jones, Z., Liu, H.Y., Zigman, J.M., Balthasar, N., Kishi, T., Lee, C.E., Aschkenasi, C.J., Zhang, C.-Y., Yu, J., Boss, O., Mountjoy, K.G., Clifton, P.G., Lowell, B.B., Friedman, J.M., Horvath, T., Butler, A.A., Elmquist, J.K., & Cowley, M.A. (2006) Serotonin reciprocally regulates melanocortin neurons to modulate food intake. *Neuron*, **51**, 239–249.

Heneka, M.T., Kummer, M.P., & Latz, E. (2014) Innate immune activation in neurodegenerative disease. *Nat. Rev. Immunol.*, **14**, 463–477.

Heppner, F.L., Ransohoff, R.M., & Becher, B. (2015) Immune attack: the role of inflammation in Alzheimer disease. *Nat Rev Neurosci*, **16**, 358–372.

Hodges, J.R., Davies, R., Xuereb, J., Kril, J., & Halliday, G. (2003) Survival in frontotemporal dementia. *Neurology*, **61**, 349–354.

Hökfelt, T., Ljungdahl, A., Steinbusch, H., Verhofstad, A., Nilsson, G., Brodin, E., Pernow, B., & Goldstein, M. (1978) Immunohistochemical evidence of substance P-like immunoreactivity in some 5-hydroxytryptamine-containing neurons in the rat central nervous system. *Neuroscience*, **3**, 517–538.

Holstege, J.C. & Kuypers, H.G.J.M. (1987) Brainstem projections to spinal motoneurons: An update. *Neuroscience*, **23**, 809–821.

Hoyer, D., Hannon, J.P., & Martin, G.R. (2002) Molecular, pharmacological and functional diversity of 5-HT receptors. *Pharmacol. Biochem. Behav.*, **71**, 533–554.

Hoyer, D., Schoeffter, P., Waeber, C., & Palacios, J.M. (1990) Serotonin 5-HT1D receptors. *Ann. N. Y. Acad. Sci.*, **600**, 168–181; discussion 181–182.

Hu, X., Li, P., Guo, Y., Wang, H., Leak, R.K., Chen, S., Gao, Y., & Chen, J. (2012) Microglia/macrophage polarization dynamics reveal novel mechanism of injury expansion after focal cerebral ischemia. *Stroke*, **43**, 3063–3070.

Imai, H., Steindler, D.A., & Kitai, S.T. (1986) The organization of divergent axonal projections from the midbrain raphe nuclei in the rat. *J. Comp. Neurol.*, **243**, 363–380.

Ingre, C., Roos, P.M., Piehl, F., Kamel, F., & Fang, F. (2015) Risk factors for amyotrophic lateral sclerosis. *Clin. Epidemiol.*, **7**, 181–193.

Iwamoto, K., Bundo, M., Kasai, K., & Kato, T. (2011) Measuring RNA editing of serotonin 2C receptor. *Biochem Biophys Res Commun*, **76**, 912–914.

Janssen, W., Schymura, Y., Novoyatleva, T., Kojonazarov, B., Boehm, M., Wietelmann, A., Luitel, H., Murmann, K., Krompiec, D.R., Tretyn, A., Pullamsetti, S.S., Weissmann, N., Seeger, W., Ghofrani, H.A., & Schermuly, R.T. (2015) 5-HT2B receptor antagonists inhibit fibrosis and protect from RV heart failure. *Biomed Res. Int.*, **2015**, 1–9.

Jelsone-Swain, L., Persad, C., Votruba, K.L., Weisenbach, S.L., Johnson, T., Gruis, K.L., & Welsh, R.C. (2012) The Relationship between Depressive Symptoms, Disease State, and Cognition in Amyotrophic Lateral Sclerosis. *Front. Psychol.*, **3**, 542.

Jones, S.L. & Light, A.R. (1992) Serotoninergic medullary raphespinal projection to the lumbar spinal cord in the rat: a retrograde immunohistochemical study. *J. Comp. Neurol.*, **322**, 599–610.

Julien, J.P.A role for neurofilaments in the pathogenesis of amyotrophic lateral sclerosis. *Biochem (2001). Cell Biol.*, **73**, 593–597.

Julien, J.-P. (2001) Amyotrophic Lateral Sclerosis. *Cell*, **104**, 581–591.

Kabashi, E., El Oussini, H., Bercier, V., Gros-Louis, F., Valdmanis, P.N., McDearmid, J., Mejier, I.A., Dion, P.A., Dupre, N., Hollinger, D., Sinniger, J., Dirrig-Grosch, S., Camu, W., Meininger, V., Loeffler, J.-P., Rene, F., Drapeau, P., Rouleau, G.A., & Dupuis, L. (2013) Investigating the contribution of VAPB/ALS8 loss of function in amyotrophic lateral sclerosis. *Hum. Mol. Genet.*, **22**, 2350–2360.

Kaplan, A., Spiller, K.J., Towne, C., Kanning, K.C., Choe, G.T., Geber, A., Akay, T., Aebischer, P., & Henderson, C.E. (2014) Neuronal matrix metalloproteinase-9 is a determinant of selective neurodegeneration. *Neuron*, **81**, 333–348.

Kasarskis, E.J., Berryman, S., Vanderleest, J.G., Schneider, A.R., & McClain, C.J. (1996) Nutritional status of patients with amyotrophic lateral sclerosis: relation to the proximity of death. *Am. J. Clin. Nutr.*, **63**, 130–137.

Katz, R. (1999) Presynaptic inhibition in humans: A comparison between normal and spastic patients. *J. Physiol.*, **93**, 379–385.

Kazakov, V.N., Kravtsov PYa, Krakhotkina, E.D., & Maisky, V.A. (1993) Sources of cortical, hypothalamic and spinal serotonergic projections: topical organization within the nucleus raphe dorsalis. *Neuroscience*, **56**, 157–164.

Kim, S.J., Veenstra-VanderWeele, J., Hanna, G.L., Gonen, D., Leventhal, B.L., & Cook, E.H. (2000) Mutation screening of human 5-HT2B receptor gene in early-onset obsessive-compulsive disorder. *Mol. Cell. Probes*, **14**, 47–52.

Kitzman, P. (2005) Alteration in axial motoneuronal morphology in the spinal cord injured spastic rat. *Exp. Neurol.*, **192**, 100–108.

Klein, M.T., Dukat, M., Glennon, R.A., & Teitler, M. (2011) Toward selective drug development for the human 5-hydroxytryptamine 1E receptor: a comparison of 5-hydroxytryptamine 1E and 1F receptor structure-affinity relationships. *J. Pharmacol. Exp. Ther.*, **337**, 860–867.

Klein, M.T. & Teitler, M. (2012) Distribution of 5-ht(1E) receptors in the mammalian brain and cerebral vasculature: an immunohistochemical and pharmacological study. *Br. J. Pharmacol.*, **166**, 1290–1302.

Köhler, C., Chan-Palay, V., & Steinbusch, H. (1982) The distribution and origin of serotonin-containing fibers in the septal area: a combined immunohistochemical and fluorescent retrograde tracing study in the rat. *J. Comp. Neurol.*, **209**, 91–111.

Köhler, C. & Steinbusch, H. (1982) Identification of serotonin and non-serotonin-containing neurons of the mid-brain raphe projecting to the entorhinal area and the hippocampal formation. A combined immunohistochemical and fluorescent retrograde tracing study in the rat brain. *Neuroscience*, **7**, 951–975.

Kolodziejczak, M., Béchade, C., Gervasi, N., Irinopoulou, T., Banas, S.M., Cordier, C., Rebsam, A., Roumier, A., & Maroteaux, L. (2015) Serotonin Modulates Developmental Microglia via 5-HT2B Receptors: Potential Implication during Synaptic Refinement of Retinogeniculate Projections. *ACS Chem. Neurosci.*, **6**, 1219–1230.

Kriegstein, A. & Alvarez-buylla, A. (2011) The Glial Nature of Embryonic and Adult Neural Stem Cells. *Annu. Rev. Neurosci.*, 149–184.

Kwiatkowski, T.J., Bosco, D.A., Leclerc, A.L., Tamrazian, E., Vanderburg, C.R., Russ, C., Davis, A., Gilchrist, J., Kasarskis, E.J., Munsat, T., Valdmanis, P., Rouleau, G.A., Hosler, B.A., Cortelli, P., de Jong, P.J., Yoshinaga, Y., Haines, J.L., Pericak-Vance, M.A., Yan, J., Ticozzi, N., Siddique, T., McKenna-Yasek, D., Sapp, P.C., Horvitz, H.R., Landers, J.E., & Brown, R.H. (2009) Mutations in the FUS/TLS gene on chromosome 16 cause familial amyotrophic lateral sclerosis. *Science*, **323**, 1205–1208.

Lagier-Tourenne, C., Polymenidou, M., & Cleveland, D.W. (2010) TDP-43 and FUS/TLS: emerging roles in RNA processing and neurodegeneration. *Hum. Mol. Genet.*, **19**, R46–R64.

Lagier-Tourenne, C., Polymenidou, M., Hutt, K.R., Vu, A.Q., Baughn, M., Huelga, S.C., Clutario, K.M., Ling, S.-C., Liang, T.Y., Mazur, C., Wancewicz, E., Kim, A.S., Watt, A., Freier, S., Hicks, G.G., Donohue, J.P., Shiue, L., Bennett, C.F., Ravits, J., Cleveland, D.W., & Yeo, G.W. (2012) Divergent roles of ALS-linked proteins FUS/TLS and TDP-43 intersect in processing long pre-mRNAs. *Nat. Neurosci.*, **15**, 1488–1497.

Lam, D.D., Garfield, A.S., Marston, O.J., Shaw, J., & Heisler, L.K. (2010) Brain serotonin system in the coordination of food intake and body weight. *Pharmacol. Biochem. Behav.*, **97**, 84–91.

Lam, D.D., Przydzial, M.J., Ridley, S.H., Yeo, G.S.H., Rochford, J.J., O'Rahilly, S., & Heisler, L.K. (2008) Serotonin 5-HT2C receptor agonist promotes hypophagia via downstream activation of melanocortin 4 receptors. *Endocrinology*, **149**, 1323–1328.

Lance, J.W. (1980) The control of muscle tone, reflexes, and movement: Robert

Wartenberg Lecture. *Neurology*, **30**, 1303–1313.

Launay, J.-M., Hervé, P., Callebert, J., Mallat, Z., Collet, C., Doly, S., Belmer, A., Diaz, S.L., Hatia, S., Côté, F., Humbert, M., & Maroteaux, L. (2012) Serotonin 5-HT2B receptors are required for bone-marrow contribution to pulmonary arterial hypertension. *Blood*, **119**, 1772–1780.

Leanza, G., Pellitteri, R., Russo, A., & Stanzani, S. (1991) Neurons in raphe nuclei pontis and magnus have branching axons that project to medial preoptic area and cervical spinal cord. A fluorescent retrograde double labeling study in the rat. *Neurosci. Lett.*, **123**, 195–199.

Leanza, G., Perez, S., Pellitteri, R., Russo, A., & Stanzani, S. (1995) Branching serotonergic and non-serotonergic projections from caudal brainstem to the medial preoptic area and the lumbar spinal cord, in the rat. *Neurosci. Lett.*, **200**, 5–8.

Lee, E.B., Lee, V.M., & Trojanowski, J.Q. (2012) Gains or losses: molecular mechanisms of TDP43-mediated neurodegeneration. TL - 13. *Nat. Rev. Neurosci.*, **13 VN - r**, 38–50.

Li, Y. & Bennett, D.J. (2003) Persistent sodium and calcium currents cause plateau potentials in motoneurons of chronic spinal rats. *J. Neurophysiol.*, **90**, 857–869.

Li, Y.Q., Takada, M., & Mizuno, N. (1993) The sites of origin of serotoninergic afferent fibers in the trigeminal motor, facial, and hypoglossal nuclei in the rat. *Neurosci. Res.*, **17**, 307–313.

Li, Y.R., King, O.D., Shorter, J., & Gitler, A.D. (2013) Stress granules as crucibles of ALS pathogenesis. *J. Cell Biol.*, **201**, 361–372.

Lidov, H.G. & Molliver, M.E (1990) .Immunohistochemical study of the development of serotonergic neurons in the rat CNS. *Brain Res. Bull.*, **9**, 559–604.

Lillo, P. & Hodges, J.R. (2009) Frontotemporal dementia and motor neurone disease: overlapping clinic-pathological disorders. *J. Clin. Neurosci.*, **16**, 1131–1135.

Ling, S., Polymenidou, M., & Cleveland, D.W. (2013) Converging mechanisms in ALS and FTD: disrupted RNA and protein homeostasis. *Neuron*, **79**, 416–438.

Lobsiger, C.S., Boillee, S., McAlonis-Downes, M., Khan, A.M., Feltri, M.L., Yamanaka, K., & Cleveland, D.W. (2009) Schwann cells expressing dismutase active mutant SOD1 unexpectedly slow disease progression in ALS mice. *Proc. Natl. Acad. Sci. U. S. A.*, **106**, 4465–4470.

Loewy, A.D. (1981) Raphe pallidus and raphe obscurus projections to the intermediolateral cell column in the rat. *Brain Res.*, **222**, 129–133.

Loewy, A.D. & McKellar, S. (1981) Serotonergic projections from the ventral medulla to the intermediolateral cell column in the rat. *Brain Res.*, **211**, 146–152.

Machacek, D.W., Garraway, S.M., Shay, B.L., & Hochman, S. (2001) Serotonin 5-HT2

receptor activation induces a long-lasting amplification of spinal reflex actions in the rat. *J. Physiol.*, **537**, 201–207.

Mackenzie, I.R.A., Neumann, M., Bigio, E.H., Cairns, N.J., Alafuzoff, I., Kril, J., Kovacs, G.G., Ghetti, B., Halliday, G., Holm, I.E., Ince, P.G., Kamphorst, W., Revesz, T., Rozemuller, A.J.M., Kumar-Singh, S., Akiyama, H., Baborie, A., Spina, S., Dickson, D.W., Trojanowski, J.Q., & Mann, D.M.A. (2010) Nomenclature and nosology for neuropathologic subtypes of frontotemporal lobar degeneration: an update. *Acta Neuropathol.*, **119**, 1–4.

Magran, J., Cortez, C., Gan, W.B., & Manfredi, G. (2014) Abnormal mitochondrial transport and morphology are common pathological denominators in SOD1 and TDP43 ALS mouse models. *Hum. Mol. Genet.*, **23**, 1413–1424.

Manabe, N., Wong, B.S., & Camilleri, M. (2010) New-generation 5-HT4 receptor agonists: potential for treatment of gastrointestinal motility disorders. *Expert Opin. Investig. Drugs*, **19**, 765–775.

Marchetto, M.C.N., Muotri, A.R., Mu, Y., Smith, A.M., Cezar, G.G., & Gage, F.H. (2008) Non-Cell-Autonomous Effect of Human SOD1G37R Astrocytes on Motor Neurons Derived from Human Embryonic Stem Cells. *Cell Stem Cell*, **3**, 649–657.

Marek, G.J., Carpenter, L.L., McDougle, C.J., & Price, L.H. (2003) Synergistic action of 5-HT2A antagonists and selective serotonin reuptake inhibitors in neuropsychiatric disorders. *Neuropsychopharmacology*, **28**, 402–412.

Maricq, A. V, Peterson, A.S., Brake, A.J., Myers, R.M., & Julius, D. (1991) Primary structure and functional expression of the 5HT3 receptor, a serotonin-gated ion channel. *Science*, **254**, 432–437.

Marin, B., Desport, J.C., Kajeu, P., Jesus, P., Nicolaud, B., Nicol, M., Preux, P.M., & Couratier, P. (2011) Alteration of nutritional status at diagnosis is a prognostic factor for survival of amyotrophic lateral sclerosis patients. *J. Neurol. Neurosurg. Psychiatry*, **82**, 628–634.

Mather, K., Watts, F.Z., Carroll, M., Whitehead, P., Swash, M., Cairn, N., & Burke, J. (1993) Antibody to an abnormal protein in amyotrophic lateral sclerosis identifies Lewy body-like inclusions in ALS and Lewy bodies in Parkinson's disease. *Neurosci. Lett.*, **160**, 13–16.

Maxwell, L., Maxwell, D.., Neilson, M., & Kerr, R. (1996) A confocal microscopic survey of serotoninergic axons in the lumbar spinal cord of the rat: co-localization with glutamate decarboxylase and neuropeptides. *Neuroscience*, **75**, 471–480.

Medina, I., Friedel, P., Rivera, C., Kahle, K.T., Kourdougli, N., Uvarov, P., & Pellegrino, C. (2014) Current view on the functional regulation of the neuronal K(+)-Cl(-) cotransporter KCC2. *Front. Cell. Neurosci.*, **8**, 27.

Mitsikostas, D.D. & Tfelt-Hansen, P. (2012) Targeting to 5-HT1F receptor subtype for migraine treatment: lessons from the past, implications for the future. *Cent. Nerv.*

Syst. Agents Med. Chem., **12**, 241–249.

Mnie-Filali, O., Faure, C., Lambás-Señas, L., El Mansari, M., Belblidia, H., Gondard, E., Etiévant, A., Scarna, H., Didier, A., Berod, A., Blier, P., & Haddjeri, N. (2011) Pharmacological blockade of 5-HT7 receptors as a putative fast acting antidepressant strategy. *Neuropsychopharmacology*, **36**, 1275–1288.

Mòdol, L., Mancuso, R., Alé, A., Francos-Quijorna, I., & Navarro, X. (2014) Differential effects on KCC2 expression and spasticity of ALS and traumatic injuries to motoneurons. *Front. Cell. Neurosci.*, **8**, 7.

Moor, H. & Rehabilitation, R. (1998) Management of spasticity_2009.pdf 239–245.

Morton, G.J., Cummings, D.E., Baskin, D.G., Barsh, G.S., & Schwartz, M.W. (2006) Central nervous system control of food intake and body weight. *Nature*, **443**, 289–295.

Moses, L. (2008) Serotonin : a review 187–199.

Murray, K.C., Stephens, M.J., Ballou, E.W., Heckman, C.J., & Bennett, D.J. (2011) Motoneuron excitability and muscle spasms are regulated by 5-HT2B and 5-HT2C receptor activity. *J. Neurophysiol.*, **105**, 731–748.

Nakamura, K., Matsumura, K., Kaneko, T., Kobayashi, S., Katoh, H., & Negishi, M. (2002) The rostral raphe pallidus nucleus mediates pyrogenic transmission from the preoptic area. *J. Neurosci.*, **22**, 4600–4610.

Nardone, A. & Schieppati, M. (2005) Reflex contribution of spindle group Ia and II afferent input to leg muscle spasticity as revealed by tendon vibration in hemiparesis. *Clin. Neurophysiol.*, **116**, 1370–1381.

Naumenko, V.S., Popova, N.K., Lacivita, E., Leopoldo, M., & Ponimaskin, E.G. (2014) Interplay between serotonin 5-HT1A and 5-HT7 receptors in depressive disorders. *CNS Neurosci. Ther.*, **20**, 582–590.

Nayak, D., Roth, T.L., & McGavern, D.B. (2014) Microglia Development and Function. *Annu. Rev. Immunol.*, **32**, 367–402.

Nebigil, C.G., Choi, D.S., Dierich, A., Hickel, P., Le Meur, M., Messaddeq, N., Launay, J.M., & Maroteaux, L. (2000) Serotonin 2B receptor is required for heart development. *Proc. Natl. Acad. Sci. U. S. A.*, **97**, 9508–9513.

Nebigil, C.G., Jaffré, F., Messaddeq, N., Hickel, P., Monassier, L., Launay, J.-M., & Maroteaux, L. (2003) Overexpression of the serotonin 5-HT2B receptor in heart leads to abnormal mitochondrial function and cardiac hypertrophy. *Circulation*, **107**, 3223–3229.

Neeb, L., Meents, J., & Reuter, U. (2010) 5-HT(1F) Receptor agonists: a new treatment option for migraine attacks? *Neurotherapeutics*, **7**, 176–182.

Nelson, D.L. (2004) 5-HT5 receptors. *Curr. Drug Targets. CNS Neurol. Disord.*, **3**, 53–58.

Neumann, M., Sampathu, D.M., Kwong, L.K., Truax, A.C., Micsenyi, M.C., Chou, T.T., Bruce, J., Schuck, T., Grossman, M., Clark, C.M., McCluskey, L.F., Miller, B.L., Masliah, E., Mackenzie, I.R., Feldman, H., Feiden, W., Kretzschmar, H.A., Trojanowski, J.Q., & Lee, V.M. (2006) Ubiquitinated TDP-43 in frontotemporal lobar degeneration and amyotrophic lateral sclerosis. *Science (80-.).*, **314**, 130–133.

Ng, A.S.L., Rademakers, R., & Miller, B.L. (2015) Frontotemporal dementia: a bridge between dementia and neuromuscular disease. *Ann. N. Y. Acad. Sci.*, **1338**, 71–93.

Ni, Y.G. & Miledi, R. (1997) Blockage of 5HT2C serotonin receptors by fluoxetine (Prozac). *Proc. Natl. Acad. Sci. U. S. A.*, **94**, 2036–2040.

Nichols, D.E. & Nichols, C.D. (2008) Serotonin receptors. *Chem Rev*, **108**, 1614–1641.

Nikiforuk, A., Kos, T., Fijał, K., Hołuj, M., Rafa, D., & Popik, P. (2013) Effects of the selective 5-HT7 receptor antagonist SB-269970 and amisulpride on ketamine-induced schizophrenia-like deficits in rats. *PLoS One*, **8**, e66695.

Okamoto, K., Mizuno, Y., & Fujita, Y. (2008) Bunina bodies in amyotrophic lateral sclerosis. *Neuropathology*, **28**, 109–115.

Olesen, J. (2010) 5-Hydroxyptryptamine 1F (5-HT1F) receptor agonism. A possible new treatment principle for acute migraine attacks. *Cephalalgia*, **30**, 1157–1158.

Olivier, B. & van Oorschot, R. (2005) 5-HT1B receptors and aggression: a review. *Eur. J. Pharmacol.*, **526**, 207–217.

Orihuela, R., Mcpherson, C.A., & Harry, G.J. (2015) Microglial M1/M2 polarization and metabolic states. *Br. J. Pharmacol.*, 649–665.

Papadeas, S.T., Kraig, S.E., O'Banion, C., Lepore, A.C., & Maragakis, N.J. (2011) Astrocytes carrying the superoxide dismutase 1 (SOD1G93A) mutation induce wild-type motor neuron degeneration in vivo. *Proc. Natl. Acad. Sci. U. S. A.*, **108**, 17803–17808.

Phadke, C.P., Balasubramanian, C.K., Holz, A., Davidson, C., Ismail, F., & Boulias, C. (2015) Adverse Clinical Effects of Botulinum Toxin Intramuscular Injections for Spasticity. *Can. J. Neurol. Sci.*, 1–13.

Philips, T. & Robberecht, W. (2011) Neuroinflammation in amyotrophic lateral sclerosis: Role of glial activation in motor neuron disease. *Lancet Neurol.*, **10**, 253–263.

Picelli, A., Bonetti, P., Fontana, C., Barausse, M., Dambruoso, F., Gajofatto, F., Tamburin, S., Girardi, P., Gimigliano, R., & Smania, N. (2012) Accuracy of botulinum toxin type A injection into the gastrocnemius muscle of adults with spastic equinus: manual needle placement and electrical stimulation guidance compared using ultrasonography. *J. Rehabil. Med.*, **44**, 450–452.

Plassat, J.L., Boschert, U., Amlaiky, N., & Hen, R. (1992) The mouse 5HT5 receptor

reveals a remarkable heterogeneity within the 5HT1D receptor family. *EMBO J.*, **11**, 4779–4786.

Polymenidou, M., Lagier-Tourenne, C., Hutt, K.R., Bennett, C.F., Cleveland, D.W., & Yeo, G.W. (2012) Misregulated RNA processing in amyotrophic lateral sclerosis. *Brain Res.*, **1462**, 3–15.

Polymenidou, M., Lagier-Tourenne, C., Hutt, K.R., Huelga, S.C., Moran, J., Liang, T.Y., Ling, S.-C., Sun, E., Wancewicz, E., Mazur, C., Kordasiewicz, H., Sedaghat, Y., Donohue, J.P., Shiue, L., Bennett, C.F., Yeo, G.W., & Cleveland, D.W. (2011) Long pre-mRNA depletion and RNA missplicing contribute to neuronal vulnerability from loss of TDP-43. *Nat. Neurosci.*, **14**, 459–468.

Pratt, A.J., Getzoff, E.D., & Perry, J.P. (2012) Amyotrophic lateral sclerosis : update and new developments. *Degener Neurol Neuromuscul Dis*, **2**, 1–14.

Prinz, M. & Priller, J. (2014) Microglia and brain macrophages in the molecular age: from origin to neuropsychiatric disease. *Nat. Rev. Neurosci.*, **15**, 300–312.

Puskarjov, M., Ahmad, F., Kaila, K., & Blaesse, P. (2012) Activity-Dependent Cleavage of the K-Cl Cotransporter KCC2 Mediated by Calcium-Activated Protease Calpain. *J. Neurosci.*, **32**, 11356–11364.

Pytliak, M., Vargová, V., Mechírová, V., & Felšöci, M. (2011) Serotonin receptors - from molecular biology to clinical applications. *Physiol. Res.*, **60**, 15–25.

Radunović, A., Mitsumoto, H., & Leigh, P.N. (2007) Clinical care of patients with amyotrophic lateral sclerosis. *Lancet. Neurol.*, **6**, 913–925.

R.D. Henderson. (2011). The Role of Immune and Inflammatory Mechanisms in ALS. Current Molecular Medicine., **11**, 246-254

Ramadan, N.M., Skljarevski, V., Phebus, L.A., & Johnson, K.W. (2003) 5-HT1F receptor agonists in acute migraine treatment: a hypothesis. *Cephalalgia*, **23**, 776–785.

Ramírez, M.J. (2013) 5-HT6 receptors and Alzheimer's disease. *Alzheimers. Res. Ther.*, **5**, 15.

Ransohoff, R.M. (2011) Microglia and monocytes: 'tis plain the twain meet in the brain. *Nat. Neurosci.*, **14**, 1098–1100.

Ransohoff, R.M. & Perry, V.H. (2009) Microglial physiology: unique stimuli, specialized responses. *Annu. Rev. Immunol.*, **27**, 119–145.

Raote, I., Bhattacharya, A., & Panicker, M.M. (2007) Serotonin 2A (5-HT2A) Receptor Function: Ligand-Dependent Mechanisms and Pathways.

Raymond, J.R., Mukhin, Y. V, Gelasco, A., Turner, J., Collinsworth, G., Gettys, T.W., Grewal, J.S., & Garnovskaya, M.N. (2001) Multiplicity of mechanisms of serotonin receptor signal transduction. *Pharmacol. Ther.*, **92**, 179–212.

Rekling, J.C., Funk, G.D., Bayliss, D. a, Dong, X.W., & Feldman, J.L. (2000) Synaptic

control of motoneuronal excitability. *Physiol. Rev.*, **80**, 767–852.

Release, S., During, V., Of, R., Function, M., Spinal, A.A., Injury, C., & Rats, I.N. (2010) Serotonin release variations during recovery of motor function after a spinal cord injury in rats. *Synapse*, **64**, 855–861.

Renton, A.E., Chiò, A., & Traynor, B.J. (2013) State of play in amyotrophic lateral sclerosis genetics. *Nat. Neurosci.*, **17**, 17–23.

Renton, A.E., Chiò, A., & Traynor, B.J. (2014) State of play in amyotrophic lateral sclerosis genetics. *Nat. Neurosci.*, **17**, 17–23.

Renton, A.E., Majounie, E., Waite, A., Simón-Sánchez, J., Rollinson, S., Gibbs, J.R., Schymick, J.C., Laaksovirta, H., van Swieten, J.C., Myllykangas, L., Kalimo, H., Paetau, A., Abramzon, Y., Remes, A.M., Kaganovich, A., Scholz, S.W., Duckworth, J., Ding, J., Harmer, D.W., Hernandez, D.G., Johnson, J.O., Mok, K., Ryten, M., Trabzuni, D., Guerreiro, R.J., Orrell, R.W., Neal, J., Murray, A., Pearson, J., Jansen, I.E., Sondervan, D., Seelaar, H., Blake, D., Young, K., Halliwell, N., Callister, J.B., Toulson, G., Richardson, A., Gerhard, A., Snowden, J., Mann, D., Neary, D., Nalls, M.A., Peuralinna, T., Jansson, L., Isoviita, V.-M., Kaivorinne, A.-L., Hölttä-Vuori, M., Ikonen, E., Sulkava, R., Benatar, M., Wuu, J., Chiò, A., Restagno, G., Borghero, G., Sabatelli, M., Heckerman, D., Rogaeva, E., Zinman, L., Rothstein, J.D., Sendtner, M., Drepper, C., Eichler, E.E., Alkan, C., Abdullaev, Z., Pack, S.D., Dutra, A., Pak, E., Hardy, J., Singleton, A., Williams, N.M., Heutink, P., Pickering-Brown, S., Morris, H.R., Tienari, P.J., & Traynor, B.J. (2011) A Hexanucleotide Repeat Expansion in C9ORF72 Is the Cause of Chromosome 9p21-Linked ALS-FTD. *Neuron*, **72**, 257–268.

Ridet, J.L., Rajaofetra, N., Teilhac, J.R., Geffard, M., & Privat, A. (1993) Evidence for nonsynaptic serotonergic and noradrenergic innervation of the rat dorsal horn and possible involvement of neuron-glia interactions. *Neuroscience*, **52**, 143–157.

Ripps, M.E., Huntley, G.W., Hof, P.R., Morrison, J.H., & Gordon, J.W. (1995) Transgenic mice expressing an altered murine superoxide dismutase gene provide an animal model of amyotrophic lateral sclerosis. *Proc. Natl. Acad. Sci. U. S. A.*, **92**, 689–693.

Rothman, R.B., Baumann, M.H., Savage, J.E., Rauser, L., McBride, a, Hufeisen, S.J., & Roth, B.L. (2000) Evidence for possible involvement of 5-HT(2B) receptors in the cardiac valvulopathy associated with fenfluramine and other serotonergic medications. *Circulation*, **102**, 2836–2841.

Rotunno, M.S. & Bosco, D.A. (2013) An emerging role for misfolded wild-type SOD1 in sporadic ALS pathogenesis. *Front. Cell. Neurosci.*, **7**, 1–16.

Rushworth, G. (1960) Spasticity and Rigidity: an Experimental Study and Review. *J. Neurol. Neurosurg. Psychiatry*, **23**, 99–118.

Saijo, K. & Glass, C.K. (2011) Microglial cell origin and phenotypes in health and disease. *Nat. Rev. Immunol.*, **11**, 775–787.

Satkunam, L.E. (2003) Rehabilitation medicine: 3. Management of adult spasticity. *CMAJ*, **169**, 1173–1179.

Savitz, J., Lucki, I., & Drevets, W.C. (2009) 5-HT1A receptor function in major depressive disorder. *Prog. Neurobiol.*, **88**, 17–31.

Saxena, S. & Caroni, P. (2011) Selective neuronal vulnerability in neurodegenerative diseases: from stressor thresholds to degeneration. *Neuron*, **71**, 35–48.

Schmidt, B.J. & Jordan, L.M. (2000) The role of serotonin in reflex modulation and locomotor rhythm production in the mammalian spinal cord. *Brain Res. Bull.*, **53**, 689–710.

Schmidt, B.J. & Jordan, L.M. (2001) Locomotor Rhythm Production in the Mammalian Spinal Cord **53**, 689–710.

Schmuck, K., Ullmer, C., Engels, P., & Lfibbert, H. (1994) Cloning and functional characterization of the human 5-HT2B serotonin receptor. *FEBS Lett.*, **342**, 85–90.

Schwartz, M.W., Woods, S.C., Porte, D., Seeley, R.J., & Baskin, D.G. (2000) Central nervous system control of food intake. *Nature*, **404**, 661–671.

Shay, B.L., Sawchuk, M., Machacek, D.W., & Hochman, S. (2005) Serotonin 5-HT2 receptors induce a long-lasting facilitation of spinal reflexes independent of ionotropic receptor activity. *J. Neurophysiol.*, **94**, 2867–2877.

Sheean, G. (2002) The pathophysiology of spasticity. *Eur. J. Neurol.*, **9 Suppl 1**, 3–9; dicussion 53–61.

Sheean, G. & McGuire, J.R. (2009) Spastic hypertonia and movement disorders: pathophysiology, clinical presentation, and quantification. *PM R*, **1**, 827–833.

Skagerberg, G. & Björklund, A. (1985) Topographic principles in the spinal projections of serotonergic and non-serotonergic brainstem neurons in the rat. *Neuroscience*, **15**, 445–480.

Slowie, L.A., Paige, M.S., & Antel, J.P. (1983) Nutritional considerations in the management of patients with amyotrophic lateral sclerosis (ALS). *J. Am. Diet. Assoc.*, **83**, 44–47.

Sofic, E., Riederer, P., Gsell, W., Gavranovic, M., Schmidtke, A., & Jellinger, K. (1991) Biogenic amines and metabolites in spinal cord of patients with Parkinson's disease and amyotrophic lateral sclerosis. *J. Neural Transm. Park. Dis. Dement. Sect.*, **3**, 133–142.

Sohn, J.-W., Xu, Y., Jones, J.E., Wickman, K., Williams, K.W., & Elmquist, J.K. (2011) Serotonin 2C receptor activates a distinct population of arcuate pro-opiomelanocortin neurons via TRPC channels. *Neuron*, **71**, 488–497.

Sorimachi, H., Hata, S., & Ono, Y. (2011) Calpain chronicle--an enzyme family under multidisciplinary characterization. *Proc. Jpn. Acad. Ser. B. Phys. Biol. Sci.*, **87**, 287–327.

Sorimachi, H. & Ono, Y. (2012) Regulation and physiological roles of the calpain system in muscular disorders. *Cardiovasc. Res.*, **96**, 11–22.

Steinbusch, H.W., van der Kooy, D., Verhofstad, A.A., & Pellegrino, A. (1980) Serotonergic and non-serotonergic projections from the nucleus raphe dorsalis to the caudate-putamen complex in the rat, studied by a combined immunofluorescence and fluorescent retrograde axonal labeling technique. *Neurosci. Lett.*, **19**, 137–142.

Stieber, A., Gonatas, J.O., & Gonatas, N.K. (2000) Aggregation of ubiquitin and a mutant ALS-linked SOD1 protein correlate with disease progression and fragmentation of the Golgi apparatus. *J. Neurol. Sci.*, **173**, 53–62.

Stifani, N. (2014) Motor neurons and the generation of spinal motor neuron diversity. *Front. Cell. Neurosci.*, **8**, 293.

Strong, M.J. & Yang, W. (2011) The frontotemporal syndromes of ALS. Clinicopathological correlates. *J. Mol. Neurosci.*, **45**, 648–655.

Swinnen, B. & Robberecht, W. (2014) The phenotypic variability of amyotrophic lateral sclerosis. *Nat. Rev. Neurol.*, **10**, 661–670.

Tafuri, F., Ronchi, D., Magri, F., Comi, G.P., & Corti, S. (2015) SOD1 misplacing and mitochondrial dysfunction in amyotrophic lateral sclerosis pathogenesis. *Front. Cell. Neurosci.*, **9**, 336.

Takanashi, K. & Yamaguchi, A. (2014) Aggregation of ALS-linked FUS mutant sequesters RNA binding proteins and impairs RNA granules formation. *Biochem. Biophys. Res. Commun.*, **452**, 600–607.

Tang, Y. & Le, W. (2015) Differential Roles of M1 and M2 Microglia in Neurodegenerative Diseases. *Mol. Neurobiol.*,.

Tanis, J.E., Bellemer, A., Moresco, J.J., Forbush, B., & Michael, R. (2010) NIH Public Access **29**, 9943–9954.

Teng, P., Bateman, N.W., Darcy, K.M., Hamilton, C.A., Maxwell, G.L., Bakkenist, C.J., Conrads, T.P., Service, O., Reed, W., Military, N., & Hospital, I.F. (2015) HHS Public Access. *Gynecol Oncol.*, **136**, 554–561.

Taylor, J.P. (2002). Toxic proteins in neurodegenerative disease. Science., **14**, 1991–1995.

Tepper, S.J., Rapoport, A.M., & Sheftell, F.D. (2002) Mechanisms of action of the 5-HT1B/1D receptor agonists. *Arch. Neurol.*, **59**, 1084–1088.

THILMANN, A.F., FELLOWS, S.J., & GARMS, E. (1991) THE MECHANISM OF SPASTIC MUSCLE HYPERTONUS: VARIATION IN REFLEX GAIN OVER THE TIME COURSE OF SPASTICITY. *Brain*, **114A**, 233–244.

Thompson, A.J. & Lummis, S.C.R. (2006) 5-HT3 receptors. *Curr. Pharm. Des.*, **12**, 3615–3630.

Thompson, A.J. & Lummis, S.C.R. (2007) The 5-HT3 receptor as a therapeutic target. *Expert Opin. Ther. Targets*, **11**, 527–540.

Thuret, S., Moon, L.D.F., & Gage, F.H. (2006) Therapeutic interventions after spinal cord injury. *Nat. Rev. Neurosci.*, **7**, 628–643.

Törk, I. (1990) Anatomy of the serotonergic system. *Ann. N. Y. Acad. Sci.*, **600**, 9–34; discussion 34–35.

Traynor, B.J., Codd, M.B., Corr, B., Forde, C., Frost, E., & Hardiman, O.M. (2000) Clinical features of amyotrophic lateral sclerosis according to the El Escorial and Airlie House diagnostic criteria: A population-based study. *Arch. Neurol.*, **57**, 1171–1176.

Trias, E., Díaz-Amarilla, P., Olivera-Bravo, S., Isasi, E., Drechsel, D. a, Lopez, N., Bradford, C.S., Ireton, K.E., Beckman, J.S., & Barbeito, L. (2013) Phenotypic transition of microglia into astrocyte-like cells associated with disease onset in a model of inherited ALS. *Front. Cell. Neurosci.*, **7**, 274.

Trompetto, C., Marinelli, L., Mori, L., Pelosin, E., Currà, A., Molfetta, L., & Abbruzzese, G. (2014) Pathophysiology of spasticity: Implications for neurorehabilitation. *Biomed Res. Int.*, **2014**.

Turnbull, I.R. & Colonna, M. (2007) Activating and inhibitory functions of DAP12. *Nat. Rev. Immunol.*, **7**, 155–161.

TURNER, B. & TALBOT, K. (2008) Transgenics, toxicity and therapeutics in rodent models of mutant SOD1-mediated familial ALS. *Prog. Neurobiol.*, **85**, 94–134.

Turner, M.R., Rabiner, E.A., Hammers, A., Al-Chalabi, A., Grasby, P.M., Shaw, C.E., Brooks, D.J., & Leigh, P.N. (2005) [11C]-WAY100635 PET demonstrates marked 5-HT1A receptor changes in sporadic ALS. *Brain*, **128**, 896–905.

Upton, N., Chuang, T.T., Hunter, A.J., & Virley, D.J. (2008) 5-HT6 receptor antagonists as novel cognitive enhancing agents for Alzheimer's disease. *Neurotherapeutics*, **5**, 458–469.

Van Bockstaele, E.J., Biswas, A., & Pickel, V.M. (1993) Topography of serotonin neurons in the dorsal raphe nucleus that send axon collaterals to the rat prefrontal cortex and nucleus accumbens. *Brain Res.*, **624**, 188–198.

Vercruysse, P., Sinniger, J., El Oussini, H., Scekic-Zahirovic, J., Dieterle, S., Dengler, R., Meyer, T., Zierz, S., Kassubek, J., Fischer, W., Dreyhaupt, J., Grehl, T., Hermann, A., Grosskreutz, J., Witting, A., Van Den Bosch, L., Spreux-Varoquaux, O., the GERP ALS Study Group, Ludolph, A.C., & Dupuis, L. (2016) Alterations in the hypothalamic melanocortin pathway in amyotrophic lateral sclerosis. *Brain*, aww004 – .

Vertes, R.P. (1991) A PHA-L analysis of ascending projections of the dorsal raphe nucleus in the rat. *J. Comp. Neurol.*, **313**, 643–668.

Vertes, R.P. & Crane, A.M. (1997) Distribution, quantification, and morphological characteristics of serotonin-immunoreactive cells of the supralemniscal nucleus (B9) and pontomesencephalic reticular formation in the rat. *J. Comp. Neurol.*, **378**, 411–424.

Vertes, R.P., Fortin, W.J., & Crane, A.M. (1999) Projections of the median raphe nucleus in the rat. *J. Comp. Neurol.*, **407**, 555–582.

Vinsant, S., Mansfield, C., Jimenez-Moreno, R., Moore, V.D.G., Yoshikawa, M., Hampton, T.G., Prevette, D., Caress, J., Oppenheim, R.W., & Milligan, C. (2013) Characterization of early pathogenesis in the SOD1G93A mouse model of ALS: Part II, results and discussion. *Brain Behav.*, **3**, 431–457.

WADE, D. Upper motor neurone syndrome and spasticity. Clinical management and neurophysiology (2001). *J. Neurol. Neurosurg. Psychiatry*, **71**, 822d – 822.

Wang, J., Slunt, H., Gonzales, V., Fromholt, D., Coonfield, M., Copeland, N.G., Jenkins, N.A., & Borchelt, D.R. (2003) Copper-binding-site-null SOD1 causes ALS in transgenic mice: aggregates of non-native SOD1 delineate a common feature. *Hum. Mol. Genet.*, **12**, 2753–2764.

Wang, J., Xu, G., Li, H., Gonzales, V., Fromholt, D., Karch, C., Copeland, N.G., Jenkins, N.A., & Borchelt, D.R. (2005) Somatodendritic accumulation of misfolded SOD1-L126Z in motor neurons mediates degeneration: alphaB-crystallin modulates aggregation. *Hum. Mol. Genet.*, **14**, 2335–2347.

Wang, W., Li, L., Lin, W.-L., Dickson, D.W., Petrucelli, L., Zhang, T., & Wang, X. (2013) The ALS disease-associated mutant TDP-43 impairs mitochondrial dynamics and function in motor neurons. *Hum. Mol. Genet.*, **22**, 4706–4719.

Wang, X., Zhou, S., Ding, X., Ma, M., Zhang, J., Zhou, Y., Wu, E., & Teng, J. (2015) Activation of ER stress and autophagy induced by TDP-43 A315T as pathogenic mechanism and the corresponding histological changes in skin as potential biomarker for ALS with the mutation. *Int. J. Biol. Sci.*, **11**, 1140–1149.

Waterhouse, B.D., Mihailoff, G.A., Baack, J.C., & Woodward, D.J. (1986) Topographical distribution of dorsal and median raphe neurons projecting to motor, sensorimotor, and visual cortical areas in the rat. *J. Comp. Neurol.*, **249**, 460–476, 478–481.

Wijesekera, L.C. & Leigh, P.N. (2009) Amyotrophic lateral sclerosis. *Orphanet J. Rare Dis.*, **4**, 3.

Williams, G. V, Rao, S.G., & Goldman-Rakic, P.S. (2002) The physiological role of 5-HT2A receptors in working memory. *J. Neurosci.*, **22**, 2843–2854.

Wilson, L.R., Gracies, J.M., Burke, D., & Gandevia, S.C. (1999) Evidence for fusimotor drive in stroke patients based on muscle spindle thixotropy. *Neurosci. Lett.*, **264**, 109–112.

Wong, P.C., Pardo, C.A., Borchelt, D.R., Lee, M.K., Copeland, N.G., Jenkins, N.A.,

Sisodia, S.S., Cleveland, D.W., & Price, D.L. (1995) An adverse property of a familial ALS-linked SOD1 mutation causes motor neuron disease characterized by vacuolar degeneration of mitochondria. *Neuron*, **14**, 1105–1116.

Wu, W. & Wessendorf, M.W. (1992) Organization of the serotonergic innervation of spinal neurons in rats--I. Neuropeptide coexistence in varicosities innervating some spinothalamic tract neurons but not in those innervating postsynaptic dorsal column neurons. *Neuroscience*, **50**, 885–898.

Xanthos, D.N. & Sandkühler, J. (2014) Neurogenic neuroinflammation: inflammatory CNS reactions in response to neuronal activity. *Nat. Rev. Neurosci.*, **15**, 43–53.

Yamanaka, K., Chun, S.J., Boillee, S., Fujimori-Tonou, N., Yamashita, H., Gutmann, D.H., Takahashi, R., Misawa, H., & Cleveland, D.W. (2008) Astrocytes as determinants of disease progression in inherited amyotrophic lateral sclerosis. *Nat. Neurosci.*, **11**, 251–253.

Zarei, S., Carr, K., Reiley, L., Diaz, K., Guerra, O., Altamirano, P.F., Pagani, W., Lodin, D., Orozco, G., & Chinea, A. (2015) A comprehensive review of amyotrophic lateral sclerosis. *Surg. Neurol. Int.*, **6**, 171.

Zwiegers, P., Lee, G., & Shaw, C. a (2014) Reduction in hSOD1 copy number significantly impacts ALS phenotype presentation in G37R (line 29) mice: implications for the assessment of putative therapeutic agents. *J. Negat. Results Biomed.*, **13**, 14.

Publication #3 :

Investigating the contribution of VAPB/ALS8 loss of function in amyotrophic lateral sclerosis.

Edor Kabashi, **Hajer El Oussini**, Valérie Bercier, François Gros-Louis, Paul N. Valdmanis, Jonathan McDearmid, Inge A. Mejier, Patrick A. Dion, Nicolas Dupre, David Hollinger, Jérôme Sinniger, Sylvie DirrigGrosch, William Camu, Vincent Meininger, Jean-Philippe Loeffler , Frédérique René, Pierre Drapeau, Guy A. Rouleau, and Luc Dupuis

Human Molecular Genetics, 2013, Vol. 22, No. 12 **2350–2360**
doi:10.1093/hmg/ddt080
Advance Access published on February 26, 2013

Investigating the contribution of *VAPB/ALS8* loss of function in amyotrophic lateral sclerosis

Edor Kabashi[1,2,†], Hajer El Oussini[3,4], Valérie Bercier[1], François Gros-Louis[2], Paul N. Valdmanis[2], Jonathan McDearmid[5], Inge A. Mejier[2], Patrick A. Dion[2,6], Nicolas Dupre[8], David Hollinger[3,4], Jérome Sinniger[3,4], Sylvie Dirrig-Grosch[3,4], William Camu[9], Vincent Meininger[10,11], Jean-Philippe Loeffler[3,4], Frédérique René[3,4], Pierre Drapeau[6,7], Guy A. Rouleau[2,12] and Luc Dupuis[3,4,*,†]

[1]Centre de Recherche de l'Institut du Cerveau et de la Moelle Épiniere (CRICM), Paris, France, [2]Center of Excellence in Neuromics, Centre Hospitalier de l'Universite de Montreal, Montreal, Canada, [3]INSERM, U1118, Mécanismes centraux et périphériques de la neurodégénérescence, Strasbourg F-67085, France, [4]Faculté de Médecine, Université de Strasbourg, UMRS1118, Strasbourg F-67085, France, [5]Department of Biology, University of Leicester, Leicester, UK, [6]Department of Pathology and Cell Biology and [7]Groupe de Recherche Sur le Système Nerveux Central, University of Montreal, Montreal, Canada, [8]Département des sciences neurologiques, CHA—Hôpital de l'Enfant-Jésus, Quebec, Canada, [9]Service de Neurologie, CHU de Montpellier, Montpellier, France, [10]Département des Maladies du Système Nerveux, Centre Référent Maladie Rare SLA Hôpital de la Pitié-Salpêtrière (AP-HP), Paris, France, [11]Université Pierre et Marie Curie, Paris, France and [12]Faculty of Medicine, Department of Medicine, University de Montreal, Montreal, Canada

Received January 22, 2013; Revised and Accepted February 14, 2013

The mutations P56S and T46I in the gene encoding vesicle-associated membrane protein-associated protein B/C (*VAPB*) cause ALS8, a familial form of amyotrophic lateral sclerosis (ALS). Overexpression of mutant forms of VAPB leads to cytosolic aggregates, suggesting a gain of function of the mutant protein. However, recent work suggested that the loss of *VAPB* function could be the major mechanism leading to ALS8. Here, we used multiple genetic and experimental approaches to study whether *VAPB* loss of function might be sufficient to trigger motor neuron degeneration. In order to identify additional ALS-associated *VAPB* mutations, we screened the entire *VAPB* gene in a cohort of ALS patients and detected two mutations (A145V and S160Δ). To directly address the contribution of *VAPB* loss of function in ALS, we generated zebrafish and mouse models with either a decreased or a complete loss of *Vapb* expression. *Vapb* knockdown in zebrafish led to swimming deficits. Mice knocked-out for *Vapb* showed mild motor deficits after 18 months of age yet had innervated neuromuscular junctions (NMJs). Importantly, overexpression of *VAPB* mutations were unable to rescue the motor deficit caused by *Vapb* knockdown in zebrafish and failed to cause a toxic gain-of-function defect on their own. Thus, *Vapb* loss of function weakens the motor system of vertebrate animal models but is on its own unable to lead to a complete ALS phenotype. Our findings are consistent with the notion that *VAPB* mutations constitute a risk factor for motor neuron disease through a loss of VAPB function.

INTRODUCTION

Amyotrophic lateral sclerosis (ALS) is a neurodegenerative disorder characterized by progressive muscular atrophy and the simultaneous degeneration of lower (spinal and bulbar) and upper (corticospinal) motor neurons (1,2). This combined degeneration leads to muscle weakness, fasciculation, speech and swallowing disabilities, and progressive paralysis.

*To whom correspondence should be addressed at: INSERM U1118, Faculté de Médecine, bat 3, 8e étage, 11 rue Humann, Strasbourg F-67085, France. Tel: +33 368853091; Fax: +33 368853065; Email: ldupuis@unistra.fr
†The authors wish it to be known that, in their opinion that E.K and L.D. are joint Senior Authors.

Approximately 10% of ALS cases, clinically indistinguishable from sporadic cases, are genetically inherited and are termed as familial ALS (fALS) (3) with more than 10 loci currently identified. *ALS8* was mapped in a large white Brazilian family and corresponds to a C→T substitution in exon 2 of the gene encoding vesicle-associated membrane protein-associated protein B/C (*VAPB*) leading to a missense mutation in the encoded protein (4). Since then, one other missense mutation (T46I) has been discovered in an independent fALS family (5).

VAPB is a member of the VAP family, which also includes VAPA, an established regulator of vesicle trafficking (6), and is a protein resident of the endoplasmic reticulum of poorly characterized function, possibly involved in an unfolded protein response (UPR) (7–9). Overexpression of mutant VAPB in cultured cells led to aggregation of the protein in the cytosol and trapping of the wild-type protein in these aggregates, suggesting that *VAPB* mutations might act as a dominant negative of *VAPB* function (4,7–10). However, transgenic mice that overexpress mutant VAPB specifically in the nervous system were created and despite displaying obvious VAPB aggregates did not show an apparent behavioural phenotype (11,12), suggesting that the overexpression of mutant VAPB is not sufficient to lead to an ALS phenotype in mammals by toxic gain of function. Interestingly, induced pluripotent stem (iPS) cells prepared from fibroblasts of ALS8 patients displayed decreased levels of VAPB protein, and did not show the cytoplasmic aggregates observed upon overexpression (13). These results suggested that the phenotype associated with *VAPB* mutations could be due to a loss of VAPB protein function rather than to a toxic gain of function of the mutant VAPB. Supporting this notion are reports of decreased VAPB levels in motor neurons of animal models of ALS1 and in sporadic ALS patients (10,14). Hence, it is currently thought that the partial loss of VAPB protein function through *VAPB* mutations causes ALS and that a similar loss might be involved in other forms of the disease. Here, we tested the contribution of *VAPB* loss of function to ALS pathogenesis through multiple genetic and experimental approaches. Our results show that the partial or complete loss of VAPB function is sufficient to lead to motor deficit but is unable to trigger a full-blown ALS phenotype, either in the mouse or in the zebrafish models.

RESULTS

Detection of new *VAPB* mutations in ALS patients

Two heterozygous mutations were identified in the *VAPB* gene in the 169 ALS cases screened (Fig. 1A). The Fam113 patient has an in-frame deletion in exon 5 (750_752delCTT) resulting in the loss of a serine amino acid (p.S160Δ), the last of three consecutive serine residues in the protein (Fig. 1B and C). Unfortunately, other affected members have not been collected to confirm the segregation of the mutation with disease in Fam113. While the serine 160 residue is not particularly conserved in other VAP proteins, no other species have an amino acid loss at this position (Fig. 1F). This mutation has been previously described in a cohort of ALS patients and at a very low frequency in the corresponding control cohort (15). In addition, an sALS patient had a nucleotide substitution (c.705C>T) causing an alanine to valine missense mutation (p.A145V), also in exon 5 (Fig. 1D). Alanine 145 is conserved in VAPB protein homologues of all species except zebrafish, which has a lysine at this position (Fig. 1F). The two patients were negative for mutations in *SOD1, FUS, TARDBP* and/or *C9ORF72*. Neither of these mutations were detected in the chromosomes of 380 ethnically matched control individuals. Conversely, the variation in the 5′ untranslated region of VAPB (c.239C>G), 33 bp before the ATG start codon, was detected in one sALS patient and also in one of the 380 control individuals. The fALS Fam113 consists of 20 members, including three affected individuals diagnosed with definite ALS of bulbar onset. Symptom onset occurred in the collected patient at age 59 with a 3-year progression. The sALS patient is a male from Quebec, Canada with spinal-onset definite ALS, initially presenting disease at the age of 58. Again no DNA was available from the other members of this family.

Vapb knockdown leads to motor deficits in zebrafish

To investigate the pathogenicity and mechanism of action of *VAPB* mutations, we first employed the zebrafish model. Zebrafish have a single *VAPB* orthologue that is closely related to the human gene (75% nucleotide identity). In order to determine loss-of-function properties of these mutations, we injected an antisense morpholino oligonucleotide (AMO) that knocked down the expression of the zebrafish homologue of *VAPB*, *Vapb*. Approximately 20% of embryos injected showed developmental and morphological abnormalities and were excluded from motor analysis. The remaining embryos were morphologically normal with no observable abnormalities in major organ development. We tested for motor deficits upon knock down (KD) of zebrafish *Vapb* using a well-characterized larval behavioural landmark: the touch-evoked escape response (TEER) (Supplementary Material, Fig. S1). Embryos injected with *Vapb* AMO were separated into three groups: (a) zebrafish lacking a proper TEER and representing motor deficits (motor) (see the image sequence in Supplementary Material, Fig. S1B), (b) zebrafish able to respond to the TEER but with mild motor defects and (c) zebrafish with a normal TEER. Furthermore, we performed a quantitative analysis of the TEER as previously described (16). The duration (Supplementary Material, Fig. S2C), the distance (Supplementary Material, Fig. S2D) and the maximal velocity of TEER swimming episodes (Supplementary Material, Fig. S2E) were significantly reduced solely upon *Vapb* KD (Supplementary Material, Fig. S2A versus Supplementary Material, Fig. S2B).

Mutant VAPB is unable to rescue the motor phenotype due to *Vapb* knock down in zebrafish

Upon co-injection of mRNA of human wild-type VAPB with *Vapb* AMO, we were able to significantly rescue both the mild and severe motor phenotypes (Fig. 2B; as seen in the image sequence in Supplementary Material, Fig. S1C), indicating that these phenotypes are most likely due to KD of the zebrafish *Vapb*. On the other hand, the percentage of zebrafish with developmental anomalies was not affected upon co-injection of WT human VAPB mRNA (Fig. 2B). These results indicate that the developmental abnormalities obtained are most likely due to non-specific toxicity associated with AMO injection.

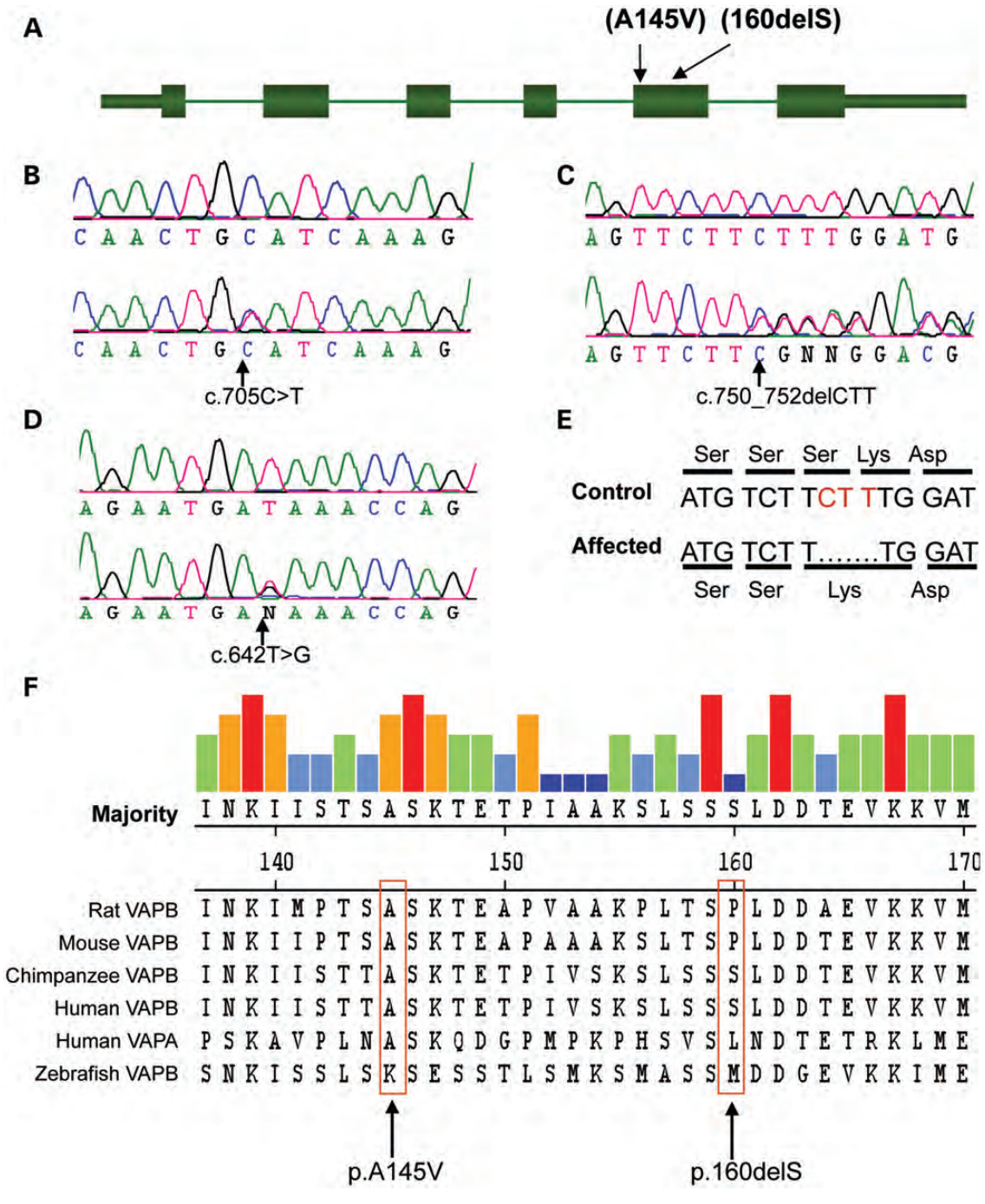

Figure 1. *VAPB* mutations in ALS patients. (**A**) Representation of the *VAPB* gene. The six exons are represented as boxes, untranslated regions (UTRs) as thick bars and introns as a line (introns and UTRs are not drawn to scale). (**B**–**D**) Genomic traces of ALS patients are aligned with a control sequence (above). Mutations are indicated by arrows. (**E**) Nucleotide sequence surrounding the CTT deletion (in red) of an ALS patient, and the resulting serine amino acid loss in affected individuals. (**F**) Conservation profile of *VAPB* mutations. The MegAlign programme (Lasergene) was used to align VAPB protein amino acid sequences from various species, including zebrafish and human VAPB and human VAPB using the Clustal-W method. The two mutated amino acids identified in ALS cases are boxed, and the conservation proportion between species is indicated above each amino acid.

We next tested whether *VAPB* mutations identified in ALS patients were able to rescue the motor phenotypes caused by *Vapb* KD. Co-injection of the VABP RNA containing a well-characterized P56S mutation was unable to rescue the motor phenotype (Fig. 3B and C). These RNA co-injections were also unable to rescue the percentage of developmentally abnormal zebrafish (Fig. 3A). The two mutations identified in this study, A145V and S160Δ, were similarly unable to rescue the motor phenotype, suggesting similar pathogenic mechanisms for these mutations (Fig. 3B and C). Interestingly, each of the ALS-related *VAPB* mutations described here, P56S, A145V and S160, were unable to induce a motor

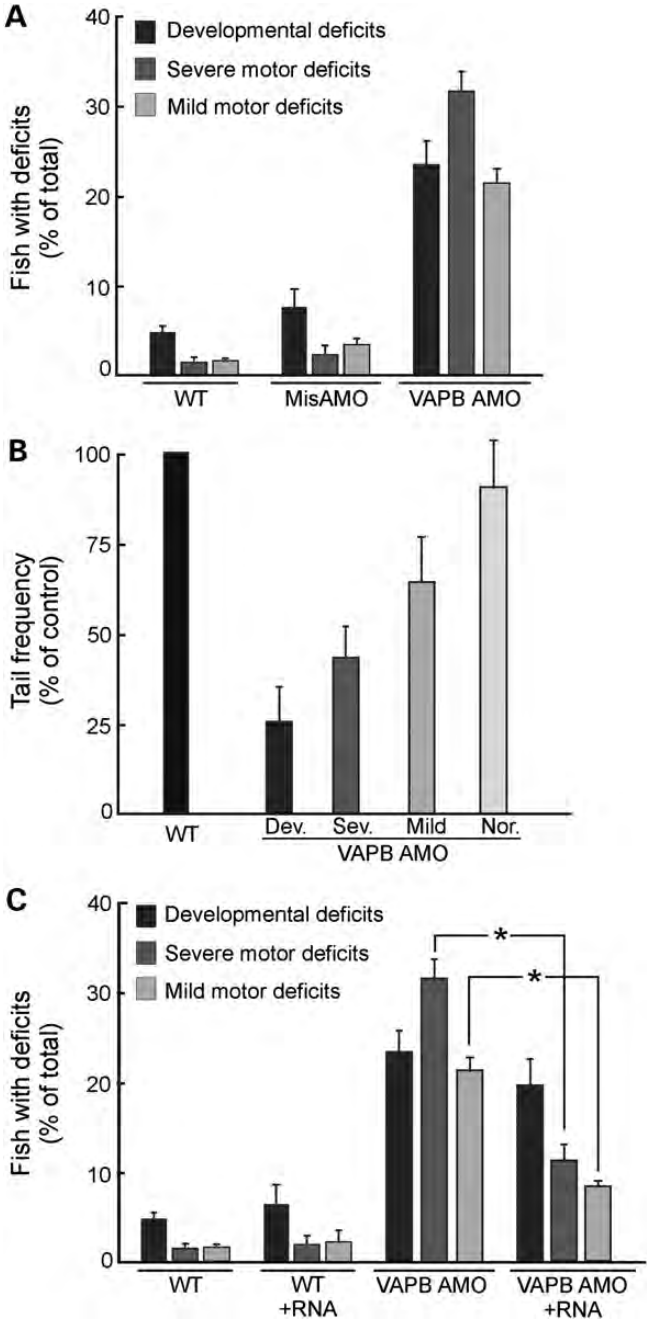

Figure 2. Quantification of behavioural deficits caused by KD of *Vapb* and rescue by wild-type VAPB in the zebrafish model. Zebrafish were tested for the TEER 48 h post-fertilization. (**A**) The percentage of fish with developmental deficits (dark grey), severe (grey) or mild (light grey) motor deficits in the TEER was minimal in non-injected embryos (WT) or in mismatch AMO injected embryos (misAMO). However, following injection with vapb AMO, TEER was markedly impaired in all the three categories. (**B**) Quantification of the tail frequency during swimming episodes following embedding the head of the embryo in agar revealed a significantly reduced tail frequency in all the three conditions when compared with non-injected embryos. (**C**) Upon co-injection of the AMO with human wild-type VAPB mRNA (indicated +RNA), the percentage of developmentally delayed embryos produced is maintained, but the motor phenotypes quantified by TEER were significantly decreased. Injection of the mRNA alone did not lead to any discernable phenotype.

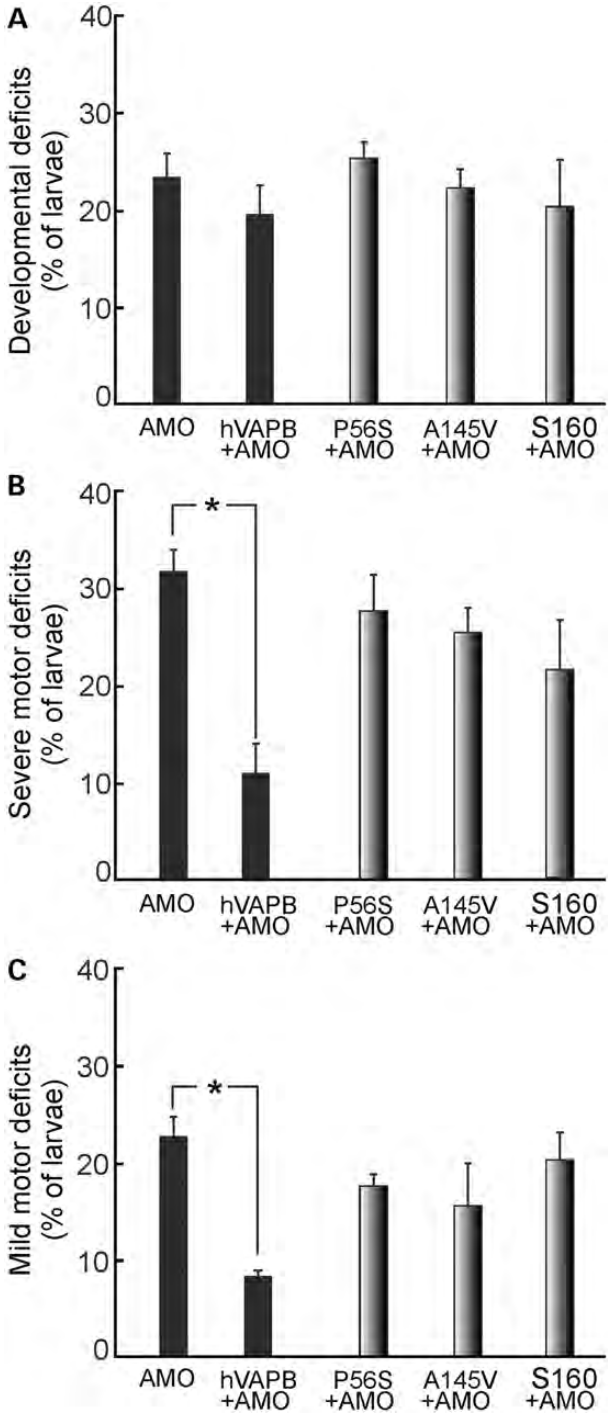

Figure 3. Mutant human VAPB RNA fails to rescue loss-of-function phenotype in the zebrafish model. Zebrafish were separated in the three conditions described in Figure 2: (**A**) The percentage of zebrafish displaying developmental abnormalities remained unchanged upon co-injection of the *Vapb* AMO with human wild-type VAPB RNA (indicated hVAPB), or with three human VAPB mRNAs bearing ALS-related mutations P56S, A145V and S160. (**B** and **C**) Both motor phenotypes observed upon the TEER assessment at 48 h post-fertilization were not significantly altered upon co-injections of P56S, A145V and S160 mutant RNAs with the *Vapb* AMO. Only co-injections of the human wild-type VAPB mRNA were able to rescue the TEER deficits.

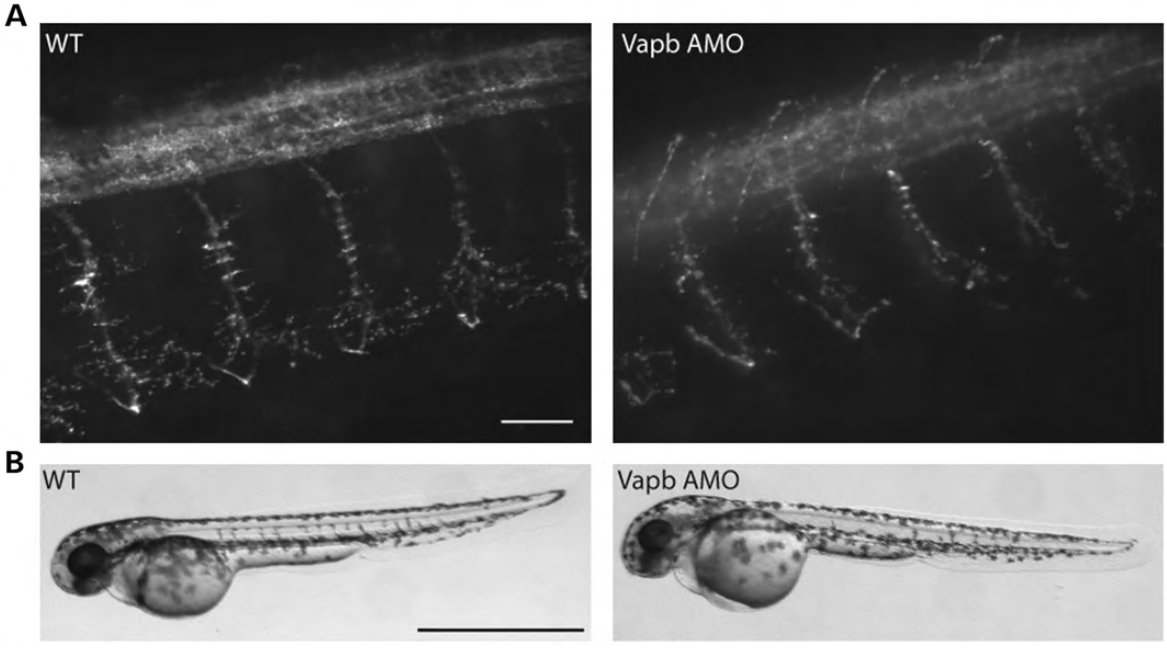

Figure 4. *Vapb* knockdown in zebrafish leads to slight morphological abnormalities of motor neurons. (**A**) Immunohistochemical analysis of the axonal projections of motor neurons revealed minor deficits in outbranching and axonal length in 48 h post-fertilization embryos injected with *vapb* AMO displaying behavioural deficits. (**B**) Embryos that displayed behavioural deficits upon TEER appeared morphologically normal.

phenotype when injected on their own (Supplementary Material, Fig. S3), suggesting that loss-of-function rather than toxic gain-of-function mechanisms of toxicity are at play for these mutations.

Vapb knockdown leads to minor axonal defects in zebrafish

To assess whether TEER deficits played a functional role in the formation and maintenance of the neuromuscular junction (NMJ), we performed immunohistochemical analysis of axonal projections from the motor neurons. We observed a similar length and arborization of axonal projections of motor neurons in larvae injected with *Vapb* AMO when compared with control embryos (non-injected and mismatch AMO) (Fig. 4A). As mentioned previously, the embryos injected with *Vapb* AMO did not display any morphological abnormalities (Fig. 4B).

Targeted ablation of exon 3 in murine *Vapb* generates *Vapb* −/− mice

We next sought to determine whether the loss of *VAPB* function could also lead to motor deficits in a mammalian model. To this aim, we generated mice with insertion of loxP sites flanking both sides of exon 3 because the presence of an ATG codon in exon 3 could lead to the generation of an almost complete VAPB protein (Fig. 5A). On the contrary, excision of exon 3 yielded an out-of-frame mRNA putatively leading to the generation of an aberrant 84 amino-acid long VAPB-derived peptide. *Vapb*-loxP animals were crossed with CMV-CRE mice to obtain germline transmission and obtain $Vapb^{\Delta exon3}$ mice in their progeny. Such $Vapb^{\Delta exon3}$ mice were obtained, viable and transmitted the Δexon3 allele to their progeny. We next generated and studied mice with one or two Δexon3 alleles. RT–PCR analysis from spinal cord tissue using primers spanning the exon 3 sequence detected the presence of mRNA lacking exon 3 in both heterozygous and homozygous $Vapb^{\Delta}$exon3 mice (Fig. 5B). RT-qPCR analysis using primers outside exon 3 revealed that the deletion led to a strong decrease in total *Vapb* mRNA in heterozygous mice, and to barely detectable *Vapb* mRNA levels in homozygous mice in both cerebral cortex and tibialis anterior (TA) muscle (Fig. 5C), which is likely due to non-sense mRNA decay. To further check that $Vapb^{\Delta exon3}$ mice were indeed *Vapb* −/− mice, we raised a polyclonal rabbit antibody against a peptide located in exon 1/2 of Vapb since all commercially available antibodies yielded non-specific bands in our hands. Western blot analysis of $Vapb^{\Delta}$exon3 mice showed a complete loss of the VAPB signal in homozygous mice and a strong reduction in heterozygous mice (Fig. 5D). We were unable to detect the potential 84-amino acid long $Vapb^{\Delta exon3}$-derived peptide (predicted MW 9 kDa). *Vapa* mRNA levels were unchanged by *Vapb* exon 3 ablation (Fig. 5E), suggesting that *Vapb* loss was not compensated by *Vapa* transcriptional upregulation. Thus, $Vapb^{\Delta}$exon3 mice are complete knockout of *Vapb*, and are termed *Vapb* −/− mice in the rest of this report.

Vapb ablation leads to mild, late-onset motor deficits in mice

Vapb −/− mice were fully viable, fertile and appeared healthy. We then sought to determine whether they displayed behavioural abnormalities. To this aim, we performed a SHIRPA protocol, consisting of a battery of simple tests to rapidly evaluate the existence of a phenotype (phenome.jax.org). The results of the SHIRPA screening in two cohorts of 4–6 months ($n = 8$) and 18–22 months ($n = 8$) of +/+,

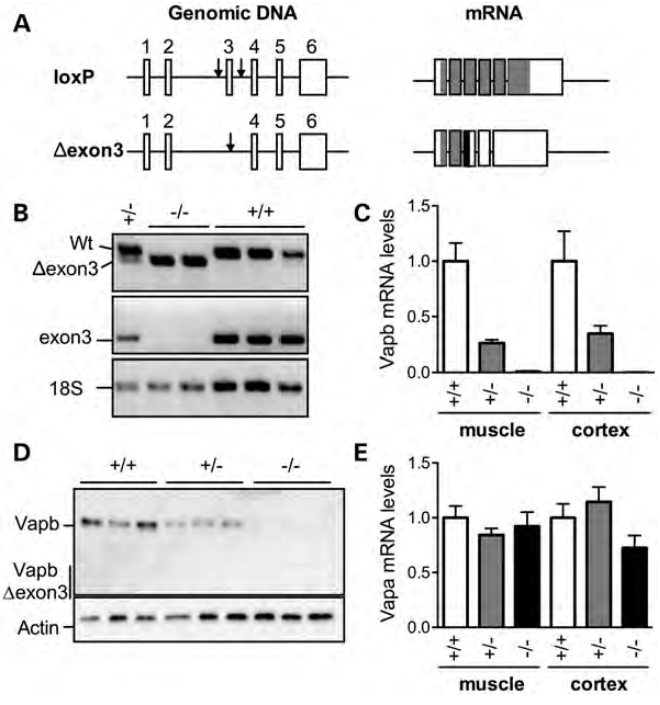

Figure 5. Generation of *Vapb* −/− mice. (**A**) Genomic DNA organization of the *Vapb*-loxP locus (left) and resulting mRNA species before (upper) and after (lower) CRE-mediated excision with loxP sites shown as arrows. Removal of exon 3 generates a transcript with an open reading frame leading to the potential generation of an aberrant 84 amino-acid long peptide. (**B**) RT–PCR analysis of the cerebral cortex from one *Vapb* +/−, two *Vapb*−/− and three *Vapb* +/+ mice using primers spanning exon 3 (upper panel), within exon 3 (middle panel) or targeting 18S rRNA. Exon 3 deletion either in one (+/−) or both alleles (−/−) leads to the detection of a smaller PCR product due to deletion of exon 3. (**C**) RT–qPCR of *Vapb* mRNA levels relative to RNA polymerase II in mouse cerebral cortex or TA muscle. (**D**) Western blot analysis of VAPB protein in the cerebral cortex of three *Vapb* +/+, three *Vapb* +/− and three *Vapb* −/− mice using an antibody targeting exons 1 to 2. Note the complete disappearance of the VAPB signal in −/− mice and that there are no detectable levels of the putative 84-amino acid long VAPB-derived peptide which could have been produced from the *Vapb* −/− locus. (**E**) RT–qPCR of *Vapa* mRNA levels relative to RNA polymerase II in mouse cerebral cortex or TA muscle.

+/− and −/− mice are presented in Supplementary Material, Table S2. Body position appeared unaffected at both ages, as well as negative geotaxis, catalepsy and toe withdrawal upon pinching. However, older *Vapb* −/− mice displayed lower hind limb and ventral tone, meaning that their spontaneous resistance against a small hand pressure on their hind limb and abdomen was decreased. Furthermore, we observed that multiple *Vapb* +/− and −/− mice displayed mild tremors in the open field. Thus, *Vapb* −/− mice seemed roughly normal but might develop age-related central nervous system defects. To further quantify this observation, we performed an accelerating Rotarod protocol to test for motor function, balance and coordination. This test showed that *Vapb* −/− mice were unable to remain on the Rotarod for as long as *Vapb* +/+ at 18 months of age, but not at 4 months of age ($P < 0.05$) (Fig. 6A). However, grip test analysis (Fig. 6B) did not demonstrate significant differences in muscle strength between the three groups at any age tested. Thus, the knockout of *Vapb* leads to mild, late onset defects in motor performance without affecting muscle strength.

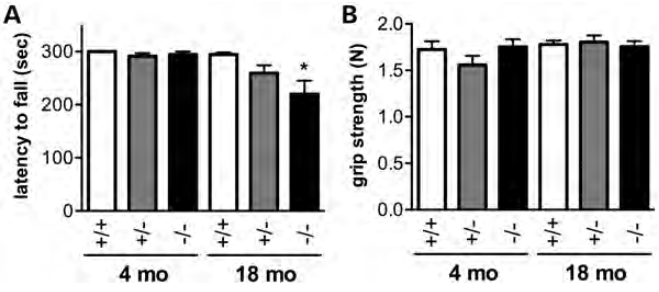

Figure 6. Behavioural analysis of *Vapb* −/− mice. Rotarod test (**A**) and grip strength test (**B**) performed with *Vapb* +/+, +/− and −/− mice at 4 and 18 months of age versus corresponding wild-type mice. $N = 8$ per group.

Vapb ablation does not lead to morphological defects at the neuromuscular junction or to muscle denervation in mice

To determine whether this mild behavioural phenotype could be due to an underlying motor neuron disease, we performed electromyographical analysis on *Vapb* −/− mice. We did not observe stereotypical denervation-related electrical activities in gastrocnemius (GA) or TA muscle of *Vapb* +/− and −/− mice (Supplementary Material, Fig. S3A), but irregular abnormal electrical activities were sparsely observed in some TA, but not GA, muscles of *Vapb* −/− mice (not shown). Diseased $SOD1^{G86R}$ mice analysed in parallel showed typical fibrillations and fasciculations in both muscles. Consistent with the lack of gross denervation in muscle, mRNA levels of denervation-related markers, including the alpha and gamma subunits of the cholinergic receptor, *myogenin* and *Musk* were unchanged in *Vapb* +/− and −/− tibialis muscle when compared with +/+, while the upregulation of these markers was obvious in muscles of paralysed $SOD1^{G86R}$ mice (Supplementary Material, Fig. S3B). To determine whether individual NMJs were morphologically normal, we studied the morphology of the NMJ in the TA of 18 months and of 12 months mice. The morphology of the post-synaptic apparatus appeared to be normal up to 18 months (Supplementary Material, Fig. S4A). We performed morphometric analysis of the post-synaptic apparatus in these mice and found that the area of the NMJ was stable with age and was not modified by the genotype (Supplementary Material, Fig. S4B). NMJs of 18 months old mice were more fragmented and tended to be less complex, but there was no obvious effect of *Vapb* genotype (Supplementary Material, Fig. S4C and D). Consistently, NMJs of *Vapb* −/− and +/− mice appear to be normally innervated in the GA (Fig. 7A) or the soleus muscles (Fig. 7B). Thus, ablation of *Vapb* does not trigger denervation of muscles or morphological defects in NMJs up to 18 months of age.

Vapb ablation does not lead to abnormal UPR

VAPB has been involved in UPR and endoplasmic reticulum homeostasis (5,7–9,17). An abnormal UPR is involved in ALS (18,19) and it is therefore possible that loss of *VAPB* function interferes with UPR signalling. The basal expression levels of BiP (GRP78), CHOP, ATF4 and ATF6 alpha, four master genes in UPR, were, however, similar to controls in 12 months *Vapb* −/− and +/− mice in spinal cord (Supplementary Material, Fig. S6A) or TA muscle (Supplementary

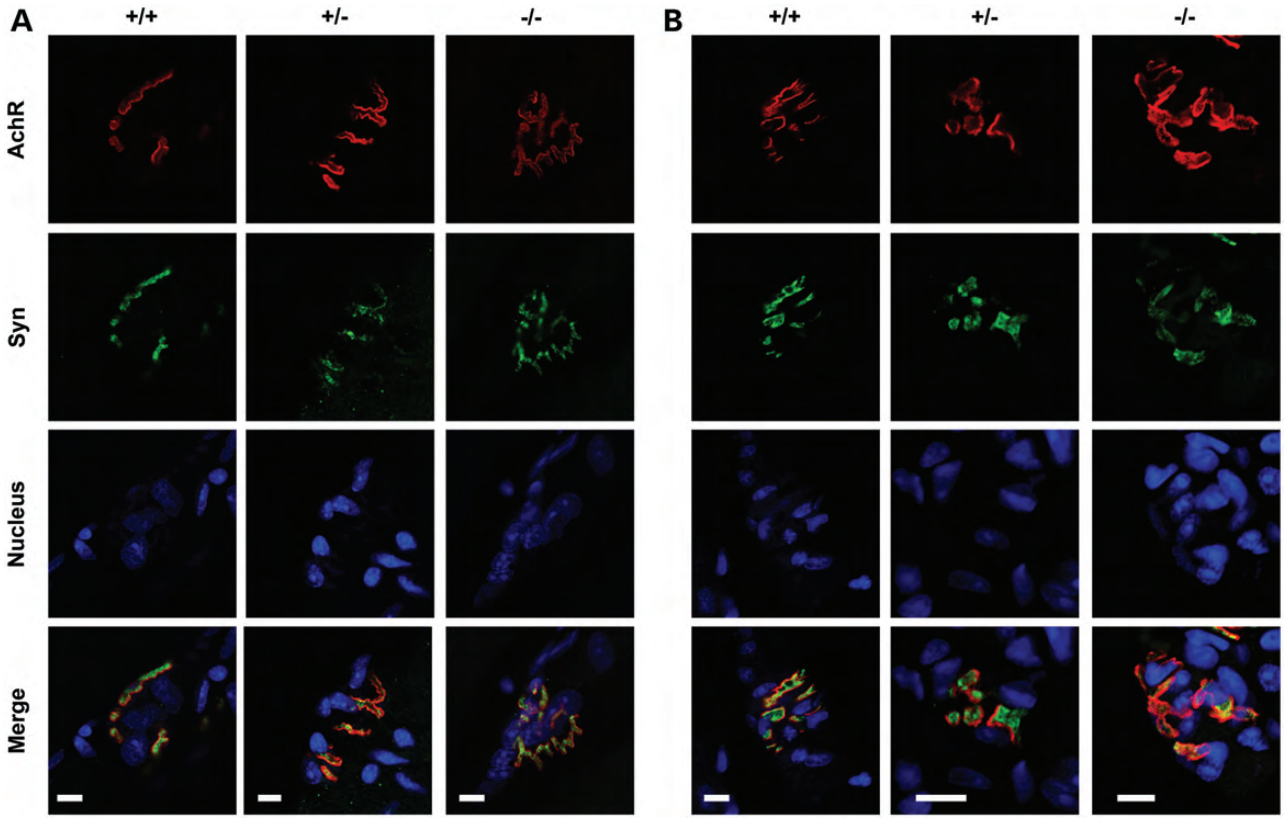

Figure 7. *Vapb* +/− and −/− mice present normal NMJ innervation. Representative photomicrographs showing AchR (red), synaptophysin (green) and nuclear staining (blue) in GA (**A**) or soleus (**B**) muscle from *Vapb* +/+, +/− and −/− mice at 18 months (18 mo) of age. Merged images are shown in the lower panels. Scale bar = 10 μm, $n = 3–6$ mice per group.

Material, Fig. S6B). UPR activation can be elicited with 1 mg/kg of tunicamycine injection and is sustained during several days in mice (20). We found similar levels of UPR gene activation in *Vapb* +/+, +/− and −/− mice 48 h after tunicamycine injection (Supplementary Material, Fig. S7C). These results suggest that *Vapb* is dispensable for both basal and tunicamycin-induced UPR.

DISCUSSION

We provide evidence in this study that the loss of function of *Vapb* weakens the motor system of vertebrate animals without recapitulating the full ALS phenotype. These data suggest that *VAPB* mutations likely constitute a risk factor for developing ALS.

A first important result of our study is that *VAPB* mutations, although rare, are found in ALS patients. We found a p.S160Δ mutation in a fALS patient (family 113) that was previously identified by Landers *et al*. in another fALS case (15). These authors also observed this deletion variant in about 1% of the control cases studied. We did not detect it in 380 controls, suggesting that this variant is rare in the general population. We further identified a novel p.A145V mutation in an apparently sporadic case, also not detected in our control individuals. Recently a family with a p.V234I mutation (21) and several others with P56S mutations were described (21–25). Altogether, this study and others indicate that *VAPB* mutations exist in rare cases of ALS and are not restricted to the initial P56S and T46I mutations. Pathogenicity of these *VAPB* mutations has, however, been conclusively shown only for the P56S mutation. To date, co-segregation was not shown for any other *VAPB* mutation.

Determining whether *VAPB* mutations are gain or loss of function is an important step in understanding ALS8. Two lines of argument suggested a potential gain of function: first, the two known mutations were situated very close one from the other, in the MSP domain that, in worms, is cleaved and secreted by neurons to regulate nerve/muscle signalling (26). Second, both P56S and T46I mutations generated large cytosolic aggregates upon overexpression *in vitro* (8,10,17) and *in vivo* (11). The p.A145V and p.S160Δ mutations we identified here lie outside the MSP domain, as does the p.V234I previously identified (21), indicating that ALS mutations spread through the whole coding sequence of *VAPB* and do not cluster within the MSP domain. This discovery argues against *VAPB* mutations directly interfering with the signalling elicited by a cleaved MSP domain. These newly identified mutations could, however, modulate, either positively or negatively, VAPB protein levels and/or MSP domain regulation. A second hypothesis recently proposed a loss of function or haploinsufficiency of the protein resulting from ALS-related mutations. This mechanism is indirectly supported by the lack of detectable phenotype in mice overexpressing wild-type or mutant VAPB (11,12). In addition, *Caenorhabditis elegans* and *Drosophila melanogaster* showed strong phenotypes upon decreased expression of VAP proteins (26–29). Furthermore, iPS cells-derived neurons

from P56S patients do not show VAPB cytosolic protein aggregates as observed upon overexpression, but present decreased VAPB protein levels (13). Our results in both mouse and fish models support the idea that a loss of function of *VAPB* contributes to ALS pathogenesis. Knockdown of fish *vapb* led to motor impairments, while the complete knockout of *Vapb* in mice led to a mild age-dependent decrease in motor performance. Haploinsufficiency experiments, through the loss of one copy of *Vapb* gene in *Vapb* +/− mice, did not lead to any detectable phenotype. Furthermore, overexpression of wild-type human VAPB RNA was able to rescue the phenotype of knockdown zebrafish VAPB, while overexpression of a VAPB mutant RNA did not. Despite a motor phenotype being observed in both animal models, neither *Vapb* knocked down fish nor *Vapb* −/− mice progressed to a full-blown ALS phenotype. In zebrafish, the phenotype observed upon *vapb* KD was milder than that observed upon *Tardbp* KD or human TARDBP mutant overexpression (30). In mice, the NMJ was spared even at very old ages, contrasting with observations from mutant SOD1 mice that develop a stereotypical ALS phenotype (31). The mild phenotypes presented here contrast with the very strong phenotypes observed in the previous invertebrate models. However, invertebrates, and in particular *C. elegans* and *D. melanogaster,* possess only one orthologue accounting for both *VAPB* and *VAPA* genes. Loss-of-function experiments in these species result in a complete loss of VAP proteins, and are thus more drastic than in single VAPB knock-out vertebrates that retain VAPA normal expression. We did not observe transcriptional upregulation of *Vapa* upon *Vapb* ablation. This, however, does not exclude that VAPA and VAPB protein functions are sufficiently redundant for VAPA to compensate for VAPB loss. Thus, we suggest that compensation for the loss of *VAPB* function through *VAPA* might underlie the difference in phenotype severity between vertebrates and invertebrates.

The mechanisms underlying the motor phenotype observed in *vapb* KD fish and *Vapb* −/− mice warrant further investigation. Since VAPB has been involved in UPR and endoplasmic reticulum homeostasis (5,7–9,17) and an abnormal UPR is involved in ALS (18,19), we hypothesized that a loss of *VAPB* could interfere with UPR signalling. However, we did not find any transcriptional evidence of UPR activation or deficit in *Vapb* −/− mice, nor observed massive UPR deficit upon tunicamycine injection. Consistently, recent work showed that VAPB overexpression, either wild-type or mutant, did not modify the UPR (11). Alternatively, the VAPB protein is involved in the regulation of Eph/Ephrin signalling, a major pathway regulating sensory-motor axonal development and regeneration (32). That *Vapb* silencing might affect the formation and maintenance of the sensory-motor system through altered Eph/Ephrin would be consistent with the recent observation that EphA4 is a risk factor for ALS (33). VAPB is also a key regulator of axonal vesicle transport (6) and its loss could also alter axonal transport leading to axonal deficits, perhaps causative of the observed phenotypes in *Vapb* KD zebrafish. Future studies using other endoplasmic reticulum homeostasis stressors or axonal transport in loss-of-function animal models could shed light on the function of *VAPB* in disease-relevant stresses.

In summary, we show here that *VAPB* mutations are present at low rates in ALS patients, and act, at least partially, through loss of function to impair the vertebrate motor system. Incomplete penetrance of ALS genes might be due to complex inheritance of multiple risk variants (oligogenic theory) (34). In such a scenario, *VAPB* mutations could be found in patients in combination with other ALS-relevant mutations. Indeed, a fALS patient was recently found to display a double *VAPB* and *C9ORF72* mutation (21). We thus postulate that *VAPB* mutations should be considered as strong risk factors that may lead to ALS, when placed in combination with other genetic risk factors or with environmental agents (35) or nutritional alterations (36) predisposing to ALS.

MATERIALS AND METHODS

Human genetic studies

Patient and control sample collection

Neurologists specialized in ALS diagnosed all cases as definite ALS according to El Escorial criteria and collected all samples. Informed written consent was obtained from each individual and blood samples were collected for DNA extraction. All fALS patients were initially screened for mutations in the *SOD1* gene prior to inclusion in this study. In total, DNA from 69 fALS and 100 sALS patients was collected. In the fALS panel, 31 individuals were French, 29 were Canadian and 9 were American. The sALS panel was composed of 44 French patients, 52 Canadian patients and 4 American patients. Ethnically matched and unrelated individuals were used as controls in this study.

Gene screening and variation analysis

The coding region of all six exons of *VAPB* (accession number NM_004738.3) was sequenced in each patient including at least 50 bp of the intronic region at each intron–exon junction. Primers were designed using the PrimerSelect programme (Lasergene) and synthesized by Invitrogen Canada Inc. PCR products were sequenced at the McGill University and Genome Quebec Centre for Innovation. In each case, the forward primer was used for sequencing and variations were confirmed by reverse sequencing. The presence of observed variants was analysed in control individuals. Variants in exon 5 were screened by direct sequencing, while allele-specific oligomerization was employed for variants in exons 1 and 4 as previously described (37,38). Oligomers used for exon 1 were 5′-AGGGGTCTCCCCGCCAA-3′ to detect the common allele and 5′-AGGGGTGTCCCCGCCAA-3′ for the rare allele and oligomers used for exon 4 were 5′-GAGAATGATAAACCAG-3′ and 5′-GAGAATGAGAAACCAG-3′. The MegAlign programme of the DNASTAR package (Lasergene) was used to align proteins homologous to VAPB from various species by the ClustalW method.

Zebrafish studies

Zebrafish were raised from a colony maintained according to the established procedures, and all experiments were carried out in compliance with the Canadian Council for Animal Care.

Constructs

Each mutation (P56S, A145V, and S160Δ) was introduced into the human *VAPB* clone by site-directed mutagenesis. The three mutant VAPB cDNAs, as well as the wild-type cDNA, were cloned into a pCS2 vector and were transcribed *in vitro* using the SP6 mMESSAGE mMachine kit (Ambion). The protein expression from each of these constructs was validated by western blot analysis with an anti-VAPB antibody (kindly provided by Dr Kanekura). A band at the appropriate molecular weight (~27 kDa for VAPB) was observed (result not shown).

Antisense morpholino oligonucleotide (AMO) injections

The morpholino sequences were designed against the zebrafish *Vapb* orthologue located on chromosome 6. The oligonucleotide 5′-CCATCTCCCACTGCAAACGCTCGGA-3′ (*Vapb* AMO) binds to the ATG of the *Vapb* gene, which prevents its translation, and a 5 bp mismatch oligonucleotide was used as a control. Both were designed and purchased from Gene Tools (Gene Tools, Oregon, USA). AMO injections were performed in one-to-four cell stage zebrafish eggs as previously described, at an optimal concentration of 1.0 mM (30). The rescue experiments were performed as mentioned above, with simultaneous injections of the AMO and human VAPB mRNA at concentrations of 1.0 mM and 80 ng/μl respectively.

Behavioural and immunocytochemical analysis

Morphology and behavioural touch responses were assessed with a stereomicroscope (Zeiss, Oberkochen, Germany). To elicit the escape response at 48 hpf, embryos were touched lightly on the tail with a pair of blunt forceps and their swimming episodes were recorded using a Photron (San Diego, CA, USA) Fastcam PCI high-speed video camera at 125 frames/s. For immunohistochemical analysis of axonal projections of motor neurons, monoclonal antibodies against synaptic vesicle 2 (anti-SV2m Developmental Studies Hybridoma) was used to label pre-synaptic axons at the NMJ and anti-acetylated alpha-tubulin (Sigma) was used to label all neuronal tubulins.

Mouse studies

Animal housing

Transgenic mice were housed in the animal facility of the medicine faculty of Strasbourg University, with 12 h/12 h of light/dark and unrestricted access to food and water. In all experiments, littermates were used for comparison. Transgenic *SOD1*^{G86R} mice were used at onset of symptoms as previously defined (39) to provide a positive control for ALS-like phenotype.

Generation of Vapb-loxP and Vapb −/− mice

Floxed exon 3 *Vapb* mice were generated in the Institut Clinique de la Souris (ICS, Illkirch) using standard procedures. The Neomycin cassette was deleted through a FRT recombination step. Complete *Vapb* −/− mice were generated through crossing with CMV-Cre animals. The recombination in double transgenic animals was total and germline transmission of the deleted allele was obtained. The genetic background of all mice used in this study is >99% C57Bl6/N Tac.

Behavioural analysis

We used the SHIRPA (SmithKline Beecham, Harwell, Imperial College School of Medicine at St Mary's; Royal London Hospital, St Bartholomew's and the Royal London School of Medicine; Phenotype Assessment) screening procedure to grossly characterize the phenotype of mice. These tests consist of using standard methods such as open field, jar view and grid tests to provide a behavioural and functional profile by rapid and simple observational assessment. The SHIRPA procedure is commonly used for phenotyping purposes (40). Mouse motor performance was assessed using Rotarod (model 7650, Ugo Basile, Comerio, Italy). Each session consisted of three tests of 330 s with an acceleration period (4 to 20 rpm during 150 s) followed by 150 s at constant speed. Results are the mean of four consecutive weekly sessions performed after 2 weeks of habituation. To evaluate muscle strength, we used a gripmeter (ALG01; Bioseb, Vitrolles, France). The muscle force (in Newton) was measured three times per mouse. Results are the mean of three consecutive weekly sessions.

Electromyography

Electromyography was performed as previously described (41,42). Mice ($n = 9$ +/+; $n = 9$ +/−; $n = 9$ −/−) were anaesthetized with a solution of ketamine/xylasine (100 mg/kg; 5 mg/kg) and electrical activity was recorded using a monopolar needle electrode (diameter 0.3 mm; 9013R0312; Medtronic, Minneapolis, MN) inserted into the tail of the mouse. Recordings were made with a concentric needle electrode (diameter 0.3 mm; 9013S0011; Medtronic). Electrical activity was monitored in both GA and TA on both legs for at least 2 min. Spontaneous activity was differentiated from voluntary activity by visual and auditory inspection.

Immunostaining

Immediately after sacrifice, muscle tissues were dissected and fixed by immersion in 4% paraformaldehyde in 0.1 M phosphate buffer pH 7.4 (1 h). Tissues were then rinsed three times with PBS and stored at 4°C until use. The prepared muscles bundles were stained using fluorescently labeled α-Bungarotoxin-TRITC (Sigma, Saint-Quentin Fallavier, France) and an anti-synaptophysin antibody (Epitomics). For post-synaptic morphology quantification, bungarotoxin signals from more than 25 NMJs per animal were imaged under a fluorescent microscope. The data were analysed as previously described (42). For double labelling or post- and pre-synaptic parts of the NMJs, images were acquired using a laser scanning microscope (LSM 510; Carl Zeiss, Thornwood,NY) equipped with a Plan-Apochromat 63x oil DIC immersion lens (numerical aperture 1,4). Synaptophysin-Alexa 488 was excited using the 488 nm ray of the argon laser. The emission signal of Alexa 488 was filtered with a BP505-530nm. Bungarotoxin-TRITC was excited using a 543-nm Helium Neon laser. The emission signal of TRITC was filtered with a BP560-615nm. Fluorescent DNA dye-Draq5 was excited using a 633-nm Helium Neon laser. The emission signal of Draq5 was filtered with a LP 650 nm.

VAPB Antibody and western blotting
A rabbit polyclonal antibody directed against mouse VAPB was prepared using the double X programme of Eurogentec (Belgium) and the following epitope (SLEPQHELKFRGPFT +C) present in exons 1/2 of murine VAPB. Antisera were immuno-purified against the peptide. Western blotting was performed as previously described (43). Pre-incubation with an excess of the peptide extinguished the signal in western blots (data not shown).

Real-Time PCR
RNA was reverse transcribed using 1 μg of RNA and the iScript cDNA synthesis kit (Bio-Rad, Marne La Coquette, France). We performed a real-time PCR (IQSYBR GREEN Supermix, BioRad, France) on the cDNA obtained from the RNA samples. Three reference genes were used to compute a normalization factor using Genorm software v3.5: *18S* (18S Ribosomal RNA), *Pol2* (Polr2 polymerase RNA 2 DNA directed polypeptide A) and *Tbp* (TATA-box binding protein) (44). Primer sequences are provided in Supplementary Material, Table S1.

Statistical analysis
Statistical comparisons were accomplished with the unpaired Student *t*-test or ANOVA followed by the *post-hoc* Newman–Keuls multiple comparisons test using PRISM version 5 for MacOS X software (GraphPad, San Diego) unless otherwise indicated.

SUPPLEMENTARY MATERIAL

Supplementary Material is available at *HMG* online.

ACKNOWLEDGEMENTS

We would like to thank the families involved in this study, and Melanie Benard for sample collection and organization. Annie Picchinenna, Marie-Jo Ruivo and Stéphane Dieterle provided technical support for this study. We thank the 'plateforme d'imagerie' from IFR37/INSERM/UDS for technical assistance with confocal imaging.

Conflict of Interest statement. None declared.

FUNDING

This work was supported by the Amyotrophic Lateral Sclerosis Association (ALSA) (grant #1698 to L.D.); Agence Nationale de la Recherche (ANR JCJC Dynemit to L.D.); Association pour la recherche sur la SLA et les autres maladies du motoneurone (ARSla) (to L.D., F.R. and J.P.L.); Thierry Latran Foundation (1st call to J.P.L., 4th call to L.D.); Association Pour La Recherche Et le Développement de Moyens de Lutte Contre les Maladies Neurodégénératives (AREMANE); the European Community's Health Seventh Framework Programme (FP7/2007-2013) (No 259867 to J.P.L.); Helmholtz Institute (RNA dysmetabolism in ALS and FTD, WP2, to L.D.); the Canadian Institutes of Health Research (CIHR) (to F-G.L., P.D., P.N.V. and G.A.R.); and the Muscular Dystrophy Association USA (to G.A.R. and E.K.). E.K. is supported by an Atip/Avenir Inserm award, as well as grants from the Robert Packard Foundation, ARSla, Marie Curie Actions, and AFM. The team of E.K. is part of the École des Neurosciences de Paris Ile-de-France (ENP) network. L.D. is supported by a Mercator Professorship (DFG, 2011–2012) and a contrat d'interface INSERM/AP-HP. P.D. and G.A.R. are supported by Canada Research Chairs. V.B. is a recipient of the ENP Graduate Programme fellowship of the École des Neurosciences de Paris Ile-de-France.

REFERENCES

1. Kiernan, M.C., Vucic, S., Cheah, B.C., Turner, M.R., Eisen, A., Hardiman, O., Burrell, J.R. and Zoing, M.C. (2011) Amyotrophic lateral sclerosis. *Lancet*, **377**, 942–955.
2. Wijesekera, L.C. and Leigh, P.N. (2009) Amyotrophic lateral sclerosis. *Orphanet J. Rare Dis.*, **4**, 3.
3. Gros-Louis, F., Gaspar, C. and Rouleau, G.A. (2006) Genetics of familial and sporadic amyotrophic lateral sclerosis. *Biochim. Biophys. Acta*, **1762**, 956–972.
4. Nishimura, A.L., Mitne-Neto, M., Silva, H.C., Richieri-Costa, A., Middleton, S., Cascio, D., Kok, F., Oliveira, J.R., Gillingwater, T., Webb, J. *et al.* (2004) A mutation in the vesicle-trafficking protein VAPB causes late-onset spinal muscular atrophy and amyotrophic lateral sclerosis. *Am. J. Hum. Genet.*, **75**, 822–831.
5. Chen, H.J., Anagnostou, G., Chai, A., Withers, J., Morris, A., Adhikaree, J., Pennetta, G. and de Belleroche, J.S. (2010) Characterisation of the properties of a novel mutation in VAPB in familial ALS. *J. Biol. Chem.*, **285**, 40266–40281.
6. Rocha, N., Kuijl, C., van der Kant, R., Janssen, L., Houben, D., Janssen, H., Zwart, W. and Neefjes, J. (2009) Cholesterol sensor ORP1L contacts the ER protein VAP to control Rab7-RILP-p150 Glued and late endosome positioning. *J. Cell Biol.*, **185**, 1209–1225.
7. Gkogkas, C., Middleton, S., Kremer, A.M., Wardrope, C., Hannah, M., Gillingwater, T.H. and Skehel, P. (2008) VAPB interacts with and modulates the activity of ATF6. *Hum. Mol. Genet.*, **17**, 1517–1526.
8. Kanekura, K., Nishimoto, I., Aiso, S. and Matsuoka, M. (2006) Characterization of amyotrophic lateral sclerosis-linked pro56ser mutation of vesicle-associated membrane protein-associated protein B (VAPB/ALS8). *J. Biol. Chem.*, **281**, 30223–30233.
9. Suzuki, H., Kanekura, K., Levine, T.P., Kohno, K., Olkkonen, V.M., Aiso, S. and Matsuoka, M. (2009) ALS-linked P56S-VAPB, an aggregated loss-of-function mutant of VAPB, predisposes motor neurons to ER stress-related death by inducing aggregation of co-expressed wild-type VAPB. *J. Neurochem.*, **108**, 973–985.
10. Teuling, E., Ahmed, S., Haasdijk, E., Demmers, J., Steinmetz, M.O., Akhmanova, A., Jaarsma, D. and Hoogenraad, C.C. (2007) Motor neuron disease-associated mutant vesicle-associated membrane protein-associated protein (VAP) B recruits wild-type VAPs into endoplasmic reticulum-derived tubular aggregates. *J. Neurosci.*, **27**, 9801–9815.
11. Qiu, L., Qiao, T., Beers, M., Tan, W., Wang, H., Yang, B. and Xu, Z. (2013) Widespread aggregation of mutant VAPB associated with ALS does not cause motor neuron degeneration or modulate mutant SOD1 aggregation and toxicity in mice. *Mol. Neurodegener.*, **8**, 1.
12. Tudor, E.L., Galtrey, C.M., Perkinton, M.S., Lau, K.F., De Vos, K.J., Mitchell, J.C., Ackerley, S., Hortobagyi, T., Vamos, E., Leigh, P.N. *et al.* (2010) Amyotrophic lateral sclerosis mutant vesicle-associated membrane protein-associated protein-B transgenic mice develop TAR-DNA-binding protein-43 pathology. *Neuroscience*, **167**, 774–785.
13. Mitne-Neto, M., Machado-Costa, M., Marchetto, M.C., Bengtson, M.H., Joazeiro, C.A., Tsuda, H., Bellen, H.J., Silva, H.C., Oliveira, A.S., Lazar, M. *et al.* (2011) Downregulation of VAPB expression in motor neurons derived from induced pluripotent stem cells of ALS8 patients. *Hum. Mol. Genet.*, **20**, 3642–3652.
14. Anagnostou, G., Akbar, M.T., Paul, P., Angelinetta, C., Steiner, T.J. and de Belleroche, J. (2010) Vesicle associated membrane protein B (VAPB) is decreased in ALS spinal cord. *Neurobiol. Aging*, **31**, 969–985.
15. Landers, J.E., Leclerc, A.L., Shi, L., Virkud, A., Cho, T., Maxwell, M.M., Henry, A.F., Polak, M., Glass, J.D., Kwiatkowski, T.J. *et al.* (2008) New

VAPB deletion variant and exclusion of VAPB mutations in familial ALS. *Neurology*, **70**, 1179–1185.
16. Vaccaro, A., Patten, S.A., Ciura, S., Maios, C., Therrien, M., Drapeau, P., Kabashi, E. and Parker, J.A. (2012) Methylene blue protects against TDP-43 and FUS neuronal toxicity in C. Elegans and D. Rerio. *PLoS One*, **7**, e42117.
17. Langou, K., Moumen, A., Pellegrino, C., Aebischer, J., Medina, I., Aebischer, P. and Raoul, C. (2010) AAV-mediated expression of wild-type and ALS-linked mutant VAPB selectively triggers death of motoneurons through a Ca^{2+}-dependent ER-associated pathway. *J. Neurochem.*, **114**, 795–809.
18. Saxena, S., Cabuy, E. and Caroni, P. (2009) A role for motoneuron subtype-selective ER stress in disease manifestations of FALS mice. *Nat. Neurosci.*, **12**, 627–636.
19. Kikuchi, H., Almer, G., Yamashita, S., Guegan, C., Nagai, M., Xu, Z., Sosunov, A.A., McKhann, G.M. 2nd and Przedborski, S. (2006) Spinal cord endoplasmic reticulum stress associated with a microsomal accumulation of mutant superoxide dismutase-1 in an ALS model. *Proc. Natl Acad. Sci. USA*, **103**, 6025–6030.
20. Wu, J., Rutkowski, D.T., Dubois, M., Swathirajan, J., Saunders, T., Wang, J., Song, B., Yau, G.D. and Kaufman, R.J. (2007) ATF6alpha optimizes long-term endoplasmic reticulum function to protect cells from chronic stress. *Dev. Cell*, **13**, 351–364.
21. van Blitterswijk, M., van Es, M.A., Koppers, M., van Rheenen, W., Medic, J., Schelhaas, H.J., van der Kooi, A.J., de Visser, M., Veldink, J.H. and van den Berg, L.H. (2012) VAPB and C9orf72 mutations in 1 familial amyotrophic lateral sclerosis patient. *Neurobiol. Aging*, **33**, 2950.
22. Nishimura, A.L., Al-Chalabi, A. and Zatz, M. (2005) A common founder for amyotrophic lateral sclerosis type 8 (ALS8) in the Brazilian population. *Hum. Genet.*, **118**, 499–500.
23. Tomiyama, H., Kokubo, Y., Sasaki, R., Li, Y., Imamichi, Y., Funayama, M., Mizuno, Y., Hattori, N. and Kuzuhara, S. (2008) Mutation analyses in amyotrophic lateral sclerosis/parkinsonism-dementia complex of the Kii peninsula, Japan. *Mov. Disord.*, **23**, 2344–2348.
24. Funke, A.D., Esser, M., Kruttgen, A., Weis, J., Mitne-Neto, M., Lazar, M., Nishimura, A.L., Sperfeld, A.D., Trillenberg, P., Senderek, J. *et al.* (2010) The p.P56S mutation in the VAPB gene is not due to a single founder: the first European case. *Clin. Genet.*, **77**, 302–303.
25. Millecamps, S., Salachas, F., Cazeneuve, C., Gordon, P., Bricka, B., Camuzat, A., Guillot-Noel, L., Russaouen, O., Bruneteau, G., Pradat, P.F. *et al.* (2010) SOD1, ANG, VAPB, TARDBP, and FUS mutations in familial amyotrophic lateral sclerosis: genotype–phenotype correlations. *J. Med. Genet.*, **47**, 554–560.
26. Tsuda, H., Han, S.M., Yang, Y., Tong, C., Lin, Y.Q., Mohan, K., Haueter, C., Zoghbi, A., Harati, Y., Kwan, J. *et al.* (2008) The amyotrophic lateral sclerosis 8 protein VAPB is cleaved, secreted, and acts as a ligand for Eph receptors. *Cell*, **133**, 963–977.
27. Pennetta, G., Hiesinger, P.R., Fabian-Fine, R., Meinertzhagen, I.A. and Bellen, H.J. (2002) Drosophila VAP-33A directs bouton formation at neuromuscular junctions in a dosage-dependent manner. *Neuron*, **35**, 291–306.
28. Chai, A., Withers, J., Koh, Y.H., Parry, K., Bao, H., Zhang, B., Budnik, V. and Pennetta, G. (2008) hVAPB, the causative gene of a heterogeneous group of motor neuron diseases in humans, is functionally interchangeable with its Drosophila homologue DVAP-33A at the neuromuscular junction. *Hum. Mol. Genet.*, **17**, 266–280.
29. Han, S.M., Tsuda, H., Yang, Y., Vibbert, J., Cottee, P., Lee, S.J., Winek, J., Haueter, C., Bellen, H.J. and Miller, M.A. (2012) Secreted VAPB/ALS8 major sperm protein domains modulate mitochondrial localization and morphology via growth cone guidance receptors. *Dev. Cell*, **22**, 348–362.
30. Kabashi, E., Lin, L., Tradewell, M.L., Dion, P.A., Bercier, V., Bourgouin, P., Rochefort, D., Bel Hadj, S., Durham, H.D., Vande Velde, C. *et al.* (2010) Gain and loss of function of ALS-related mutations of TARDBP (TDP-43) cause motor deficits in vivo. *Hum. Mol. Genet.*, **19**, 671–683.
31. Dupuis, L. and Loeffler, J.P. (2009) Neuromuscular junction destruction during amyotrophic lateral sclerosis: insights from transgenic models. *Curr. Opin. Pharmacol.*, **9**, 341–346.
32. Gallarda, B.W., Bonanomi, D., Muller, D., Brown, A., Alaynick, W.A., Andrews, S.E., Lemke, G., Pfaff, S.L. and Marquardt, T. (2008) Segregation of axial motor and sensory pathways via heterotypic trans-axonal signaling. *Science*, **320**, 233–236.
33. Van Hoecke, A., Schoonaert, L., Lemmens, R., Timmers, M., Staats, K.A., Laird, A.S., Peeters, E., Philips, T., Goris, A., Dubois, B. *et al.* (2012) EPHA4 is a disease modifier of amyotrophic lateral sclerosis in animal models and in humans. *Nat. Med.*, **18**, 1418–1422.
34. van Blitterswijk, M., van Es, M.A., Hennekam, E.A., Dooijes, D., van Rheenen, W., Medic, J., Bourque, P.R., Schelhaas, H.J., van der Kooi, A.J., de Visser, M. *et al.* (2012) Evidence for an oligogenic basis of amyotrophic lateral sclerosis. *Hum. Mol. Genet.*, **21**, 3776–3784.
35. Valdmanis, P.N. and Rouleau, G.A. (2008) Genetics of familial amyotrophic lateral sclerosis. *Neurology*, **70**, 144–152.
36. Dupuis, L., Pradat, P.F., Ludolph, A.C. and Loeffler, J.P. (2011) Energy metabolism in amyotrophic lateral sclerosis. *Lancet Neurol.*, **10**, 75–82.
37. Labuda, D., Krajinovic, M., Richer, C., Skoll, A., Sinnett, H., Yotova, V. and Sinnett, D. (1999) Rapid detection of CYP1A1, CYP2D6, and NAT variants by multiplex polymerase chain reaction and allele-specific oligonucleotide assay. *Anal. Biochem.*, **275**, 84–92.
38. Bourgeois, S. and Labuda, D. (2004) Dynamic allele-specific oligonucleotide hybridization on solid support. *Anal. Biochem.*, **324**, 309–311.
39. Dentel, C., Palamiuc, L., Henriques, A., Lannes, B., Spreux-Varoquaux, O., Gutknecht, L., Rene, F., Echaniz-Laguna, A., Gonzalez De Aguilar, J.L., Lesch, K.P. *et al.* (2013) Degeneration of serotonin neurons in amyotrophic lateral sclerosis: a link to spasticity. *Brain*, **136** (Pt 2), 483–493.
40. Rogers, D.C., Fisher, E.M., Brown, S.D., Peters, J., Hunter, A.J. and Martin, J.E. (1997) Behavioral and functional analysis of mouse phenotype: SHIRPA, a proposed protocol for comprehensive phenotype assessment. *Mamm. Genome*, **8**, 711–713.
41. Dupuis, L., Fergani, A., Braunstein, K.E., Eschbach, J., Holl, N., Rene, F., Gonzalez De Aguilar, J.L., Zoerner, B., Schwalenstocker, B., Ludolph, A.C. *et al.* (2009) Mice with a mutation in the dynein heavy chain 1 gene display sensory neuropathy but lack motor neuron disease. *Exp. Neurol.*, **215**, 146–152.
42. Dupuis, L., Gonzalez de Aguilar, J.L., Echaniz-Laguna, A., Eschbach, J., Rene, F., Oudart, H., Halter, B., Huze, C., Schaeffer, L., Bouillaud, F. *et al.* (2009) Muscle mitochondrial uncoupling dismantles neuromuscular junction and triggers distal degeneration of motor neurons. *PLoS One*, **4**, e5390.
43. Eschbach, J., Fergani, A., Oudart, H., Robin, J.P., Rene, F., Gonzalez de Aguilar, J.L., Larmet, Y., Zoll, J., Hafezparast, M., Schwalenstocker, B. *et al.* (2011) Mutations in cytoplasmic dynein lead to a Huntington's disease-like defect in energy metabolism of brown and white adipose tissues. *Biochim. Biophys. Acta*, **1812**, 59–69.
44. Vandesompele, J., De Preter, K., Pattyn, F., Poppe, B., Van Roy, N., De Paepe, A. and Speleman, F. (2002) Accurate normalization of real-time quantitative RT-PCR data by geometric averaging of multiple internal control genes. *Genome Biol.*, **3**, research0034.0031–0034.0011.

Supplementary Material

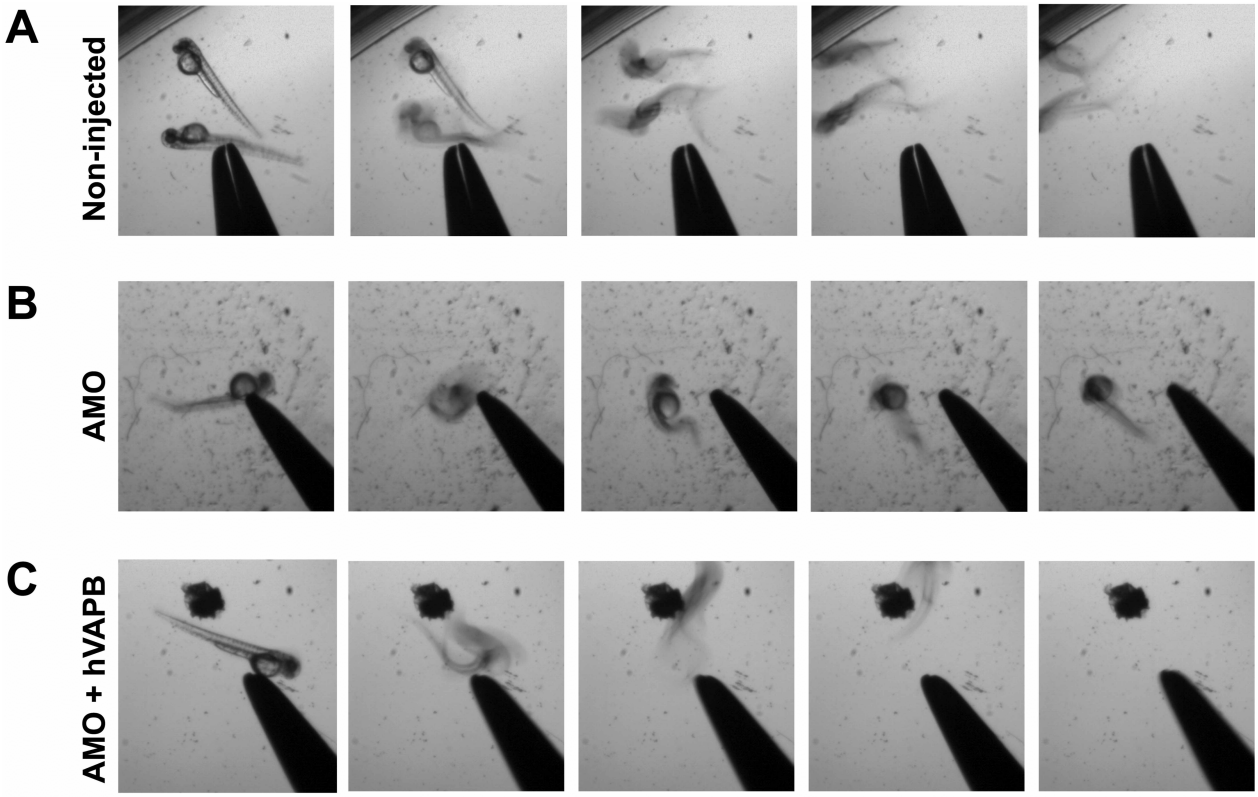

Supplementary Figure 1: Motor deficits associated with *vapb* loss of function in knock down zebrafish embryos.

A and B: Knockdown of *vapb* by AMO led to behavioural deficits observed during TEER swimming bouts (as quantified i
Supplementary Figure 2).
C: These deficits were reduced upon co-injection of human wild-type VAPB mRNA with the *vapb*AMO.

Supplementary Figure 2

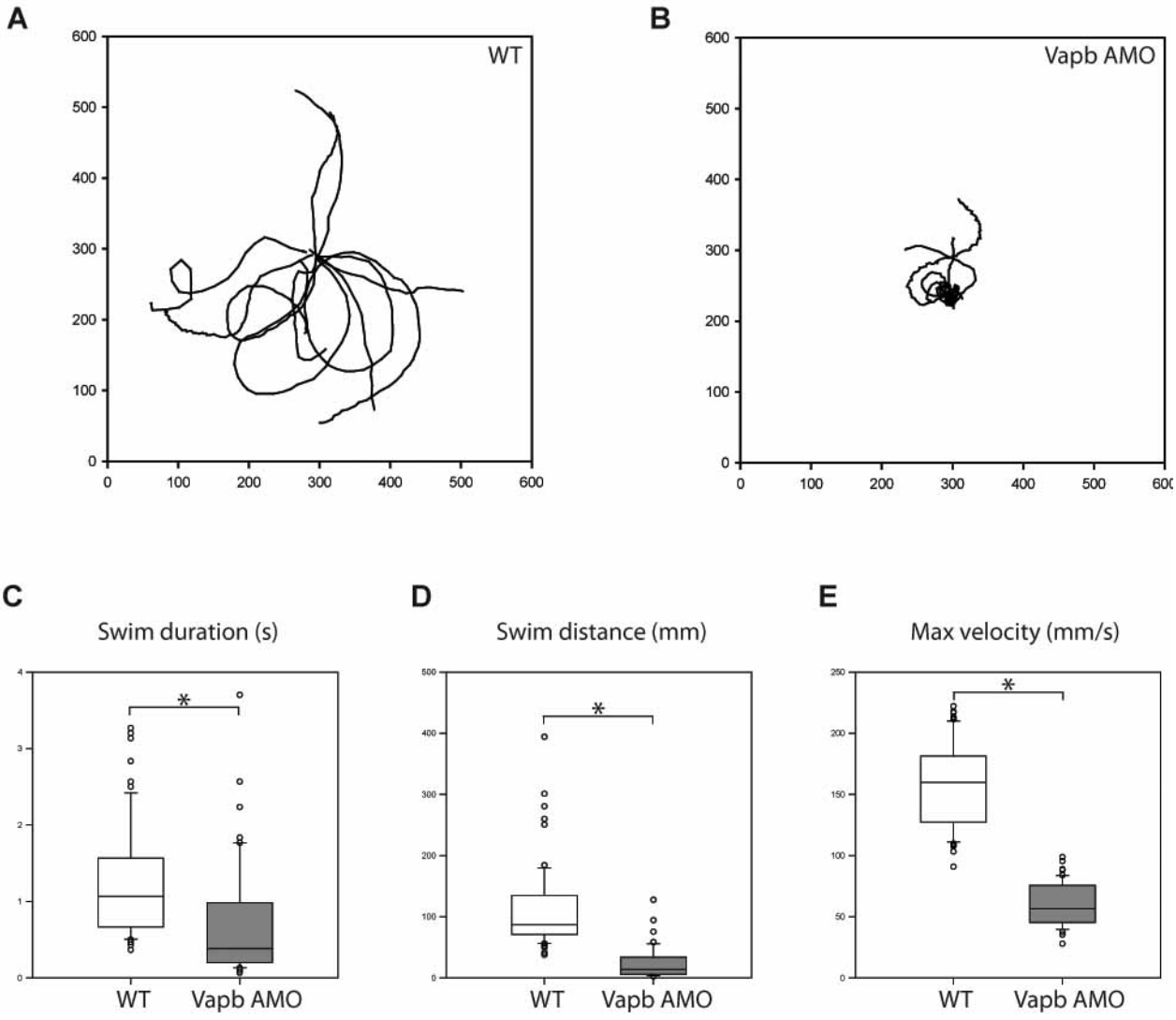

Supplementary Figure 2: Quantification of behavioural deficits associated with *vapb* loss of function in knock dow zebrafish embryos.

A and B: Traces of embryo movement during TEER induced swimming bouts revealed major behavioural deficits in th *vapb* knock down embryos (traces shown for 10 embryos) .

C, D and E: The swimming duration, distance swam and maximum velocity of the *vapb* knock down embryos swimmin episode were significantly reduced. (n=10-15 embryos for each condition, N=4)

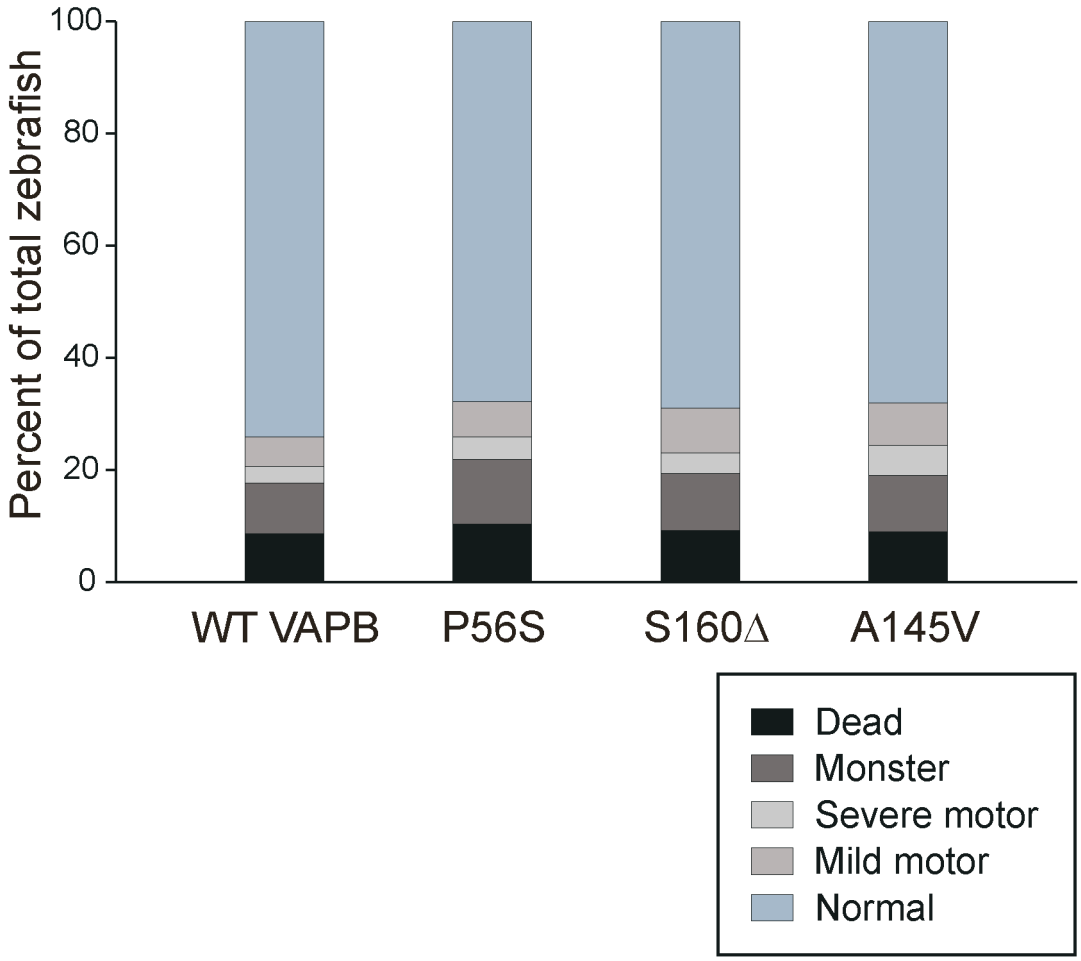

Supplementary Figure 3: Quantification of developmental and behavioural deficits associated with overexpression o wild type or mutant VAPB RNAs.

The percentage of zebrafish displaying developmental or motor abnormalities was not significantly altered and similar upo injection of human wild-type VAPB RNA (WT), or of the three human VAPB mRNAs bearing ALS-related mutation P56S, S160Δ and A145V.

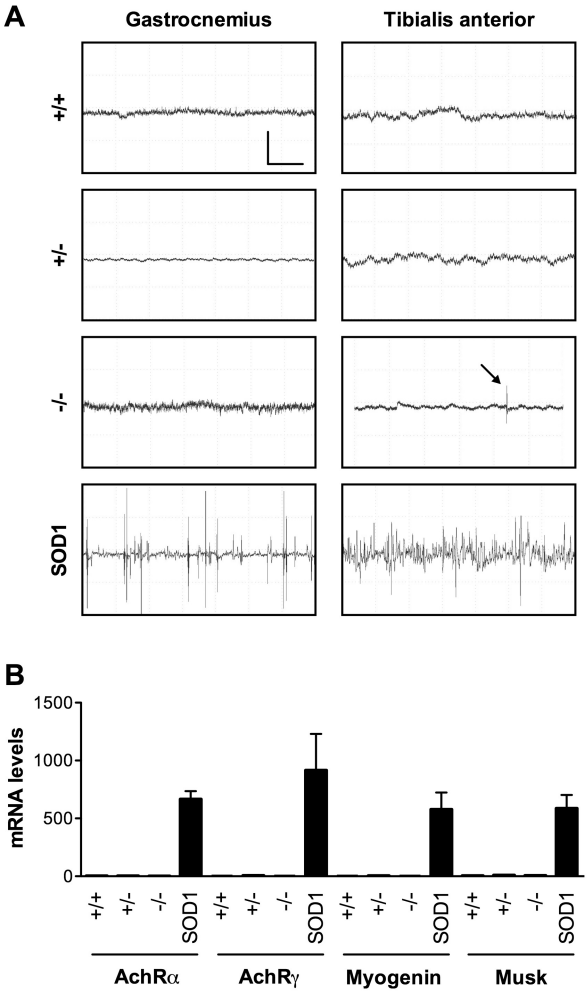

Supplementary Figure 4: Absence of muscle denervation in *Vapb* +/- and -/- mice

A: Representative electromyograms of *Vapb* +/+, +/- and -/- mice in gastrocnemius (left) and tibialis (right) muscles. Lowe panels show representative traces obtained in early symptomatic SOD1(G86R) mice as references. Note the absence o typical spontaneous denervation activities in +/- and -/- mice muscles. N=8 per group; scale bars= 50ms and 50µV.

B: RT-qPCR analysis of the alpha and gamma subunits of the cholinergic receptor (AchRα and AchRγ), of *myogenin* an *musk* in *Vapb* +/+, +/- and -/- mice against early symptomatic *Sod1*(G86R) (SOD1) mice used as a positive control. Not that the expression of these denervation related markers is barely detectable for cell types, except in SOD1 mice.

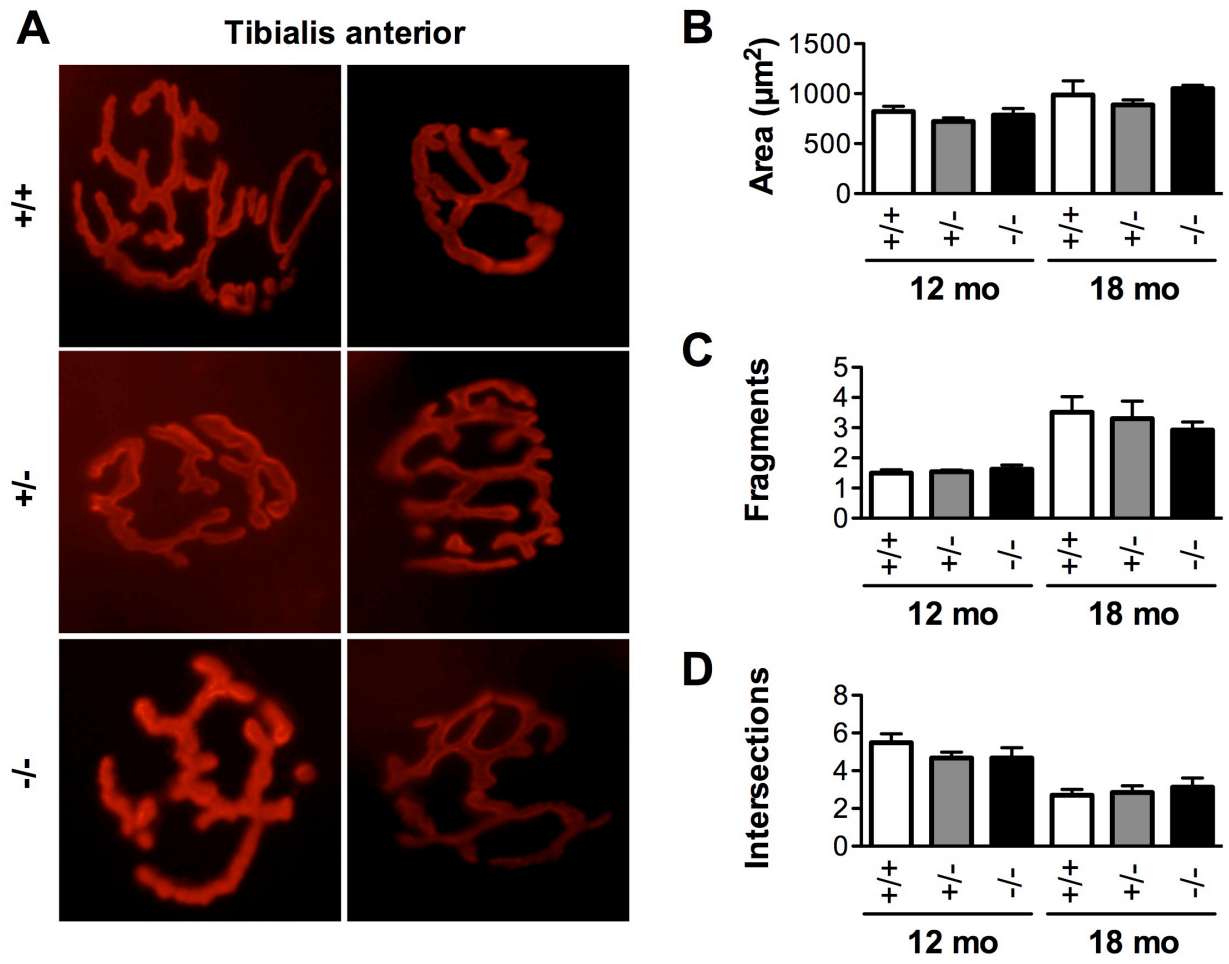

Supplementary Figure 5: Normal neuromuscular junction morphology in *Vapb* +/- and -/- mice.
A: Representative microphotographs of NMJ post-synaptic apparatus in tibialis anterior muscles from *Vapb* +/+, +/- and -/- mice at 18 months of age. Note the normal pretzel-shaped morphology of NMJs. Scale bar, 20 µm.
B-D: Quantitative morphometry of NMJs in gastrocnemius muscle from *Vapb* +/+, +/- and -/- mice at 12 (12 mo) and 18 months (18 mo) of age. (n = 3-8 mice per group).

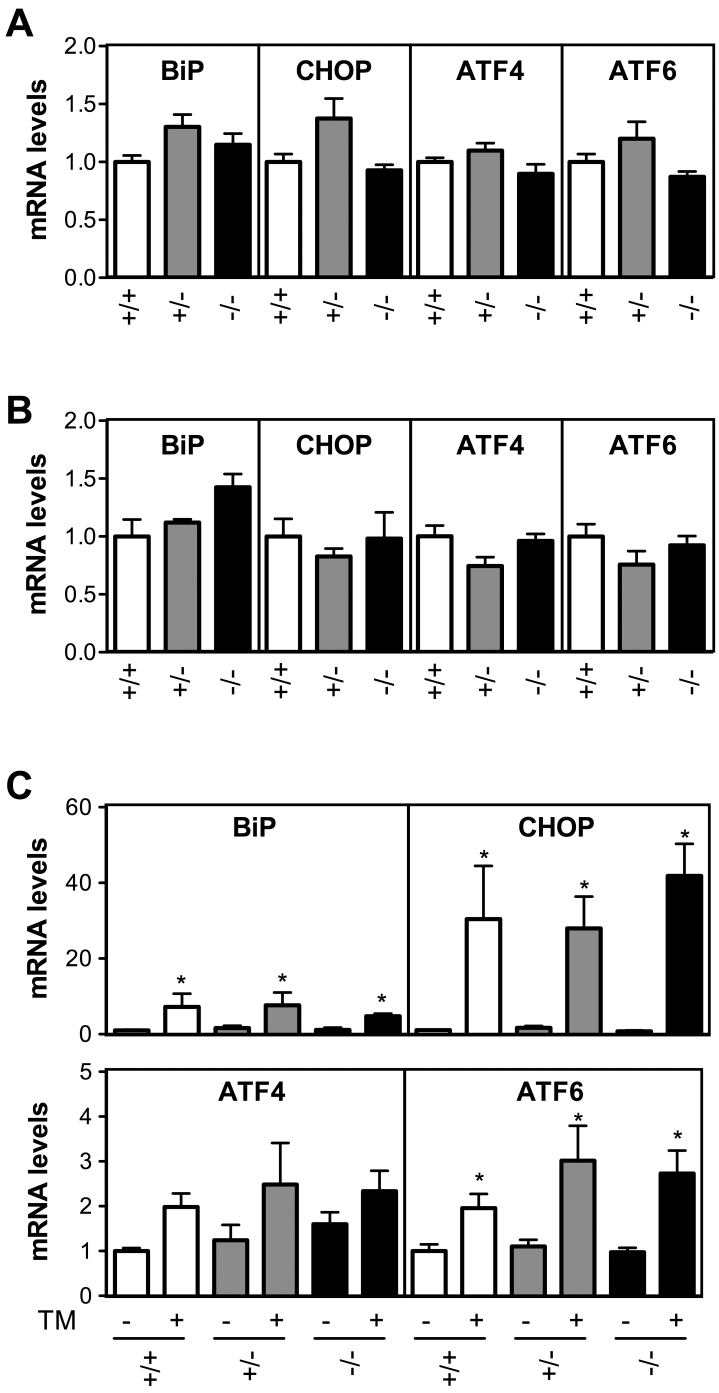

Supplementary Figure 6: Normal basal and induced UPR in *Vapb* +/- and -/- mice.
A-B: RT-qPCR analysis of the chaperone BiP/GRP78, and the UPR master genes CHOP, ATF4 and ATF6alpha in spinal cord (A) and tibialis anterior (B) of 12 months of *Vapb* +/+, +/- and -/- mice (n=5).
C: RT-qPCR of the same genes as in A-B in the liver of *Vapb* +/+, +/- and -/- mice 48 hours after injection with either vehicle or tunicamycine 1 mg/kg (TM). TM injections led to expected upregulations of BiP, CHOP and ATF6, similarly in each genotype. N=5-6 in each group.

Supplementary Table 1: qPCR primers

mRNA	Forward primer	Reverse primer
AchR, alpha subunit	CCACAGACTCAGGGGAGAAG	AACGGTGGTGTGTGTTGATG
AchR, gamma subunit	GAGAGCCACCTCGAAGACAC	GACCAACCTCATCTCCCTGA
ATF4	ATGGCCGGCTATGGATGAT	CGAAGTCAAACTCTTTCAGATCCATT
ATF6alpha	GAGTCGACGTTGTTTGCTGA	CCAAGGCATCAAATCCAAAT
BiP	CTGAGGCGTATTTGGGAAAG	TCATGACATTCAGTCCAGCAA
CHOP	CTGCCTTTCACCTTGGAGAC	CGTTTCCTGGGGATGAGATA
Musk	TTCAGCGGGACTGAGAAACT	TGTCTTCCACGCTCAGAATG
Myogenin	CGTTGCTCAGCTCCCTCA	TGGGAGTTGCATTCACTGG

Supplementary table 2: SHIRPA results per mouse

Item	4-6 mo			18-22 mo		
	+/+	+/-	-/-	+/+	+/-	-/-
Body position						
Lying	2	0	1	3	2	2
Sitting or standing	5	8	6	1	4	1
Restated	1	0	1	4	3	5
Pelvis position						
Normal (3 mm)	6	7	7	5	6	2
Touch the ground	1	1	1	3	2	4
Elevated (+ 3 mm)	1	0	0	0	1	2
Abdominal tone						
Flaccid	0	0	0	0	0	0
Weak tone	6	8	7	3	9	8
Important tone	2	1	0	5	0	0
Limb tone						
No tone	0	0	0	0	0	0
Weak tone	3	1	6	2	6	8
Moderate tone	4	7	2	5	3	0
Important tone	1	0	0	0	0	0
Catalepsy						
Climbs	6	7	2	4	5	4
Moves then stops	2	1	4	0	0	0
Moves after 5-15s	0	0	2	0	1	0
Moves after 15-30s	0	0	0	0	0	1
Descends	0	0	0	0	2	2
Falls	0	0	0	3	1	1
Negative geotaxis						
Returns and moves up	4	4	2	3	2	1
Returns and freezes	1	0	0	1	0	1
Freezes during 30s	3	1	2	0	0	0
Falls	0	0	0	0	3	3
Moves down	0	3	4	4	4	2
Toe withdrawal						
None	0	0	0	1	1	0
Weak	6	3	1	3	3	2
Moderate	0	3	3	2	3	3
Fast	2	2	4	2	2	3
Tremors						
None	7	4	1	8	7	4
Mild	1	4	7	0	2	4
Severe	0	0	0	0	0	0

Publication #4 :

VAPB/ALS8 MSP Ligands Regulate Striated Muscle Energy Metabolism Critical for Adult Survival in Caenorhabditis elegans

Sung Min Han, **Hajer El Oussini**, Jelena Scekic-Zahirovic, Jack Vibbert, Pauline Cottee, Jeevan K. Prasain, Hugo J. Bellen, Luc Dupuis, Michael A. Miller

OPEN ACCESS Freely available online

PLOS | GENETICS

VAPB/ALS8 MSP Ligands Regulate Striated Muscle Energy Metabolism Critical for Adult Survival in *Caenorhabditis elegans*

Sung Min Han[1], Hajer El Oussini[2,3], Jelena Scekic-Zahirovic[2,3], Jack Vibbert[1], Pauline Cottee[1], Jeevan K. Prasain[4], Hugo J. Bellen[5,6,7], Luc Dupuis[2,3], Michael A. Miller[1]*

1 Department of Cell, Developmental, and Integrative Biology, University of Alabama School of Medicine, Birmingham, Alabama, United States of America, **2** INSERM, U1118, Mécanismes centraux et périphériques de la neurodégénérescence, Strasbourg, France, **3** Faculté de Médecine, Fédération de Médecine Translationnelle de Strasbourg, Université de Strasbourg, UMRS1118, Strasbourg, France, **4** Department of Pharmacology and Toxicology, University of Alabama School of Medicine, Birmingham, Alabama, United States of America, **5** Howard Hughes Medical Institute, Chevy Chase, Maryland, United States of America, **6** Department of Molecular and Human Genetics, Baylor College of Medicine, Houston, Texas, United States of America, **7** Program in Developmental Biology, Baylor College of Medicine, Houston, Texas, United States of America

Abstract

Mutations in VAPB/ALS8 are associated with amyotrophic lateral sclerosis (ALS) and spinal muscular atrophy (SMA), two motor neuron diseases that often include alterations in energy metabolism. We have shown that *C. elegans* and Drosophila neurons secrete a cleavage product of VAPB, the N-terminal major sperm protein domain (vMSP). Secreted vMSPs signal through Roundabout and Lar-like receptors expressed on striated muscle. The muscle signaling pathway localizes mitochondria to myofilaments, alters their fission/fusion balance, and promotes energy production. Here, we show that neuronal loss of the *C. elegans* VAPB homolog triggers metabolic alterations that appear to compensate for muscle mitochondrial dysfunction. When vMSP levels drop, cytoskeletal or mitochondrial abnormalities in muscle induce elevated DAF-16, the Forkhead Box O (FoxO) homolog, transcription factor activity. DAF-16 promotes muscle triacylglycerol accumulation, increases ATP levels in adults, and extends lifespan, despite reduced muscle mitochondria electron transport chain activity. Finally, *Vapb* knock-out mice exhibit abnormal muscular triacylglycerol levels and FoxO target gene transcriptional responses to fasting and refeeding. Our data indicate that impaired vMSP signaling to striated muscle alters FoxO activity, which affects energy metabolism. Abnormalities in energy metabolism of ALS patients may thus constitute a compensatory mechanism counterbalancing skeletal muscle mitochondrial dysfunction.

Citation: Han SM, El Oussini H, Scekic-Zahirovic J, Vibbert J, Cottee P, et al. (2013) VAPB/ALS8 MSP Ligands Regulate Striated Muscle Energy Metabolism Critical for Adult Survival in *Caenorhabditis elegans*. PLoS Genet 9(9): e1003738. doi:10.1371/journal.pgen.1003738

Editor: Kaveh Ashrafi, University of California San Francisco, United States of America

Received April 5, 2013; **Accepted** July 8, 2013; **Published** September 5, 2013

Funding: This project was funded by the Muscular Dystrophy Association (MDA186119, to MAM), UAB Clinical Nutrition Center Nutrition or Obesity-Related Pilot Feasibility Studies grant (UAB NORC grant P30DK056336, to MAM), Amyotrophic Lateral Sclerosis Association (grant #1698, to LD), Agence Nationale de la Recherche (ANR JCJC Dynemit, to LD), Association pour la recherche sur la SLA et les autres maladies du motoneurone (to LD), Thierry Latran Foundation (SpastALS, to LD), and Association Pour La Recherche Et le Développement de Moyens de Lutte Contre les Maladies Neurodégénératives (to LD). JSZ is supported by the ERASMUS Neurotime project. The UAB Targeted Metabolomics and Proteomics Laboratory has been supported in part by the UAB Skin Disease Research Center (P30 AR050948), the UAB-UCSD O'Brien Acute Kidney Injury Center (P30 DK079337), and the UAB Lung Health Center (R01 HL114439, R01 HL110950). Support for the mass spectrometer was from a NCRR Shared Instrumentation grant (S10 RR19261). The Caenorhabditis Genetics Center is supported by the NIH Office of Research Infrastructure Programs (P40 OD010440) and the Japanese National Bioresource Project is supported by the Ministry of Education, Culture, Science, Sports and Technology. HJB is an investigator of the HHMI. The funders had no role in study design, data collection and analysis, decision to publish, or preparation of the manuscript.

Competing Interests: The authors HJB and MAM declare a potential conflict of interest. A patent application has been filed and HJB is part of HEALS Biopharma.

* E-mail: mamiller@uab.edu

Introduction

ALS is a lethal neurodegenerative disease characterized by the combined degeneration of lower and upper motor neurons [1]. Most ALS cases occur sporadically, but about 10% are familial. These genetic cases are caused by mutations in multiple genes, including in the *Vapb* (VAMP/synaptobrevin-associated protein B) gene. Mutations in *Vapb* lead to ALS8 that manifests as ALS or late-onset SMA, a motor neuron disease restricted to lower motor neurons [2–4]. While *Vapb* mutations are rare, reduced VAPB mRNA or protein levels have been reported in sporadic ALS patients, a mSOD1 ALS mouse model, and *ALS8* patient motor neurons derived from induced pluripotent stem cells [5–7]. Hence, a loss of VAPB might be relevant in non-*ALS8* patients.

VAPB, and its paralog VAPA, are broadly expressed type II membrane proteins that are evolutionarily conserved. These VAPs have been implicated in regulating lipid transport and homeostasis at intracellular organelle contact sites, endoplasmic reticulum (ER) dynamics, and membrane trafficking [8–12]. In addition to these cell autonomous functions, the VAP vMSP is cleaved from the transmembrane domain in the cytoplasm and secreted in a cell-type specific fashion [13–15]. Secreted vMSPs antagonize Eph receptor signaling through a direct interaction with the extracellular domain [13]. More recently, we have shown in *C. elegans* and Drosophila that neurons secrete vMSPs to regulate mitochondrial

Author Summary

ALS patients often present with systemic alterations in energy metabolism, such as dyslipidemia and hypermetabolism of unknown origin. Reduction of *Vapb* function is thought to cause motor neuron disease in *ALS8* patients and may predispose individuals to ALS, in general. We have shown that neurons secrete the N-terminal VAPB vMSP into the extracellular environment. The secreted vMSPs signal through Roundabout and Lar-like receptors on striated muscles. This neuron to muscle signaling pathway localizes mitochondria to myofilament I-bands and promotes mitochondrial function. Here we show that loss of VAPB in *C. elegans* neurons causes metabolic changes in muscles, including altered fat metabolism and elevated DAF-16 FoxO transcription factor activity. DAF-16 promotes muscle triacylglycerol accumulation, increases ATP levels, and prolongs survival in *Vapb* mutants. However, it does not influence muscle mitochondrial localization nor does it affect oxygen consumption. We also show that *Vapb* knockout mice exhibit disrupted muscular triacylglycerol and FoxO target gene transcriptional responses to fasting and refeeding. These data indicate that impaired vMSP signaling to muscle triggers an energy deficiency, which induces a protective metabolic response involving FoxO. Hence, some energy metabolism alterations observed in ALS patients might be a consequence of striated muscle mitochondrial dysfunction.

localization and function in striated muscle [15]. vMSPs interact with muscle SAX-3 Roundabout and CLR-1 Lar-like protein-tyrosine phosphatase receptors to down-regulate CLR-1 signaling. VAP loss causes uncontrolled CLR-1 Lar-like receptor activation in body wall muscle. CLR-1 stimulates actin filament assembly in the muscle belly that requires the actin-related protein 2/3 (Arp2/3) complex. These ectopic actin filaments displace mitochondria from I-bands, cause aberrant fission and fusion balance, and impair respiratory chain activity. Hence, vMSPs secreted by neurons promote muscle mitochondrial localization and function, perhaps in an effort to modulate energy homeostasis.

vMSP signaling to muscle mitochondria might be relevant for the energy balance in *ALS8* disease. Out of five *ALS8* patients studied, five had increased cholesterol levels, four had reduced HDL, three had elevated triacylglycerol levels, and one was diabetic [16]. More generally, ALS is associated with a spectrum of abnormalities in energy metabolism, including mitochondrial defects in neurons and skeletal muscle, insulin resistance, dyslipidemia, and hypermetabolism [17]. These metabolic abnormalities are positively correlated with survival. For instance, increased prediagnostic body fat is associated with decreased risk of ALS mortality [18] and in some patient populations, higher LDL/HDL ratios correlate with increased survival time [19,20]. However, the cause(s) of the metabolic defects and their relationship to each other are not well understood.

Here we show in *C. elegans* that loss of the VAP homolog VPR-1 causes triacylglycerol (TAG) accumulation in striated body wall muscle. Mosaic analysis and tissue-specific expression studies provide compelling evidence that VPR-1 acts in neurons, not muscles to regulate fat levels. Multiple lines of evidence support the model that impaired vMSP signaling from neurons to muscle increases TAG levels in muscle. We propose that this fat metabolism alteration is part of a compensatory response mediated by the DAF-16/FoxO transcription factor. FoxO promotes muscle fat accumulation, maintains ATP levels during aging, and extends lifespan without influencing muscle mitochondrial morphology, localization, or function. Finally, we provide evidence that skeletal muscle metabolism is abnormal in *Vapb* mutant mice. Our results support the model that disrupting vMSP signaling to muscle triggers a compensatory response involving FoxO transcription factors.

Results

vpr-1/vap loss increases fat levels in adult body wall muscle

In our studies of *vpr-1(tm1411)* null mutant hermaphrodites, we noticed that body wall muscles often contain large lipid-like droplets not observed in wild-type controls. These apparent lipid-like droplets were visible in young adults (1–3 days post L4 stage) by differential interference contrast (DIC) microscopy (Figure 1A). In transgenic *vpr-1* mutants expressing mitochondrial matrix-targeted GFP (mitoGFP) in muscle, droplets are observed in the muscle belly surrounded by mitochondria (Figure S1). The vast majority of visible droplets in peripheral tissues are found in muscle. Transmission electron microscopy (TEM) of *vpr-1(tm1411)* mutant muscle shows an expanded muscle belly filled with mitochondria, as previously reported [15], and large droplets (Figures 1B and S2). The droplets are often found in close proximity to mitochondria and ER. Large muscle droplets were not observed in young adult wild-type muscle (Figures 1B and S2). However, muscle lipid droplets and abnormal mitochondria are observed in very old (18 day) wild-type adults [21,22]. In these old worms, large lipid droplets accumulate in the muscle, intestine, and epidermis. We did not detect abnormally large droplets in young *vpr-1* mutant intestinal and epidermal tissues by TEM. Instead, intestinal and epidermal tissues looked similar to wild-type controls, although it is difficult to assess minor differences (Figure S2). Hence, muscle droplets accumulate in aging *vpr-1* mutant worms.

To directly test whether these droplets contain lipid, we fed *vpr-1* mutant worms *E. coli* incubated with Bodipy-conjugated fatty acids (Bodipy-FAs). These fluorescent compounds can be used to directly visualize fat stores in live tissue [23,24]. In wild-type hermaphrodite controls, dietary Bodipy-FAs were observed primarily in the intestine with a few small droplets present in muscle. In contrast, muscles of *vpr-1(tm1411)* null mutants contained numerous large Bodipy-FA-stained droplets (Figure 1C). The fluorescent droplets fully overlapped with those observed in muscle by DIC microscopy (Figure 1D). Similar results are observed with Sudan Black B, which darkly stains neutral TAGs in fixed opaque worms (Figure S3). Bodipy-FAs are continuously transported from the diet, to the worm's intestinal cells, and then to the muscle, where they are tightly packed in membrane-bound vesicles. Bodipy-FAs are also incorporated into yolk lipoprotein complexes [23], which are specifically endocytosed by oocytes [25]. Although yolk accumulates in the pseudocoelom of *vpr-1* mutants (due to defective oogenesis), it is not up-taken by muscle (Figure S4). Both Bodipy-FA and Sudan Black staining show a mild increase in intestinal fat content in *vpr-1* mutants. Whether this apparent increase is due to fat accumulation or increased fat synthesis is not clear.

We also performed mass spectrometry of lipid extracts to determine the lipid composition of wild-type and *vpr-1* mutant adult hermaphrodites. Lipids were analyzed by electrospray ionization tandem mass spectrometry (ESI-MS/MS). ESI-MS/MS analysis of the extracts detected a robust increase in TAGs in *vpr-1* mutant extracts, but not in the membrane phospholipids phosphatidylethanolamine and phosphatidylcholine (Figure 1E and data not shown). These data indicate that loss of *vpr-1* causes TAG accumulation in muscle of adult hermaphrodite worms.

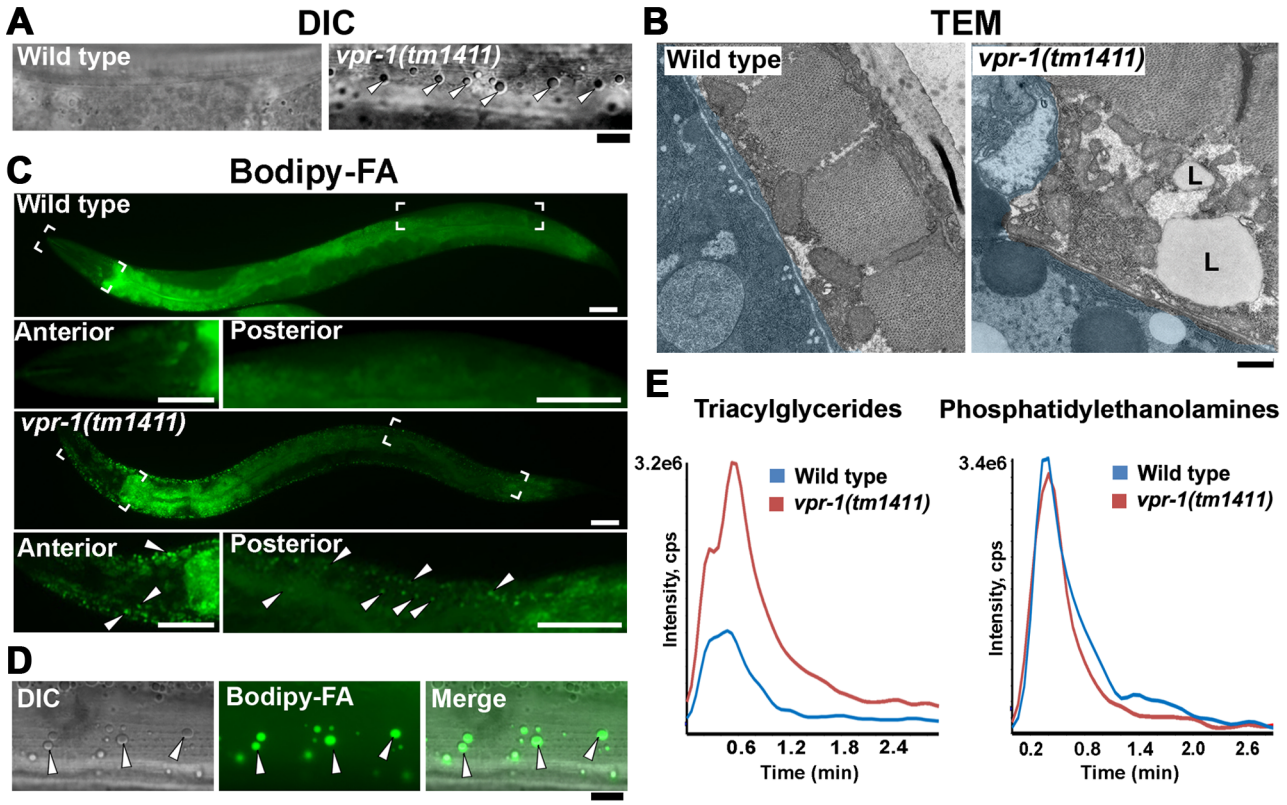

Figure 1. Fat levels in body wall muscle of wild-type and *vpr-1* mutant worms. (A) DIC images of muscle in live adult hermaphrodites. Arrowheads indicate lipid-like droplets. Bar, 5 μm. (B) Transmission electron micrographs of body wall muscle cytoplasm in wild-type and *vpr-1(tm1411)* mutant hermaphrodites. Light blue color demarcates muscle boundary. L, Lipid-like droplet. Bar, 0.5 μm. (C) Fluorescent images of muscle in live adult hermaphrodites fed Bodipy-FAs. Close-up images of boxed areas are shown below. Arrowheads indicate examples of Bodipy-FA-stained droplets. Anterior is to the left in all panels. Bars, 50 μm. (D) High magnification images of muscle showing Bodipy-FA-stained fluorescent droplets and droplets observed by DIC microscopy. Bar, 5 μm. (E) Comparison of total ion chromatograms of wild-type and *vpr-1(tm1411)* mutant adults extracts for 18:0 TAG (Neutral Loss 284) and phosphatidylethanolamine (Neutral Loss 141).
doi:10.1371/journal.pgen.1003738.g001

Increased ER stress does not cause muscle TAG accumulation in *vpr-1/vap* mutants

VAP homologs have been implicated in ER stress pathways [13,26,27], which can modulate lipid metabolism and homeostasis [28]. Furthermore, mitochondrial dysfunction is sometimes associated with ER stress. We considered the possibility that increased ER stress might cause the high muscle fat levels in *vpr-1* mutants. Three lines of evidence argue against this possibility. First, an integrated *hsp-4/BiPp::gfp* ER stress reporter [29] did not show elevated stress levels in *vpr-1* mutants (Figure S5A). Second, *vpr-1* mutants are not more sensitive than wild type to tunicamycin treatment, which induces ER stress (Figure S5B). Third, RNA-mediated interference (RNAi) of *xbp-1*, an ER stress-responsive transcription factor, in *vpr-1* mutants had no effect on muscle fat levels in 3-day old adults (18.0 ± 3.6 droplets/mm^2 for *vpr-1(tm1411)* [n = 12] versus 17.3 ± 3.6 droplets/mm^2 for *vpr-1(tm1411) xbp-1 RNAi* [n = 10]; $P = 0.28$). These data indicate that increased ER stress does not cause the muscle TAG defect in *vpr-1* mutants.

vpr-1/vap acts cell nonautonomously to regulate fat accumulation

vpr-1 is ubiquitously expressed and its homologs have been implicated in regulating lipid dynamics via a cell autonomous mechanism [10,30–32]. To determine in which cell type(s) VPR-1 functions to regulate muscle fat, we first used genetic mosaic analysis. Transgenic *vpr-1(tm1411)* mutant hermaphrodites were generated containing the *vpr-1* genomic locus and the lineage marker *sur-5::GFP* expressed from an extrachromosomal array [33]. In *C. elegans*, extrachromosomal arrays are spontaneously lost at low frequency during cell division, thereby generating mosaic worms. When these events occur early in development, mosaic worms can be generated with losses in neurons, body wall muscles, intestinal cells, and the germ line.

Expressing the *vpr-1* genomic locus in *vpr-1(tm1411)* null worms rescued the fat metabolism defect in muscle (Figure 2), as well as the muscle mitochondrial defects, sterility, slow growth, and other phenotypes. Body wall muscles are generated from multiple cell lineages, including the EMS lineage. Transgene array loss in the EMS lineage generates mosaic worms that have a subset of muscles lacking *vpr-1* expression. These muscle cells exhibited low fat levels, identical to muscle cells that express *vpr-1* (Figure 2). Therefore, VPR-1 is not required in body wall muscle for fat accumulation. Mosaic worms lacking *vpr-1* in the E lineage, which generates the intestine, also did not exhibit elevated muscle fat droplets, indicating that *vpr-1* is not required in the intestine. In contrast to muscle and intestine loss, *vpr-1* loss in the AB lineage, which generates the neurons, did cause increased fat droplets in muscles (Figure 2). Unexpectedly, we also found that *vpr-1* loss in the germ cell lineage causes muscle fat accumulation (Figure 2). These results indicate that VPR-1 acts cell nonautonomously in

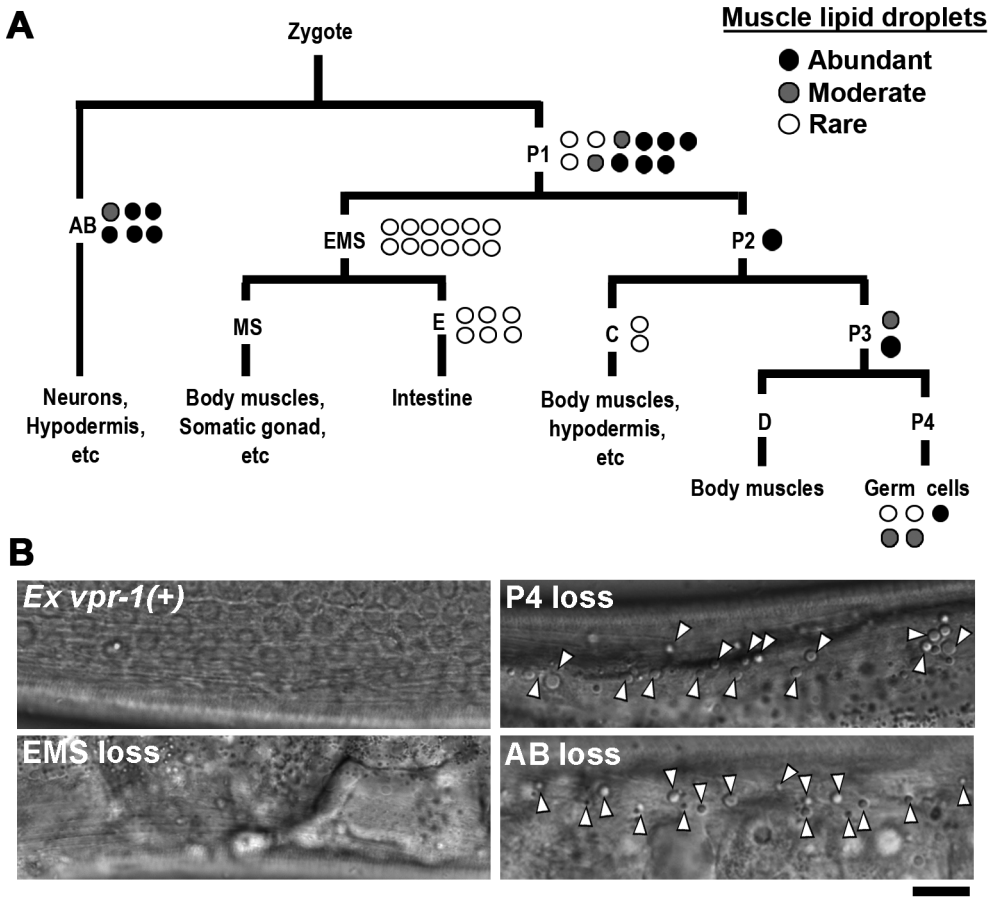

Figure 2. *vpr-1* mosaic analysis. (A) Analysis of vpr-1 genetic mosaics showing the lineages of major tissues. Each circle indicates one genetic mosaic worm. Points at which the genomic copy of *vpr-1(+)* was lost and the resulting phenotype are shown. (B) Representative DIC images of muscle in *vpr-1(tm1411)* mutant mosaic worms. *Ex vpr-1(+)* indicates expression of the vpr-1 genomic locus via an extrachromosomal array. Arrowheads indicate fat droplets. Bar, 5 μm.
doi:10.1371/journal.pgen.1003738.g002

neurons and germ cells (or their differentiation products) to modulate fat levels in muscle.

vpr-1 null mutants are sterile, due to a failure of germ cells to differentiate into sperm and oocytes. Sperm secrete signaling molecules, such as MSPs that may influence fat metabolism [14]. To test whether sperm affect fat levels, we mated sterile 1-day-old adult *vpr-1(tm1411)* hermaphrodites to wild-type males. Supplying sperm to the reproductive tract reduces muscle fat levels in *vpr-1(tm1411)* mutants, as visualized with Bodipy-FAs (Figure S6A). Sperm did not rescue the sterility or muscle mitochondrial defects of *vpr-1* mutants (data not shown). However, preventing spermatogenesis in wild-type hermaphrodites using the *fog-3(q443)* null mutation causes mild muscle fat accumulation, as well as mild mitochondrial morphology defects (Figure S6B), without affecting oxygen consumption [34]. These data indicate that the spermatogenesis defects in *vpr-1* mutants contribute to muscle fat levels and perhaps mitochondrial defects. Two mechanisms appear to affect muscle fat levels, one mechanism involving neuronal *vpr-1* and a second mechanism involving sperm, which can modify specific *vpr-1*-dependent pathways. Here, we focus on the neuronal mechanism.

Genetic mosaics assess the effect of *vpr-1* loss from cells within an otherwise *vpr-1(+)* background. To test whether VPR-1 expression is sufficient in neurons, we expressed VPR-1 under the control of tissue-specific promoters in *vpr-1* null mutants. Consistent with genetic mosaic analysis, VPR-1 expression using the *myo-3* muscle-specific promoter or the *ges-1* intestine-specific promoter did not influence muscle fat levels. In contrast, overexpressing the *vpr-1* cDNA with the *unc-119* pan-neuronal promoter completely rescued the muscle fat levels in approximately 30–40% of transgenic mutant worms (Figures 3A and 3B). These rescued transgenic mutants were still sterile. The incomplete rescue appears to be due to the germ line defects (i.e. lack of sperm) and missing *vpr-1* introns or 3′UTR in the transgene (P. Cottee and M. Miller, unpublished). Consistent with these observations, driving neuronal expression of the *vpr-1* genomic locus instead of the cDNA rescued several *vpr-1* mutant phenotypes with increased efficiency. These results indicate that VPR-1 acts cell nonautonomously in neurons to regulate muscle fat levels.

vMSP signaling to muscle regulates muscle fat levels

The VAPB P56S mutation acts as a dominant negative by inhibiting secretion of the wild-type and mutant vMSPs [13,15]. To test whether neuronal vMSP secretion affects muscle fat levels, we generated transgenic worms expressing P56S VPR-1 under the *unc-119* neuronal promoter. P56S VPR-1 overexpression in wild-type worms causes increased muscle lipid droplets in most worms (Figure 3A), suggesting that vMSP secretion from neurons influences muscle fat accumulation.

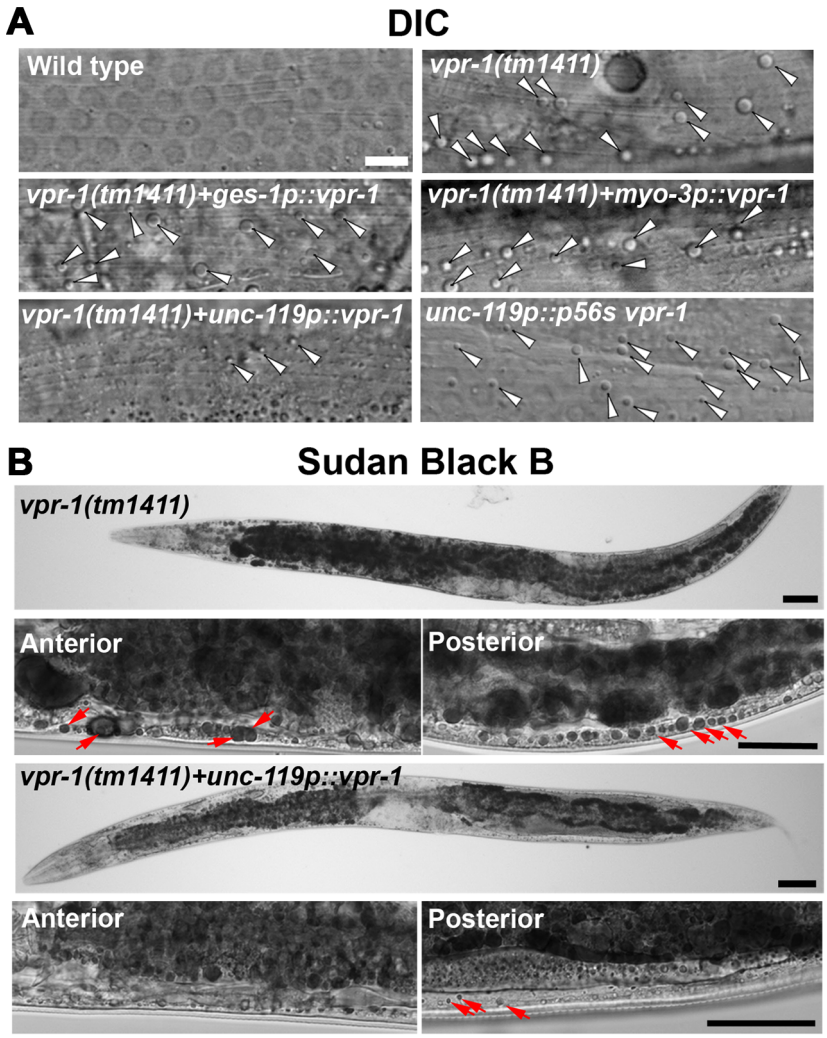

Figure 3. Effect of tissue-specific *vpr-1* expression on fat levels. (A) DIC images of muscle in live wild-type and *vpr-1(tm1411)* mutant hermaphrodites expressing wild-type VPR-1 or VPR-1(P56S) under indicated tissue-specific promoters. Arrowheads indicate lipid-like droplets. Bar, 5 μm. (B) Sudan Black B staining images of *vpr-1* mutants expressing *vpr-1* under the *unc-119* pan-neuronal promoter. Arrows indicate muscle fat droplets. Anterior is to the left in all panels. Wild-type controls (Figure S3) are similar to transgenic *vpr-1(tm1411)* mutants expressing *unc119p::vpr-1*. Low magnification bars, 50 μm; high magnification bars, 25 μm.
doi:10.1371/journal.pgen.1003738.g003

vMSP signaling to muscle is transduced via muscle SAX-3 Robo and CLR-1 Lar-like receptors [15]. *sax-3* mutations cause incompletely penetrant and variably expressed defects in muscle mitochondrial morphology [15]. Similarly, we observed incompletely penetrant defects in muscle fat accumulation by TEM and DIC microscopy (Figure S2; 11.1±13.2 fat droplets/mm^2 for *sax-3(ky123)* [n = 13] versus 0.9±1.8 droplets/mm^2 for wild type [n = 8]). Impaired vMSP signaling causes uncontrolled CLR-1 Lar receptor activity and ectopic Arp2/3-dependent actin filaments in muscle. A reduction of *clr-1* or *arx-2*, which encodes Arp2, rescues the muscle mitochondrial defects, but not the sterility in *vpr-1* mutants [15]. To test whether excess CLR-1 Lar and Arp2/3 activities cause muscle lipid accumulation, we used RNAi to down-regulate their functions in *vpr-1* mutants. *clr-1* or *arx-2* RNAi restored mitochondria to I-bands, as previously reported [15], and reduced muscle fat droplets in *vpr-1(tm1411)* mutants when compared to the mutant control (Figure 4; 18.0±3.6 droplets/mm^2 for *vpr-1(tm1411)* [n = 12] versus 0.6±1.3 droplets/mm^2 for *vpr-1(tm1411) clr-1 RNAi* [n = 9, P<0.001] and 3.1±2.0 droplets/mm^2 for *vpr-1(tm1411) arx-2 RNAi* [n = 6, P<0.001]). Similar results were observed using TEM [15]. We also found that overexpressing *arx-2/arp2* specifically in wild-type muscle causes mild mitochondrial morphology and fat accumulation defects (Figure S7). Taken together, the data strongly support the hypothesis that impaired vMSP signaling from neurons to muscle causes elevated fat levels in muscle.

DAF-16/FoxO is required for fat accumulation in *vpr-1/vap* mutants

The elevated TAGs in *vpr-1* mutants and continuous accumulation of dietary Bodipy-FAs in muscle suggested that fat metabolism and transport pathways are altered. Reduced energy production triggers enhanced activity of the DAF-16/FoxO transcription factor, which controls expression of genes involved in fat synthesis, fat transport, β-oxidation, and stress resistance [35–39]. We hypothesized that the muscle cytoskeletal or mitochondrial defects trigger elevated FoxO activity. To investi-

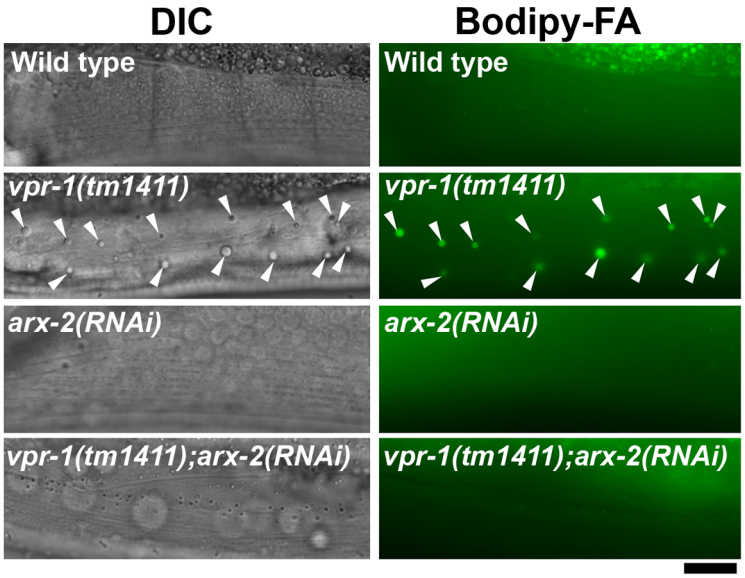

Figure 4. Effect of Arp2/3 inactivation on muscle fat levels. DIC and fluorescent images of muscle in live 3-day-old hermaphrodite worms fed Bodipy-FAs. *arx-2* encodes the Arp2 component of the Arp2/3 complex. Arrowheads indicate Bodipy-FA-stained fat droplets. Bar, 5 µm.
doi:10.1371/journal.pgen.1003738.g004

gate if DAF-16 affects fat metabolism in *vpr-1* mutants, we generated *vpr-1(tm1411) daf-16(mu86)* double mutants. Muscles of *daf-16(mu86)* null mutants contain few Bodipy-FA-stained droplets, similar to muscles of wild-type controls. However, muscle fat levels in the double mutants are also low, and strongly reduced when compared to those in *vpr-1(tm1411)* mutants alone (Figure 5A). *daf-16* loss did not affect food intake, assessed by measuring pharyngeal pumping rates (Figure 5B; $P>0.05$), muscle mitochondria (see below), or sterility of *vpr-1(tm1411)* mutants. We conclude that the elevated fat levels in *vpr-1* null mutants require DAF-16/FoxO activity.

We next examined DAF-16/FoxO transcriptional activity using an integrated transgenic line that expresses GFP under the *sod-3* promoter (*sod-3p::GFP*), a direct DAF-16 target [35,40]. When worms were cultured under normal growth conditions, about 40–50% of 1-day-old adult *vpr-1(tm1411)* transgenic worms showed increased GFP expression relative to control transgenic animals (Figure 5C). By day three of adulthood, most *vpr-1(tm1411)* mutants show broad GFP expression throughout the body, including the intestine, neurons, vulva muscles, and body wall muscles. The elevated GFP expression is due to DAF-16 because GFP expression is suppressed in transgenic *vpr-1(tm1411) daf-16(mu86)* double mutants (Figure 5C). These data indicate that *vpr-1* loss causes elevated DAF-16 activity in muscles and other cell types.

To investigate the mechanism(s) by which VPR-1 controls DAF-16/FoxO, we analyzed DAF-16 subcellular localization in *vpr-1(tm1411)* mutants. An integrated and rescuing transgenic line was used to express DAF-16::GFP under its endogenous promoter. DAF-16::GFP translocates from cytoplasm to nucleus upon loss of insulin signaling, although other mechanisms exist that regulate nuclear DAF-16 activity independent of translocation [41,42]. Under normal growth conditions at 20°C, DAF-16::GFP in *vpr-1* mutant and control transgenic strains was distributed throughout the cytoplasm and nucleus with no significant difference between the two strains (Figures 6A and 6B). However, *vpr-1* mutants appear more sensitive to higher temperatures that require increased metabolic activity (Figures 6A and 6B). We conclude that VPR-1 does not have a strong effect on DAF-16 nuclear translocation under standard conditions.

DAF-16/FoxO likely acts downstream of the Arp2/3 complex

The results thus far strongly support the model that impaired vMSP signaling to muscle triggers DAF-16-dependent muscle fat accumulation. We hypothesized that cytoskeletal or mitochondrial abnormalities in *vpr-1* mutant muscles induce elevated DAF-16 transcriptional activity. If this idea is correct, then inactivating the Arp2/3 complex in *vpr-1* mutants should attenuate DAF-16 activity. To assess DAF-16 transcriptional activity, we used the integrated *sod-3p::GFP* transgenic reporter. *arx-2/arp2* RNAi in *vpr-1(tm1411)* mutants causes a strong reduction in *sod-3p::GFP* expression in body wall muscle, the intestine, and other cells (Figure 6C). *arx-2* RNAi in wild-type worms has little effect on GFP expression. Therefore, the elevated DAF-16 activity in *vpr-1* mutants is at least partially dependent on the Arp2/3 complex.

One possibility is that DAF-16 causes the mitochondrial abnormalities in *vpr-1* mutants. To test this model, we first evaluated mitochondria using the mitoGFP transgene expressed in body wall muscle. As previously documented [15], wild-type muscles contain linear mitochondrial tubules positioned along I-bands. In contrast, *vpr-1(tm1411)* mutants contain disorganized and interconnected mitochondrial networks in the muscle belly (Figure 7A). Loss of *daf-16* in *vpr-1(tm1411)* mutants did not affect muscle mitochondrial morphology or localization (Figure 7A). Next, we examined mitochondrial functional status using MitoTracker CMXRos, which accumulates in the mitochondrial matrix depending on membrane potential, and oxygen consumption of whole worms. DAF-16 loss did not affect the reduced MitoTracker CMXRos accumulation (Figure 7B) or the low oxygen consumption rates of *vpr-1* mutants (Figures 7C and 7D). We conclude that DAF-16 does not affect the muscle mitochondrial defects in *vpr-1* mutants and likely acts downstream of Arp2/3.

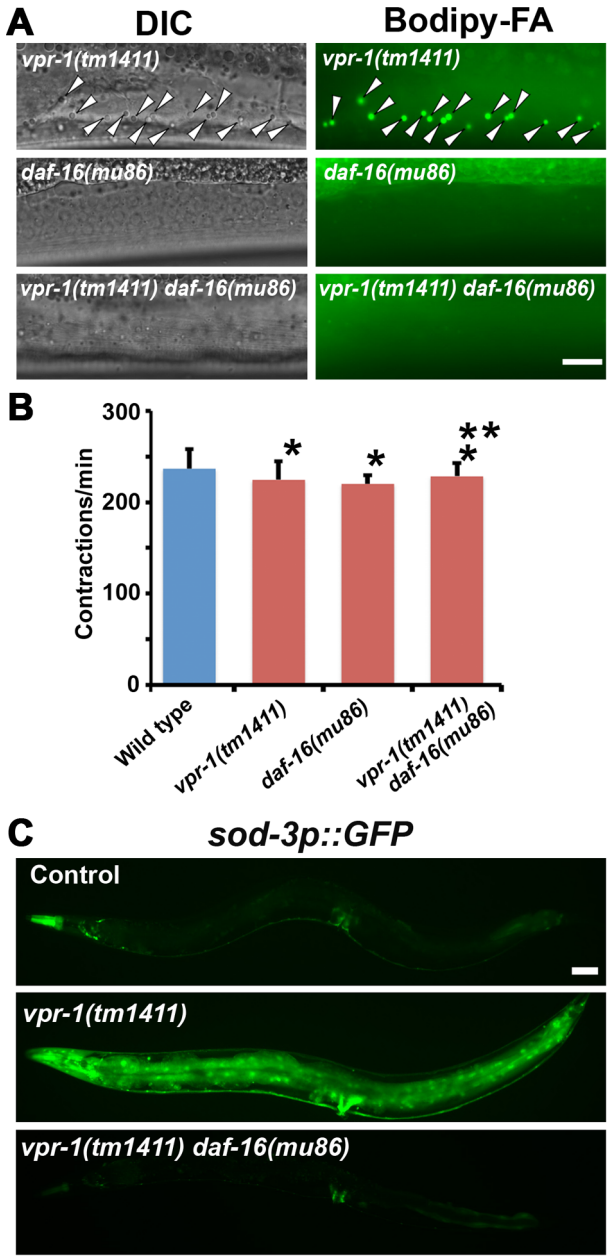

Figure 5. DAF-16 activity in *vpr-1* mutants. (A) DIC and fluorescent images of muscle in live 3-day-old hermaphrodite worms fed Bodipy-FAs. Arrowheads indicate Bodipy-FA-stained droplets. Wild-type controls (not shown) are similar to *daf-16(mu86)* mutants (See figures 1C and 4). Bar, 5 μm. (B) Pharyngeal pumping rates of 1-day-old adult hermaphrodites. Wild type (236.7±21.1 [n = 11]) and *vpr-1(tm1411)* mutants (220.1±9.6 [n = 11]) have similar pharyngeal pumping rate. Error bars represent SD. *$P>0.05$ compared to wild type. **$P>0.05$ compared to *vpr-1(tm1411)* mutant. (C) Transgenic worms expressing GFP under control of the *sod-3* promoter, a direct DAF-16/FoxO target. Anterior is to the left in all panels. Bar, 50 μm.
doi:10.1371/journal.pgen.1003738.g005

DAF-16/FoxO increases ATP levels and extends lifespan of *vpr-1/vap* mutants

As the intestine and epidermis are fat storage sites in *C. elegans*, we hypothesized that the increase in muscle fat is an attempt to provide fuel for energy production. Our previous studies showed that 1-day-old adult *vpr-1(tm1411)* mutants have reduced ATP levels when compared to controls [15]. However, the ATP levels in *vpr-1* mutants did not decrease over the next two days, as observed in the wild type (Figure 8A). 3-day-old adult *vpr-1(tm1411)* mutants had higher ATP levels than wild-type controls at the same age (Figure 8A). Similar ATP dynamics have been observed in aging worms with mutations in the *daf-2* insulin receptor or *clk-1*, a mitochondrial protein involved in ubiquinone biosynthesis [43,44]. Hence, DAF-16 may help maintain ATP levels in these aging worms. To test whether DAF-16 affects the energy balance of *vpr-1* mutants, we measured ATP levels in single and double mutant extracts. *daf-16* loss did not influence ATP levels in 1-day-old adult *vpr-1(tm1411)* mutants (Figure 8A). However, *daf-16* is required for the high ATP concentration in 3-day old mutant adults (Figure 8A; $P<0.001$). ATP levels in *daf-16* mutants are similar to wild-type controls (data not shown), as previously shown [43,44]. These data indicate that DAF-16/FoxO helps *vpr-1* mutants maintain ATP levels during aging.

Based on the abnormalities in energy metabolism, we tested whether DAF-16 influences lifespan in *vpr-1* mutants. Similar to other worm mutants with mild or tissue-specific reduction in mitochondrial function, *vpr-1(tm1411)* mutants have slightly extended adult lifespan compared to wild-type worms (Figure 8B; mean adult lifespan ± SD of 12.9±4.4 days [n = 154] for *vpr-1(tm1411)* versus 10.5±2.1 days [n = 159] for wild type, $P<0.001$). *daf-16* loss in *vpr-1(tm1411)* mutants causes a strong reduction in lifespan relative to *vpr-1* mutants and wild-type controls (Figure 8B; 6.9±2.5 days for *vpr-1(tm1411) daf-16(mu86)* [n = 250]; $P<0.001$). The lifespan of *daf-16* single mutants was similar to wild type (data not shown), as previously shown [38,45]. These data indicate that DAF-16/FoxO activity extends survival of *vpr-1* mutants.

Vapb knockout mice exhibit signs of abnormal skeletal muscle energy metabolism

The data thus far indicate that VPR-1 loss causes profound defects in muscle energy metabolism. We hypothesized that the regulatory function of vMSPs on energy metabolism was conserved in mammals, and studied energy metabolism of *Vapb* −/− mice [4]. In basal conditions, *Vapb* −/− mice do not exhibit overt defects in energy metabolism. In particular, body weight and glycemia appear normal with age (L. Dupuis, unpublished results). However, an energy metabolism defect of *Vapb* deficient mice might be unmasked by modifying insulin supply through feeding and fasting paradigms. In worms and mice, fasting reduces insulin signaling and increases FoxO activity, resulting in altered metabolic gene expression. We used *Vapb* −/− mice of 2–6 months of age to avoid any confounding effect of the motor dysfunction observed at 18 months [4]. Mice were either fasted for 24 hours (fasted group) or fasted for 16 hours and refed for 8 hours to synchronize meals (fed group). In +/+ mice, fasting decreased the TAG levels in the gastrocnemius (GA) muscle (Figure 9A; $P<0.05$). In contrast, TAG levels remained unchanged upon fasting in *Vapb* −/− GA and tibialis anterior (TA) muscles (Figure 9A and data not shown). In liver, TAG levels were unchanged upon fasting and feeding in either +/+ or −/− mice (Figure 9A). Thus, *Vapb* ablation increases the resistance of muscle lipid stores to fasting induced mobilization.

We next looked at mRNA levels of metabolic genes by quantitative RT-PCR. In liver, *Vapb* ablation potentiated induction of the direct FoxO1 target gene phosphoenolpyruvate carboxykinase (PEPCK) in response to fasting, but had no effect on fasting induction of other FoxO1 targets such as glucose 6-phosphatase (G6Pase) and pyruvate dehydrogenase kinase (PDK4) (Figure 9B). FoxO1 and FoxO3 mRNA and proteins were similar

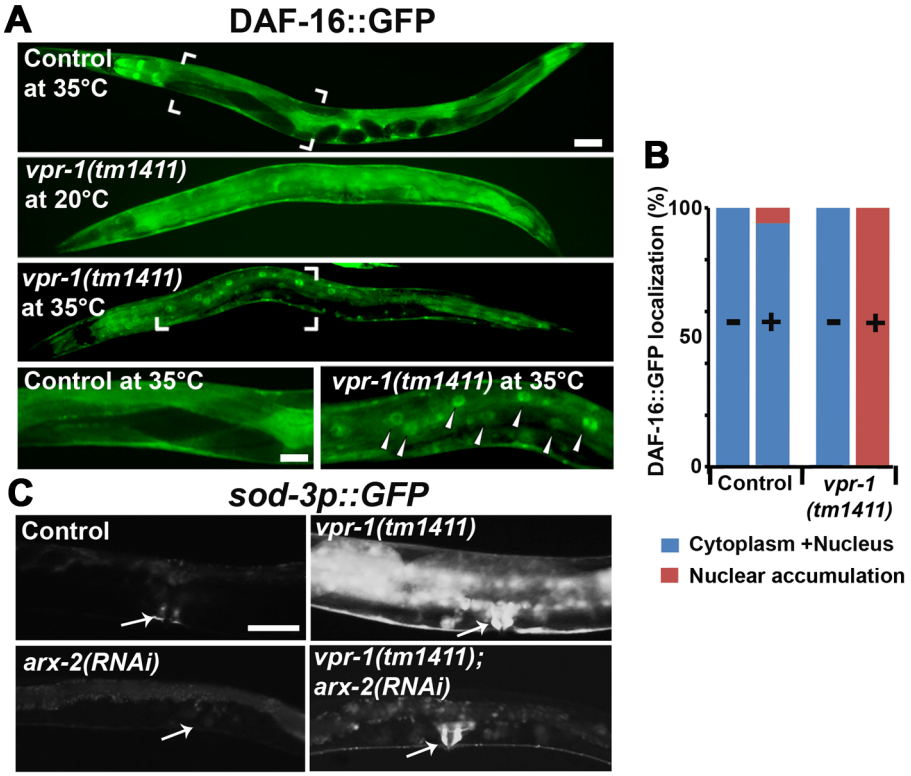

Figure 6. DAF-16 localization and activity in wild-type and mutant worms. (A) Transgenic strains expressing DAF-16::GFP under its endogenous promoter. Transgenic controls raised at 20°C are similar to those raised at 20°C then shifted to 35°C for 30 minutes (see panel B for quantification). Close up images of boxed areas are shown. Anterior is to the left in all panels. Low magnification bar, 50 μm; high magnification bar, 25 μm. (B) Quantification of DAF-16::GFP localization in control (n = 157) and *vpr-1(tm1411)* mutants (n = 49). (−), incubation under normal growth condition; (+), incubation at 35°C for 30 minutes. (C) Magnified images showing transgenic lines expressing GFP under the *sod-3* promoter. *arx-2* encodes Arp2. Arrows indicate vulva muscle region. Anterior is to the left in all panels. Bar, 50 μm.
doi:10.1371/journal.pgen.1003738.g006

in +/+ and −/− livers, and FoxO1 up-regulation by fasting appeared normal in −/− liver (Figure 9B).

We also examined putative FoxO1 and FoxO3 target genes in +/+ and mutant TA muscle. Feeding decreased expression of PEPCK, G6Pase, and lipoprotein lipase (LPL), and increased expression of the lipogenic transcription factor SREBP1c (Figure 9C). This regulation was lost in *Vapb* −/− muscles, as feeding did not modify expression of these four genes. *Vapb* genotype did not affect levels of PDK4 mRNA. FoxO1 and FoxO3 expression was down-regulated upon feeding in control TA muscles, but FoxO3 regulation was lost in −/− muscles (Figure 9C). The expression of muscle FoxO3 targets LC3 and Atrogin1 was up-regulated in fed −/− mice, while another FoxO3 target, ATG12, was unchanged. These results indicate that muscles of *Vapb* −/− mice are partially insensitive to fasting/feeding alterations in lipid mobilization and FoxO target gene expression. Hence, *Vapb* mutant worms and mice appear to have muscle energy metabolism alterations, at least in part involving FoxO targets. Whether the putative metabolic changes in mouse muscle are due to secreted vMSPs is not yet clear.

Discussion

Results from Drosophila and *C. elegans* support the model that VAP MSP domains are secreted neurogenic factors that promote striated muscle oxidative metabolism [15]. In *C. elegans*, neurons cleave the vMSP and secrete it into the surrounding environment. Secreted vMSPs signal through SAX-3 Roundabout and CLR-1 Lar-like receptors expressed in muscle, down-regulating Lar signaling to the Arp2/3 complex. This signaling pathway restricts actin filament formation to I-bands of the myofilaments, thereby localizing mitochondria to I-bands and promoting mitochondrial function [13,15]. Here we show that impaired vMSP signaling to muscle triggers increased DAF-16/FoxO transcription factor activity. FoxO promotes TAG accumulation in muscle, helps maintain ATP levels during aging, and extends lifespan. We propose that reduced vMSP signaling puts animals in an energy deficit, which triggers an altered metabolic response involving FoxO. Evidence for this model and implications for ALS are discussed below.

A VAPB cell nonautonomous mechanism for regulating muscle TAGs

VAPs physically interact with multiple proteins involved in lipid binding and transport, such as oxysterol binding protein and ceramide-transfer protein [10,11,30,46]. Although the biological role of these interactions is not well understood, VAPs have been proposed to act in macromolecular complexes for transporting lipids between organelles at membrane contact sites. This mechanism depends on VAP function in the same cell in which lipid dynamics occur (i.e. a cell autonomous function). Here we show in *C. elegans* that *vpr-1/vap* loss triggers a robust increase in striated muscle TAG levels. Unexpectedly, this function does not require VPR-1 in muscle. Genetic mosaic and cell-type specific expression studies demonstrate that VPR-1 acts in neurons,

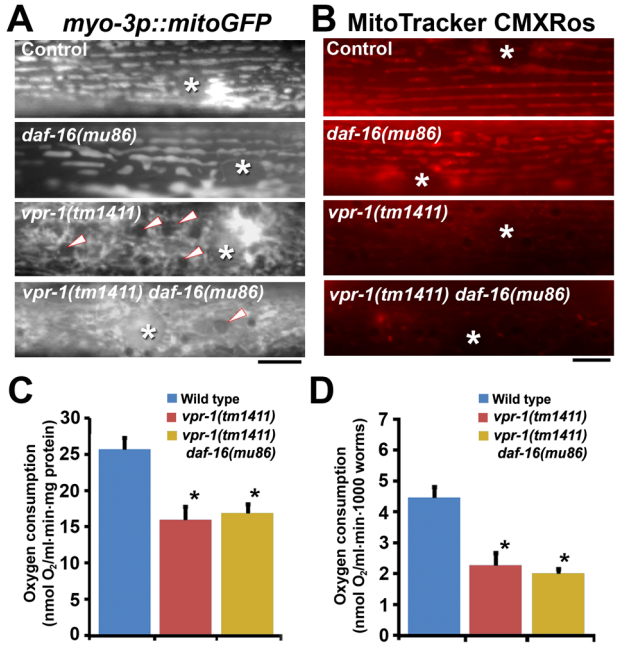

Figure 7. Effect of DAF-16 inactivation on muscle mitochondria. (A) Muscle mitochondrial tubules in indicated genotypes visualized using mitoGFP. Arrowheads indicate fat droplets. Asterisks indicate nucleus. Bar, 5 µm. (B) MitoTracker CMXRos staining of wild-type and mutant muscle. Asterisks indicate nucleus. Bar, 5 µm. (C and D) Oxygen consumption rates of wild-type and mutant hermaphrodites. Measured consumption rates were normalized by protein content (C) or number of worms (D). Error bars represent SD. *, $P<0.001$ compared to wild type. Oxygen consumption rate of wild-type and *vpr-1(tm1411)* mutants includes published data [15] measured together with *vpr-1(tm1411) daf-16(mu86)* mutants.
doi:10.1371/journal.pgen.1003738.g007

consistent with the signaling function. Indeed, muscle vMSP receptors and the downstream Arp2/3 complex mediate this lipid metabolism response. We also found that sperm presence can modulate striated muscle TAG metabolism. Neurons and sperm are two cell types capable of secreting MSP domains [15,47]. Our data do not exclude cell autonomous roles for VPR-1 in regulating lipid dynamics. Nevertheless, they highlight the importance of testing VAP autonomy when evaluating biological mechanism.

The connection between VAPB and FoxO

We show that *vpr-1/vap* loss triggers elevated DAF-16/FoxO activity, resulting in muscle TAG accumulation. Inactivating the Arp2/3 complex largely suppresses these metabolic alterations, as well as the muscle mitochondrial defects. These data support the model that impaired vMSP signaling to muscle triggers elevated FoxO activity. Consistent with this model, over-expressing Arp2 specifically in wild-type muscle causes TAG accumulation and mitochondrial defects. Although we cannot eliminate the possibility that Arp2/3 acts in other tissues, it appears to be a muscle-specific suppressor of *vpr-1* mutants. How might the Arp2/3 complex regulate FoxO? One possibility is that *vpr-1* mutants go into energy deficit as they age, as mitochondrial dysfunction is thought to increase FoxO activity [48–51]. An alternative possibility is that FoxO acts downstream of Arp2/3, but in parallel to mitochondria. In either case, reduced insulin signaling could be involved. A strong reduction in insulin causes increased FoxO nuclear translocation, which is not observed in *vpr-1* mutants under standard conditions. However, subtle changes can be more difficult to detect.

Additional mechanisms could also modulate FoxO in *vpr-1* mutants. The vMSP/ephrin receptor VAB-1 directly interacts with DAF-18/PTEN (phosphatase and tensin homolog deleted on chromosome ten), which regulates FoxO activity [52]. VAB-1 is expressed throughout the adult nervous system and in the gonad [53,54]. Previous studies have shown that sperm presence can modulate DAF-16/FoxO translocation and transcriptional activity [55], perhaps through secreted MSPs. Whether sperm act via the Arp2/3 complex is not clear. An interesting possibility is that global MSP signals from neurons and sperm are sensed through distinct mechanisms. These mechanisms might converge on muscle metabolic output to meet changes in energy requirements.

In mammals, FoxO transcription factors are critical regulators of energy metabolism, particularly under fasting conditions. We show that *Vapb* ablation in mice renders muscle lipid stores resistant to fasting, a situation analogous to lipid accumulation in *vpr-1* mutant worm muscles. Dysregulated lipid stores in mutant mice is associated with alterations in muscle gene expression consistent with abnormal FoxO1 and FoxO3 activity [56]. For instance, FoxO1 target gene mRNAs for PEPCK and G6Pase are clearly up-regulated in muscle of young *Vapb* −/− mice in the fed state (*i.e.* in the presence of insulin that decreases FoxO1 activity). Similar results are observed for FoxO3 target genes LC3 and Atrogin-1. These data suggest that FoxO1/3 are less sensitive to insulin inhibition in *Vapb* −/− mice.

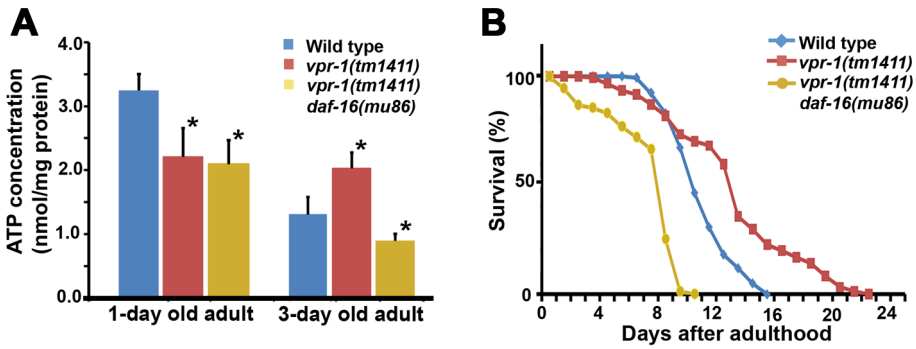

Figure 8. Effect of DAF-16 inactivation on ATP level and lifespan. (A) ATP concentration in wild-type and *vpr-1(tm1411)* mutant adult extracts. *, $P<0.001$ compared to wild type. Error bars represent SD. ATP concentration of wild-type and *vpr-1(tm1411)* mutants at 1-day-old adults include published data [15] measured together with *vpr-1(tm1411) daf-16(mu86)* mutants. (B) Lifespan measurements of indicated genotypes. The lifespan of *daf-16(mu86)* mutants (not shown) was similar to the wild type, as previously shown.
doi:10.1371/journal.pgen.1003738.g008

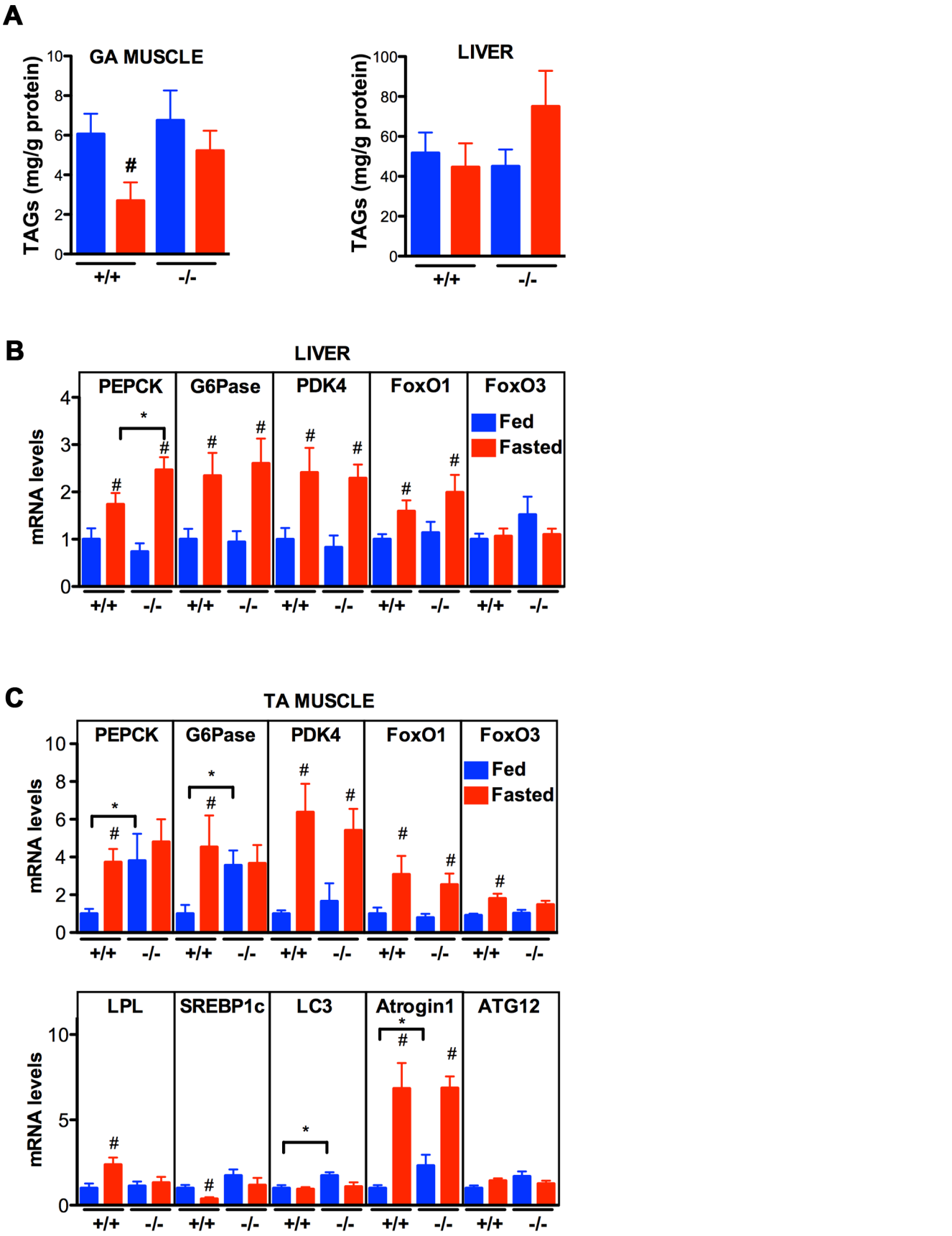
A
GA MUSCLE
TAGs (mg/g protein)
LIVER
+/+
-/-
B
LIVER
PEPCK
G6Pase
PDK4
FoxO1
FoxO3
Fed
Fasted
mRNA levels
C
TA MUSCLE
LPL
SREBP1c
LC3
Atrogin1
ATG12

Figure 9. Effect of *Vapb* ablation on fasting/refeeding energy metabolism in mice. (A) TAG concentration in GA muscle and liver of wild-type (+/+) and *Vapb* knock-out (−/−) mice after 24-hour fasting (red) or 24 hours fasting followed by 6 hours of refeeding (blue). (B and C) Quantitative RT-PCR of indicated genes in liver (B) and TA muscle (C) of wild-type (+/+) and *Vapb* knock-out (−/−) mice after 24-hour fasting (red) or 24 hours fasting followed by 6 hours of refeeding (blue). Relative mRNA levels are shown on the Y-axis. #, $P<0.05$ compared to fed mice of the same genotype. *, $P<0.05$ compared to +/+ under the same condition.
doi:10.1371/journal.pgen.1003738.g009

Not all FoxO target genes studied are sensitive to *Vapb* ablation. For instance, VAPB does not appear to influence PDK4 and ATG12 mRNAs. Additionally, some of the mRNAs studied showed uncoupling from circulating insulin levels, consistent with an insensitivity of FoxO1 to insulin. SREBP1c mRNA, which is negatively regulated by FoxO1 [57], was increased by feeding in +/+ mice, but not in −/− mice. A similar, albeit mirror situation was observed for LPL, a gene positively regulated by FoxO1 [58]. Hence, FoxO1/3 might participate in the abnormal lipid mobilization in *Vapb* −/− mice, but other mechanisms are likely at work to avoid the major consequences of chronic muscle FoxO activation, such as muscle atrophy [59]. In summary, our findings show that VAPB is involved in modulating mouse muscle energy metabolism upon fasting and refeeding, possibly via altered FoxO activity. Whether this occurs through a cell autonomous or a cell nonautonomous mechanism, like in *C. elegans* and Drosophila, remains to be determined.

FoxO is protective in *vap* mutants

A key finding in worms is that DAF-16/FoxO activity prolongs the adult lifespan of *vpr-1* mutants from 6.9±2.5 to 12.9±4.4 days. This lifespan increase may be due to metabolic alterations that compensate for mitochondrial dysfunction. Consistent with this idea, FoxO extends the lifespan of *C. elegans* with reduced mitochondrial function [48,49,60]. The FoxO-dependent fat accumulation in *vpr-1* mutant muscle may reflect an effort to increase energy production. We show that DAF-16 helps *vpr-1* mutants maintain ATP levels in 3-day old adults. Among the numerous DAF-16 metabolic genes are those involved in fat synthesis and transport, β-oxidation, the glyoxylate cycle, and gluconeogenesis [37]. However, additional DAF-16 targets may also be involved, such as stress resistance enzymes [37,38,61]. *vpr-1* mutants are more resistant than the wild type to reactive oxygen species and ER stress. Based on identified DAF-16 targets and *vpr-1* mutant phenotypes, DAF-16 might increase energy substrate availability in muscle, stimulate anaerobic metabolism, increase oxidative metabolism in non-muscle cells, or decrease ATP consumption. Further studies are necessary to distinguish among these possibilities, as well as other models.

Implications for ALS

Metabolic alterations in ALS patients and mouse models are hypothesized to compensate for mitochondrial dysfunction, particularly in skeletal muscle [17,19,62,63]. Differentially expressed gene networks involved in oxidative metabolism and the cytoskeleton, including up-regulated FoxO1 and FoxO3 mRNAs have been found in ALS patient skeletal muscles [64,65]. Our studies of VAPB in worms, flies, and mice are consistent with impaired vMSP signaling to muscle causing some of these alterations. Importantly, *vpr-1* loss in worms, *Vapb* depletion in zebrafish, or *Vapb* loss in mice does not cause motor neuron degeneration [4,15], providing strong evidence that mitochondrial and metabolic defects are not secondary consequences of neurodegeneration. These data contrast with a recent Drosophila study suggesting that *Vapb* loss causes neurodegeneration via increased phosphoinositides [66]. In humans, metabolic alterations caused by reduced VAPB function may not be sufficient to induce motor neuron degeneration, although they could strongly predispose to ALS. Redundancy could be an important consideration in the different models. The worm genome encodes a single *vap* homolog, but many genes with MSP domains. Vertebrate genomes typically encode VAPA and VAPB, which are approximately 60% identical. *Vap* mutant flies have the most severe developmental defects and the fewest MSP genes in the genome.

In summary, our results support the model that striated muscle mitochondrial dysfunction alters FoxO activity, which in turn affects energy metabolism and promotes survival. It is possible that reduced vMSP signaling causes some of the mitochondrial and metabolic alterations in ALS patients. Perhaps vMSPs might protect against ALS via effects on skeletal muscle energy metabolism.

Materials and Methods

C. elegans genetics, strains, and RNA-mediated interference

C. elegans Bristol N2 is the wild-type strain. Worms were grown on NGM plates with NA22 bacteria as the food source [67]. Strain construction and marker scoring were done as previously described [15,54]. The strains and genetic markers used or generated were as follows: CF1553 muIs84[pAD76(*sod-3::GFP*)], CF1038 *daf-16(mu86)* I, *vpr-1(tm1411)*/hT2[*bli-4(e937)* let-?(*q782*) qIs48] I;III, SJ4005 zcIs4[*hsp-4::GFP*], TJ356 zIs356[*daf-16p::daf-16::GFP; rol-6*] IV, *fog-3(q443) I*/hT2[*bli-4(e937)* let-?(*q782*) qIs48] I;III, CX3198 *sax-3(ky123) X*, and XM1004 *vpr-1(tm1411) daf-16(mu86)*/hT2[*bli-4(e937)* let-?(*q782*) qIs48] I;III. Transgenics expressing *vit-2p::vit-2::gfp* were generated by crossing into the pwIs23 integrated line. RNAi was performed using the feeding method starting at the L1 stage, as previously described [15]. *arx-2*, *clr-1*, and *xbp-1* RNAi clones are from the genome-wide library [68]. Each clone was sequenced for confirmation.

Transgenics

To generate transgenic *C. elegans*, the marker plasmids pRF4 [*rol-6*] (60 ng/µl) or *myo-3p::mito::GFP* (30–60 ng/µl) were mixed with *myo-3p::vpr-1* (60 ng/µl), *ges-1p::vpr-1*(60 ng/µl), *unc-119p::vpr-1*(60 ng/µl), *unc-119p::vpr-1* P56S (60 ng/µl), or *myo-3p::arx-2::mCherry* (60 ng/µl) and microinjected into the gonads of young adult hermaphrodites. Injected worms were incubated for 24 hours, transferred to new NGM plates, and screened for transgenic progeny. Transgenic lines were selected based on the roller phenotype or GFP expression. Multiple independent transgenic lines were generated for all strains. To conduct genetic mosaic analysis, 10 ng/µl WRM06B28 fosmid DNA containing the *vpr-1* genomic locus was mixed with 10 ng/µl pTG96 (*sur-5p::GFP*) plasmid and microinjected into the gonads of *vpr-1(tm1411)*/hT2 hermaphrodites. Transgenic lines were selected based on GFP expression. Transgenic lines were maintained as *vpr-1(tm1411)* homozygotes, as the fosmid rescued the sterility, mitochondria, fat metabolism, slow growth, and embryonic defects. For lineage scoring, approximately 15,000 worms were screened. Transgene loss in the AB lineage was scored by GFP loss in head and tail neurons, the nerve cords, and the excretory gland.

Transgene loss in the P1 lineage was scored by GFP loss in the intestine, muscle, somatic gonad, and hyp11. The P2 lineage was scored by GFP loss in numerous body wall muscle cells and hyp11, the P3 lineage was scored by GFP loss in body wall muscle, and the P4 lineage was inferred by a sterile phenotype without GFP loss. Transgene loss in the EMS lineage was scored by GFP loss in the intestine and somatic gonad, while loss in the E lineage was score by exclusive GFP loss in the intestine.

Transmission electron microscopy

TEM was performed as previously described [15].

Bodipy-FA and Sudan Black B staining

For the Bodipy-FA experiments, a 5 mM Bodipy-FA (Molecular probe, U.S.A) stock solution was prepared in DMSO and kept at −20°C. A 200 µM working solution diluted in distilled water was dropped onto seeded plates and allowed to dry. L4 stage worms were placed on the plates and incubated in the dark for 24 hours at 20°C. Bodipy-FAs can get trapped in intestinal gut granules that are not present in muscle.

Sudan Black B staining was conducted as described in previous studies [15]. Briefly, synchronized 1-day-old adult worms were collected into microfuge tubes containing M9 solution. Worms were washed five times, incubated for 40 minutes at 20°C to remove intestinal bacteria, and fixed in 1% paraformaldehyde. The fixed worms were washed three times in cold M9 solution and dehydrated through a 25%, 50%, and 70% ethanol series. Sudan Black B solution was added to the worms and incubated for 1 hour. To remove excess stain, worms were washed five times with 70% ethanol. To normalize for staining variability among experiments, wild type and *vpr-1(tm1411)* mutants were processed in the same tube and identified based on gonad morphology.

Lipid analysis by ESI-MS/MS

For the lipid analysis by ESI-MS/MS, lipids from equal masses of wild type and *vpr-1(tm1411)* mutant adults were extracted by chloroform-methanol following a modified Bligh/Dyer extraction [69]. A mixture of internal standards including T17:1 TAG was added to the chloroform-methanol phase before extraction. The extracted samples were concentrated to dryness under a nitrogen stream, reconstituted with methanol:chloroform (1:1 v/v) and transferred to HPLC auto samplers. Lipids were analyzed by ESI-MS/MS using an API 4000 (Applied Biosystems/MDS Sciex, Concord, Ontario, Canada) triple quadrupole mass spectrometer. Extracted lipid samples (5 ml) were infused into the mass spectrometer with a solvent mixture of chloroform-methanol (1:2, v/v) containing 0.1% formic acid using a Shimadzu Prominence HPLC with a refrigerated auto sampler (Shimadzu Scientific Instruments, Inc. Columbia, MD). Lipids were analyzed in positive ion mode using an API 4000 (Applied Biosystems/MDS Sciex, Concord, Ontario, Canada) triple quadruple mass spectrometer. Samples (5 µl) were directly infused into the electrospray source using a Shimadzu Prominence HPLC with a refrigerated auto sampler (Shimadzu Scientific Instruments, Inc. Columbia, MD). Neutral loss (NL) scanning (228, 254, 256, 268, 278, 280, 284, and 304) of naturally occurring aliphatic chains (i.e. building block of TAG molecular species) were utilized to determine the identities of each molecular species. NL scanning of 141 was used for profiling phosphatidylethanolamine. The following analysis parameters were used: ion spray voltage 5000 V, de-clustering potential 40 V, temperature 300°C (for TAG), collision energy 35 V, and collisionally activated dissociation 5.

Mitochondrial staining

To assess mitochondrial transmembrane potential, worms were stained using the MitoTracker CMXRos dye (Molecular Probes, U.S.A), as previously described [15]. This lipophilic cationic fluorescent dye accumulates in mitochondria in a membrane potential-dependent manner [70]. L4 larval stage worms were placed on dried plates containing a 100 µM MitoTracker CMXRos dye solution (dropped on bacteria). After 24 hours incubation in the dark, worms were transferred to a new NGM plate and incubated in the dark for 20 minutes to remove intestinal background. Worms were mounted on dried 2% agarose pads without anesthetic. Wild-type and *vpr-1(tm1411)* mutant hermaphrodites were cultured on the same plates.

ATP concentration measurement

ATP concentration was measured as described previously, with slight modification [15]. Briefly, 150 worms were individually picked and placed into tubes containing M9 buffer, washed four times, and incubated at 20°C for 40 minutes to remove intestinal bacteria. These worms were then washed four times with TE solution (100 mM Tris–Cl, pH 7.6, 4 mM EDTA) and placed into microfuge tubes containing 300 µl TE solution. Worm extracts were prepared by a series of cycles including freezing, thawing, and sonicating. These extracts were boiled for 10 minutes to release ATP and block ATPase activity. Carcasses and insoluble material were pelleted in a microcentrifuge at 20,000×g for 10 minutes. The soluble extracts were diluted in a 1:10 ratio using TE solution. ATP concentration in 60 µl of diluted extracts was measured using the ENLITEN ATP Assay System (Promega, U.S.A), according to the manufacturer's instructions. A luminometer (Berthold, Germany) was used for quantification. Protein concentration was determined using the BCA protein assay (Pierce, U.S.A). ATP measurements were repeated at least three times for each strain.

Oxygen consumption

Oxygen consumption rates were measured as previously described using the oxygraph system (Hansatech, UK) with minor modifications [15]. Worms were cultured at 20°C and synchronized to the 1-day-old adult stage. For each test, 1000 worms were individually picked and placed into a glass tube with 1 ml M9 buffer at 20°C. Collected worms were incubated for 40 min at 20°C to remove intestinal bacteria, carefully washed five times, and placed into 1 ml M9 buffer. The worm solution was loaded into the chamber equipped with a S1 Clark type polarographic oxygen electrode disc maintained at 20°C. Oxygen concentration was measured for 10 minutes. For normalization, worms were carefully collected from the chamber and protein content was measured using the BCA test kit (Pierce, U.S.A.). Rates were normalized to either total protein content or number of worms. We performed at least three independent measurements per strain.

Feeding rate and lifespan assays

To measure feeding rates, worms were cultured at 20°C and 1-day-old adult worms were placed on new NGM plates. Feeding behavior was recorded using a Zeiss Lumar stereomicroscope with AxioCam MRM digital camera. Measurements were conducted during a 30 second period at room temperature (22°C). The rhythmic contractions of the pharyngeal bulb were counted. For each strain, over 20 worms were counted. To determine lifespan of worms, L4 larval stage worms were placed on new NGM plates

seeded with NA22 bacteria and cultured at 20°C. The L4 stage was used because a small percentage of *vpr-1* mutants die during L1–L4 stages and *vpr-1* mutants develop slowly. Worms were monitored every day and transferred to flesh NGM plates. Death was scored by failure to respond to touching with a platinum wire. Wild-type worms fed NA22 bacteria have slightly shorter lifespan than worms fed OP50 bacteria.

Tunicamycin resistance

To analyze ER homeostasis, worms were cultured on plates with tunicamycin (Sigma, U.S.A) from the embryonic stage to adulthood. NGM plates with 0.1% DMSO and 0 or 5.0 µg/ml tunicamycin were prepared. About 30 adult worms were placed on each tunicamycin plate and allowed to lay embryos for 30 minutes. Adult worms were then removed. Twelve hours later the number of hatched embryos was counted and compared with the number of worms that reached the adult stage within 96 hours. We performed at least three independent measurements for each strain.

Mouse experiments

Mouse experiments were performed using the Institutional European Guidelines, under the supervision of an authorized investigator (LD), and approved by the local ethical committee for animal experiments (CREMEAS, agreement N° AL/01/08/02/13). *Vapb* −/− mice were used and genotyped as described [4]. Mice (8–10 per group) were either fasted for 24 hours from 5PM (fasted group), or fasted from 5PM to 9AM and refed until sacrifice at 5PM. GA and TA muscle and liver tissues were collected, and rapidly frozen in liquid nitrogen for subsequent analyses of gene expression and TAG levels. The tissues were stored at −80°C until the time of analysis.

For RT-qPCR, frozen liver and muscle tissues were placed into tubes containing 5 mm stainless steel beads (Qiagen, Courtaboeuf, France) and 1 ml of Trizol reagent (Invitrogen, Paisley, UK) and homogenized using a TissueLyser (Qiagen). RNA was prepared from tissue homogenates following Trizol manufacturer's instructions. RNA reverse transcription and SYBR Green real-time PCR assays were performed using the Bio-Rad (Biorad, Marnes la Coquette, France) iCycler kits and protocols. PCR conditions were 3 min at 94°C, followed by 40 cycles of 45 s at 94°C and 10 s at 60°C. Primers are shown in Table S1. For western blotting, liver and TA muscles were incubated in Lysis buffer containing complete protease and phosphatase inhibitor cocktails. Protein concentration was measured using BCA Protein Assay. Equal amount of protein (50 µg) were separated by SDS-PAGE 10% and blotted onto nitrocellulose membrane. Membranes were saturated with 10% milk and then incubated with the primary antibodies FoxO1 (Proteintech; 18592-1-AP), FoxO3a (Cell signaling; #2497), VAPB [4] and Histone H3 (Cell signaling; #9715), all diluted (1:1000) followed by anti-rabbit secondary antibody, diluted 1:5000.

For TAG analysis, tissue powder was homogenized in lysis buffer (250 mM Sucrose solution, 1 mM EDTA, 2% SDT, 1 mM DTT, 10 mM Tris HCl pH 7.4) containing protease inhibitors (Sigma P8340) and phosphatase inhibitors (Sigma 8345), centrifuged at 12000×rpm for 15 minutes at room temperature. TAG concentration was determined in duplicate for each sample in 5 µl of supernatant, using the enzymatic method of analysis (Randox *Triglyceride* Colorimetric Assay *Kit*, *Randox Laboratories Limited*, *UK*) as described by the manufacturer. Lipid values were normalized to protein concentration.

Supporting Information

Figure S1 Lipid-like droplets and mitochondria in *vpr-1* mutant striated muscle. (A) Close-up image of a live transgenic *vpr-1(tm1441)* mutant hermaphrodite expressing mitoGFP in body wall muscle. mitoGFP labels muscle mitochondrial tubules. (B) Image of a single body wall muscle in a transgenic *vpr-1(tm1441)* mutant hermaphrodite expressing mitoGFP. (C) Close-up image of the boxed region from panel B showing horizontal and vertical cross-sections. Arrowheads indicate lipid-like droplets. Asterisks indicate nucleus. Bar in A, 1 µm; Bars in B and C, 10 µm.
(TIF)

Figure S2 Transmission electron micrographs of wild-type and mutant adults. Micrographs are transverse sections showing the cuticle (C) and body wall muscle sarcomeres (S) with hypodermis sandwiched in between. A lipid droplet within the hypodermis (HL) is seen in the wild-type panel. The intestine is filled with electron dense and opaque lipid droplets (IL). Yolk lipoprotein complexes (Y) are found between muscle and intestinal tissues (also see Figure S4). Notice that yolk is electron dense, whereas muscle lipid droplets (ML) are opaque. N, muscle nucleus. Bars, 1 µm.
(TIF)

Figure S3 Sudan Black B staining in wild type and *vpr-1* mutants. 1-day-old adult wild-type and *vpr-1(tm1411)* hermaphrodites were stained using Sudan Black B. Arrowheads indicate fat droplets in body wall muscle. Anterior is to the left in all panels. Boxed regions are magnified 5× below. Low magnification bars, 50 µm; high magnification bars, 10 µm.
(TIF)

Figure S4 Yolk lipoprotein complex distribution in wild-type and *vpr-1* mutants. (A) Yolk distribution visualized with the *vit-2p::vit-2::gfp* transgene. *vpr-1* mutants accumulate yolk in the pseudocoelom due to failure of oocyte differentiation. GFP uptake is not observed in peripheral tissues. (B) Close-up image showing muscle fat droplets (arrows) in *vpr-1* mutants. Bar, 5 µm.
(TIF)

Figure S5 ER stress assays in wild-type and *vpr-1* mutant worms. (A) Integrated transgenic lines expressing GFP under the *hsp-4* promoter *(hsp-4p::GFP)* with and without tunicamycin treatment, which induces ER stress. Anterior is to the left in all panels. Bar, 5 mm. (B) Tunicamycin sensitivity in wild-type and *vpr-1(tm1411)* mutants hermaphrodites. Y-axis indicates the percentage of worms that developed to the adult stage in the presence of 5 µg/ml tunicamycin. Error bars represent SD. Three independent measurements were performed.
(TIF)

Figure S6 Effect of sperm presence on muscle fat droplets and mitochondria. (A) DIC and fluorescent images of muscle in live 3-day-old *vpr-1* mutant hermaphrodite worms fed Bodipy-FAs. Mating with wild type (WT) males provides sperm into the uterus. Sperm presence did not affect the sterility or muscle mitochondrial morphology of *vpr-1* mutants (data not shown). Anterior is to the left in all panels. Arrowheads indicate lipid-like droplets. Bar, 5 µm. (B) DIC and fluorescent images of muscle in live transgenic *fog-3(q443)/hT2* hermaphrodites containing sperm and unmated *fog-3(q443)* mutants without sperm. Muscle mitochondrial tubules were visualized using mitoGFP. Arrowheads indicate lipid-like droplets. Asterisks indicate nucleus. Bar, 5 µm.
(TIF)

Figure S7 Effect of ARX-2/Arp2 overexpression on muscle fat droplets and mitochondria. DIC and fluorescent images of muscle in live transgenic wild-type hermaphrodites expressing *arx-2* under

control of the muscle specific *myo-3* promoter. Muscle mitochondrial tubules were visualized using mitoGFP. Notice that muscle mitochondrial morphology closely resembles the morphology seen in *vpr-1* mutants [15]. See Figures 7A, S6B and [15] for controls. Arrows indicate lipid-like droplets. Asterisks indicate nucleus. Bar, 5 μm.
(TIF)

Table S1 Primers used for RT-qPCR in mice.
(TIF)

Acknowledgments

We thank Se-Jin Lee and three anonymous reviewers for comments on the manuscript. We also thank the UAB Targeted Metabolomics and Proteomics Laboratory, the *Caenorhabditis* Genetics Center, and the Japanese National Bioresource Project.

Author Contributions

Conceived and designed the experiments: MAM LD HJB JKP SMH. Performed the experiments: SMH HEO JSZ JV PC JKP. Analyzed the data: SMH MAM HJB JKP LD. Wrote the paper: SMH MAM LD.

References

1. Kiernan MC, Vucic S, Cheah BC, Turner MR, Eisen A, et al. (2011) Amyotrophic lateral sclerosis. Lancet 377: 942–955.
2. Nishimura AL, Mitne-Neto M, Silva HC, Richieri-Costa A, Middleton S, et al. (2004) A mutation in the vesicle-trafficking protein VAPB causes late-onset spinal muscular atrophy and amyotrophic lateral sclerosis. Am J Hum Genet 75: 822–831.
3. Chen HJ, Anagnostou G, Chai A, Withers J, Morris A, et al. (2010) Characterization of the properties of a novel mutation in VAPB in familial amyotrophic lateral sclerosis. J Biol Chem 285: 40266–40281.
4. Kabashi E, El Oussini H, Bercier V, Gros-Louis F, Valdmanis PN, et al. (2013) Investigating the contribution of VAPB/ALS8 loss of function in amyotrophic lateral sclerosis. Hum Mol Genet 22: 2350–2360.
5. Anagnostou G, Akbar MT, Paul P, Angelinetta C, Steiner TJ, et al. (2010) Vesicle associated membrane protein B (VAPB) is decreased in ALS spinal cord. Neurobiol Aging 31: 969–985.
6. Teuling E, Ahmed S, Haasdijk E, Demmers J, Steinmetz MO, et al. (2007) Motor neuron disease-associated mutant vesicle-associated membrane protein-associated protein (VAP) B recruits wild-type VAPs into endoplasmic reticulum-derived tubular aggregates. J Neurosci 27: 9801–9815.
7. Mitne-Neto M, Machado-Costa M, Marchetto MC, Bengtson MH, Joazeiro CA, et al. (2011) Downregulation of VAPB expression in motor neurons derived from induced pluripotent stem cells of ALS8 patients. Hum Mol Genet 20: 3642–3652.
8. Loewen CJ, Levine TP (2005) A highly conserved binding site in vesicle-associated membrane protein-associated protein (VAP) for the FFAT motif of lipid-binding proteins. J Biol Chem 280: 14097–14104.
9. Amarilio R, Ramachandran S, Sabanay H, Lev S (2005) Differential regulation of endoplasmic reticulum structure through VAP-Nir protein interaction. J Biol Chem 280: 5934–5944.
10. Lev S, Ben Halevy D, Peretti D, Dahan N (2008) The VAP protein family: from cellular functions to motor neuron disease. Trends Cell Biol 18: 282–290.
11. Peretti D, Dahan N, Shimoni E, Hirschberg K, Lev S (2008) Coordinated lipid transfer between the endoplasmic reticulum and the Golgi complex requires the VAP proteins and is essential for Golgi-mediated transport. Mol Biol Cell 19: 3871–3884.
12. De Vos KJ, Morotz GM, Stoica R, Tudor EL, Lau KF, et al. (2012) VAPB interacts with the mitochondrial protein PTPIP51 to regulate calcium homeostasis. Hum Mol Genet 21: 1299–1311.
13. Tsuda H, Han SM, Yang Y, Tong C, Lin YQ, et al. (2008) The amyotrophic lateral sclerosis 8 protein VAPB is cleaved, secreted, and acts as a ligand for Eph receptors. Cell 133: 963–977.
14. Han SM, Cottee PA, Miller MA (2010) Sperm and oocyte communication mechanisms controlling C. elegans fertility. Dev Dyn 239: 1265–1281.
15. Han SM, Tsuda H, Yang Y, Vibbert J, Cottee P, et al. (2012) Secreted VAPB/ALS8 Major Sperm Protein Domains Modulate Mitochondrial Localization and Morphology via Growth Cone Guidance Receptors. Dev Cell 22: 348–362.
16. Marques VD, Barreira AA, Davis MB, Abou-Sleiman PM, Silva WA, Jr., et al. (2006) Expanding the phenotypes of the Pro56Ser VAPB mutation: proximal SMA with dysautonomia. Muscle Nerve 34: 731–739.
17. Dupuis L, Pradat PF, Ludolph AC, Loeffler JP (2011) Energy metabolism in amyotrophic lateral sclerosis. Lancet Neurol 10: 75–82.
18. Gallo V, Wark PA, Jenab M, Pearce N, Brayne C, et al. (2013) Prediagnostic body fat and risk of death from amyotrophic lateral sclerosis: The EPIC cohort. Neurology 80: 829–838.
19. Dupuis L, Corcia P, Fergani A, Gonzalez De Aguilar JL, Bonnefont-Rousselot D, et al. (2008) Dyslipidemia is a protective factor in amyotrophic lateral sclerosis. Neurology 70: 1004–1009.
20. Dorst J, Kuhnlein P, Hendrich C, Kassubek J, Sperfeld AD, et al. (2011) Patients with elevated triglyceride and cholesterol serum levels have a prolonged survival in amyotrophic lateral sclerosis. J Neurol 258: 613–617.
21. Herndon LA, Schmeissner PJ, Dudaronek JM, Brown PA, Listner KM, et al. (2002) Stochastic and genetic factors influence tissue-specific decline in ageing C. elegans. Nature 419: 808–814.
22. McGee MD, Weber D, Day N, Vitelli C, Crippen D, et al. (2011) Loss of intestinal nuclei and intestinal integrity in aging C. elegans. Aging cell 10: 699–710.
23. Kubagawa HM, Watts JL, Corrigan C, Edmonds JW, Sztul E, et al. (2006) Oocyte signals derived from polyunsaturated fatty acids control sperm recruitment in vivo. Nat Cell Biol 8: 1143–1148.
24. Klapper M, Ehmke M, Palgunow D, Bohme M, Matthaus C, et al. (2011) Fluorescence-based fixative and vital staining of lipid droplets in Caenorhabditis elegans reveal fat stores using microscopy and flow cytometry approaches. J Lipid Res 52: 1281–1293.
25. Grant B, Hirsh D (1999) Receptor-mediated endocytosis in the Caenorhabditis elegans oocyte. Mol Biol Cell 10: 4311–4326.
26. Moumen A, Virard I, Raoul C (2011) Accumulation of wildtype and ALS-linked mutated VAPB impairs activity of the proteasome. PloS One 6: e26066.
27. Gkogkas C, Middleton S, Kremer AM, Wardrope C, Hannah M, et al. (2008) VAPB interacts with and modulates the activity of ATF6. Hum Mol Genet 17: 1517–1526.
28. Basseri S, Austin RC (2012) Endoplasmic reticulum stress and lipid metabolism: mechanisms and therapeutic potential. Biochem Res Int 2012: 841362.
29. Urano F, Calfon M, Yoneda T, Yun C, Kiraly M, et al. (2002) A survival pathway for Caenorhabditis elegans with a blocked unfolded protein response. J Cell Biol 158: 639–646.
30. Wyles JP, McMaster CR, Ridgway ND (2002) VAMP-associated protein-A (VAP-A) interacts with the oxysterol binding protein (OSBP) to modify export from the endoplasmic reticulum. J Biol Chem 277: 29908–29918.
31. Jansen M, Ohsaki Y, Rita Rega L, Bittman R, Olkkonen VM, et al. (2011) Role of ORPs in sterol transport from plasma membrane to ER and lipid droplets in mammalian cells. Traffic 12: 218–231.
32. Peretti D, Dahan N, Shimoni E, Hirschberg K, Lev S (2008) Coordinated lipid transfer between the endoplasmic reticulum and the Golgi complex requires the VAP proteins and is essential for Golgi-mediated transport. Mol Biol Cell 19: 3871–3884.
33. Yochem J, Herman RK (2003) Investigating C. elegans development through mosaic analysis. Development 130: 4761–4768.
34. Yang Y, Han SM, Miller MA (2010) MSP hormonal control of the oocyte MAP kinase cascade and reactive oxygen species signaling. Dev Biol 342: 96–107.
35. Oh SW, Mukhopadhyay A, Dixit BL, Raha T, Green MR, et al. (2006) Identification of direct DAF-16 targets controlling longevity, metabolism and diapause by chromatin immunoprecipitation. Nat Genet 38: 251–257.
36. Halaschek-Wiener J, Khattra JS, McKay S, Pouzyrev A, Stott JM, et al. (2005) Analysis of long-lived C. elegans daf-2 mutants using serial analysis of gene expression. Genome Res 15: 603–615.
37. Murphy CT (2006) The search for DAF-16/FOXO transcriptional targets: approaches and discoveries. Exp Gerontol 41: 910–921.
38. Murphy CT, McCarroll SA, Bargmann CI, Fraser A, Kamath RS, et al. (2003) Genes that act downstream of DAF-16 to influence the lifespan of Caenorhabditis elegans. Nature 424: 277–283.
39. McElwee J, Bubb K, Thomas JH (2003) Transcriptional outputs of the Caenorhabditis elegans forkhead protein DAF-16. Aging Cell 2: 111–121.
40. Henderson ST, Bonafe M, Johnson TE (2006) daf-16 protects the nematode Caenorhabditis elegans during food deprivation. J Gerontol A Biol Sci Med Sci 61: 444–460.
41. Landis JN, Murphy CT (2010) Integration of diverse inputs in the regulation of Caenorhabditis elegans DAF-16/FOXO. Dev Dyn 239: 1405–1412.
42. Williams TW, Dumas KJ, Hu PJ (2010) EAK proteins: novel conserved regulators of C. elegans lifespan. Aging 2: 742–747.
43. Houthoofd K, Braeckman BP, Lenaerts I, Brys K, Matthijssens F, et al. (2005) DAF-2 pathway mutations and food restriction in aging Caenorhabditis elegans differentially affect metabolism. Neurobiol Aging 26: 689–696.
44. Braeckman BP, Houthoofd K, De Vreese A, Vanfleteren JR (2002) Assaying metabolic activity in ageing Caenorhabditis elegans. Mech Ageing Dev 123: 105–119.
45. Lin K, Hsin H, Libina N, Kenyon C (2001) Regulation of the Caenorhabditis elegans longevity protein DAF-16 by insulin/IGF-1 and germline signaling. Nat Genet 28: 139–145.
46. Stefan CJ, Manford AG, Baird D, Yamada-Hanff J, Mao Y, et al. (2011) Osh proteins regulate phosphoinositide metabolism at ER-plasma membrane contact sites. Cell 144: 389–401.

47. Kosinski M, McDonald K, Schwartz J, Yamamoto I, Greenstein D (2005) C. elegans sperm bud vesicles to deliver a meiotic maturation signal to distant oocytes. Development 132: 3357–3369.
48. Dillin A, Hsu AL, Arantes-Oliveira N, Lehrer-Graiwer J, Hsin H, et al. (2002) Rates of behavior and aging specified by mitochondrial function during development. Science 298: 2398–2401.
49. Lee SS, Lee RY, Fraser AG, Kamath RS, Ahringer J, et al. (2003) A systematic RNAi screen identifies a critical role for mitochondria in C. elegans longevity. Nat Genet 33: 40–48.
50. Billing O, Kao G, Naredi P (2011) Mitochondrial function is required for secretion of DAF-28/insulin in C. elegans. PloS One 6: e14507.
51. Greer EL, Banko MR, Brunet A (2009) AMP-activated protein kinase and FoxO transcription factors in dietary restriction-induced longevity. Ann N Y Acad Sci 1170: 688–692.
52. Brisbin S, Liu J, Boudreau J, Peng J, Evangelista M, et al. (2009) A role for C. elegans Eph RTK signaling in PTEN regulation. Dev Cell 17: 459–469.
53. George SE, Simokat K, Hardin J, Chisholm AD (1998) The VAB-1 Eph receptor tyrosine kinase functions in neural and epithelial morphogenesis in C. elegans. Cell 92: 633–643.
54. Miller MA, Ruest PJ, Kosinski M, Hanks SK, Greenstein D (2003) An Eph receptor sperm-sensing control mechanism for oocyte meiotic maturation in Caenorhabditis elegans. Genes Dev 17: 187–200.
55. Miyata S, Begun J, Troemel ER, Ausubel FM (2008) DAF-16-dependent suppression of immunity during reproduction in Caenorhabditis elegans. Genetics 178: 903–918.
56. Cheng Z, White MF (2011) Targeting Forkhead box O1 from the concept to metabolic diseases: lessons from mouse models. Antioxid Redox Signal 14: 649–661.
57. Kamei Y, Miura S, Suganami T, Akaike F, Kanai S, et al. (2008) Regulation of SREBP1c gene expression in skeletal muscle: role of retinoid X receptor/liver X receptor and forkhead-O1 transcription factor. Endocrinology 149: 2293–2305.
58. Kamei Y, Ohizumi H, Fujitani Y, Nemoto T, Tanaka T, et al. (2003) PPARgamma coactivator 1beta/ERR ligand 1 is an ERR protein ligand, whose expression induces a high-energy expenditure and antagonizes obesity. Proc Natl Acad Sci U S A 100: 12378–12383.
59. Kamei Y, Miura S, Suzuki M, Kai Y, Mizukami J, et al. (2004) Skeletal muscle FOXO1 (FKHR) transgenic mice have less skeletal muscle mass, down-regulated Type I (slow twitch/red muscle) fiber genes, and impaired glycemic control. J Biol Chem 279: 41114–41123.
60. Rea SL, Ventura N, Johnson TE (2007) Relationship between mitochondrial electron transport chain dysfunction, development, and life extension in Caenorhabditis elegans. PLoS Biol 5: e259.
61. Honda Y, Honda S (1999) The daf-2 gene network for longevity regulates oxidative stress resistance and Mn-superoxide dismutase gene expression in Caenorhabditis elegans. FASEB J 13: 1385–1393.
62. Crugnola V, Lamperti C, Lucchini V, Ronchi D, Peverelli L, et al. (2010) Mitochondrial respiratory chain dysfunction in muscle from patients with amyotrophic lateral sclerosis. Arch Neurol 67: 849–854.
63. Zhou J, Yi J, Fu R, Liu E, Siddique T, et al. (2010) Hyperactive intracellular calcium signaling associated with localized mitochondrial defects in skeletal muscle of an animal model of amyotrophic lateral sclerosis. J Biol Chem 285: 705–712.
64. Bernardini C, Censi F, Lattanzi W, Barba M, Calcagnini G, et al. (2013) Mitochondrial network genes in the skeletal muscle of amyotrophic lateral sclerosis patients. PloS One 8: e57739.
65. Leger B, Vergani L, Soraru G, Hespel P, Derave W, et al. (2006) Human skeletal muscle atrophy in amyotrophic lateral sclerosis reveals a reduction in Akt and an increase in atrogin-1. FASEB J 20: 583–585.
66. Forrest S, Chai A, Sanhueza M, Marescotti M, Parry K, et al. (2013) Increased levels of phosphoinositides cause neurodegeneration in a Drosophila model of amyotrophic lateral sclerosis. Hum Mol Genet 22: 2689–2704.
67. Brenner S (1974) The genetics of Caenorhabditis elegans. Genetics 77: 71–94.
68. Kamath RS, Ahringer J (2003) Genome-wide RNAi screening in Caenorhabditis elegans. Methods 30: 313–321.
69. Bligh EG, Dyer WJ (1959) A rapid method of total lipid extraction and purification. Can J Biochem Physiol 37: 911–917.
70. Gilmore K, Wilson M (1999) The use of chloromethyl-X-rosamine (Mitotracker red) to measure loss of mitochondrial membrane potential in apoptotic cells is incompatible with cell fixation. Cytometry 36: 355–358.

Publication #5 :

Alterations in the hypothalamic melanocortin pathway in amyotrophic lateral sclerosis.

Pauline Vercruysse, Jérôme Sinniger, **Hajer El Oussini**, Jelena ScekicZahirovic, Stéphane Dieterlé, Reinhard Dengler, Thomas Meyer, Stephan Zierz, Jan Kassubek, Wilhelm Fischer, Jens Dreyhaupt, Torsten Grehl, Andreas Hermann, Julian Grosskreutz, Anke Witting, Ludo Van Den Bosch, Odile Spreux-Varoquaux, the GERP ALS Study Group, Albert C. Ludolph and Luc Dupuis.

doi:10.1093/brain/aww004 BRAIN 2016: 139; 1106–1122 | 1106

BRAIN
A JOURNAL OF NEUROLOGY

Alterations in the hypothalamic melanocortin pathway in amyotrophic lateral sclerosis

Pauline Vercruysse,[1,2,3] Jérôme Sinniger,[1,2] Hajer El Oussini,[1,2] Jelena Scekic-Zahirovic,[1,2] Stéphane Dieterlé,[1,2] Reinhard Dengler,[4] Thomas Meyer,[5] Stephan Zierz,[6] Jan Kassubek,[3] Wilhelm Fischer,[3] Jens Dreyhaupt,[7] Torsten Grehl,[8] Andreas Hermann,[9] Julian Grosskreutz,[10] Anke Witting,[3] Ludo Van Den Bosch,[11] Odile Spreux-Varoquaux,[12,13,14] the GERP ALS Study Group,[†] Albert C. Ludolph[3] and Luc Dupuis[1,2]

[†]See Appendix 1

Amyotrophic lateral sclerosis, the most common adult-onset motor neuron disease, leads to death within 3 to 5 years after onset. Beyond progressive motor impairment, patients with amyotrophic lateral sclerosis suffer from major defects in energy metabolism, such as weight loss, which are well correlated with survival. Indeed, nutritional intervention targeting weight loss might improve survival of patients. However, the neural mechanisms underlying metabolic impairment in patients with amyotrophic lateral sclerosis remain elusive, in particular due to the lack of longitudinal studies. Here we took advantage of samples collected during the clinical trial of pioglitazone (GERP-ALS), and characterized longitudinally energy metabolism of patients with amyotrophic lateral sclerosis in response to pioglitazone, a drug with well-characterized metabolic effects. As expected, pioglitazone decreased glycaemia, decreased liver enzymes and increased circulating adiponectin in patients with amyotrophic lateral sclerosis, showing its efficacy in the periphery. However, pioglitazone did not increase body weight of patients with amyotrophic lateral sclerosis independently of bulbar involvement. As pioglitazone increases body weight through a direct inhibition of the hypothalamic melanocortin system, we studied hypothalamic neurons producing proopiomelanocortin (POMC) and the endogenous melanocortin inhibitor agouti-related peptide (AGRP), in mice expressing amyotrophic lateral sclerosis-linked mutant SOD1(G86R). We observed lower *Pomc* but higher *Agrp* mRNA levels in the hypothalamus of presymptomatic SOD1(G86R) mice. Consistently, numbers of POMC-positive neurons were decreased, whereas AGRP fibre density was elevated in the hypothalamic arcuate nucleus of SOD1(G86R) mice. Consistent with a defect in the hypothalamic melanocortin system, food intake after short term fasting was increased in SOD1(G86R) mice. Importantly, these findings were replicated in two other amyotrophic lateral sclerosis mouse models based on TDP-43 (*Tardbp*) and FUS mutations. Finally, we demonstrate that the melanocortin defect is primarily caused by serotonin loss in mutant SOD1(G86R) mice. Altogether, the current study combined clinical evidence and experimental studies in rodents to provide a mechanistic explanation for abnormalities in food intake and weight control observed in patients with amyotrophic lateral sclerosis. Importantly, these results also show that amyotrophic lateral sclerosis progression impairs responsiveness to classical drugs leading to weight gain. This has important implications for pharmacological management of weight loss in amyotrophic lateral sclerosis.

1 Inserm U1118, Mécanismes centraux et périphétiques de la neurodégénérescence, Strasbourg, F-67085 France
2 Université de Strasbourg, Faculté de Médecine, UMRS1118, Strasbourg, F-67085 France
3 Department of Neurology, University of Ulm, Germany
4 Department of Neurology, Hannover Medical School, Hannover, Germany
5 Department of Neurology, Charité University Hospital, Berlin, Germany
6 Department of Neurology, University of Halle-Wittenberg, Germany
7 Institute of Epidemiology and Medical Biometry, University of Ulm, Germany

Received July 27, 2015. Revised November 13, 2015. Accepted December 04, 2015. Advance Access publication March 16, 2016

8 Department of Neurology, BG University Hospital Bergmannsheil, Bochum, Germany
9 Department of Neurology, Technische Universität Dresden, and German Center for Neurodegenerative Disease (DZNE), Dresden, Germany
10 Department of Neurology, University Hospital, Jena, Germany
11 Laboratory of Neurobiology, KU Leuven and Vesalius Research Center, VIB, Leuven, Belgium
12 Faculté de Médecine Paris-Ile de France-Ouest, France
13 Université de Versailles Saint-Quentin-en-Yvelines, France
14 Centre Hospitalier Versailles, Le Chesnay, France

Correspondence to: Luc Dupuis,
INSERM U1118, Faculté de médecine, bat 3, 8e etage, 11 rue Humann, 67085 Strasbourg, Cedex, France
E-mail: ldupuis@unistra.fr

Correspondence may also be addressed to: Albert C. Ludolph,
RKU, Universitatsklinik Ulm, Oberer Eselsberg 45, 89081 Ulm, Germany
E-mail: albert-c.ludolph@uni-ulm.de

Keywords: amyotrophic lateral sclerosis; calorie intake; hypothalamus; thiazolinediones; weight loss

Abbreviations: ALS = amyotrophic lateral sclerosis; TZD = thiazolinedione

Introduction

Amyotrophic lateral sclerosis (ALS), the most common adult-onset motor neuron disease, is characterized by the simultaneous degeneration of upper and lower motor neurons, leading to muscle atrophy and paralysis, and death within 3 to 5 years after onset. A subset of ALS cases are of familial origin and five major genes are currently associated with familial ALS (*C9orf72*, *SOD1*, *FUS*, *TARDBP* and *TBK1*) (Leblond *et al.*, 2014; Cirulli *et al.*, 2015; Freischmidt *et al.*, 2015; Lattante *et al.*, 2015). The *SOD1* gene was the first associated with ALS and most ALS mouse models currently used are based upon overexpression of mutant forms of *SOD1* (Gurney *et al.*, 1994; Ripps *et al.*, 1995).

Beyond progressive motor impairment, patients with ALS suffer from major, yet incompletely characterized, defects in energy metabolism (Dupuis *et al.*, 2011). First, ALS is more likely to occur with lower premorbid body fat (Gallo *et al.*, 2013; O'Reilly *et al.*, 2013) or better cardiovascular or physical fitness (Turner *et al.*, 2012; Huisman *et al.*, 2013). Second, weight loss is negatively correlated with survival (Desport *et al.*, 1999; Marin *et al.*, 2011; Paganoni *et al.*, 2011). This weight loss is associated with, and likely caused by, intrinsic hypermetabolism (Desport *et al.*, 2001; Bouteloup *et al.*, 2009), and is exacerbated by dysphagia occurring with bulbar involvement. Third, ALS patients develop abnormalities in lipid (Dupuis *et al.*, 2008; Dorst *et al.*, 2011; Lindauer *et al.*, 2013) and glucose (Pradat *et al.*, 2010) metabolisms. Interestingly, these metabolic alterations are largely replicated in transgenic mice expressing mutant SOD1 (Dupuis *et al.*, 2004; Fergani *et al.*, 2007; Palamiuc *et al.*, 2015). Not much is known on the underlying mechanisms of energy metabolism impairment despite the fact that elucidation of such mechanisms would offer therapeutic strategies to treat weight loss pharmacologically. Furthermore, deciphering the mechanisms of energy metabolism impairment could identify disease-modifying interventions as a hypercaloric diet was recently found to increase survival of patients with ALS under gastrostomy (Wills *et al.*, 2014; Dorst *et al.*, 2015).

Most of the studies to date have characterized energy metabolism in patients with ALS in steady state, at one single time point. The dynamic nature of energy metabolism and its homeostatic regulation thus severely limit the interpretation of these studies. Interventions performed during randomized clinical trials often have metabolic effects, and such studies include long term follow-up of patients for many months. These clinical studies thus provide high-quality information useful to understand the metabolic defects of patients with ALS.

Here, we performed a *post hoc* analysis of samples obtained during the clinical trial of pioglitazone (Dupuis *et al.*, 2012) to characterize energy metabolism of ALS patients on a metabolic challenge. Indeed, pioglitazone, like other thiazolinediones (TZDs), has pleiotropic effects on energy metabolism that have been extremely well characterized in both mouse models and human patients. In the periphery, pioglitazone sensitizes to insulin, leading to decreased glycaemia, and decreases circulating levels of liver enzymes (Promrat *et al.*, 2004; Belfort *et al.*, 2006; Sanyal *et al.*, 2010; DeFronzo *et al.*, 2011). In the CNS, pioglitazone inhibits the hypothalamic melanocortin system to increase food intake (Diano *et al.*, 2011; Lu *et al.*, 2011; Ryan *et al.*, 2011; Long *et al.*, 2014). Specifically, pioglitazone decreases activity of the hypothalamic neurons producing proopiomelanocortin (POMC), the precursor of a number of anorexigenic peptides such as α-MSH (melanocyte stimulating hormone) (Diano *et al.*, 2011; Lu *et al.*, 2011; Ryan *et al.*, 2011; Long *et al.*, 2014). In humans, this leads to a robust (3–5 kg) weight gain that was repeatedly

observed in multiple clinical trials (Promrat *et al.*, 2004; Belfort *et al.*, 2006; Sanyal *et al.*, 2010; DeFronzo *et al.*, 2011). Here, we show that patients with ALS display normal peripheral action of pioglitazone, while they lack weight gain. In transgenic mice expressing mutant SOD1, pioglitazone failed to increase food intake. This was associated with prominent involvement of the hypothalamic melanocortin system, also observed in other mouse models of ALS, independent of mutant SOD1 overexpression. Last, we show that the melanocortin defect occurs downstream of the previously documented serotonin loss (Dentel *et al.*, 2013). Altogether, our analysis of the data from the pioglitazone trial disclosed a previously unanticipated defect in patients with ALS that could account for a subset of ALS-related metabolic defects.

Materials and methods

Patients and treatments

All the biological materials from human ALS patients were sampled as part of the GERP-ALS trial (clinicaltrials.gov reference: NCT00690118) (Dupuis *et al.*, 2012). Briefly, patients with possible, probable (clinically or laboratory-supported) or definite ALS according to the revised version of the El Escorial criteria were considered for enrolment into the study. Included patients displayed onset of progressive weakness within 36 months prior to study and had disease duration of > 6 months and < 3 years (inclusive) with disease onset defined as date of first muscle weakness, excluding fasciculation and cramps. They reached a best-sitting slow vital capacity between 50% and 95% of predicted normal. They were capable of thoroughly understanding the information provided and gave written informed consent. All included patients had been treated with 100 mg riluzole daily for at least 3 months prior to inclusion. Detailed exclusion and inclusion criteria have been described earlier (Dupuis *et al.*, 2012). The study protocol was approved by the ethics committee of the University of Ulm and all other participating centres.

The two treatment groups were 100 mg riluzole plus 45 mg pioglitazone (pioglitazone group) and 100 mg riluzole plus placebo (placebo group). Patients were randomly assigned to one of the two treatment groups and both groups were matched for age, gender and site of onset (Dupuis *et al.*, 2012).

Procedures and biochemical analysis of human samples

After inclusion, patients underwent a screening phase and a treatment phase (18 months), with stepwise increase in dosage (Dupuis *et al.*, 2012). Clinical and physical examinations, blood sampling, and drug compliance were recorded at on-site visits (1, 2, 6, 12 and 18 months after baseline visit). Body weight was recorded at on-site visits, except for 3-, 9- and 15-month time points (telephone contacts). There were no differences in results when excluding these three time points. Routine clinical laboratory tests were performed at each on-site visit (baseline and 1, 2, 6, 12 and 18 months after baseline). All tests were carried out according to standard laboratory procedures at each study centres' locally accredited laboratory, which defined the normal reference range for each analyte. The following laboratory tests were performed using standard methods: alanine aminotransferase (ALAT), aspartate aminotransferase (ASAT), fasting blood glucose. Adiponectin measurements were done in the neurochemical laboratory in Ulm (MSD assay).

Animals

Transgenic mice were housed in the animal facility of the medicine faculty of Strasbourg University, with 12 h/12 h light/dark and unrestricted access to food and water. In all experiments, littermates were used for comparison. Transgenic SOD1(G86R) were maintained in their initial FVB/N genetic background according to previous studies (Dentel *et al.*, 2013). Transgenic mice expressing TDP43(A315T) were previously described and were maintained as heterozygous in their initial C57Bl6/J background (Wegorzewska *et al.*, 2009). Heterozygous $Fus^{\Delta NLS/+}$ are knock-in mice expressing FUS protein deleted from its C-terminal nuclear localization signal (NLS) from one copy of the endogenous *Fus* gene. These mice were generated and maintained in C57Bl6/J background. The motor phenotype of these mice will be described elsewhere (Scekic-Zahirovic, submitted for publication). Tph2-YFP mice were purchased from Jackson laboratories (Bar Harbor; strain 014555) and maintained in their initial genetic background. Female Tph2-YFP mice were crossed with male SOD1(G86R) to generate compound transgenic mice.

For biochemical analysis, animals were sacrificed at the ages indicated at 2 pm, and tissues were quickly dissected, frozen in liquid nitrogen, and stored at -80°C until use. For histological analysis, animals were anaesthetized by intraperitoneal injection of ketamine (Imalgène 1000®, Merial; 90 mg/kg body weight) and xylazine (Rompun 2%®, Bayer; 10 mg/kg body weight) at the ages indicated at 2 pm. After perfusion of 4% paraformaldehyde (v/v PFA, Sigma), brains were removed, stored in the same fixative overnight at 4°C and stored in phosphate-buffered saline (PBS) until used. These experiments were authorized by the local ethical committee of Strasbourg University (CREMEAS).

Drugs and treatments

Pioglitazone (Actos®, Takeda) was dissolved in 10% (v/v) dimethyl sulphoxide (DMSO, Fisher Scientific) and a single oral administration was given by gavage at a dose of 40 mg/kg body weight. Fluoxetine (Sigma) was dissolved in 0.9% (w/v) NaCl (Sigma) and administrated intraperitoneally at a dose of 20 mg/kg body weight.

Measurements of food intake

For the pioglitazone experiment, mice were fasted from 9 am to 3 pm, and pioglitazone was administrated at 3 pm. Food was reintroduced 1 h after gavage and food intake was recorded for 24 h.

For short-term fasting experiments, mice were fasted from 8 am to 3 pm (7 h fasting conditions) or from 2 pm to 3 pm (1 h fasting conditions) and food was reintroduced after 7 h or 1 h

of fasting. Food intake was measured 1 h and 24 h after refeeding.

For fluoxetine experiment, mice were fasted from 1 pm to 2 pm, and fluoxetine was injected at 2 pm. Food was reintroduced 30 min after fluoxetine injection and food intake was measured for 1 h. For biochemical analysis, a second injection of fluoxetine was done after 1 h of feeding and mice were sacrificed 30 min later.

Histology

Fixed brains were included in 6% (w/v) agar (Sigma) and sectioned from Bregma 0.02mm to Bregma −2.90 mm into 40 µm coronal sections on a vibratome. Arcuate nucleus was identified according to Paxinos Brain Atlas. POMC immunohistochemistry was performed on half of the selected brain sections. AGRP and green fluorescent protein (GFP) immunohistochemistries were performed each on anatomically matched sections. Immunohistochemistry was performed on floating sections using standard histological techniques. Endogenous peroxidases were inactivated using 3% (v/v) H_2O_2. For POMC immunohistochemistry, permeabilization and saturation of non-specific sites were done with 0.25% (v/v) Triton™ (Sigma) and 50 mg/ml bovine serum albumin (BSA, Sigma). For GFP immunohistochemistry, permeabilization and saturation of non-specific sites were done with 0.5% (v/v) Triton™ (Sigma) and 5% (v/v) horse serum (Gibco, Life Technologies). For AGRP immunohistochemistry, antigen retrieval with citrate buffer was done before permeabilization and saturation of non-specific sites with 0.5% (v/v) Triton™ (Sigma) and 5%(v/v) horse serum (Gibco, Life Technologies). Rabbit anti-POMC primary antibody (Phoenix Peptide; 1:2000), rabbit anti-AgRP primary antibody (Phoenix Peptide; 1:2000) or rabbit anti-GFP primary antibody (Invitrogen, Life Technologies, 1:1000) were incubated overnight at room temperature. Biotinylated donkey anti-Rabbit secondary antibody (Jackson; 1:500) was incubated for 90 min at room temperature. Staining was performed using Vectastain Elite ABC kit (Vector). After revelation with 3,3'-diaminobenzidine (DAB, Sigma; 0.5 mg/ml), sections were mounted and images of all sections were taken.

For quantification, bright-field images of lower brain part for POMC and AgRP stainings or bright-field images of right arcuate nucleus part for GFP staining were acquired with a Nikon DS –Ri1 camera attached to a Nikon microscope (Nikon Eclipse E800) fitted with a Plan Apo 4× lens (N.A. = 0.20, Nikon) and a plan Apo 10× lens (N.A. = 0.45, Nikon), respectively. White balance, gain, exposure, and light settings were kept the same when acquiring all images of a given staining.

Image analysis

An operator blinded to the genotype quantified all experiments. Total numbers of POMC-positive cell bodies in the arcuate nucleus were determined for each animal and normalized per section. Quantification of GFP staining and AGRP staining was processed to binary images using NIH ImageJ as described previously (Grider *et al.*, 2006). Briefly, after changing tiff images to 8-bit images, images were inverted and processed with Feature J plugin for ImageJ (version 1.50d) to select the smallest Hessian values and « smoothing scale » of 1.0. The resulting images were transformed into binary images by thresholding. Threshold was determined on one cut and same threshold was applied to every image. Occupied area for AGRP or GFP staining was measured.

RNA extraction and quantitative reverse transcription-polymerase chain reaction

RNA was extracted from mouse hypothalami using TRIzol® reagent (Life Technologies). After reverse transcription with iScript™ reverse transcription Supermix for RT-qPCR (Bio-Rad), cDNA was obtained from 1 µg of RNA. Messenger RNA levels were obtained by quantitative PCR using Sso Advanced Universal SYBR Green Supermix (Bio-Rad) with corresponding sense and antisense primers. Standard curves were constructed by amplifying serial dilutions of cDNA. Starting quantities of samples were calculated with Bio-Rad software. Messenger RNA levels of genes of interest were normalized to expression levels of the 18S ribosomal, *Tbp* and *Pola2* RNA housekeeping genes using GeNorm (Vandesompele *et al.*, 2002). Primer sequences are shown in Supplementary Table 1.

Serotonin levels

Hypothalamic serotonin levels were measured using high performance liquid chromatography, as previously described (Dentel *et al.*, 2013).

Statistical analysis

For statistical analyses in ALS patients, group comparisons were performed using mixed effects regression model analysis by the Institute of Epidemiology and Medical Biometrics at the University of Ulm using the statistical software package SAS Version 9.2 under Windows.

For animal experiments, comparison of two groups was performed using unpaired Student's *t*-test, except for experiments with pioglitazone in which paired *t*-test was used. Comparison of three or four groups was performed using one-way ANOVA and Tukey *post hoc* test. Statistics in animal experiments were performed using Prism version 6.0.

All results from analysis were regarded as hypothesis generating only. All statistical tests were carried out two-sided at a significance level of 5%.

Results

Normal peripheral response to pioglitazone in patients with ALS

We took advantage of data collected during the pioglitazone GERP-ALS trial to investigate energy metabolism in ALS patients in response to pioglitazone.

In this clinical trial, 219 patients with ALS were enrolled and randomly allocated to either placebo ($n = 110$; bulbar: $n = 33$, spinal: $n = 77$), or pioglitazone ($n = 109$;

bulbar: $n = 32$, spinal: $n = 77$) treatment after stratification based on site of onset (bulbar or spinal) (Dupuis *et al.*, 2012).

The metabolic effects of TZDs, including pioglitazone are well understood in models and their effects are largely described in patients (Fig. 1A and Supplementary Table 2). Pioglitazone treatment is known to increase levels of adiponectin, an adipose-derived hormone through direct transcriptional activation of the adiponectin gene in adipocytes (Maeda *et al.*, 2001). Consistently, pioglitazone treatment increased the levels of circulating adiponectin 4-fold in patients with ALS after 6 months of treatment, and this was maintained after 12 months of treatment (Fig. 1B). Pioglitazone decreases glycaemia through hepatic and skeletal muscle PPARγ (encoded by *PPARG*). In patients with ALS, pioglitazone decreased glycaemia (Fig. 1C), although this effect was milder than observed in other populations, including non-diabetic patients (Belfort *et al.*, 2006; Sanyal *et al.*, 2010; DeFronzo *et al.*, 2011). Consistent with a direct action on liver, pioglitazone decreased levels of ASAT and more robustly levels of ALAT (Fig. 1D and E). In all, pioglitazone displayed the expected metabolic effects on adipocytic, muscular, and hepatic biomarkers, and was likely able to activate PPARγ in these tissues.

Pioglitazone does not lead to weight gain in patients with ALS

TZDs are also known to act in hypothalamic melanocortin neurons to promote feeding (Diano *et al.*, 2011; Long *et al.*, 2014), and this activation of PPARγ in melanocortin neurons is responsible for the robust weight gain associated with TZD treatment (Lu *et al.*, 2011; Ryan *et al.*, 2011; Long *et al.*, 2014). Thus, the evolution of body weight upon pioglitazone treatment represents a reliable proximal marker of PPARγ action in hypothalamic melanocortin neurons. In ALS patients, pioglitazone had no effect on weight loss (Fig. 2A), or body mass index (BMI) (Fig. 2B and Supplementary Table 2). Increased weight in response to pioglitazone is due to increased food intake, and a subset of ALS patients experience dysphagia. However, pioglitazone had also no effect on BMI and weight loss when considering spinal onset patients (Fig. 2C and D), or patients with preserved everyday life during at least 6 months (results from EuroQoL EQ-5D questionnaire, Fig. 2E and F). Lastly, patients with preserved bulbar function during at least 6 months after inclusion [as assessed using ALS functional rating scale-revised (FRS-R) bulbar subscale] did not lose weight, yet pioglitazone had no effect on their BMI (Fig. 2G and H). Importantly, there were no differences among groups for intake of drugs affecting body weight and food intake, in particular anti-epileptics, anti-diabetics, anti-psychotics or selective serotonin reuptake inhibitors (Supplementary Table 4). Thus, pioglitazone did not increase weight in ALS patients, and this was not related with dysphagia nor confounded by intake of other drugs.

Pioglitazone does not increase food intake in mutant SOD1 mice

We hypothesized that the lack of weight gain for patients with ALS under pioglitazone was due to defects in stimulating food intake. To test this hypothesis, we used transgenic mice expressing mutant SOD1(G86R) (SOD1m mice) as a model of ALS and examined food intake in response to pioglitazone. In rodents, pioglitazone has various effects on food intake depending on genetic background, dose, route and associated diet (Diano *et al.*, 2011; Ryan *et al.*, 2011; Long *et al.*, 2014). Using a protocol (Fig. 3A) adapted from Ryan *et al.* (2011), we observed that a single oral dose of pioglitazone (40 mg/kg) increased food intake by 10–15% in wild-type FVB/N mice (Fig. 3B and C). However, food intake was not increased in littermate SOD1m mice either 1 month before motor symptoms (Fig. 3 B) or at disease onset (Fig. 3C). Thus, pioglitazone was not able to increase food intake in SOD1m mice.

Defects in melanocortin neurons in mutant SOD1 mice

Hypothalamic melanocortin neurons constitute the primary target of TZDs to promote food intake (Diano *et al.*, 2011; Long *et al.*, 2014). The melanocortin system mainly comprises two antagonistic neuronal types located in the arcuate nucleus: POMC neurons, which secrete the anorexigenic peptide alpha melanocyte-stimulating hormone (αMSH), and AGRP neurons, which promote food intake, mostly through production of AGRP, an endogenous αMSH antagonist. *Pomc* mRNA levels were 2-fold lower in SOD1m mice at 75 days of age (Fig. 4A) or at onset (Fig. 4B), whereas *Agrp* mRNA levels were higher in non-symptomatic mice, but not at onset (Fig. 4A and B). This involvement of the melanocortin system was relatively selective, as we did not observe expression changes in multiple neuropeptides involved in energy homeostasis, in particular CART (*Cartpt*), NPY, CRF (*Crh*), AVP, TRH, galanin (GAL), somatostatin (SST) and BDNF. Importantly however, we observed decreased expression of MCH (*Pmch*) at both ages, and orexin, at onset (Fig. 4C). Consistent with decreased POMC expression, we observed ~30% fewer POMC-positive neurons in the arcuate nucleus of SOD1m mice as compared with their wild-type littermates at 75 days of age and almost 50% fewer at onset (Fig. 5). Furthermore, we observed increased density of AGRP-positive fibres in arcuate nucleus as well as in projection regions present on the same sections such as dorso-medial hypothalamus and lateral hypothalamus (Fig. 6). In all, the melanocortin system appears shifted towards decreased melanocortin tone in SOD1m mice.

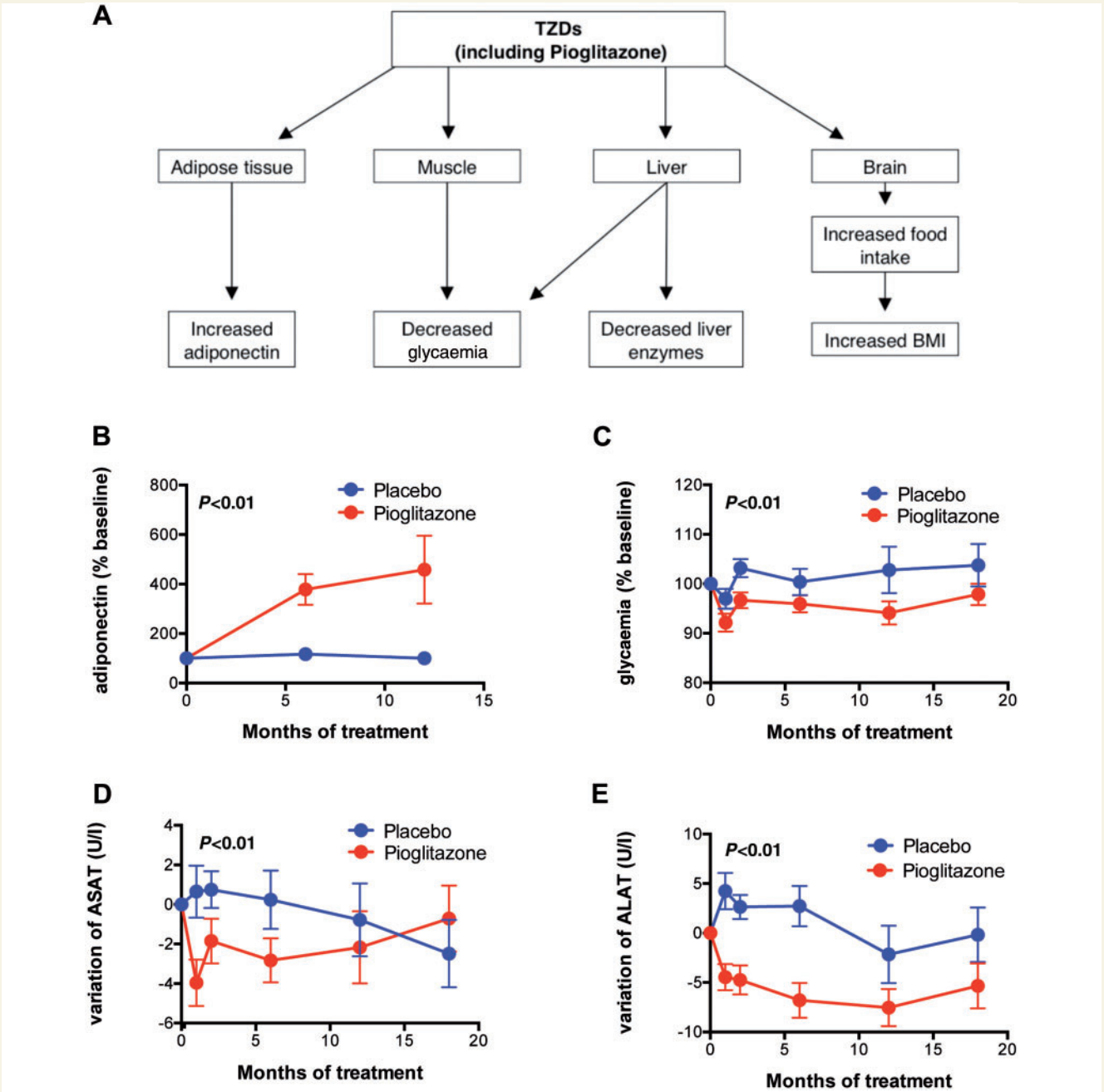

Figure 1 Effects of pioglitazone on peripheral biomarkers in ALS patients. (**A**) Summary of metabolic effects of pioglitazone (and TZDs) in humans. (**B**–**E**) Changes in plasma adiponectin (% from the baseline, **B**), glycaemia (% from the baseline, **C**), circulating aspartate amino-transferase (ASAT, changes in U/l from the baseline, **D**), and alanine amino-transferase (ALAT, changes in U/l from the baseline, **E**). Pioglitazone treated patients are significantly different from placebo treated patients for these items as assessed using a mixed effects regression model analysis. Data are presented as mean and standard error (SE).

Multiple ALS mouse models display functional and molecular alterations in hypothalamic melanocortin system

We then asked whether the observed melanocortin defects translated into functional abnormalities. Indeed, the combination of decreased POMC with increased AgRP is usually found in situations of promotion of food intake, such as during fasting or in the case of leptin deficiency (Mizuno *et al.*, 1998, 1999; Ziotopoulou *et al.*, 2000), and compromised melanocortin system is likely to affect food intake behaviour, in particular during refeeding (Perez-Tilve *et al.*, 2010). Thus, we measured food intake after short-term fasting in SOD1m mice. Consistent with decreased POMC levels, 1 h food intake of SOD1m mice was 2-fold higher than wild-type littermates after 7 h (Fig. 7A) or 1 h (Fig. 7B)

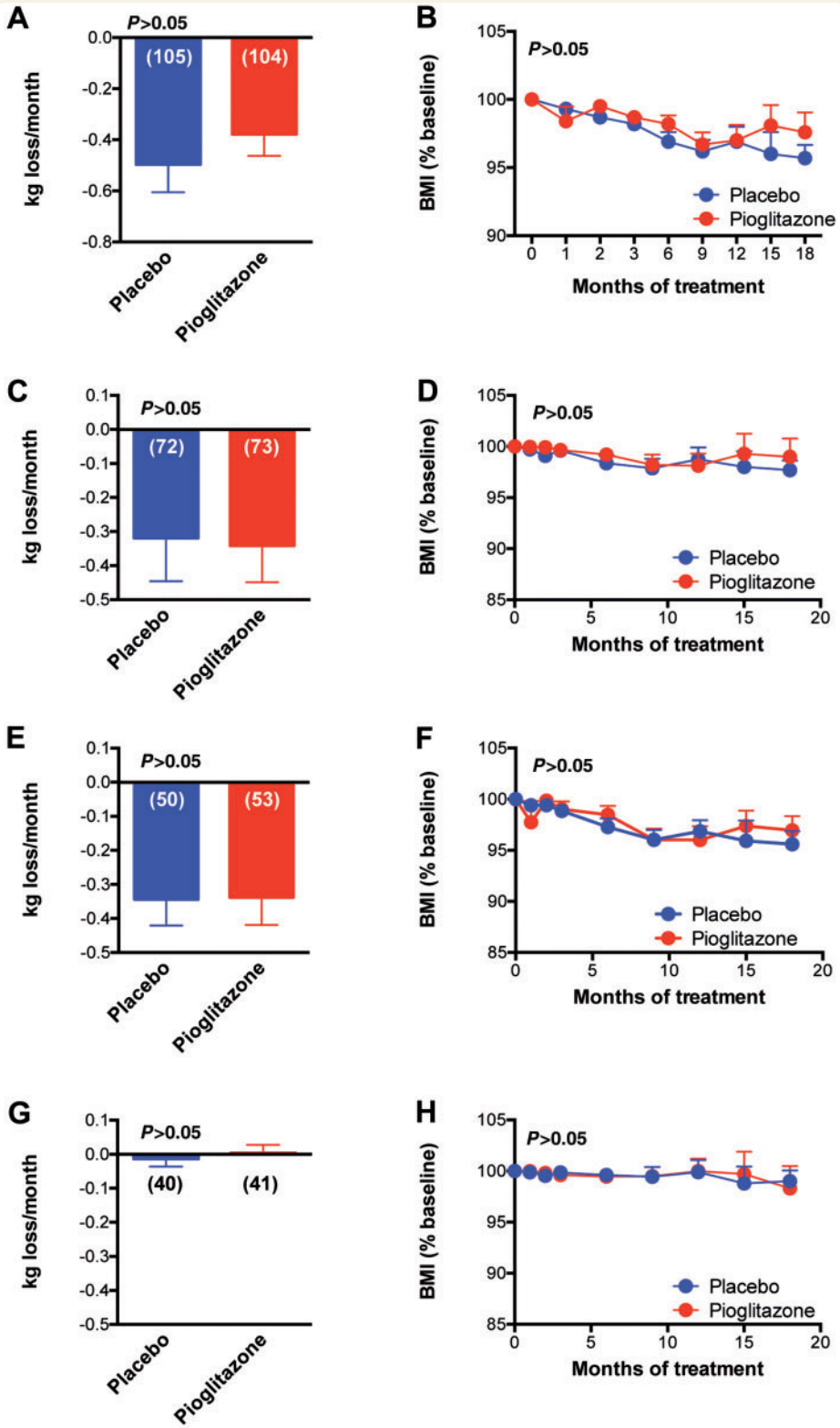

Figure 2 Effects of pioglitazone on weight loss in ALS patients. Weight loss (kg loss per month, **A**, **C**, **E** and **G**) and changes in BMI from the baseline (**B**, **D**, **F** and **H**) in the whole ALS population (**A** and **B**), spinal onset patients (**C** and **D**), in patients with relatively preserved quality of life (**E** and **F**) and in patients with preserved bulbar function (**G** and **H**). To select the patients with preserved quality of life, we used the results from the EuroQoL questionnaire to identify patients that had no or only few problems with their everyday life. Selected patients answered that they had either no or few problems in their everyday life during at least 6 months after their allocation to a group. To select the patients with preserved bulbar function, we used the results from ALS-FRS-R bulbar subscale and selected patients with a score equal or superior to 10 (maximum: 12) 6 months after inclusion. No significant difference is noted for these items. Data are presented as mean and SE.

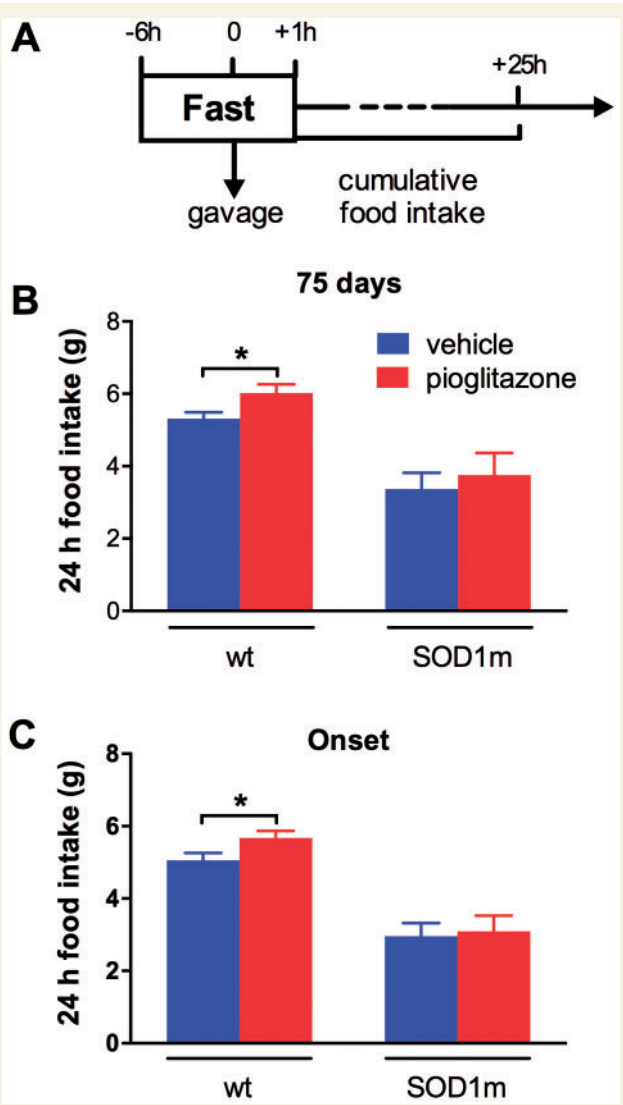

Figure 3 No effect of piogliotazone on SOD1m mice food intake. (**A**) Experimental scheme: pioglitazone was provided *per os* after 6 h of fasting. Food was reintroduced 1 h after gavage, and food intake recorded for the next 24 h. (**B** and **C**) Food intake after pioglitazone treatment in SOD1(G86R) mice (SOD1m) and control littermates (wt) at 75 days of age ($n = 12$, **B**) and symptom onset ($n = 13$, **C**), either treated with vehicle (blue) or pioglitazone 40 mg/kg body weight (red).$^{*}P < 0.05$, Paired Student's *t*-test for the drug. Data are presented as mean and SE.

of fasting. Mutations in *SOD1* only account for 20% of familial ALS cases, and alterations in hypothalamic melanocortin pathways could be SOD1-specific. However, *Pomc* mRNA levels were decreased in transgenic mice expressing A315T mutant *Tardbp* (Wegorzewska *et al.*, 2009) (Fig. 7C), and these mice also displayed transient hyperphagia in response to fasting (Fig. 7D). Last, *Pomc* mRNA levels tended to be lower in 10-month-old knock-in mice expressing a truncated FUS protein retained in the cytoplasm ($Fus^{\Delta NLS/+}$ mice) (Fig. 7E) (Scekic-Zahirovic, submitted for publication), and $Fus^{\Delta NLS/+}$ mice displayed increased food intake after short-term fasting as compared with their littermates (Fig. 7F). Thus, abnormal food intake behaviour and defects in the melanocortin system are hallmarks of ALS mouse models.

Involvement of serotonin loss in melanocortin defects associated with ALS

We then sought to understand the mechanisms underlying melanocortin defects in ALS. POMC neurons are affected by multiple stressors that could ultimately underlie the observed defects. We did not observe changes in expression of a series of genes related with oxidative or endoplasmic reticulum stress (e.g. gp47, splicing of *Xbp1* mRNA), peroxisome biogenesis [*Gpx1*, catalase (*Cat*)] or mitochondrial function (*Mfn2*; not shown) indirectly suggesting that neither overt oxidative stress, nor endoplasmic reticulum stress, nor defective peroxisomal biogenesis, nor mitochondrial abnormalities might account for decreased POMC neuronal counts. We hypothesized that the previously observed serotonin neuron degeneration (Turner *et al.*, 2005; Dentel *et al.*, 2013) could contribute to the observed melanocortin defects. Indeed, serotonin is known to promote POMC expression in arcuate nucleus through the 5-HT_{2C} receptor (encoded by *HTR2C*) (Heisler *et al.*, 2006; Lam *et al.*, 2008). Interestingly, serotonin levels tended to decrease at onset in the hypothalamus of SOD1m mice (Fig. 8A). To determine whether loss of serotonin axons occurred in the arcuate nucleus, we crossed SOD1m mice with Tph2-YFP mice, expressing yellow fluorescent protein (YFP) under the control of the *Tph2* promoter targeting expression in central serotonin neurons (Zhao *et al.*, 2011). We observed a sharp and profound decrease in the density of YFP-positive fibres in the arcuate nucleus of SOD1m mice, as compared with their littermates (Fig. 8B). Hypothalamic 5-HT_{2C} expression was increased suggesting that the hypothalamus sought to compensate for loss of serotonergic innervation (Fig. 8C). To probe for serotonergic involvement in defects of the melanocortin system, we used fluoxetine, a selective serotonin reuptake inhibitor to rescue serotonin signalling, using previously published doses and protocols (Kaur and Kulkarni, 2002; Liou *et al.*, 2012). Interestingly fluoxetine pretreatment completely abrogated the increased food intake in response to short-term fasting (Fig. 8D) and increased *Pomc* mRNA levels back to normal in SOD1m mice (Fig. 8E). Fluoxetine had no effect on *Agrp* upregulation (Fig. 8E). Thus, loss of serotonin innervation is contributing to the melanocortin defects observed in SOD1m mice.

Discussion

In this combined mouse and human study, we showed that ALS is associated with defects in the melanocortin system,

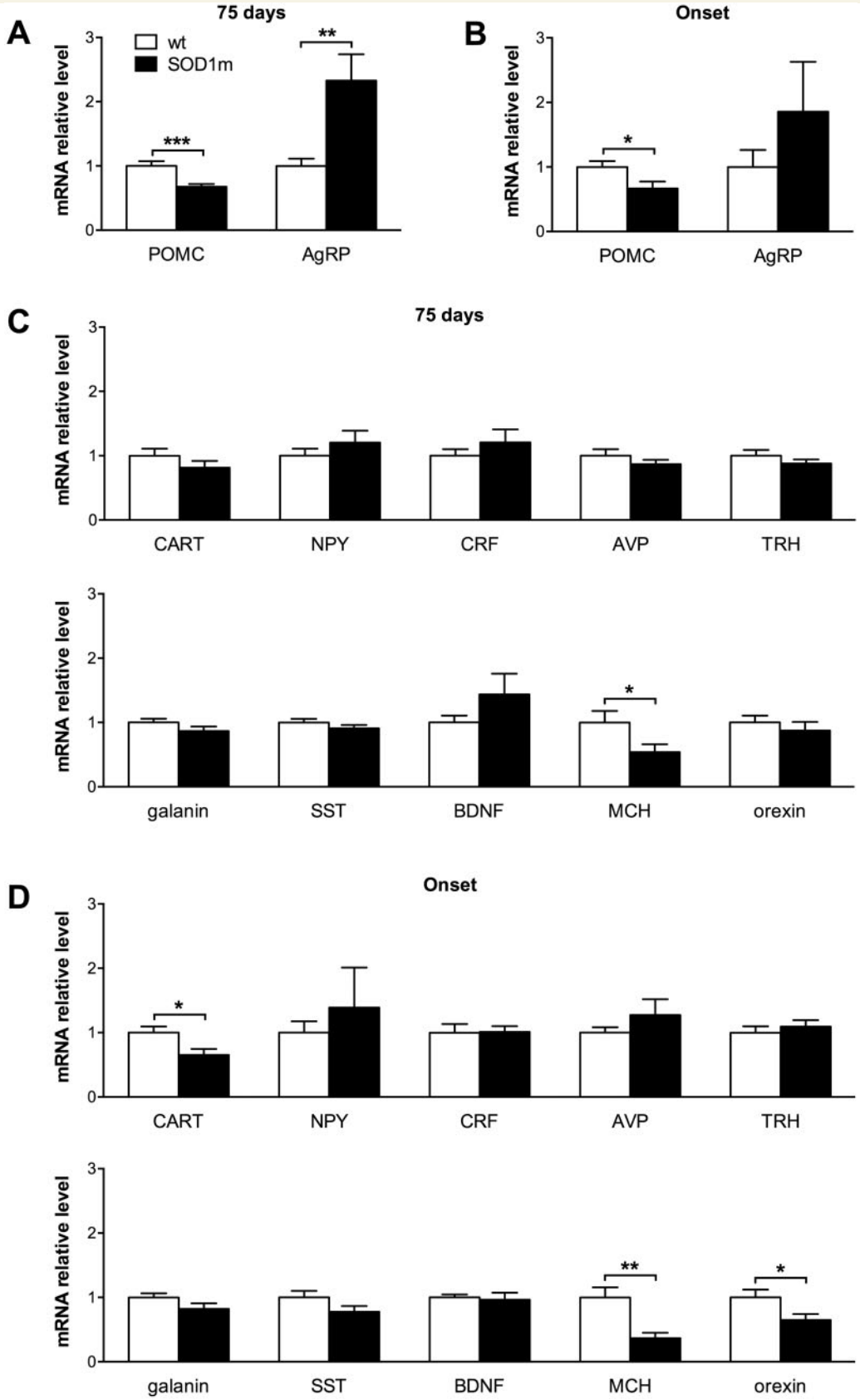

Figure 4 Altered melanocortin-related gene expression in SOD1m mice. (**A** and **B**) Messenger RNA levels of *Pomc* and *Agrp* in the hypothalamus of SOD1(G86R) mice (black, SOD1m) and control littermates (white, wt) at 75 days of age ($n = 15$, **A**) and symptom onset ($n = 11$, **B**). $^{*}P < 0.05$. $^{**}P < 0.005$. $^{***}P < 0.0005$, Student's *t*-test. Data are presented as mean and SE. (**C** and **D**) Messenger RNA levels of hypothalamic neuropeptides in the hypothalamus of SOD1(G86R) mice (black columns, SOD1m) and control littermates (white columns, wt) at 75 days of age ($n = 15$, **C**) and symptom onset ($n = 11$, **D**). $^{*}P < 0.05$; $^{**}P < 0.005$, Student's *t*-test. Data are presented as mean and SE.

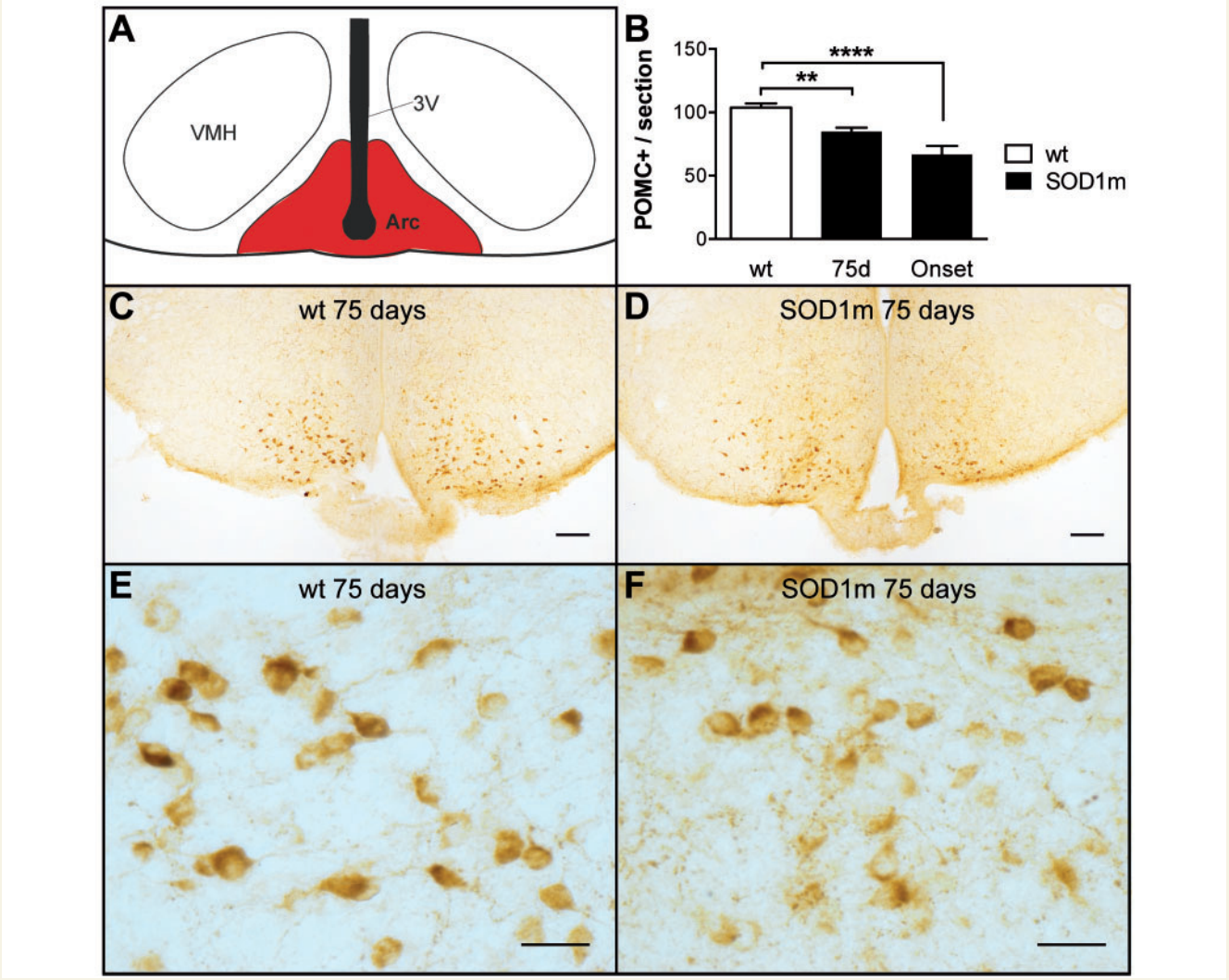

Figure 5 Decreased POMC-positive neurons in SOD1m mice. (**A** and **B**) Quantification of POMC neurons in the arcuate nucleus. The whole region was sectioned and half of these sections were stained for POMC immunohistochemistry after identification of arcuate nucleus according to Paxinos Brain Atlas (scheme of identified regions, in red, **A**). Total numbers of POMC-positive cell bodies in the arcuate nucleus were determined in SOD1m mice at 75 days of age ($n = 8$, **B–F**) and at symptom onset ($n = 7$, **B**) as compared with their wild-type littermates. $^{**}P < 0.005$, $^{****}P < 0.0001$, one-way ANOVA followed by Tukey *post hoc* test. Data are presented as mean and SE. (**C–F**) Representative images are shown for SOD1(G86R) mice (**D** and **F**) and control littermates (**C** and **E**) at 75 days of age at two magnifications. Scale bar = 200 μm (**C** and **D**); 20 μm (**E** and **F**).

the major hypothalamic circuit controlling food intake and energy expenditure. Pioglitazone did not increase weight in ALS patients, thus providing indirect evidence of altered hypothalamic melanocortin pathway. Pathological and functional deficits of melanocortin system were found in ALS mouse models directly demonstrating these defects. These findings further extend the spectrum of defects in ALS and provide a mechanistic explanation for a subset of metabolic signs observed in these patients. Our study also has important implications for the design of therapies to target weight loss in this disease.

We first observed that pioglitazone did not increase body weight or slow down weight loss in patients with ALS. This was a surprising observation as progressive weight gain has been repeatedly observed in all clinical trials of pioglitazone in multiple non-neurological diseases (Promrat *et al.*, 2004; Belfort *et al.*, 2006; Sanyal *et al.*, 2010; DeFronzo *et al.*, 2011). Despite this lack of weight gain, ALS patients under pioglitazone displayed all other biomarkers of efficacy, including decreased glycaemia, decreased circulating liver enzymes or increased adiponectin, thus ruling out that patients with ALS simply did not respond to the drug. Interestingly, a series of recent studies dissected out how TZDs lead to weight gain through activation of PPARγ in hypothalamic POMC neurons leading to increased food intake (Diano *et al.*, 2011; Lu *et al.*, 2011; Ryan *et al.*, 2011; Long *et al.*, 2014). Consistent with the notion that pioglitazone hypothalamic response was blunted in

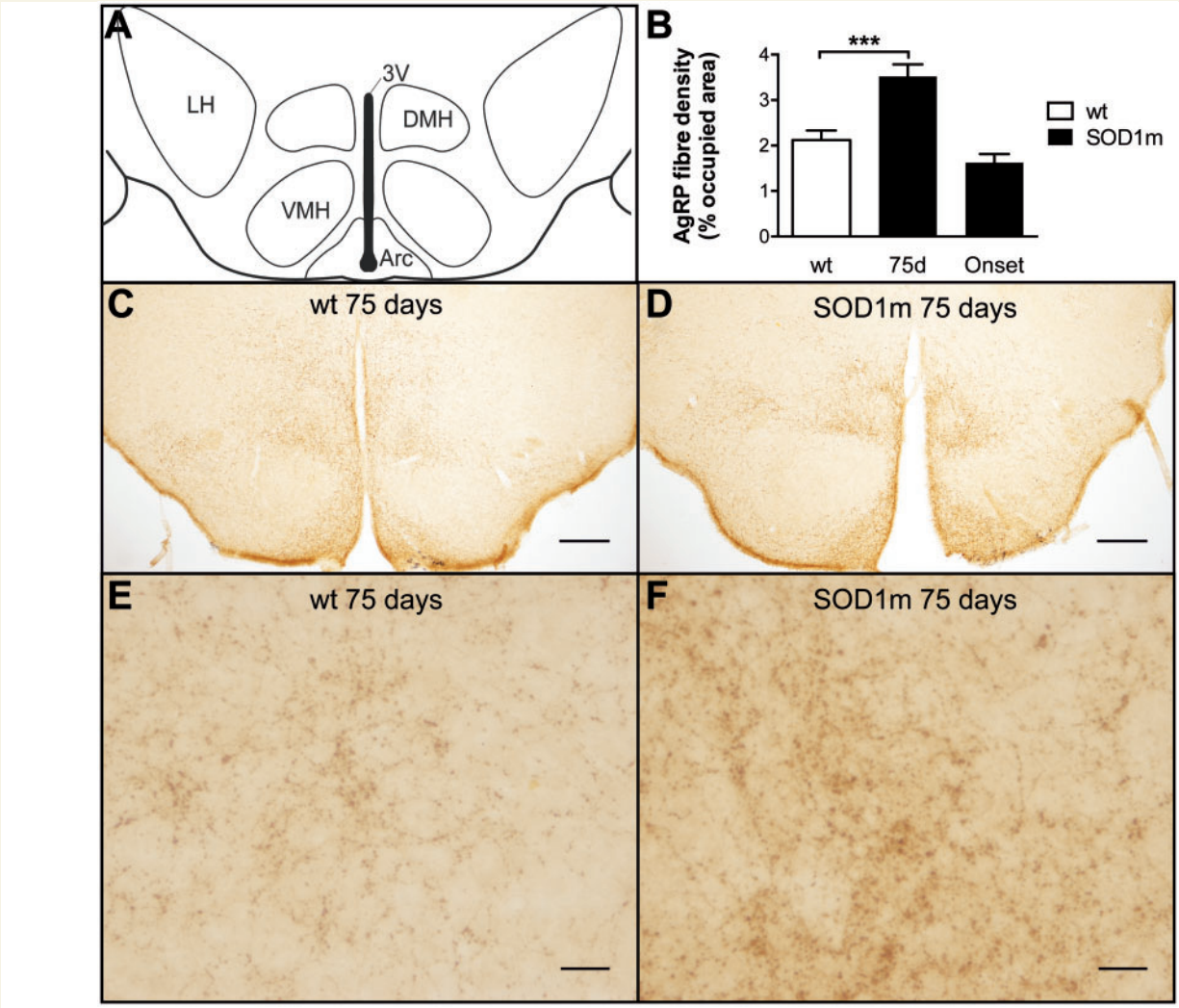

Figure 6 Defect in AGRP neurons in SOD1m mice. (**A** and **B**) Quantification of AGRP immunoreactive neurites in the hypothalamus. For each animal, one section (Bregma −1.58 mm) was identified according to Paxinos Brain Atlas (**A**, scheme of identified regions) and stained for AGRP immunohistochemistry. AGRP fibre density was determined in SOD1m mice at 75 days of age ($n = 7$, **B** and **F**) and at symptom onset ($n = 4$, **B**) as compared with their wild-type littermates. $^{***}P < 0.001$, one-way ANOVA followed by Tukey *post hoc* test. Data are presented as mean and SE. (**C–F**) Representative images are shown for SOD1(G86R) mice (**D** and **F**) and control littermates (**C** and **E**) at 75 days of age at two magnifications. Scale bar = 200 μm (**C** and **D**), 20 μm (**E** and **F**).

ALS patients, pioglitazone was not able to promote food intake in SOD1m mice. Indeed, the melanocortin system is dramatically affected in these mice, with decreased POMC expression and loss of POMC positive neurons; similar alterations were observed in TDP-43- and FUS-based mouse models pointing out that such defects are a general feature in ALS. As pioglitazone decreases the activity of POMC neurons thus increasing food intake (Diano *et al.*, 2011), we propose that the already decreased melanocortin tone in ALS prevents the silencing of POMC neurons by pioglitazone. Consistent with this, SOD1 mice displayed hyperphagia in response to short-term fasting, an orexigenic stimulus that also leads to decreased POMC neuronal activity (Perez-Tilve *et al.*, 2010; Diano *et al.*, 2011). Thus, our results point to a general decrease in melanocortin tone in ALS, leading to both a lack of response to TZDs, and abnormal food intake behaviour in response to fasting.

What is the contribution of impaired melanocortin system to the metabolic phenotypes associated with ALS? The melanocortin system exerts multiple actions on energy metabolism, either dependent on or independent of food intake. First, an expected consequence of decreased melanocortin tone is increased energy intake, especially in response to an orexigenic stimulus such as food deprivation. This is indeed what has been observed in multiple transgenic mouse models of ALS, suggesting that the defect in the melanocortin system translates into a functional deficit. Furthermore, consistent with the observed melanocortin defect, we previously observed slightly increased cumulative food intake in SOD1m mice (Dupuis *et al.*, 2004).

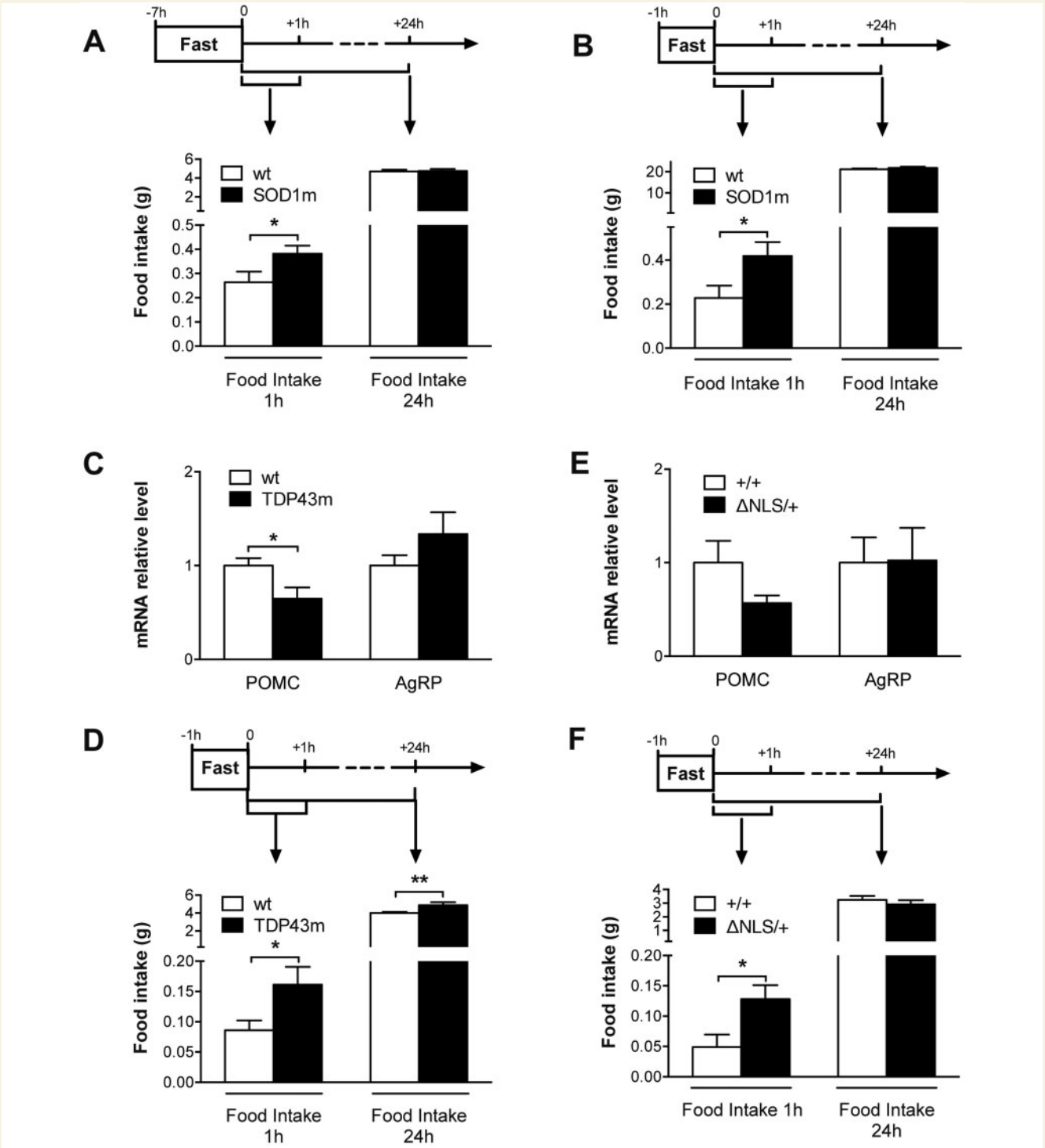

Figure 7 Multiple ALS mouse models display functional and molecular alterations in hypothalamic melanocortin system. (**A** and **B**) Food intake was measured for 1 h, after either 7 h (**A**) or 1 h (**B**) of fasting in SOD1(G86R) mice (black columns, SOD1m) and control littermates (white columns, wt) at 75 days of age ($n = 10$ and $n = 14$, respectively, for **A** and **B**). $^{*}P < 0.05$, Student's *t*-test. Data are presented as mean and SE. (**C**) Messenger RNA levels of *Pomc* and *Agrp* in the hypothalamus of transgenic mice expressing A315T TDP-43 mutation (black columns, TDP43m) and control littermates (white columns, wt) at non-symptomatic stage ($n = 6$). Unpaired *t*-test. $^{*}P < 0.05$. (**D**) Food intake was measured 1 h after refeeding in TDP43m mice ($n = 8$). $^{*}P < 0.05$, $^{**}P < 0.01$, Multiple *t*-test. Data are presented as mean and SE. (**E**) Messenger RNA levels of *Pomc* and *Agrp* in the hypothalamus of transgenic mice *Fus* ΔNLS/+ knock-in mice (black columns, ΔNLS/+) and control littermates (white columns, +/+) at 10 months of age ($n = 4$). Data are presented as mean and SE. (**F**) Food intake was measured 1 h after refeeding in ΔNLS/+ mice ($n = 10$) at 10 months of age. $^{*}P < 0.05$, Student's *t*-test. Data are presented as mean and SE.

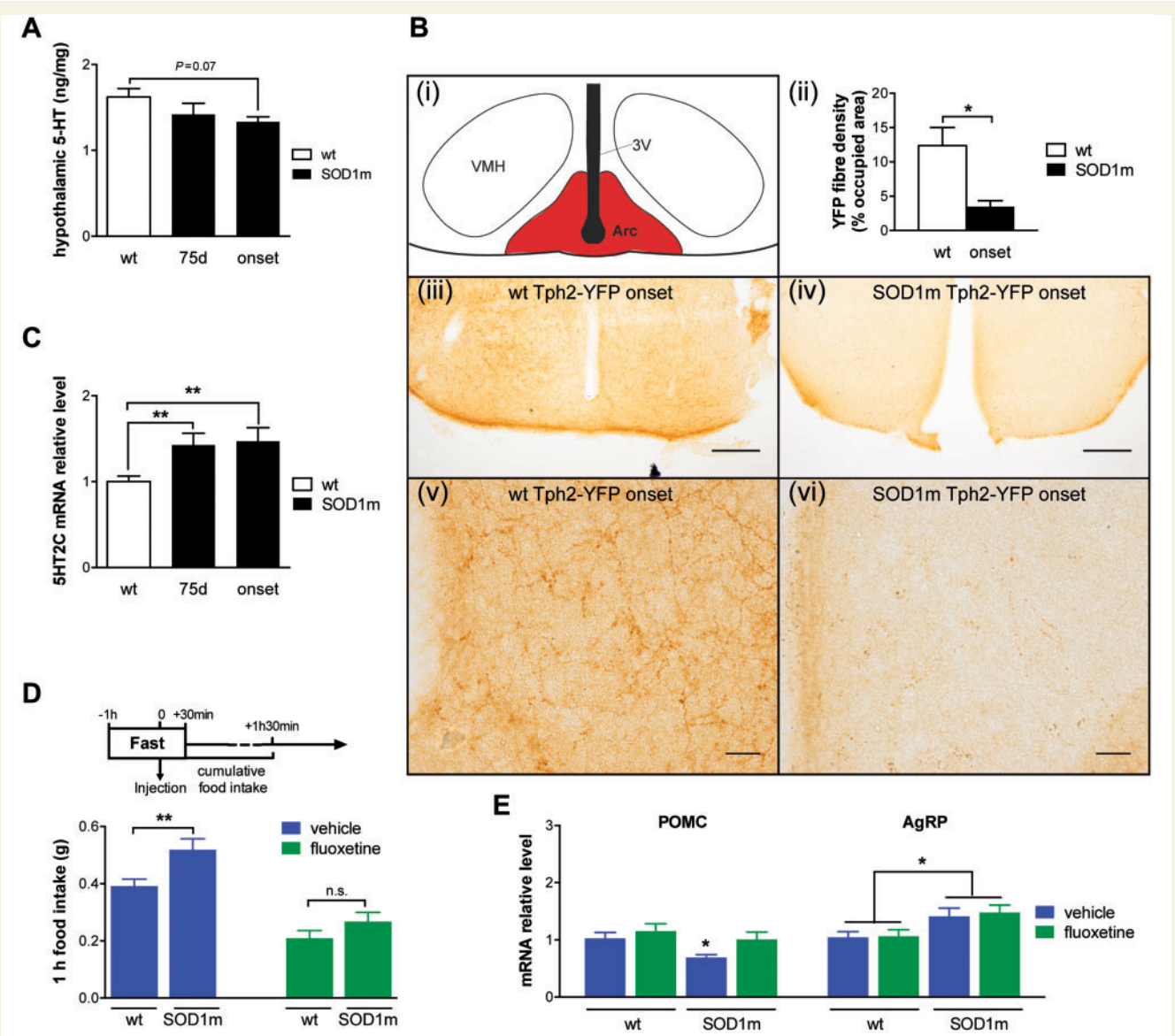

Figure 8 Involvement of serotonin loss in melanocortin defects of mutant SOD1 mice. (**A**) Serotonin levels in the hypothalamus of SOD1(G86R) mice (black columns, SOD1m) and control littermates (white columns, wt) ($n = 5$ at 75 days and $n = 5$ at onset). One-way ANOVA followed by Tukey *post hoc* test. Data are presented as mean and SE. (**B**) Serotonergic innervation in the arcuate nucleus. GFP immunohistochemistry was performed on Tph2-YFP mice on arcuate nucleus cuts after identification on Paxinos Brain Atlas (**i**, scheme of identified regions, in red, in the upper left column). Representative images are shown for SOD1(G86R) Tph2-YFP mice and control littermates at onset at two magnifications. Scale bar = 200 μm (**iii**, **iv**), 20 μm (**v** and **vi**). Serotonergic fibre densities in the arcuate nucleus were quantified by a blind observer as described previously (Grider *et al.*, 2006) in SOD1m mice at symptom onset (**ii**–**vi**, $n = 4$) as compared with their wild-type littermates. $^{*}P < 0.05$, Student's *t*-test. Data are presented as mean and SE. (**C**) Messenger RNA levels of *Htr2c* (5-HT_{2C} receptor) in the hypothalamus of SOD1(G86R) mice (black, SOD1m) at 75 days of age and onset and in control littermates (white, wt) ($n = 8$). $^{**}P < 0.01$, one-way ANOVA. Data are presented as mean and SE. (**D**) Food intake was measured 1 h after refeeding in SOD1(G86R) mice (SOD1m) at 80 days of age and control littermates (wt) after fluoxetine 20 mg/kg body weight (red) or vehicle (blue) injection ($n = 38$). $^{**}P < 0.005$, Multiple *t*-test. Data are presented as mean and SE. (**E**) Messenger RNA levels of *Pomc* and *Agrp* in the hypothalamus of SOD1(G86R) mice (SOD1m) and control littermates (wt) at 85 days of age after fluoxetine 20 mg/kg body weight (red) or vehicle (blue) injection ($n = 20$). $^{*}P < 0.05$, one-way ANOVA. Data are presented as mean and SE.

The situation in ALS patients is less clear with respect to energy intake due to a relative lack of studies reporting dietary intake accurately and to confounding effects of dysphagia in advanced ALS patients. However, two case-control studies reported that increased dietary fat intake was associated with ALS (Nelson *et al.*, 2000; Huisman *et al.*, 2015). Moreover, Huisman *et al.* (2015) and collaborators observed that presymptomatic daily energy intake was increased in ALS patients as compared with controls, and this would be consistent with both melanocortin

impairment and lack of weight gain under pioglitazone. Second, the melanocortin defect could be responsible for alterations in peripheral metabolic pathways. Indeed, the melanocortin system regulates peripheral lipid metabolism in rodents, by activating cholesterol reuptake by the liver (Perez-Tilve *et al.*, 2010) and reduces hepatic lipogenesis (Leckstrom *et al.*, 2011) independently of food intake. In the same line, the melanocortin system is controlling glucose metabolism and insulin response (Obici *et al.*, 2001). Interestingly, ALS patients have been reported to display increased circulating cholesterol levels (Dupuis *et al.*, 2008), and glucose intolerance (Pradat *et al.*, 2010). Third, the melanocortin defect could impair regulation of the autonomic nervous system (Sohn *et al.*, 2013), and autonomic abnormalities have sometimes been found in ALS patients (Baltadzhieva *et al.*, 2005). The relationships between these different phenotypes and melanocortin defects are unclear and will have to be clarified in further studies. Importantly, the observed melanocortin defect is unable to explain the weight loss associated with ALS, as, on the contrary, the increased orexigenic drive triggered by POMC deficiency likely compensates for weight loss by increasing food intake. Other mechanisms, either peripheral or central, have still to be identified to explain weight loss.

What causes the melanocortin defect in ALS? A first obvious potential mechanism is energy deficit. Indeed, SOD1m mice display weight loss due to hypermetabolism, leading to decreased fat mass. These mice also display decreased circulating insulin and leptin levels (Dupuis *et al.*, 2004). Ablation of leptin in *ob/ob* mice or fasting is indeed sufficient to cause decreased *Pomc* mRNA (Mizuno *et al.*, 1998, 1999; Ziotopoulou *et al.*, 2000). However, leptin levels are only decreased by 30% in 75-day-old mice (Dupuis *et al.*, 2004), an age at which we already observe strong *Pomc* mRNA decreases. We and others had previously observed serotonin loss in ALS (Turner *et al.*, 2005; Dentel *et al.*, 2013), and we hypothesized that this contributed to melanocortin impairment in SOD1m mice. Indeed, serotonin is a major activator of POMC neurons through the 5-HT_{2C} receptor, and this occurs through direct electrical stimulation (Heisler *et al.*, 2002) but also trough transcriptional activation (Zhou *et al.*, 2007; Lam *et al.*, 2008; Xu *et al.*, 2008). Consistently, loss of 5-HT_{2C} receptor leads to decreased *Pomc* mRNA in the hypothalamus (Wang and Chehab, 2006). Our observation of restoration of *Pomc* mRNA levels, as well as reversal of transient hyperphagia in SOD1m mice by fluoxetine argues for serotonin loss being a primary cause of melanocortin defect. This, however, does not exclude that direct modulation of electrical activity by either decreased leptin or other cues, either extrinsic or intrinsic, further exacerbate the observed defect. Brain serotonin system is itself affected by organismal energy status (Dwarkasing *et al.*, 2015; Zemdegs *et al.*, 2015) and our data do not exclude that defects in serotonin levels found in ALS patients and models is caused, or contributed by, weight loss and hypermetabolism. Consistent with this notion, decreasing leptin, whose major action is on the melanocortin system, was able to revert partial weight loss and increased energy expenditure in SOD1m mice (Lim *et al.*, 2014), suggesting that the melanocortin system can be further inhibited by leptin ablation.

What are the consequences of our current findings in ALS? There are at least three consequences of our finding for ALS research. First, melanocortin impairment seems to be a general event occuring in sporadic ALS patients, as well as in animal models caused by disparate mutations leading to ALS. Interestingly, a series of recent studies demonstrated the occurence of similar hypothalamic abnormalities in FTD (Piguet *et al.*, 2011; Ahmed *et al.*, 2014*a*, *b*, 2015), and in particular, increased AGRP (Ahmed *et al.*, 2015). Thus, melanocortin impairment appears associated with overall ALS/FTD continuum. It remains to be determined how melanocortin impairment relates with motor neuron degeneration in ALS. Second, this study reinforces the notion of systemic involvement in ALS. That melanocortin impairment appears downstream of serotonin loss, also brings about the notion that circuitry dysfunction might contribute to aspects of ALS phenotype. How these serotonin and melanocortin defects might be related to the spreading of TDP-43 aggregates (Brettschneider *et al.*, 2013) remains to be resolved. Second, these results have consequences for the design of pharmacological strategies to combat weight loss in ALS. Weight loss in ALS is likely to be multi-factorial, with primary causes such as hypermetabolism, and bulbar involvement, and could be exacerbated secondary to other symptoms such as deficit in upper limbs or depression. Treating weight loss could identify disease-modifying interventions as a hypercaloric diet was recently found to increase survival of ALS patients under gastrostomy (Wills *et al.*, 2014; Dorst *et al.*, 2015). Many drugs that could be used to prevent weight loss, including atypical antipsychotics (e.g. olanzapine) inhibit POMC neurons (Kirk *et al.*, 2009; Weston-Green *et al.*, 2012; Lian *et al.*, 2014). Drugs targeting the cannabinoid system increase body weight by increasing beta-endorphin release from POMC neurons (Koch *et al.*, 2015). As beta-endorphin is derived from POMC, which is decreased in ALS mice, it appears likely that cannabinoids might not be able to promote food intake through this mechanism in ALS. Thus, our current study provides a note of caution for the use of these drugs to counteract weight loss in the specific context of ALS patients, and suggest that disease progression might impair responsiveness of ALS patients to classical drugs leading to weight gain. A number of neural pathways controlling energy homeostasis have not yet been studied in the context of ALS and could be potential targets for treating weight loss (Morton *et al.*, 2014). First, pathways involved in the emergency response to glucose deprivation (glucopaenia) such as NPY might be useful, although the precise neurochemical pathways still need to be elucidated. Second, drugs affecting food reward might be of interest to improve the attractability of food during the disease. Last, the existence of emergency neuronal circuits involved in stress-

induced anorexia was recently elucidated. Inhibiting these pathways in ALS might also be a possible target for treating weight loss (Morton *et al.*, 2014). Alternatively, and besides pharmacological treatments, increasing caloric density of the diet is likely an efficient strategy to counteract weight loss (Wills *et al.*, 2014; Dorst *et al.*, 2015), although current results do not allow us to determine whether lipid enriched or carbohydrate enriched would be more efficient.

In all, our *post hoc* analysis of the pioglitazone trial revealed that the melanocortin system is profoundly altered in ALS, and that this might be important for understanding and preventing impairment of energy metabolism in ALS patients.

Acknowledgements

We acknowledge the technical help of Marie Jo Ruivo, Annie Picchinenna, Coraline Kostal, Marc Antoine Goy and Paul Rochet.

Funding

This work was supported by Association de recherche sur la SLA (ARSLA) and Fondation Thierry Latran (SpastALS, to LD). Work in our laboratories is supported by ALS Association Investigator Initiated Award (grants 2235, 3209 and 8075; to L.D.); the Frick Foundation (award 2013 to L.D.); Association Française contre les Myopathies (grant #18280; to L.D.); Virtual Helmholtz Institute "RNA dysmetabolism in ALS and FTD VI-510" (WP2, to L.D., A.W., A.C.L. and A.H.); Fondation « recherche sur le cerveau » (call 2015, to L.D.). Research leading to these results has received funding from the European Community's Health Seventh Framework Programme (FP7/2007-2013; EuroMOTOR grant agreement n° 259867).

Supplementary material

Supplementary material is available at *Brain* online.

References

Ahmed RM, Irish M, Kam J, van Keizerswaard J, Bartley L, Samaras K, et al. Quantifying the eating abnormalities in frontotemporal dementia. JAMA Neurol 2014a; 71: 1540–6.

Ahmed RM, Latheef S, Bartley L, Irish M, Halliday GM, Kiernan MC, et al. Eating behavior in frontotemporal dementia: peripheral hormones vs hypothalamic pathology. Neurology 2015; 85: 1310–7.

Ahmed RM, MacMillan M, Bartley L, Halliday GM, Kiernan MC, Hodges JR, et al. Systemic metabolism in frontotemporal dementia. Neurology 2014b; 83: 1812–8.

Baltadzhieva R, Gurevich T, Korczyn AD. Autonomic impairment in amyotrophic lateral sclerosis. Curr Opin Neurol 2005; 18: 487–93.

Belfort R, Harrison SA, Brown K, Darland C, Finch J, Hardies J, et al. A placebo-controlled trial of pioglitazone in subjects with nonalcoholic steatohepatitis. N Engl J Med 2006; 355: 2297–307.

Bouteloup C, Desport JC, Clavelou P, Guy N, Derumeaux-Burel H, Ferrier A, et al. Hypermetabolism in ALS patients: an early and persistent phenomenon. J Neurol 2009; 256: 1236–42.

Brettschneider J, Del Tredici K, Toledo JB, Robinson JL, Irwin DJ, Grossman M, et al. Stages of pTDP-43 pathology in amyotrophic lateral sclerosis. Ann Neurol 2013; 74: 20–38.

Cirulli ET, Lasseigne BN, Petrovski S, Sapp PC, Dion PA, Leblond CS, et al. Exome sequencing in amyotrophic lateral sclerosis identifies risk genes and pathways. Science 2015; 347: 1436–41.

DeFronzo RA, Tripathy D, Schwenke DC, Banerji M, Bray GA, Buchanan TA, et al. Pioglitazone for diabetes prevention in impaired glucose tolerance. N Engl J Med 2011; 364: 1104–15.

Dentel C, Palamiuc L, Henriques A, Lannes B, Spreux-Varoquaux O, Gutknecht L, et al. Degeneration of serotonergic neurons in amyotrophic lateral sclerosis: a link to spasticity. Brain 2013; 136(Pt 2): 483–93.

Desport JC, Preux PM, Magy L, Boirie Y, Vallat JM, Beaufrere B, et al. Factors correlated with hypermetabolism in patients with amyotrophic lateral sclerosis. Am J Clin Nutr 2001; 74: 328–34.

Desport JC, Preux PM, Truong TC, Vallat JM, Sautereau D, Couratier P. Nutritional status is a prognostic factor for survival in ALS patients. Neurology 1999; 53: 1059–63.

Diano S, Liu ZW, Jeong JK, Dietrich MO, Ruan HB, Kim E, et al. Peroxisome proliferation-associated control of reactive oxygen species sets melanocortin tone and feeding in diet-induced obesity. Nat Med 2011; 17: 1121–7.

Dorst J, Dupuis L, Petri S, Kollewe K, Abdulla S, Wolf J, et al. Percutaneous endoscopic gastrostomy in amyotrophic lateral sclerosis: a prospective observational study. J Neurol 2015; 262: 849–58.

Dorst J, Kühnlein P, Hendrich C, Kassubek J, Sperfeld AD, Ludolph AC. Patients with elevated triglyceride and cholesterol serum levels have a prolonged survival in Amyotrophic Lateral Sclerosis. J Neurol 2011; 258: 613–7.

Dupuis L, Corcia P, Fergani A, Gonzalez De Aguilar JL, Bonnefont-Rousselot D, Bittar R, et al. Dyslipidemia is a protective factor in amyotrophic lateral sclerosis. Neurology 2008; 70: 1004–9.

Dupuis L, Dengler R, Heneka MT, Meyer T, Zierz S, Kassubek J, et al. A randomized, double blind, placebo-controlled trial of pioglitazone in combination with riluzole in amyotrophic lateral sclerosis. PLoS One 2012; 7: e37885

Dupuis L, Oudart H, Rene F, Gonzalez de Aguilar JL, Loeffler JP. Evidence for defective energy homeostasis in amyotrophic lateral sclerosis: benefit of a high-energy diet in a transgenic mouse model. Proc Natl Acad Sci USA 2004; 101: 11159–64.

Dupuis L, Pradat PF, Ludolph AC, Loeffler JP. Energy metabolism in amyotrophic lateral sclerosis. Lancet Neurol 2011; 10: 75–82.

Dwarkasing JT, Boekschoten MV, Argiles JM, van Dijk M, Busquets S, Penna F, et al. Differences in food intake of tumour-bearing cachectic mice are associated with hypothalamic serotonin signalling. J Cachexia Sarcopenia Muscle 2015; 6: 84–94.

Fergani A, Oudart H, Gonzalez De Aguilar JL, Fricker B, Rene F, Hocquette JF, et al. Increased peripheral lipid clearance in an animal model of amyotrophic lateral sclerosis. J Lipid Res 2007; 48: 1571–80.

Freischmidt A, Wieland T, Richter B, Ruf W, Schaeffer V, Muller K, et al. Haploinsufficiency of TBK1 causes familial ALS and frontotemporal dementia. Nat Neurosci 2015; 18: 631–6.

Gallo V, Wark PA, Jenab M, Pearce N, Brayne C, Vermeulen R, et al. Prediagnostic body fat and risk of death from amyotrophic lateral sclerosis: the EPIC cohort. Neurology 2013; 80: 829–38.

Grider MH, Chen Q, Shine HD. Semi-automated quantification of axonal densities in labeled CNS tissue. J Neurosci Methods 2006; 155: 172–9.

Gurney ME, Pu H, Chiu AY, Dal Canto MC, Polchow CY, Alexander DD, et al. Motor neuron degeneration in mice that express a human Cu,Zn superoxide dismutase mutation. Science 1994; 264: 1772–5.

Heisler LK, Cowley MA, Tecott LH, Fan W, Low MJ, Smart JL, et al. Activation of central melanocortin pathways by fenfluramine. Science 2002; 297: 609–11.

Heisler LK, Jobst EE, Sutton GM, Zhou L, Borok E, Thornton-Jones Z, et al. Serotonin reciprocally regulates melanocortin neurons to modulate food intake. Neuron 2006; 51: 239–49.

Huisman MH, Seelen M, de Jong SW, Dorresteijn KR, van Doormaal PT, van der Kooi AJ, et al. Lifetime physical activity and the risk of amyotrophic lateral sclerosis. J Neurol Neurosurg Psychiatry 2013; 84: 976–81.

Huisman MH, Seelen M, van Doormaal PT, de Jong SW, de Vries JH, van der Kooi AJ, et al. Independent associations of presymptomatic body mass index, and consumption of fat and alcohol with amyotrophic lateral sclerosis. JAMA Neurol 2015; 72: 1155–62.

Kaur G, Kulkarni SK. Evidence for serotonergic modulation of progesterone-induced hyperphagia, depression and algesia in female mice. Brain Res 2002; 943: 206–15.

Kirk SL, Glazebrook J, Grayson B, Neill JC, Reynolds GP. Olanzapine-induced weight gain in the rat: role of 5-HT2C and histamine H1 receptors. Psychopharmacology 2009; 207: 119–25.

Koch M, Varela L, Kim JG, Kim JD, Hernandez-Nuno F, Simonds SE, et al. Hypothalamic POMC neurons promote cannabinoid-induced feeding. Nature 2015; 519: 45–50.

Lam DD, Przydzial MJ, Ridley SH, Yeo GS, Rochford JJ, O'Rahilly S, et al. Serotonin 5-HT2C receptor agonist promotes hypophagia via downstream activation of melanocortin 4 receptors. Endocrinology 2008; 149: 1323–8.

Lattante S, Ciura S, Rouleau GA, Kabashi E. Defining the genetic connection linking amyotrophic lateral sclerosis (ALS) with frontotemporal dementia (FTD). Trends Genet 2015; 31: 263–73.

Leblond CS, Kaneb HM, Dion PA, Rouleau GA. Dissection of genetic factors associated with amyotrophic lateral sclerosis. Exp Neurol 2014; 262 (Pt B): 91–101.

Leckstrom A, Lew PS, Poritsanos NJ, Mizuno TM. Central melanocortin receptor agonist reduces hepatic lipogenic gene expression in streptozotocin-induced diabetic mice. Life Sciences 2011; 88: 664–9.

Lian J, Huang XF, Pai N, Deng C. Betahistine ameliorates olanzapine-induced weight gain through modulation of histaminergic, NPY and AMPK pathways. Psychoneuroendocrinology 2014; 48: 77–86.

Lim MA, Bence KK, Sandesara I, Andreux P, Auwerx J, Ishibashi J, et al. Genetically altering organismal metabolism by leptin-deficiency benefits a mouse model of amyotrophic lateral sclerosis. Hum Mol Genet 2014; 23: 4995–5008.

Lindauer E, Dupuis L, Muller HP, Neumann H, Ludolph AC, Kassubek J. Adipose Tissue Distribution Predicts Survival in Amyotrophic Lateral Sclerosis. PLoS One 2013; 8: e67783.

Liou YJ, Chen CH, Cheng CY, Chen SY, Chen TJ, Yu YW, et al. Convergent evidence from mouse and human studies suggests the involvement of zinc finger protein 326 gene in antidepressant treatment response. PLoS One 2012; 7: e32984

Long L, Toda C, Jeong JK, Horvath TL, Diano S. PPARgamma ablation sensitizes proopiomelanocortin neurons to leptin during high-fat feeding. J Clin Invest 2014; 124: 4017–27.

Lu M, Sarruf DA, Talukdar S, Sharma S, Li P, Bandyopadhyay G, et al. Brain PPAR-gamma promotes obesity and is required for the insulin-sensitizing effect of thiazolidinediones. Nat Med 2011; 17: 618–22.

Maeda N, Takahashi M, Funahashi T, Kihara S, Nishizawa H, Kishida K, et al. PPARgamma ligands increase expression and plasma concentrations of adiponectin, an adipose-derived protein. Diabetes 2001; 50: 2094–9.

Marin B, Desport JC, Kajeu P, Jesus P, Nicolaud B, Nicol M, et al. Alteration of nutritional status at diagnosis is a prognostic factor for survival of amyotrophic lateral sclerosis patients. J Neurol Neurosurg Psychiatry 2011; 82: 628–34.

Mizuno TM, Kleopoulos SP, Bergen HT, Roberts JL, Priest CA, Mobbs CV. Hypothalamic pro-opiomelanocortin mRNA is reduced by fasting and [corrected] in ob/ob and db/db mice, but is stimulated by leptin. Diabetes 1998; 47: 294–7.

Mizuno TM, Makimura H, Silverstein J, Roberts JL, Lopingco T, Mobbs CV. Fasting regulates hypothalamic neuropeptide Y, agouti-related peptide, and proopiomelanocortin in diabetic mice independent of changes in leptin or insulin. Endocrinology 1999; 140: 4551–7.

Morton GJ, Meek TH, Schwartz MW. Neurobiology of food intake in health and disease. Nat Rev Neurosci 2014; 15: 367–78.

Nelson LM, Matkin C, Longstreth WT Jr, McGuire V. Population-based case-control study of amyotrophic lateral sclerosis in western Washington State. II. Diet Am J Epidemiol 2000; 151: 164–73.

O'Reilly EJ, Wang H, Weisskopf MG, Fitzgerald KC, Falcone G, McCullough ML, et al. Premorbid body mass index and risk of amyotrophic lateral sclerosis. Amyotroph Lateral Scler Frontotemporal Degener 2013; 14: 205–11.

Obici S, Feng Z, Tan J, Liu L, Karkanias G, Rossetti L. Central melanocortin receptors regulate insulin action. J Clin Invest 2001; 108: 1079–85.

Paganoni S, Deng J, Jaffa M, Cudkowicz ME, Wills AM. Body mass index, not dyslipidemia, is an independent predictor of survival in amyotrophic lateral sclerosis. Muscle Nerve 2011; 44: 20–4.

Palamiuc L, Schlagowski A, Ngo ST, Vernay A, Dirrig-Grosch S, Henriques A, et al. A metabolic switch toward lipid use in glycolytic muscle is an early pathologic event in a mouse model of amyotrophic lateral sclerosis. EMBO Mol Med 2015; 7: 526–46.

Perez-Tilve D, Hofmann SM, Basford J, Nogueiras R, Pfluger PT, Patterson JT, et al. Melanocortin signaling in the CNS directly regulates circulating cholesterol. Nat Neurosci 2010; 13: 877–82.

Piguet O, Petersen A, Yin Ka Lam B, Gabery S, Murphy K, Hodges JR, et al. Eating and hypothalamus changes in behavioral-variant frontotemporal dementia. Ann Neurol 2011; 69: 312–9.

Pradat PF, Bruneteau G, Gordon PH, Dupuis L, Bonnefont-Rousselot D, Simon D, et al. Impaired glucose tolerance in patients with amyotrophic lateral sclerosis. Amyotroph Lateral Scler 2010; 11: 166–71.

Promrat K, Lutchman G, Uwaifo GI, Freedman RJ, Soza A, Heller T, et al. A pilot study of pioglitazone treatment for nonalcoholic steatohepatitis. Hepatology 2004; 39: 188–96.

Ripps ME, Huntley GW, Hof PR, Morrison JH, Gordon JW. Transgenic mice expressing an altered murine superoxide dismutase gene provide an animal model of amyotrophic lateral sclerosis. Proc Natl Acad Sci USA 1995; 92: 689–93.

Ryan KK, Li B, Grayson BE, Matter EK, Woods SC, Seeley RJ. A role for central nervous system PPAR-gamma in the regulation of energy balance. Nat Med 2011; 17: 623–6.

Sanyal AJ, Chalasani N, Kowdley KV, McCullough A, Diehl AM, Bass NM, et al. Pioglitazone, vitamin E, or placebo for nonalcoholic steatohepatitis. N Engl J Med 2010; 362: 1675–85.

Sohn JW, Harris LE, Berglund ED, Liu T, Vong L, Lowell BB, et al. Melanocortin 4 receptors reciprocally regulate sympathetic and parasympathetic preganglionic neurons. Cell 2013; 152: 612–9.

Turner MR, Rabiner EA, Hammers A, Al-Chalabi A, Grasby PM, Shaw CE, et al. [11C]-WAY100635 PET demonstrates marked 5-HT1A receptor changes in sporadic ALS. Brain 2005; 128(Pt 4): 896–905.

Turner MR, Wotton C, Talbot K, Goldacre MJ. Cardiovascular fitness as a risk factor for amyotrophic lateral sclerosis: indirect evidence from record linkage study. J Neurol Neurosurg Psychiatry 2012; 83: 395–8.

Vandesompele J, De Preter K, Pattyn F, Poppe B, Van Roy N, De Paepe A, et al. Accurate normalization of real-time quantitative RT-PCR data by geometric averaging of multiple internal control genes. Genome Biol 2002; 3: research0034.

Wang B, Chehab FF. Deletion of the serotonin 2c receptor from transgenic mice overexpressing leptin does not affect their lipodystrophy but exacerbates their diet-induced obesity. Biochem Biophys Res Commun 2006; 351: 418–23.

Wegorzewska I, Bell S, Cairns NJ, Miller TM, Baloh RH. TDP-43 mutant transgenic mice develop features of ALS and frontotemporal lobar degeneration. Proc Natl Acad Sci USA 2009; 106: 18809–14.

Weston-Green K, Huang XF, Deng C. Alterations to melanocortinergic, GABAergic and cannabinoid neurotransmission associated with olanzapine-induced weight gain. PLoS One 2012; 7: e33548.

Wills AM, Hubbard J, Macklin EA, Glass J, Tandan R, Simpson EP, et al. Hypercaloric enteral nutrition in patients with amyotrophic lateral sclerosis: a randomised, double-blind, placebo-controlled phase 2 trial. Lancet 2014; 383: 2065–72.

Xu Y, Jones JE, Kohno D, Williams KW, Lee CE, Choi MJ, et al. 5-HT2CRs expressed by pro-opiomelanocortin neurons regulate energy homeostasis. Neuron 2008; 60: 582–9.

Zemdegs J, Quesseveur G, Jarriault D, Penicaud L, Fioramonti X, Guiard BP. High fat diet-induced metabolic disorders impairs serotonergic function and anxiety-like behaviours in mice. Br J Pharmacol 2015. Advance Access published on October 16, 2015, doi: 10.1111/bph.13343.

Zhao S, Ting JT, Atallah HE, Qiu L, Tan J, Gloss B, et al. Cell type-specific channelrhodopsin-2 transgenic mice for optogenetic dissection of neural circuitry function. Nat Methods 2011; 8: 745–52.

Zhou L, Sutton GM, Rochford JJ, Semple RK, Lam DD, Oksanen LJ, et al. Serotonin 2C receptor agonists improve type 2 diabetes via melanocortin-4 receptor signaling pathways. Cell Metab 2007; 6: 398–405.

Ziotopoulou M, Erani DM, Hileman SM, Bjorbaek C, Mantzoros CS. Unlike leptin, ciliary neurotrophic factor does not reverse the starvation-induced changes of serum corticosterone and hypothalamic neuropeptide levels but induces expression of hypothalamic inhibitors of leptin signaling. Diabetes 2000; 49: 1890–6.

Appendix 1

Collaborators: GERP ALS Study Group

All centres were located in Germany. Investigators are listed by alphabetical order of centre and investigator:

Berlin (Department of Neurology, Charité University Hospital): Nadja Borisow; Theresa Holm; Andre Maier; Thomas Meyer; Bochum (Department of Neurology, University Hospital Bergmannsheil): Paula Budde; Torsten Grehl; Kai Gruhn; Bonn (Department of Neurology, University Hospital of Bonn): Malte Bewersdorff; Michael Heneka; Dresden (Department of Neurology, University Hospital Carl Gustav Carus, Technische Universität Dresden): Andreas Hermann; Alexander Storch; Göttingen (Department of Neurology, University Hospital of Göttingen): Tobias Frank; Bettina Göricke; Jochen Weishaupt; Halle (Department of Neurology, University Hospital of Halle/Saale): Katharina Eger; Frank Hanisch; Stephan Zierz; Hannover (Department of Neurology and Clinical Neurophysiology, Hannover Medical School (MHH), University Clinic): Anna-Lena Boeck; Reinhard Dengler; Sonja Koerner; Katja Kollewe; Susanne Petri; Jena (Department of Neurology, University Hospital Jena): Julian Grosskreutz; Tino Prell; Thomas Ringer; Jan Zinke; Munich (Department of Neurology, University of Munich): Johanna Anneser; Gian Domenico Borasio; Christine Chahli; Andrea S. Winkler; Muenster (Department of Neurology, University of Muenster): Matthias Boentert; Bianca Stubbe-Draeger; Peter Young; Regensburg (Department of Neurology, University of Regensburg): Ulrich Bogdahn; Steffen Franz; Verena Haringer; Norbert Weidner; Rostock (Department of Neurology, University of Rostock): Reiner Benecke; Stefanie Meister; Johannes Prudlo; Matthias Wittstock; Ulm (Department of Neurology, University of Ulm): Johannes Dorst; Corinna Hendrich; Albert C. Ludolph; Anne-Dorte Sperfeld; Ulrike Weiland; Wiesbaden (Department of Neurology, Neurological clinic, DKD): Sabine Neidhardt; Berthold Schrank; Wurzburg (Department of Neurology, University of Wurzburg): Marcus Beck; Peter Kraft; Klaus Toyka; Jochen Ulzheimer; Carsten Wessig.

Supplementary Table 1: primers used for RT-qPCR

Target	forward primer	reverse primer
18s	F-TCTGATAAATGCACGCATCC	R-GCCATGCATGTCTAAGTACGC
AgRP	F- CAGGCTCTGTTCCCAGAGTT	R- TCTAGCACCTCCGCCAAA
AVP	F- TCTGACATGGAGCTGAGACAG	R- GAAGCAGCCCAGCTCGT
BDNF	F- GCCTTTGGAGCCTCCTCTAC	R- GCGGCATCCAGGTAATTTT
CART	F- CGAGAAGAAGTACGGCCAAG	R- CTGGCCCCTTTCCTCACT
CRH	F- GAGGCATCCTGAGAGAAGTCC	R- TGTTAGGGGCGCTCTCTTC
Galanin	F- AGAAGAGAGGTTGGACCCTGA	R- GAGGCCATGCTTGTCGCTAA
MCH	F-GCAGAAAGATCCGTTGTCGC	R-CGGATCCTTTCAGAGCGAGG
NPY	F- CCGCTCTGCGACACTACAT	R- TGTCTCAGGGCTGGATCTCT
NTS	F-AGCCCTGGAGGCAGATCTAT	R-CCAAGACGGAGGACTTGCTT
Orexin	F-CTTCAGGCCAACGGTAACCA	R-GGTGCTAAAGCGGTGGTAGT
PC1	F- GCTGGTGTGTCTCTGATCTTG	R- GAGTCCAACCTCTTTGCTCCA
PC2	F- AAAATACCACCCACCGGCAA	R- CCAGGTAGCGGACGAAGTTT
POMC	F- AGTGCCAGGACCTCACCA	R- CAGCGAGAGGTCGAGTTTG
POL2	F-GCTGGGAGACATAGCACCA	R-TTACTCCCCTGCATGGTCTC
SST	F- GGGCATCATTCTCTGTCTGG	R- GGGCATCATTCTCTGTCTGG
TBP	F-CCAATGACTCCTATGACCCCTA	R-CAGCCAAGATTCACGGTAGAT
TRH	F- TGCAGAGTCTCCACCTTGC	R- GGGGATACCAGTTAGCACGA

Supplementary Table 2: numbers of patients for Figure 1

	0	1	2	6	12	18
Adiponectin						
Placebo	58			58	38	
Pioglitazone	57			56	35	
Glycemia						
Placebo	100	84	90	70	47	41
Pioglitazone	104	89	95	79	44	44
ASAT						
Placebo	104	92	93	76	46	43
Pioglitazone	106	98	96	79	48	47
ALAT						
Placebo	104	92	93	76	46	44
Pioglitazone	107	99	97	80	48	47

Supplementary Table 3: numbers of patients for Figure 2

	0	1	2	3	6	9	12	15	18
Total									
Placebo	105	94	94	84	77	67	52	32	55
Pioglitazone	104	94	98	86	80	69	48	30	55
Spinal onset									
Placebo	72	64	65	56	53	46	37	24	37
Pioglitazone	72	66	67	56	56	47	34	20	40
Preserved QoL									
Placebo	50	47	48	45	49	45	36	20	36
Pioglitazone	53	49	50	47	49	45	35	21	40
Preserved bulbar function									
Placebo	40	38	39	37	39	35	30	21	26
Pioglitazone	42	40	41	39	41	34	28	18	30

Supplementary Table 4: intake of drugs affecting body weight and food intake

The number of patients taking the corresponding class of drug is shown. P value was calculated using Fisher's exact – test

Class of drugs	**n total**	**Pioglitazone**	**Placebo**	**p-value**
anti-epileptics	9	3	6	0.50
anti-diabetics	3	1	2	1.00
anti-psychotics	4	4	0	0.12
SSRIs	37	20	17	0.72

Publication #6 :

Toxic gain of function from mutant FUS protein is crucial to trigger cell autonomous motor neuron loss

Jelena Scekic-Zahirovic, Oliver Sendscheid, Hajer El Oussini, Mélanie Jambeau, Ying Sun, Sina Mersmann, Marina Wagner, Stéphane Dieterlé, Jérome Sinniger, Sylvie Dirrig-Grosch, Kevin Drenner, Marie-Christine Birling, Jinsong Qiu, Yu Zhou, Hairi Li, Xiang-Dong Fu, Caroline Rouaux, Tatyana Shelkovnikova, Anke Witting, Albert C Ludolph, Friedemann Kiefer, Erik Storkebaum, Clotilde Lagier-Tourenne, & Luc Dupuis

Published online: March 7, 2016

Article

SOURCE DATA | TRANSPARENT PROCESS | OPEN ACCESS

THE EMBO JOURNAL

Toxic gain of function from mutant FUS protein is crucial to trigger cell autonomous motor neuron loss

Jelena Scekic-Zahirovic[1,2], Oliver Sendscheid[3,4], Hajer El Oussini[1,2], Mélanie Jambeau[5,6], Ying Sun[5,6], Sina Mersmann[3,4], Marina Wagner[3,4], Stéphane Dieterlé[1,2], Jérome Sinniger[1,2], Sylvie Dirrig-Grosch[1,2], Kevin Drenner[5,6], Marie-Christine Birling[7], Jinsong Qiu[8], Yu Zhou[8], Hairi Li[8], Xiang-Dong Fu[8], Caroline Rouaux[1,2], Tatyana Shelkovnikova[9], Anke Witting[10], Albert C Ludolph[10], Friedemann Kiefer[11], Erik Storkebaum[3,4,*], Clotilde Lagier-Tourenne[5,6,†,**] & Luc Dupuis[1,2,***]

Abstract

FUS is an RNA-binding protein involved in amyotrophic lateral sclerosis (ALS) and frontotemporal dementia (FTD). Cytoplasmic FUS-containing aggregates are often associated with concomitant loss of nuclear FUS. Whether loss of nuclear FUS function, gain of a cytoplasmic function, or a combination of both lead to neurodegeneration remains elusive. To address this question, we generated knockin mice expressing mislocalized cytoplasmic FUS and complete FUS knockout mice. Both mouse models display similar perinatal lethality with respiratory insufficiency, reduced body weight and length, and largely similar alterations in gene expression and mRNA splicing patterns, indicating that mislocalized FUS results in loss of its normal function. However, FUS knockin mice, but not FUS knockout mice, display reduced motor neuron numbers at birth, associated with enhanced motor neuron apoptosis, which can be rescued by cell-specific CRE-mediated expression of wild-type FUS within motor neurons. Together, our findings indicate that cytoplasmic FUS mislocalization not only leads to nuclear loss of function, but also triggers motor neuron death through a toxic gain of function within motor neurons.

Keywords amyotrophic lateral sclerosis; frontotemporal dementia; FUS; motor neuron degeneration; PY-NLS

Subject Categories Molecular Biology of Disease; Neuroscience

DOI 10.15252/embj.201592559 | Received 26 July 2015 | Revised 28 January 2016 | Accepted 1 February 2016

Introduction

Mutations in several aggregation-prone RNA-binding proteins (RBPs) are increasingly linked to various neurodegenerative diseases. Such mutations constitute a major cause of amyotrophic lateral sclerosis (ALS), the most frequent adult-onset motor neuron disease, with mutations in TDP-43 (Gitcho *et al*, 2008; Kabashi *et al*, 2008; Sreedharan *et al*, 2008) and FUS (Kwiatkowski *et al*, 2009; Vance *et al*, 2009) accounting each for about 5% of familial ALS cases. Even in the absence of mutations, abnormal cytoplasmic inclusions of TDP-43 represent a pathological hallmark of sporadic ALS, non-SOD1 familial ALS, and frontotemporal dementia (FTD) (Neumann *et al*, 2006, 2009), a neurodegenerative condition characterized by behavioral and language deficits. Similarly, compromised FUS nuclear localization

1 Faculté de Médecine, INSERM U1118, Strasbourg, France
2 Université de Strasbourg UMR_S1118, Strasbourg, France
3 Molecular Neurogenetics Laboratory, Max Planck Institute for Molecular Biomedicine, Muenster, Germany
4 Faculty of Medicine, University of Muenster, Muenster, Germany
5 Department of Neurosciences, University of California, San Diego, La Jolla, CA, USA
6 Ludwig Institute for Cancer Research, University of California, San Diego, La Jolla, CA, USA
7 Institut Clinique de la souris, Illkirch-Graffenstaden, France
8 Department of Cellular and Molecular Medicine, University of California, San Diego, La Jolla, CA, USA
9 University of Cardiff, Cardiff, UK
10 Department of Neurology, University of Ulm, Ulm, Germany
11 Mammalian Cell Signaling Laboratory, Department of Vascular Cell Biology, Max Planck Institute for Molecular Biomedicine, Muenster, Germany
*Corresponding author. Tel: +49 251 8346895; E-mail: erik.storkebaum@mpi-muenster.mpg.de
**Corresponding author. Tel: +1 617 643 6774; E-mail: clagier-tourenne@mgh.harvard.edu
***Corresponding author. Tel: +33 3 68 85 30 82; E-mail: ldupuis@unistra.fr
†Present address: MassGeneral Institute for Neurodegenerative Disease, Department of Neurology, Massachusetts General Hospital, Harvard Medical School, Charlestown, MA, USA

and cytoplasmic FUS aggregates are found in ALS patients carrying *FUS* mutations, as well as in a subset of FTD patients without TDP-43 pathology (Mackenzie *et al*, 2010). Consistent with a central role of RNA processing misregulation in ALS and FTD pathogenesis, mutations in several other RBPs were recently identified, in particular TAF15 and EWSR1, two proteins from the same family as FUS (Couthouis *et al*, 2011, 2012), and other less closely related RBPs such as ataxin 2 (Elden *et al*, 2010), hnRNPA2B1 (Kim *et al*, 2013), hnRNPA1 (Kim *et al*, 2013), and matrin-3 (Johnson *et al*, 2014).

Disease-associated mutations in RBPs typically disrupt the normal nuclear localization of mutant proteins, with concomitant sequestration of the endogenous wild-type protein into cytoplasmic aggregates (Kim *et al*, 2013; Vance *et al*, 2013). Mutations are either located in highly unstructured prion-like protein domains, resulting in a higher propensity to aggregate (Kim *et al*, 2013), or in the vicinity of the nuclear localization signal (NLS), impairing nuclear import of the protein. For instance, the NLS of FUS is an atypical PY-NLS (Dormann *et al*, 2010) located at the C-terminus of the protein that represents a mutational hot spot in ALS patients. Along with missense mutations, several truncating or frameshift mutations deleting the FUS NLS have been identified in ALS patients (Fig EV1) and are often associated with juvenile onset and rapid disease progression (Baumer *et al*, 2010; Waibel *et al*, 2010, 2013; Zou *et al*, 2013; Calvo *et al*, 2014; Deng *et al*, 2014). In most instances, *FUS* mutations are dominantly inherited. However, it is noteworthy that a recessive inheritance pattern is occasionally observed in ALS patients (Kwiatkowski *et al*, 2009; Bertolin *et al*, 2014).

FUS and TDP-43 normally shuttle between the nucleus and cytoplasm, and defective nuclear import may lead to both loss of their nuclear functions and deregulation of their cytoplasmic roles. In the nucleus, FUS and TDP-43 are involved in regulation of pre-mRNA splicing, transcription, and microRNA biogenesis, all processes that may be affected by their depletion from the nucleus (Morlando *et al*, 2012; Ling *et al*, 2013). Consistently, reductions of TDP-43 or FUS were associated with altered expression and splicing of several hundreds of genes (Polymenidou *et al*, 2011; Tollervey *et al*, 2011; Ishigaki *et al*, 2012; Lagier-Tourenne *et al*, 2012; Rogelj *et al*, 2012; Ling *et al*, 2015), and both proteins are critically involved in the processing of long pre-mRNAs (Polymenidou *et al*, 2011; Lagier-Tourenne *et al*, 2012; Ling *et al*, 2013; Sibley *et al*, 2015). Cytosolic functions of FUS and TDP-43 include transport (Alami *et al*, 2014) and/or storage (Han *et al*, 2012) of mRNA in the cytoplasm with a crucial role in the formation of stress granules (Li *et al*, 2013).

Although several lines of evidence indicate that cytoplasmic mislocalization of RBPs is a key event in disease pathogenesis, definitive *in vivo* evidence is lacking and the relative contributions of loss and gain of function still need to be established. Indeed, it remains unknown whether loss of nuclear function of mutant RBPs is sufficient to trigger motor neuron disease or whether a cytosolic gain of function is also involved. There have been two major hurdles in answering these questions. First, ALS-associated RBPs are crucial for cell physiology, and overexpression of wild-type proteins causes widespread phenotypes (Huang *et al*, 2011; Mitchell *et al*, 2013; Sephton *et al*, 2014). This represents a major drawback when attempting to discern the pathophysiological effects of disease-causing mutations in overexpression models. Second, potent autoregulatory mechanisms control cellular levels of RBPs. For instance, both TDP-43 (Ayala *et al*, 2011; Polymenidou *et al*, 2011; D'Alton *et al*, 2015) and FUS (Lagier-Tourenne *et al*, 2012; Zhou *et al*, 2013; Dini Modigliani *et al*, 2014) control their own levels by binding to their mRNAs. As a consequence, the levels of endogenous TDP-43 or FUS proteins are strikingly reduced in animal models overexpressing wild-type or mutant TDP-43 and FUS (Wegorzewska *et al*, 2009; Huang *et al*, 2011; Arnold *et al*, 2013; Mitchell *et al*, 2013; Sephton *et al*, 2014).

Here, we use homologous recombination techniques to circumvent issues inherent to overexpression animal models. We systematically compare the pathological and molecular features of two novel mouse models either expressing a truncated FUS protein that lacks the NLS and localizes within the cytoplasm (knockin mice) or harboring a genomic mutation associated with complete absence of FUS protein (knockout mice). Both mice expressing mutant cytoplasmic FUS and mice completely devoid of FUS died at birth of respiratory insufficiency. Using genomic approaches, we determined that FUS knockin mice display expression and splicing alterations consistent with loss of FUS nuclear function. However, mice expressing truncated cytoplasmic FUS, but not FUS knockout mice, exhibit perinatal motor neuron loss, which can be rescued by motor neuron-restricted reversal of the mutant FUS gene to wild-type FUS. These findings demonstrate that cytoplasmic FUS leads to loss of nuclear FUS function, yet exerts a toxic gain of function within the cytoplasm of motor neurons necessary to trigger neuronal death.

Results

Cytoplasmic mislocalization of mutant FUS in *Fus*$^{\Delta NLS/\Delta NLS}$ mice

With the aim to investigate *in vivo* consequences of altered FUS localization, we generated a mouse model with targeted deletion of the PY-NLS, encoded by the last exon of the *Fus* gene (exon 15). This mutation closely mimics ALS-causing truncating mutations of *FUS* (Fig EV1). We opted for a strategy that would not only result in ablation of exon 15, but also allow for CRE-mediated reversal to the wild-type locus. Due to the small size of intron 14, we engineered the *Fus* locus to include, in intron 12, a floxed cDNA encoding exons 13 and 14 of *Fus*, followed by 3 transcription stop cassettes and a poly-adenylation signal (Fig 1A). Germ line transmission of the recombinant allele was obtained (Fig 1B) and mice heterozygous and homozygous for the targeted allele will hereafter be referred to as *Fus*$^{\Delta NLS/+}$ and *Fus*$^{\Delta NLS/\Delta NLS}$, respectively. Homozygous *Fus*$^{\Delta NLS/\Delta NLS}$ mice died shortly after birth, and tissues dissected at birth (P0) were analyzed for expression and localization of FUS$^{\Delta NLS}$ mRNA and protein. The ΔNLS mRNA could be detected by RT–PCR in tissues of *Fus*$^{\Delta NLS/+}$ and *Fus*$^{\Delta NLS/\Delta NLS}$ mice (Figs 1C and EV2A). FUS protein was detected by immunoblotting in *Fus*$^{\Delta NLS/+}$ and *Fus*$^{\Delta NLS/\Delta NLS}$ brain, spinal cord, and muscle protein extracts using antibodies targeting the internal or N-terminal parts of FUS (Figs 1D and EV2B). Contrastingly, no signal was found in *Fus*$^{\Delta NLS/\Delta NLS}$ protein extracts when using two different antibodies that recognize the C-terminal NLS of FUS (Figs 1D and EV2B), demonstrating that the engineered *Fus* gene leads to the generation of a FUS protein devoid of NLS. FUS protein levels were heterogeneous in *Fus*$^{\Delta NLS/+}$ brains (Fig 1D). As expected, FUS protein localized to the nucleus in cultured mouse embryonic fibroblasts

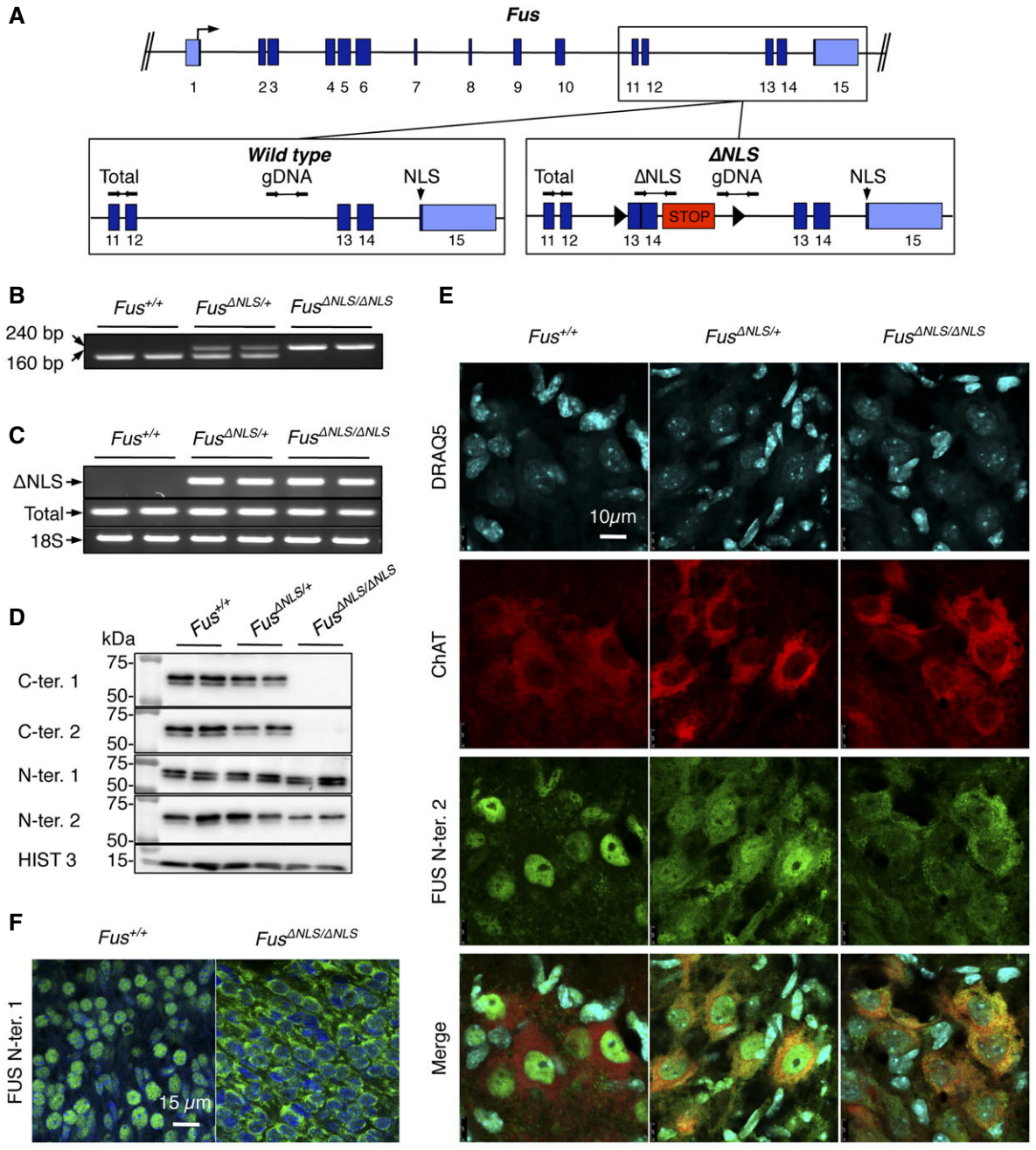

Figure 1. FUS mislocalization in *Fus$^{\Delta NLS/\Delta NLS}$* mice.

A Schematic representation of the *Fus* gene locus (upper panel). Lower panels depict exons 11–15 in the wild-type allele (left) and ΔNLS allele (right) with localization of PCR primers used for genotyping (gDNA, used in B) and for RT–PCR (Total and ΔNLS, used in C). Arrow: translational start site. STOP cassettes are indicated in red; loxP sites as black triangles; coding regions are in dark blue and UTRs in light blue. Location of the region encoding the nuclear localization signal (NLS) is indicated in exon 15.

B Representative PCR genotyping results from 2 *Fus$^{+/+}$*, 2 *Fus$^{\Delta NLS/+}$*, and 2 *Fus$^{\Delta NLS/\Delta NLS}$* knockin mice using primers designed around the distal loxP site of the *Fus$^{\Delta NLS}$* allele and shown as gDNA in (A). The expected size of the PCR product of the ΔNLS allele is 240 bp; the size of wild-type allele is 160 bp.

C RT–PCR analysis of brain from 2 *Fus$^{+/+}$*, 2 *Fus$^{\Delta NLS/+}$*, and 2 *Fus$^{\Delta NLS/\Delta NLS}$* knockin P0 mice using primers located in the STOP cassette, and thus specific to the ΔNLS mRNA (ΔNLS, upper panel), or primers located in exon 11, that is, upstream of the floxed cDNA insertion, and thus amplifying total *Fus*-derived mRNA (Total, middle panel). PCR amplification of 18S rRNA is shown as a standard gene (lower panel).

D Immunoblot analysis of FUS protein in cerebral cortex of 2 *Fus$^{+/+}$*, 2 *Fus$^{\Delta NLS/+}$*, and 2 *Fus$^{\Delta NLS/\Delta NLS}$* knockin mice using a combination of two different antibodies targeting either the C-terminal (C-ter. 1 and C-ter. 2) NLS, the N-terminal part (N-ter. 1), or an internal part (N-ter. 2) of FUS. Molecular weight markers are shown on the left, and apparent MW is indicated.

E Double immunostaining for the motor neuronal marker ChAT and Fus (N-terminal part) in the ventral horn of spinal cord.

F Double immunostaining for nuclei (DAPI, blue) and Fus (N-terminal part) in the cerebral cortex.

Source data are available online for this figure.

(MEFs) of $Fus^{+/+}$ mice. In striking contrast, FUS redistributed from the nuclear compartment to the cytoplasm in $Fus^{\Delta NLS/\Delta NLS}$ MEFs (Fig EV2C) and was detected in both the nucleus and the cytoplasm of $Fus^{\Delta NLS/+}$ MEFs (Fig EV2C). Consistently, in $Fus^{\Delta NLS/\Delta NLS}$ newborn mice, immunostaining revealed that mutant FUS is localized to the cytoplasm of spinal motor neurons and cortical neurons, contrasting with the normal nuclear localization in $Fus^{+/+}$ neurons (Fig 1E and F). In $Fus^{\Delta NLS/+}$ mice, FUS is detected in both the nucleus and the cytoplasm of motor neurons (Fig 1E). Thus, the $Fus^{\Delta NLS}$ allele effectively leads to the expression of a truncated FUS protein that lacks the NLS and localizes predominantly to the cytoplasm.

Both cytoplasmic mislocalization of FUS and complete loss of FUS result in perinatal lethality

$Fus^{\Delta NLS/\Delta NLS}$ mice were born alive, but died within minutes after birth, while $Fus^{\Delta NLS/+}$ mice survived the perinatal period. The body length and weight of $Fus^{\Delta NLS/\Delta NLS}$ pups were slightly but significantly reduced as compared to $Fus^{+/+}$ and $Fus^{\Delta NLS/+}$ newborn mice (Fig 2A–C). The cause of death appeared to be respiratory insufficiency, as $Fus^{\Delta NLS/\Delta NLS}$ animals showed poor respiratory movements and cyanosis, and H&E staining of sections through the lung revealed uninflated lungs with complete alveolar atelectasis (Fig 2D).

Cytoplasmic FUS mislocalization could have detrimental effects either through toxicity resulting from increased cytoplasmic FUS levels or through loss of its normal nuclear function. To distinguish between these possibilities, we investigated whether complete loss of FUS recapitulates the perinatal lethality phenotype of $Fus^{\Delta NLS/\Delta NLS}$ mice. Mice with a gene trap insertion in exons 8 or 12 of the *Fus* gene have been described previously (Hicks *et al*, 2000; Kuroda *et al*, 2000), yet both of these *Fus* gene trap lines express low amounts of truncated FUS protein, thus precluding their use to discriminate between loss- versus gain-of-function mechanisms. To tackle this issue, we generated a novel *Fus* knockout model (hereafter referred to as $Fus^{-/-}$) that was systematically compared to $Fus^{\Delta NLS/\Delta NLS}$ mice in the same C57Bl6 background. In this new *Fus* knockout allele, a trap cassette was inserted in intron 1 to completely disrupt transcription of the endogenous *Fus* gene (Fig 3A). Southern blot and direct sequencing confirmed the position and orientation of the gene trap insertion, and excluded additional insertion events elsewhere in the genome (not shown). FUS protein was undetectable in the central nervous system of $Fus^{-/-}$ newborn mice by Western blot using the above-described antibodies against the N-terminal and C-terminal parts of the protein (Fig 3B and C) and *Fus* mRNA could not be detected by quantitative real-time PCR (Fig 3D). Consistently, immunostaining for FUS on spinal cord sections of E18.5 $Fus^{-/-}$ mice did not detect FUS protein (Fig 3E), confirming that $Fus^{-/-}$ mice are FUS protein null. Depending on the genetic background, previously described *Fus* gene trap mice were reported either to be adult viable, to die before the age of weaning or within 16 h after birth (Hicks *et al*, 2000; Kuroda *et al*, 2000; Kino *et al*, 2015). In contrast, $Fus^{-/-}$ mice died within 30 min after birth due to respiratory insufficiency. Similar to $Fus^{\Delta NLS/\Delta NLS}$ pups, the body weight and body length of $Fus^{-/-}$ newborn mice were significantly reduced as compared to littermate controls (Fig 3F and G). Thus, both complete loss of FUS and its cytoplasmic mislocalization trigger a similar perinatal phenotype in C57Bl6 mice.

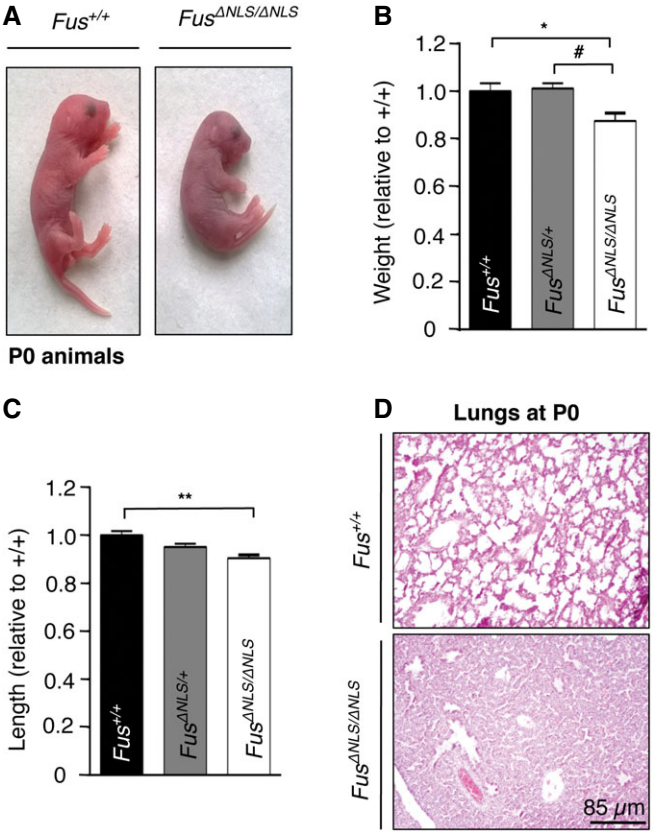

Figure 2. Perinatal lethality in $Fus^{\Delta NLS/\Delta NLS}$ mice.

A Photographs of $Fus^{+/+}$ and $Fus^{\Delta NLS/\Delta NLS}$ pups immediately after birth (P0 animals).

B, C $Fus^{\Delta NLS/\Delta NLS}$ mice showed significantly reduced body weight (B) and length (C). Weight and length values normalized to wild type ($Fus^{+/+}$) are presented (mean ± SEM). $N = 11$ $Fus^{+/+}$, $N = 26$ $Fus^{\Delta NLS/+}$ and $N = 14$ $Fus^{\Delta NLS/\Delta NLS}$; $^{*}P < 0.05$, $^{**}P < 0.01$ versus $Fus^{+/+}$, $^{\#}P < 0.05$ versus $Fus^{\Delta NLS/+}$; one-way ANOVA followed by Tukey's *post hoc* test.

D Representative hematoxylin and eosin stainings of lungs of $Fus^{+/+}$ and $Fus^{\Delta NLS/\Delta NLS}$ at birth.

Extensive overlap of RNA expression changes induced by cytoplasmic FUS mislocalization and complete loss of FUS

The phenotypic similarity of $Fus^{\Delta NLS/\Delta NLS}$ and $Fus^{-/-}$ newborn mice is consistent with FUS cytoplasmic mislocalization leading to loss of FUS nuclear function. FUS has been involved in the regulation of gene expression and alternative splicing of its mRNA targets (Polymenidou *et al*, 2011; Tollervey *et al*, 2011; Ishigaki *et al*, 2012; Lagier-Tourenne *et al*, 2012; Rogelj *et al*, 2012). In addition, FUS interacts with several proteins, including U1-snRNP (Yamazaki *et al*, 2012; Sun *et al*, 2015), SMN (Yamazaki *et al*, 2012; Groen *et al*, 2013; Tsuiji *et al*, 2013; Sun *et al*, 2015), HDAC1 (Wang *et al*, 2013), Drosha (Morlando *et al*, 2012), RNA polymerase II (Schwartz *et al*, 2012), and PRMT1 (Tibshirani *et al*, 2014), known to have profound effects on splicing and gene expression. Hence, the expression of a truncated cytoplasmic form of FUS may primarily lead to loss of nuclear FUS function and defective regulation of direct FUS RNA targets. In addition, cytoplasmic accumulation of FUS may also alter the function and/or

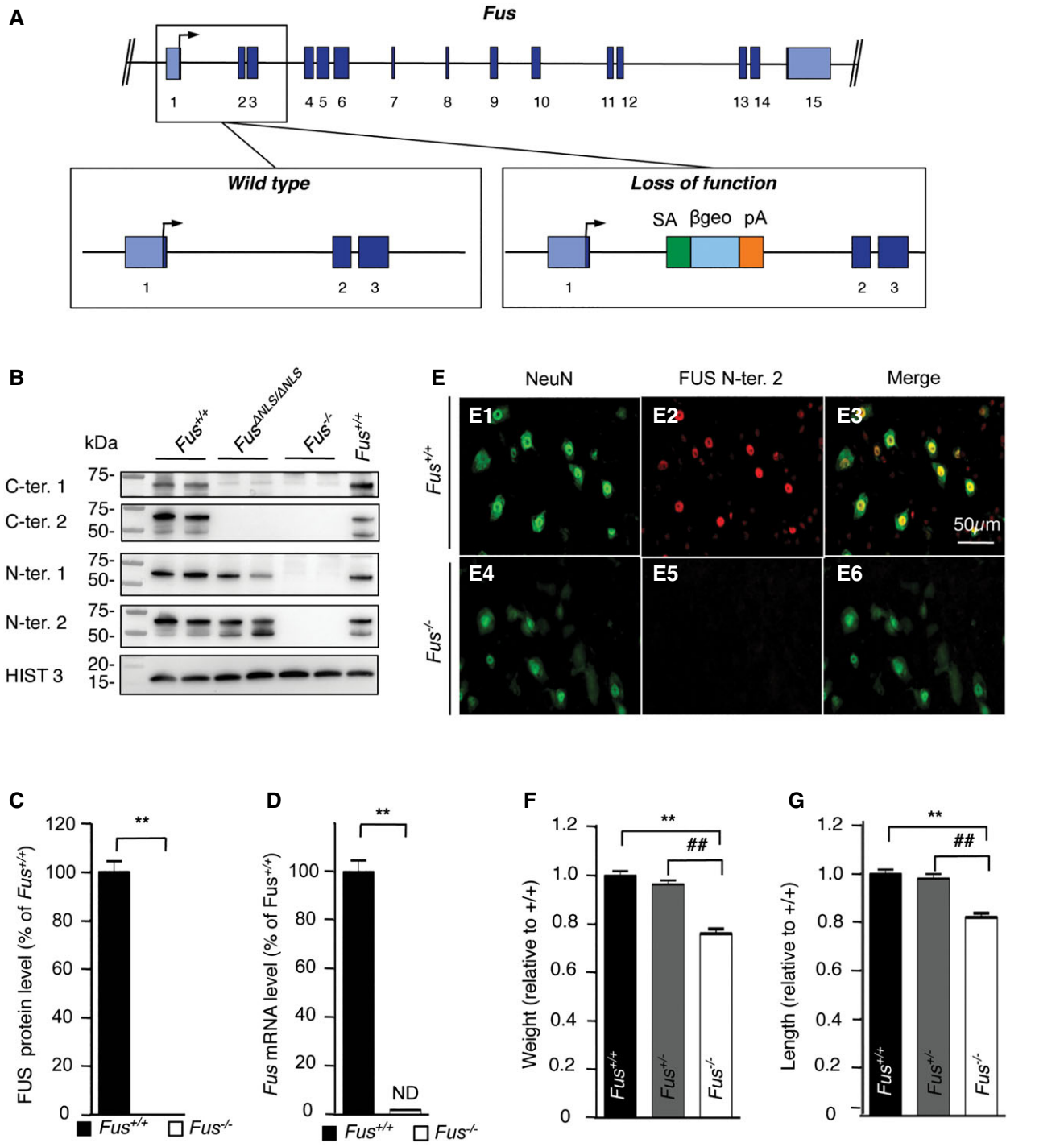

Figure 3. Generation of a complete *Fus*$^{-/-}$ loss-of-function mouse model.

A Schematic representation of the *Fus* gene locus (upper panel). Lower panels depict exons 1–3 in the wild-type allele (left) and loss-of-function allele (right). Arrow: translational start site; SA: splice acceptor; βgeo: β-galactosidase/neomycin phosphotransferase fusion gene; pA: polyA.

B Representative immunoblot for FUS on protein extracts of E18.5 brain. Histone 3 is used as a loading control.

C Quantification of FUS protein levels from immunoblots.

D Quantitative real-time PCR for *Fus* transcript in *Fus*$^{+/+}$ *and Fus*$^{-/-}$ mice. ND: not detected.

E Immunostaining for the neuronal marker NeuN and FUS on the spinal cord ventral horn of E18.5 *Fus*$^{+/+}$ and *Fus*$^{-/-}$ mice.

F, G Body weight (F) and length (G) of *Fus*$^{+/+}$, *Fus*$^{+/-}$, and *Fus*$^{-/-}$ pups at birth; $N = 14$ *Fus*$^{+/+}$, $N = 36$ *Fus*$^{+/-}$, and $N = 13$ *Fus*$^{-/-}$ for body weight; $N = 6$ per genotype for body length.

Data information: Data represent mean ± SEM. $^{**}P < 0.01$ versus *Fus*$^{+/+}$, $^{\#\#}P < 0.01$ versus *Fus*$^{+/-}$; one-way ANOVA followed by Tukey's *post hoc* test.
Source data are available online for this figure.

subcellular localization of FUS-interacting proteins and result in additional gene expression and splicing alterations. To discriminate between gain- and loss-of-function changes, we systematically compared RNA profiles in brains from $Fus^{\Delta NLS/\Delta NLS}$ and $Fus^{-/-}$ mice. First, we used strand-specific, genomewide sequencing of RNAs (Parkhomchuk *et al*, 2009) (RNA-seq) to evaluate RNA expression levels in brains of $Fus^{\Delta NLS/\Delta NLS}$ and $Fus^{-/-}$ mice. Total RNA was extracted from E18.5 embryonic brains of $Fus^{\Delta NLS/\Delta NLS}$ mice ($N = 5$), and wild-type littermates ($N = 4$), as well as homozygous $Fus^{-/-}$ ($N = 5$) and their control $Fus^{+/+}$ littermates ($N = 5$). Expression levels for each annotated protein-coding gene were determined by the number of mapped fragments per kilobase of exon, per million mapped reads (FPKM) (Mortazavi *et al*, 2008; Trapnell *et al*, 2012). The FPKM ratio of the *Fus* gene confirmed that *Fus* was expressed in $Fus^{\Delta NLS/\Delta NLS}$ mice, but not in $Fus^{-/-}$ mice (Fig EV3A). Inspection of the reads mapped on the *Fus* gene demonstrated the absence of reads throughout all exons for the $Fus^{-/-}$ mice, while only exon 15 was not integrated in *Fus* transcripts of $Fus^{\Delta NLS/\Delta NLS}$ mice (Fig 4A). *Fus* transcript levels as determined by FPKM ratio were not significantly different in $Fus^{\Delta NLS/\Delta NLS}$ and $Fus^{+/+}$ mice (Fig EV3A). Unsupervised hierarchical clustering with all genes reliably discriminated mutant genotypes from their controls (Fig EV3B and C), indicating that both *Fus* mutation and *Fus* deletion displayed RNA expression profiles divergent from wild type. Statistical comparison of FPKM values identified 237 genes upregulated and 549 genes downregulated in $Fus^{\Delta NLS/\Delta NLS}$ mice (Dataset EV1 and Fig 4B). Of note, only nine genes and 56 genes were upregulated and downregulated more than 1.5-fold, respectively (Dataset EV1). Identical analysis in $Fus^{-/-}$ mice identified 669 upregulated genes (29 genes more than 1.5-fold) and 889 downregulated genes (72 genes more than 1.5-fold) (Dataset EV2 and Fig 4C). Comparison of both models identified 353 genes that were altered in the same direction, consistent with loss of FUS nuclear function underlying the altered levels of these transcripts (Fig 4D and Dataset EV3).

Downregulation of selected genes in both mouse models was confirmed by qRT–PCR (Appendix Fig S1A) yielding data similar to the RNA-seq results (Fig 4E). Out of these, several genes have been previously involved in neurological diseases such as the *Abelson helper integration site 1* (*Ahi1*) gene mutated in the neurodevelopmental Joubert syndrome (Ferland *et al*, 2004), the *Dystrophia myotonica protein kinase* (*Dmpk*) gene implicated in myotonic dystrophy type 1, the *low* and *medium* molecular weight *neurofilament* subunits (*Nefl* and *Nefm*) (Bergeron *et al*, 1994), and the gene encoding tubulin alpha 4A (*Tuba4a*) that was recently implicated in ALS (Smith *et al*, 2014). Similarly, selected upregulated genes were confirmed by qRT–PCR (Fig 4E and Appendix Fig S1A), including *Taf15,* a FUS family member also mutant in ALS (Couthouis *et al*, 2011). Increased levels of *Taf15* in $Fus^{\Delta NLS/\Delta NLS}$ and $Fus^{-/-}$ mice are consistent with the presence of FUS binding sites on the *Taf15* transcript (Lagier-Tourenne *et al*, 2012) and may illustrate a mechanism of compensation induced by loss of FUS nuclear function. Overall, an extensive overlap in RNA expression changes was found in $Fus^{\Delta NLS/\Delta NLS}$ and $Fus^{-/-}$ brains consistent with loss of FUS nuclear function in knockin mice.

Cytoplasmic mislocalization of FUS leads to unique RNA expression changes

A subset of transcripts were altered uniquely in $Fus^{\Delta NLS/\Delta NLS}$ animals (Fig 4F and Appendix Fig S1B), including the *Vitronectin* (*Vtn*) gene, the *small nuclear ribonucleoprotein polypeptides B and B1* (*Snrpb*) gene, the *Trove2* gene encoding for the 60 kDa SS-A/Ro ribonucleoprotein, and the *U2AF homology motif kinase 1* (*Uhmk1*) gene encoding for the kinase interacting with stathmin (KIS) protein that was implicated in schizophrenia and the regulation of splicing (Manceau *et al*, 2008) and local translation in neuritic projections (Cambray *et al*, 2009; Pedraza *et al*, 2014). Interestingly, $Fus^{\Delta NLS/\Delta NLS}$ animals displayed increased mRNA levels of *Ephb3*, a member of Eph/ephrin signaling pathways crucial in synaptogenesis and previously involved in Alzheimer's disease (Sheffler-Collins & Dalva, 2012), while *EphA4,* another member of Eph/ephrin system, has been recently involved in ALS (Van Hoecke *et al*, 2012) (Fig 4F and Appendix Fig S1B). Thus, $Fus^{\Delta NLS/\Delta NLS}$ expression profiles largely recapitulated expression profiles of $Fus^{-/-}$ brains, yet a subset of genes was found specifically associated with the expression of cytoplasmic truncated FUS in $Fus^{\Delta NLS/\Delta NLS}$ brains.

Gene ontology analysis showed that transcripts whose expression was upregulated in $Fus^{\Delta NLS/\Delta NLS}$ animals were enriched for genes involved in mRNA translation and extracellular matrix constituents (Dataset EV4). In contrast, transcripts upregulated in $Fus^{-/-}$ brains revealed enrichment for nuclear and nucleolar proteins involved in the regulation of transcription, DNA replication, or regulation of RNA metabolic processes (Dataset EV5). Gene ontology

Figure 4. FUS-dependent expression changes in mouse brain.

A RNA-seq reads from brain of homozygous knockin ($Fus^{\Delta NLS/\Delta NLS}$, upper panel), homozygous knockout ($Fus^{-/-}$, middle panel), and control ($Fus^{+/+}$, lower panel) mice showing the absence of exon 15 (red arrow) in *Fus* mRNA in $Fus^{\Delta NLS/\Delta NLS}$ mice, while the entire *Fus* transcript is absent in $Fus^{-/-}$ mice (green arrows).

B Heat map with hierarchical clustering of RNA-seq data from biological replicates of $Fus^{\Delta NLS/\Delta NLS}$ ($N = 5$) and control littermates ($N = 4$), showing genes differentially regulated between both genotypes among which 237 are upregulated and 549 are downregulated in $Fus^{\Delta NLS/\Delta NLS}$ animals as defined by $P < 0.05$ adjusted for multiple testing.

C Heat map with hierarchical clustering of RNA-seq data from biological replicates of $Fus^{-/-}$ ($N = 5$) and control littermates ($N = 5$), showing genes differentially regulated between both genotypes, among which 669 are upregulated and 889 are downregulated in $Fus^{-/-}$ animals as defined by $P < 0.05$ adjusted for multiple testing.

D Venn diagram showing the number of overlapping genes misregulated in $Fus^{\Delta NLS/\Delta NLS}$ (blue circle) and $Fus^{-/-}$ (red circle) brains with 353 genes similarly downregulated or upregulated upon cytoplasmic mislocalization or complete loss of FUS.

E Normalized expression (based on FPKM from RNA-seq) of genes identified by RNA-seq to be significantly downregulated (*Ahi1, Kcnip1, Nefm, Nefl, Tuba4a, Dmpk, Rad9b, Stac3, Hist1h2bc, Hist1h1c*) or upregulated (*Fam193b, Pmm2, Bphl, Taf15*) in both $Fus^{\Delta NLS/\Delta NLS}$ and $Fus^{-/-}$ compared to their control. Error bars represent SEM in 4-5 biological replicates. $^{**}P < 0.01$, two-tailed student's *t*-test.

F Normalized expression (based on FPKM from RNA-seq) of genes identified by RNA-seq to be uniquely changed in $Fus^{\Delta NLS/\Delta NLS}$ mice (*Trove2, Uhmk1, Ssh3, Vtn, Snrpb, Ephb3*). Error bars represent SEM in 4–5 biological replicates. $^{*}P < 0.05$, $^{**}P < 0.01$, two-tailed Student's *t*-test.

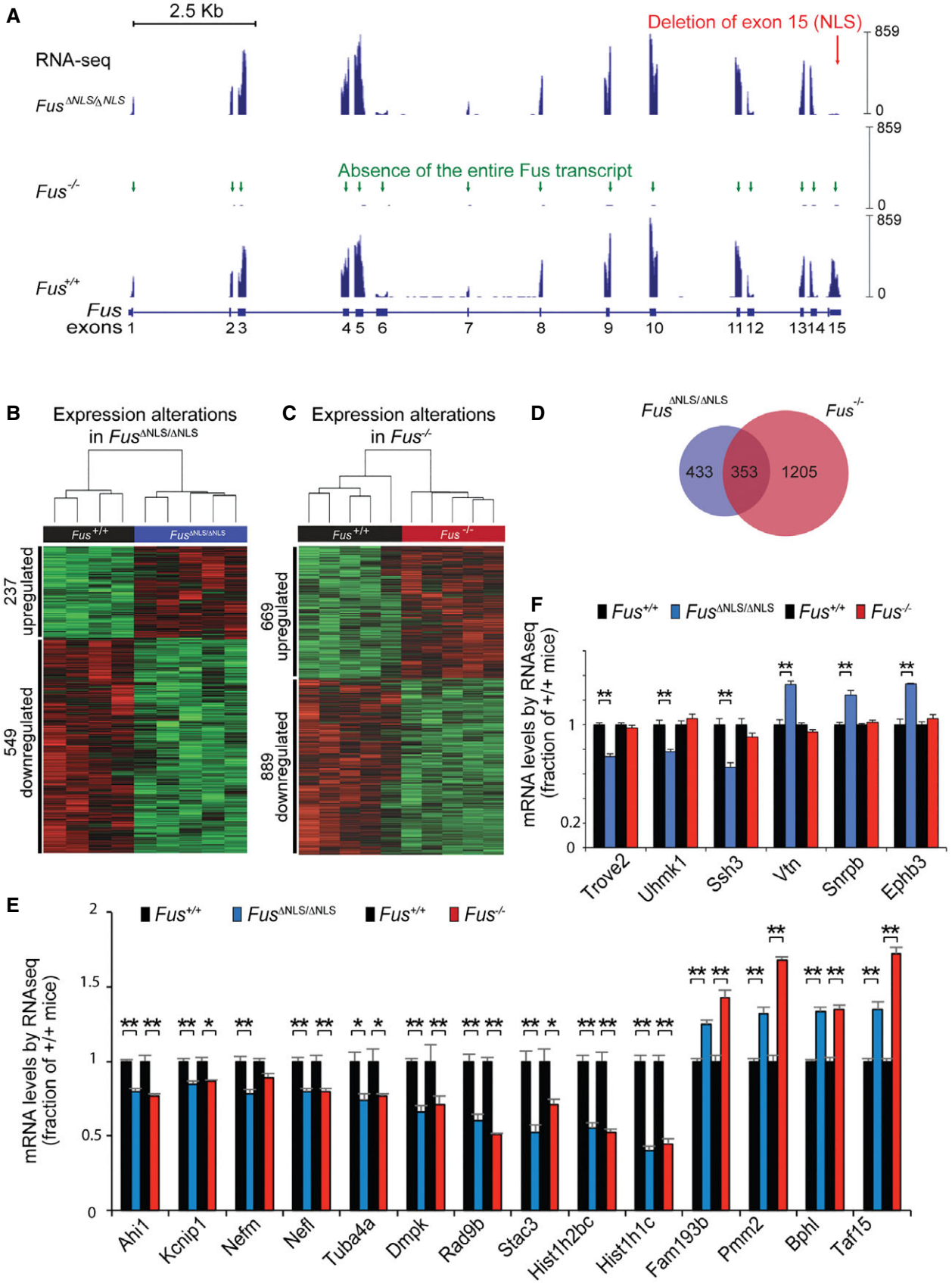
A
2.5 Kb
RNA-seq
Deletion of exon 15 (NLS)
Absence of the entire Fus transcript
Fus exons 1 2 3 4 5 6 7 8 9 10 11 12 13 14 15
B
Expression alterations in FusΔNLS/ΔNLS
237 upregulated
549 downregulated
C
Expression alterations in Fus-/-
669 upregulated
889 downregulated
D
433
353
1205
E
mRNA levels by RNAseq (fraction of +/+ mice)
Ahi1
Kcnip1
Nefm
Nefl
Tuba4a
Dmpk
Rad9b
Stac3
Hist1h2bc
Hist1h1c
Fam193b
Pmm2
Bphl
Taf15
F
mRNA levels by RNAseq (fraction of +/+ mice)
Trove2
Uhmk1
Ssh3
Vtn
Snrpb
Ephb3

Figure 4.

analysis revealed a similar enrichment for synaptic activity and function among transcripts downregulated in $Fus^{\Delta NLS/\Delta NLS}$ and $Fus^{-/-}$ animals (Datasets EV4 and EV5), supporting that cytoplasmic mislocalization of FUS alters the expression of genes involved in synaptogenesis, as a direct consequence of FUS loss of function. Contrastingly, gain of function elicited by cytoplasmic FUS might be more related to alterations in genes related to mRNA translation and extracellular matrix.

Widespread splicing alterations induced by cytoplasmic mislocalization and loss of FUS

To further compare the molecular changes elicited by cytoplasmic FUS mislocalization and FUS loss of function, we asked whether regulation of mRNA splicing was similarly affected in E18.5 brains of $Fus^{\Delta NLS/\Delta NLS}$ mice and $Fus^{-/-}$ mice. To characterize mRNA splicing, we exploited the RNA-mediated oligonucleotide annealing, selection, and ligation with next-generation sequencing (RASL-seq) method (Li *et al*, 2012; Zhou *et al*, 2012). This approach allowed us to quantitatively profile 3,859 unique alternative splicing events that correspond to exon inclusion or skipping events conserved between mouse and human (Fig EV4). Ratios of shorter to longer mRNA isoform counts were calculated and used to statistically compare the splicing changes between different groups. Unsupervised hierarchical clustering for all splicing events showed that mutant and deleted *Fus* mice clustered apart from their controls (Fig EV4B and C). In $Fus^{\Delta NLS/\Delta NLS}$ brains, 9.3% (173 events) of the 1,852 detected splicing events were different from controls, with 101 increased long splicing isoforms and 72 enhanced short isoforms (defined by *t*-test with $P < 0.05$ and average fold change > 1.5) (Fig 5A and Dataset EV6). Heterozygous $Fus^{\Delta NLS/+}$ mice clustered with wild-type mice demonstrating that their splicing profile is not significantly altered (Appendix Fig S2). Nevertheless, heat map of the 173 events significantly changed in homozygous $Fus^{\Delta NLS/\Delta NLS}$ mice showed an intermediate pattern in $Fus^{\Delta NLS/+}$ heterozygous littermates supporting a partial loss of FUS function in these mice (Appendix Fig S2). In $Fus^{-/-}$ brains, 17.9% (252 events) of the 1,406 detected splicing events were different from control littermates, with 118 increased long isoforms and 134 enhanced short isoforms (Fig 5B and Dataset EV7).

Comparison of the splicing changes between $Fus^{\Delta NLS/\Delta NLS}$ and $Fus^{-/-}$ mice revealed a striking overlap between both models. Seventy-five splicing events were commonly regulated in $Fus^{\Delta NLS/\Delta NLS}$ and $Fus^{-/-}$ mice, 100% of which were differentially included or excluded in the same direction (Fig EV4D and E and Dataset EV8).

Semi-quantitative RT–PCR of selected RNAs confirmed these FUS-dependent splicing changes (Figs 5C and EV4F), including transcripts previously implicated in neurodegenerative diseases such as the N-myc downstream-regulated gene 2 (*Ndrg2*) that is misaccumulated in Alzheimer's disease (Mitchelmore *et al*, 2004), the microtubule-associated protein tau (*Mapt*) gene mutated in frontotemporal dementia (Hutton *et al*, 1998), the ataxin 2 (*Atxn2*) gene mutated in ALS (Elden *et al*, 2010), spinocerebellar ataxia type 2 (SCA2) (Imbert *et al*, 1996), and the pro-neurotrophin receptor sortilin 1 (*Sort1*) (Hu *et al*, 2010). Interestingly, inclusion of sortilin 1 exon 17b [also referred to as exon 18 in Polymenidou *et al* (2011)] was previously associated with low levels of TDP-43 (Polymenidou *et al*, 2011; Prudencio *et al*, 2012) and found significantly increased in cortex of FTD patients with TDP-43 proteinopathy (Prudencio *et al*, 2012). Here, we observe that *Fus* mutation and deletion have an opposite effect on sortilin 1 as compared to TDP-43, with decreased inclusion of exon 17b in embryonic brains from both $Fus^{\Delta NLS/\Delta NLS}$ and $Fus^{-/-}$ mice (Figs 5C and EV4F).

Despite expected developmental differences in the alternative splicing patterns of embryonic and adult brains, 57 splicing events found misregulated by RASL-seq in $Fus^{\Delta NLS/\Delta NLS}$ and $Fus^{-/-}$ mice were also identified by Affymetrix microarrays in striatum from adult wild-type mice with antisense oligonucleotide-mediated depletion of *Fus* (Lagier-Tourenne *et al*, 2012), or in embryonic brains from another *Fus* knockout model that expresses low levels of truncated FUS protein (Hicks *et al*, 2000; Lagier-Tourenne *et al*, 2012). Among FUS-dependent alterations, abnormal splicing of *Mapt* exon 10 (Figs 5C and EV4F) is of particular relevance for disease pathogenesis as mutations enhancing exon 10 inclusion are linked to frontotemporal dementia (Liu & Gong, 2008). While in embryonic mouse brains the predominant mRNA isoforms of *Mapt* do not include exon 10 and encode for tau protein with three microtubule binding repeats (3R-tau) (McMillan *et al*, 2008; Dillman *et al*, 2013), we observed increased inclusion of exon 10 encoding for the 4-repeat tau isoform (4R tau) in both $Fus^{\Delta NLS/\Delta NLS}$ and $Fus^{-/-}$ mice. In all, splicing alterations caused by cytoplasmic FUS mislocalization are largely overlapping with those elicited by complete loss of FUS. Nevertheless, a subset of events were uniquely found in $Fus^{\Delta NLS/\Delta NLS}$ (Fig EV4D), which may be the consequence of functional disruption of other RNA-binding proteins by abnormal accumulation of FUS in the cytoplasm.

Cytoplasmic mislocalization of FUS leads to increased perinatal motor neuron apoptosis

We next asked whether perinatal death of $Fus^{\Delta NLS/\Delta NLS}$ and $Fus^{-/-}$ mice was accompanied by loss of motor neurons in the lumbar spinal cord. Immunostaining for choline acetyltransferase (ChAT), which specifically labels large motor neurons in the spinal cord ventral horn, revealed that the number of motor neurons was reduced by approximately 30% in $Fus^{\Delta NLS/\Delta NLS}$ mice as compared with both $Fus^{+/+}$ and $Fus^{\Delta NLS/+}$ mice (Fig 6A and B). To exclude

Figure 5. FUS-dependent alternative splicing alterations in mouse brain.

A Heat map with hierarchical clustering of RASL-seq data from biological replicates of $Fus^{\Delta NLS/\Delta NLS}$ ($N = 4$) and control littermates ($N = 4$), showing 173 alternative splicing alterations associated with expression of cytoplasmic FUS in knockin animals.

B Heat map with hierarchical clustering of RASL-seq data from biological replicates of $Fus^{-/-}$ ($N = 5$) and control littermates ($N = 5$), showing 252 alternative splicing alterations associated with loss of FUS in knockout animals.

C Semi-quantitative RT–PCR analyses of selected targets. Left panels show representative acrylamide gel pictures of RT–PCR products. Quantification of splicing changes from at least three biological replicates of $Fus^{\Delta NLS/\Delta NLS}$ (blue bars) and $Fus^{-/-}$ (red bars) compared to their control littermates ($Fus^{+/+}$, black bars) by semi-quantitative RT–PCR (middle panel) and RASL-seq (right panel) are shown. Error bars represent SEM. $^{*}P < 0.05$, $^{**}P < 0.01$, two-tailed Student's *t*-test.

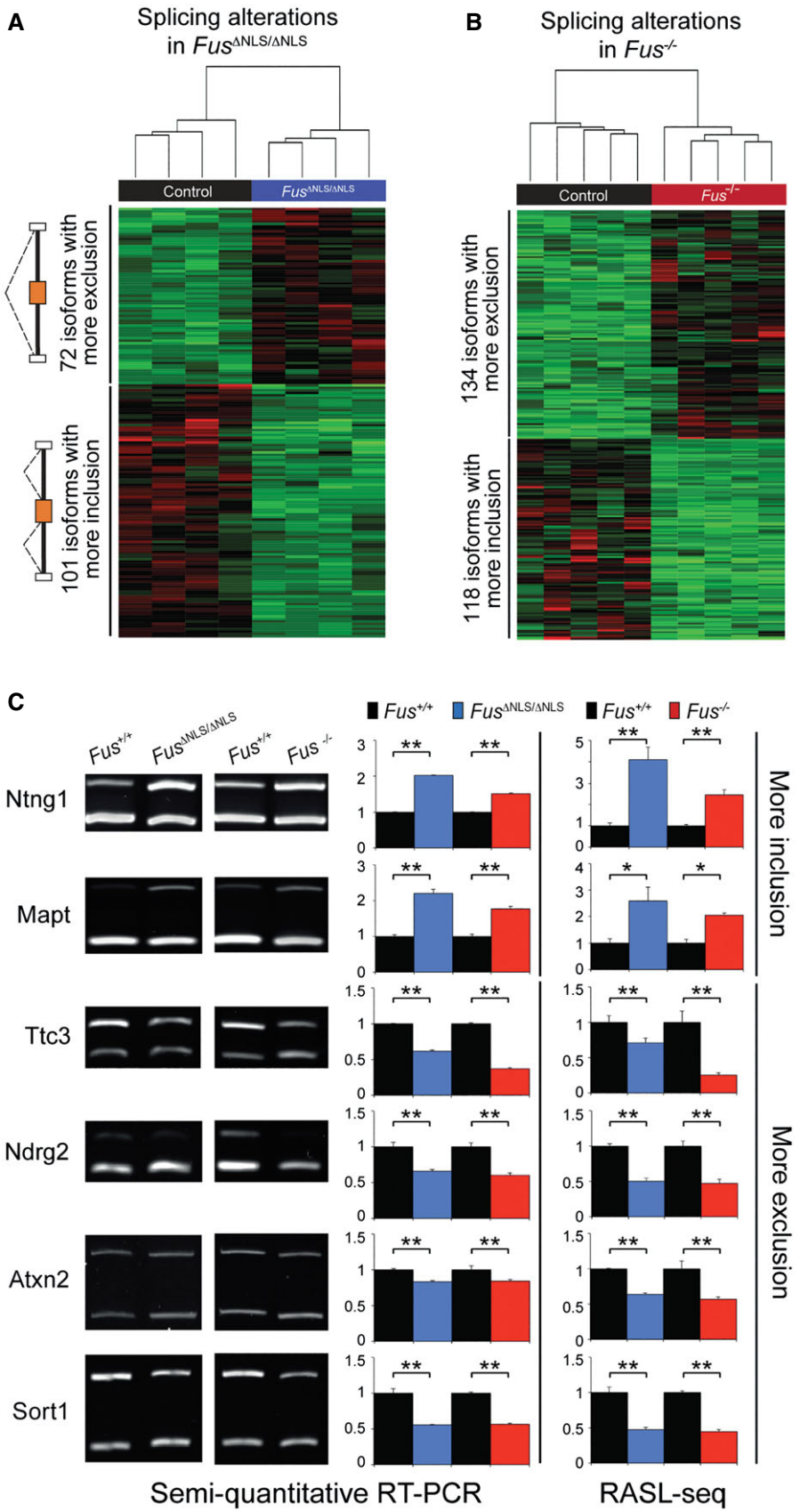

Figure 5.

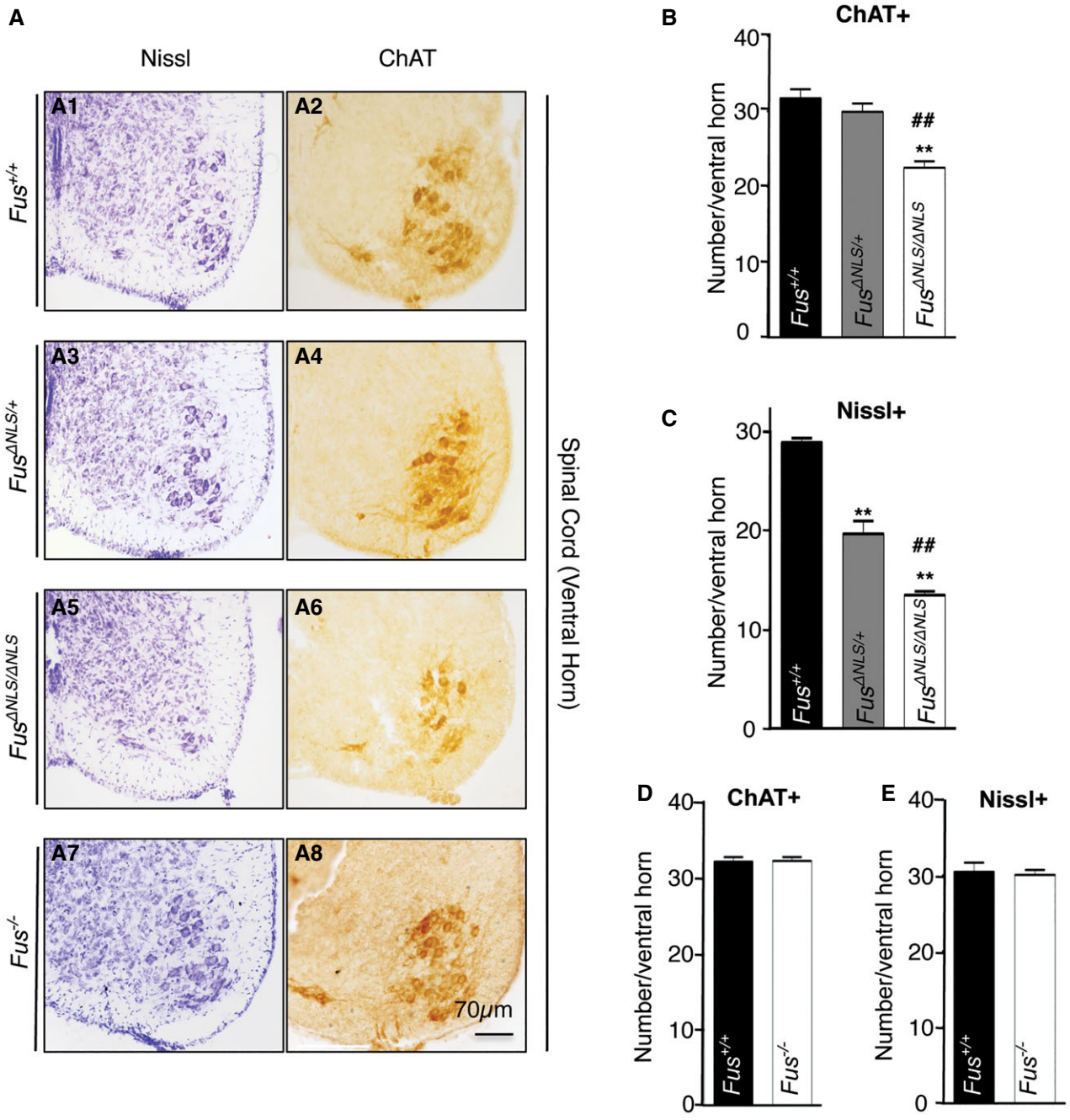

Figure 6. Motor neuron loss in $Fus^{\Delta NLS/\Delta NLS}$ mice.

A Representative light microscopy images of spinal cord sections of $Fus^{+/+}$, $Fus^{\Delta NLS/+}$, $Fus^{\Delta NLS/\Delta NLS}$, and $Fus^{-/-}$ mice at birth stained with cresyl violet (Nissl, A^1, A^3 A^5, A^7), or anti-choline acetyltransferase (ChAT, A^2, A^4 A^6, A^8).

B, C Quantification of $ChAT^+$ motor neurons (B) and $Nissl^+$ motor neurons (defined as Nissl-positive cells with a soma area > 80 μm^2) (C) per spinal cord ventral horn in $Fus^{\Delta NLS/\Delta NLS}$ mice (mean ± SEM). For $Nissl^+$ $N = 8$ $Fus^{+/+}$, $N = 5$ $Fus^{\Delta NLS/+}$, $N = 7$ $Fus^{\Delta NLS/\Delta NLS}$, and for $ChAT^+$ $N = 7$ per genotype, $^{**}P < 0.01$ versus $Fus^{+/+}$, $^{\#\#}P < 0.01$ versus $Fus^{\Delta NLS/+}$; one-way ANOVA followed by Tukey's *post hoc* test.

D–E Quantification of $ChAT^+$ (D) and $Nissl^+$ (E) motor neurons per spinal cord ventral horn in $Fus^{-/-}$ mice (mean ± SEM). $N = 6$ per genotype, no significant differences were found, by Student's unpaired *t*-test.

the possibility that this reduced number of ChAT-positive motor neurons reflected downregulation of ChAT expression rather than loss of motor neurons, we also performed Nissl staining, a histochemical stain that does not rely on the expression level of a specific marker. Quantification of neurons with an area of ≥ 80 μm^2 revealed a 50% reduction in the number of large motor neurons in the ventral horn of $Fus^{\Delta NLS/\Delta NLS}$ newborn mice (Fig 6C). Interestingly, $Fus^{\Delta NLS/+}$ mice displayed a smaller but statistically significant

loss of large Nissl-stained cells, suggesting that motor neurons were also affected in these mice despite showing normal numbers of ChAT-positive cells. In striking contrast with the situation in $Fus^{\Delta NLS/\Delta NLS}$ mice, spinal motor neuron counts were similar between $Fus^{-/-}$ mice and their wild-type littermates (Fig 6A, D and E), demonstrating that the mutant FUS protein expressed in $Fus^{\Delta NLS/\Delta NLS}$ mice is toxic to motor neurons during development. Besides motor neuron degeneration, neither $Fus^{\Delta NLS/\Delta NLS}$ nor $Fus^{-/-}$ mice displayed gross developmental abnormalities of the brain. Indeed, cortical thickness appeared normal in both mouse strains (Appendix Fig S3). In addition, the thickness of layers II-IV and layers V-VI defined by CUX1 and CTIP2 immunofluorescence, respectively, was normal in both mouse strains (Appendix Fig S4).

At birth, mouse motor neurons are still in the developmental period, and motor neurons that did not efficiently create synaptic contacts with muscles undergo apoptosis until P10 (Kanning *et al*, 2010). Supporting an increased perinatal motor neuron apoptosis in $Fus^{\Delta NLS/\Delta NLS}$ mice, the number of apoptotic cells detected by terminal deoxynucleotidyl transferase dUTP nick end labeling (TUNEL) was threefold higher in lumbar spinal cord sections of $Fus^{\Delta NLS/\Delta NLS}$ newborn mice than in wild-type littermates (Fig 7A and B). Furthermore, double immunostaining for ChAT and active caspase-3, labeling motor neurons actively undergoing apoptosis, revealed that motor neuron apoptosis was three times more frequent in $Fus^{\Delta NLS/\Delta NLS}$ than in wild-type littermates (Fig 7C–E). Together, these data indicate that cytoplasmic mislocalization of FUS leads to increased motor neuron death resulting in reduced numbers of lower motor neurons. The absence of motor neuron loss in $Fus^{-/-}$ mice indicates that cytoplasmic FUS accumulation leads to motor neuron death through a toxic gain-of-function mechanism.

Cytoplasmic mislocalization of FUS alters SMN and HDAC1 localization and induces eIF2α phosphorylation

We then asked whether cytoplasmic mislocalization of FUS in $Fus^{\Delta NLS/\Delta NLS}$ mice would affect the subcellular localization of some of its interaction partners. Immunostaining for SMN1 revealed that SMN1-positive nuclear gems were lost in motor neurons of $Fus^{\Delta NLS/\Delta NLS}$ mice (Fig 8A), as in cells from ALS patients and mouse models (Yamazaki *et al*, 2012; Tsuiji *et al*, 2013; Sun *et al*, 2015; Yu *et al*, 2015) and consistent with enhanced interaction between mutant FUS and SMN1 (Yamazaki *et al*, 2012; Gerbino *et al*, 2013; Groen *et al*, 2013; Sun *et al*, 2015; Yu *et al*, 2015). Furthermore, HDAC1, another FUS interaction partner (Wang *et al*, 2013), showed profoundly abnormal immunoreactivity in $Fus^{\Delta NLS/\Delta NLS}$ mice. Indeed, HDAC1 was diffusely nuclear in cells from wild-type spinal cords, while in $Fus^{\Delta NLS/\Delta NLS}$ animals HDAC1 immunoreactivity was condensed in 1–3 nuclear foci per cell (Fig 8B). Double immunofluorescence in spinal cords from control animals found a weak HDAC1 staining in ChAT-positive motor neurons contrasting with a strong nuclear signal in neighboring cells. The pattern was strikingly different in $Fus^{\Delta NLS/\Delta NLS}$ animals with HDAC1 aggregation into nuclear foci in ChAT-positive motor neurons (Fig 8C). In contrast to SMN1 and HDAC1, the binding partner of FUS TAF15 remained mostly nuclear in motor neurons from $Fus^{\Delta NLS/\Delta NLS}$ mice (Appendix Fig S5). Thus, cytoplasmic mislocalization of FUS perturbs the localization, and potentially the function, of specific interaction partners in motor neurons.

In autopsy material of ALS-FUS patients, FUS-containing cytoplasmic aggregates are found in neurons and glial cells. These aggregates are usually also immunopositive for ubiquitin (Vance *et al*, 2009; Baumer *et al*, 2010; Huang *et al*, 2010; Kobayashi *et al*, 2010; Tateishi *et al*, 2010). Despite motor neuron loss in $Fus^{\Delta NLS/\Delta NLS}$ mice, we did not observe FUS-positive (Fig 1E and F) aggregates in motor neurons or cortical neurons of newborn $Fus^{\Delta NLS/\Delta NLS}$ mice. We also did not observe ubiquitin-positive, poly-ubiquitin-positive, or neurofilament-positive aggregates in the ventral spinal cord of $Fus^{\Delta NLS/\Delta NLS}$ mice (Fig EV5A and B). As FUS is recruited to stress granules, and since neuropathology revealed that cytoplasmic protein aggregates in ALS-FUS patients stain positive for stress granule markers (Baumer *et al*, 2010; Dormann *et al*, 2010; Liu-Yesucevitz *et al*, 2010), we evaluated the distribution of TIAR, a stress granule marker in the spinal cord ventral horn in $Fus^{\Delta NLS/\Delta NLS}$ mice. TIAR displayed a similar diffuse cytosolic pattern in motor neurons of $Fus^{\Delta NLS/\Delta NLS}$ and control mice (Fig EV5C). As an additional marker for cellular stress, we evaluated eIF2α phosphorylation, which occurs in response to cellular stress and results in decreased global protein translation (Holcik & Sonenberg, 2005; Sonenberg & Hinnebusch, 2009). Immunostaining for the phosphorylated form of eIF2α revealed a diffuse cytoplasmic staining that was substantially more intense in spinal motor neurons of $Fus^{\Delta NLS/\Delta NLS}$ mice as compared to controls (Fig 8D) reflecting cellular stress in $Fus^{\Delta NLS/\Delta NLS}$ motor neurons, with consequent repression of protein translation.

Taken together, cytoplasmic mislocalization of FUS in motor neurons led to altered subcellular localization of several of its binding partners accompanied by stress-induced translational repression, but without the induction of protein aggregation or stress granule formation.

Cytoplasmic FUS mislocalization is intrinsically toxic to motor neurons

We subsequently asked whether FUS mislocalization within motor neurons is necessary to induce motor neuron loss in $Fus^{\Delta NLS/\Delta NLS}$ mice and therefore evaluated whether restricted expression of wild-type FUS in motor neurons could rescue their survival despite accumulation of the mutant protein in neighboring cells. We exploited the presence of loxP sites flanking the STOP cassette (Fig 1A) to selectively revert the ΔNLS allele to wild type in motor neurons. For this purpose, $Fus^{\Delta NLS/+}$ mice were crossed to mice expressing the CRE recombinase from the *ChAT* locus, which leads to CRE recombinase activity in virtually all cholinergic neurons (Rossi *et al*, 2011; Saxena *et al*, 2013). We expected that $Fus^{\Delta NLS/\Delta NLS}$/ChAT-CRE mice would express truncated FUS protein ubiquitously, except for cholinergic neurons. Double immunostaining for FUS and ChAT on spinal cord sections of $Fus^{\Delta NLS/\Delta NLS}$/*ChAT*-CRE newborn mice revealed that FUS nuclear localization was indeed largely restored in cholinergic neurons in the ventral spinal cord, but not in other neighboring cells, consistent with motor neuron selective CRE expression (Fig 9A). The rescue of FUS nuclear localization was either complete or only partial, with in the latter case motor neurons showing mixed cytoplasmic/nuclear FUS localization (Fig 9A), consistent with CRE having successfully recombined at least one $Fus^{\Delta NLS}$ allele to wild type. Neonatal lethality of $Fus^{\Delta NLS/\Delta NLS}$ mice was not rescued by the

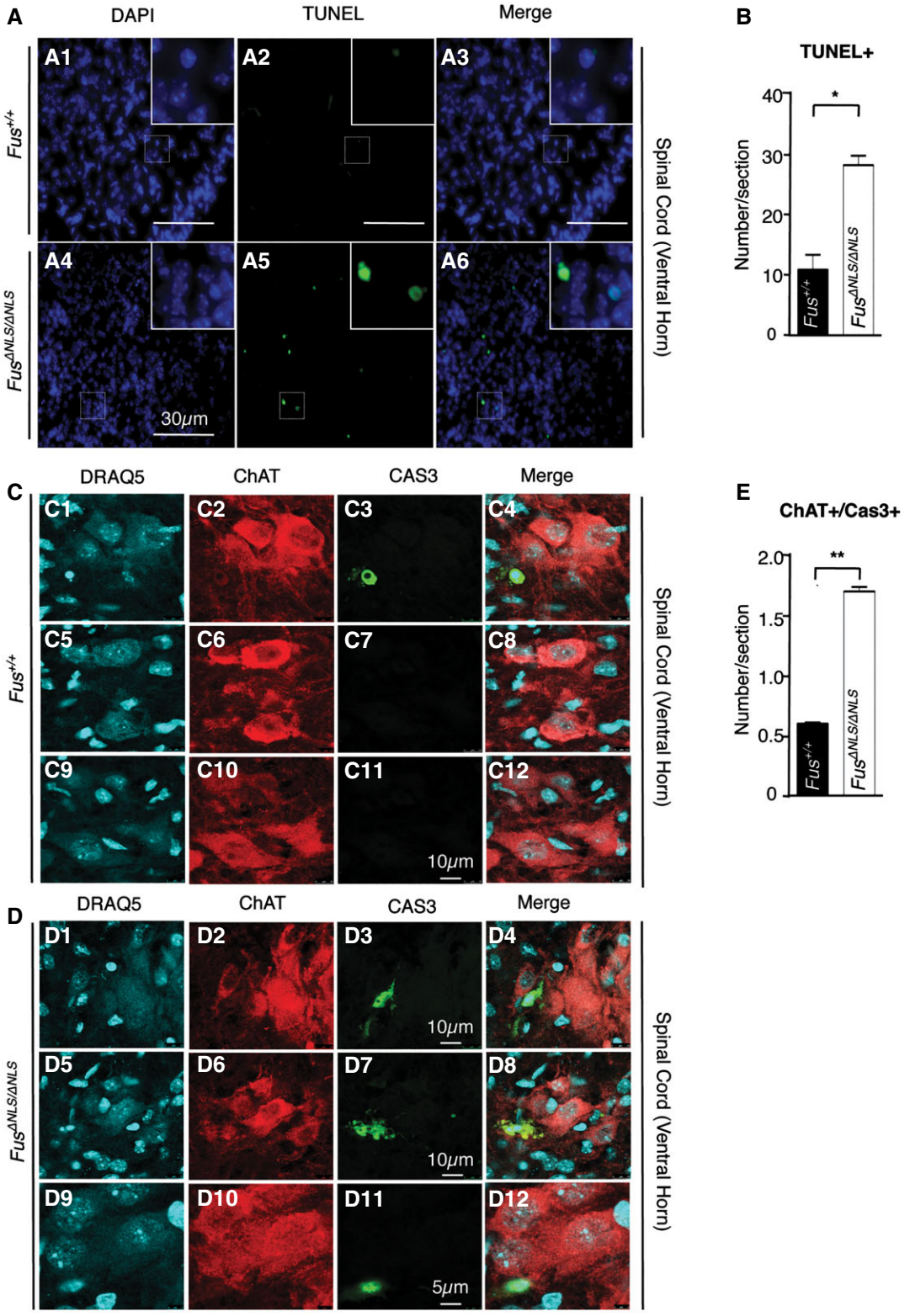

Figure 7. Motor neuron apoptosis in *Fus*$^{\Delta NLS/\Delta NLS}$ mice.

A Representative images of TUNEL assay in spinal cord of *Fus*$^{\Delta NLS/\Delta NLS}$ mice (A^4-A^6) and *Fus*$^{+/+}$ mice (A^1-A^3).

B Quantification of the total number of TUNEL and DRAQ5 (blue) double-positive cells in *Fus*$^{\Delta NLS/\Delta NLS}$ and *Fus*$^{+/+}$ per spinal cord section. Mean ± SEM, $N = 3$ per genotype, $^*P < 0.05$, by Student's unpaired *t*-test.

C, D Immunofluorescence microscopy of spinal cord of *Fus*$^{+/+}$ (C) and *Fus*$^{\Delta NLS/\Delta NLS}$ (D) mice showing active caspase-3 (green), ChAT (red), and DNA (cyan, DRAQ5).

E Quantification of caspase-3 (Cas3)/ChAT/DRAQ5 triple-positive cells in *Fus*$^{\Delta NLS/\Delta NLS}$ mice. Mean ± SEM, $N = 7$ per genotype, $^{**}P < 0.01$, by Student's unpaired *t*-test.

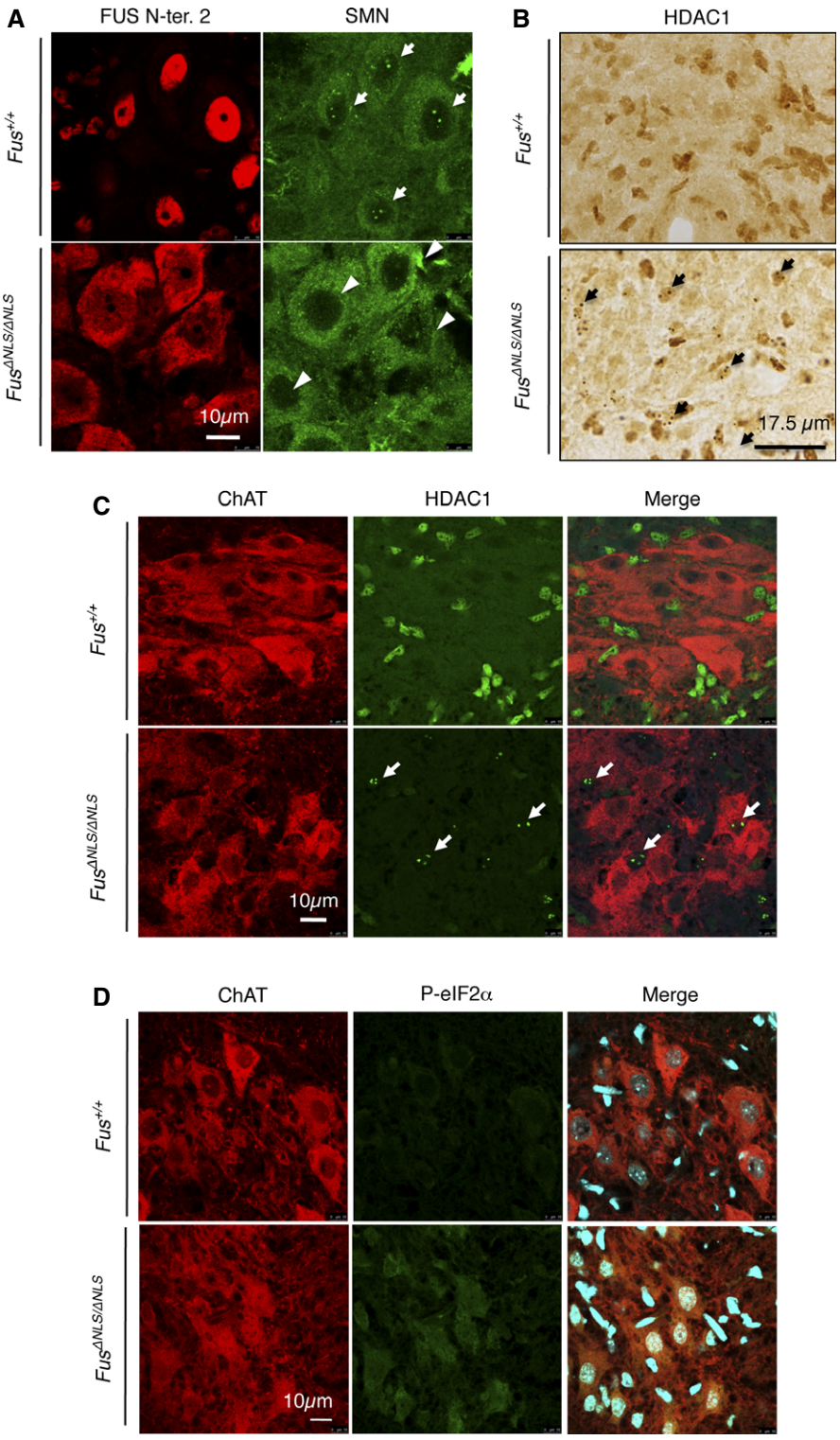

Figure 8. Alterations of SMN, HDAC1, and eIF2α in *Fus*$^{\Delta NLS/\Delta NLS}$ mice.

A Representative images of SMN (green) immunofluorescence in spinal cord. Nuclear gems, corresponding to SMN-immunoreactive foci in nuclei, are marked by arrows.

B HDAC1 immunoreactivity in spinal cord sections of *Fus*$^{+/+}$ and *Fus*$^{\Delta NLS/\Delta NLS}$ mice. Arrows point to HDAC1-immunoreactive nuclear foci.

C Representative images of immunofluorescence staining of motor neurons, labeled with ChAT (red) and HDAC1 (green). Examples of HDAC1 immunoreactive foci in motor neurons are indicated by arrows.

D Representative images of immunofluorescence staining of motor neurons labeled with ChAT (red) and phosphorylated eIF2α (green), a general translational stress response marker. DRAQ5 (cyan) was used to label nuclei.

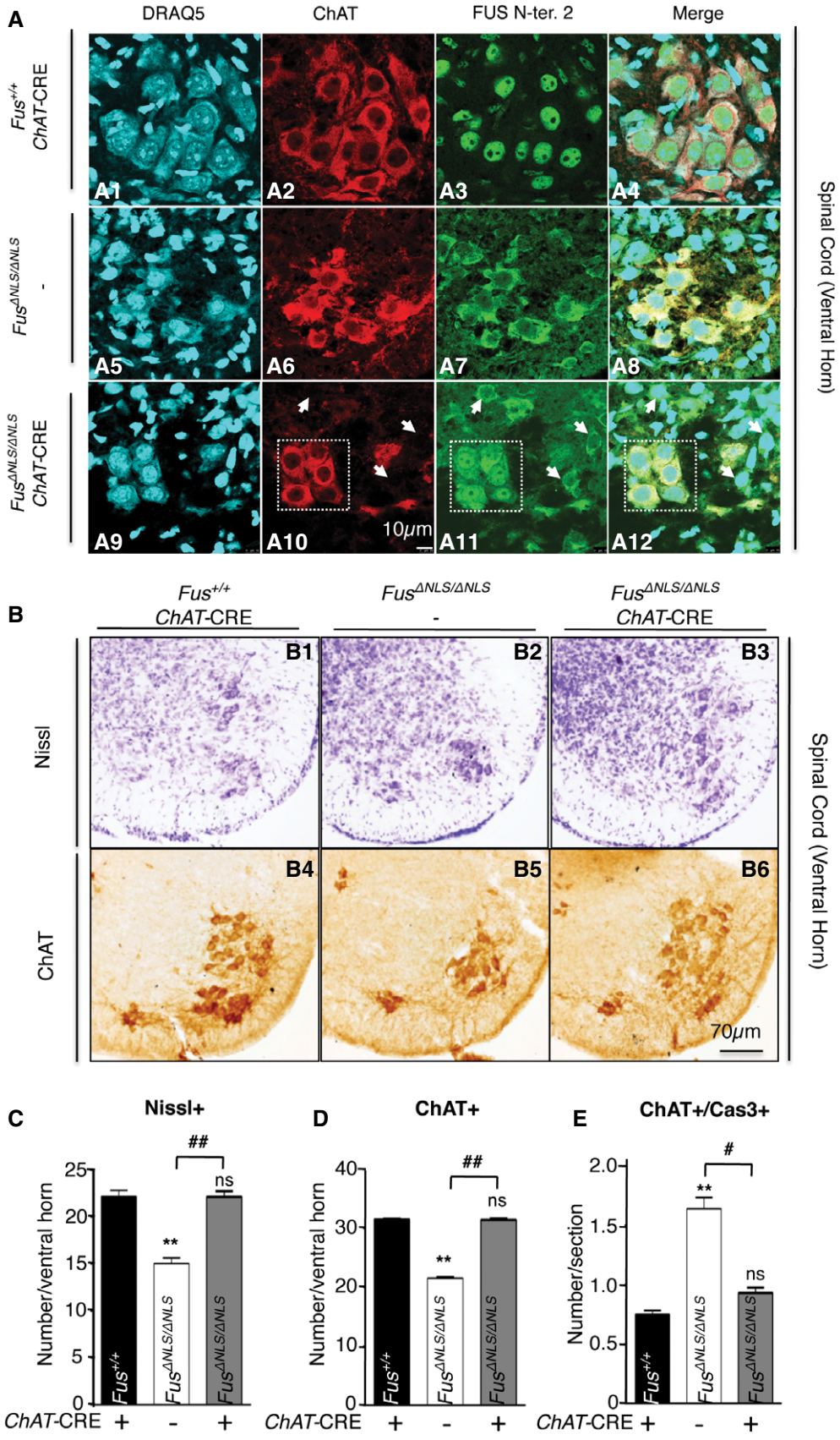

Figure 9.

Figure 9. Selective restoration of FUS nuclear import in motor neurons rescues motor neuron loss.

A Double immunolabeling of spinal cord neurons with ChAT (red) and N-terminal FUS antibody (green). Nuclei were visualized with DRAQ5 (blue). Cellular localization of FUS was analyzed in the ventral spinal cord of $Fus^{+/+}$/*ChAT*-CRE (A^1-A^4), $Fus^{\Delta NLS/\Delta NLS}$/− ($A^5$-$A^8$), and $Fus^{\Delta NLS/\Delta NLS}$/*ChAT*-CRE ($A^9$-$A^{12}$). FUS was completely nuclear in ChAT$^+$ neurons of $Fus^{+/+}$/*ChAT*-CRE, while cytoplasmic in $Fus^{\Delta NLS/\Delta NLS}$/−. In the ventral horn of $Fus^{\Delta NLS/\Delta NLS}$/*ChAT*-CRE mice, ChAT$^+$ neurons (motor neurons, e.g., within the dashed square) displayed nuclear FUS immunoreactivity, while ChAT-negative cells retained cytoplasmic FUS immunoreactivity (arrows).

B Representative light microscopy images of spinal cord sections of $Fus^{+/+}$/*ChAT*-CRE (B^1, B^4), $Fus^{\Delta NLS/\Delta NLS}$/− ($B^2$, B^5), and $Fus^{\Delta NLS/\Delta NLS}$/*ChAT*-CRE ($B^3$, B^6) mice at birth stained with cresyl violet (Nissl, B^1-B^3) or anti-choline acetyltransferase (ChAT, B^4-B^6).

C, D Quantification of Nissl$^+$ (C) and ChAT$^+$ (D) motor neurons per spinal cord ventral horn. Mean ± SEM, $N = 9$ $Fus^{+/+}$/*ChAT*-CRE, $N = 8$ $Fus^{\Delta NLS/\Delta NLS}$/−, and $N = 4$ $Fus^{\Delta NLS/\Delta NLS}$/*ChAT*-CRE for Nissl$^+$, and $N = 11$ $Fus^{+/+}$/*ChAT*-CRE, $N = 7$ $Fus^{\Delta NLS/\Delta NLS}$/−, and $N = 8$ $Fus^{\Delta NLS/\Delta NLS}$/*ChAT*-CRE for ChAT$^+$; (**) $P < 0.01$ versus $Fus^{+/+}$, $^{\#\#}P < 0.01$ versus $Fus^{\Delta NLS/+}$; (ns) non-significant; one-way ANOVA followed by Tukey's *post hoc* test.

E Total numbers of caspase-3 (Cas3)/ChAT/DAPI triple-positive cells in $Fus^{+/+}$/*ChAT*-CRE, $Fus^{\Delta NLS/\Delta NLS}$/−, and $Fus^{\Delta NLS/\Delta NLS}$/*ChAT*-CRE mice. $N = 9$ $Fus^{+/+}$/*ChAT*-CRE, $N = 7$ $Fus^{\Delta NLS/\Delta NLS}$/−, and $N = 8$ $Fus^{\Delta NLS/\Delta NLS}$/*ChAT*-CRE; $^{**}P < 0.01$ versus $Fus^{+/+}$, $^{\#}P < 0.05$ versus $Fus^{\Delta NLS/+}$; (ns) non-significant; one-way ANOVA followed by Tukey's *post hoc* test.

ChAT-CRE allele, suggesting that expression of mutant FUS in motor neurons is not the main contributor of neonatal lethality in homozygous mice. Last, we evaluated whether restoration of FUS nuclear localization in motor neurons would prevent motor neuron loss in $Fus^{\Delta NLS/\Delta NLS}$ mice. This approach revealed that the presence of a *ChAT*-CRE allele was indeed sufficient to fully rescue motor neuron loss (Fig 9B–D), as well as restore a normal number of caspase-3-positive motor neurons (Fig 9E). These findings establish that cytoplasmic FUS mislocalization within motor neurons is required to induce their loss in $Fus^{\Delta NLS/\Delta NLS}$ mice.

Discussion

FUS and other related RBPs form cytoplasmic inclusions associated with nuclear clearance in affected cells from ALS and FTD patients. An outstanding question is whether disease is caused by gain of cytoplasmic toxicity or by loss of the nuclear function of the respective RBP. To gain insight into this conundrum, we targeted the FUS locus to generate two novel mouse models. In the first model, the last exon of *Fus* is no longer transcribed, resulting in the production of a truncated FUS protein that lacks the NLS and localizes almost exclusively to the cytoplasm (Fig 1). The second model results in complete loss of FUS expression (Fig 3). A thorough comparison of these two models allowed us to determine whether a gain of a toxic cytoplasmic function is required for the observed phenotypes.

Interestingly, this approach revealed that $Fus^{\Delta NLS/\Delta NLS}$ and $Fus^{-/-}$ mice share several features: both mouse models die shortly after birth due to respiratory insufficiency and exhibit reduced body weight and size. Transcriptomic analysis also revealed overlapping alterations in RNA levels and splicing. However, a reduced number of spinal motor neurons associated with increased perinatal motor neuron apoptosis and a subset of expression and splicing changes were uniquely found in $Fus^{\Delta NLS/\Delta NLS}$ mice (Figs 4, 5, 6 and 7). Thus, FUS mislocalization to the cytoplasm with reduced levels of nuclear FUS is associated with phenotypes linked to loss of FUS function, but also with motor neuron death induced by a gain of toxicity mechanism that is not recapitulated in the knockout mouse model (Fig 6). The notion that loss of FUS function may not be sufficient to induce motor neuron degeneration is also supported by two recent reports. First, in an outbred genetic background, homozygous *Fus* gene trap mice reached 2 years of age without manifesting ALS-like phenotypes or motor neuron loss (Kino *et al*, 2015). Second, selective inactivation of the FUS homolog *cabeza* in neurons of adult *Drosophila* did not affect motor performance or life span, indicating that *cabeza* is not required for maintenance of neuronal function in adults (Frickenhaus *et al*, 2015). Here, we demonstrate that loss of FUS function is not sufficient and that gain of function by cytoplasmic redistribution of FUS is necessary to elicit motor neuron apoptosis. Notably, RNA-seq and RASL-seq experiments showed that the ΔNLS mutation triggered a partial loss of FUS function in splicing and gene expression regulation. Loss of function, although not sufficient, may be necessary in $Fus^{\Delta NLS/\Delta NLS}$ mice to induce motor neuron death. Indeed, a number of genes involved in synaptogenesis and/or in neurodegenerative diseases show altered expression (*Ahi1, Dmpk, Nefl, Nefm, Tuba4a, Taf15*) or splicing (*Ndrg2, Mapt, Atxn2, Sort1*) in $Fus^{\Delta NLS/\Delta NLS}$ and $Fus^{-/-}$ mice (Figs 4 and 5), and these alterations linked to loss of FUS nuclear function may weaken the motor neuron and sensitize it to the toxic effects of cytoplasmic FUS accumulation.

Importantly, we showed that motor neuron death in $Fus^{\Delta NLS/\Delta NLS}$ mice could be prevented by selectively restoring FUS nuclear import in motor neurons (Fig 9), demonstrating that FUS cytoplasmic mislocalization within motor neurons is required to induce motor neuron loss. The observation that cytoplasmic mislocalization of FUS is intrinsically toxic to motor neurons contrasts with the non-cell-autonomous contribution to motor neuron degeneration demonstrated for *SOD1* mutations (Boillee *et al*, 2006). Indeed, abrogation of mutant SOD1 expression in motor neurons delayed, but did not prevent, motor neuron degeneration, and a contribution of neighboring cells to SOD1 mediated toxicity is well established (Ilieva *et al*, 2009). Moreover, our data support a degenerative rather than developmental origin of motor neuron loss in newborn $Fus^{\Delta NLS/\Delta NLS}$ mice. The reduced number of motor neurons could have a developmental origin, either by impaired proliferation of motor neuron progenitors or defects in acquisition of motor neuron fate. However, this scenario is unlikely since motor neuron loss in $Fus^{\Delta NLS/\Delta NLS}$ mice can be prevented by ChAT-CRE-induced reversal of the $Fus^{\Delta NLS}$ locus to wild type (Fig 9). Expression of the ChAT gene, which encodes choline acetyl transferase, an enzyme essential for the biosynthesis of acetylcholine, is detectable in postmitotic motor neurons from E11.5 onwards, thus after exit from the cell cycle and acquisition of motor neuron fate at E.9.5 (Chen & Chiu, 1992; Alaynick *et al*, 2011; Cho *et al*, 2014). Therefore, the pathogenic events driving motor neuron loss in $Fus^{\Delta NLS/\Delta NLS}$ mice occur after motor neuron specification. It should be noted that a large proportion of motor neurons showed an incomplete rescue of FUS

nuclear localization. This could be either due to the rescue of one single allele or to the persistence of truncated FUS produced before CRE-mediated recombination. In any case, only a partial rescue of FUS subcellular localization was sufficient to abrogate motor neuron loss.

An attractive hypothesis to explain motor neuron loss in $Fus^{\Delta NLS/\Delta NLS}$ mice is that excessive motor neuron apoptosis happens during the so-called natural cell death period. During development, motor neurons are generated in excess and approximately 40% of the initially generated motor neurons are progressively removed. This process ensures the generation of the appropriate number of motor neurons and guarantees the elimination of motor neurons that did not establish proper neuromuscular junctions. According to the "neurotrophin hypothesis", developing motor neurons compete for limited amounts of neurotrophic factors produced by the muscle targets. Only motor axons that establish stable and functional neuromuscular junctions receive sufficient survival signals and are maintained (Oppenheim, 1991; Kanning *et al*, 2010). Importantly, we found that motor neuron loss elicited by cytoplasmic FUS mislocalization is associated with increased apoptosis of spinal motor neurons (Fig 7). Several motor neuron intrinsic mechanisms may underlie increased motor neuron apoptosis in $Fus^{\Delta NLS/\Delta NLS}$ mice and future studies are needed to investigate these possible mechanisms. For instance, expression of axon guidance receptors may be deregulated in $Fus^{\Delta NLS/\Delta NLS}$ mice, leading to defects in motor axon targeting and failure to receive neurotrophic support. Alternatively, $Fus^{\Delta NLS/\Delta NLS}$ motor axons may reach their targets, but reduced expression of receptors for muscle-derived neurotrophic factors may render a fraction of motor neurons insensitive to survival signals.

Previous work suggested various potential toxic mechanisms for cytoplasmic FUS, and our study sheds light on several of these candidate pathways. First, cytoplasmic FUS could generate toxic FUS aggregates in the cytosol, as shown in yeast models of FUSopathies (Ju *et al*, 2011; Sun *et al*, 2011). Here, we detected neither FUS-positive nor ubiquitin-positive aggregates expected to occur in case of strong ubiquitin proteasome system (UPS) impairment. Thus, at least in this model and at this perinatal age, FUS aggregation or robust FUS-mediated impairment of protein clearance pathways is dispensable for toxicity toward motor neurons. Cytoplasmic FUS could also alter stress granule (SG) dynamics through its localization to SGs upon stress and its regulatory properties toward SG assembly (Li *et al*, 2013). In $Fus^{\Delta NLS/\Delta NLS}$ mice, we did not observe formation of SGs in spinal cord motor neurons using TIAR as a marker, suggesting that major impairment of SG biology is not required for FUS toxicity *in vivo* in this model. However, we observed increased phosphorylation of the translation initiation factor eIF2α, an event known to be caused by cellular stress and to lead to repression of global protein translation (Holcik & Sonenberg, 2005; Sonenberg & Hinnebusch, 2009). Consistent with this scenario, gene ontology analysis of differentially expressed genes also pointed to alterations in mRNA translation as a potential function uniquely altered in $Fus^{\Delta NLS/\Delta NLS}$ mice.

In addition to increased eIF2α phosphorylation, several FUS binding partners are affected in their subcellular localization upon cytoplasmic FUS mislocalization. Firstly, SMN1-positive nuclear gems were lost in $Fus^{\Delta NLS/\Delta NLS}$ motor neurons, likely as a consequence of FUS loss of function, as FUS was shown to be required for gem formation in HeLa cells and primary hippocampal neurons (Yamazaki *et al*, 2012; Tsuiji *et al*, 2013). Intriguingly, nuclear gems were also reduced in fibroblasts from ALS patients with FUS or TDP-43 mutations, and in motor neurons in postmortem lumbar spinal cord from ALS patients (Yamazaki *et al*, 2012; Tsuiji *et al*, 2013; Sun *et al*, 2015). Furthermore, we observed a dramatic concentration of HDAC1 in nuclear foci in $Fus^{\Delta NLS/\Delta NLS}$ neurons. The exact consequences of this abnormal HDAC1 localization remain to be determined, but the pleiotropic functions of HDAC1 in cell survival, axonal damage, and repair of DNA damage (Kim *et al*, 2010; Wang *et al*, 2013) suggest that downstream consequences of abnormal HDAC1 distribution might underlie toxicity. In any case, the abnormal subcellular localizations of HDAC1 and SMN in $Fus^{\Delta NLS/\Delta NLS}$ neurons provide evidence that FUS cytoplasmic mislocalization could lead to alterations in splicing or gene expression through cytoplasmic retention or abnormal trafficking of its interaction partners.

An interesting observation is that both $Fus^{\Delta NLS/\Delta NLS}$ and $Fus^{-/-}$ mice die shortly after birth of respiratory insufficiency, presumably caused by loss of FUS function. A concerted action of several physiological systems is required for newborn mice to breathe normally, and defects in any of these systems can lead to neonatal lethality (Turgeon & Meloche, 2009). Firstly, the respiratory rhythm is generated in the respiratory center in the brainstem and transmitted through the spinal motor neurons to the respiratory muscles (diaphragm and intercostals muscles). Therefore, structural or functional defects of neurons in the respiratory center, motor neurons, neuromuscular junctions, and/or respiratory muscles can lead to respiratory distress. Our observation that neonatal lethality of $Fus^{\Delta NLS/\Delta NLS}$ mice is not rescued by restoration of FUS nuclear import in motor neurons indicates that loss of FUS function in cell types other than motor neurons is sufficient to trigger neonatal lethality. Alternatively, the expression of CRE under the *ChAT* promoter may occur too late in the development to provide a complete rescue of the motor neurons functionality. The remaining cytoplasmic FUS observed in rescued motor neurons could result either from a long half-life of FUS protein in motor neurons or from CRE-mediated recombination of only one allele. Thus, rescued motor neurons, despite being histologically normal, could remain functionally altered due to residual cytoplasmic FUS. This would be analogous to results observed in Nova double knockout animals rescued with neuronal agrin (Ruggiu *et al*, 2009). Electrophysiological characterization of neuromuscular transmission could help discriminate between these two possibilities. Apart from neuromuscular alterations, defects in lung morphogenesis or maturation, cardiovascular defects, hematological defects, or skeletal defects can all result in poor blood oxygenation and the characteristic cyanosis observed in $Fus^{\Delta NLS/\Delta NLS}$ and $Fus^{-/-}$ neonates. It will be important to investigate these possible causes of neonatal lethality due to loss of FUS function in future studies. In particular, generation of conditional *Fus* knockout mice would provide a valuable tool to evaluate whether selective FUS inactivation in neurons, muscle, lung epithelium, or the vasculature would result in respiratory insufficiency and neonatal death. Possibly, loss of FUS function in a combination of these tissues is necessary to induce this phenotype.

While a few FUS mutations have a recessive pattern of inheritance (Kwiatkowski *et al*, 2009; Bertolin *et al*, 2014), the vast majority are dominantly inherited, and most ALS patients are affected in

their 5th to 7th decade. Thus, our observation of perinatal death is not fully representative of the disease state as occurs in ALS patients and some changes observed here might be deleterious through developmental rather than degenerative effects. In this respect, it will be crucial to further analyze heterozygous $Fus^{\Delta NLS/+}$ mice that closely mimic the genetic situation in the vast majority of ALS-FUS patients. These mice are viable and show no obvious motor phenotype until 6 months of age (Scekic-Zahirovic, unpublished results). Nevertheless, $Fus^{\Delta NLS/+}$ mice showed cytoplasmic mislocalization of FUS and subtle alterations in mRNA splicing at birth. Aging might exacerbate these defects, consistent with a late-onset disease such as ALS, and it will be highly interesting to characterize a potential age-dependent phenotype of $Fus^{\Delta NLS/+}$ mice and $Fus^{+/-}$ mice.

The very severe phenotype of $Fus^{\Delta NLS/\Delta NLS}$ mice resembles spinal muscular atrophy, which is caused by mutations in the *SMN1* gene, whose product SMN interacts directly with FUS and is an integral component of the spliceosome (Yamazaki *et al*, 2012; Gerbino *et al*, 2013; Groen *et al*, 2013; Tsuiji *et al*, 2013; Sun *et al*, 2015; Yu *et al*, 2015). This is further reinforced by the strong splicing defects observed in $Fus^{\Delta NLS/\Delta NLS}$ mice and is consistent with juvenile onset in many ALS-*FUS* patients with C-terminal truncation mutations. These similarities strengthen the links between ALS and SMA, and support that SMA, ALS, and FTD may be part of the same disease spectrum with common molecular mechanisms leading to neuronal death.

In conclusion, this study provides *in vivo* genetic evidence that cytoplasmic mislocalization of FUS triggers apoptotic motor neuron degeneration and demonstrates a crucial role for a gain of toxic function in this process. Motor neuron loss occurs at least partially through a cell autonomous gain-of-function mechanism, since complete loss of FUS is not associated with motor neuron death, and rescue of nuclear FUS within motor neurons prevents neuronal death.

Materials and Methods

Generation of conditional knockin $Fus^{\Delta NLS/\Delta NLS}$ and $Fus^{-/-}$ mice

Knockin *Fus* mice with the conditional ablation of exon 15 were generated in the Institut Clinique de la Souris (ICS, Illkirch, Strasbourg) using standard procedures. The *Fus* locus was engineered to include, in between the exons 12 and 13 of the gene, an inserted floxed cDNA encoding exons 13 and 14 of *FUS*, followed by 3 STOP cassettes. We obtained germ line transmission of the recombinant allele. Homozygous $Fus^{\Delta NLS/\Delta NLS}$ mice were generated by intercrossing $Fus^{\Delta NLS/+}$ animals.

For generation of $Fus^{-/-}$ mice, the mouse ES cell clone EUCE0131_G08 was obtained from the European Conditional Mouse Mutagenesis Consortium (EUCOMM) (Friedel *et al*, 2007). Southern blotting and sequencing of PCR-amplified genomic sequences confirmed a single gene trap insertion event in the first intron of *Fus*. Blastocyst injection of ES cells resulted in chimeric mice, which allowed for germ line transmission of the mutant *Fus* allele. As the ES cells were generated in a 129P2 background, the resulting offspring was backcrossed at least five times to C57Bl6 mice. The genetic background of all mice used in this study is C57Bl6.

Western blot

Western blotting and antibodies used are presented in Appendix Supplementary Methods.

Histology and motor neuron counts

Spinal cords were removed and immersed in fixative for 2 h at 4°C. Samples were transferred overnight into 30% sucrose in 0.1 M phosphate buffer (PB) at 4°C for cryoprotection, embedded in medium (Tissue-Tek® O.C.T. Compound, SAKURA#4583), and cut with a cryostat (Leica CM 3050S). P0 spinal cords were cut in serial 25-μm-thick sections and mounted onto 2% gelatin-coated slides to be processed for immunostaining.

For Nissl staining, slides were air-dried overnight. Sections were then hydrated through 100% and 95% alcohol to distilled water, immersed in 0.1% Cresyl violet acetate (Certistain®, MERCK#5235), and coverslipped with Roti-Histokitt (Roth, 6638.1).

For immunohistochemistry (IHC), unspecific binding sites were blocked with 5% horse serum (HS), 0.5% Triton X-100 for 30 min at room temperature (RT), immersed in 3% hydrogen peroxide (H_2O_2) to remove the endogenous peroxidase activity, rinsed in phosphate buffered saline (PBS), and incubated with goat polyclonal anti-choline acetyltransferase (ChAT) antibody (Millipore, AB144-P; diluted 1:50) overnight at RT in a humidified chamber. After rinsing in PBS, sections were incubated with biotinylated donkey anti-goat IgG (Jackson, 705-066-147; 1:250) for 1.5 h, rinsed in PBS, and then incubated with ABC kit (Vector, PK7200; 1:4,000) for 1 h. All antibodies were diluted in 0.01 M PBS, 0.1% Triton X-100. Peroxidase staining was obtained by incubating the sections in 0.075% 3,3′-diaminobenzidine tetrahydrochloride (DAB; Sigma Aldrich) and 0.002% H_2O_2 in 50 mM Tris–HCl pH 7.5. Sections were dehydrated, air-dried, and coverslipped with Roti-Histokitt (Roth, 6638.1).

Motor neurons were counted at L1–L5 on both cresyl violet- and ChAT-stained sections at 20× magnification (for each genotype: Exact numbers of animals per group are provided in figure legends). The counting was performed per ventral horn in every tenth section for ten sections in total per animal. In Nissl-stained sections, only neurons with an area ≥ 80 μm^2 and located in a position congruent with that of motor neuron groups were counted (d'Errico *et al*, 2013). All $ChAT^+$ profiles located in the ventral horns of immunostained sections clearly displayed on the plane of the section were counted. Total estimated motor neuron numbers were obtained using a computer-assisted microscope (Nikon Eclipse E800) and the software (Nis Elements version 4.0). Cells were counted on the computer screen using a digital camera (Nikon Digital Sight DS-U3) mounted on a microscope. The soma size of Nissl+ motor neurons was also analyzed by measuring cross-sectional areas at 20× magnification using ImageJ software (Schneider *et al*, 2012).

Other histological techniques are described in Appendix Supplementary Methods.

Analysis of expression changes by RNA-seq

Total RNA from brains of $Fus^{\Delta NLS/\Delta NLS}$, $Fus^{-/-}$, and their control littermates were extracted with TRIzol (Invitrogen). RNA quality was measured using the Agilent Bioanalyzer system or RNA ScreenTape (Agilent technologies) according to the manufacturer's

recommendations and processed using the Illumina TruSeq Stranded mRNA Sample Preparation Kit according to manufacturer's protocol. Generated cDNA libraries were sequenced using an Illumina HiSeq 2000 sequencer with 4–5 biological replicates sequenced per condition using single read, 50 cycle runs. Quality of sequencing reads was assessed using FastQC (Babraham Bioinformatics) and then aligned to a mouse reference genome (mm9, UCSC Genome Browser) using TopHat (version v2.0.10). Sequencing yielded, on average, 15 million non-redundant reads per sample with a 48.4–58.7% mapping rate. Cufflinks (version v2.1.1) was used to generate transcript abundance for each annotated protein-coding gene as fragments per kilobase of transcript per million mapped reads (FPKM), and statistical analysis and comparison of FPKM values were calculated using Cuffdiff (version v2.1.1). Genomewide unsupervised clustering analysis and heat maps with significant changes between different groups were generated using R (Bioconductor). qRT–PCR techniques used to confirm RNA-seq changes are described in Appendix Supplementary Methods and oligonucleotides sequences are provided in Dataset EV9.

Analysis of splicing alterations by RASL-seq

RNA-mediated oligonucleotide annealing, selection, and ligation with next-generation sequencing (RASL-seq) analysis of alternative splicing changes was carried out as already described elsewhere (Li *et al*, 2012; Zhou *et al*, 2012). In brief, a pool of oligonucleotides was designed to detect 3,859 alternative splicing events in mice. One hundred fmol of RASL-seq oligos were annealed to 1 μg of total RNA isolated from brains of $Fus^{\Delta NLS/\Delta NLS}$, $Fus^{-/-}$, and their control littermates. After ligation, 5 μl eluted ligated oligos were used for 16–18 cycles of PCR amplification, and the barcoded PCR products were sequenced using an Illumina HiSeq 2000 sequencer with 24–30 samples per lanes. Sequencing data were decoded allowing no mismatch with each barcode, and target sequences were mapped with RASL-seq oligo pool sequences using the short read alignment software Bowtie allowing for 1 mismatch at both the left and right side of the ligated oligos. An average of ~5 million reads from each sample was mapped, with events with < 4 counts in one of the isoforms removed. Ratios of the counts of shorter to longer isoforms were calculated. The significantly changed events were identified by *t*-test and average fold change. Unsupervised clustering analysis and heat maps with significant changes between different groups were generated using R (Bioconductor). Semi-quantitative PCR techniques used to confirm RASL-seq changes are described in Appendix Supplementary Methods. Oligonucleotides sequences are provided in Dataset EV9.

Statistics

For the animal experiments, the values from each animal were averaged for each genotype group and analyzed by Student's unpaired two-tailed *t*-test. Comparison of three or four groups was performed using one-way ANOVA and Tukey's *post hoc* test. Data were analyzed by using the Graphics Prism Program (Graph Pad Software, San Diego, CA) and expressed as mean ± SEM (standard error of the mean) and differences were considered significant when $P \leq 0.05$.

Data accession

RNA-seq and RASL-seq data have been deposited in GEO, under entry GSE78730.

Expanded View for this article is available online.

Acknowledgements
We thank Dr. Pico Caroni for providing the ChAT-CRE knockin mice and helpful discussions. We thank Marlene Bartos for her help in achieving this project. We are grateful to Dr. Don W. Cleveland and the members of his group for tremendous support and fruitful discussions. This work is supported by an ALS Association Investigator Initiated Award (grants 2235 and 3209; to LD and CLT); the Frick Foundation (award 2013 to LD and CLT, award 2010 to ES); Association Française contre les Myopathies (grant #18280; to LD, CLT and ES); Target ALS (grant 13-0840; to CLT); Virtual Helmholtz Institute "RNA dysmetabolism in ALS and FTD" (WP2, to LD, AW and ACL); Association de recherche sur la SLA (ArSLA; to LD); State North Rhine Westphalia (to ES); Minna-James-Heineman-Stiftung (to ES); and the Max Planck Society (to ES). JSZ received a Erasmus Mundus Neurotime Fellowship to perform these studies. OS received a fellowship from the German National Academic Foundation. CLT received salary support from the Ludwig Institute for Cancer Research.

Author contributions
JSZ, OS, ES, CLT, and LD designed research; JSZ, OS, HEO, MJ, SM, MW, SD, JS, SDG, KD, NM, MCB, JQ, CR, TS, and ES performed research; SY, JQ, YZ, HL, XDF, AW, ACL, and FK contributed reagents and data analysis; JSZ, OS, MJ, SY, KD, ES, CLT, and LD analyzed data and made figures; and JSZ, ES, CLT, and LD wrote the manuscript.

Conflict of interest
The authors declare that they have no conflict of interest.

References

Alami NH, Smith RB, Carrasco MA, Williams LA, Winborn CS, Han SS, Kiskinis E, Winborn B, Freibaum BD, Kanagaraj A, Clare AJ, Badders NM, Bilican B, Chaum E, Chandran S, Shaw CE, Eggan KC, Maniatis T, Taylor JP (2014) Axonal transport of TDP-43 mRNA granules is impaired by ALS-causing mutations. *Neuron* 81: 536 – 543

Alaynick WA, Jessell TM, Pfaff SL (2011) SnapShot: spinal cord development. *Cell* 146: 178 – 178 e1

Arnold ES, Ling SC, Huelga SC, Lagier-Tourenne C, Polymenidou M, Ditsworth D, Kordasiewicz HB, McAlonis-Downes M, Platoshyn O, Parone PA, Da Cruz S, Clutario KM, Swing D, Tessarollo L, Marsala M, Shaw CE, Yeo GW, Cleveland DW (2013) ALS-linked TDP-43 mutations produce aberrant RNA splicing and adult-onset motor neuron disease without aggregation or loss of nuclear TDP-43. *Proc Natl Acad Sci USA* 110: E736 – E745

Ayala YM, De Conti L, Avendano-Vazquez SE, Dhir A, Romano M, D'Ambrogio A, Tollervey J, Ule J, Baralle M, Buratti E, Baralle FE (2011) TDP-43 regulates its mRNA levels through a negative feedback loop. *EMBO J* 30: 277 – 288

Baumer D, Hilton D, Paine SM, Turner MR, Lowe J, Talbot K, Ansorge O (2010) Juvenile ALS with basophilic inclusions is a FUS proteinopathy with FUS mutations. *Neurology* 75: 611 – 618

Bergeron C, Beric-Maskarel K, Muntasser S, Weyer L, Somerville MJ, Percy ME (1994) Neurofilament light and polyadenylated mRNA levels are decreased

in amyotrophic lateral sclerosis motor neurons. *J Neuropathol Exp Neurol* 53: 221 – 230

Bertolin C, D'Ascenzo C, Querin G, Gaiani A, Boaretto F, Salvoro C, Vazza G, Angelini C, Cagnin A, Pegoraro E, Soraru G, Mostacciuolo ML (2014) Improving the knowledge of amyotrophic lateral sclerosis genetics: novel SOD1 and FUS variants. *Neurobiol Aging* 35: 1212 e7 – 1212 e10.

Boillee S, Vande Velde C, Cleveland DW (2006) ALS: a disease of motor neurons and their nonneuronal neighbors. *Neuron* 52: 39 – 59

Calvo A, Moglia C, Canosa A, Brunetti M, Barberis M, Traynor BJ, Carrara G, Valentini C, Restagno G, Chio A (2014) *De novo* nonsense mutation of the FUS gene in an apparently familial amyotrophic lateral sclerosis case. *Neurobiol Aging* 35: 1513 e7 – 11

Cambray S, Pedraza N, Rafel M, Gari E, Aldea M, Gallego C (2009) Protein kinase KIS localizes to RNA granules and enhances local translation. *Mol Cell Biol* 29: 726 – 735

Chen EW, Chiu AY (1992) Early stages in the development of spinal motor neurons. *J Comp Neurol* 320: 291 – 303

Cho HH, Cargnin F, Kim Y, Lee B, Kwon RJ, Nam H, Shen R, Barnes AP, Lee JW, Lee S, Lee SK (2014) Isl1 directly controls a cholinergic neuronal identity in the developing forebrain and spinal cord by forming cell type-specific complexes. *PLoS Genet* 10: e1004280

Couthouis J, Hart MP, Shorter J, DeJesus-Hernandez M, Erion R, Oristano R, Liu AX, Ramos D, Jethava N, Hosangadi D, Epstein J, Chiang A, Diaz Z, Nakaya T, Ibrahim F, Kim HJ, Solski JA, Williams KL, Mojsilovic-Petrovic J, Ingre C *et al* (2011) A yeast functional screen predicts new candidate ALS disease genes. *Proc Natl Acad Sci USA* 108: 20881 – 20890

Couthouis J, Hart MP, Erion R, King OD, Diaz Z, Nakaya T, Ibrahim F, Kim HJ, Mojsilovic-Petrovic J, Panossian S, Kim CE, Frackelton EC, Solski JA, Williams KL, Clay-Falcone D, Elman L, McCluskey L, Greene R, Hakonarson H, Kalb RG *et al* (2012) Evaluating the role of the FUS/TLS-related gene EWSR1 in amyotrophic lateral sclerosis. *Hum Mol Genet* 21: 2899 – 2911

D'Alton S, Altshuler M, Lewis J (2015) Studies of alternative isoforms provide insight into TDP-43 autoregulation and pathogenesis. *RNA* 21: 1419 – 1432

Deng H, Gao K, Jankovic J (2014) The role of FUS gene variants in neurodegenerative diseases. *Nat Rev Neurol* 10: 337 – 348

Dillman AA, Hauser DN, Gibbs JR, Nalls MA, McCoy MK, Rudenko IN, Galter D, Cookson MR (2013) mRNA expression, splicing and editing in the embryonic and adult mouse cerebral cortex. *Nat Neurosci* 16: 499 – 506

Dini Modigliani S, Morlando M, Errichelli L, Sabatelli M, Bozzoni I (2014) An ALS-associated mutation in the FUS 3′-UTR disrupts a microRNA-FUS regulatory circuitry. *Nat Commun* 5: 4335

Dormann D, Rodde R, Edbauer D, Bentmann E, Fischer I, Hruscha A, Than ME, Mackenzie IR, Capell A, Schmid B, Neumann M, Haass C (2010) ALS-associated fused in sarcoma (FUS) mutations disrupt Transportin-mediated nuclear import. *EMBO J* 29: 2841 – 2857

Elden AC, Kim HJ, Hart MP, Chen-Plotkin AS, Johnson BS, Fang X, Armakola M, Geser F, Greene R, Lu MM, Padmanabhan A, Clay-Falcone D, McCluskey L, Elman L, Juhr D, Gruber PJ, Rub U, Auburger G, Trojanowski JQ, Lee VM *et al* (2010) Ataxin-2 intermediate-length polyglutamine expansions are associated with increased risk for ALS. *Nature* 466: 1069 – 1075

d'Errico P, Boido M, Piras A, Valsecchi V, De Amicis E, Locatelli D, Capra S, Vagni F, Vercelli A, Battaglia G (2013) Selective vulnerability of spinal and cortical motor neuron subpopulations in delta7 SMA mice. *PLoS ONE* 8: e82654

Ferland RJ, Eyaid W, Collura RV, Tully LD, Hill RS, Al-Nouri D, Al-Rumayyan A, Topcu M, Gascon G, Bodell A, Shugart YY, Ruvolo M, Walsh CA (2004) Abnormal cerebellar development and axonal decussation due to mutations in AHI1 in Joubert syndrome. *Nat Genet* 36: 1008 – 1013

Frickenhaus M, Wagner M, Mallik M, Catinozzi M, Storkebaum E (2015) Highly efficient cell-type-specific gene inactivation reveals a key function for the Drosophila FUS homolog cabeza in neurons. *Sci Rep* 5: 9107

Friedel RH, Seisenberger C, Kaloff C, Wurst W (2007) EUCOMM–the European conditional mouse mutagenesis program. *Brief Funct Genomic Proteomic* 6: 180 – 185

Gerbino V, Carri MT, Cozzolino M, Achsel T (2013) Mislocalised FUS mutants stall spliceosomal snRNPs in the cytoplasm. *Neurobiol Dis* 55: 120 – 128

Gitcho MA, Baloh RH, Chakraverty S, Mayo K, Norton JB, Levitch D, Hatanpaa KJ, White CL III, Bigio EH, Caselli R, Baker M, Al-Lozi MT, Morris JC, Pestronk A, Rademakers R, Goate AM, Cairns NJ (2008) TDP-43 A315T mutation in familial motor neuron disease. *Ann Neurol* 63: 535 – 538

Groen EJ, Fumoto K, Blokhuis AM, Engelen-Lee J, Zhou Y, van den Heuvel DM, Koppers M, van Diggelen F, van Heest J, Demmers JA, Kirby J, Shaw PJ, Aronica E, Spliet WG, Veldink JH, van den Berg LH, Pasterkamp RJ (2013) ALS-associated mutations in FUS disrupt the axonal distribution and function of SMN. *Hum Mol Genet* 22: 3690 – 3704

Han TW, Kato M, Xie S, Wu LC, Mirzaei H, Pei J, Chen M, Xie Y, Allen J, Xiao G, McKnight SL (2012) Cell-free formation of RNA granules: bound RNAs identify features and components of cellular assemblies. *Cell* 149: 768 – 779

Hicks GG, Singh N, Nashabi A, Mai S, Bozek G, Klewes L, Arapovic D, White EK, Koury MJ, Oltz EM, Van Kaer L, Ruley HE (2000) Fus deficiency in mice results in defective B-lymphocyte development and activation, high levels of chromosomal instability and perinatal death. *Nat Genet* 24: 175 – 179

Holcik M, Sonenberg N (2005) Translational control in stress and apoptosis. *Nat Rev Mol Cell Biol* 6: 318 – 327

Hu F, Padukkavidana T, Vaegter CB, Brady OA, Zheng Y, Mackenzie IR, Feldman HH, Nykjaer A, Strittmatter SM (2010) Sortilin-mediated endocytosis determines levels of the frontotemporal dementia protein, progranulin. *Neuron* 68: 654 – 667

Huang EJ, Zhang J, Geser F, Trojanowski JQ, Strober JB, Dickson DW, Brown RH Jr, Shapiro BE, Lomen-Hoerth C (2010) Extensive FUS-immunoreactive pathology in juvenile amyotrophic lateral sclerosis with basophilic inclusions. *Brain Pathol* 20: 1069 – 1076

Huang C, Zhou H, Tong J, Chen H, Liu YJ, Wang D, Wei X, Xia XG (2011) FUS transgenic rats develop the phenotypes of amyotrophic lateral sclerosis and frontotemporal lobar degeneration. *PLoS Genet* 7: e1002011

Hutton M, Lendon CL, Rizzu P, Baker M, Froelich S, Houlden H, Pickering-Brown S, Chakraverty S, Isaacs A, Grover A, Hackett J, Adamson J, Lincoln S, Dickson D, Davies P, Petersen RC, Stevens M, de Graaff E, Wauters E, van Baren J *et al* (1998) Association of missense and 5′-splice-site mutations in tau with the inherited dementia FTDP-17. *Nature* 393: 702 – 705

Ilieva H, Polymenidou M, Cleveland DW (2009) Non-cell autonomous toxicity in neurodegenerative disorders: ALS and beyond. *J Cell Biol* 187: 761 – 772

Imbert G, Saudou F, Yvert G, Devys D, Trottier Y, Garnier JM, Weber C, Mandel JL, Cancel G, Abbas N, Durr A, Didierjean O, Stevanin G, Agid Y, Brice A (1996) Cloning of the gene for spinocerebellar ataxia 2 reveals a locus with high sensitivity to expanded CAG/glutamine repeats. *Nat Genet* 14: 285 – 291

Ishigaki S, Masuda A, Fujioka Y, Iguchi Y, Katsuno M, Shibata A, Urano F, Sobue G, Ohno K (2012) Position-dependent FUS-RNA interactions regulate alternative splicing events and transcriptions. *Sci Rep* 2: 529

Johnson JO, Pioro EP, Boehringer A, Chia R, Feit H, Renton AE, Pliner HA, Abramzon Y, Marangi G, Winborn BJ, Gibbs JR, Nalls MA, Morgan S, Shoai M, Hardy J, Pittman A, Orrell RW, Malaspina A, Sidle KC, Fratta P *et al* (2014) Mutations in the Matrin 3 gene cause familial amyotrophic lateral sclerosis. *Nat Neurosci* 17: 664 – 666

Ju S, Tardiff DF, Han H, Divya K, Zhong Q, Maquat LE, Bosco DA, Hayward LJ, Brown RH Jr, Lindquist S, Ringe D, Petsko GA (2011) A yeast model of FUS/TLS-dependent cytotoxicity. *PLoS Biol* 9: e1001052

Kabashi E, Valdmanis PN, Dion P, Spiegelman D, McConkey BJ, Vande Velde C, Bouchard JP, Lacomblez L, Pochigaeva K, Salachas F, Pradat PF, Camu W, Meininger V, Dupre N, Rouleau GA (2008) TARDBP mutations in individuals with sporadic and familial amyotrophic lateral sclerosis. *Nat Genet* 40: 572 – 574

Kanning KC, Kaplan A, Henderson CE (2010) Motor neuron diversity in development and disease. *Annu Rev Neurosci* 33: 409 – 440

Kim JY, Shen S, Dietz K, He Y, Howell O, Reynolds R, Casaccia P (2010) HDAC1 nuclear export induced by pathological conditions is essential for the onset of axonal damage. *Nat Neurosci* 13: 180 – 189

Kim HJ, Kim NC, Wang YD, Scarborough EA, Moore J, Diaz Z, MacLea KS, Freibaum B, Li S, Molliex A, Kanagaraj AP, Carter R, Boylan KB, Wojtas AM, Rademakers R, Pinkus JL, Greenberg SA, Trojanowski JQ, Traynor BJ, Smith BN *et al* (2013) Mutations in prion-like domains in hnRNPA2B1 and hnRNPA1 cause multisystem proteinopathy and ALS. *Nature* 495: 467 – 473

Kino Y, Washizu C, Kurosawa M, Yamada M, Miyazaki H, Akagi T, Hashikawa T, Doi H, Takumi T, Hicks GG, Hattori N, Shimogori T, Nukina N (2015) FUS/TLS deficiency causes behavioral and pathological abnormalities distinct from amyotrophic lateral sclerosis. *Acta Neuropathol Commun* 3: 24

Kobayashi Z, Tsuchiya K, Arai T, Aoki M, Hasegawa M, Ishizu H, Akiyama H, Mizusawa H (2010) Occurrence of basophilic inclusions and FUS-immunoreactive neuronal and glial inclusions in a case of familial amyotrophic lateral sclerosis. *J Neurol Sci* 293: 6 – 11

Kuroda M, Sok J, Webb L, Baechtold H, Urano F, Yin Y, Chung P, de Rooij DG, Akhmedov A, Ashley T, Ron D (2000) Male sterility and enhanced radiation sensitivity in TLS(−/−) mice. *EMBO J* 19: 453 – 462

Kwiatkowski TJ Jr, Bosco DA, Leclerc AL, Tamrazian E, Vanderburg CR, Russ C, Davis A, Gilchrist J, Kasarskis EJ, Munsat T, Valdmanis P, Rouleau GA, Hosler BA, Cortelli P, de Jong PJ, Yoshinaga Y, Haines JL, Pericak-Vance MA, Yan J, Ticozzi N *et al* (2009) Mutations in the FUS/TLS gene on chromosome 16 cause familial amyotrophic lateral sclerosis. *Science* 323: 1205 – 1208

Lagier-Tourenne C, Polymenidou M, Hutt KR, Vu AQ, Baughn M, Huelga SC, Clutario KM, Ling SC, Liang TY, Mazur C, Wancewicz E, Kim AS, Watt A, Freier S, Hicks GG, Donohue JP, Shiue L, Bennett CF, Ravits J, Cleveland DW *et al* (2012) Divergent roles of ALS-linked proteins FUS/TLS and TDP-43 intersect in processing long pre-mRNAs. *Nat Neurosci* 15: 1488 – 1497

Li H, Qiu J, Fu XD (2012) RASL-seq for massively parallel and quantitative analysis of gene expression. *Curr Protocols Mol Biol*/edited by Ausubel FM, Brent R, Kingston RE, Moore DD, Seidman JG, Smith JA, Struhl K. Chapter 4: Unit 4.13.1 – 9

Li YR, King OD, Shorter J, Gitler AD (2013) Stress granules as crucibles of ALS pathogenesis. *J Cell Biol* 201: 361 – 372

Ling SC, Polymenidou M, Cleveland DW (2013) Converging mechanisms in ALS and FTD: disrupted RNA and protein homeostasis. *Neuron* 79: 416 – 438

Ling JP, Pletnikova O, Troncoso JC, Wong PC (2015) TDP-43 repression of nonconserved cryptic exons is compromised in ALS-FTD. *Science* 349: 650 – 655

Liu F, Gong CX (2008) Tau exon 10 alternative splicing and tauopathies. *Mol Neurodegener* 3: 8

Liu-Yesucevitz L, Bilgutay A, Zhang YJ, Vanderweyde T, Citro A, Mehta T, Zaarur N, McKee A, Bowser R, Sherman M, Petrucelli L, Wolozin B (2010) Tar DNA binding protein-43 (TDP-43) associates with stress granules: analysis of cultured cells and pathological brain tissue. *PLoS ONE* 5: e13250

Mackenzie IR, Rademakers R, Neumann M (2010) TDP-43 and FUS in amyotrophic lateral sclerosis and frontotemporal dementia. *Lancet Neurol* 9: 995 – 1007

Manceau V, Kielkopf CL, Sobel A, Maucuer A (2008) Different requirements of the kinase and UHM domains of KIS for its nuclear localization and binding to splicing factors. *J Mol Biol* 381: 748 – 762

McMillan P, Korvatska E, Poorkaj P, Evstafjeva Z, Robinson L, Greenup L, Leverenz J, Schellenberg GD, D'Souza I (2008) Tau isoform regulation is region- and cell-specific in mouse brain. *J Comp Neurol* 511: 788 – 803

Mitchell JC, McGoldrick P, Vance C, Hortobagyi T, Sreedharan J, Rogelj B, Tudor EL, Smith BN, Klasen C, Miller CC, Cooper JD, Greensmith L, Shaw CE (2013) Overexpression of human wild-type FUS causes progressive motor neuron degeneration in an age- and dose-dependent fashion. *Acta Neuropathol* 125: 273 – 288

Mitchelmore C, Buchmann-Moller S, Rask L, West MJ, Troncoso JC, Jensen NA (2004) NDRG2: a novel Alzheimer's disease associated protein. *Neurobiol Dis* 16: 48 – 58

Morlando M, Dini Modigliani S, Torrelli G, Rosa A, Di Carlo V, Caffarelli E, Bozzoni I (2012) FUS stimulates microRNA biogenesis by facilitating co-transcriptional Drosha recruitment. *EMBO J* 31: 4502 – 4510

Mortazavi A, Williams BA, McCue K, Schaeffer L, Wold B (2008) Mapping and quantifying mammalian transcriptomes by RNA-Seq. *Nat Methods* 5: 621 – 628

Neumann M, Sampathu DM, Kwong LK, Truax AC, Micsenyi MC, Chou TT, Bruce J, Schuck T, Grossman M, Clark CM, McCluskey LF, Miller BL, Masliah E, Mackenzie IR, Feldman H, Feiden W, Kretzschmar HA, Trojanowski JQ, Lee VM (2006) Ubiquitinated TDP-43 in frontotemporal lobar degeneration and amyotrophic lateral sclerosis. *Science* 314: 130 – 133

Neumann M, Rademakers R, Roeber S, Baker M, Kretzschmar HA, Mackenzie IR (2009) A new subtype of frontotemporal lobar degeneration with FUS pathology. *Brain* 132: 2922 – 2931

Oppenheim RW (1991) Cell death during development of the nervous system. *Annu Rev Neurosci* 14: 453 – 501

Parkhomchuk D, Borodina T, Amstislavskiy V, Banaru M, Hallen L, Krobitsch S, Lehrach H, Soldatov A (2009) Transcriptome analysis by strand-specific sequencing of complementary DNA. *Nucleic Acids Res* 37: e123

Pedraza N, Ortiz R, Cornado A, Llobet A, Aldea M, Gallego C (2014) KIS, a kinase associated with microtubule regulators, enhances translation of AMPA receptors and stimulates dendritic spine remodeling. *J Neurosci* 34: 13988 – 13997

Polymenidou M, Lagier-Tourenne C, Hutt KR, Huelga SC, Moran J, Liang TY, Ling SC, Sun E, Wancewicz E, Mazur C, Kordasiewicz H, Sedaghat Y, Donohue JP, Shiue L, Bennett CF, Yeo GW, Cleveland DW (2011) Long pre-mRNA depletion and RNA missplicing contribute to neuronal vulnerability from loss of TDP-43. *Nat Neurosci* 14: 459 – 468

Prudencio M, Jansen-West KR, Lee WC, Gendron TF, Zhang YJ, Xu YF, Gass J, Stuani C, Stetler C, Rademakers R, Dickson DW, Buratti E, Petrucelli L (2012) Misregulation of human sortilin splicing leads to the generation of a nonfunctional progranulin receptor. *Proc Natl Acad Sci USA* 109: 21510 – 21515

Rogelj B, Easton LE, Bogu GK, Stanton LW, Rot G, Curk T, Zupan B, Sugimoto Y, Modic M, Haberman N, Tollervey J, Fujii R, Takumi T, Shaw CE, Ule J (2012) Widespread binding of FUS along nascent RNA regulates alternative splicing in the brain. *Sci Rep* 2: 603

Rossi J, Balthasar N, Olson D, Scott M, Berglund E, Lee CE, Choi MJ, Lauzon D, Lowell BB, Elmquist JK (2011) Melanocortin-4 receptors expressed by cholinergic neurons regulate energy balance and glucose homeostasis. *Cell Metab* 13: 195 – 204

Ruggiu M, Herbst R, Kim N, Jevsek M, Fak JJ, Mann MA, Fischbach G, Burden SJ, Darnell RB (2009) Rescuing Z+ agrin splicing in Nova null mice restores synapse formation and unmasks a physiologic defect in motor neuron firing. *Proc Natl Acad Sci USA* 106: 3513 – 3518

Saxena S, Roselli F, Singh K, Leptien K, Julien JP, Gros-Louis F, Caroni P (2013) Neuroprotection through excitability and mTOR required in ALS motoneurons to delay disease and extend survival. *Neuron* 80: 80 – 96

Schneider CA, Rasband WS, Eliceiri KW (2012) NIH Image to ImageJ: 25 years of image analysis. *Nat Methods* 9: 671 – 675

Schwartz JC, Ebmeier CC, Podell ER, Heimiller J, Taatjes DJ, Cech TR (2012) FUS binds the CTD of RNA polymerase II and regulates its phosphorylation at Ser2. *Genes Dev* 26: 2690 – 2695

Sephton CF, Tang AA, Kulkarni A, West J, Brooks M, Stubblefield JJ, Liu Y, Zhang MQ, Green CB, Huber KM, Huang EJ, Herz J, Yu G (2014) Activity-dependent FUS dysregulation disrupts synaptic homeostasis. *Proc Natl Acad Sci USA* 111: E4769 – E4778

Sheffler-Collins SI, Dalva MB (2012) EphBs: an integral link between synaptic function and synaptopathies. *Trends Neurosci* 35: 293 – 304

Sibley CR, Emmett W, Blazquez L, Faro A, Haberman N, Briese M, Trabzuni D, Ryten M, Weale ME, Hardy J, Modic M, Curk T, Wilson SW, Plagnol V, Ule J (2015) Recursive splicing in long vertebrate genes. *Nature* 521: 371 – 375

Smith BN, Ticozzi N, Fallini C, Gkazi AS, Topp S, Kenna KP, Scotter EL, Kost J, Keagle P, Miller JW, Calini D, Vance C, Danielson EW, Troakes C, Tiloca C, Al-Sarraj S, Lewis EA, King A, Colombrita C, Pensato V *et al* (2014) Exome-wide rare variant analysis identifies TUBA4A mutations associated with familial ALS. *Neuron* 84: 324 – 331

Sonenberg N, Hinnebusch AG (2009) Regulation of translation initiation in eukaryotes: mechanisms and biological targets. *Cell* 136: 731 – 745

Sreedharan J, Blair IP, Tripathi VB, Hu X, Vance C, Rogelj B, Ackerley S, Durnall JC, Williams KL, Buratti E, Baralle F, de Belleroche J, Mitchell JD, Leigh PN, Al-Chalabi A, Miller CC, Nicholson G, Shaw CE (2008) TDP-43 mutations in familial and sporadic amyotrophic lateral sclerosis. *Science* 319: 1668 – 1672

Sun Z, Diaz Z, Fang X, Hart MP, Chesi A, Shorter J, Gitler AD (2011) Molecular determinants and genetic modifiers of aggregation and toxicity for the ALS disease protein FUS/TLS. *PLoS Biol* 9: e1000614

Sun S, Ling SC, Qiu J, Albuquerque CP, Zhou Y, Tokunaga S, Li H, Qiu H, Bui A, Yeo GW, Huang EJ, Eggan K, Zhou H, Fu XD, Lagier-Tourenne C, Cleveland DW (2015) ALS-causative mutations in FUS/TLS confer gain- and loss-of-function by altered association with SMN and U1-snRNP. *Nat Commun* 6: 6171

Tateishi T, Hokonohara T, Yamasaki R, Miura S, Kikuchi H, Iwaki A, Tashiro H, Furuya H, Nagara Y, Ohyagi Y, Nukina N, Iwaki T, Fukumaki Y, Kira JI (2010) Multiple system degeneration with basophilic inclusions in Japanese ALS patients with FUS mutation. *Acta Neuropathol* 119: 355 – 364

Tibshirani M, Tradewell ML, Mattina KR, Minotti S, Yang W, Zhou H, Strong MJ, Hayward LJ, Durham HD (2014) Cytoplasmic sequestration of FUS/TLS associated with ALS alters histone marks through loss of nuclear protein arginine methyltransferase 1. *Hum Mol Genet* 24: 773 – 786

Tollervey JR, Curk T, Rogelj B, Briese M, Cereda M, Kayikci M, Konig J, Hortobagyi T, Nishimura AL, Zupunski V, Patani R, Chandran S, Rot G, Zupan B, Shaw CE, Ule J (2011) Characterizing the RNA targets and position-dependent splicing regulation by TDP-43. *Nat Neurosci* 14: 452 – 458

Trapnell C, Roberts A, Goff L, Pertea G, Kim D, Kelley DR, Pimentel H, Salzberg SL, Rinn JL, Pachter L (2012) Differential gene and transcript expression analysis of RNA-seq experiments with TopHat and Cufflinks. *Nat Protoc* 7: 562 – 578

Tsuiji H, Iguchi Y, Furuya A, Kataoka A, Hatsuta H, Atsuta N, Tanaka F, Hashizume Y, Akatsu H, Murayama S, Sobue G, Yamanaka K (2013) Spliceosome integrity is defective in the motor neuron diseases ALS and SMA. *EMBO Mol Med* 5: 221 – 234

Turgeon B, Meloche S (2009) Interpreting neonatal lethal phenotypes in mouse mutants: insights into gene function and human diseases. *Physiol Rev* 89: 1 – 26

Van Hoecke A, Schoonaert L, Lemmens R, Timmers M, Staats KA, Laird AS, Peeters E, Philips T, Goris A, Dubois B, Andersen PM, Al-Chalabi A, Thijs V, Turnley AM, van Vught PW, Veldink JH, Hardiman O, Van Den Bosch L, Gonzalez-Perez P, Van Damme P *et al* (2012) EPHA4 is a disease modifier of amyotrophic lateral sclerosis in animal models and in humans. *Nat Med* 18: 1418 – 1422

Vance C, Rogelj B, Hortobagyi T, De Vos KJ, Nishimura AL, Sreedharan J, Hu X, Smith B, Ruddy D, Wright P, Ganesalingam J, Williams KL, Tripathi V, Al-Saraj S, Al-Chalabi A, Leigh PN, Blair IP, Nicholson G, de Belleroche J, Gallo JM *et al* (2009) Mutations in FUS, an RNA processing protein, cause familial amyotrophic lateral sclerosis type 6. *Science* 323: 1208 – 1211

Vance C, Scotter EL, Nishimura AL, Troakes C, Mitchell JC, Kathe C, Urwin H, Manser C, Miller CC, Hortobagyi T, Dragunow M, Rogelj B, Shaw CE (2013) ALS mutant FUS disrupts nuclear localisation and sequesters wild-type FUS within cytoplasmic stress granules. *Hum Mol Genet* 22: 2676 – 2688

Waibel S, Neumann M, Rabe M, Meyer T, Ludolph AC (2010) Novel missense and truncating mutations in FUS/TLS in familial ALS. *Neurology* 75: 815 – 817

Waibel S, Neumann M, Rosenbohm A, Birve A, Volk AE, Weishaupt JH, Meyer T, Muller U, Andersen PM, Ludolph AC (2013) Truncating mutations in FUS/TLS give rise to a more aggressive ALS-phenotype than missense mutations: a clinico-genetic study in Germany. *Eur J Neurol* 20: 540 – 546

Wang WY, Pan L, Su SC, Quinn EJ, Sasaki M, Jimenez JC, Mackenzie IR, Huang EJ, Tsai LH (2013) Interaction of FUS and HDAC1 regulates DNA damage response and repair in neurons. *Nat Neurosci* 16: 1383 – 1391

Wegorzewska I, Bell S, Cairns NJ, Miller TM, Baloh RH (2009) TDP-43 mutant transgenic mice develop features of ALS and frontotemporal lobar degeneration. *Proc Natl Acad Sci USA* 106: 18809 – 18814

Yamazaki T, Chen S, Yu Y, Yan B, Haertlein TC, Carrasco MA, Tapia JC, Zhai B, Das R, Lalancette-Hebert M, Sharma A, Chandran S, Sullivan G, Nishimura AL, Shaw CE, Gygi SP, Shneider NA, Maniatis T, Reed R (2012) FUS-SMN protein interactions link the motor neuron diseases ALS and SMA. *Cell Rep* 2: 799 – 806

Yu Y, Chi B, Xia W, Gangopadhyay J, Yamazaki T, Winkelbauer-Hurt ME, Yin S, Eliasse Y, Adams E, Shaw CE, Reed R (2015) U1 snRNP is mislocalized in ALS patient fibroblasts bearing NLS mutations in FUS and is required for motor neuron outgrowth in zebrafish. *Nucleic Acids Res* 43: 3208 – 3218

Zhou Z, Qiu J, Liu W, Zhou Y, Plocinik RM, Li H, Hu Q, Ghosh G, Adams JA, Rosenfeld MG, Fu XD (2012) The Akt-SRPK-SR axis constitutes a major pathway in transducing EGF signaling to regulate alternative splicing in the nucleus. *Mol Cell* 47: 422 – 433

Zhou Y, Liu S, Liu G, Ozturk A, Hicks GG (2013) ALS-associated FUS mutations result in compromised FUS alternative splicing and autoregulation. *PLoS Genet* 9: e1003895

Zou ZY, Cui LY, Sun Q, Li XG, Liu MS, Xu Y, Zhou Y, Yang XZ (2013) *De novo* FUS gene mutations are associated with juvenile-onset sporadic amyotrophic lateral sclerosis in China. *Neurobiol Aging* 34: 1312 e1 – 8

Scekic-Zahirovic and collaborators
Toxic gain of function from mutant FUS protein is crucial to trigger cell autonomous motor neuron loss

Table of contents:

Appendix supplementary methods

Animal breeding and genotyping

Fus $^{\Delta NLS}$ and *ChAT-CRE* mice were housed in the animal facility of the Faculty of medicine from Strasbourg University, with 12/12 hours of light/dark cycle. The animals had unrestricted access to standard diet and water. *Fus*$^{+/+}$, *Fus* $^{\Delta NLS/+}$ and *Fus* $^{\Delta NLS/\Delta NLS}$ mice were produced by interbreeding *Fus* $^{\Delta NLS/+}$ mice, and littermates were systematically used as controls. *Fus* $^{\Delta NLS/\Delta NLS}$/ChAT-CRE mice were generated by a two-step breeding strategy. First, heterozygous *Fus* $^{\Delta NLS/+}$ mice were crossed with ChAT-CRE mice. *Fus* $^{\Delta NLS/+}$/ChAT-CRE mice were then crossed with heterozygous *Fus* $^{\Delta NLS/+}$ mice and these F2 litters were used in experiments. *Fus* $^{\Delta NLS}$ mice were genotyped by PCR on tail DNA using following primers: GAT TTG AAG TGG GTA GAT AGA TAG TGC AGG and CCT TTC CAC ACT TTA GGT TAG TCA CAG. *ChAT-CRE* mice were genotyped by PCR on tail DNA using following primers: CCA TCT GCC ACC AGC CAG and TCG CCA TCT TCC AGC AGG.

Fus$^{-/-}$, *Fus*$^{+/-}$ and *Fus*$^{+/+}$ mice were generated by crossing *Fus*$^{+/-}$ mice and PCR genotyped using a combination of three primers: (i) a common forward primer (CTC TCC TGG CCC GGT CAC) which anneals upstream of the gene trap insertion, (ii) a reverse primer (GCC AGA GGA GCG CGT GC) which anneals downstream of the gene trap insertion and gives rise to a 150 bp band for wild type *Fus*, but no band for the gene trap allele under the cycling conditions used, and (iii) a reverse primer (CTG GAC TAC TGC GCC CTA C) which anneals in the gene trap and gives rise to a 715 bp band when the gene trap allele is present.

All experiments were approved by the local ethical committees of Strasbourg and Muenster universities.

Western blotting

For western blotting, tissue powder (brain, spinal cord and gastrocnemius muscle) was homogenized in lysis buffer (250 mM Sucrose solution, 1 mM EDTA, 2% SDT, 1 mM DTT, 10 mM Tris HCl pH 7.4) containing protease inhibitor (Sigma P8340) and phosphatase inhibitor cocktail (Sigma 8345) and centrifuged at 12000 x rpm for 15 minutes at room temperature. Protein concentration was measured using BCA Protein Assay. Equal amounts of protein (20μg) were separated by SDS-PAGE 10% and blotted onto a nitrocellulose membrane. Membranes were saturated with 10% non-fat milk and then incubated with the primary

antibodies against the internal or N-terminal part of FUS (Proteintech™, 11570-1-AP; 1:1000 and Bethyl A303-839A; 1:1000) diluted in 3% non-fat milk, and antibodies against the C-terminal part of FUS (Bethyl A300-294A; 1:10000 and Bethyl A300-302A; 1:10000), followed by anti-rabbit (P.A.R.I.S.; BI2413) or anti-goat (Sigma A5420) secondary antibody diluted 1:5000. Of note, the Bethyl antibody A300-302A is reported by the company as raised against the N-terminal part of the protein, but evidence supports either that this antibody recognizes the C-terminal NLS of FUS or that its binding to FUS is altered by the presence of mutation. An antibody against Histone 3 (Cell signaling, #9715; 1:1000) was used as loading control. All blots were analyzed with chemiluminescence (ECL; Luminata Forte Kit, Millipore WBLUF0500) using the Molecular Imager Chemidoc XRS (Biorad) as detection system.

Immunodetection of FUS in mouse embryonic fibroblasts, motor neurons and cerebral cortex

Localization of FUS protein was analyzed in spinal cord motor neurons on cryosections prepared as described below and double stained for FUS (Proteintech™; 11570-1-AP; 1:100), and ChAT (Millipore, AB144-P; 1:50) or for FUS (Proteintech™; 11570-1-AP; 1:100 and NeuN (Millipore, ABN78; 1:100). Localization of FUS in the cerebral cortex was analyzed on 30 µm coronal cryosections of the brain of newborn *Fus* $^{\Delta NLS/\Delta NLS}$ and *Fus* $^{+/+}$ mice using a rabbit anti-FUS antibody (Bethyl A300-302A, 1:150).

Fus immunoreactivity was visualized with a confocal microscope (LSM 510; Carl Zeiss, Thornwood, NY), within mouse embryonic fibroblasts (MEF) double stained with antibodies against the internal or N-terminal part of FUS (Proteintech™, 11570-1-AP; 1:100 and Bethyl A303-839A; 1:100) and Draq5 (Cell Signaling, 4084; 1:1000) followed by fluorescent secondary antibodies donkey anti-rabbit Alexa 488 (Jackson, A21206) and donkey anti-goat Alexa 594 (Molecular Probes, A11058) diluted 1:500. This experiment was repeated three times; data shown are from one representative experiment.

Quantification of cortical thickness

For quantification of cortical thickness, brains of newborn *Fus* $^{\Delta NLS/\Delta NLS}$, *Fus* $^{-/-}$ and their respective *Fus* $^{+/+}$ littermate controls were dissected and fixed for two hours in 4% paraformaldehyde at room temperature. Brains were subsequently cryoprotected in 30% sucrose at 4°C overnight, washed in PBS and embedded in cryo medium. 30 µm coronal cryosections were made, air-dried for several hours, and stored at -80°C or directly used for histochemical or immunostaining. Cortical thickness was quantified on images of Nissl-

stained sections, using the first section on which the hippocampus could be identified for quantification. ImageJ software was used to measure the cortical thickness, which was normalized to the area of the cerebral hemisphere to take brain size into account. The ratio of cortical thickness to hemisphere area was determined for each animal and compared between genotypes.

Immunostaining for Cux1 and Ctip2 was performed to visualize cortical layers II-IV and V-VI, respectively. For antigen retrieval, 30 μm coronal cryosections were incubated in hot sodium citrate buffer pH 6.0, followed by blocking and overnight incubation at 4°C with primary antibodies against Cux1 (Santa Cruz Biotechnology, sc-13024, 1:250) or Ctip2 (Abcam, 25B6, 1:500). After incubation with Alexa488-labeled secondary antibodies for two hours, a cover slip was mounted onto the sections using mounting medium with DAPI. The first section on which the hippocampus could be identified was selected for confocal imaging, and ImageJ was used to generate maximal intensity Z-projections of the resulting confocal sections. The thickness of the cortical layers was measured and normalized to the hemisphere area which had been determined on Nissl stained sections.

***In situ* detection of apoptosis in spinal cord cells by TUNEL assay**

For TUNEL staining, the spinal cord cryosections prepared as described above were treated with TUNEL reagent (Trevigen, 4812-30-K) according to the kit instructions. The tissue sections were permeabilized with Cytonnin™. All TUNEL-positive cells were counted and examined for the typical pathological feature of apoptosis under a fluorescent microscope (Nikon Eclipse E800) at a 20x magnification. The numbers in each set of sections were summed up and divided by number of the sections in a set. The mean number of TUNEL-positive cells for each genotype group was calculated.

Caspase 3 immunostaining and apoptotic events

Apoptotic bodies across the lumbar spinal cord cross-sectional area were determined by fluorescence microscopy. For detection of caspase-positive motor neurons sections were double-stained with goat-anti-ChAT (Millipore, AB144-P; diluted 1:50) and rabbit-anti-cleaved caspase-3 (R&D Systems, AF835; 1:100) and combination of secondary antibodies Alexa 594 anti-goat (Molecular Probes, A11058; 1:500) and Alexa 488 anti-rabbit (Jacson, A21206; 1:500) and Draq5 (Cell Signaling, 4084; 1:1000). Total number of apoptotic bodies was counted all over the cross sectional area for every tenth section for 10 sections in total

per animal. Apoptotic motor neurons were counted as cells triple positive for ChAT, caspase and condensed chromatin by Draq5. Information on the total numbers of apoptotic counts and further details are presented along with the description of the results. This experiment was repeated two times for both groups of animals *Fus* $^{\Delta NLS}$ and *ChAT-CRE* mice; images shown are from one representative experiment.

Lung histology

Lungs were harvested and fixed with 4% formaldehyde solution (Sigma 47608) for 24 h and embedded in paraffin; Sections of 6 μm were stained with hematoxylin (Vector H-3401) and eosin (Eosin Y-solution 0.5%; Roth X883.1) for light microscope observation (Nikon Eclipse E800) at a 40x magnification.

Other immunostainings

For detection of protein aggregation spinal cord sections were double immunostained with N-terminal part of FUS (Bethyl A303-839A; 1:100) and anti-Sqstm1 (p62, Abcam 56416; 1:100) followed by fluorescent secondary antibodies donkey anti-mouse Alexa 488 (Jackson, 715-545-150) and donkey anti-goat Alexa 594 (Molecular Probes, A11058) diluted 1:500. Anti Neurofilament (Abcam 24574; 1:100) , anti Ubiquitin (Cell signaling 3933; 1:100) and anti Ubiquitin (Millipore, MAB1510; 1:100) were used for studing corresponding proteins. For stress granule markers we used following antibodies anti eIF2α phosphorylated (Cell signaling 9722; 1:100), and anti TIAR (Santa Cruz 1751; 1:100).

Imunoreactivity for SMN positive germs was studied using anti SMN (BD 610646; 1:100) and HDAC1 was visualized by anti HDAC1 (Bethyl A300-713A; 1:100).

Double immunostaining with anti ChAT (Millipore, AB144-P; diluted 1:50) was performed at the spinal cord for analyzing the localization of TAF15 (Abcam 134916; 1:100).

Imaging

Single-layer images (except for mouse embryonic fibroblasts (MEF) were acquired using a laser-scanning microscope (confocal Leica SP5 Leica Microsystems CMS GmbH) equipped with 63×oil objective (NA1.4). Excitation rays are sequential argon laser 488nm, diode 561nm, Helium Neon laser 633nm. Emission bandwidths are 500-550nm for Alexa488, 570-620nm for Alexa594, and 650-750nm for Draq5.

Confirmation of expression changes by quantitative RT-PCR

RNA samples from brains of *Fus*$^{\Delta NLS/\Delta NLS}$, *Fus*$^{-/-}$ and their control littermates were treated with DnaseI (Invitrogen) and converted to cDNA using SuperScript III kit (Invitrogen) with random hexamers or the Iscript Reverse Transcriptase (Bio-Rad). qRT-PCR reactions were performed with 3-5 mice for each group and two technical replicates using the iQ SYBR green Supermix (Bio-Rad) on either the IQ5, the CFX96 Touch or the CFX384 Touch Real-Time PCR detection system (Bio-Rad). Analysis was performed using the iQ5 optical system software (Bio-Rad; version 2.1) or the CFX manager system software (Bio-Rad; version 3.1). Expression values were normalized to the control gene Rsp9, and were expressed as a percentage of the average expression of the control samples. Primer sequences were designed using Primer3 software (http://frodo.wi.mit.edu/primer3/) and are available in **Dataset S9**.

Confirmation of splicing changes by semi-quantitative RT-PCR

Semi-quantitative RT-PCR (25-30 cycles) was used to validate alternative splicing changes. Isoform products were separated on 10% polyacrylamide gels and stained with SYBR gold (Invitrogen) and quantified with ImageJ software to record the intensity of the bands corresponding to different splicing isoforms. Intensity ratios of long and short isoforms were averaged from three biological replicates per group. Primer sequences were designed using Primer3 software (http://frodo.wi.mit.edu/primer3/) in exons flanking the alternatively spliced exon. PCR primer sequences are shown in **Dataset S9**.

Supplementary figures

Fig S1: Validation of expression changes identified by RNA-seq in *Fus*$^{\Delta NLS/\Delta NLS}$ and *Fus*$^{-/-}$ mouse brain

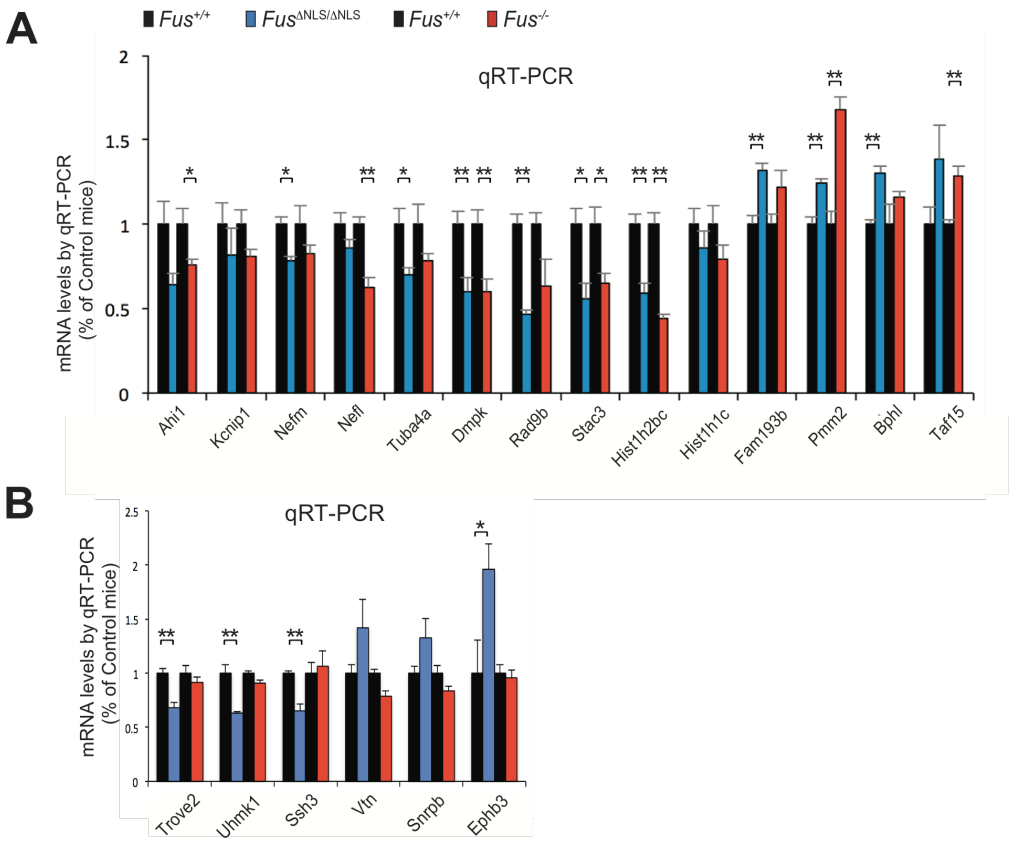

Expression levels of selected genes in *Fus*$^{\Delta NLS/\Delta NLS}$ (blue bars) and *Fus*$^{-/-}$ (red bars) compared to their control littermates (*Fus*$^{+/+}$, black bars).

(A) Quantitative RT-PCR (qRT-PCR) for genes identified by RNA-seq to be significantly downregulated (*Ahi1, Kcnip1, Nefm, Nefl, Tuba4a, Dmpk, Rad9b, Stac3, Hist1h2bc, Hist1h1c)* or upregulated (*Fam193b, Pmm2, Bphl, Taf15*) in both *Fus*$^{\Delta NLS/\Delta NLS}$ (blue bars) and *Fus*$^{-/-}$ (red bars) compared to their control littermates (*Fus*$^{+/+}$, black bars). Error bars represent SEM in 3-5 biological replicates.

(B) qRT-PCR for *Trove2, Uhmk1, Ssh3, Vtn, Snrpb* and *Ephb3* in brains from *Fus*$^{\Delta NLS/\Delta NLS}$ (blue bars), *Fus*$^{-/-}$ (red bars) and control littermates (*Fus*$^{+/+}$, black bars), showing genes identified by RNA-seq to be associated with the presence of truncated FUS in *Fus*$^{\Delta NLS/\Delta NLS}$ animals and not modified by loss of FUS in *Fus*$^{-/-}$ mice. Error bars represent SEM in 3-5 biological replicates.

Fig S2: Intermediate splicing pattern in heterozygous *Fus*$^{\Delta NLS/+}$mice

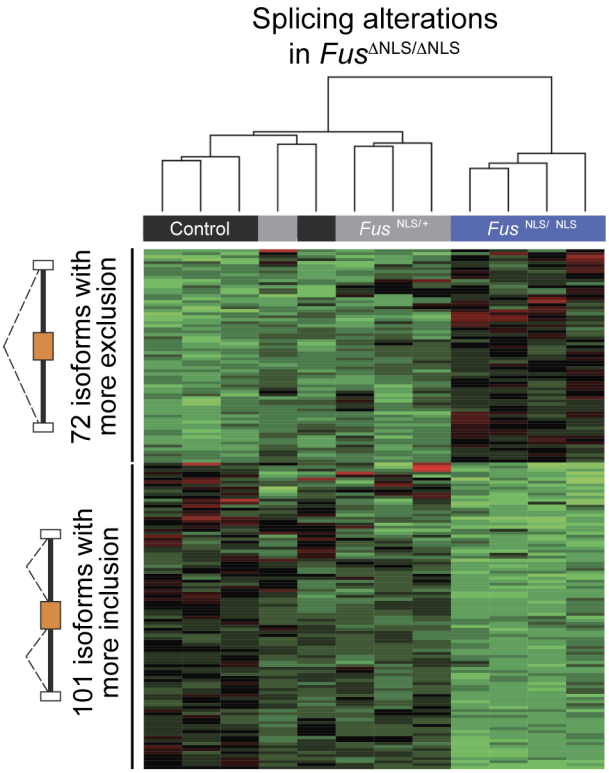

Heatmap with hierarchical clustering of RASL-seq data from biological replicates of *Fus*$^{\Delta NLS/\Delta NLS}$ (N=4), *Fus*$^{\Delta NLS/+}$ (N=4) and control littermates (N=4), showing 173 alternative splicing alterations associated with expression of cytoplasmic FUS in knock-in animals (defined by t-test with $p<0.05$ and average fold change >1.5).

Fig S3: Normal cortical development in *Fus* knock-in and knock-out mice

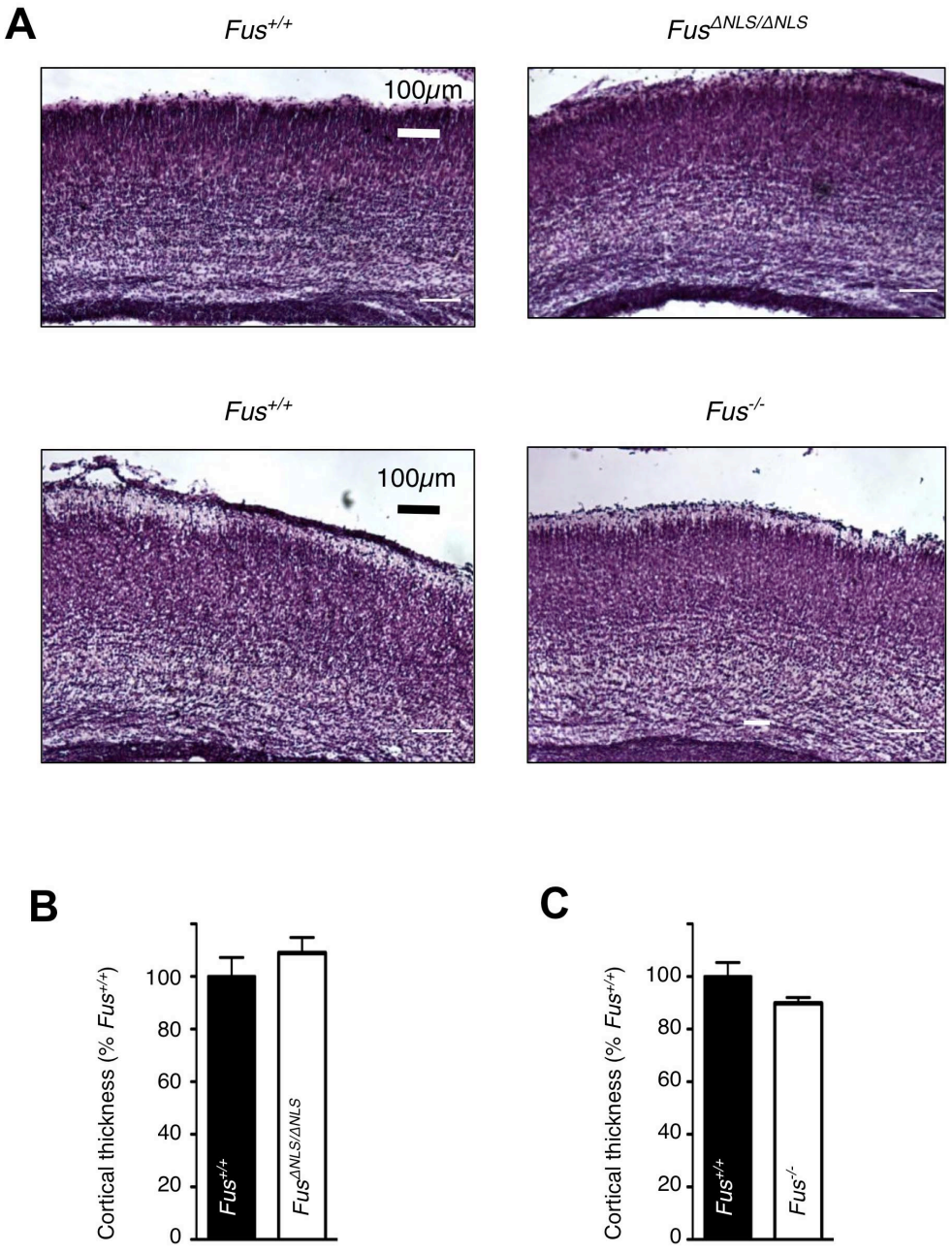

(A) Representative Nissl staining of cerebral cortex of $Fus^{-/-}$ mice and $Fus^{\Delta NLS/\Delta NLS}$ mice, and their respective controls at birth. Note that the cerebral cortex appear grossly normal in all 4 groups.
(B-C) Quantification of cerebral cortical thickness, relative to wild type littermates in $Fus^{\Delta NLS/\Delta NLS}$ mice (n=6 for $Fus^{+/+}$ and n=8 for $Fus^{\Delta NLS/\Delta NLS}$; **B)** and $Fus^{-/-}$ mice (n=9 for $Fus^{+/+}$ and n=9 for $Fus^{-/-}$; **C).** Scale bar: 100μm

Fig S4: Normal cortical layering in *Fus* knock-in and knock-out mice

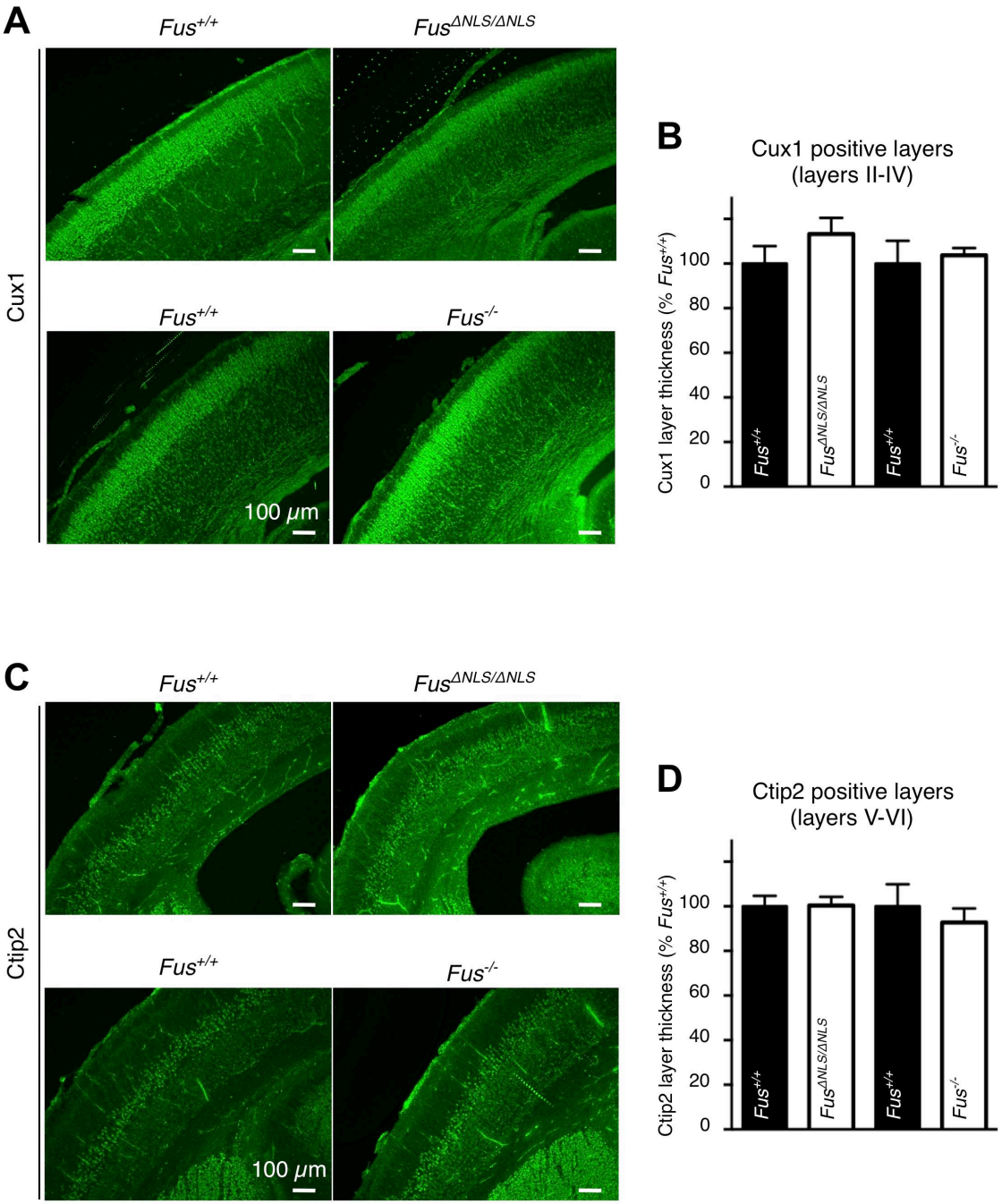

(A, B) representative immunofluorescent staining of Cux1 (**A**, marker of neurons from layers II-IV) and Ctip2 (**B**, marker of neurons from layers V-VI) in the cerebral cortex of *Fus*$^{-/-}$ mice and *Fus*$^{\Delta NLS/\Delta NLS}$ mice, and their respective controls at birth.

(C, D) Measurement of the thickness of Cux1 positive layers (B) and Ctip2 positive layers (D), in the cerebral cortex of *Fus*$^{-/-}$ mice and *Fus*$^{\Delta NLS/\Delta NLS}$ mice, and their respective controls at birth.

Scale bar: 100μm.

Fig S5: Normal subcellular distribution of TAF15 in *Fus*$^{\Delta NLS/\Delta NLS}$ mice

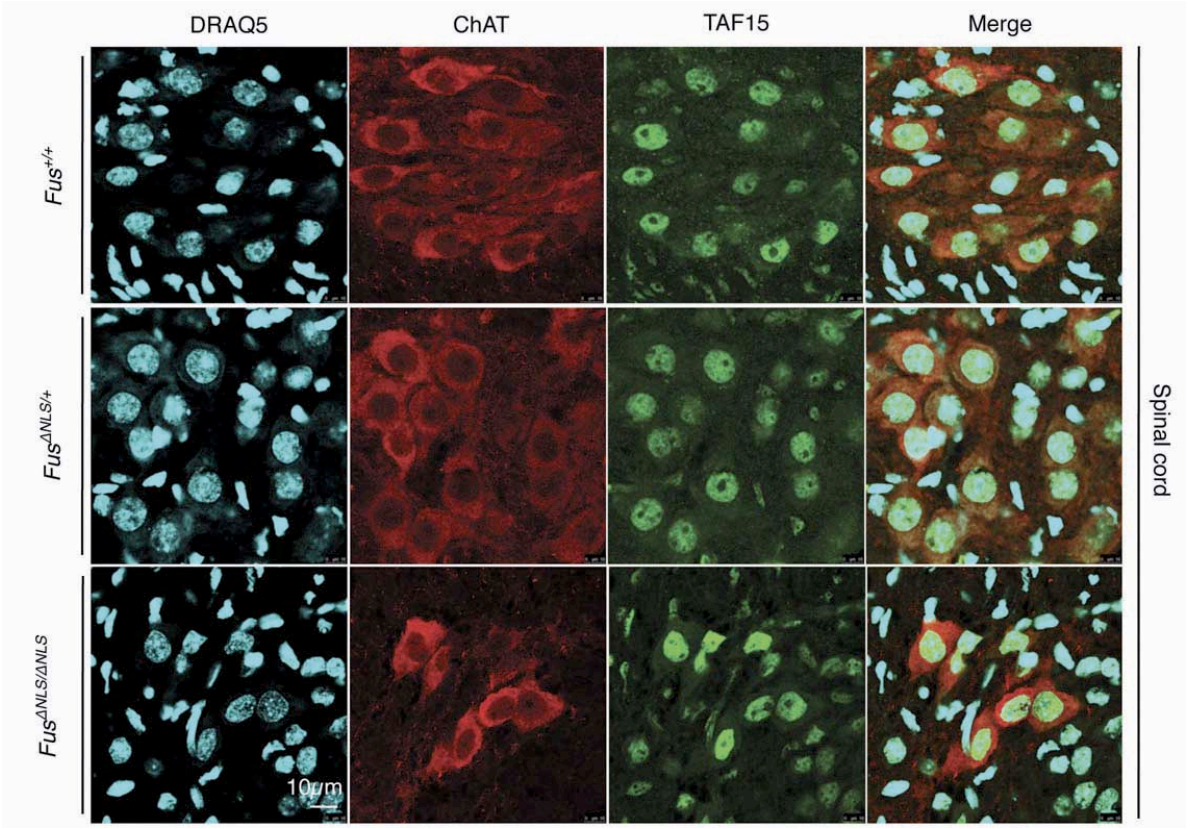

Representative images of immunofluorescent staining of motor neurons, labelled with DRAQ5 (nuclei, blue), ChAT (red) and TAF15 (green), a binding partner of FUS, that is also a FET family member.
Scale bar: 10μm.

Expanded View Figures

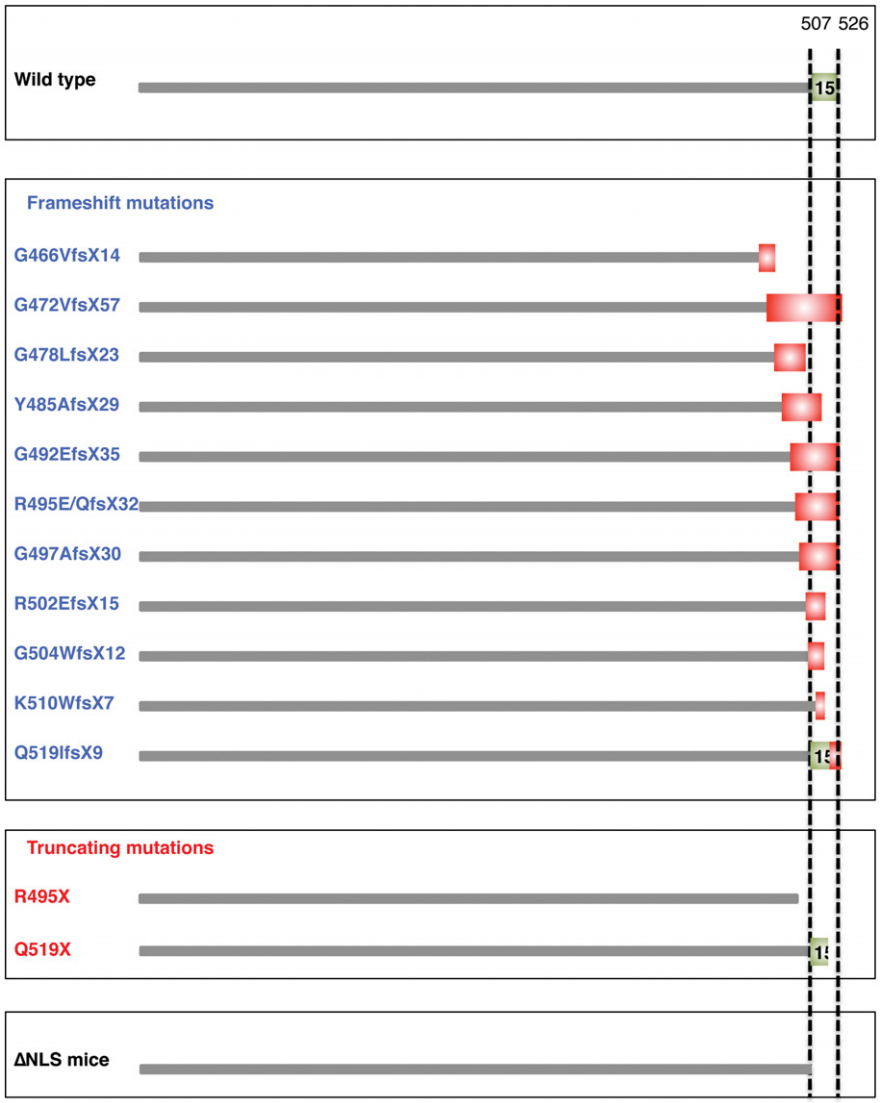

Figure EV1. Relevance of *Fus*$^{\Delta NLS}$ mice to human ALS.

Upper panel: Scheme of the wild-type FUS protein. The NLS, encoded by exon 15, includes the C-terminal amino acids (aa 507–526, boundaries shown by the two dashed lines). Middle panels: 11 frameshift mutations (upper middle panel) and 2 truncating mutations (lower middle panel) in the *FUS* gene have been identified in ALS families. The corresponding mutant FUS proteins are shown. Insertions of abnormal polypeptide sequences induced by frameshift mutations are shown as red boxes. Lower panel: structure of FUS$^{\Delta NLS}$ protein in *Fus*$^{\Delta NLS}$ mice.

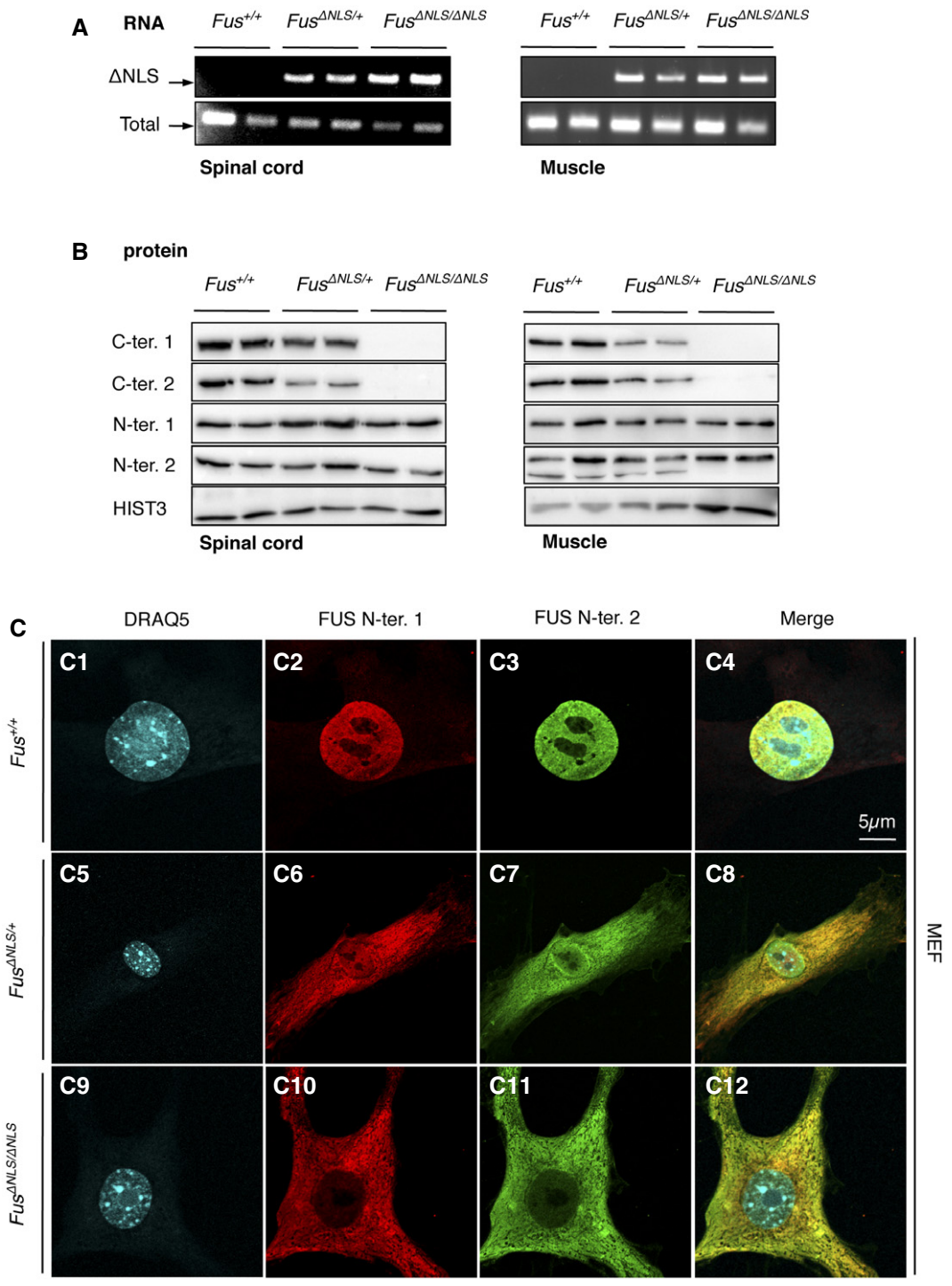

Figure EV2. Expression of the *Fus* gene in various tissues of *Fus*$^{\Delta NLS}$ mice.

A RT–PCR analysis of spinal cord and gastrocnemius muscle from 2 *Fus*$^{+/+}$, 2 *Fus*$^{\Delta NLS/+}$, and 2 *Fus*$^{\Delta NLS/\Delta NLS}$ P0 mice using primers located in the STOP cassette, and thus specific to the *Fus* ΔNLS mRNA (ΔNLS, upper panel), or primers located in exon 11 and 12, that is, upstream of the floxed cDNA insertion, and thus amplifying total *Fus* mRNA (Total, lower panel).

B Immunoblot analysis of FUS protein in spinal cord and gastrocnemius of 2 *Fus*$^{+/+}$, 2 *Fus*$^{\Delta NLS/+}$, and 2 *Fus*$^{\Delta NLS/\Delta NLS}$ mice using two different antibodies targeting the C-terminal (C-ter. 1 and C-ter. 2) NLS or antibodies targeting the N-terminal (N-ter. 1) and internal parts (N-ter. 2) of FUS.

C Representative confocal images for fluorescence immunocytochemical localization of FUS protein in mouse embryonic fibroblasts (MEFs).

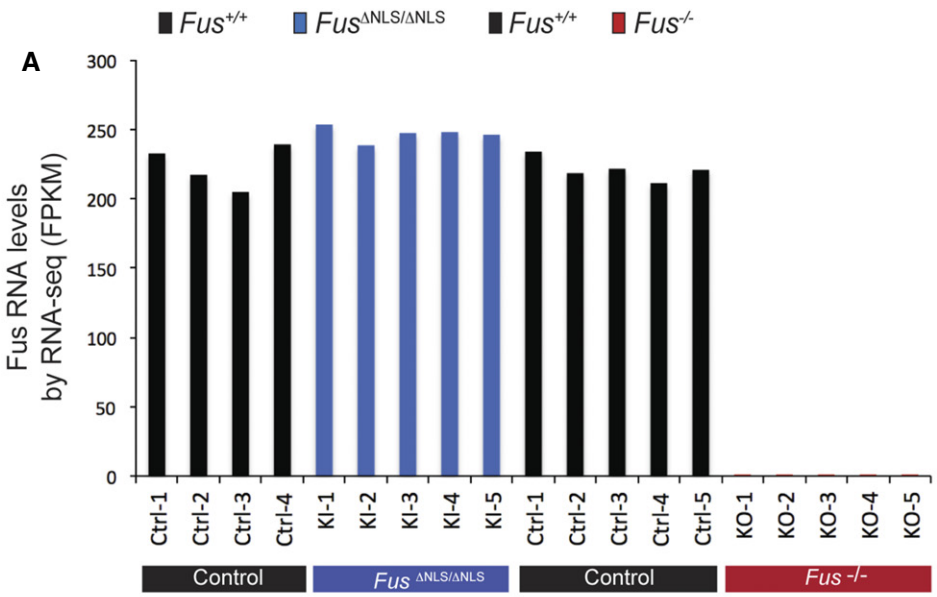

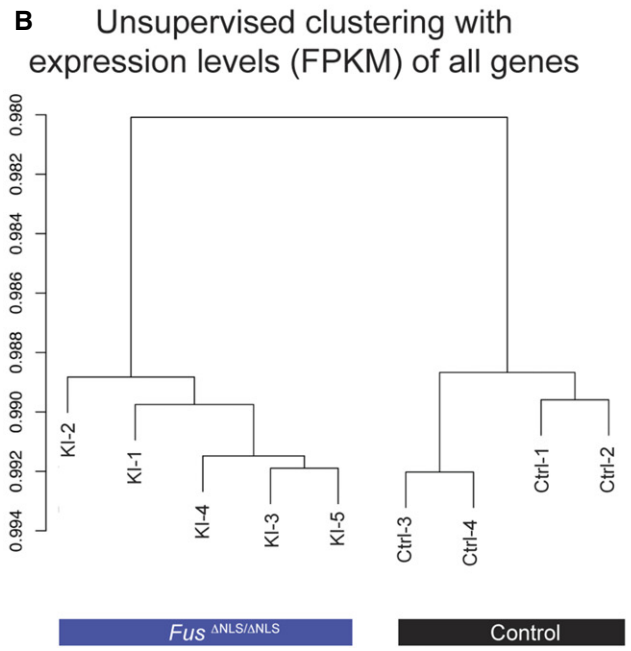

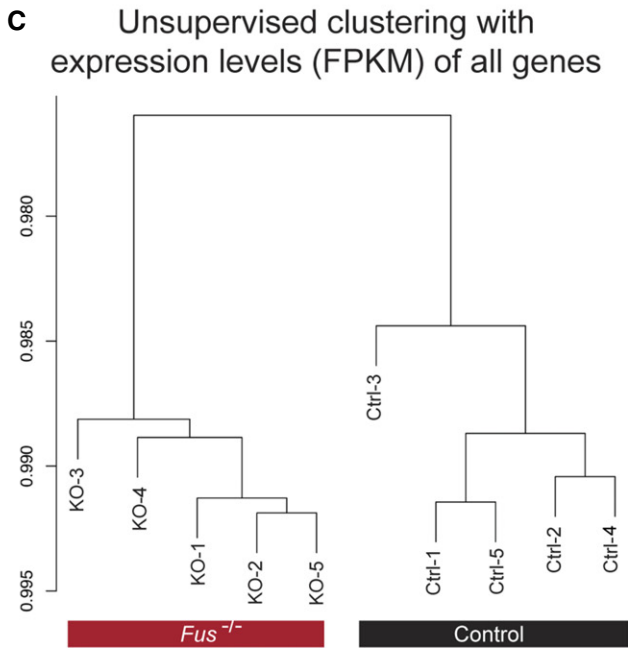

Figure EV3. Genomewide expression changes identified by RNA-seq in *Fus*$^{\Delta NLS/\Delta NLS}$ and *Fus*$^{-/-}$ brains.

A Quantification of *Fus* RNA levels by strand-specific RNA sequencing in brains from *Fus*$^{\Delta NLS/\Delta NLS}$ (blue bars), *Fus*$^{-/-}$ (red bars), and control littermates (*Fus*$^{+/+}$, black bars). RNA levels were determined by fragments per kilobase of transcript per million mapped reads (FPKM) value.

B Unsupervised hierarchical cluster analysis using all RNAs expressed in brains of *Fus*$^{\Delta NLS/\Delta NLS}$ mice (KI-1 to KI-5) and their control littermates (Ctrl-1 to Ctrl-4).

C Unsupervised hierarchical cluster analysis using all RNAs expressed in brains of *Fus*$^{-/-}$ mice (KO-1 to KO-5) and their control littermates (Ctrl-1 to Ctrl-5).

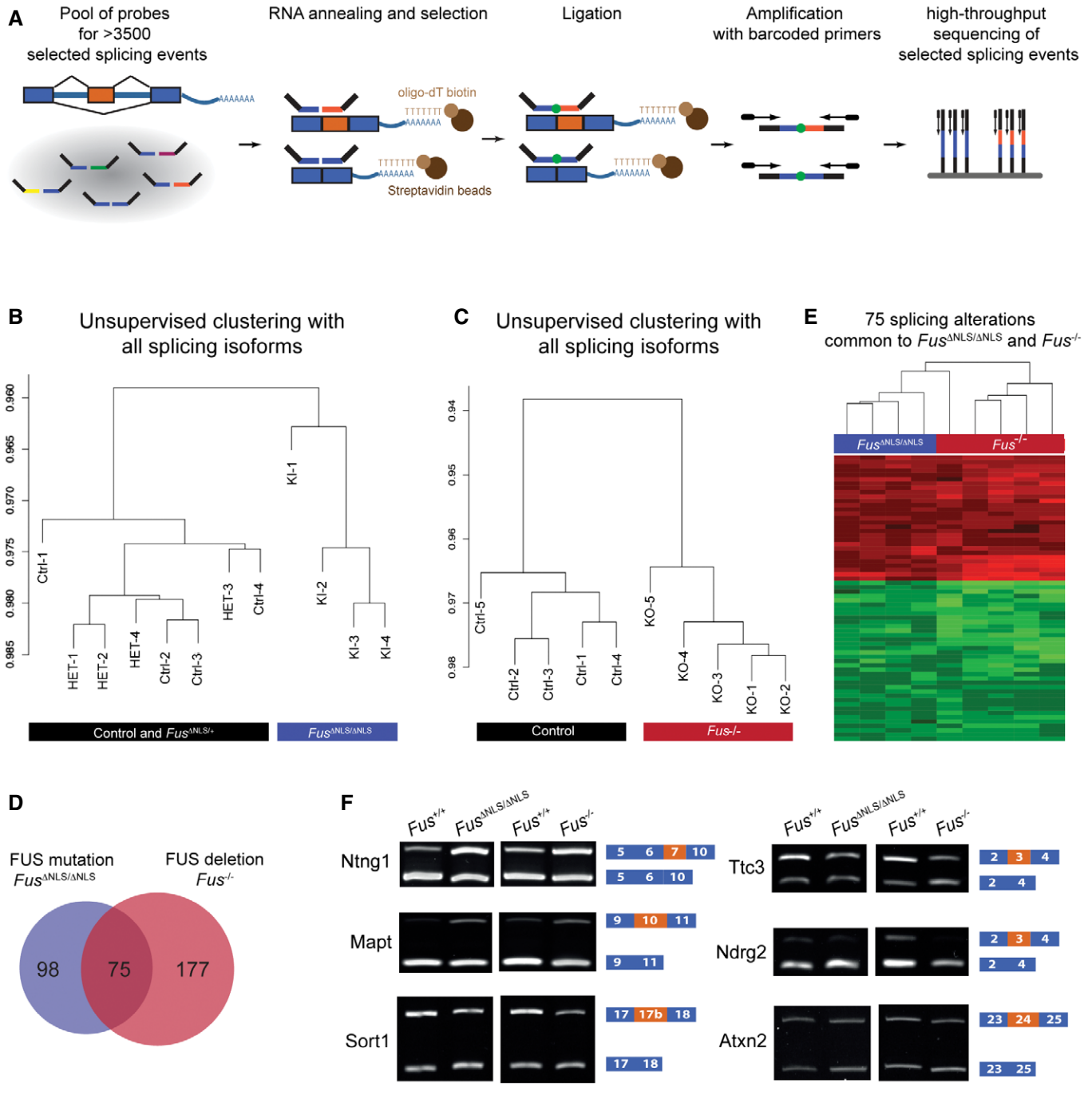

Figure EV4. FUS-dependent splicing alterations identified by RASL-seq.

A Schematic representation of the RASL-seq strategy to measure ratios of alternative splicing isoforms from thousands of selected splicing events by high-throughput sequencing.

B Unsupervised hierarchical cluster analysis using all splicing events sequenced in brains of $Fus^{\Delta NLS/\Delta NLS}$ mice (KI-1 to KI-4), $Fus^{\Delta NLS/+}$ (HET-1 to HET-4), and their control littermates (Ctrl-1 to Ctrl-4).

C Unsupervised hierarchical cluster analysis using all splicing events sequenced in brains of $Fus^{-/-}$ mice (KO-1 to KO-5) and their control littermates (Ctrl-1 to Ctrl-5).

D Venn diagram showing the number of overlapping splicing events that are misregulated in $Fus^{\Delta NLS/\Delta NLS}$ (blue circle) and $Fus^{-/-}$ (red circle) brains with 75 exons similarly altered upon cytoplasmic mislocalization or complete loss of FUS.

E Heat map using the fold changes of the 75 splicing events commonly regulated in $Fus^{\Delta NLS/\Delta NLS}$ and $Fus^{-/-}$ mice showing that 100% of the events were differentially included or excluded in the same direction.

F Semi-quantitative RT–PCR analyses of selected targets shown in Fig 5C with alternatively spliced exons depicted in orange boxes with their flanking constitutive exons in blue boxes.

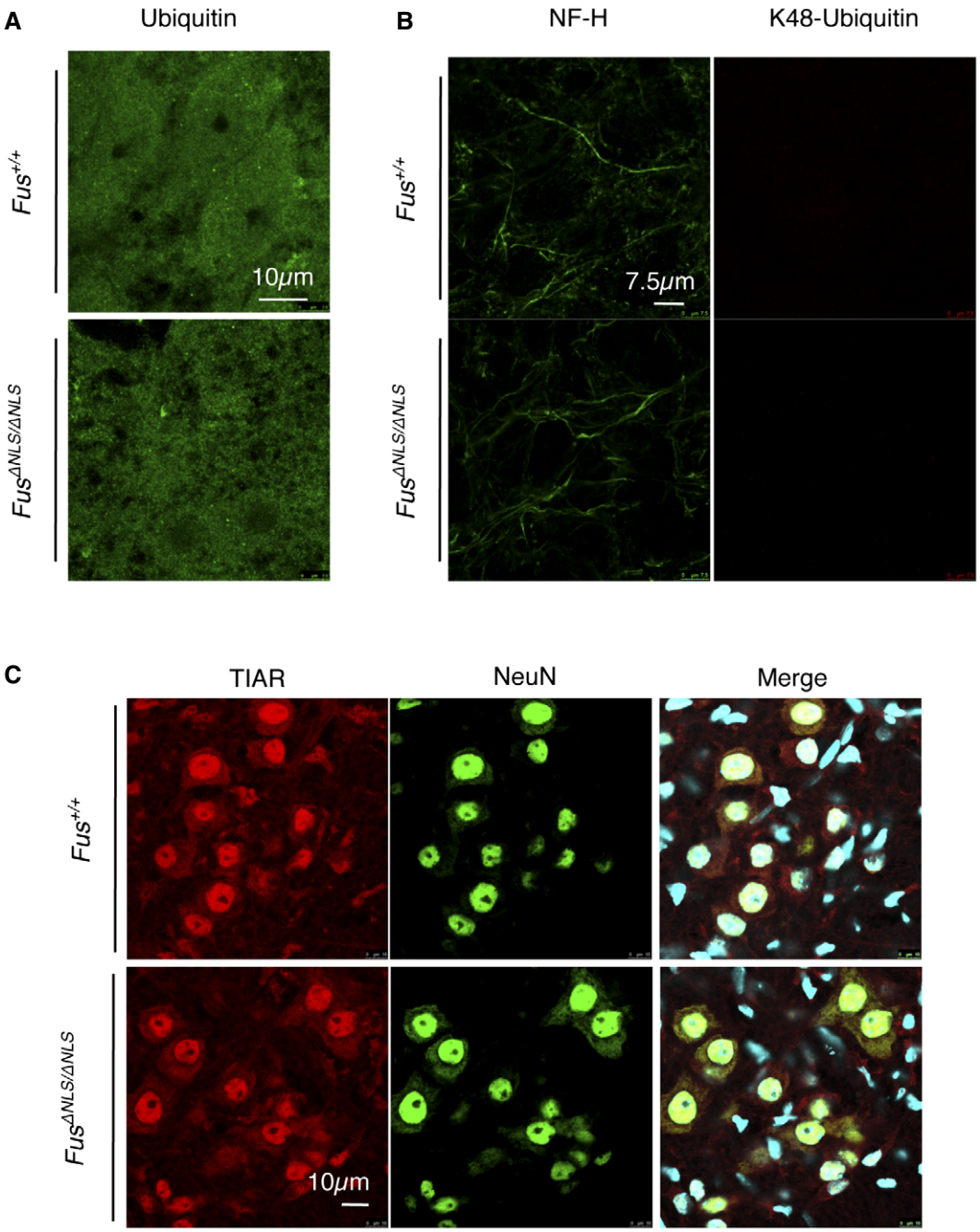

Figure EV5. The absence of protein aggregates and stress granules in *Fus*$^{\Delta NLS/\Delta NLS}$ mice.

A Representative images of ubiquitin staining (green) in the ventral spinal cord.

B Representative images of immunofluorescence staining of neurofilament heavy chain (green) and poly-ubiquitin (lysine 48; red). The neurofilament immunostaining shows normal filamentous staining, and the poly-ubiquitin staining is very weak and shows no positive aggregates.

C Representative images of immunofluorescence staining of neurons labeled with NeuN (green) and TIAR (red), a stress granule marker.

Dataset EV9: Primers for quantitative and semi-quantitative RT-PCR

Target	Sequence	
mouse Ntng1	Forward	GTATCCCCAGCATTTCCAGT
	Reverse	CTCTTCGCACCGTAGCTTCT
mouse Mapt	Forward	TCAGGTCGAAGATTGGCTCT
	Reverse	GGAGGTCACTTTGCTCAGGT
mouse Ttc3	Forward	TGCTGAGGGAGGTCTCAGTT
	Reverse	GGAGAGTGGCTTACTGCACC
mouse Ndrg2	Forward	AGGACAAACACCCGAGACTG
	Reverse	ATGGTAGGTGAATATCGCCG
mouse Atxn2	Forward	CTTCCATGACACCTGCCTCT
	Reverse	TCCACTGCAAGTGAGCTGTT
mouse Sort1	Forward	CAGGAGACAAATGCCAAGGT
	Reverse	TGGCCAGGATAATAGGGACA
mouse Ahi1	Forward	AGGGCAAAGATCAAAACGTG
	Reverse	TCTGCTTCGTCTCCAGCTTT
mouse Kcnip1	Forward	TGGCATTGTAACGTTAGATGAAT
	Reverse	GAATGGCCAGTGTCCTCAGT
mouse Nefm	Forward	CCATCCAGCAGTTGGAAAAT
	Reverse	CGGTGATGCTTCCTGAAAAT
mouse Nefl	Forward	GAGGCTACGAAAGCTGAGGA
	Reverse	TCACCCTCACCACCTTCTTC
mouse Dmpk	Forward	AGGAAGCCCTGGAAGAAGAG
	Reverse	TCTCCATCCGTTCCTGTAGC
mouse Rad9b	Forward	TTTCCCAAGGATTCTCCTGA
	Reverse	CGGCATACTCTTGCTGTTCA
mouse Stac3	Forward	TGACGTAACCACCAGCTTCA
	Reverse	CGGATTCTTCCCTCCAAACT
mouse Hist1h1c	Forward	CCGAAGCGCTTGCTTTATAC
	Reverse	CAGATAGCCAATTTAACATTTTGG
mouse Fam193b	Forward	CTGCAAAGCAAACTCGTCAG
	Reverse	CAGGGCACGTCAGAACTACA
mouse Pmm2	Forward	GGATAAGCGGTATTGCCTGA
	Reverse	CACAGATCCTGCGTGTGTCT
mouse Bphl	Forward	CAGTGCCCTACCCTCATTGT
	Reverse	TCGTCTGCAAAGCGTAAGTG
mouse Taf15	Forward	GTGGCTATGGAGGCAAAATG
	Reverse	GAAAGCAGCAGGCACACTCT
mouse Vtn	Forward	GTTCTCCAGCGAGGAGAGTG
	Reverse	GGGAGGATTCACAGAGTCCA
mouse Snrnpb	Forward	CTCCTGGCCGAGGAACTC
	Reverse	TCGCCTCTGAGCTACTGACA
mouse Hist1h2bc	Forward	ACACCAGCTCCAAGTGATCC
	Reverse	CACCCATTTGCACTGTCTTG
mouse Slc39a2	Forward	GTCATCACCACAGGGTCCTC
	Reverse	GAAGCAGCATCACGAGAAGA
mouse Dok3	Forward	GTGATCGTGCAGAGGACAGA
	Reverse	CAGCCTCAAACGAGAACACA
mouse Slc2a4rg-ps	Forward	GGCTAGGATCTGACCAGCAG
	Reverse	TCTCTGCATCCCAGACACTG
mouse Dnase1l2	Forward	CCACTCAGCCTCAGTTCACA
	Reverse	GTCTGCAGGTGGCATATCCT
mouse Ccdc24	Forward	AAGCCTTCTGGAGGAAGAGTG
	Reverse	GGCATTTGGGTGTCCTTAGA
mouse Mmp9	Forward	CATTCGCGTGGATAAGGAGT
	Reverse	TCACACGCCAGAAGAATTTG
mouse Ipw	Forward	CAGCAGCTTCACCAAAACAA
	Reverse	TGTAACTGGAGAGGGTTGCAG
mouse Trove2	Forward	CGCAGATGTCTTCGTTGTGT
	Reverse	TGCCTCTATCGTCTGGGTCT

mouse Uhmk1	Forward	CAAAGGAAAATCCTGGCAGA
	Reverse	CCCTCTTGTAGGCACTCAGC
mouse Tuba4a	Forward	GTCAGCTCTTCCACCCAGAG
	Reverse	AGGAAGCCCTGAAGTCCTGT
mouse Ephb3	Forward	GGTTTGCATCCTTTGACCTG
	Reverse	CTCGTTGGAGCTGAGTGTCA
mouse Ssh3	Forward	CCAGGAAACCCCAAAAGAAG
	Reverse	CCTTTGGCTCTTGAAAGCTG
mouse ΔNLS	Forward	AAACTATGGAGATGATCGACGTG
	Reverse	GATCCTCTAGAGTCGCAGATCCT
mouse Total Fus	Forward	TTATGGACAGACCCAAAACACA
	Reverse	TGCTGCCCATAAGAAGATTGT
mouse 18S	Forward	TCTGATAAATGCACGCATCC
	Reverse	GCCATGCATGTCTAAGTCGC
mouse Pol2	Forward	AATCCGCATGAACAGTG
	Reverse	TCATCCATTTTATCCACCACC
mouse Tbp	Forward	CCAATGACTCCTATGACCCCTA
	Reverse	CAGCCAAGATTCACGGTAGAT

Résumé de thèse

Hajer EL OUSSINI, Inserm UMR-S1118

« Contribution des neurones sérotonergiques à la sclérose latérale amyotrophique »

Introduction

La sclérose amyotrophique latérale (SLA) est une maladie neurodégénérative affectant 2 à 3 nouveaux patients par an pour 100 000 habitants, pour 15000 personnes atteintes de SLA au sein de l'union européenne. La SLA est due à la dégénérescence des motoneurones, situés dans la moëlle épinière et le tronc cérébral, qui contrôlent la contraction musculaire. Les neurones moteurs supérieurs, situés dans le cortex moteur sont aussi atteints, et l'hypothèse prévalente est que cette dégénérescence provoque l'apparition de spasmes musculaires et une hyper-réflexie.

La SLA est une maladie fatale, provoquant une insuffisance respiratoire fatale causée par l'atrophie et la paralysie progressive des muscles. Une grande partie des cas de SLA est associée à des mutations génétiques dans 5 gènes principaux (*SOD1, C9ORF72, TARDBP, FUS* et *TBK1*). Des modèles murins sont principalement caractérisés pour les mutations du gène *SOD1*. De tels modèles ont été utilisés au cours de cette thèse.

Contexte et axes de recherches

Notre laboratoire a démontré en 2013 que la dégénérescence associée à la SLA n'était pas limitée aux motoneurones et aux neurones moteurs supérieurs. Dentel et collaborateurs ont observé la dégénérescence des neurones sérotoninergiques présents dans le tronc cérébral, aussi bien dans les modèles animaux de SLA, que dans une cohorte de patients[1]. Ces auteurs ont aussi observé une augmentation de l'expression du gène codant pour le récepteur 2B de la sérotonine (5-HT2B) au moment du déclenchement des symptômes. Les neurones sérotonergiques centraux ont des actions régulatrices sur de nombreuses fonctions physiologiques, notamment la prise alimentaire, la mémoire ou la contraction musculaire, et leur dégénérescence pourrait donc affecter de nombreuses régions cérébrales et spinales.

L'objectif de ma thèse a été de caractériser le rôle des neurones sérotonergiques dans la SLA. Pour cela, nous avons décidé de baser notre projet d'étude sur trois questions principales.

1. Quelle est l'étendue de la dégénérescence sérotonergique ?
2. Quel est le rôle des neurones sérotonergiques dans le développement des symptômes liés à la SLA ?
3. Quel est le rôle du récepteur 5-HT2B dans la SLA ?

Les résultats obtenus pour ces trois questions sont présentés dans les pages suivantes.

Résultats

1/ Caractérisation de la dégénérescence des neurones sérotoninergiques

Tout d'abord, nous avons cherché à caractériser la dégénérescence des neurones sérotonergiques au cours de la progression de la maladie car les fonctions des régions affectées sont différentes. Pour ce faire, nous avons croisé un modèle murin de SLA (SOD1(G86R)) avec une souche de souris exprimant la protéine fluorescente YFP (Yellow fluorescente protein) sous le contrôle du promoteur Tph2 (tryptophane hydroxylase 2) spécifique aux neurones sérotoninergiques. Les souris SOD1(G86R) développent des symptômes similaires aux patients, notamment une paralysie et une perte de poids progressive dès 90 jours et un stade final de la maladie à partir de 105 jours.

Nous avons observé une dégénérescence massive des projections sérotoninergiques dans l'hypothalamus, le striatum et l'hippocampe. Cette perte axonales était observée même à un âge symptomatique (90 jours). Une partie de ces résultats a été publiée dans l'étude de Vercruysse et collaborateurs (Brain, 2016).

2/ Rôle des neurones sérotoninergiques dans la progression de la SLA

Nous avons ensuite étudié le rôle de la toxicité de la SOD1 mutée dans les neurones sérotoninergiques. Pour cela, nous avons utilisé un modèle de SLA conditionnel exprimant un gène SOD1 humain muté en position G37R, et flanqué de sites loxP [2]. Ce modèle exprime donc la SOD1(G37R) de façon ubiquitaire, sauf dans les cellules ayant exprimé la recombinase CRE.

Nous avons croisé ce modèle avec des souris exprimant la CRE sous le contrôle du promoteur Tph2. Nous avons tout d'abord vérifié, par différentes méthodes, que la recombinaison générée est bien spécifique des neurones serotonergiques centraux. Nous vons ensuite généré une cohorte importante de souris SOD1(G37R) (G37R) et de souris SOD1(G37R)/Tph2-CRE ($G37R^{\Delta Tph2}$) qui ont été suivi pendant l'intégralité de leur vie (>15 mois). Nous avons observé que les souris $G37R^{\Delta Tph2}$ présentaient une dégénérescence des neurones sérotonergiques plus faible que les souris G37R. La préservation des neurones sérotonergiques chez les souris $G37R^{\Delta Tph2}$ diminue très fortement la spasticité, ce qui accélère l'établissement de la paralysie. La survie n'est par contre pas affectée. Ces résultats, encore préliminaires seront consolidés par des analyses histologiques et moléculaires, et soumis à publication au cours du printemps 2016.

D'ores et déjà, nos résultats suggèrent que la spasticité, un symptôme fréquent en cas de SLA, est causée par la dégénérescence des neurones sérotoninergiques.

3/ Rôle du récepteur 5-HT_{2B} dans le cas SLA:

En dernier lieu, nous avons caractérisé le rôle du récepteur 5-HT2B dans la progression de la SLA.

Tout d'abord, nous avons analysé l'expression des récepteurs sérotoninergiques principaux (5-HTr) a été réalisé dans différents souris transgéniques modèles de SLA. Seule la surexpression de 5-HT_{2B}, précédemment observée par Dentel et collaborateurs, a été systématiquement observée dans les différents modèles animaux. Nous avons donc focalisé nos études fonctionnelles sur ce récepteur.

Le récepteur 5-HT_{2B} (5-HT_{2B}R) est impliqué dans la physiopathologie de l'hypertension artérielle pulmonaire, les fonctions cardiaques et la réponse inflammatoire. Au niveau central, 5-HT_{2B}R est impliqué dans de nombreuses fonctions comme la prise alimentaire ou l'impulsivité. Au niveau du système nerveux central, 5-HT_{2B}R est exprimé dans quelques rares populations neuronales, et est exprimé de façon prédominante dans les cellules microgliales.

Pour caractériser le rôle du 5-HT_{2B}R, nous avons croisé les souris SOD1(G86R) avec des souris knock-out (KO) du récepteur 5-HT_{2B}. L'ablation du récepteur 5-HT_{2B} chez les souris modèle de SLA a accéléré la progression de la maladie. Les souris SOD1 sans le récepteur 5-HT_{2B} présentaient une perte de poids plus importante et une diminution des performances motrices. Au niveau histologique la perte de 5-HT_{2B}R a provoqué une atrophie des motoneurones.

Par des expériences de tri cellulaire, nous avons montré que la surexpression de 5-HT_{2B}R avait pour origine les cellules CD11+, probablement les microglies. De fait, l'ablation de 5-HT2B a diminué l'expression de nombreux marqueurs inflammatoires et diminué l'activation microgliale. Les microglies de souris SOD1(G86R) sans 5-HT_{2B}R étaient plus fréquemment fragmentées, traduisant une dégénérescence accélérée de ce type cellulaire en absence de 5-HT_{2B}.

Nous avons ensuite étudié les polymorphismes génétiques du gène codant pour 5-HT_{2B}R (HT2BR) chez les patients SLA. Dans une cohorte de patients néerlandais, nous avons observé que l'allèle C du SNP rs10199752 présent dans le gène HTR2B était associé à une survie plus longue des patients. De plus, les patients porteurs d'une copie de cet allèle C du SNP rs10199752 présentent des niveaux augmentés de l'ARNm de 5-HT_{2B}R dans la moelle épinière et une diminution de la fréquence de la dégénérescence des microglies que les patients présentant deux copies de l'allèle A.

Ces résultats démontrent que le récepteur à la sérotonine 2B tarde la progression de la maladie et empêche la dégénérescence des microglies dans le cas d'une SLA. Ils ont été publiés dans la revue Acta Neuropathologica (El Oussini, 2016).

Conclusion et perspectives

Au cours de cette thèse, nous avons démontré que la dégénérescence des neurones sérotonergiques était importante dans les différentes régions de projection. Nous avons de plus montré que la spasticité était essentiellement d'origine sérotonergique au cours de la SLA, et que le récepteur 2B de la serotonine protégeait les microglies de la dégénérescence au cours de la SLA.

Ces trois principaux ouvrent la voie à des approches thérapeutiques qui ciblent cette population neuronale affectée lors de la maladie pour traiter la spasticité, la perte de poids et la neuroinflammation au cours de la maladie.

Publications en rapport avec le sujet de thèse:

Vercruysse P, Sinniger J, **El Oussini H**, Scekic-Zahirovic J, Dieterlé S, Dengler R, Meyer T, Zierz S, Kassubek J, Fischer W, Dreyhaupt J, Grehl T, Hermann A, Grosskreutz J, Witting A, Van Den Bosch L, Spreux-Varoquaux O, Ludolph A.C. & Dupuis L.

Alterations in the hypothalamic melanocortin pathway in amyotrophic lateral sclerosis**,**
Brain. 2016, in press (IF : 9,2)

El Oussini H, Bayer H, Scekic-Zahirovic J, Vercruysse P, Sinniger J, Dirrig-Grosch S, Dieterlé S, Echaniz-Laguna A, Larmet Y, Müller K, Weishaupt JH, Thal DR, van Rheenen W, van Eijk K, Lawson R, Monassier L, Maroteaux L, Roumier A, Wong PC, van den Berg LH, Ludolph AC, Veldink JH, Witting A & Dupuis L.

Serotonin 2B receptor slows disease progression and prevents degeneration of spinal cord mononuclear phagocytes in amyotrophic lateral sclerosis
Acta Neuropathol. 2016, in press (IF: 10,8)

Autres publications

Scekic-Zahirovic J., Sendscheid O., **El Oussini H**., Jambeau M., Ying S., Mersmann S., Wagner M., Dieterlé S., Sinniger J., Dirrig-Grosch S., Drenner K., Birling M.C., Qiu J., Zhou Y., Li H., Fu X.D., Rouaux C., Shelkovnikova T., Witting A., Ludolph A.C., Kiefer F., Storkebaum E., Lagier-Tourenne C. & Dupuis L.

Toxic gain of function from mutant FUS protein is crucial to trigger cell autonomous motor neuron loss
EMBO J, 2016, in press (IF : 10.4)

Kabashi E, **El Oussini H,** Bercier V, Gros-Louis F, Valdmanis PN, McDearmid J, Mejier IA, Dion PA, Dupre N, Hollinger D, Sinniger J, Dirrig-Grosch S, Camu W, Meininger V, Loeffler JP, René F, Drapeau P, Rouleau GA, Dupuis L.

Investigating the contribution of VAPB/ALS8 loss of function in amyotrophic lateral sclerosis.
Hum Mol Genet. 2013 Jun 15;22(12):2350-60. (IF : 6.7)

Han SM, **El Oussini H**, Scekic-Zahirovic J, Vibbert J, Cottee P, Prasain JK, Bellen HJ, Dupuis L, Miller MA.

VAPB/ALS8 MSP ligands regulate striated muscle energy metabolism critical for adult survival in caenorhabditis elegans.
PLoS Genet. 2013;9(9):e1003738. (IF : 8.2)

Communication:

Presentation orale:
Journée de l'école doctorale ED414 2014 (prix de la meilleure présentation)
ENCALS Dublin 2015 (communication sélectionnée sur résumé)

Poster:
Journée de l'école doctorale ED414 2013 (Présentation du sujet de thèse)
ENCALS Leuven 2014

References

1. Dentel, C. *et al.* Degeneration of serotonergic neurons in amyotrophic lateral sclerosis: a link to spasticity. *Brain* **136**, 483-93 (2013).
2. Boillee, S. *et al.* Onset and progression in inherited ALS determined by motor neurons and microglia. *Science* **312**, 1389-92 (2006).

Hajer EL OUSSINI

Rôle des neurones sérotoninergiques dans la sclérose latérale amyotrophique

Résumé

La sclérose amyotrophique latérale (SLA) est une maladie neurodégénérative due à la dégénérescence des motoneurones supérieurs dans le cortex moteur et des motoneurones inférieurs situés dans la moelle épinière et le tronc cérébral. La perte des neurones moteurs provoque l'atrophie et la paralysie progressive des muscles. Notre laboratoire a démontré en 2013 que la dégénérescence associée à la SLA n'était pas limitée aux motoneurones mais aussi aux neurones sérotoninergiques chez les patients et les modèles animaux de SLA. L'objectif de ma thèse a été de caractériser le rôle des neurones sérotoninergiques dans la SLA.

On a observé une augmentation de l'expression du gène codant pour le récepteur 2B de la sérotonine (5-HT_{2B}) chez les modèles murins de SLA. L'analyse du rôle du récepteur 5-HT_{2B} dans le cas de SLA a montré que ce dernier est un modulateur de la maladie. La perte du récepteur 5-HT_{2B} accélère la progression de la maladie et modifie la régulation de la réponse inflammatoire.

En plus, nos travaux ont révélé que la perte des neurones sérotoninergiques est à l'origine du développement de la spasticité, un symptôme douloureux chez les patients SLA. Ces résultats ouvrent la voie à des approches thérapeutiques qui ciblent cette population neuronale affectée lors de la maladie pour traiter la spasticité et la neuroinflammation au cours de la maladie.

Résumé en anglais

Amyotrophic lateral sclerosis (SLA) is a neurodegenerative disease characterize by the loss of upper motor neurons in the motor cortex and lower motor neurons in the brainstem and spinal cord. The loss of motor neurons leads to muscle atrophy and progressive paralysis. In 2013 our laboratory identified a new neuronal population affected in ALS. They observed the degeneration of serotoninergic neurons in ALS patients and animal models. For this, the aim of my PhD is to identify the role of serotoninergic neurons in case of ALS.

We observed an upregulation of serotonin receptor 5-HT_{2B} in ALS mice models. The investigation of the role of 5-HT_{2B} receptor in case of ALS showed its role as a disease modulator. The loss of 5-HT_{2B} receptor accelerated disease progression and modulated neuroinflammatory response.

Moreover, our results showed that the loss of serotoninergic neurons is responsible of the development of spasticity, a painful symptom observed in ALS patients. All these opened the way for therapeutic strategies targeting spasticity and neuroinflammation in case of ALS.